

*motion*

FACILITY FORM 602	N67-15850	N67-15880
	(ACCESSION NUMBER)	(THRU)
	422	1
	(PAGES)	(CODE)
		05
	(NASA CR OR TMX OR AD NUMBER)	(CATEGORY)

# SECOND ANNUAL NASA-UNIVERSITY CONFERENCE ON MANUAL CONTROL

GPO PRICE \$ 2.50

CFSTI PRICE(S) \$ \_\_\_\_\_

Hard copy (HC) \_\_\_\_\_

Microfiche (MF) 4.55

ff 653 July 65

MASSACHUSETTS INSTITUTE  
OF TECHNOLOGY

Cambridge, Massachusetts

February 28 - March 2, 1966



NATIONAL AERONAUTICS AND SPACE ADMINISTRATION

# SECOND ANNUAL NASA-UNIVERSITY CONFERENCE ON MANUAL CONTROL

*Massachusetts Institute of Technology  
Cambridge, Massachusetts  
February 28 - March '2, 1966*



*Scientific and Technical Information Division*

OFFICE OF TECHNOLOGY UTILIZATION

NATIONAL AERONAUTICS AND SPACE ADMINISTRATION

Washington, D.C.

1966



FOR SALE BY THE SUPERINTENDENT OF DOCUMENTS, U.S. GOVERNMENT PRINTING OFFICE

WASHINGTON, D. C., 20402 - PRICE \$2.50

*Library of Congress Catalog Card Number 66-61934*

## FOREWORD

This volume contains the proceedings of the Second Annual NASA-University Conference on Manual Control held February 28 to March 2, 1966, at Cambridge, Massachusetts. The program was divided into the following nine sessions: discrete and continuous models, adaptive control, information theory, multivariable control, display, motion and stress, applications, optimal control, and analysis and design methods. Both formal and informal presentations were made. All of the formal and some of the informal papers are included in this volume. The session on applications contained only informal presentations, and it is not included in these proceedings although the major points of that session are reviewed in the summary.

# CONTENTS

	<i>page</i>	
Summary.....	1	✓

## DISCRETE AND CONTINUOUS MODELS

1. Summary of Sine-Wave Tracking Studies .....	15	✓
R. W. Pew, J. C. Duffendack, and L. K. Fensch		
2. Asynchronous Finite State Models of Manual Control Systems .....	25	✓
G. A. Bekey and E. S. Angel		
3. Some Neuromuscular Subsystem Dynamics .....	39	✓
Duane McRuer		

## ADAPTIVE CONTROL

4. Process of Adaptation by the Human Controller .....	47	✓
Jerome I. Elkind and Duncan C. Miller		
5. Model of Human-Operator Response to Step Transitions in Controlled Element Dynamics .....	65	✓
D. H. Weir and A. V. Phatak		
6. Adaptive Model of the Human Operator in a Time-Varying Control Task .....	85	✓
E. E. Gould and K. S. Fu		
7. Man in an Adaptive and Multiloop Control System .....	99	✓
Y. T. Li		
8. Time Varying and Nonlinear Models of Human Operator Dynamics .....	107	✓
W. W. Wierwille and G. A. Gagné		

## INFORMATION THEORY

9. Usefulness of Transinformation as a Measure of Human Tracking Performance ----	111	✓
T. Wempe and D. Baty		
10. Measured Information Capacity as a Performance Index in Manual Tracking Tasks .....	131	✓
Patrick A. Gainer		

## MULTIVARIABLE CONTROL

11. Human Performance in Single- and Two-Axis Tracking Systems .....	143	✓
E. P. Todosiev, R. E. Rose, and L. G. Summers		

	<i>page</i>	
12. Two-Dimensional Manual Control Systems -----	159	✓
William H. Levison		
13. Pilot Describing Function Measurements in a Multiloop Task-----	181	✓
R. L. Stapleford, D. T. McRuer, and R. Magdaleno		
14. Pilot Response in Multiloop Tracking Tasks in Combination With Side Tasks -----	205	✓
James J. Adams		

### DISPLAY

15. Symbolic and Pictorial Displays for Submarine Control -----	213	✓
Robert C. McLane and James D. Wolf		

### MOTION AND STRESS

16. Some Effects of Motion Cues on Manual Tracking -----	231	✓
Laurence R. Young		
17. Acceleration Stress Effects on Pilot Performance and Dynamic Response-----	241	✓
Melvin Sadoff and C. B. Dolkas		
18. The Effect of Minor Alcohol Stress on Tracking Skill -----	259	✓
C. B. Gibbs		
19. An Evaluation of Three Types of Hand Controllers Under Random Vertical Vibration -----	269	✓
A. Z. Weisz, R. W. Allen, and C. J. Goddard		
20. Human Describing Functions Measured in Flight and on Simulators -----	279	✓
Harriet J. Smith		

### OPTIMAL CONTROL

21. Preview Control Behavior and Optimal Control Norms-----	293	✓
T. B. Sheridan, B. F. Fabis, and R. D. Roland		
22. Studies in Optimal Behavior in Manual Control Systems: The Effect of Four Performance Criteria in Compensatory Rate-Control Tracking -----	311	✓
Richard W. Obermayer, Raymond B. Webster, and Frederick A. Muckler		
23. Human Decision-Making in Manual Control Systems -----	325	✓
R. E. Thomas and J. T. Tou		
24. Differential Games and Manual Control -----	335	✓
Sheldon Baron		
25. Dynamic System Modeling of Human Operators—A Preliminary Report -----	345	✓
Peter L. Falb and George Kovatch		

### ANALYSIS AND DESIGN METHODS

26. A "Critical" Tracking Task for Man-Machine Research Related to Operator's Effective Delay Time -----	361	✓
H. R. Jex, J. D. McDonnell, and A. V. Phatak		
27. Design Applications of Adaptive (Self-Adjusting) Simulators -----	379	✓
Charles R. Kelley		

## CONTENTS

	<i>page</i>	
28. Discussion of Spectral Human-Response Analysis -----	403	✓
Lawrence W. Taylor, Jr.		
29. Analysis and Prediction of Performance of a Digital Computer Facility for Flight Simulation Studies -----	413	✓
M. C. Grignetti and J. I. Elkind		

N67-15851

## SUMMARY

*Lawrence R. Young*  
*Massachusetts Institute of Technology*  
*and*

*Roger Windblade*  
*Office of Advanced Research and Technology, NASA*

The growing complexity of advanced vehicles developed in recent years for transportation on or near the surface of the earth, as well as in outer space and in the ocean, places enormously increasing demands of the man-machine interactions associated with piloting these vehicles. The development of versatile and reliable automatic control equipment also forces a reexamination of the appropriate roles of men in controlling these complex systems. The consequence of this trend has been the desire of systems engineers to seek more quantitative descriptions of the behavior of humans in tracking and control tasks—descriptions which would be compatible with conventional engineering design specifications so that the effect of the "man in the loop" might be readily evaluated and potential problem areas avoided.

Although application of control theory to manual systems was begun both in England and in the United States during the Second World War, it was not until the 1950's in the United States that a significant number of researchers turned their attention to the problem of generating mathematical models for the human operator. A series of informal conferences of the engineers and psychologists working on these problems, known as the "Annual Manuals," were begun in the late 1950's. In 1964, the growing number of interdisciplinary workers in the field convened at the University of Michigan-NASA Manual Control Conference held in Ann Arbor.

In 1966 an attempt was made to bring together the engineering psychology specialists who have been developing more advanced models of the pilot in a control loop and some of the engineers concerned with application of such models to designs of advanced man-vehicle systems. Approximately one hundred people attended the 3-day NASA-University Conference on Manual Control at the Massachusetts Institute of Technology in Cambridge, from February 28 to March 2. The conference was organized and chaired by the authors of this summary.

Most of the manual control experts agree on the adequacy of a quasi-linear describing-function model for the human operator when he is displayed only the error signal in a single-axis tracking task with reasonably well behaved and nontime-varying plant dynamics. (Such models consist of a variable dead time, variable lead and/or lag time constants, a fixed neuromuscular delay and variable gains, and an additive remnant term representing the portion of the operator's output not linearly correlated with the input. The variable parameters have been cataloged for a wide variety of plant dynamics and input spectra.) The emphasis in the conference, consequently, was on the development of other models to describe human operator behavior in greater detail or in multiple-loop, multiaxis, time-varying or deliberately nonlinear tracking situations, as well as the application of our notions of tracking

ability to a variety of vehicle control tasks. The formal program was divided into nine sessions, some of the highlights of which are described in the following paragraphs.

## DISCRETE AND CONTINUOUS MODELS

With the general acceptance of the quasi-linear model for design purposes, as mentioned above, the emphasis in this session was on the "fine structure" of the operator's behavior. Curiously enough, there was no further discussion of simple sampled data models to describe either transient tracking behavior or the "sampling peak" in the operator's remnant power spectrum. G. A. Bekey and E. S. Angel proposed a class of synchronous, finite-state models in which the input and output of the operator are assumed quantized rather than continuous, and the operator himself is modeled by a simple finite-state machine performing asynchronous switching among states. Although input and output quantization and bang-bang operation have long been observed, the techniques for synthesizing finite-state models are in their infancy and, consequently, no judgments as to the possible usefulness of such an approach can be made at this time.

In a new study of an old problem, R. W. Pew, J. C. Duffendack, and L. K. Fensch investigated tracking of single sinusoids under various control and display gains and display modes. They verified a prediction of the McRuer and Krendel "successive organization of perception" model, showing that with increasing practice the subjects used the coherency of the input to track with a compensatory (error only) display in a manner similar to tracking with a pursuit (input, output, and error) display. In an attempt to create a "rational parameter model" which would tie the properties of the mathematical describing function to known descriptions of the biophysics of the system, D. T. McRuer presented a preliminary neuromuscular model for hand movement. Considerable interest was shown in the relations between the "neuromuscular wiring diagram" and observed tracking performance.

## ADAPTIVE CONTROL

In parallel with the interest in automatic adaptive control, the study of these characteristics of man, the archetype adaptive controller, began recently and has been intensified in the past few years. Attempts to observe or explain the changes in human tracking behavior as the plant dynamics suddenly fail or otherwise undergo a rapid change have been hampered by the inability to track the "human control law" during the brief period of active adaptation. Three papers in this session specifically treated the problem of modeling human adaptive behavior following rapid changes in plant dynamics. The phases of the adaptive process are detection of a change in plant dynamics, identification of the nature of the new dynamics, modification of the operator's control law to reduce the accumulated error consistent with the new situation, and optimization of tracking characteristics to bring the long-term performance up on a symptotic level. J. I. Elkind and D. C. Miller emphasized the first of these phases. Using a model reference-type adaptive control scheme, they proposed a model in which the man compares the actual error rate over a sampling period to the error rate he would have expected based on his knowledge of his control movements and an internal representation of the plant dynamics. When the difference between these predicted and observed error rates exceeds some criterion level, the model predicts detection of a change in plant dynamics, and enters an identification phase. Experiments on actual detection time following controlled element transitions support this theory. E. E. Gould and K. S. Fu directed their attention to the modeling of the identification phase of the adaptive process, proposing that the operator uses pattern recognition techniques to identify the order of the system being controlled. A model based on linear decision theory to choose among position, derivative,

and integral control is presented. Although no experimental validation was available, the combination of the approaches of these two papers would yield a testable model for the detection and identification phases.

D. H. Weir and A. V. Phatak modeled the human adaptive response to transitions in controlled element dynamics in a descriptive manner which avoids the question of how the operator decides when a change occurred and what the change was. It may prove quite useful for ad hoc studies of accumulated error during particular system failures. They assumed that the appropriate human control behavior for the pretransition and posttransition dynamics are known and that the main problem is merely when and how the operator switches between the two. System error typically diverges while the operator continues tracking with his pretransition control law. Weir and Phatak hypothesized that once detection and identification occur, the operator reduces the accumulated error in an optimal, or near optimal, manner until it reaches a level where steady-state transition control may be used. Such an approach, if validated experimentally and supported by reliable tables of expected duration of pretransition retention periods, could permit an estimation of what happens to a manual control system following changes in vehicle dynamics.

A more general approach to the man-machine adaptive control problem was taken by Y. T. Li who emphasized the trade-off between speed of adaptive control and the use of precisely defined performance indices.

## INFORMATION THEORY

Since Shannon popularized the information theory approach to transmission and processing of signals and noise in communication systems nearly 20 years ago, there have been repeated attempts in mathematical psychology to characterize the human as a fixed channel-capacity information processor. The obvious advantage of such a characterization would be the ability to assess the work load imposed by a variety of subtasks in terms of the number of bits/sec they required and the human capacity. Human transinformation capacity was measured for simple decision tasks and jobs such as sending or receiving code, typing, and piano playing. As regards characterization of human operators in a tracking task, however, the application of information theory had yielded disappointingly few usable results and has been virtually neglected in the literature for the past 5 years.

T. Wempe and D. Baty took a fresh look at this problem in an effort to determine the usefulness of transinformation as a human tracking measure. In attempting to define an appropriate measure of information for the human tracking task, they concluded that the traditional communication concept, which examines how closely the operator's output reproduces the input, is not appropriate since it does not penalize the instantaneous error or shifting of the waveform resulting from the operator's delay. An alternate definition of transinformation, considering the effective bandwidth of the input signal and the correlation between input and the inphase component of output, is proposed and compared with experimental tracking results. Although this transinformation formulation agreed with the subjective opinion about task difficulty and ability to accomplish the task, it was not successful in predicting the operator's control law. Rather, the control characteristics assumed by the operator seemed to be of the type to minimize relative error, just as that assumed in most of the quasi-linear describing function models for the operator. Figure 1 shows how the operator chooses a time constant ( $T_f$ ) and gain crossover frequency ( $f_{XO}$ ) for a given task, which seem to minimize the relative error. The tentative information-processing model suggested by Wempe





error scores for the relatively simple dynamics considered; however, an interesting difference in the pilot model was found for the case of two-axis tracking with the more sluggish system. In order to maintain the same level of error performance as in single-axis tracking, the operator was forced to adopt a significantly greater lead-time constant for two-axis tracking. (This increased lead might reflect the effect of sampling two input channels, which requires the operator to extrapolate the error on the unattended channel by means of velocity estimates.) In a related set of experiments, W. H. Levison verified that two-axis performance degradation was small when the tracking conditions were homogeneous, whether the inputs to the two axes were the same or different. However, when the dynamics in the two axes were different (position control and acceleration control), the effects on system error were large and significant, increasing the normalized mean-squared error from 15 to 125 percent. Furthermore, the subject describing functions showed important changes in this case. Levison suggests that visual motor interaction, differential allocation of attention, and nonhomogeneity of required equalization must all be considered in deciding upon modification of the single-axis models for multiaxis tasks.

A somewhat different problem is presented by the multiloop task, which was investigated by R. L. Stapleford, D. T. McRuer, and R. Magdaleno, using lateral aircraft control (bank angle and yaw velocity) as a test situation. They recorded error, describing functions, and pilot opinion for the multiloop control situation, and concluded that the quasi-linear pilot model and adjustment rules, which had been developed for single-loop systems, are in general applicable to multiloop system command loops. For simultaneous closure of an inner loop, however, the single-loop pilot models may be applied only with some reservations, and the ability to increase performance through use of a crossfeed from one loop to the other must be accounted for. These authors also found that in this multiloop situation the tracking errors can be kept down to the level of a single-loop task; however, subjective opinion is degraded.

The final paper in the session, by J. J. Adams, reported on experiments involving the pilot in multiloop tracking tasks in combination with side tasks. Adams used multiloop tasks representative of altitude and horizontal translation control of an Apollo lunar excursion module. For multiple-loop control of vehicle pitch and translation, simple pilot models for each loop were shown to be useful. He showed that some of the multiloop characteristics could be easily reproduced if one included switching in the model of the human controller, representing a duty cycle, or periods of neglect of control in the inner loop.

## DISPLAYS

Human performance in a control task is directly affected by the method used to display information about the controlled element. The fifth session of the conference, entitled "Displays," considered three very different approaches to the problem of information display.

R. L. McLane discussed the results of a program designed to examine differences in submarine control performance as a function of display format. The two formats investigated were the pictorial contact analog shown in figure 2 and the symbolic depth azimuth display. The results of this very thorough study point up the lack of sensitivity in current performance measurement techniques. The lower tracking error scores achieved on the pictorial display could only be considered a general trend, rather than a statistically significant difference in all cases.

The first of the two informal presentations in this session was made by J. C. Bliss, who described the results of a series of tracking experiments using the tactile sense modality as the channel for displaying information to the controller. The technique used to generate the tactile information consisted of a series of air jets located above the outstretched index finger when the hand was placed on the manipulator. The subject attempted to maintain the air jet above the first knuckle of the index finger. Comparisons were made between performance with the tactile display and a comparable visual display in which the air jets were replaced by small light bulbs. The results of these experiments indicate that the reaction times in tracking tactile step inputs may be slightly less than with the visual system, and in addition the tactile display appears to reduce the tendency to overshoot when presented with more complex dynamics. While currently more difficult to mechanize, the tactile display appears to offer a feasible means of providing control information, particularly in situations where visual information can not be presented.

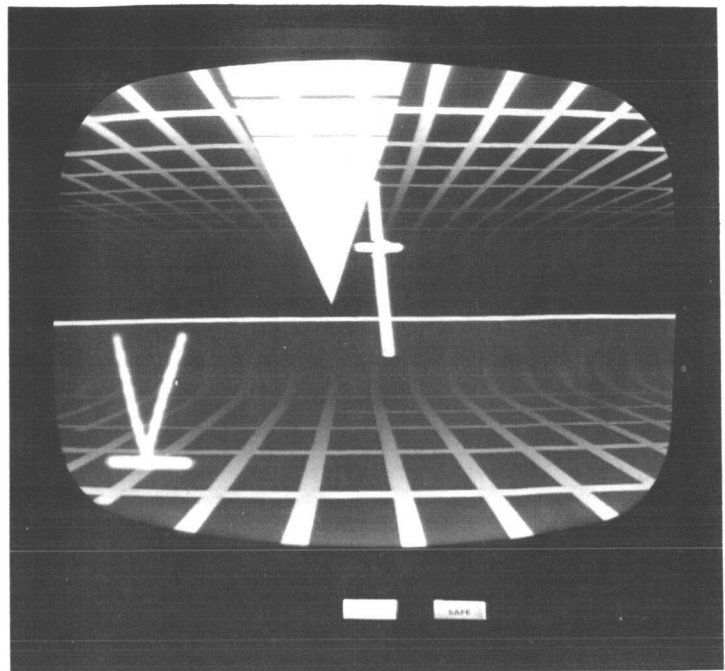


Figure 2.—Simulation of the Norden Contact Analog perspectively quickened display for submarine control. (McLane and Wolf)

The final presentation in this session was made by W. R. Ferrell, in which he described the results of a study that examined delayed force feedback. The experiment described was a simulated remote manipulation task with force feedback through the controller. The objective of the study was to examine the effect of the force feedback cue when faced with a relatively long transmission delay in the system. The apparatus described was a one-dimensional remote positioning device with forces measured by strain gages and feedback to the operator by means of a motor connected to the controller.

This study indicates that the inclusion of force feedback in remote manipulators is feasible in spite of long transmission delays. However, the forces should be displayed to the operator in such a way that they do not affect the movements of the master control.

## MOTION AND STRESS

The effects of motion and stress on control performance is a complex subject. The physiological limits are reasonably well known from a design criteria point of view; or at any rate, limits have been established and accepted by system designers. Below these limits, however, the effect on control performance of various types and levels of stress is not clearly defined.

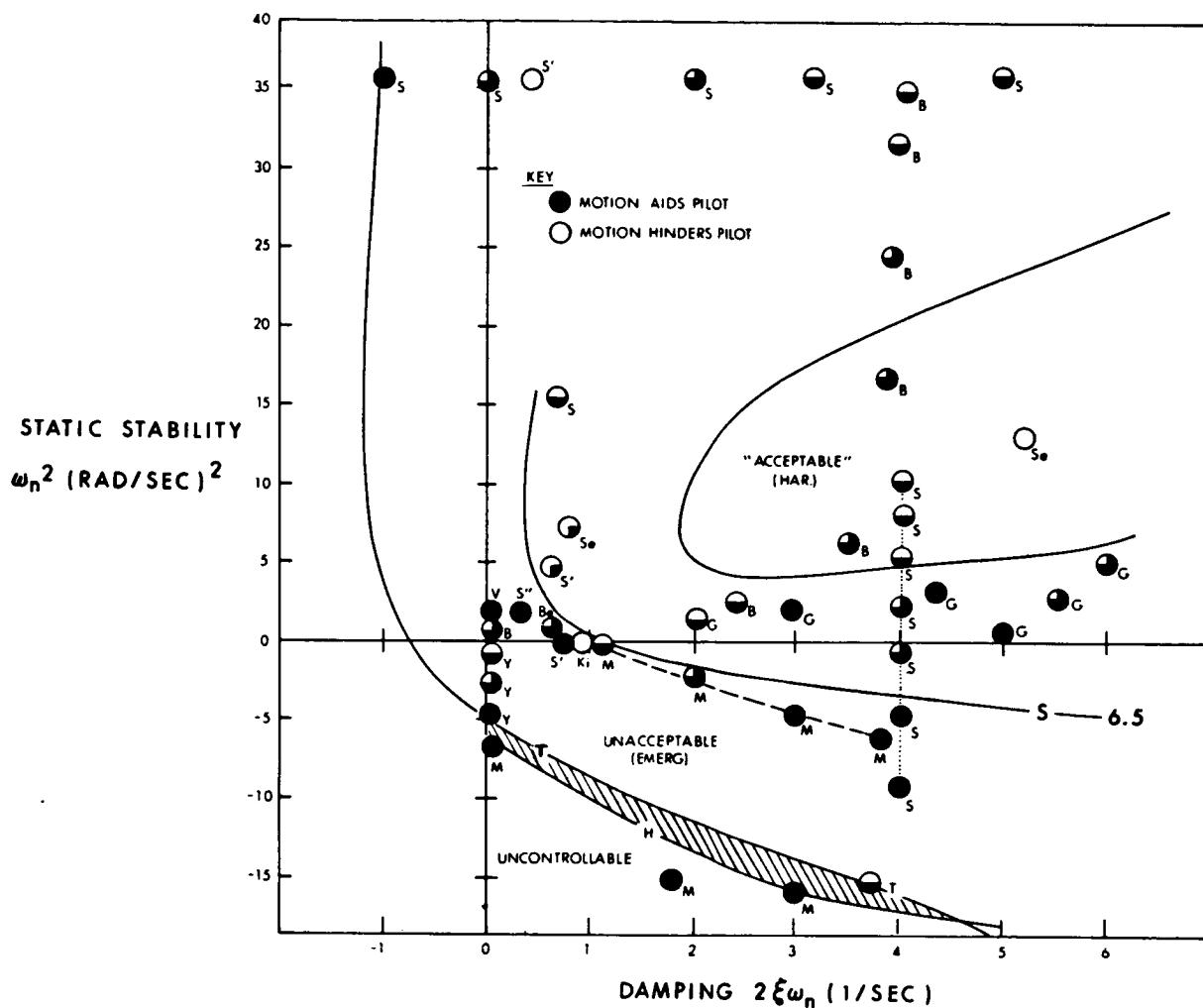


Figure 3.—Effect of motion cues on pilot performance. (Young)

While it is certainly true that the addition of high levels of sustained acceleration or vibration to a control task will degrade performance, L. R. Young's paper describes several areas where control performance is enhanced through the use of motion cues by the controller. Specifically, the control tasks that appear to benefit most from the addition of acceleration and motion cues are those situations requiring more lead compensation than is easily developed from visual displays. The additional information being presented to the controller through vestibular and tactile sensations is also shown to be of significant value in adapting to a rapid change in controlled element dynamics. A plot of a compilation of data from several sources, shown in figure 3, indicates the relative effect of motion cues on controllability as a function of the controlled element dynamics.

Not all acceleration cues are beneficial even though they are well below the accepted physiological limits. Included in the studies reported by M. Sadoff were data to show that under short-term zero gravity, while simple reaction time is essentially unaffected, the

complex reaction time is significantly increased. The increase in percentage of control reversals that occur at zero g and +3 g parallels the increase in complex reaction time for those same levels, and lends additional support to the possibility of "central processor" changes due to weightlessness. On the opposite end of the scale, the results of an analysis of pilot performance under sustained linear acceleration with a superimposed 1.5 g, 11-cps vibration suggest that the required lead equalization disappears during severe vibration.

Pursuing the vibration environment as a very probable stressor on the control task, A. Z. Weisz presented an evaluation of three types of hand controllers under random vertical vibration. In general, the results of the study agree with previous efforts in that the force stick concept did provide superior performance. A subsequent analysis using the transfer function description of the controller confirms the conclusions reached when using tracking efficiency as a performance measure.

Indicating the complex interactions and substitutions of cues that occur within the human controller, H. L. Smith presented the results of a series of tests conducted in the Cornell Aero Labs Variable Stability T-33. As described, the tests were conducted in flight, on the ground using the aircraft as a fixed-base simulator, and in a conventional analog simulator that included a contact analog-type visual display. Analysis of the pilot response data indicated that the analog simulator and visual display gave results closer to the flight situation than did the actual flight hardware when operated as a ground-based simulator, even though the controlled-element dynamics were identical in all three cases.

In attempting to measure the effect of stress on performance not only is the problem compounded by the multiplicity of types, but as the levels of application are reduced, the investigator rapidly encounters a problem in sensitivity of the available performance measures. As a means of relieving this latter problem, C. B. Gibbs presented the results of studies aimed at evaluating the effects of minor stress, such as low levels of alcohol or minor frustration, on automobile driving performance. The measures used by Gibbs were the response latency and correct versus incorrect responses while the subjects were tracking step functions. The sensitivities achieved were quite impressive, being able to identify performance impairment of one bottle of beer several hours after consumption.

## APPLICATIONS

Several examples of the use of human dynamics in the analysis and design of systems were presented in the session on applications. Four of the five informal presentations in this session dealt with the design or analysis of specific systems, including manual launch-vehicle control and VTOL handling qualities. The other presentation, by C. B. Westbrook, was a discussion of the present and future applications of pilot dynamics data in flight control system design and development. The salient point of this presentation was that while valid controversy still exists over specific details, and much work is still needed to relax the constraints on existing techniques, the current capability has been proven, and more emphasis should now be shifted toward design applications.

## OPTIMAL CONTROL

Modern optimal control theory generally requires that the criteria to be optimized be specified prior to system synthesis. Since theory makes no attempt to define a universally optimal system, it is possible for any control system to be optimal if the criteria are defined

appropriately. Consideration of the human in a manual control task as an optimal controller then must center about determining what criteria are being adopted since system synthesis is a somewhat remote possibility.

The studies presented by T. B. Sheridan propose a model of human behavior in a preview control task in which the "road ahead" may be seen. The model was used in two exploratory experiments which illustrate some relevant experimental variables and provide a rough comparison of the human operator to an optimal preview controller. The results of the experiments suggest that for a relatively difficult control task, the human operator is reasonably close to optimal and trades off error with effort in a rational fashion. Further, human control in a preview task may be suboptimal for several reasons, for example, insufficient experience with the controlled process or explicit cost function, use of an implicit cost function which differs from that stipulated, or inability to see and remember the previewed input adequately.

The paper presented by F. A. Muckler discussed an experiment designed to investigate further the ability to state explicitly the performance criteria to be used in a tracking task. The study employed a constant set of dynamics and used the same control and displays throughout, with the variable being the explicit performance criteria. From the data presented, it is clear that while no changes in forcing function or controlled elements were made, several distinct shifts in operator behavior occurred. It is evident that the same subjects can perform the same basic task differently. It follows that if a particular performance criterion is desired, it must be adequately conveyed to the subject.

In addition, as evidenced in this study, it is possible for subjects to perform according to some implicit criteria regardless of what is requested, resulting in extreme intersubject variability.

"Human Decision Making in Manual Control Systems" is the title of a paper by R. E. Thomas and J. T. Tou in which an approach to modeling the decision process is proposed. The model attempts to describe the manner in which a human operator exhibits on-line adaptive behavior in a control system. No repeated trial is permitted in the decision-making process while solving the optimal control problem; consequently, the model is only concerned with on-line learning. The primary difficulty seems to center around the question of the extent to which a human controller can be characterized by a Bayesian decision maker.

The characteristic framework of the proposed model results in a search algorithm that generates a control strategy and finally control actions by minimizing the incremental "cost."

The pursuit-evasion differential game examined by S. Baron gave a direct comparison between an optimal pursuer and a human controller. The studies were not directed toward a study of manual control; as a result the information gleaned from this effort was mostly qualitative. A point of significance, consistent with the early papers in this session by Sheridan and Muckler, was the marked improvement toward optimal control as the test subject became more aware of the required strategy. This was evident after the subject was permitted to view the optimal pursuer several times before making manually controlled runs.

## ANALYSIS AND DESIGN METHODS

The final session of the conference covered a broad range of subjects, from the application of modern control theory to human-operator model development to the development of a performance prediction of a digital computer facility for flight simulation studies. Five papers were presented in this session that started with a description of dynamical system modeling by P. L. Falb and G. Kovatch. In this paper, the authors suggest the possibility of using results from modern control theory in developing differential, difference, and integral equation models for human-operator behavior in a control system. The very powerful analytical techniques developed in the modern control theory field have the potential of giving greater insight into human performance modeling problem than previously possible. The authors discuss the possible techniques for application of the B. L. Ho identification procedures to planned simulation studies and to some previously obtained experimental data.

The following two papers described the use of variable system dynamics as means of analyzing human performance. The "critical task" described by H. R. Jex records subject tracking performance in a task with a programed variation in dynamics that increases in difficulty until control is lost. Data taken in this manner, represented by figure 4, show that when the subject is operating near the limit of control, his behavior is adequately represented by the more recent human operator models and adaptation laws. The adaptive simulator technique described by C. R. Kelly again uses variable system dynamics. However, in this instance, the difficulty of the controlled element dynamics is established as a function of the subject's instantaneous error resulting in a self-paced task. The steady-state level of difficulty a subject accepts appears to be an effective means for comparing control and display systems. As was pointed out by Kelly, great care must be taken in selecting and mechanizing the parameters and rationale of the task adjustment.

The paper presented by L. W. Taylor entitled "Discussions of Spectral Human Responses Analysis," was one of the most controversial presentations at the conference. Taylor's approach states that the pilot describing function estimate, which consists of the ratio of the cross spectral densities from input to pilot output and displayed error, is equal to the ratios of the Fourier transforms of pilot output and error. The estimate using the power spectral densities was thought to be free of bias, and is shown to be equal to the ratio of Fourier transforms under certain conditions, especially when the input is a sum of sine waves.

The discussion from the floor was quite thorough and in summary concluded that the expressions presented for the pilot describing function as a ratio of Fourier transforms are a valid interpretation under the following conditions:

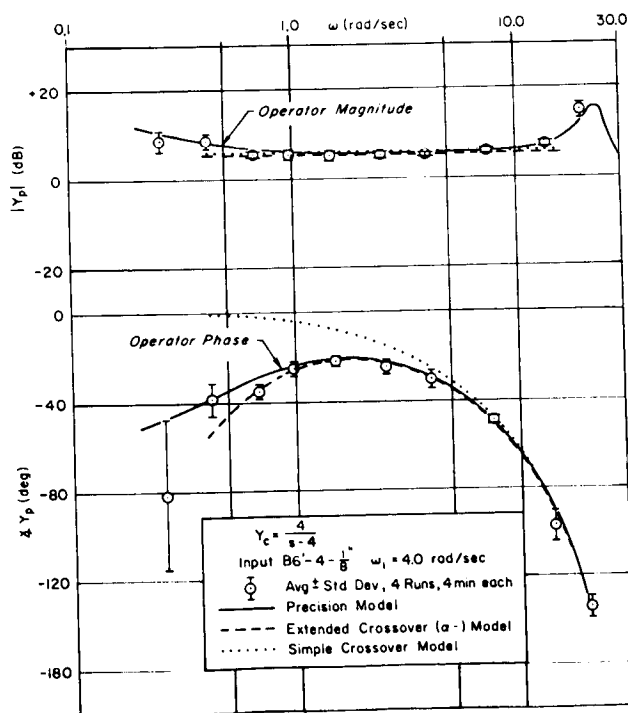


Figure 4.—Mean data and curve fits for one operator's describing function in a critical task ( $\lambda = 4$ ). (Jex)

- (1) The input is a sum of sine waves.
- (2) The transforms are evaluated using the same sine and cosine functions for both transforms over the same run length.
- (3) The transforms are evaluated only at the input frequencies.

Within these restrictions, the technique presented will yield valid results and does offer some computational advantage; however, the validity of any generalization beyond these restrictions is questionable.

The final paper of this conference did follow the session title, "Analysis and Design Methods;" however, the attack was not upon the human describing-function problem, but rather on the analysis and design of a computer facility for flight simulator studies. As presented by M. C. Grignetti, the paper described the analysis and performance prediction for a computer facility using a Markov model of the system.



**DISCRETE AND  
CONTINUOUS MODELS**

N67-158521

PRECEDING PAGES BLANK NOT FILMED.

## 1. SUMMARY OF SINE-WAVE TRACKING STUDIES

*R. W. Pew, J. C. Duffendack, L. K. Fensch  
University of Michigan*

The highlights of a study of sine-wave tracking are reported which illustrate the extent to which the predictability of the input and of the control device dynamics can be utilized with extended practice. Analysis of the error power spectra establishes the presence of a stable source of noise power in the operator's output that has implications for deriving models of manual tracking performance.

In terms of the present level of understanding of manual control performance, there are two reasons for wanting to study further performance with predictable input signals. First, it is of interest to know more about the development of the operator's ability to make use of the predictability of signal and system characteristics. Second, studies with simple, deterministic input signals provide the least contaminated data for revealing the fine structure of the operator's output.

Among studies examining performance with predictable input signals, there have been at least four previous experiments on sine-wave tracking with simple system dynamics in which the effect of input signal frequency was one of the primary variables of interest (refs. 1 to 4). The two major findings of all of these studies were that, as a function of frequency, the amplitude ratio of output to input was essentially unity; and that the phase shift was negligible up to an input frequency of approximately 2 cps with erratic timing performance beyond that frequency. In short, the system did not behave like a linear control system because of the operator's ability to make use of input signal coherence.

Studies of ramp tracking by Craik in reference 5 (data reported by Vince (ref. 6)) and by Ellson, Hill, and Gray (ref. 7) in which distributions of the time between axis-crossings were obtained are also relevant to consideration of the effects of predictable input signals. Craik pointed to a peak in the axis-crossing distributions in the range of 0.5 sec and argued that operators make discrete response corrections on the average every 1/2 second.

It was desired to expand on several aspects of these earlier studies: to look at longer-term learning effects especially as they relate to certain system design variables; to attempt to examine in more detail the transition region between very low and very high sine-wave input frequencies; and to make use of power spectral analysis methods to get a more analytic look at the fine structure of the operator's output. This paper summarizes some selected results from this study.

### METHOD

Subjects viewed the horizontal motion of a target on an oscilloscope and attempted to track a constant-frequency sine wave with either a compensatory or pursuit display mode and

pure gain system dynamics. The subject rested his arm on a control stick that was pivoted at the elbow to permit a lateral rotation of the lower arm over the range of  $\pm 45^\circ$ . In addition to integrated-absolute-error scores reported to the subject at the end of each 2-minute trial, he listened to a tone having a pitch inversely proportional to his integrated absolute error performance continuously averaged over the most recent 2-second period. This tone served as a source of augmented concurrent performance feedback.

Three subjects practiced for 32 daily 1-hour sessions divided into eight blocks of 4 days each. Within each block they received all combinations of four variables: pursuit versus compensatory display mode; 1.42- versus 3.12-volts/deg control gain; 0.066- versus 0.132-cm/volt display gain; and control-stick spring constants of 0.023 lb/deg and 0.065 lb/deg at the control handle. The stick had negligible damping and small inertia ( $0.006 \text{ slug-ft}^2/\text{rad}$ ). Each subject tracked sine-wave input frequencies of 0.098, 0.51, 1.14, 2.05, and 3.62 cps under all of these combinations of variables, producing a total of eighty 2-minute trials in each 4-day block. Input-signal peak amplitude was fixed at  $\pm 30$  volts so that the actual peak amplitude of target motion on the display was  $\pm 2.0$  and  $\pm 4.0$  cm for the two display gain conditions. Following the 32 practice sessions, terminal performance was measured at 11 input frequencies spanning the range from 0.1 to 5.0 cps and at the original 5 frequencies with the springs removed from the control stick.

## RESULTS

Figure 1 shows the performance scores obtained as a joint function of input frequency and 4-day blocks of practice for the two display modes. Each data point represents the average of four 2-minute trials for each of the three subjects. With no control input the integrated absolute error was 100 volt-sec at all frequencies. By block four, even at 3.62 cps, the subjects reduced the error substantially

over that which would have been obtained without responding at all. In the subsequent test at 11 frequencies, the integrated error at 5.0 cps was 80.6, which still reflects some ability to reduce the error by active control. Analysis of variance of the last two blocks of practice revealed a significant main effect of frequency but no significant main effect of display mode, control gain, display gain, or spring constant.

Note that with extended practice, performance with the compensatory display mode approached that obtained with the pursuit mode. This result is consistent with the predictions of the Krendel and McRuer "Successive Organization of Perception" (SOP) model (refs. 8 and 9). These authors suggest that with extended practice operators using a compensatory display to track

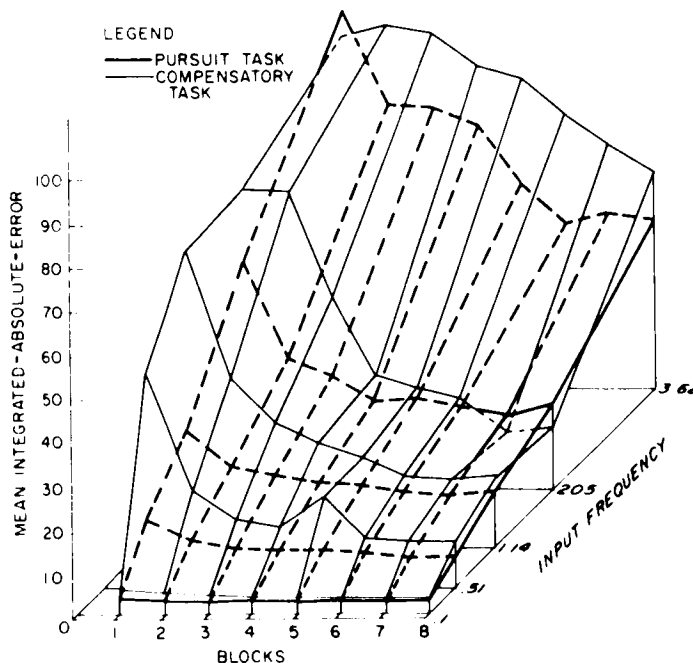
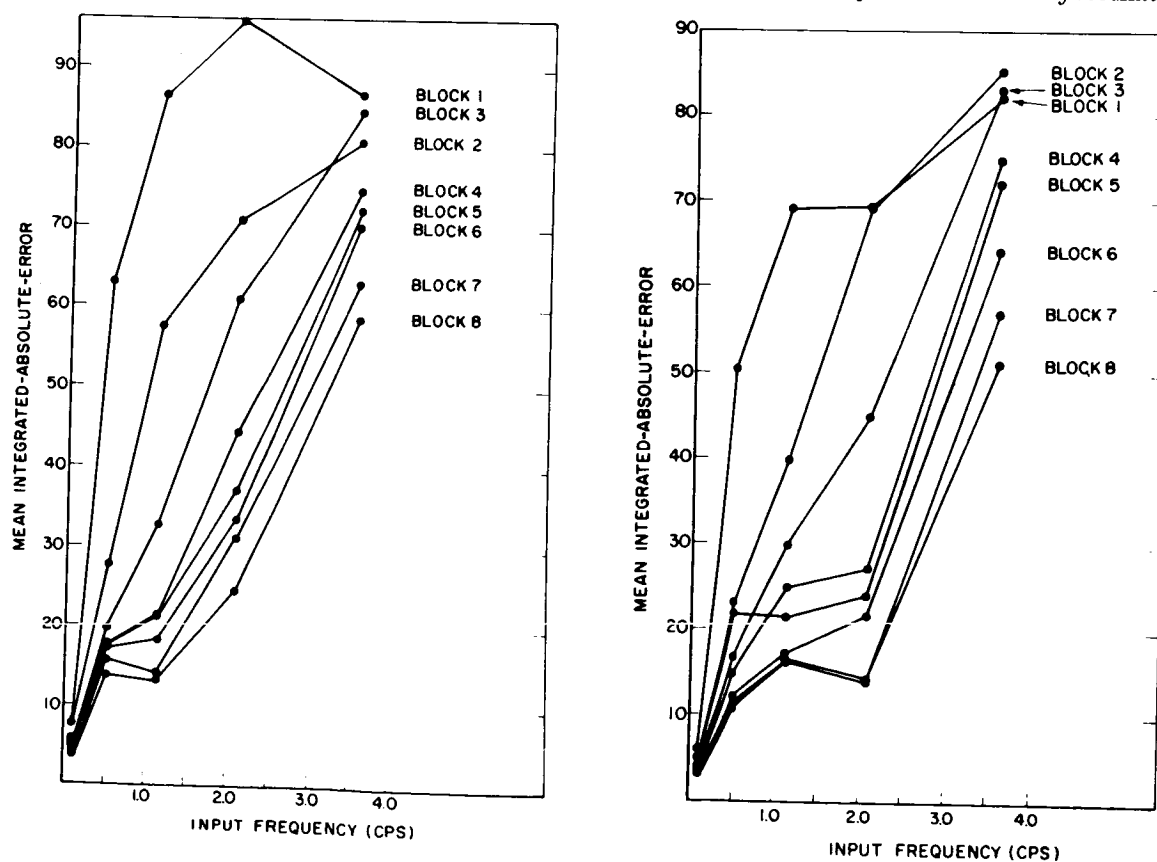


Figure 1.—Mean performance score as a function of blocks of practice and input frequency for pursuit and compensatory display modes.

coherent inputs achieve an effective restructuring of the display which permits pursuit-like operation. The information on which this restructuring is based may be derived from attention to the output motion of the arm, probably through proprioceptive cues.

An alternative view based on the SOP model is that, with this much practice, performance with both pursuit and compensatory displays approaches the precognitive level at which the operator is essentially performing short-term open-loop tracking. This interpretation seems appropriate for the higher input frequencies, but error power spectra at low frequencies, described in a later section, did not show the changes with practice that would be required to support this position.

The effect of the two spring constants on error performance with the compensatory display is shown in figure 2 in which error performance as a function of frequency is presented with blocks of practice as a parameter. Figures 2(a) and 2(b) show performance with spring constants of 0.023 and 0.065 lb/deg, respectively. Note that with extended practice performance was disproportionately better at certain critical frequencies. Furthermore, the input frequency that showed greatest improvement was different for the two spring conditions. It appeared that the subject was able to learn to make the natural resonant frequency of the arm-stick combination work to his advantage. This figure shows clearly the slow but systematic



(a) Spring constant = 0.023 lb/deg.

(b) Spring constant = 0.065 lb/deg.

Figure 2.—Average performance scores for three subjects for practice blocks 1-8 as a function of input frequency with the compensatory display.

learning of this rather specific system characteristic. The statistical significance of the two-way interaction between input frequency and spring constant confirms the reliability of the finding. Two other facts are pertinent to the interpretation of this frequency selectivity as a function of control-stick spring constant. First, the effect was very much more pronounced for the compensatory display than for the pursuit display; and second, in the follow-up testing with no spring, this frequency selectivity was not observed.

These findings taken together emphasize the ability of an operator to make use of proprioceptive cues provided by the motion of the arm-stick combination. That they were more effective in the compensatory mode probably reflects the greater need to rely on proprioceptive cues in order to infer the input signal characteristics with this display mode. However, in this case, more than the simple restructuring of the display as suggested by the SOP model was taking place because the ability to take advantage of the arm-stick system natural frequencies involved making use of knowledge gained about the system dynamics as well as about the coherence of the input. It is interesting to note that this was more effectively accomplished with the compensatory display which otherwise has been found to produce poorer performance than its pursuit counterpart.

Perhaps the most interesting data were obtained from power spectral analysis of the operator's output. Figure 3 shows samples of time histories of a subject's performance late in training at input frequencies of 0.098, 0.51 and 2.05 cps. From top to bottom are shown operator's output, error, output velocity, and error velocity. At the lowest frequency the error records have been substantially amplified to show evidence of power uncorrelated with the input signal. At 0.51 cps there is still some indication of higher frequency power but it is beginning to be confounded with power contributed by phase error at the input frequency. At 2.05 cps there is primarily error power at the input frequency and evidence of frequency mistuning and beats that have been reported previously as the subject generates a sine wave and attempts to synchronize it in amplitude and phase with the input frequency.

In order to quantify these observations, an estimate of the power spectrum of the error-velocity signal was computed by a standard single-pass analog harmonic-analysis technique utilizing 10 narrow-band filters distributed logarithmically over the range from 0.10 to 5.0 cps. The error-velocity spectrum was analyzed instead of the output directly in order to (1) suppress the input signal power at low frequencies and (2) obtain a scaling advantage at high frequencies. The analyzer had a dynamic range of approximately 30 dB, and the  $\pm 1\sigma$  confidence bands for the specified filter bandwidth, damping ratio, and run length varied from  $\pm 1.5$  dB at 0.10 cps to  $\pm 0.2$  dB at 5.0 cps. Unless otherwise noted, the spectra are presented in terms of error-velocity power directly and have been normalized with respect to the total error-velocity signal power. They may be translated into error spectra by subtracting  $20 \log 2\pi f$  throughout the range of  $f$ , the measurement frequency. Figure 4 shows the error-velocity power spectra for the data at the 11 input frequencies obtained during the testing phase after 32 days of practice. Since negligible differences were observed among subjects, the spectra reported are the averages of three subjects' data with 0.066 lb/deg spring constant, 0.132 cm/volt display gain, and 1.42 volts/deg control gain. Pursuit and compensatory data are shown separately, but the differences were very small.

At low frequencies there was a broad band of power in the range from 0.5 to 2.0 cps that appeared to be uncorrelated with the input frequency since it remained relatively fixed in position and shape with input frequencies up to 0.5 cps. As the input frequency was further increased, the error power at or near the input frequency increased and either obscured or

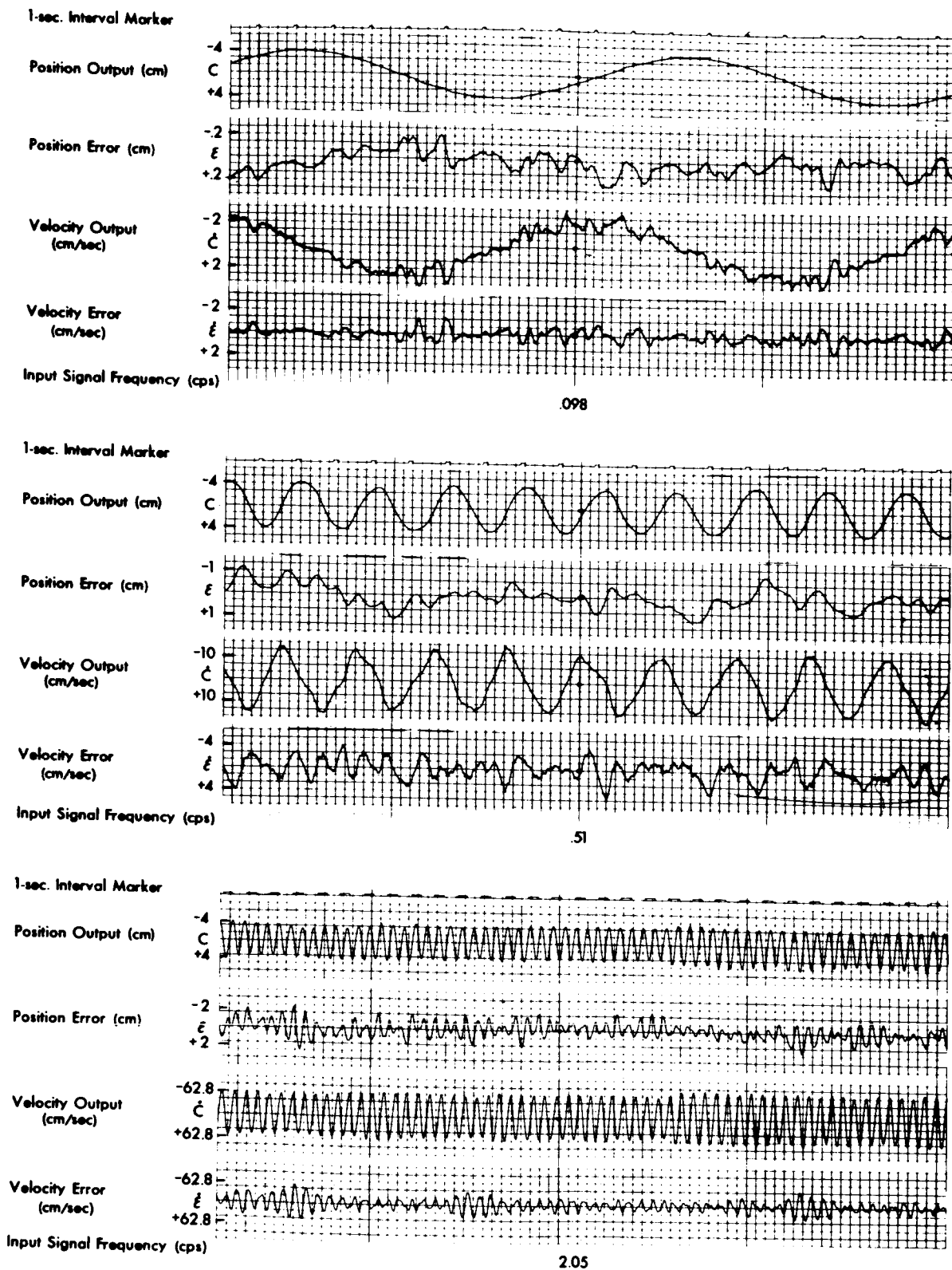


Figure 3.—Time histories of an operator's output.

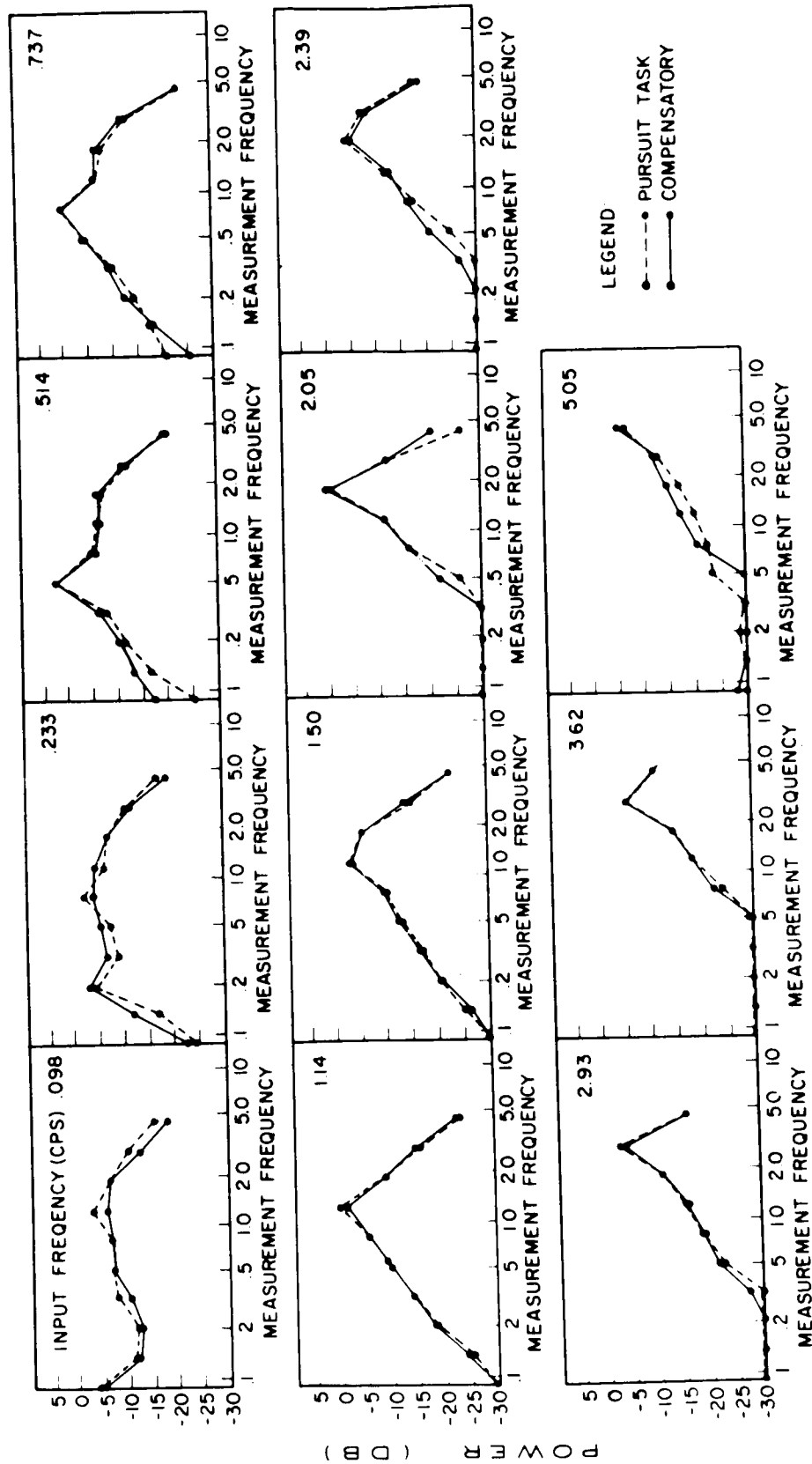


Figure 4.—Error velocity power spectra at 11 input frequencies averaged over three subjects. Data were obtained with control spring constant of 0.066 lb/deg, display gain of 0.132 cm/volt, and control gain of 1.42 volts/deg.

replaced this uncorrelated band of power. Instead, a relatively narrowly tuned spectrum that was centered on the input frequency appeared. At low input frequencies examination of the time histories suggested that the error spectrum was relatively stationary; but at high frequencies more and more time variation was evident, and it was no longer clear that a valid stationary spectrum was being measured. Although the obtained high input-frequency spectra were relatively repeatable from run to run and subject to subject, less reliance should be placed on these data. They are, however, consistent with the previously reported observations that at high input frequencies the subject generates, in a precognitive fashion, a sine wave of frequency approximately equal to the input frequency and then attempts to synchronize that sine wave with the input signal. The remaining discussion will be focused on the properties of the band of power that characterized the subjects' performance with relatively low frequency inputs.

With respect to the other system variables studied, it can be seen that display mode had little effect on the shape of the spectrum. Similarly, for the values studied, display gain and control gain had little effect. Modifying the spring constant had a small but consistent effect suggesting that the dynamics of the arm-stick combination can serve to shape the high frequency end of the spectrum. Significantly, in relation to the effects of the springs on overall error scores, the power spectrum obtained with no spring was only slightly different from that with either spring installed. The broad band of power could not be attributed to a natural resonance of the arm-stick combination alone.

Finally, figure 5 shows the error-velocity power spectrum during block 2, block 4, and block 8 stages of practice. Again there are essentially no differences except a very slight tendency toward sharpening of the peak. The picture that emerges from these data is one of a very stable source of noise power in the operator's output having a high-frequency cutoff that is determined by the dynamics of the arm and control stick taken together. If one is inclined toward sampled-data models, he can attribute this noise to a variable-rate sampling element in the system. On the other hand, the data are adequately described by a noise-injection representation directly.

Two analyses have been directed toward tie-in of these data with those of previous investigators. When Vince's axis-crossing data (ref. 6) were converted to the frequency domain by assuming that the time between axis crossings corresponded to the period of one-half cycle of the predominate frequency in the data, the distribution shown superimposed on the power spectra in figure 5 was obtained. The amplitude and vertical displacement of this distribution are irrelevant, but the position in frequency is entirely consistent with the power spectra shown. It is believed that this distribution could have been obtained equally well from the time histories reported here. It is argued that these power spectra reflect the same periodicities originally reported by references 1 and 5.

To provide a second point of tie-in, several of the output power spectra obtained with random input signals and reported in reference 9 were replotted on a logarithmic frequency scale for comparison with the error power spectrum obtained with the present 0.098-cps sine-wave input signal data. The sine-wave spectrum was transformed from velocity to position coordinates. This comparison is shown in figure 6 for one of the spectra from reference 9. The curves have been translated vertically because of the differing reference power levels, but the dB and frequency scales have been maintained intact. The only point of difference between the two is the lower frequency cutoff of the sine-wave data, an effect to be expected in light of the differing stick dynamics and limb involvement in the two studies.



Both curves roll off at approximately 3 dB per octave up to the break point and then break at 12 dB per octave.

This comparison serves to emphasize the relevance of the noise-injection interpretation of at least a portion of the remnant as suggested frequently by the quasi-linear describing-function modelers. However, this finding suggests only that there is a relatively invariant source of noise in the operator's output. It does not say that with random input tracking it is the most important source, in comparison with time variation, for example. It seems likely that, as the tracking task is made easier, for example, by reducing the input signal bandwidth, this noise will constitute an increasing percentage of the total remnant.

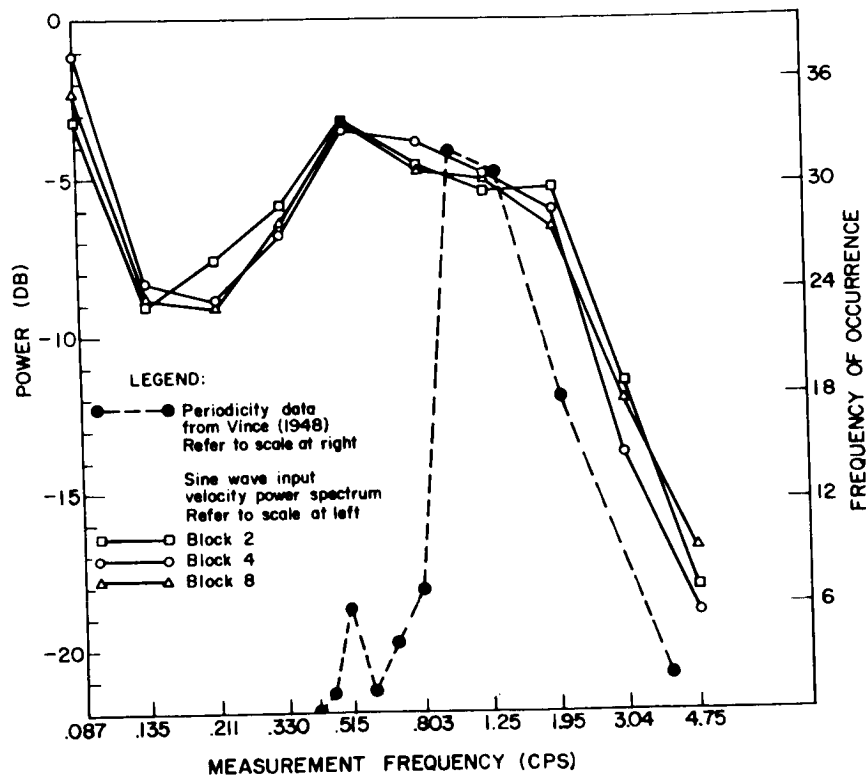


Figure 5.—Error velocity power spectrum at three stages of practice averaged over three subjects and two display gains. Data were obtained at 0.098 cps input frequency with pursuit display mode, control gain of 1.42 volts/deg, and spring constant of 0.023 lb/deg. Also shown is one of Vince's (ref. 6) axis-crossing distributions converted into the frequency domain (from figure 2 of ref. 6, 50 mm/sec ramp input).

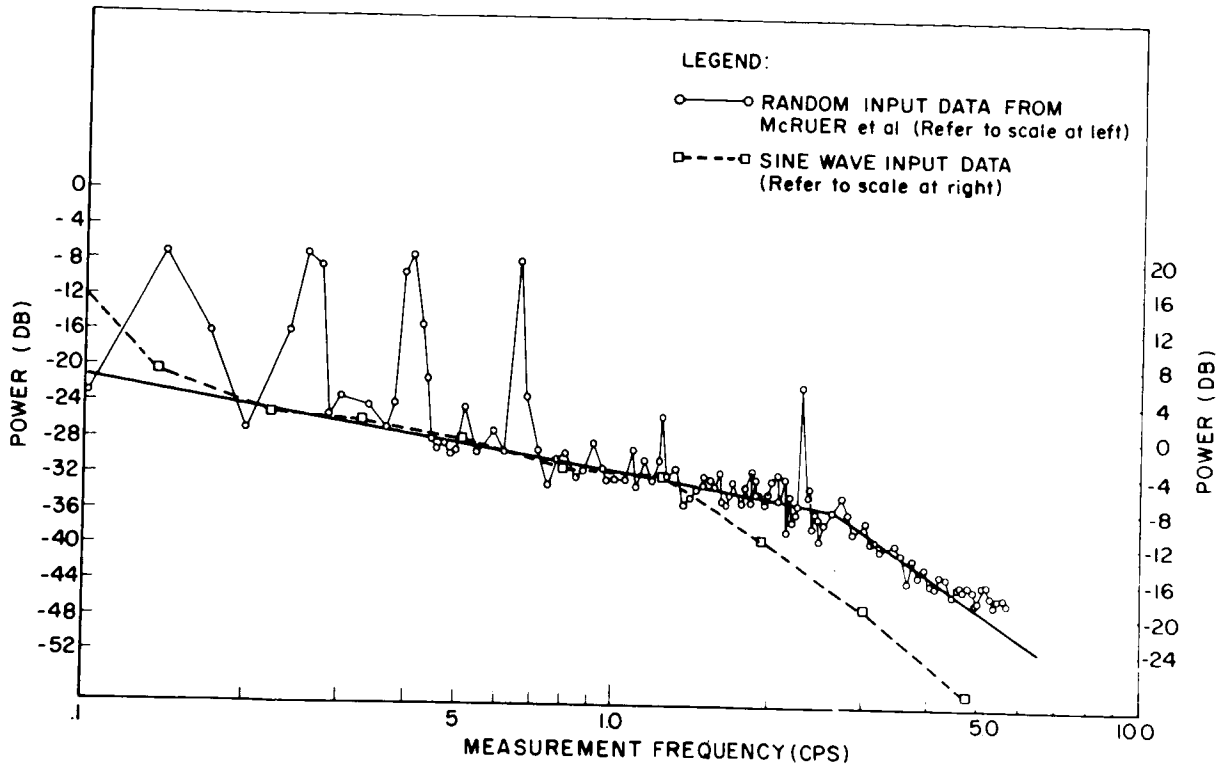


Figure 6.—Output power spectrum obtained from a random input signal tracking study of reference 9 (fig. 67). Also shown is the error power spectrum from sine-wave tracking with pursuit display and 0.098-cps input frequency. Data are for same conditions as those shown in figure 4. Heavy lines indicate 3 dB and 12 dB slopes respectively.

Finally, identifying and isolating a source of noise in the operator's output serves only to make the investigator wish to delve further into determining the origin of this noise. Is the noise simply the result of inadequate control of the neuromuscular system? Is it the result of the explicit or implicit discrete commands to the neuromuscular system that could be interpreted in terms of a sampling element somewhere in the overall system? Is it produced by the operator's inherent time delay in processing feedback information? Further studies that make a start toward its analysis will be reported subsequently.

### SUMMARY

It was hoped that further analysis of the effects of extended practice on tracking of sine waves would provide insight into the process of acquisition of skilled performance. Since the normalized power spectra do not change substantially with practice, it can only be concluded that much of what is learned is concerned with improved utilization of the predictability of the signals and system dynamics to which the operator is exposed. However, this study has revealed an underlying processing limitation that restricts the ultimate accuracy of tracking performance that can be achieved.

## REFERENCES

1. Ellson, D. G.; and Gray, F. E.: Frequency Responses of Human Operators Following a Sine-Wave Input. Memo. Rep. MCREXD-694-2N, Eng. Div., Air Material Command, Dec. 1948.
2. Mayne, R.: Some Engineering Aspects of the Mechanism of Body Control. Elec. Eng., vol. 70, 1951, pp. 207-212.
3. Noble, M.; Fitts, P. M.; and Warren, C. E.: The Frequency Response of Skilled Subjects in a Pursuit Tracking Task. J. Exp. Psychol., vol. 49, 1955, pp. 249-256.
4. Stark, L.; Iida, M.; and Willis, P. A.: Dynamic Characteristics of the Motor Coordination System in Man. Biophysical J., vol. 1, 1961, pp. 279-300.
5. Craik, K. J. W.: Theory of the Human Operator in Control Systems - II. Man as an Element in a Control System. Brit. J. Psychol., vol. 38, 1948, pp. 142-148.
6. Vince, M. A.: The Intermittency of Control Movements and the Psychological Refractory Period. Brit. J. Psychol., vol. 38, 1948, pp. 149-157.
7. Ellson, D. G.; Hill, H.; and Gray, F. E.: Wave Length and Amplitude Characteristics of Tracking Error Curves. Memo. Rep. TSEAA-694-2D, Eng. Div., Air Material Command, Apr. 1947.
8. Krendel, E. S.; and McRuer, D. T.: A Servomechanisms Approach to Skill Development. J. Franklin Inst., vol. 269, 1960, pp. 24-42.
9. McRuer, D. T.; and Krendel, E. S.: Human Pilot Dynamics in Compensatory Systems. Tech. Rep. AFFDL-65-15, Res. and Tech. Div., Air Force Systems Command, May 1965.

N67-15853

## 2. ASYNCHRONOUS FINITE STATE MODELS OF MANUAL CONTROL SYSTEMS\*

*G. A. Bekey and E. S. Angel  
University of Southern California*

The mathematical models most commonly used to represent human operator behavior in manual control systems are based on the assumption that the operator observes and makes use of a continuum of input states. In contrast to those approaches, this paper is based on the assumption that the operator quantizes his input and output into a limited number of states and that data processing is performed on asynchronous samples of this coarsely quantized input; that is, the human operator behaves as a finite-state machine. A hybrid output element or hybrid actuator is used to achieve a continuous variation of output position.

In order to provide for the generation of timed output waveforms in manual tracking, the paper shows that the concept of the hybrid actuator also provides a bridge between binary decisions and continuous time. The application of standard logical design techniques to the synthesis and minimization of the resulting mathematical models is discussed. It is shown that for the particular case of compensatory control of a pure inertia plant, a human controller model can be synthesized by using only threshold gates, flip-flops, gates, and hybrid actuators.

The paper concludes with a discussion of proposed research in further applications of finite-state machine theory to manual control.

The mathematical models most commonly used to represent human operators in manual control systems are based on the assumption that the operator observes a continuum of input states. This assumption is basic to both continuous modeling, whether done by spectral analysis or orthonormal filter representations (refs. 1 and 2), and to sampled-data modeling (ref. 3). The latter models assume that input information is continuous in amplitude but sampled at discrete times. In contrast to these approaches, this paper presents an approach to modeling of manual control behavior with the fundamental assumption that the operator quantizes his input into a finite (and very limited) number of states by means of threshold gates. It is then assumed that his data processing is performed on asynchronous samples of this coarsely quantized input and only a finite number of outputs is possible. That is, he operates as a finite-state machine. Finally, in order to obtain a continuous variation of output position, a hybrid actuator is utilized in the model. This output element will be called a "finite-state actuator" in this paper. It was formulated originally by Tomovic and McGhee (ref. 4) and termed a "cybernetic actuator" in the context of applications to prosthetics.

\*This research was sponsored in part by the National Aeronautics and Space Administration under Grant No. NGR-05-018-022 and in part by the U.S. Air Force Office of Scientific Research under Grant No. AF-AFOSR-1018-66.

The model developed here also makes use of the concept of a "force program," as used by LeMay and Westcott (ref. 5) and Elkind et al. (ref. 6). This concept suggests that the trained human controller possesses a file of possible timed responses, all of which are constantly available to him. On the basis of perceptual quantities such as error and error rate (in a compensatory task), one of these programs is chosen and used.

Mathematical modeling of a force program in this paper requires the generation of a timed waveform (a force-time history) using asynchronous sequential circuits. Boolean algebra, as used in logical design procedure, makes no provision for the generation of timed waveforms occurring at arbitrary intervals. The paper also shows how a finite-state actuator can be used to obtain the required timing sequence.

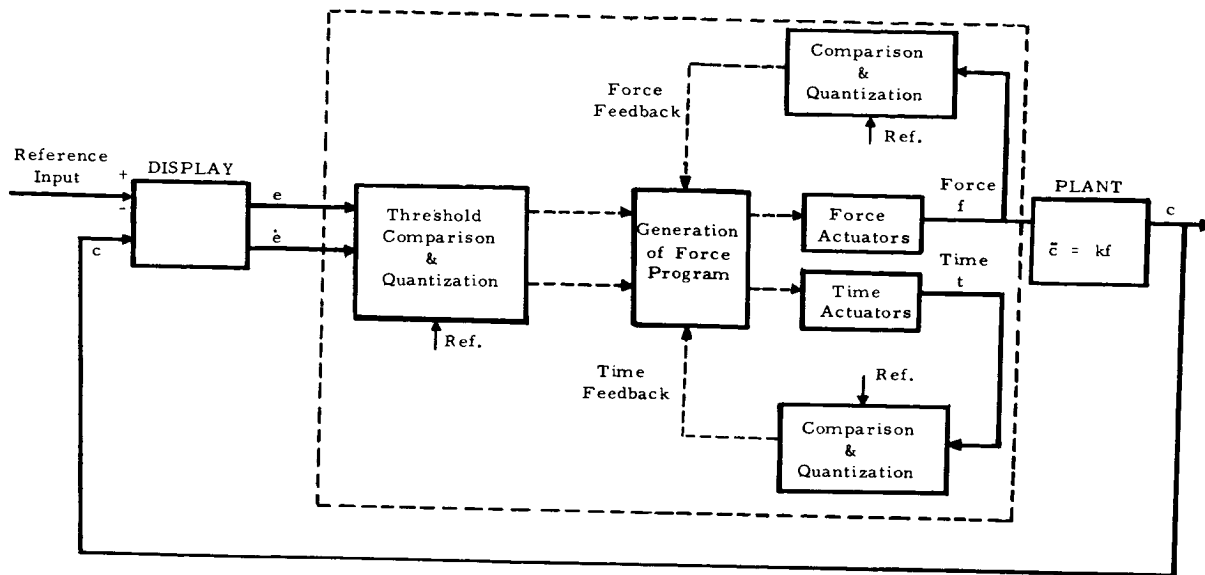
The paper is intended to show the feasibility of a new concept in the study of manual control systems. Consequently, attention has been focused on a specific control system, namely, a compensatory task with a pure inertia (double-integration) plant and a hand controller with negligible dynamics.

### BASIC REQUIREMENTS AND ASSUMPTIONS

The formulation of the new model was based on examination of the literature on manual control in compensatory tracking tasks. Consequently, the following requirements were selected:

- (1) Inputs: The inputs to the operator are assumed to be error  $e$  and error rate  $\dot{e}$ . However, it is assumed that the operator does not detect actual values of  $e$  and  $\dot{e}$ , but rather that he receives binary information on the relation of  $e$  and  $\dot{e}$  to one or more threshold levels.
- (2) Outputs: Human operator output is assumed to be a force applied to a hand controller or similar positioning device. If the plant is purely inertial, and the controller has a negligible dynamics, then the output force is proportional to the plant acceleration. The output force is assumed to be available in only a finite number of levels ( $+A$ ,  $-A$ , and  $0$ ) where  $A$  is a given constant, with the transition between these levels being made in a time interval which is short compared with the duration of a given force level.
- (3) Force programs: The human operator is assumed to accomplish his tracking task by the generation of a series of force-time programs, whose basic patterns are prestored and available. For the purposes of this paper, only four such programs will be assumed to exist in the "library": (a) a positive force pulse of given duration (velocity compensation), (b) a positive force pulse followed after a preset interval by a negative-force pulse (position compensation), (c) and (d) the negatives of (a) and (b). It is assumed that a given program, once triggered, runs to completion regardless of input signal changes and that a new program may only be initiated after the  $T$  seconds duration of last force program. This assumption is consistent with the classical work of Craik (ref. 7) and with the models of LeMay and Westcott (ref. 5). The control of the force program is based on binary information obtained from the input and output of the system.

Based on these assumptions, the human operator may be represented in block diagram form by the diagram of figure 1. It is evident from an examination of this diagram that this model of human performance requires the following elements:



Legend

Continuous Signals ———  
Discrete Signals - - - - -

Figure 1.—Human operator problem.

- (1) Devices for receiving continuous inputs and generating binary outputs
- (2) Devices for generating continuous outputs from binary inputs
- (3) A network for combining the discrete information as required to generate the required control for the force program.

Figure 1 also shows that the operator model is assumed to have an interval mechanism for timing the force program.

It should be noted that the above assumptions and requirements for the model are specifically suited to single-axis compensatory control of an inertial plant. They are consistent with published literature which indicates that human controllers in such systems tend to use an on-off, or "bang-bang," mode of control (refs. 8 and 9). However, human controllers may use more than three fixed levels of output force, as given in (2) above. This requirement was introduced in order to keep the model structure as simple as possible. Relaxation of this and other assumptions is discussed in the concluding section of the paper.

### IMPLEMENTATION OF THE BASIC ELEMENTS OF THE MODEL

**THRESHOLD GATES.**—Transformation of continuous to binary information is characterized by the input-output relations of table 1:

TABLE 1.—THRESHOLD GATE  
CHARACTERISTICS

Input, $x$	Output, $z$
$x < x_{ref}$	0
$x \geq x_{ref}$	1

**FINITE STATE ACTUATORS.**—Transformation of discrete to continuous output is achieved with finite-state or hybrid actuators. A finite-state actuator is a memoryless (combinatorial) device with  $n$  discrete inputs and  $m$  continuous outputs. The number of inputs and outputs and their coding are arbitrary and depend on the particular application.

A two-input, single-output actuator may be visualized as illustrated in figure 2. The discrete inputs  $x_1$  and  $x_2$  control an analog integrator with two possible fixed input voltages  $+K$  and  $-K$ . The integrator is assumed to introduce no sign changes. Depending on the state of the discrete input, the output increases at a rate  $K$ , decreases at a rate  $K$ , or holds its value. The fourth input condition connects a small resistor  $r$  from output to input, thus causing the output level to reset exponentially to zero. The input-output table for the hybrid actuator is given in table 2.

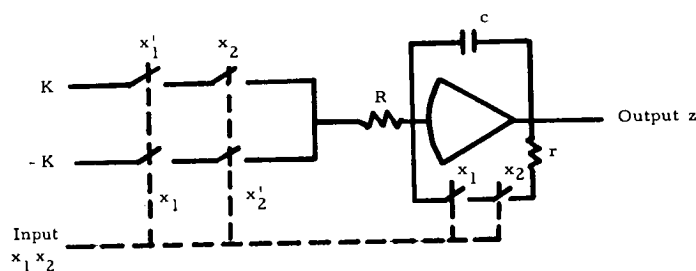
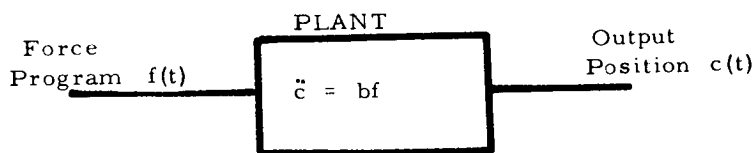


Figure 2.—Finite state actuator.

TABLE 2.—FINITE STATE ACTUATOR CHARACTERISTICS

Input, $x_1x_2$	Output $z$	$\frac{dz}{dt}$
0 0	Constant	0
0 1	Increases	$+K$
1 0	Decreases	$-K$
1 1	Resets	$-z/rc$

**PRE-STORED FORCE PROGRAMS.**—In order to provide the model with an ability to track arbitrary inputs, two basic minimum force programs were chosen. They are termed the "velocity correction program" and the "position correction program." These two basic force programs may be illustrated by figure 3. Since the force represents an acceleration input to the plant, the final position is obtained from a double integration of the force program



The two basic programs of figure 3 were suggested by observations of human tracking behavior in systems such as figure 1. Human controllers sometimes comment that they pulse the system in one direction in reducing the error rate to zero and then they pulse it alternately to provide position corrections. It is evident that a position-correction program does not affect the error rate, while a velocity correction changes the output rate by an increment  $\pm AT/2$ . Further, it is assumed that neither correction can be applied more than once every  $T$  seconds, but that the interval during which the force is applied need not cover the entire interval, that is,

$$\tau_v \min \leq \tau_v \leq T$$

$$\tau_p \min \leq \tau_p \leq T$$

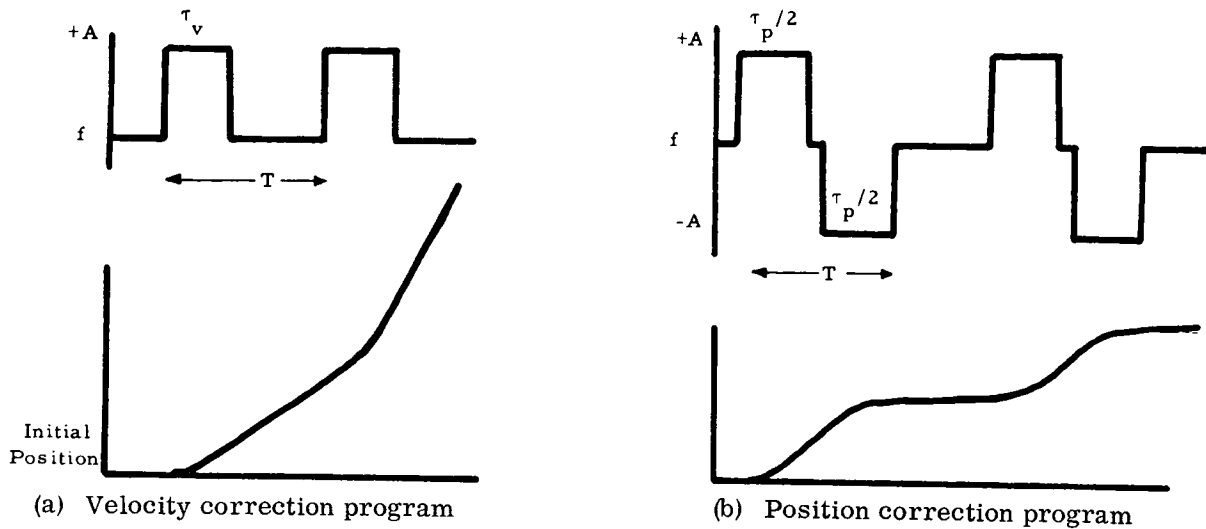


Figure 3.—Basic force programs.

If both position and rate thresholds are available, a table of combinations can be derived to show whether a velocity or position movement is desirable. Table 3 below shows such choices, with the further assumption that two levels of error magnitude thresholds are available.

TABLE 3.—COMBINATIONS FOR POSITION AND VELOCITY CORRECTIONS

$-\epsilon_2$	$-\epsilon_1$	0	0	$\epsilon_1$	$\epsilon_2$	
+p	+p	-v	-v	-v	-p	$\dot{\epsilon}$
+p	+p	0	0	-p	-p	0
+p	+p	0	0	-p	-p	0
+p	+v	+v	+v	-p	-p	$-\dot{\epsilon}$

### ASYNCHRONOUS GENERATION OF FORCE PROGRAMS AT ARBITRARY TIMES

Between the inputs (threshold gates) and output devices (finite-state actuators) it is desired to have a finite state machine which, given the input conditions, will generate the proper output, that is, a force program. The main difficulty in the synthesis of such a machine is that the force programs, each of which involves exact time durations, will be initiated at arbitrary times. Thus, synchronous logic circuits are unsuitable. Conversely, the need of the exact time duration of the force program itself make asynchronous logic circuits similarly unsuitable.

The basis of the method used is to add an extra finite-state actuator to generate timing ramps. The reset capability of the actuator allows a force program to be started at arbitrary times. Threshold gating of the timing ramp reduces the design of the desired circuit to one



of asynchronous techniques. This technique makes a wide range of problems amenable to standard logical design procedures (ref. 10).

To avoid unrealistic jumps in the force output, such as those shown in figure 3, an approximation to the force program will be generated using finite-state actuators, as shown in figure 4.

It will be sufficient to design a circuit which will generate a position-correcting force program and one which will generate a velocity-correcting program. A single bit of additional information (one relay or flip-flop) added to these networks can be used to invert the outputs at the proper time. Figure 5 shows a block diagram of the logical circuitry necessary to generate the four force programs at the proper times. The force program generators consist of asynchronous circuitry and actuators and possess internal digital feedback. These designs are discussed in the following sections. Feedback from these generators to the inverter and selector is necessary so the inverter cannot change state until completion of a force program. Two alternatives are to construct separate generators for all four force programs or to construct a single force generator in one large machine.

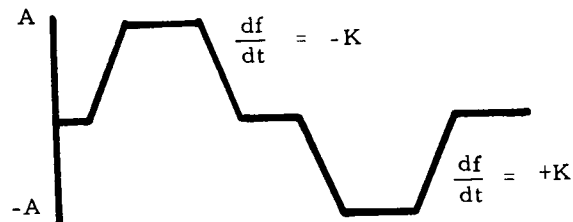


Figure 4.—Approximation to force program.

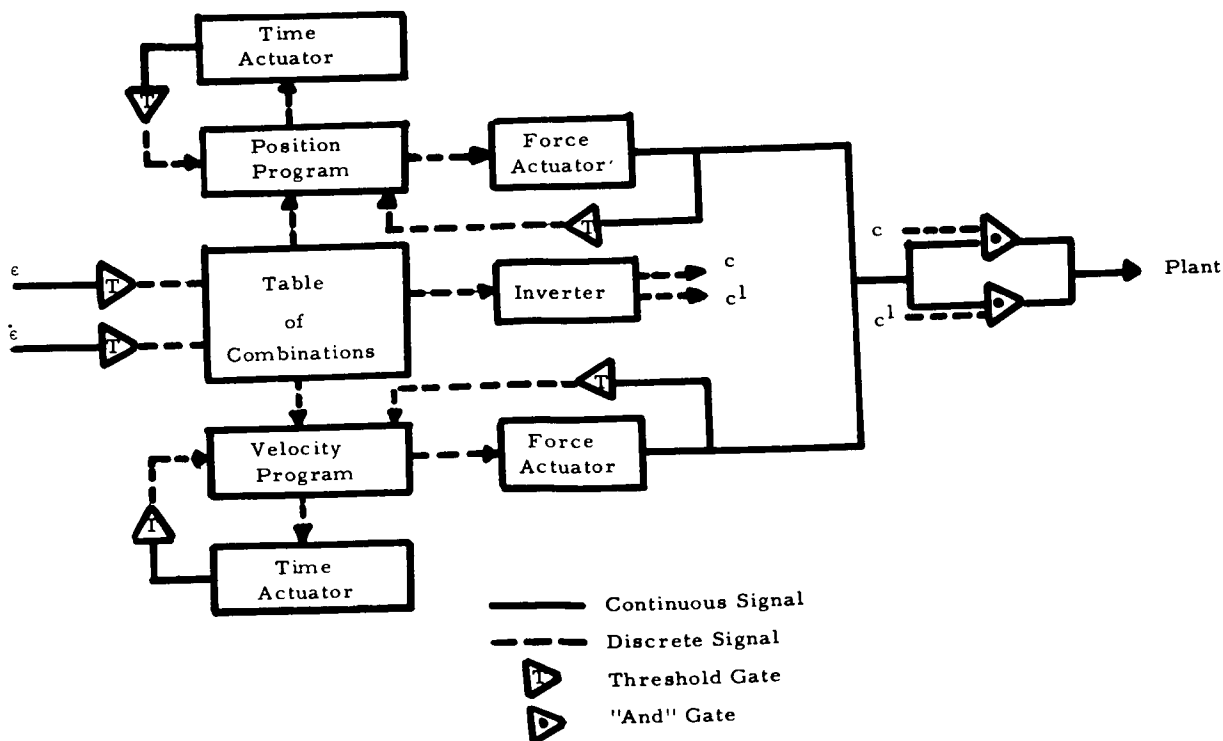


Figure 5.—Block diagram of asynchronous network.

## CODING AND STATE DIAGRAMS

The asynchronous sequential machine to generate a position-correcting force program needs as binary inputs a start signal  $x_e$ , two force actuator feedback signals,  $x_T$  and  $x_\tau$ . These signals are shown in table 4. The feedback signals are obtained by threshold gates on actuator outputs. The outputs of the finite state machine are  $z_1$  and  $z_2$  (the inputs to the force actuator), and  $z_3$  and  $z_4$  (the inputs to the timing actuator). Actuator coding is the same as that in table 2.

TABLE 4.—THRESHOLD GATE OUTPUT CODING

Gate Output	Condition
$x_e = 1$	If program is to start
$x_A = 1$	If $ \text{Force}  \geq  \text{Pulse height} $
$x_O = 1$	If $\text{Force} \geq 0$
$x_T = 1$	If $t \geq T$ , ( $t$ = Length of timing ramp)
$x_\tau = 1$	If $-t \leq -\tau$

In order to visualize the sequential behavior of the model, consider the generation of a positive position-correcting program only. This portion of the model is shown in figure 6(a), with all gate outputs and actuator inputs labelled in accordance with the coding of table 4. The force program is shown in figure 6(b). The sequential operation of the model is described by the state diagram of figure 6(c). The output states ( $z_1, z_2, z_3, z_4$ ) are shown in the circles and the arrows indicate the input changes leading to a change in output. Thus, output state 0010 is interpreted (with reference to table 2) as follows: The first two digits ( $00 = z_1 z_2$ ) refer to the force actuator and indicate that the force output is remaining fixed, while the second two digits ( $10 = z_3 z_4$ ) refer to the time actuator and indicate that a timing ramp is being generated.

In terms of output states, the sequence in figure 6(c) is as follows:

- (1) Start with force output being held at zero and time ramp reset to zero:

$$z_1 z_2 z_3 z_4 = 0011$$

- (2) Error exceeds threshold ( $x_e \rightarrow 1$ ) and the force begins to increase:

$$z_1 z_2 z_3 z_4 = 0111$$

- (3) Force reaches the desired value A ( $x_A \rightarrow 1$ ), holds its value, and timing starts:

$$z_1 z_2 z_3 z_4 = 0001$$

- (4) Time reaches  $T/2$  ( $x_T \rightarrow 1$ ) so that force must now decrease and timer resets to zero:

$$z_1 z_2 z_3 z_4 = 1011$$

(5) Force becomes just negative ( $x_o \rightarrow 0$ ), holds this value, and the timing starts:

$$z_1 z_2 z_3 z_4 = 0010$$

(6) Time reaches  $\tau$  ( $x_T \rightarrow 1$ ), timer is reset, and force starts decreasing:

$$z_1 z_2 z_3 z_4 = 1011$$

(7) Force reaches  $-A$  ( $x_A \rightarrow 1$ ), holds its value, and timer starts:

$$z_1 z_2 z_3 z_4 = 0001$$

(8) Time reaches  $T/2$  ( $x_T \rightarrow 1$ ) so that force starts increasing and the time resets:

$$z_1 z_2 z_3 z_4 = 0111$$

(9) Force becomes barely positive ( $x_o \rightarrow 1$ ) and holds this value:

$$z_1 z_2 z_3 z_4 = 0011$$

This completes one cycle of the program. It can be noted that in step (6) the time actuator generates a negative ramp which is compared with the value  $-\tau$  in a threshold gate. This approach was selected strictly for coding convenience and economy of components in the model. The use of an additional gate providing a second threshold on the positive time ramp at  $t = T/2 + \tau$  could have been used as well.

The sequence for the velocity correction program is much simpler. The force waveform and state diagram are shown in figures 7(a) and 7(b).

The detailed synthesis of the sequential network which achieves the behavior symbolized in the state diagrams is given in the appendix to this paper. For the position-correcting program, the minimal design reduces to three internal states requiring two R-S flip-flops and 17 gates for mechanization.

## PERFORMANCE OF THE MODEL

The response of velocity and position correction force programs were simulated on the IBM 1620 digital computer. Results of these preliminary investigations are shown in figures 8 and 9. The response using solely velocity corrections enables the model to track a ramp input. However, a large initial displacement causes large overshoots since as the velocity

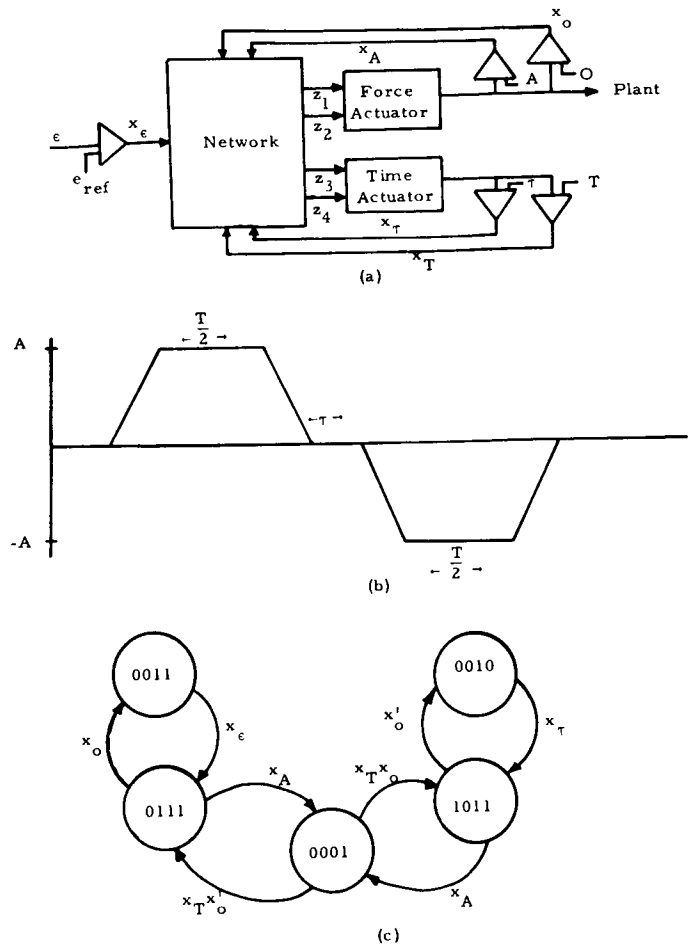


Figure 6.—Generation of position program.

builds up due to a series of velocity corrections, the distance traveled during a single correction grows as the square of the incremental velocity. Thus, a combination of position and velocity corrections is necessary as suggested in table 2.

Use of position corrections until the error is reduced and then application of velocity corrections result in a maximum time between corrections as the error is decreased. The lower bound of the average error is, of course, determined by the number and values of the error and error rate thresholds. Figures 8 and 9 show responses of the model to various input step and ramp combinations, with several values of the position increment and several threshold values. These results have a strong resemblance to human tracking data under similar conditions.

## CONCLUSIONS

It has been shown that the concepts and techniques of finite-state machine or automata theory are applicable to the study of manual control systems. In particular, models of human control performance in a particular task were constructed using threshold gates, finite-state actuators and sequential networks. The realistic responses of this model illustrate the feasibility of the concept.

It is evident that in its present form the model is not capable of representing the more complex aspects of tracking behavior. Consequently, the following modifications will be investigated in the future:

(1) The threshold levels used in the present model are all constant. The next step will be to make these thresholds dependent on other level sensors. For instance, Fu and Knoop (ref. 9) showed that the force magnitude  $A$  during a correction program depends on the magnitude of the tracking error  $e$  at the beginning of the correction. Similar work by M. J. Merritt at the University of Southern California shows that  $A$  depends on both  $e$  and  $\dot{e}$ , that is,

$$A = A(e, \dot{e})$$

It is evident that selection of a number of levels for  $A$  is possible in this model.

(2) The duration of the force pulses was taken as fixed during the present study. However, this value likewise represents only a threshold level and can be made adaptive as well.

(3) Performance of the model must be compared with that of trained human controllers, and model parameters must be selected for a variety of tasks.

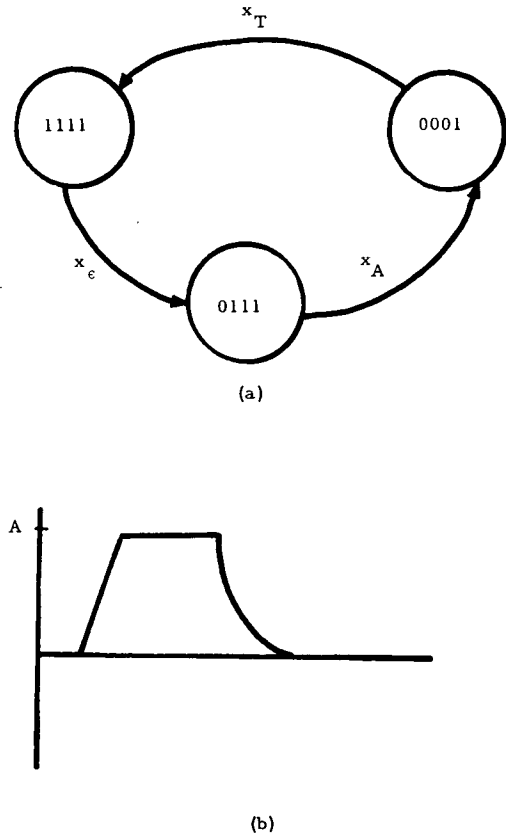


Figure 7.—Generation of velocity program.

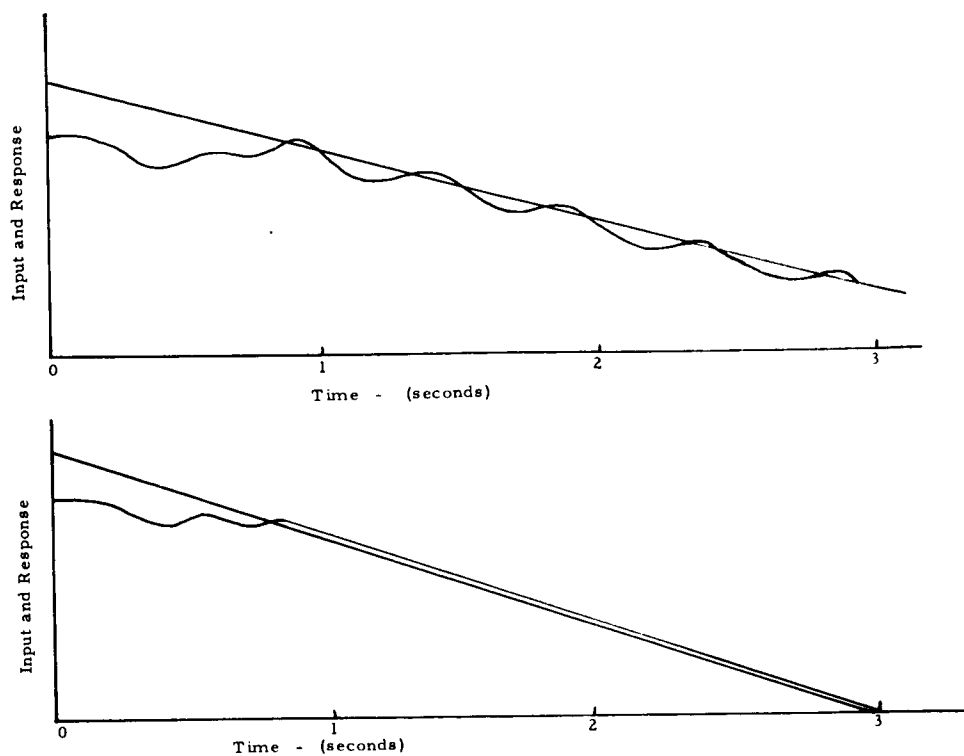


Figure 8.—Responses to decreasing ramps.

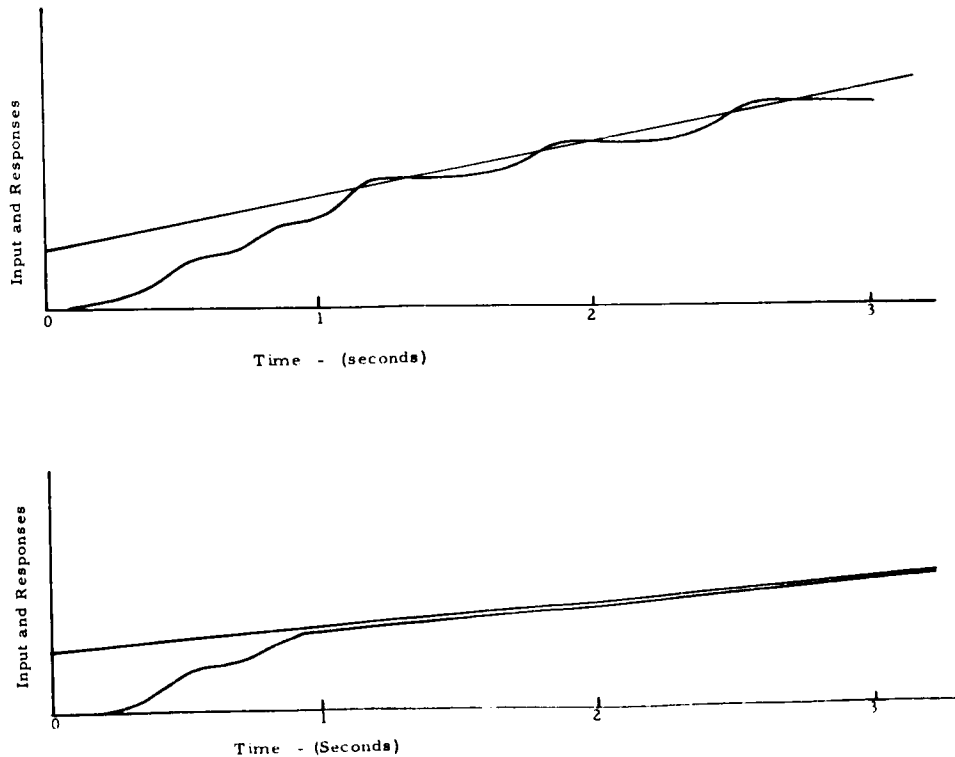


Figure 9.—Responses to increasing ramps.

It is interesting to note that the adaptation of the model to more realistic performance requirements requires no basic modifications in the fundamental approach. It is for this reason that the finite-state approach appears to be a hopeful new technique for the study of manual control systems, especially in its adaptive and time-varying aspects.

## APPENDIX

The sequential machine for the position correction was synthesized using a primitive flow table. Merger of the table leaves three states requiring only two secondary variables,  $y_1$  and  $y_2$ . The circuit requires 2 RS flip-flops and 17 gates. The equations are:

$$S_1 = y_1 y_2 x_T$$

$$R_1 = y_1 x_T x_T x_A x_e$$

$$S_2 = y_2 x_T$$

$$R_2 = y_1 y_2 x_T + y_2 x_T x_O$$

$$Z_1 = y_1 y_2' + y_1 x_T' x_T' x_A' x_O'$$

$$Z_2 = y_2 x_T' x_T' x_A' x_O' + y_1 x_T' x_A' x_O' + y_1 x_T' x_A' x_e + y_1 x_T' x_O' + y_1 x_T$$

$$Z_3 = y_1' + y_2 + x_A x_T'$$

$$Z_4 = x_T'$$

The sequential machine for the velocity correction reduces to only two states and one secondary variable,  $y$ . This requires one RS flip-flop and four gates. The equations are:

$$S = x_e x_T' x_A'$$

$$R = y x_T$$

$$Z_1 = y'$$

$$Z_2 = Z_3 = y' + x_T' x_A'$$

$$Z_4 = 1$$

The circuits are shown in figures 10 and 11.

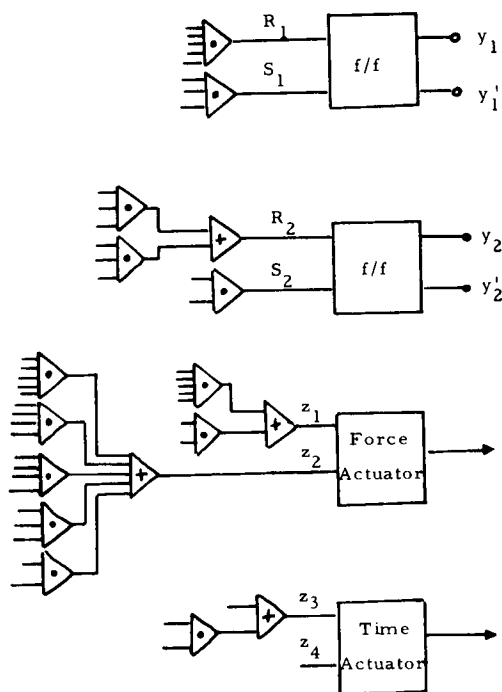


Figure 10.—Position machine.

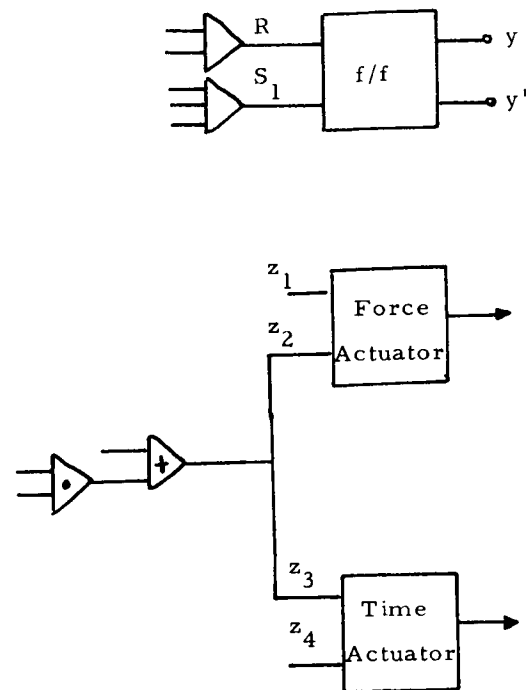


Figure 11.—Velocity machine.

## REFERENCES

1. McRuer, D. T.; and Krendel, E.: The Human Operator as a Servo System Element. J. Franklin Inst., vol. 267, May 1959, pp. 381-403, and vol. 267, June 1959, pp. 511-536.
2. Elkind, J. I.; and Green, D. M.: Measurement of Time-Varying and Nonlinear Dynamic Characteristics of Human Pilots. ASD Tech. Rep. 61-225, Dec. 1961.
3. Bekey, G. A.: The Human Operator as a Sampled-Data System. IRE Trans. on Human Factors in Electronics, vol. HFE-3, 1962, pp. 43-51.
4. Tomovic, R.; and McGhee, R. B.: A Finite-State Approach to the Synthesis of Bioengineering Control Systems. IEEE Trans. on Human Factors in Electronics, vol. HFE-7, no. 2, June 1966, pp. 65-69.
5. LeMay, L. P.; and Westcott, J. H.: The Simulation of Human Operator Tracking Using an Intermittent Model. Proc. International Congress on Human Factors in Electronics (Long Beach, Calif.), May 1962.
6. Elkind, J. I.; Kelly, J. A.; and Payne, R. A.: Adaptive Characteristics of the Human Controller in Systems Having Complex Dynamics. Proc. Fifth National Symposium on Human Factors in Electronics (San Diego, Calif.), May 1964.

7. Craik, K. J. W.: Theory of the Human Operator in Control Systems. Brit. J. Psychol., vol. 38, 1947, pp. 56-61, and vol. 38, 1948, pp. 142-148.
8. Young, L. R.; and Meiry, J. L.: Bang-Bang Aspects of Manual Control in High-Order Control Systems. IEEE Trans. on Automatic Control, AC-10, July 1965, pp. 336-341.
9. Fu, K. S.; and Knopp, D. E.: An Adaptive Model of the Human Operator in a Control System. Report No. TR-EE 64-15, Control and Information Sciences Laboratory, Purdue University, Sept. 1964.
10. McCluskey, E. J.: Introduction to the Theory of Switching Circuits. McGraw-Hill Book Co., Inc., 1965.



N67-15854

PRECEDING PAGE BLANK NOT FILMED.

### 3. SOME NEUROMUSCULAR SUBSYSTEM DYNAMICS\*

*Duane McRuer  
Systems Technology, Inc.*

The neuromuscular actuation properties of the human operator have always been considered to be an essential element in the operator's dynamic characteristics. In the past, however, the available data for systems with random-appearing inputs have permitted the description of the neuromuscular system only as a low-frequency approximation to higher frequency dynamics. Typical approximations have included a lag or a pure time delay. Recently, refined data of low variability and large dynamic range have become available (ref. 1). These provide the basis for better neuromuscular system descriptions and a greater scope in model-building activities.

The two reasons for interest in more refined neuromuscular system data and descriptions are as follows:

- (1) Practical ramifications of neuromuscular dynamics in manual control systems
- (2) Implications of these data on the structural organization of the neurological apparatus which make up the neuromuscular system

The single simple example discussed in this paper bears on both of these points.

#### DISCUSSION

To describe the operator dynamics data, several levels of approximation have been used. Two of these are shown in figure 1. These describing function models are descriptive of the transfer dynamics for the complete human operator. The so-called precision model is a minimum form compatible with all the fine-detail, low-variability data for random-appearing forcing functions and also compatible with such things as the dynamics of the movement component in step responses. The approximate model is a much simpler form in which the number of parameters is reduced without too serious a degradation in the analytical description of the data. Both models exhibit the same gain, equalization, and basic latency elements. They differ in their neuromuscular system aspects. For these the high-frequency effects are third-order in the precision model. In the approximate model low-frequency approximations are used for the high-frequency effects—either a first-order lag (so-called neuromuscular lag) or a pure time delay. The low-frequency effects are modeled by a lag-lead or lead-lag in the precision model, which are approximated by  $e^{-j\alpha/\omega}$  in the approximate

\*This paper includes research which was supported, in whole or in part, by the Air Force Flight Dynamics Laboratory of the Research and Technology Division, Air Force Systems Command, USAF, under Contract AF 33(657)-10835 and by the National Aeronautics and Space Administration under Contract NAS2-2824.

### Precision Model

$$\begin{array}{c}
 \begin{array}{|c|c|c|} \hline \text{Equalization} & \text{Basic} & \text{Neuromuscular System} \\ \hline \text{and Gain} & \text{Latencies} & \\ \hline \end{array} \\
 \\
 Y_p = K_p \left( \frac{T_L j\omega + 1}{T_I j\omega + 1} \right) e^{-j\omega\tau} \left\{ \underbrace{\left( \frac{\pm T_K j\omega + 1}{T'_K j\omega + 1} \right)}_{e^{-j\alpha/\omega}} \underbrace{\frac{1}{(T_{N1} j\omega + 1) \left[ \left( \frac{j\omega}{\omega_N} \right)^2 + \frac{2\zeta_N j\omega}{\omega_N} + 1 \right]}}_{(T_N j\omega + 1)^{-1} \text{ or } e^{-j\omega T_N}} \right\} \\
 \\
 \text{where} \qquad \qquad \qquad \text{where} \\
 \alpha \doteq \frac{1}{T'_K} \pm \frac{1}{T_K} \qquad \qquad T_N \doteq T_{N1} + \frac{2\zeta_N}{\omega_N}
 \end{array}$$

### Approximate Model

$$\begin{aligned}
 Y_p &= K_p \left( \frac{T_L j\omega + 1}{T_I j\omega + 1} \right) e^{-j\omega\tau} \frac{e^{-j\alpha/\omega}}{T_N j\omega + 1} \\
 &\doteq K_p \left( \frac{T_L j\omega + 1}{T_I j\omega + 1} \right) e^{-j[\omega(\tau + T_N) + (\alpha/\omega)]} \quad ; \quad \tau_{eq} = \tau + T_N
 \end{aligned}$$

Figure 1.—Describing function models.

model. This is an approximation for the higher frequency effects of very low frequency leads and lags, that is,

$$\begin{aligned}
 \Delta\phi_{low} &= \sum_{i=1}^m \tan^{-1} T_{lead_i} \omega - \sum_{i=1}^m \tan^{-1} T_{lag_i} \omega \\
 &\doteq \sum_{i=1}^m \left( \frac{\pi}{2} - \frac{1}{\omega T_{lead_i}} \right) - \sum_{i=1}^m \left( \frac{\pi}{2} - \frac{1}{\omega T_{lag_i}} \right) \\
 &\doteq \frac{1}{\omega} \sum_{i=1}^m \left( \frac{1}{T_{lag_i}} - \frac{1}{T_{lead_i}} \right) = \frac{\alpha}{\omega}
 \end{aligned}$$

The emphasis in the following discussion is on the  $\alpha$  and equivalent time-delay quantities.

Figure 2 illustrates the nature of typical pilot describing-function data and the application of the previously given precision and approximate model forms as descriptors of these

data. The typical data shown are from a so-called subcritical task involving the control of a controlled element consisting of a first-order divergence. The  $\alpha$  and  $\tau_{eq}$  aspects do not affect the amplitude ratio at all, although they are clearly shown in the phase. The  $\tau_{eq}\omega$  phase due to time delay dominates the high frequencies, whereas the  $\alpha/\omega$  phase lag is the major low-frequency effect. Their joint action tends to make the phase look like an umbrella, with  $\alpha$  controlling the left and  $\tau_{eq}$  the right. Changes in  $\tau_{eq}$  shift the right side of the umbrella, while changes in  $\alpha$  shift the left. Simultaneous increases or decreases in both  $\alpha$  and  $1/\tau_{eq}$  shift the umbrella to the right or left.

To see how  $\alpha$  and  $\tau_{eq}$  do vary, and to discover any connection between them, we are interested in experiments which force a variation in one or both. We have such data from two recent large-scale Systems Technology, Inc.—Franklin Institute experimental series (ref. 1). They are—

(1)  $Y_C = K_C/(j\omega)^2$ , with three different forcing-function bandwidths, eight subjects. In these experiments a principal effect noted was a decrease in equivalent time delay forced by the increase in forcing function bandwidth. This was accompanied by an increase in low-frequency phase lag.

(2)  $Y_C = K_C/j\omega(j\omega - 1/T)$ , with three different values of  $1/T$ ,  $\omega_i = 1.5$  rad/sec, six subjects. A major effect found was a decrease in equivalent time delay forced by the increase in the divergent tendency of the controlled element—again accompanied by an increase in low frequency phase lag.

A more quantitative indication of these variations is shown in figure 3 which shows in a very compact fashion that, to a first approximation,  $\alpha$  and  $1/\tau_{eq}$  vary together for these experiments. In terms of the describing-function phase curve previously shown, the umbrella is moved to the right with either an increase in forcing function bandwidth in the first experimental series mentioned, or a decrease in divergence time constant for the second.

The phenomenon illustrated has some impact on manual control operations. Typically, a decrease in equivalent time delay is used by the operator in one of two ways:

(1) To increase the phase margin while the crossover frequency is held constant (as in the  $K_C/(j\omega)^2$  series)

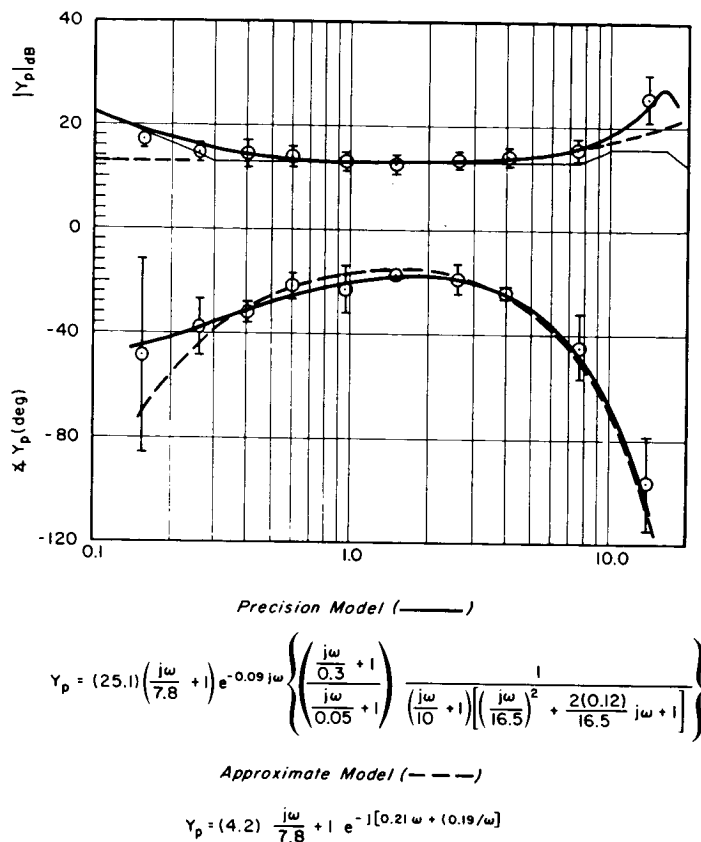


Figure 2.—Typical pilot describing function data and models.

$$(Y_C = K_C/(j\omega - 2); \omega_i = 4.0 \text{ rad/sec})$$

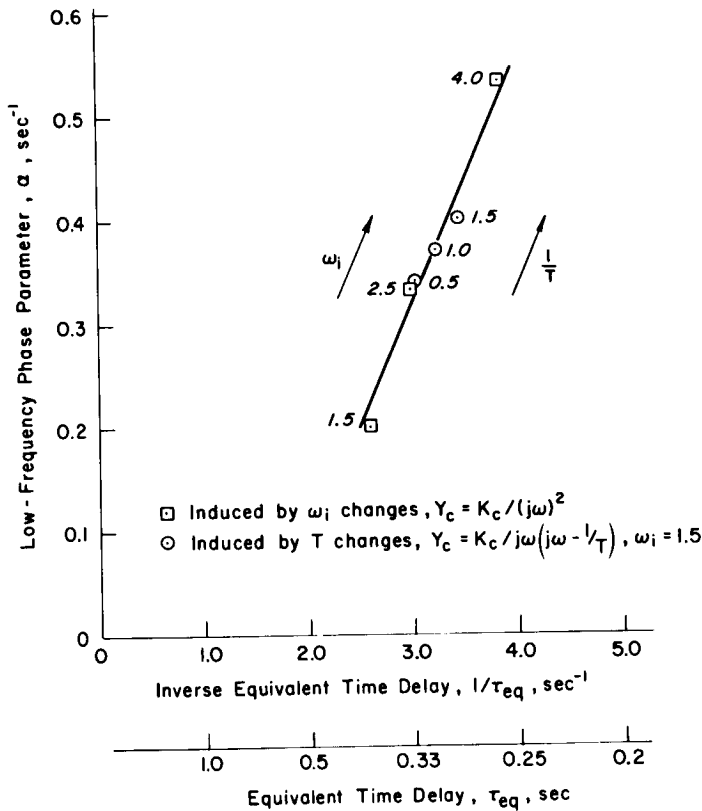


Figure 3.—Connection between equivalent time delay and low-frequency phase lag.

proposed models for the neuromuscular system's actions. An example of such a model is shown in figure 4. This model is based on many more considerations and data than the factors just mentioned, but these considerations are not discussed in this paper. The point to be made in connection with the model at this time is that, among other things, the model was made to be compatible with the data described previously. In this particular simplified version only one system parameter, the neuromuscular system loop gain, need vary to create a covariant connection between the equivalent time delay and the low-frequency phase-lag parameter. The actual mechanism of the neuromuscular gain change is a change in an operating point on the ensemble of nuclear bag spindles, induced by a change in  $\gamma$  bias, as supplied by  $\gamma_c$ . This mechanism is akin to that proposed by Stark (ref. 2) about 5 years ago. Although figure 4 alone does not show this (without consideration of the actual characteristics for the muscle and manipulator elements,  $GM$ ), the operating-point change causes an increase in the average tension in the muscles, which in turn leads to the decreased time constant. In the speculative neuromuscular system model shown, low-frequency characteristics are also modified by the change in neuromuscular gain. Thus the required covariation of  $\tau_{eq}$  and  $\alpha$  is accounted for as it should be.

(2) To permit an extension in the crossover frequency, thereby increasing the bandwidth of available control (as in the  $K_c/j\omega(j\omega - 1/T)$  series).

In either of these limiting cases the change noted is made possible by a time delay decrease. Since this serves an important functional purpose, it is highly desirable. But, along with this time delay decrease, there is the low frequency phase increase. For many systems this is of little significance, but for conditionally stable systems it can have important effects, particularly for higher order controlled elements.

Another practical consideration is introduced by the  $\alpha$  effect for measurements with parameter trackers or orthonormal filters in that they should be tailored to show up the effect when it is present.

Finally, besides these practical aspects, the covariation of the two quantities becomes a property which must be accounted for by any

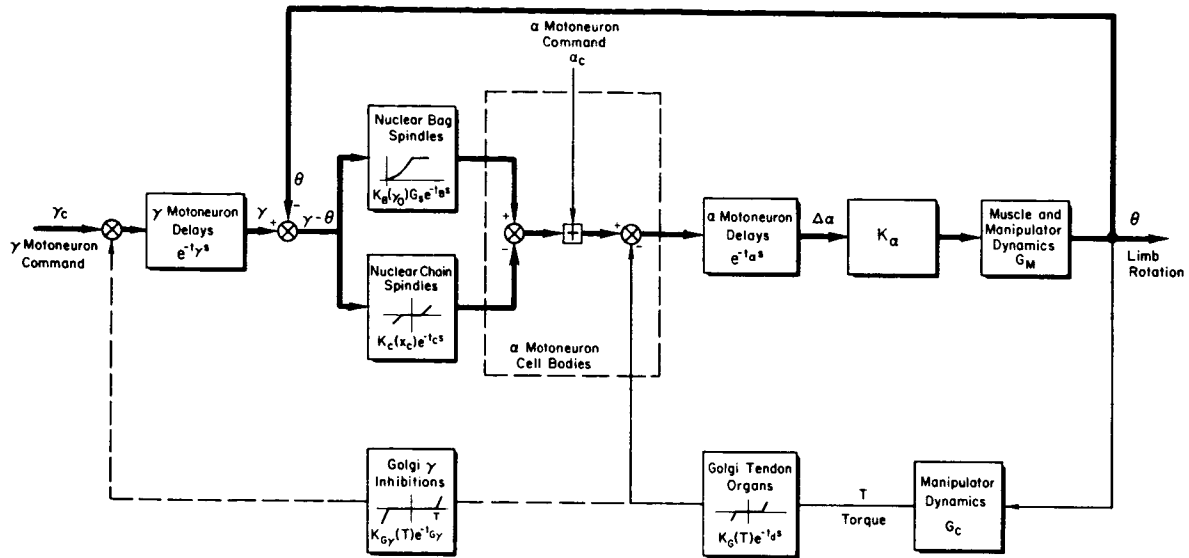


Figure 4.—Elementary neuromuscular system model.

## REFERENCES

1. McRuer, Duane; Graham, Dunstan; Krendel, Ezra; and Reisener, William, Jr.: Human Pilot Dynamics in Compensatory Systems—Theory, Models, and Experiments With Controlled Element and Forcing Function Variations. AFFDL-TR-65-15, Jan. 1965.
2. Stark, L.: Neurological Organization of the Control System for Movement. Quar. Prog. Rept. 61, Res. Lab. Elec., MIT, Apr. 1961, pp. 234-238.

# ADAPTIVE CONTROL

N67-15855

## 4. PROCESS OF ADAPTATION BY THE HUMAN CONTROLLER\*

*Jerome I. Elkind and Duncan C. Miller  
Bolt Beranek and Newman, Inc.*

The ability of human controllers of dynamic systems to adapt to changes in control situation is of considerable practical importance. Human-controlled vehicles, such as aircraft and automobiles, frequently undergo abrupt changes in dynamic characteristics. These might result from malfunctions in a flight control system, a change in road surface conditions, or other similar causes. An understanding of the process of human adaptation to such changes in dynamics would be valuable for the design of these vehicles, or for the specification of the limits of their operation.

The literature on human adaptation in time-varying control situations is not extensive (refs. 1 to 5). The first study of this problem was by Sheridan (ref. 1) who investigated adaptation to changes in input and plant dynamics. Young et al. (ref. 2) sought to determine the speed of adaptation and the process of adaptation with very simple plants. Elkind et al. (ref. 3) extended these results to more complex plants and proposed a four-phase model for the adaptive process involving detection, identification, mode switching modification of controller dynamics, and parameter adjustment optimizing. Knoop and Fu (ref. 4) proposed an adaptive model for very simple plants in which the human controller is assumed to have an internal model for the plant being controlled and in which modification is accomplished by a parameter adjustment technique.

None of these studies has led to good quantitative models for human controller adaptation. In an attempt to develop a more comprehensive model, we performed an extensive experimental study of the adaptation of human controllers to sudden changes in plant dynamics. These experiments and the model that we have developed are discussed in this paper.

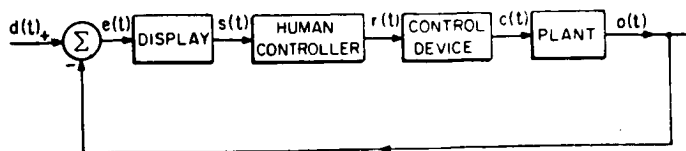
### HUMAN CONTROLLER CHARACTERISTICS IN TIME-INVARIANT SITUATIONS

SYSTEM CONFIGURATION.—Our studies of human controller characteristics were performed with a control system that can be represented by the block diagram of figure 1(a). In this system only the system error is presented to the human controller and his task is to minimize, that is, to compensate, this error. He does this by moving the control device which provides control inputs to the plant. If the control device has small mass and friction, and if the display is nearly ideal, the system can be represented by the simplified diagram of figure 1(b).

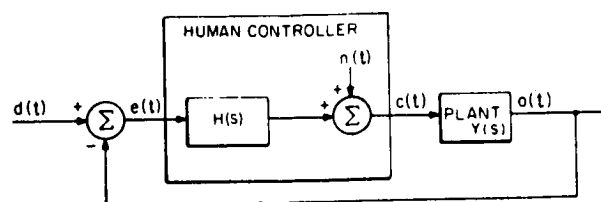
In most of our experiments the display was a cathode-ray oscilloscope of 12 cm diameter. It was positioned about 50 cm from the subject at eye level. The displacement of a dot

\*The research upon which this paper is based was supported by the Air Force under Contract No. AF33(657)-10124.

from the center of the display represented the system error  $e(t)$ . The control was located on the subject's right and was moved horizontally to control the horizontal movement of the error dot. The control had a linear spring restraint. In all the experiments the system had one degree of freedom and the error dot moved along the horizontal axis of the display. The input forcing function in these experiments was an approximation to low-frequency gaussian noise.



(A)



(B)

Figure 1.—Control system.

#### QUASI-LINEAR TIME-INVARIANT MODELS.

—In linear systems of the kind described above, the human controller's characteristics can be represented by the quasi-linear model

shown in the human controller block of figure 1(b) (refs. 6 to 9). The quasi-linear model consists of a single equivalent linear element represented by the describing function  $H(s)$  and a remnant  $n(t)$ . For a large class of control situations the human controller's describing function can be approximated very well by an analytic function of the form

$$H(s) = \frac{K_h e^{-\tau s} (T_L s + 1)}{(T_I s + 1)(T_N s + 1)} \quad (1)$$

The term  $(T_L s + 1)/(T_I s + 1)$  is an equalizer. The delay  $\exp(-\tau s)$  is analogous to a reaction time delay and has been found to be approximately constant with a value of between 0.15 second and 0.2 second (refs. 6 to 9). The lag  $1/(T_N s + 1)$  represents the dynamics of the neuromuscular system (refs. 7 to 9).  $K_h(T_L s + 1)/(T_I s + 1)$  plays the major role in the human controller's adaptation to different control situations and is of principal interest to us in studies of human adaptation.

McRuer et al. (ref. 7) have shown that the human controller adjusts his characteristics so as to maintain  $HY(s)$  in the neighborhood of the gain crossover frequency  $\omega_c$ , approximately invariant to changes in  $Y(s)$ . To a first approximation  $HY(s)$  in the region of crossover can be represented by

$$HY(s) = \frac{\omega_c e^{-\tau_e s}}{s} \quad (2)$$

where  $\tau_e$  is a delay term that includes the reaction time delay plus the low-frequency effects of the lead and lag terms that are not otherwise included in this simple crossover model. The human controller attempts to maintain the crossover frequency,  $\omega_c$ , as high as possible consistent with the requirements of stability and good performance. The principal constraint on the maximum value of the crossover frequency is imposed by the delay  $\exp(-\tau_e s)$  and the phase lag that it produces.



## A TYPICAL ADAPTIVE RESPONSE

A control situation in which abrupt unpredictable changes in plant occur imposes a vigilance or monitoring task upon the human controller. He must control the plant and at the same time monitor its behavior to detect changes in plant characteristics. If a change occurs, he must identify the new plant dynamics and then modify his own characteristics in order to achieve stability and control of the plant. Finally, he must optimize his characteristics to achieve good system performance.

These four elements of the adaptive process—detection, identification, modification, and optimization—are evident in records of human-controller adaptation. Figure 2 is the record of a typical response of a highly-trained human controller to a change in plant dynamics. At the time marked  $t_0$  on the record, the plant dynamics change abruptly from  $+8/s^2$  to  $-16/s^2$ . Figure 2 shows the time histories of the input disturbance, the plant response, the stick movement and the error before and after this change in plant dynamics.

In spite of the fact that after  $t_0$  the closed-loop system was unstable, its state at  $t_0$  and the input after  $t_0$  were such that the error and error rate remained small until  $t_0 + 1.2$  seconds. It is clear from the character of the stick movements that the controller had not detected the change in dynamics prior to  $t_0 + 1.2$  seconds. After  $t_0 + 1.2$  seconds the error rate became large, and the fact that the plant dynamics had changed must have been apparent to the controller. He made one or two more movements of wrong polarity, apparently to identify the plant dynamics, and then at  $t_0 + 1.7$  seconds he reversed the polarity of his control movements. Since the second overshoot in the error is smaller than the first, he must also

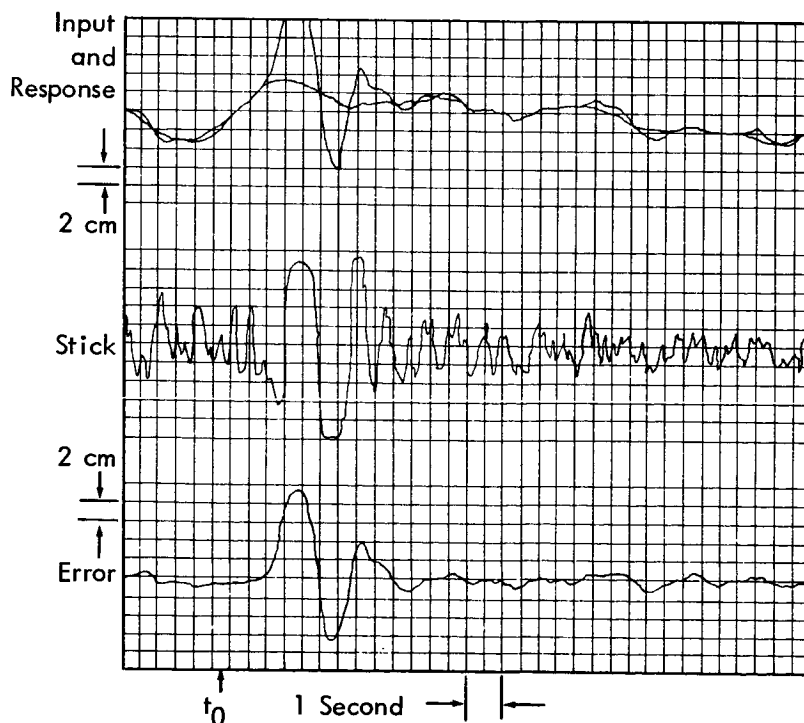


Figure 2.—Tracking record for a change in  $Y(s)$  from  $+8/s^2$  to  $-16/s^2$ .

have compensated for the increase in plant gain at least partially before the beginning of the large negative stick movement at  $t_0 + 2.5$  seconds. Thus, in less than 1.3 seconds from detection, the controller had made a sufficient adjustment in the polarity and gain of his own characteristics to render the system stable. By  $t_0 + 4$  seconds most of the errors had been nulled and the system was well under control. At about  $t_0 + 12$  seconds there appears to be an adjustment in the character of the controller's movements which perhaps represents an attempt to optimize the system's performance.

## A MODEL FOR THE ADAPTATION BY HIGHLY-TRAINED CONTROLLERS

In a control situation like that of figure 1 the human has only two sources of information about the system: the error signal  $e(t)$  presented to him on the display, and the displacement of the control device  $c(t)$ . The only way that the human can ascertain that the plant's characteristics have changed is by observing the response of the error signal to his stick movements.

If we accept the crossover model of equation (2) as an adequate approximation to the open-loop characteristics of the system prior to any change in dynamics, then we may consider the human controller's adaptation problem to be simply the establishment of the correct relation between the system response rate and the error  $\tau_e$  seconds earlier. Under this assumption, we would expect that the error rate would be the principal quantity used by the controller for monitoring the state of the system and for identifying changes in it. Output rate is not available to the controller and must be estimated from the error rate. However, estimates of the output rate made from observations of the error will be masked by the input and therefore subject to random errors.

Figure 3 is a signal flow diagram of the model we propose for the process of human controller adaptation. This model is based upon the use of error rate information for detection and identification. The detection, identification, and modification portions of the model are shown separately. In the following discussion we explain the behavior of the model and justify its design.

**DETECTION OF A CHANGE IN PLANT DYNAMICS.**—If the human controller is skilled at controlling the plant and has been operating it for a long time, it is reasonable to assume that he can predict how the plant will respond to his control movements and, therefore, how the error rate will respond to his control movements. Miller (ref. 10) suggests that the quantity the controller uses for monitoring is the difference between the observed change in error rate and the predicted change due to a stick movement. If this difference is small, it is reasonable for the controller to assume that the system dynamics have not changed. If the difference is large, the controller can properly assume that a change in dynamics has occurred.

To predict the system response, the human controller, in effect, must have an internal representation for the plant dynamics  $Y_m$ , the element shown in figure 3(a). By differentiating the output of this model, the predicted error rate  $\dot{e}_p(t)$  is obtained. We assume that the human controller makes a movement every  $T$  seconds, where  $T$  is approximately equal to  $\tau_e$  in equation (2). The change in  $\dot{e}_p$ , due to movements made during this  $T$ -second-long interval, is obtained by subtracting  $\dot{e}_p(t-T)$  from  $\dot{e}_p(t)$  as shown in the figure. This increment in  $\dot{e}_p$  is designated  $\Delta\dot{e}_p(t)$ . The actual error  $e(t)$  is also differentiated and the increment  $\Delta\dot{e}(t)$  during the period  $T$  is obtained. A comparison is then made between  $\Delta\dot{e}$  and

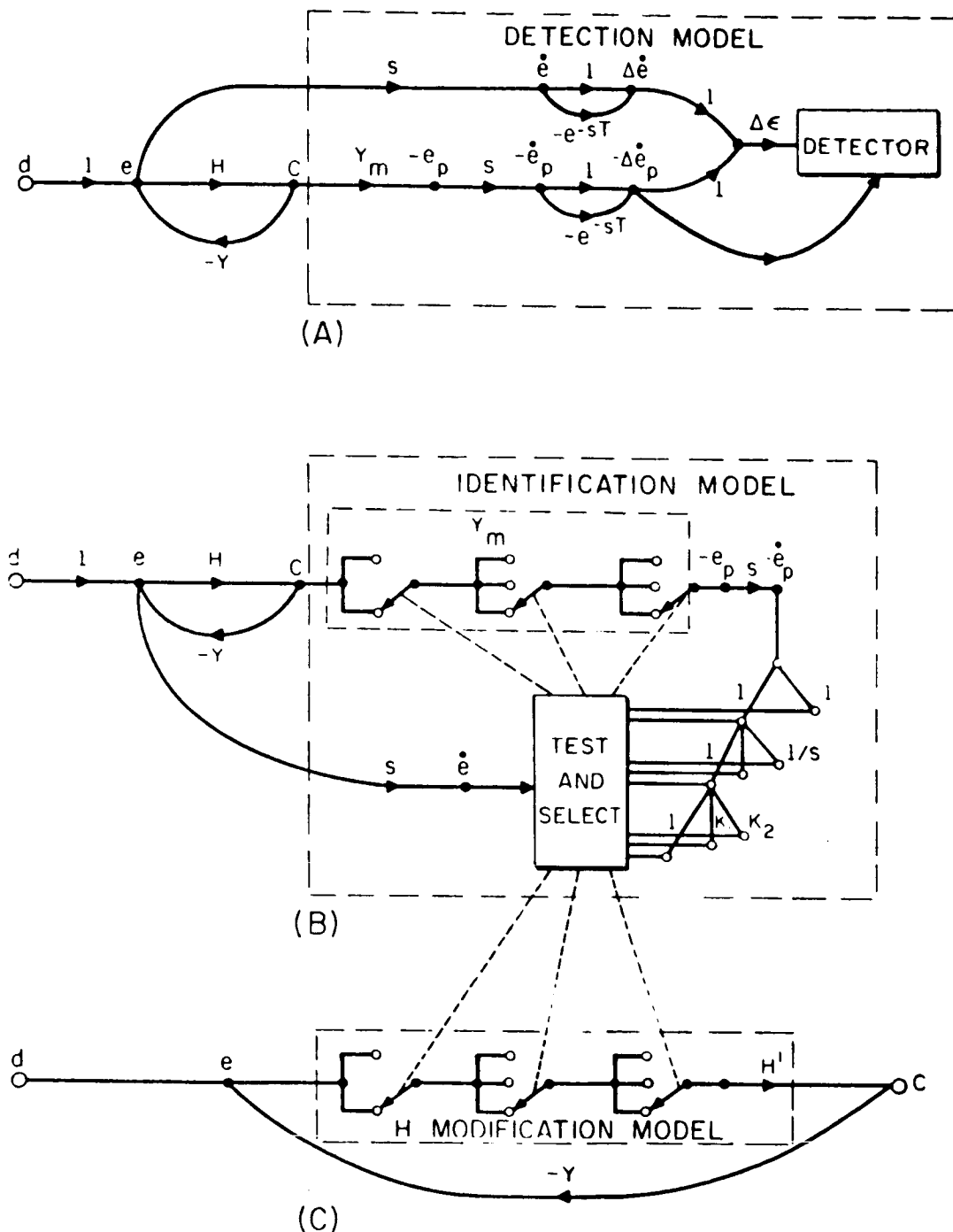


Figure 3.—Signal flow diagram of model for human adaptation.

$\Delta \dot{e}_p$ . The observed  $\Delta \epsilon$  is evaluated relative to  $\sigma_{\Delta \epsilon}$  the standard deviation of  $\Delta \epsilon$  with time-invariant plant dynamics. If the ratio  $\Delta \epsilon / \sigma_{\Delta \epsilon}$  exceeds some criterion  $t$ , the model will report a change in  $Y(s)$ . If  $\Delta \epsilon / \sigma_{\Delta \epsilon}$  is less than  $t$ , it will report no change.

Miller (ref. 10) found that for  $Y = K/s$ , the detection criterion depends upon the magnitude of the stick movement. This implies that  $\sigma_{\Delta \epsilon}$  has two components: one that results

from the change in input rate during the interval  $T$ ; the second that results from the stick movement. For the general case of plants whose dynamics are not simply  $K/s$ , this second component may be proportional to  $\Delta\dot{e}_p$ . In figure 3 the dependence of the detection criterion on  $\Delta\dot{e}_p$  is shown by the connection between  $\Delta\dot{e}_p$  and the detector.

If we assume that the internal model  $Y_m$  has been adjusted to match the plant dynamics  $Y$  and that no prediction of input is made,  $\Delta\dot{e}_p$  can be obtained by a simulation of figure 3(a), or can be computed directly using standard methods (ref. 11). For the case of a pure first-order plant  $Y = K/s$  which is of special interest since many of our experiments were performed with this kind of a plant

$$\Delta\dot{e}_p(t) = -K_m \Delta c(t) \quad (3)$$

where  $K_m$  is the gain of the plant model. For more complex plants we can often obtain a satisfactory estimate of  $\Delta\dot{e}_p$  from the crossover model of equation (2). To use this model we assume that

$$HY_m(s) \doteq \frac{\omega_c m e^{-\tau_e s}}{s} \quad (4)$$

From the inverse Laplace transform of equation (4) it follows that

$$\Delta\dot{e}_p(t) = \omega_c m \Delta e(t - \tau_e) \quad (5)$$

where  $\Delta e(t - \tau_e) = e(t - \tau_e) - e(t - 2\tau_e)$ , and  $\tau_e$  is taken as movement time  $T$ . The difference between the estimates of  $\Delta\dot{e}_p$  and the observed values of  $\Delta\dot{e}$  forms the basis for the detection of a change in dynamics.

**IDENTIFICATION OF CHANGE IN DYNAMICS.**—Previous experiments (refs. 2 and 3) showed that a well-trained human controller is able to identify changes in dynamics very rapidly, in times of order of a reaction time from the time of detection. This identification process is a classification or pattern recognition process by which the human controller decides which of a finite number of previously encountered plant dynamics is currently in operation. We assume that signals used for this classification process are the control stick movement  $c(t)$  and the system error rate  $\dot{e}(t)$ .

The human controller is capable of a partial identification of plant dynamics. When several properties of the plant have changed, say, a change in both the polarity and a gain of a plant, the human controller attempts to identify and to compensate first for the change in plant that has the greatest influence on system performance. Subsequently, he attends to less important plant parameters. We find that the polarity of control movements is always adjusted first and then the gain and lead time constants are adjusted (refs. 2 and 3). The sequence in which adjustments are made implies an identification sequence.

A model for the identification process is shown in figure 3(b). The identification is performed by a decision tree that operates on  $\dot{e}_p$ , the output of  $Y_m$ . The branches of the tree are arranged in levels, each level composed of a group of signal processing elements. The signal transformations performed by the branches of a group are similar but have different parameters. Thus, one group of branches may be composed of gain elements of different values, another of lead or lag terms.

The purpose of the tree is to determine how  $Y_m$  should be modified to obtain a better match between  $\dot{e}$  and  $\dot{e}_p$ . The branches of the tree represent the changes that must be made to  $Y_m$ . From each group of branches one must be selected. Our present data indicate that the selection rule may consist of simply choosing the branch whose change in output  $\Delta \dot{e}_i$  matches most closely the change in observed error rate  $\Delta \dot{e}$ . To mechanize this rule, the test and select box would compute

$$\Delta \epsilon_i = \Delta \dot{e} - \Delta \dot{e}_i \quad (6)$$

for every branch and would select the branch yielding the smallest  $\Delta \epsilon_i$ .

The selection of a branch implies a modification to  $Y_m$ . Note that  $Y_m$  in figure 3(b) is constructed from a switching tree whose branches are also signal processing elements. They are arranged in groups that are compatible with those of the decision tree. Thus, when a branch of the decision tree is selected, the change to  $Y_m$  implied by that selection can be made by operating the appropriate switch of the  $Y_m$  tree.

The trees are arranged so that groups representing characteristics that have both the greatest influence on the system performance and the greatest probability of being changed are tested and modified first. Thus, the uppermost level of the decision tree and the left-most group of the  $Y_m$  tree would include a sign reversal when such a change of dynamics is considered by the controller to be likely. As the identification process proceeds down the tree, testing for changes of decreasing importance,  $Y_m$  is adjusted to match more and more closely the plant dynamics.

MODIFICATION OF CONTROLLER CHARACTERISTICS.—The identification process and the modification process interact very closely. Whenever an identification decision has been made, a corresponding modification is made in the human controller's characteristics. For highly-trained controllers this modification process is very fast (within a reaction time or two) and appears to be essentially a switching process (ref. 3).

Accordingly, we represent this modification process by a switching tree shown in figure 3(c). The branches are signal processing operators arranged in groups. The selection of an operator within a group is made by the switches and corresponds to the selection made in the identification process. As the selection process proceeds from left to right, the human controller's characteristics converge to the required characteristics. The most important changes (i.e., polarity reversal) are made first provided, of course, the human controller has arranged his selection tree in the most efficient manner. The adjustment tree represents the equalizer portion of the human controller's characteristics. Fixed elements  $H'$  are treated separately in the model as shown in the figure.

OPTIMIZATION OF CONTROLLER CHARACTERISTICS.—The mode switching adjustment, because it is fast, is not likely to be very accurate. Given more time to evaluate the performance of the system, the human controller should be able to adjust the parameters of his characteristics to optimize the system performance. We have not studied this aspect of the adaptive process in detail as yet and are not ready to propose a model for optimization. We would expect, however, that one of the conventional parameter adjustment optimizing techniques might serve as a prototype for a model (ref. 12).

## MEASUREMENTS OF HUMAN ADAPTIVE PERFORMANCE

We, together with our colleagues, have performed a number of experimental studies to measure the ability of human controllers to adapt to sudden changes in controlled-element dynamics. We will cite the results obtained in three of these studies and discuss the extent to which the model presented in the previous section accounts for the behavior observed in them.

**MILLER'S EXPERIMENT.**—Miller (ref. 10) conducted a set of experiments with pure first order plant dynamics such that  $\dot{y}(t) = K_y(t)c(t)$ .  $K_y(t)$  was allowed to change suddenly in three ways: increase, decrease, and change sign. This is a particularly good choice of plant dynamics because it leads to a very simple human controller describing function. From the crossover model (eq. (2)), for  $Y = K_y/s$ ,

$$H(s, t) = \frac{\omega_c e^{-\tau s}}{K_y(t)} = K_h(t) e^{-\tau s} \quad (7)$$

In this case, the impulse response corresponding to the human controller's describing function is

$$h(t, \tau) = K_h(t) \delta(t - \tau) \quad (8)$$

where  $\delta(t)$  is a unit impulse. Because of the simple form of  $h(t, \tau)$ ,  $K_h(t)$  is very easy to estimate from the observed error and stick movements.

Miller had his subjects indicate explicitly when they detected a change in plant dynamics by releasing a button. Thus, from the button release time, we were able to obtain a direct indication of the time of detection. From measurements of  $K_h(t)$  we can infer when identification is completed, the nature of the modification process, and perhaps something about the nature of the optimization process.

Miller used an input disturbance that was an approximation to low-frequency gaussian noise. The spectrum was rectangular in shape and had a cut-off frequency of 1.5 rad/sec. The rms of the input was 2.1 cm; the display diameter was 12 cm. The changes of dynamics were synchronized with the input by a control signal that was recorded on the input tape. In each experimental session 18 changes in plant gain were made, all but six of which were presented in randomized order. For these six, the ones on which most of the analysis was performed, the input signal was identical from session to session. This procedure was followed to reduce the variability of the results obtained.

**Detection Results.**—In the detection model, detection of a change is made whenever  $\Delta\epsilon$  exceeds the criterion  $t$ . The criterion depends upon the standard deviation of  $\Delta\epsilon$ , which, in turn, was assumed to depend upon both the input and  $\Delta c$ . The values of  $\Delta\epsilon$  versus  $\Delta c$  are plotted in figure 4. These values were obtained one reaction time before the button release as  $K_y$  was decreased from 10 to 2. This figure gives the data for three subjects for two changes in dynamics of this type. The linear dependence of the criterion value of  $\Delta\epsilon$  upon  $\Delta c$  is evident. The smallest value of  $\Delta c$  for which a detection was indicated was about 0.15 cm. The corresponding value of  $\Delta\epsilon$  was about 1 cm/sec. For this experiment  $\sigma_{\Delta d}$ , the standard

deviation of the change in input rate during a standard measurement time, was about 0.6 cm/sec. Thus, the minimum observed value of the detection criterion was about 2.0 times  $\sigma \Delta d$

Figure 4 can be used to estimate the detection criterion given  $\Delta c$ . This estimated detection criterion can then be compared with  $\Delta \epsilon$  to predict the point at which detection of a change in plant gain will be made. Figure 5 is a plot of the button release time versus the time at which  $\Delta \epsilon$  first exceeds the criterion for the three different kinds of changes in dynamics with one subject. The data for the other subjects are similar. The button release time on the average is 0.4 second greater than the time at which  $\Delta \epsilon$  exceeds criterion. The 0.4-second difference is presumably the subject's reaction time.

These results tend to confirm the part of the model concerned with detection of a change in dynamics. A more complete discussion of the detection model and tests of it are reported by Miller (ref. 10).

**Identification.**—For  $Y = K_Y/s$  the identification procedure reduces to finding the model gain  $K_m$  that gives the minimum  $\Delta \epsilon$ . Three estimates of  $\Delta \epsilon(t)$  obtained using  $K_m = -10, +10, -2$  to estimate  $\Delta \dot{e}_p$  and thus  $\Delta \epsilon$  following a change in dynamics from  $-10/s$  to  $-2/s$  are plotted in figure 6. In Miller's experiment these three gain values are the only permissible ones for a base condition of  $Y = -10/s$ . It is clear in the figure that  $K_m = -2$  gives the minimum  $\Delta \epsilon$ , and once a detection has been made the model will correctly select this value of gain as its estimate of the new dynamics. Detection will occur

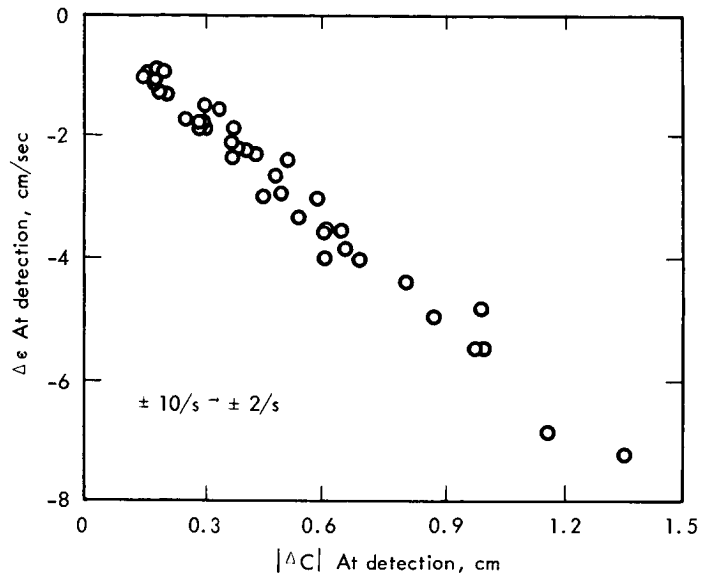


Figure 4.—Relation between  $\Delta c$  and  $\Delta \epsilon$  0.2 sec before detection button release; dynamics changed from  $Y(s) = 10/s$  to  $2/s$ .

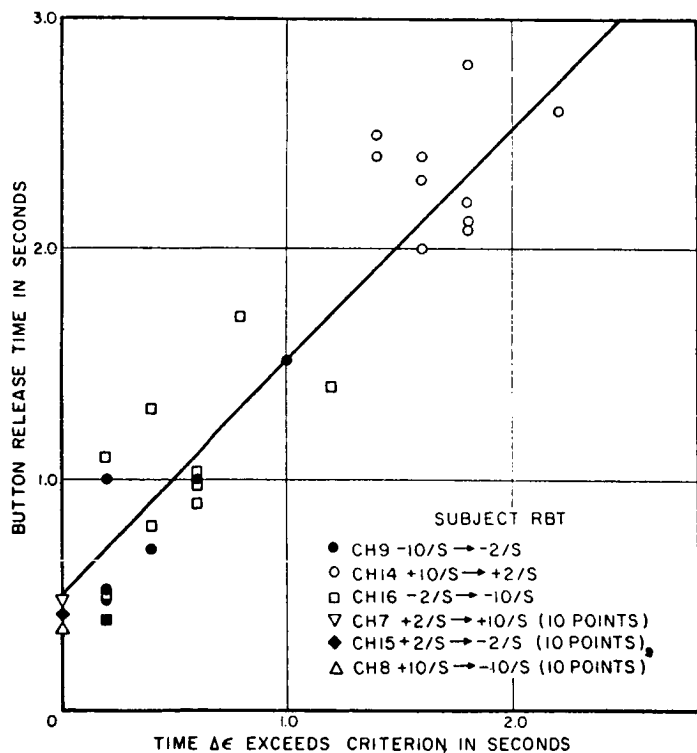


Figure 5.—Verification of detection model; relation between button release time and the time  $\Delta \epsilon$  first exceeds the detection criterion; data are from tests with six kinds of changes and with one subject.

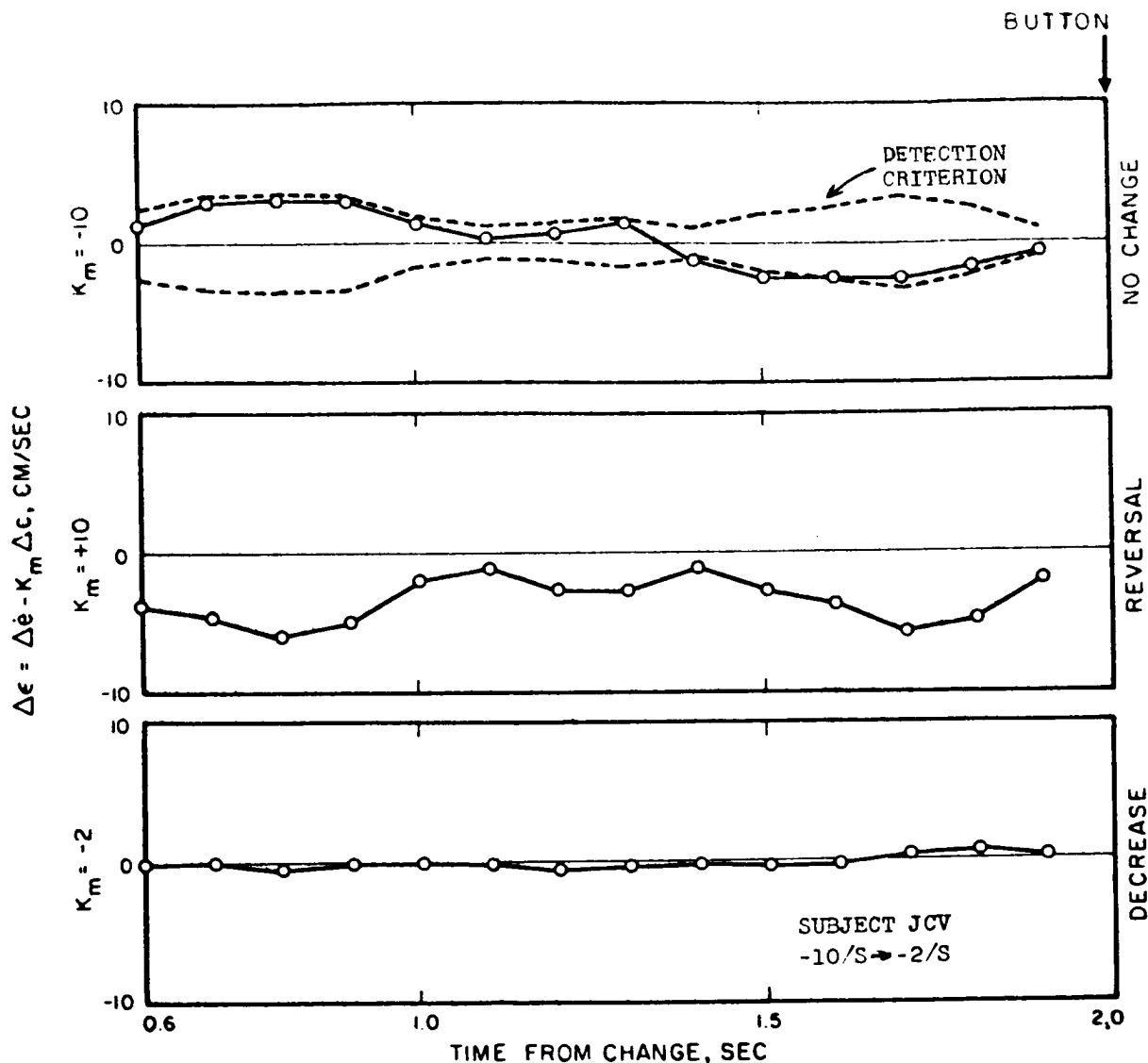


Figure 6.—Verification of identification model versus time for the three allowable values of  $K_m$  for a change from  $-10/s$  to  $-2/s$ .

when  $\Delta\epsilon$  for  $K_m = -10$  exceeds criterion. This occurs in this example about 1.4 seconds after the change in dynamics as shown in the upper curve of figure 6. The button release actually occurred 0.6 second after the criterion was exceeded. This is reasonably consistent with the model estimates. The example of the identification in figure 6 is typical of those observed by Miller.

Modification.—For  $Y = K_y/s$ , the human controller's gain can be estimated from the relation

$$K_h(t) = \frac{\langle c(t)e(t-.2) \rangle}{\langle e^2(t-.2) \rangle} \quad (9)$$



where  $\langle ce \rangle$  and  $\langle e^2 \rangle$  are averages taken over an ensemble of runs. The reaction time is assumed to be 0.2 second. Figure 7 shows  $K_h(t)$  versus time for a change of  $K_y$  from 2 to -2. The brackets shown about the  $K_h$  data points are estimates of the standard deviation of  $K_h$ . The curve at the bottom of the figure shows the squared correlation between model output and human controller output. It indicates the extent to which the model of equation (8) accounts for the human controller's responses.

The human controller changes his gain from -4 to about +1.5 starting just prior to the release of detection button. The gain changes polarity about 0.1 second after the button release. The change in  $K_h$  is abrupt and is approximately of the correct magnitude. This result is typical of those obtained and illustrates that a well-practiced controller adjusts his characteristics by switching from one well-practiced control mode to another.

**Optimization.**—Figure 7 shows that at about 1.7 seconds after the button release,  $K_h$  increases gradually from about 1.5 to about 4. This final value is equal in magnitude and opposite in sign to the pretransition  $K_h$  of -4. The gradual increase in  $K_h$  extending from about 1.7 to 2.5 seconds is evidence of the relatively slow optimization behavior of the human controller.

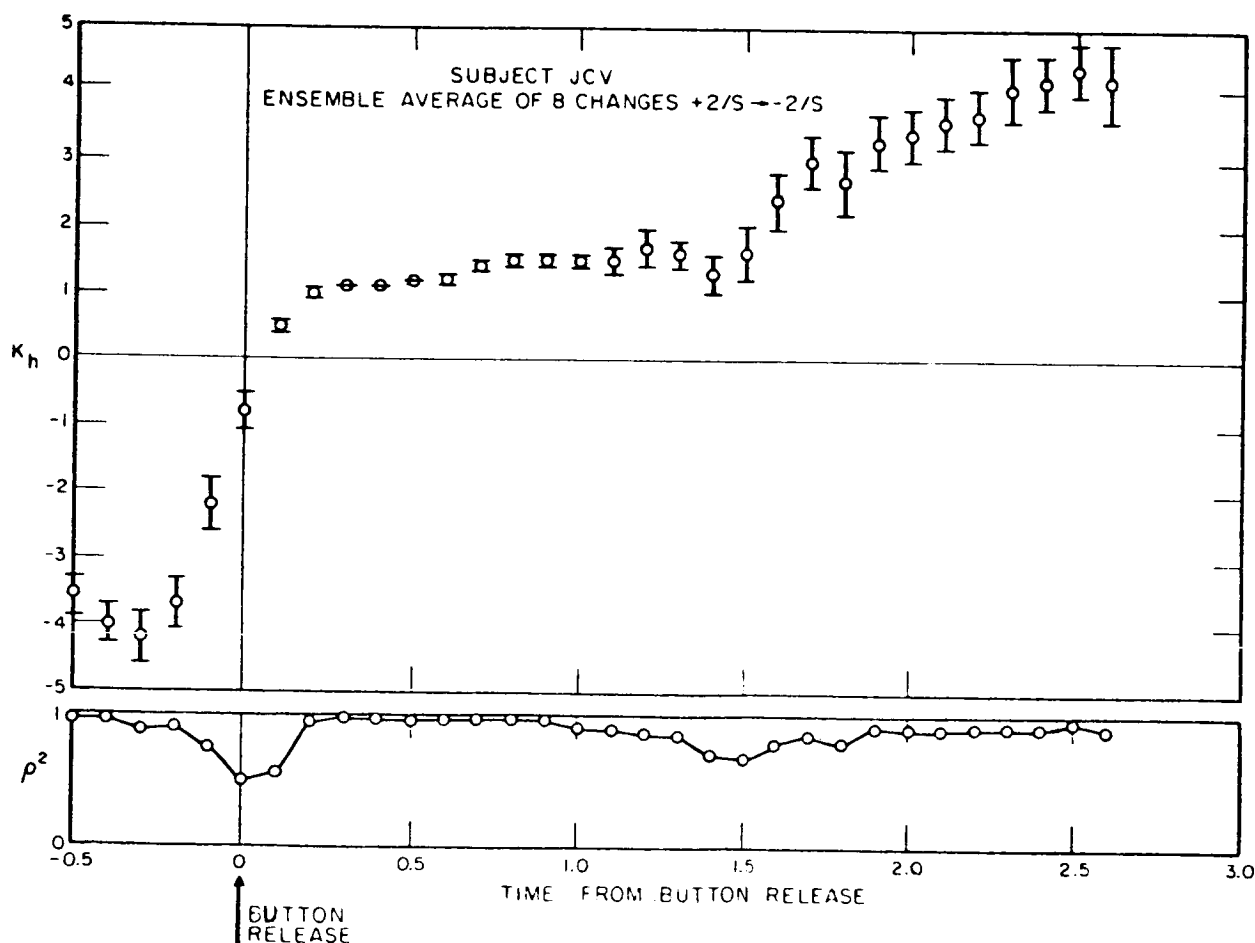


Figure 7.—Ensemble average  $K_h$ ,  $\sigma_K$ , and  $\rho^2$  following a change in dynamics from +2/s to -2/s.

**THE ELKIND-KELLY EXPERIMENT.**—Prior to Miller's experiments, Elkind and Kelly (ref. 3) performed similar experiments except that they used a variety of plant dynamics and did not have a detection button. The adaptive model of figure 3 can also be used to represent the results obtained from these experiments which involved more complex plant dynamics. For example, the results for a change in plant from  $4/s$  to  $8/s^2$  are plotted in figure 8. Since the plant was  $K_y/s$  prior to the change, equation (3) can be used to estimate  $\Delta\dot{e}_p$ .

Figure 8 shows that at 0.4 second after the change in dynamics  $\Delta\dot{e}$  increased to 2.2 cm/sec, a magnitude much larger than observed prior to the change. Although the subject had no means of indicating explicitly when he thought the plant changed, we can determine from the tracking record (not shown here) the time at which he changed the character of his responses. Since detection must occur before this change in response, it is an upper bound on the detection time. This upper bound we call the apparent detection time. For the trial of figure 8, the apparent detection time was at 1.0 second which is reasonably close to that predicted by the detection model.

We can also determine approximately how the subject adapted to this change by computing an estimate of loop gain  $\hat{K}_l$  as defined by the crossover model, equation (2),

$$\hat{K}_l \doteq \dot{o}(t)/e(t-\tau_e) \quad (10)$$

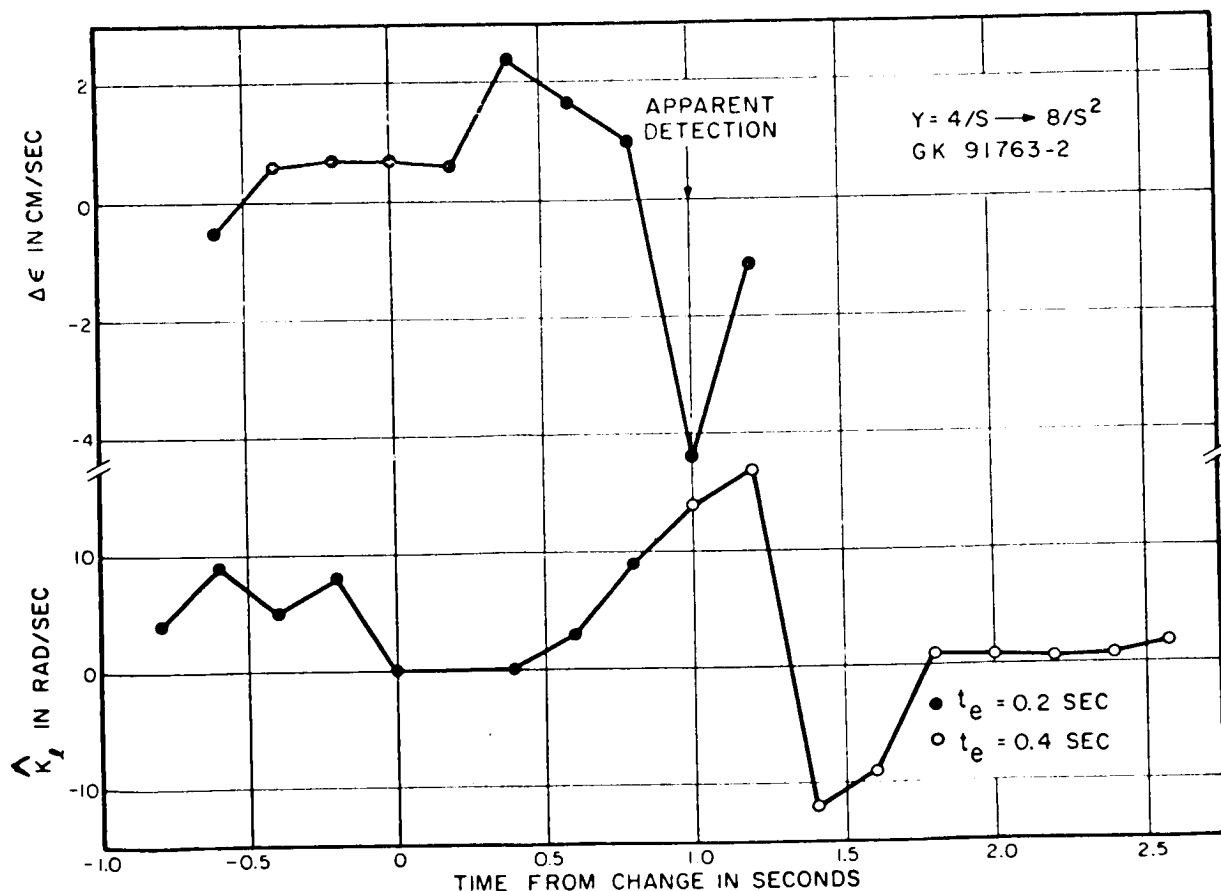


Figure 8.— $\Delta\dot{e}$  and  $\hat{K}_l$  for a change in plant from  $Y(s) = 4/s$  to  $8/s^2$ .

where  $\tau_e$  is taken to be 0.2 second prior to detection and 0.4 second after detection. The lower value is appropriate for  $K/s$  dynamics and the higher for  $K/s^2$ . Values of  $\hat{K}_1$  are plotted in figure 8. Prior to the change  $\hat{K}_1$  is approximately 5, a typical value for  $Y=K/s$ . From time 0 to 1.6 seconds  $\hat{K}_1$  varies greatly. At 1.8 seconds  $\hat{K}_1$  becomes slightly less than 1 and then increases gradually to 1.5. This value is somewhat low for  $K/s^2$  dynamics, but within the range of values observed for these dynamics.

Thus, within 0.8 second of the apparent detection time, the subject had made the necessary adjustment to his characteristics to compensate approximately for the change in plant dynamics. The adjustment is less rapid in this case of a change in the order of the dynamics than previously observed when only the plant gain changed. This longer adjustment implies a longer identification time. The decision tree model for identification predicts that a longer time is required when several properties of the internal model must be modified in order to complete the identification. In this case, the gain and order of the internal model and of the controller's characteristics must be changed.

In figure 9 are plotted  $\Delta e$  and  $\hat{K}_1$  for a change in plant from  $8/s^2$  to  $4/s^2$ . The model predicts detection at 1.2 seconds (plus the reaction time). The tracking records indicate an apparent detection at 1.4 seconds. During the interval from 0 to 1.2 seconds,  $\hat{K}_1$  is either indeterminate (because  $e(t-\tau_e)$  in equation (10) is zero) or negative. The negative  $\hat{K}_1$  results from the fact that the error increased in spite of the subject's efforts to control it, because of a large input rate and the decreased control effectiveness. This ever-increasing error or negative  $\hat{K}_1$  was interpreted by the subject to be a polarity reversal in  $Y(s)$ , an incorrect identification. He momentarily reversed the direction of his movements at 1.3 seconds, immediately noticed that the identification was wrong, and changed back to positive polarity.

At 1.4 seconds  $\hat{K}_1$  is positive, but small, indicating that the subject had not yet compensated for the gain decrease. By 2.0 seconds,  $\hat{K}_1$  starts to increase and reaches a satisfactory value of 2.5 at 2.4 seconds. Thus, adjustment is completed 1 second after the apparent detection during which time a false identification and false adjustment were made and had to be corrected. The false identification was predicted by the model.

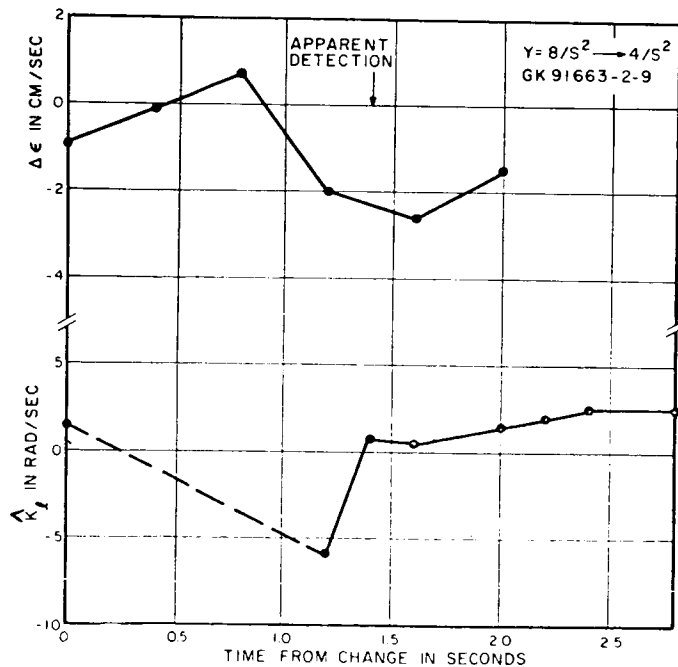


Figure 9.  $-\Delta e$  and  $\hat{K}_1$  for a change in plant from  $Y(s) = 8/s^2$  to  $4/s^2$ .

Elkind and Kelly also investigated the effects of an audio alerting signal on the adaptive process. The onset of the signal coincided with the change in dynamics. Their data are presented in table 1 which compares the apparent detection times with and without the alerting signal in a situation in which the plant switched back and forth between the pairs of dynamics

shown in the table. Thus, the subject knew what change in plant would occur, but he did not know when it would occur.

For this situation of certainty about the change, the alerting signal reduced the detection times. The difference between the mean alerted and nonalerted times is statistically significant.<sup>1</sup> The alerting signal also reduced the apparent detection time when the subject was uncertain about the nature of the changes in plant dynamics, but not by a statistically significant amount.

The apparent detection times obtained from these experiments include some fraction of the identification process. Typically, the subjects did not change the character of their responses immediately after the onset of the alerting signal. This is apparent from the data in table 1. They waited until  $\Delta\epsilon$  had become large. The effect of alerting was to lower the detection criterion. Once the detection decision had been made, the controller merely had to change his dynamics to a second predetermined form. When there was uncertainty about the change in plant, the controller had to wait until he had identified the plant before changing his own characteristics. This need for identification is no doubt the reason for the lack of a significant effect of the alerting signal when the plant changes were uncertain.

TABLE 1. —EFFECT OF ALERTING SIGNAL ON APPARENT DETECTION TIME

Plant change	Detection time, sec	
	Alerted certain	Non-alerted certain
$8/s^2 \rightarrow -16/s^2$	0.82	0.90
$8/s^2 \rightarrow +16/s^2$	.52	1.25
$8/s^2 \rightarrow -16/s$	.50	.61
$8/s^2 \rightarrow +16/s$	.64	.79
$8/s^2 \rightarrow 4$	.30	.51
Mean	0.55	0.77

In some unreported experiments performed by the authors, the effects of plant change uncertainty on the apparent detection times and on the percentage of false identifications was investigated. In these experiments the plant could change from  $+5/s$  to  $-5/s$ , or to  $2/s$ . In addition, a transient disturbance input could occur which produced an error waveform similar to that obtained when the polarity reversed.

When the type of plant change that could occur was uncertain, the controller often incorrectly identified reversals as transients and vice-versa. The apparent detection times were longer than when there was no uncertainty about the change in dynamics. A typical set of results obtained with one subject is shown in table 2. About 15 percent of the reversals were identified as transient inputs in the uncertain case. There were no mistakes in the

<sup>1</sup>A two-tailed sign test was used to test significance. For one of the two subjects whose data are summarized in table 1, the level of significance was 0.002. For the other subject it was 0.05.

certain case. The mean apparent detection time  $\bar{t}$  for the uncertain case was 0.24 second longer than for the certain case. This is about the time required for one movement which the subject could have used to obtain the information required to differentiate between the transient and the reversal.

TABLE 2. -EFFECT OF CERTAINTY ON DETECTION

	System change 5/s to -5/s	
	Certain reversal	Uncertain reversal
Reversal	$N = 33$ $\bar{t} = .39 \text{ sec}$ $\sigma_t = .09 \text{ sec}$	$N = 28$ $\bar{t} = .63 \text{ sec}$ $\sigma_t = .10 \text{ sec}$
Subject's response transient	$N = 0$	$N = 5$ $\bar{t} = 1.08 \text{ sec}$ $\sigma_t = .37 \text{ sec}$

This result is consistent with our identification model. The human controller makes use of a priori information, or of his recent experience to restructure his identification decision tree so that the identification procedure is most efficient for the particular experiment being performed. An average of only one additional movement was required to distinguish between one of two plant changes and the input transient input. Of course, his error rate, as indicated in table 2 is still fairly high. To reduce this would require more information and, therefore, more control movements.

**THE YOUNG-GREEN-ELKIND EXPERIMENT.**—Young et al. (ref. 2) performed some experiments with very simple plants of the form  $Y=K$ . They measured the time required to reduce system error to a criterion which was based upon the rms error prior to the change in dynamics (they called this the adjustment time), and they computed the ensemble average of the error following the change in dynamics. The adjustment time includes the times to detect, identify, and correct for the accumulated errors produced by the change. The ensemble average error curves provide some information about the details of the adaptive process.

With the simple plants used in these experiments all changes, except gain decreases, produced a large discrepancy between observed and predicted error rates immediately after the change occurred (provided there was a stick movement). Detection, therefore, should have occurred within 0.2 to 0.4 second after the change. The average error curves indicate that this, in fact, was the case. For a gain decrease the discrepancy in error rates should have been small, and we would expect detection to be delayed. This was also observed.

They also observed that a change of both polarity and gain led to longer adjustment times than a change of only the polarity or of only the gain. This result is consistent with our identification model in which tests on the internal model are made in a sequential manner.

They investigated the effects of plant change uncertainty and found that increasing the number of possible values of gain which the plant could assume produced some slight

lengthening of the adjustment times. The initial adjustment in controller gain did not appear to be affected by the uncertainty, but the secondary or vernier adjustments took longer when there were eight possible values of gain than when there were only two. This result is consistent with our model which would require more time and data to discriminate among the larger number of values of gain.

## CONCLUSIONS

We have presented a model for three phases of the process by which the human controller adapts to changes in dynamics—detection, identification, and modification. The key features of the model are (1) an internal, adjustable model for the plant dynamics; (2) a threshold detector which operates upon the difference between the observed change in error rate due to control movement and that predicted by the internal model; (3) a decision tree that identifies the change in dynamics by determining in a sequential manner what modifications to the internal model are necessary in order that the observed error rate and the predicted error rate correspond; and (4) a switching tree that allows for rapid and sequential changes in human controller characteristics as determined by the identification procedure.

The detection and identification models have been found to predict accurately the time at which the human controller will detect a change in plant. Most of the verification data are for plants of the form  $Y=K/s$ . However, application of the model to a few more complex plants has also been successful. The model predicts the kind of dependence of identification time upon such factors as plant change uncertainty and plant change complexity that has been observed in previously reported experiments. The mode switching adjustment model has been verified by analysis of the adjustment process of well-trained controllers who show very rapid changes in characteristics once they have detected a change in plant dynamics.

Further development and testing of the model are required. More detailed study of the identification and adjustment process is necessary to determine the effects of nonpredictable changes in plant. The process by which the human controller optimizes his characteristics has received little attention. Finally, the effects of relatively infrequent exposure to changes in plant dynamics, the problem of forgetting, should be investigated because of the practical importance of this aspect of the adaptive behavior of human controllers.

## REFERENCES

1. Sheridan, T. B.: Time Variable Dynamics of Human Operator Systems. AFCRC-TN-60-169, Air Force Cambridge Research Center, 1960.
2. Young, L. R.; Green, D. M.; Elkind, J. I.; and Kelly, J. A.: Adaptive Dynamic Response Characteristics of the Human Operator in Simple Manual Control. IEEE Trans. on Human Factors in Electronics, vol. HFE-5, no. 1, Sept. 1964.
3. Elkind, J. I.; Kelly, J. A.; and Payne, R. V.: Adaptive Characteristics of the Human Controller in Systems Having Complex Dynamics. IEEE Proc. 5th National Symposium on Human Factors in Electronics (San Diego, Calif.), May 1964.
4. Knoop, D. E.; and Fu, K. S.: An Adaptive Model of the Human Operator in a Control System. IEEE Proc. 5th National Symposium on Human Factors in Electronics (San Diego, Calif.), May 1964.

5. Naslin, P.; and Raoult, J. C.: Models Continus et Chantillones de l'operateur Humain place dans une Boude de Commande. Pres. 2nd Intern. Congress, International Federation of Automatic Control (Basel, Switzerland), Sept. 1963.
6. Elkind, J. I.; and Forgie, C. D.: Characteristics of the Human Operator in Simple Manual Control Systems. IRE Trans. on Automatic Control, vol. AC-4, May 1959.
7. McRuer, D. T.; Graham, D.; Krendel, E. S.; and Reissner, W., Jr.: Human Pilot Dynamics in Compensatory Systems. Systems Technology, Inc., Oct. 1964.
8. Elkind, J. I.: A Survey of the Development of Models for the Human Controller. Prog. in Astronaut. and Aeronaut., vol. 13, 1964, pp. 623-643.
9. McRuer, D. T.; and Krendel, E. S.: Dynamic Response of Human Operations. WADC TR-56-524, Wright Air Development Center, Oct. 1957.
10. Miller, D. C.: A Model for the Adaptive Response of the Human Controller to Sudden Changes in Controlled Process Dynamics. M.S. Thesis, Dept. Mech. Eng., MIT, May 1965.
11. Bellman, R.: Introduction to Matrix Analysis. McGraw-Hill Series in Matrix Theory, McGraw-Hill Book Co., Inc., 1960.
12. Osburn, P. V.: Investigation of a Method of Adaptive Control. Sc.D. Thesis, Dept. of Aeronaut. and Astronaut., MIT. Jan. 1962.

## 5. MODEL OF HUMAN-OPERATOR RESPONSE TO STEP TRANSITIONS IN CONTROLLED ELEMENT DYNAMICS\*

*D. H. Weir and A. V. Phatak  
Systems Technology, Inc.*

A critical control problem involving the vehicle/controlled-element system results from a step transition (sudden change) in the controlled element. Practical examples include failure of a manned aircraft stability augments, or the large changes in center of gravity which might occur during staging in the manual control of boost. This paper summarizes the derivation of an analytical model useful in predicting operator transition response. Extensive use is made of experimental data from a variety of sources. Other topics, such as detection criteria and the effects of learning, alerting, and uncertainty about the new dynamics, are included by reference only.

Data are available from past research on several aspects of operator response to changes in controlled element dynamics. Initial studies by Sheridan (refs. 2 and 3) featured gradual changes in the controlled element from pure gain  $K$  to pure integration  $K/s$  and vice versa in both compensatory and pursuit tracking. Later, Sadoff (ref. 4) investigated the response of skilled pilots to sudden (steplike) changes in the controlled element in both fixed- and moving-cab simulators. A longitudinal pitch-attitude tracking task was used, and the transition simulated failures of systems which augmented either static stability or pitch damping. Concurrently, extensive experimental research on operator response to step controlled element transitions was accomplished by Elkind and associates (refs. 5 to 8). These latter studies all involved single-axis compensatory tracking tasks in the presence of low-frequency random-appearing forcing functions.

In the experimental situation to which the model applies, the operator is assumed to be performing a single-axis compensatory tracking task in the presence of a low-frequency random-appearing forcing function. Controlled element dynamics such as the forms  $K$ ,  $K/s$ , or  $K/s^2$  are used. At the time of transition a step change is made to another form and/or to a different gain (magnitude or polarity). When only the controlled element form  $K$  is used, the task is called a "pure gain transition." When other controlled dynamics are involved, together with a possible change in order and/or gain, the transition is called "complex." The problem is to determine the operator response from the time of transition until the system error returns to and remains within an acceptable threshold level following operator adaptation to the new dynamics.

The pure-gain transitions and complex transitions exhibit important differences. In the pure-gain transitions the operator knows that the only possible changes are a sign reversal and/or a magnitude change. Rapid stick movements are immediately evident in the display

\*This work was sponsored by the National Aeronautics and Space Administration under Contract NAS 2-1868-4 and is documented more thoroughly in reference 1.



as well. In the complex transitions the number of posttransition alternatives is increased greatly. The operator is potentially faced with a transition in any or all of order, sign, and magnitude. These factors have a distinct effect on his strategy and transition response.

Transitions which yield an unstable system when pretransition operator adaptation is retained are of particular interest, because they require immediate corrective action to retain control. This correction must occur for any of the following controlled element changes:

- (1) Sufficiently large gain increase
- (2) Polarity reversal
- (3) Increase in effective controlled element order (for sufficiently large gain)

Pure-gain controlled element transitions were examined first. A mode-switching model<sup>1</sup> was derived based on averaged system-error data for a large number of transitions. Its primary contribution is the structural form of its temporal phases. This model was then extended to describe complex transition response characteristics.

### PURE GAIN TRANSITIONS

The operator is assumed to be performing a single-axis compensatory tracking task in the presence of a low-frequency random-appearing forcing function. At transition the controlled element changes from one pure gain to another as shown in figure 1. Five types of change are possible:

(1) Reversal: The sign of the gain changes, but the magnitude remains constant. The loop dynamics with the pretransition human operator adaptation are always unstable.

(2) Increase: The magnitude of the gain increases. A sufficiently large increase will destabilize the system with the pretransition operator adaptation.

(3) Reversal-increase: The sign changes and the magnitude increases. The loop dynamics are unstable in the presence of the pretransition operator adaptation.

(4) Reversal-decrease: The sign changes and the magnitude decreases. The loop dynamics are unstable, unless the decrease is very large. The divergence is comparatively low frequency.

(5) Decrease: The magnitude of the gain decreases, but the sign remains the same. The loop dynamics with the pretransition operator adaptation are always stable.

Only the first three types of change are considered because the relatively high-frequency nature of their instability requires prompt operator attention and readaptation to avoid loss

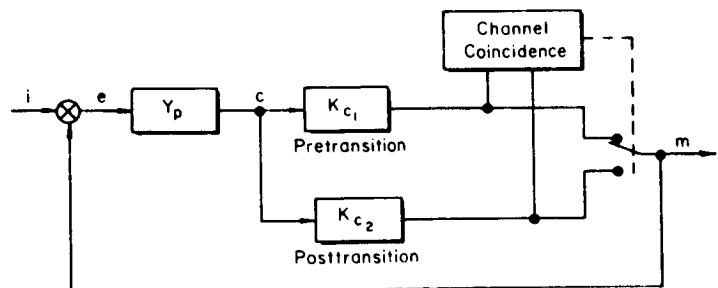


Figure 1. —Experimental configuration (ref. 5).

<sup>1</sup>Mode switching implies successive forms of response behavior.

of control. The reversal-decrease case is not included because of the relatively slow divergence. Stable transitions involving a gain decrease or small increase are less catastrophic and are also omitted.

**TYPICAL DATA.** — The most applicable pure gain transition data are derived from reference 5. The manipulator was a light control stick which protruded through a circular hole in the right arm rest of a student's chair on which the subject was seated. It had a light spring restraint, it could be moved left or right through approximately  $45^\circ$ , and it required about 1 pound for maximum deflection. A channel coincidence device was used to trigger a transition when the system forcing function  $i(t)$  was near zero in order to avoid display discontinuities which might alert the operator (see fig. 1).

The data of reference 5 consist of ensemble average error traces  $e(t)$  for two trained subjects performing the three types of pure-gain transition (reversal, increase, reversal-increase). A "representative" set of trajectories was derived from these average data to illustrate the key features of transition response, resulting in the "typical" error waveforms of figure 2. Any pure-gain transition model should incorporate the distinctive features of the figure 2 waveforms:

(1) The error increases steadily for a few tenths of a second following transition in each of the three cases.

(2) The peak error occurs sooner in the gain increase case than in the other two.

(3) The two cases involving a gain increase show an overshoot following the initial peak. The reversal curve has essentially no overshoot.

(4) The peak error amplitude in the reversal-increase case is larger than that in the other two.

(5) The sign of the initial error for the two reversal cases is opposite that of the gain increase alone.

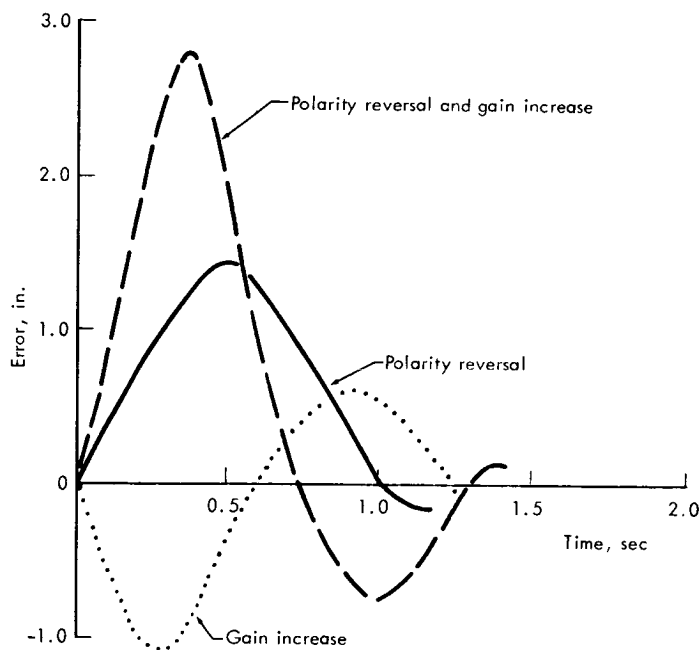


Figure 2. —Typical error waveforms.

Operator output, stick deflection, is useful in gaining a better feel for the operator's response characteristics. Average stick-deflection data are not available directly; however, typical waveforms can be deduced from the error waveforms of figure 2 in combination with the forcing function  $i(t)$ . The forcing function is well approximated by a ramp for at least 1 second after an axis crossing because of its low-frequency nature (as shown in ref. 1). Then, knowing the typical error waveforms, figure 2, and the ramplike forcing-function approximation, it is possible to estimate the operator stick deflection  $c(t)$  following transition. The

essential posttransition signals are defined in figure 1. System output  $m(t)$  can be determined, in turn, using the equation

$$c = \frac{m}{K_{c_2}} = \frac{i - e}{K_{c_2}}$$

Typical stick deflection waveforms for the three types of pure-gain transition are given in figure 3, corresponding to the figure 2 error waveforms. These show features similar to individual records of posttransition output motions given as examples in reference 5.

**TEMPORAL PHASES.** — Several qualitative features of the response data in figure 3 are worth noting. Stick deflections for the first 0.3 to 0.4 second following transition are approximately coincident for all transitions. This is followed by a fairly rapid stick movement to a point which corresponds roughly to the proper deflection for the new controlled element and the instantaneous forcing function value. Some overshoot occurs, and the operator reduces the error to a small value as the system output  $m$  once more becomes nearly equal to the forcing function. Refinement and explanation of these deflection characteristics lead directly to the pure-gain transition model.

**Retention.** — The operator is assumed to be tracking a ramplike forcing function with zero error prior to transition. This corresponds to a stick deflection given by line  $p'-0$  in figure 3. If this constant stick deflection rate were continued after transition, it would go

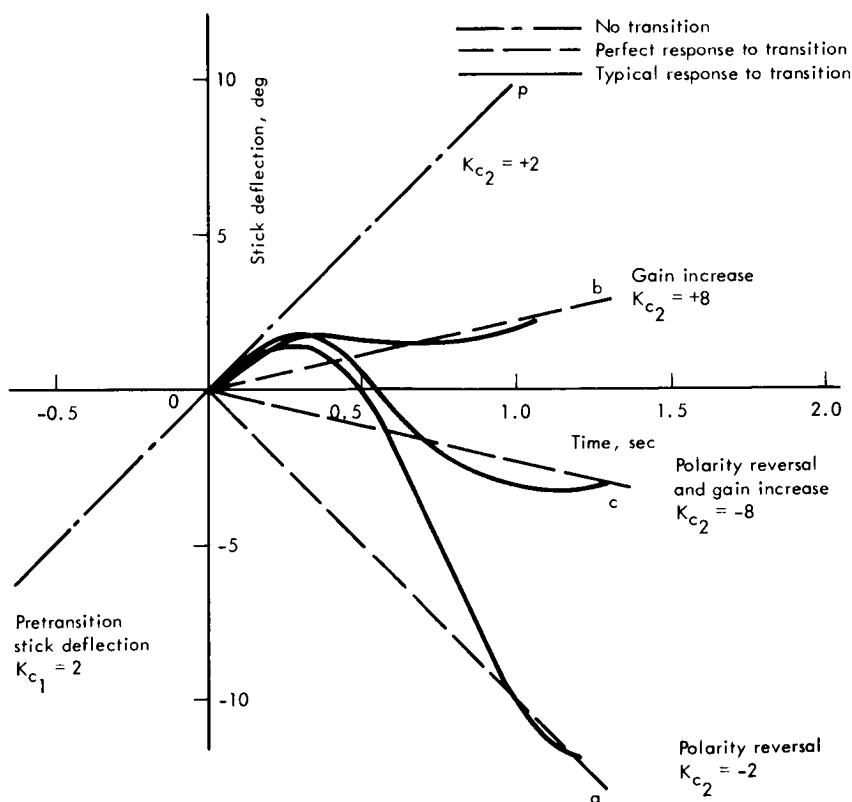


Figure 3. — Typical stick deflection.

along line 0-p in figure 3. This line does not differ significantly from the typical curves shown by solid lines for approximately the first 0.2 second. Therefore, it is reasonable to model the first  $t_q$  seconds of the transition response by a continuation of the ramp along 0-p to point q, and to call it the "retention phase." Line 0-q is shown in figure 4.

Stick deflection rate retention can be interpreted in model terms. The pretransition operator adaptation  $Y_{p_1}$  has the following approximate crossover model form (ref. 9) for a pure gain  $K_{c_1}$ :

$$Y_{p_1} \doteq \frac{K_{p_1} e^{-j\omega\tau}}{j\omega}$$

Because of the time delay, for the first  $t_q$  seconds following transition the operator's stick deflection is a linear operation on the pretransition error. For perfect tracking with  $Y_{p_1}$ , the pretransition error is constant, and the resultant stick output from  $Y_{p_1}$  is a ramp  $p_1$  for the first  $\tau$  seconds following transition. Values of  $\tau$  given in reference 8 are compatible with  $\tau \doteq t_q \doteq 0.2$  second used in the idealized result of figure 4. The open-loop retention phase dynamics become simply  $Y_{p_1} K_{c_2}$ .

Gain Change.—Following the retention phase, the operator holds the stick approximately stationary (see fig. 3) for an intermediate period before the large stick motion. This

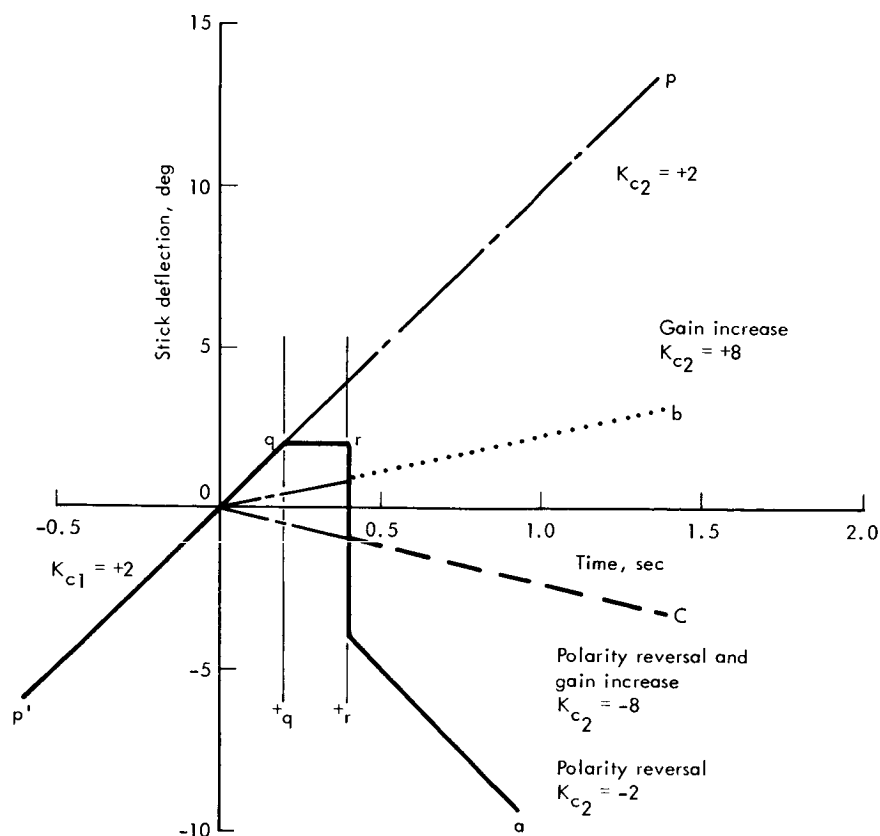


Figure 4. — Ideal stick deflection for retention and gain change phase.

period lasts for about 0.2 second and can be associated with the time delay  $\tau$  in the operator's closed-loop describing function. This time delay is shown in figure 4 by the line q-r. Following the time delay, the plots of figure 3 show a large stick deflection to the neighborhood of the appropriate posttransition value (corresponding to the forcing function). The simplest description of the large stick motion would be given by the instantaneous (steplike) change commencing at point r in figure 4. This steplike change differs from the typical results of figure 3, largely because of dynamic lag effects. The large stick motion together with the preceding time delay is called the "gain change" phase.

The lags evident in the large stick motions (fig. 3) can conceivably arise either during an operator response accomplished as an open-loop step response adjustment, or by reduction of the error in a closed-loop manner using the visual modality. This question can be resolved by examining the magnitude of the effective time constant evident in the traces of figure 3 for the large deflection. If the time constant is small, the motion is probably an open-loop correction to the "step" initial condition on the error existing at the start of the gain-change phase. Larger values of the lag time constant would imply that the stick deflection is accomplished in a closed-loop manner with visual monitoring of the displayed error.

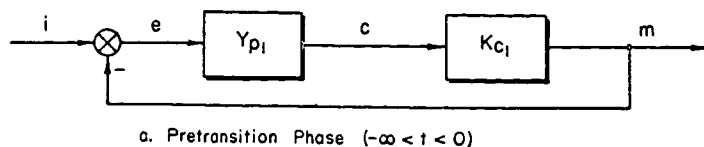
The classical operator step response is a combination of open-loop and closed-loop operation with respect to vision (e.g., ref. 10). In the classic case, the dominant rise-time (see ref. 11 for definition) characteristics following the initial time delay are visually open-loop, with the operator executing a command from the neurological system via the closed-loop neuromuscular system. This is supported by the common observation that the operator will accurately complete a practiced step response even though the visual reference input is shut off during his delay time. Typical rise times are between 0.06 and 0.1 second (ref. 10).

The stick deflection during the gain-change phase of figure 3 can be considered to be a response to a "step" initial condition on  $c(t)$  at time  $t_q$  in the presence of the forcing function  $i(t)$ . Under this assumption, the typical stick deflection data of figure 3 show rise times of about 0.3 second. Since this time is significantly longer than 0.1 second, it indicates that the stick deflection is accomplished in a closed-loop manner with respect to the visual modality. The operator time delay is the delay time  $t_r - t_q$  before the large stick deflection.

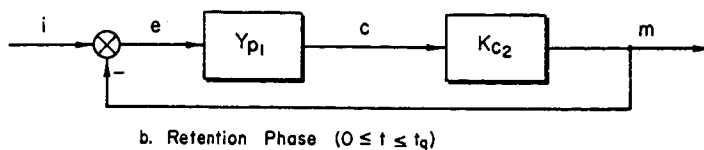
The slower rise time of figure 3 just noted is also compatible with the response that might be expected in visually closed-loop compensatory tracking if the step were a part of a random-appearing input sequence. In this case the loop dynamics are well approximated by the crossover model (ref. 9) with appropriate gain and time delay. Closing the loop yields a rise time of about 0.2 second following the time delay. Since the rise times observed in figure 3 are even longer, the contention that the large stick movement is visually closed-loop is sustained. Thus, the operator response is closed-loop with respect to vision throughout the transition, although his transfer characteristics are not necessarily constant-coefficient.

**PURE GAIN TRANSITION MODEL.** — The results of the analysis of typical stick deflections lead to the following characterization of the predictive model (corresponding block diagrams are given in fig. 5):

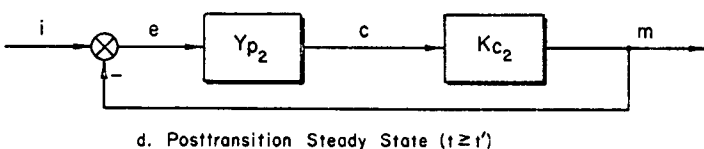
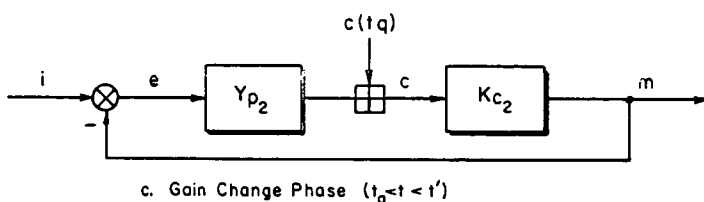
(1) Pretransition: Determine the pretransition steady-state operator adaptation  $Y_{p1}$  using conventional techniques (e.g., the crossover model of ref. 9). See figure 5(a).



(2) Retention: Retain  $Y_{p1}$  in the closed-loop with  $K_{c2}$  for  $t_q$  seconds following transition as shown in figure 5(b). For pure-gain transitions this amounts to retention of the pretransition stick deflection rate for about one reaction delay (to a first approximation).



(3) Gain change: Determine the posttransition steady-state characteristic  $Y_{p2}K_{c2}$  using conventional techniques (e.g., ref. 9). Apply both the forcing function and an initial condition  $c(t_q)$  equal to the stick deflection at the end of the retention phase at time  $t_q$ . See figure 5(c).



(4) Posttransition steady-state: When the error has been reduced to near the threshold value following the gain change transient, the posttransition steady-state describing function form applies. This occurs at time  $t'$ , which is about 1 second for the pure gain transition data of reference 1. See figure 5(d).

Figure 5.—Pure gain transition mode-switching model.

The derived pure-gain transition mode-switching model is the simplest one which accurately describes the pure-gain transition data and can be used to predict operator response. The model has the following distinctive features:

- (1) Simplicity: The model describes the ensemble average error data for the three types of pure-gain transition in the simplest way and in a minimum number of steps.
- (2) Compatibility with steady-state: The model ties in directly with the pretransition and posttransition describing function models for steady-state compensatory tracking.
- (3) Closed-loop visual characteristics: The gain-change phase dynamics are compatible with what is known about visually closed-loop stationary random input responses.
- (4) Rapidity of operator response: Transition response and adjustment to the quasi-linear describing function form  $Y_{p2}$  corresponding to the new controlled element, followed by reduction of the mean-squared tracking error to steady-state levels, are accomplished in about 1 second.

## COMPLEX TRANSITIONS

The complex transition is a more general form of step-controlled element transition. In the systems considered here the pretransition and posttransition controlled elements can take any of the forms  $K$ ,  $K/s$ , or  $K/s^2$ . The transition can involve a change in any or all of order, polarity, and magnitude.

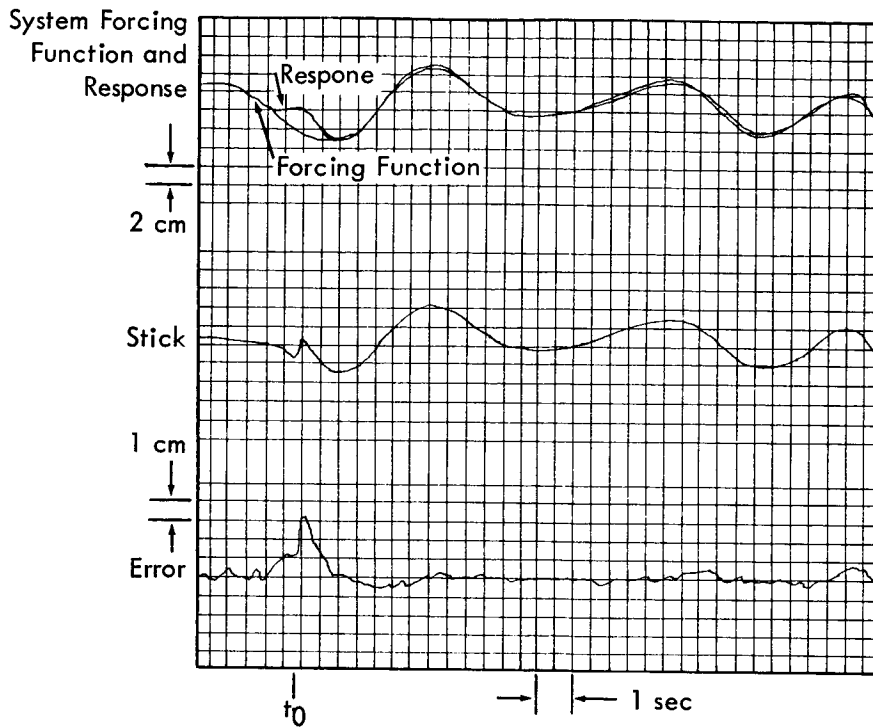
Although simplified controlled elements are used, these can be good approximations, in the region of crossover, to any of a much larger class of controlled element dynamics. Thus, extension of mode-switching model results for one of the simplified controlled element forms to this larger class of controlled elements is direct and straightforward.

**EXPERIMENTAL CONDITIONS.** —The most general complex transition data derive from Bolt Beranek and Newman, Inc. (refs. 6 to 8) and correspond to an experimental configuration similar to that of figure 1. The principal difference in the complex transition configuration is that the operator output  $c$  is not connected to the posttransition controlled element  $Y_{c_2}$  prior to transition. The controlled element transition occurred when the output channels were coincident to eliminate discontinuities in the error signal which might have alerted the operator. The operator was generally not alerted by any stimulus. A number of different transitions were presented in a random sequence, so the operator was uncertain of the nature of the next controlled element. The same manipulator was used.

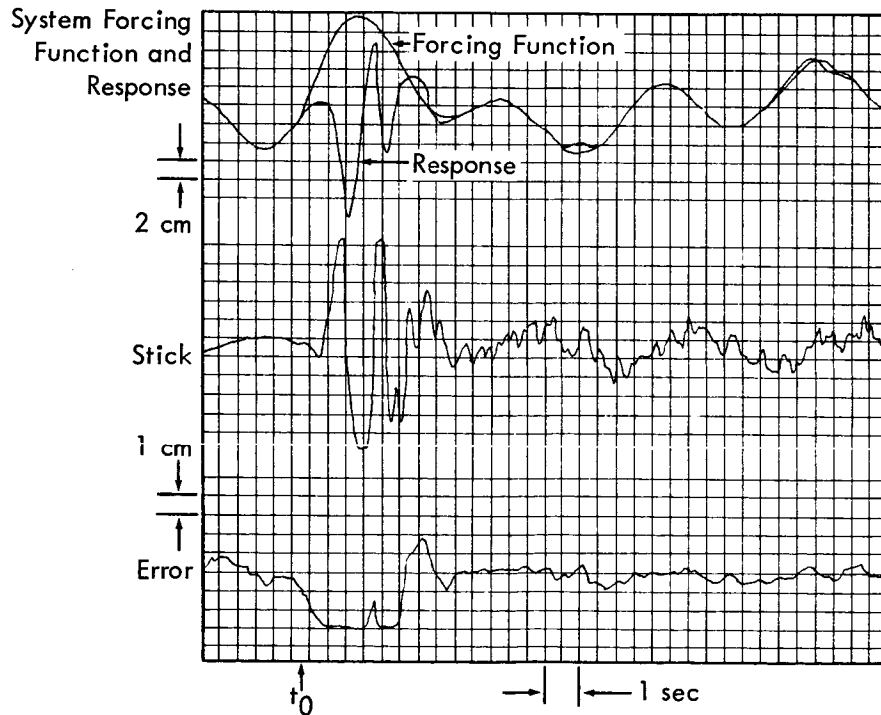
The system forcing function was a low-frequency random-appearing signal with a cut-off frequency of 1.5 rad/sec. The transitions were accomplished by the operator in about 3 seconds (ref. 6), corresponding to less than 1 cycle of the highest frequency forcing-function component. Thus, the forcing function looks quite similar to a portion of one period of a sinusoid over the transition duration.

**DATA.** —The most useful data forms for analysis are time histories of stick motion, system output, and system error. Data for the five transitions of table 1 are presented in figure 6 taken from reference 6. The records are individual runs, not ensemble averages. The run-to-run variability can be roughly estimated by comparing figures 6(c) and 6(e). Figures 6(b) and 6(d) present data for a relatively unskilled operator, and the poorer control technique is evident in the error traces. These data are more exploratory than definitive and provide a preliminary estimate of operator response technique.

Some general features of the data traces may be discussed. The top plot in each of the five figures actually presents two traces, system forcing function and system response or output. In all cases the smoother (lower frequency content) trace is the forcing function. The stick deflection traces for the higher order controlled elements (except for fig. 6(a)) exhibit large-amplitude motions with "limiting." The fact that the large peaks are perfectly "squared off" indicates that the limiting did not happen within the operator, but occurred downstream, probably in the manipulator. Manipulator limiting is reasonable because a sidearm controller involving wrist motions for lateral axis control was used (ref. 8). It has a travel of  $\pm 45^\circ$  but required only 1 pound for full deflection; thus it would be very easy for the operator to attain a limiting deflection.



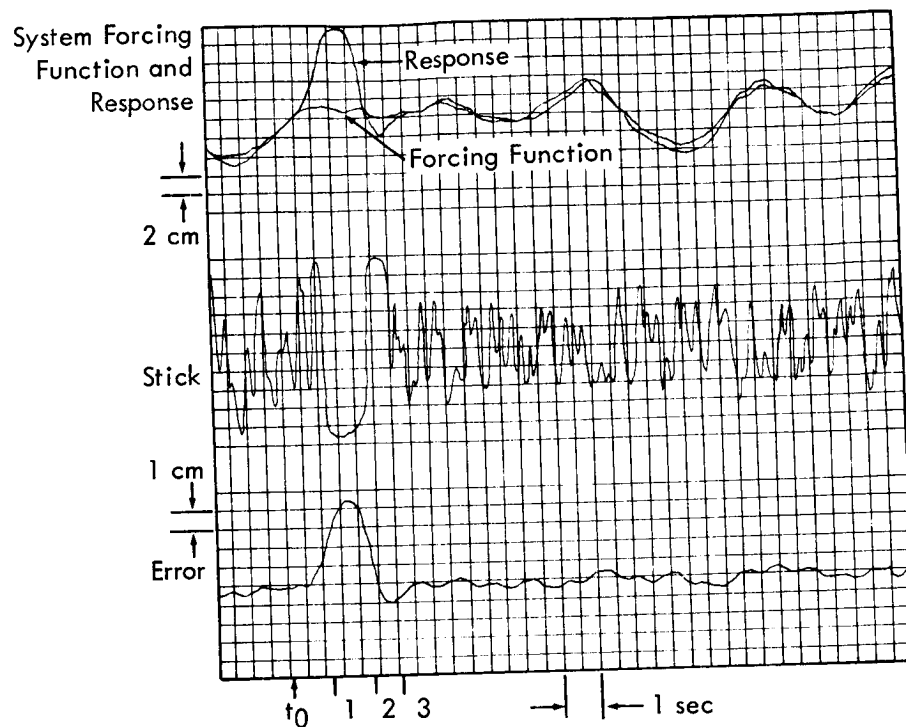
(a)  $Y_{c2}(s) = 2$ . At  $t_0$ ,  $Y_c(s)$  changed from +8 to +2.



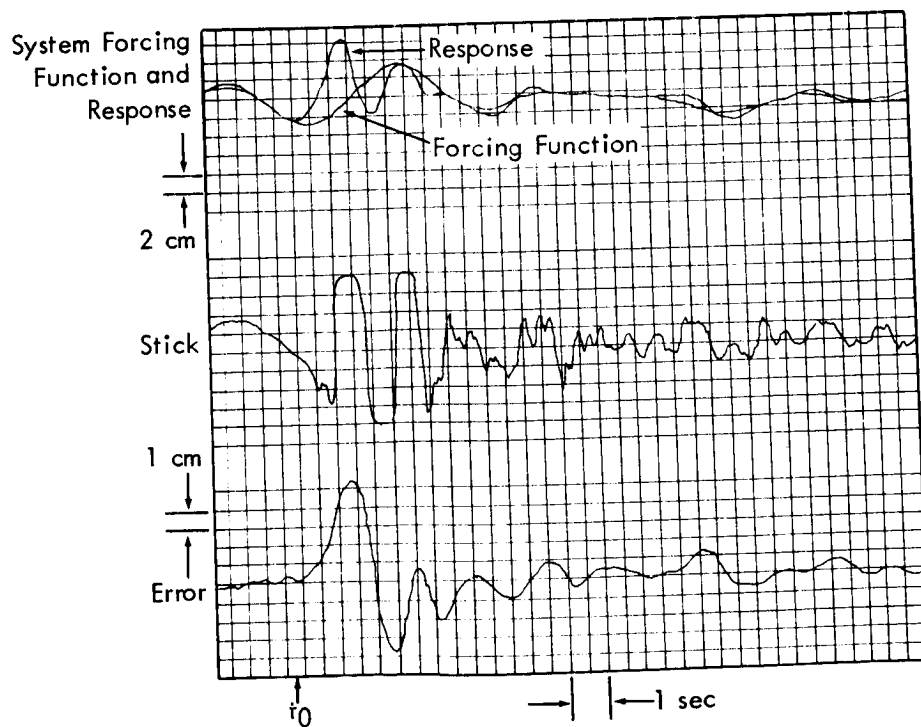
(b)  $Y_{c2}(s) = 4/s$ . At  $t_0$ ,  $Y_c(s)$  changed from +8 to +4/s.

Figure 6.—Tracking records (ref. 6).



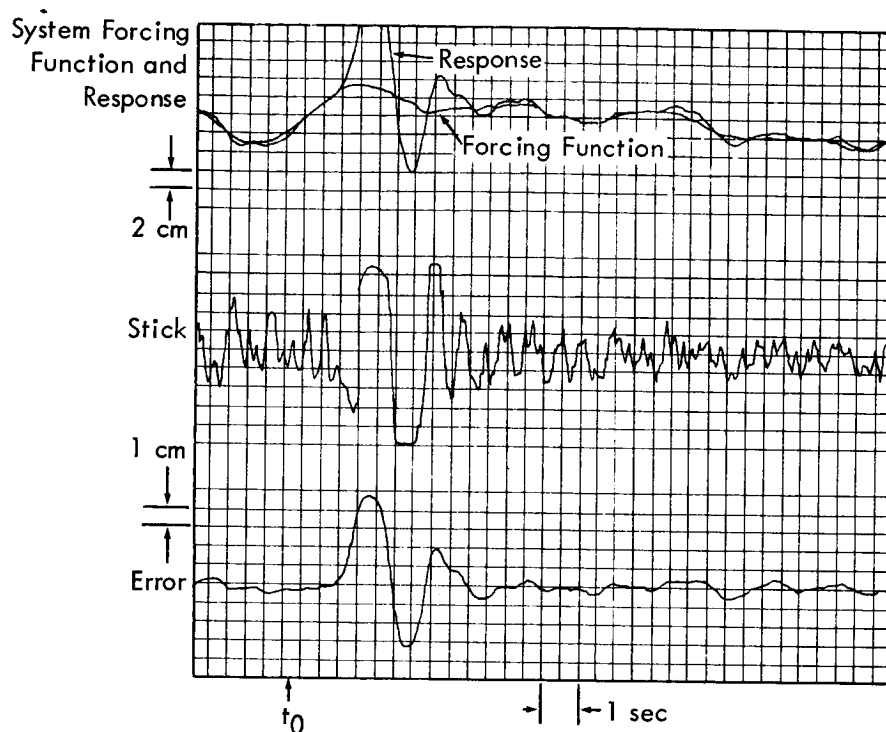


(c)  $Y_{c2}(s) = 8/s^2$ . At  $t_0$ ,  $Y_c(s)$  changed from  $-4/s^2$  to  $+8/s^2$ .



(d)  $Y_{c2}(s) = -8/s^2$ ; at  $t_0$ ,  $Y_c(s)$  changed from  $+2$  to  $-8/s^2$

Figure 6. —Continued.



(e)  $Y_{c2} = -16/s^2$ ; at  $t_0$ ,  $Y_c(s)$  changed from  $+8/s^2$  to  $-16/s^2$

Figure 6. —Concluded.

**TRANSITION DURATION.** —Transition durations are evident in the data of figure 6 with pilot adaptation<sup>2</sup> occurring within about 3 seconds in all cases. These fairly rapid transition times are representative of the average behavior observed in extensive experimental studies by Elkind et al. (refs. 5, 6, and 8) of detection and adaptation times involving a variety of controlled elements and conditions. They are also compatible with Sadoff's results for his fixed-cab series (ref. 4).

TABLE 1. —AVAILABLE COMPLEX TRANSITION DATA  
(From ref. 6)

Transition	Operator skill level
$+8 \rightarrow +2$	Well trained
$+8 \rightarrow +4/s$	Probably not well trained
$-4/s^2 \rightarrow +8/s^2$	Well trained
$+2 \rightarrow -8/s^2$	Relatively untrained
$+8/s^2 \rightarrow -16/s^2$	Probably well trained

<sup>2</sup>Adaptation time is roughly the time at which the transition response is completed, the operator has assumed the approximate form of the posttransition steady-state describing function, and has started reducing residual error to the asymptotic value.

It is evident that the operator must adapt quickly to the new dynamics in the unstable transition cases or face loss of control. The consequences of slower adaptation in the stable transition case are not at all severe, however. That stable transition adaptations are rapid as well is an experimental fact demonstrated in reference 1 for both pure-gain and complex transitions, where it is shown that adaptation is accomplished in 2 or 3 seconds, even when the operator is not consciously aware that a transition has occurred.

While there appears to be a large amount of data showing rapid adaptation times, these results are by no means universal. Rapid adaptation times were generally not observed by Sadoff (ref. 4) in his moving-cab cases with the center-stick controller. In the data shown for the side-stick controller under moving-cab conditions, however, the mean square error increases only a small amount following transition and remains constant for about 20 to 30 seconds. This suggests that the adaptation may have been rapid, and the significant features of the data correspond to the posttransition adjustment phase. As already mentioned, the fixed-cab conditions are generally compatible with the data cited in figure 6. Specifically, in three out of the five cases for fixed-cab center stick control shown in reference 4, adaptation was accomplished in 3 to 6 seconds. Thus, reasonably good correlation between data acquired under similar experimental conditions appears to be obtained.

The transition times observed by Sheridan (ref. 2) were not rapid either; however, the controlled element variations occurred slowly with respect to typical adaptation times for step transitions. It may be concluded that he observed the posttransition adjustment phase characteristics rather than the type of transition phenomenon studied herein.

TEMPORAL PHASES OF THE COMPLEX TRANSITION MODEL.—The pure-gain-transition mode-switching model suggests that there may be several temporal phases in the operator's response to a complex transition. The data of figure 6 also provide support for this hypothesis. With these factors in mind, the several phases of a complex-transition mode-switching model are defined and examined in the following discussion.

Pretransition Retention.—Initially, the operator acts as if the controlled element dynamics have not changed, and his adapted form  $Y_{p1}$  remains that pertinent to  $Y_{c1}$ . An incorrect stick deflection  $c(t)$  results, and the error increases according to  $Y_{p1} Y_{c2}$  and the forcing function. The duration of this retention phase is governed by the time to exceed some error amplitude. At the end of the retention phase the operator has detected that the controlled element has changed, but he does not know its form or gain.

Retention behavior following  $t_0$  and prior to the first corrective response is clearly evident in the stick deflection traces of figure 6. In figure 6(a) stick deflection rate is approximately constant after  $t_0$  and before the first small upward movement on the trace. This is in agreement with the response predicted by the retention phase of the pure-gain-transition model. Similarly, in the  $K_{c2}/s$  case (fig. 6(b)) the retention is apparent during 0.5 second following  $t_0$  and before the sharp upward movement on the stick-deflection trace.

The higher order transitions, figures 6(c) to 6(e), all involve a sign reversal in the controlled element which leads to a well defined stick reversal at the end of the retention phase. Thus, the retention duration is readily recognizable in the data.

Optimal Control.—The operator's tasks following transition detection are to arrest the rate of divergence and reduce the error to some tolerable level. The best way in which this

can be accomplished is to switch to an optimal mode of control following transition detection. For minimum transition time, a time-optimal or bang-bang model is hypothesized for this phase.

There is experimental evidence to support the time-optimal response model hypothesis as an appropriate idealization or limiting case. The available data for  $Y_{C2} = K_{C2}/s^2$  presented in figures 6(c) and 6(e) suggest that a well-trained operator responds in a way that is approximately time optimal. The data of figure 6(c) show a reversal at  $t_1$  followed by a relatively long-duration deflection or bang between  $t_1$  and  $t_2$ . This corresponds to the trajectory between points  $t_1$  and  $t_2$  for fixed-bang amplitude on the illustrative phase plane of figure 7 (the forcing function effect is assumed to be negligible here). At time  $t_2$  another reversal occurs, and the system follows the zero trajectory into the phase plane origin, arriving at time  $t_3$ , corresponding to the bang between times  $t_2$  and  $t_3$  in figure 6(c). At time  $t_3$  the error and error rate are within the threshold region, the operator's deflection goes to zero, and he effectively "shuts off" this phase of the transition response. Thus, the data of figure 6(c) exhibit nearly time-optimal response as evidenced by the following:

- (1) The fixed bang amplitudes
- (2) The minimum number of reversals
- (3) Only one error peak with essentially no overshoot

The data in figure 6(d) and 6(e) show one extra reversal and an additional bang of short duration. This may result from an error in operator switching time  $t_2$  caused by the forcing function. It could correspond to chatter in a suboptimal control mode near the error threshold region.

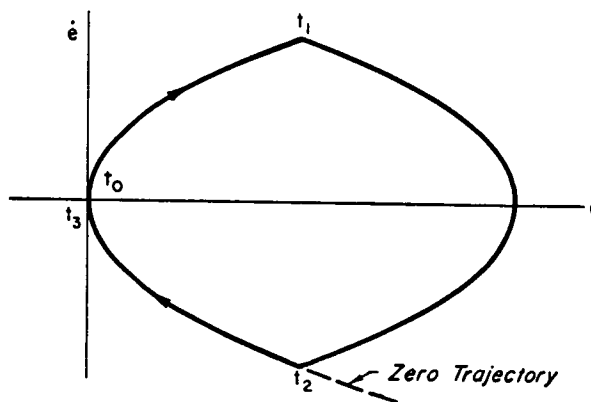


Figure 7. —Phase plane trajectory for time-optimal control of  $K_{C2}/s^2$  (ref. 12).

In figures 6(a) and 6(b) the polarity of the controlled element does not change, and the time-optimal response following retention would be to make a steplike increase in the magnitude of the stick deflection  $c(t)$  to the bang amplitude. The stick would not be reversed. This, however, is not evident in these data; instead, the operator reverses the stick incorrectly in each case, followed shortly by a second corrective reversal. The cause of these "reversal errors" appears to be that these nonpolarity reversal  $Y_C$  transitions were mixed in an experimental sequence with the others (figs. 6(c) to 6(e)). Perhaps the operator adopts this reversal strategy only for this particular purpose because the penalty in terms of loss of control for failing to reverse in the reversal cases is sufficiently greater than that incurred by a reversal error. This is particularly evident in the sample of figure 6 where all  $Y_C$  polarity reversal cases were of high order and difficult to control, while the nonreversal cases were of lower order and the error response to  $c(t)$  was prompt, easily recognized, and readily controlled.

In the ideal case the operator should not make the reversal error, and it will not be included as an essential feature of the model. The possibility ought to be considered in an application nevertheless, particularly when the odds, penalties, or training favor the likelihood of a sign reversal at the time of  $Y_c$  transition.

In a series of experiments conducted by Smith (ref. 13) the operator was told to track a "friction plus mass" controlled element "as fast as possible, or with the minimum of delay time." In 25 percent of these cases the operator response was that of a nonlinear time-optimal controller. Further evidence of a nonlinear time-optimal control capability is provided by the results of Platzer (ref. 14) and Pew (ref. 15).

Identification of  $Y_{c_2}$  is important in determining the appropriate time-optimal control law to use during this phase. One method by which the operator may identify the controlled element is to use the basic property of the change in error due to his step change (or reversal) in  $c(t)$  following retention. These properties are summarized in table 2 for various orders of  $Y_{c_2}$ . Notice that the identification is only a function of the posttransition controlled element under this hypothesis.

The operator's response is assumed to be time optimal in this phase, so that the models derived are suitable for approximating the ideal circumstances observed. Much of the transition data are suboptimal, however, and the consequences of suboptimal linear response during this control phase are explored in reference 1.

Adjustment to Steady-State Tracking.—At the end of the time-optimal control phase, the error and its derivatives are reduced to within some threshold level. The operator then makes a mode switch to the describing function form appropriate to the new controlled element the transition is completed, and compensatory tracking under steady-state conditions is resumed.

The verbal descriptions of the three temporal phases discussed in the previous paragraphs permit a preliminary definition of hypothesized operator response for the various types of complex transitions. These predictions of gross response characteristics are summarized in table 3, and form the general framework for the model. Additional experimental validation together with a detailed examination of the analytical consequences of nonlinear time-optimal control are presented in reference 1. The effect of the forcing function on transition response behavior is also analytically examined at some length.

TABLE 2.—EFFECT OF STICK REVERSAL ON ERROR SIGNAL

Controlled element, $Y_{c_2}$	Change in error signal due to step stick reversal
$K_{c_2}$	Step change in error, $e(t)$
$K_{c_2}/s$	Step change in error rate, $\dot{e}(t)$
$K_{c_2}/s^2$	Step change in error acceleration, $\ddot{e}(t)$

TABLE 3. — PREDICTION OF COMPLEX TRANSITION RESPONSE

Posttransition controlled element, $Y_{c_2}$	Temporal phases			Remarks
	Retention	Optimal control	Adjustment to steady-state tracking	
$K_{c_2}$	$Y_p(Y_{c_1})$	No bangs; switch directly to post- transition steady state	Small corrections to $Y_p(Y_{c_2})$	Behavior differs from that pre- dicted by pure-gain mode- switching model. Reversal error followed by a correc- tive error may occur in a sequence of complex transi- tions.
$\frac{K_{c_2}}{s}$		One bang		Reversal error followed by a corrective error may occur in a sequence of complex transi- tions. Forcing function may have large effect on response.
$\frac{K_{c_2}}{s^2}$		Two bangs		Low-frequency forcing func- tion has only a small effect.

## SUMMARY OF THE MODELS

Mode-switching models of the human operator during pure-gain and complex controlled-element transitions have been derived on the basis of extant data. The primary contribution of the pure-gain model is its structural form in terms of temporal phases or modes. The complex transition model replaces and supersedes it and comprises the principal result.

The gross characteristics of operator response in the pure-gain case are described by the complex transition model as well, and the differences between models are at the detail level. Specifically, the stick deflection following retention is steplike or ideal in the complex model, while it contains appropriate dynamic lags in the pure gain version. Thus, the model selection can be based on the type of transitions anticipated and the desired fidelity.

The complex transition model uses three successive control modes to explain operator response actions following a step change in controlled element among the forms  $K$ ,  $K/s$ , and  $K/s^2$ . The control modes or response phases are summarized in table 4. Operator behavior in the entire period between pretransition and posttransition steady-state tracking is defined in terms of either duration, solution to an optimal control problem, or  $Y_{p_1}$  and  $Y_{p_2}$ .

The model is ultimately intended for use in the design of aerospace vehicles and their control systems to predict the response to a sudden change in dynamic characteristics. Analysis would proceed in the stepwise manner outlined in table 4. The retention phase has a duration based on data for various controlled elements. The next phase might involve a phase plane analysis with a selected form of controller. When error and error rate are reduced to within some threshold level, the adjustment to the posttransition steady-state describing function is made.

The duration of the retention phase is not given by the model. This depends on the operator transition-detection criterion. A detailed investigation of detection criteria is reported by Miller in reference 16.

The amplitude of the bangs is not given by the model. Some maximum deflection will be used with a free-moving manipulator, while a maximum force level will be used with an isometric device.

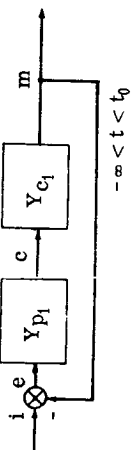
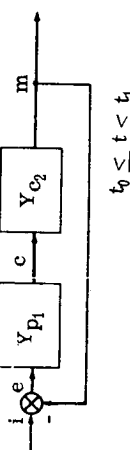
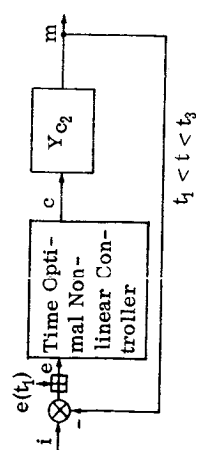
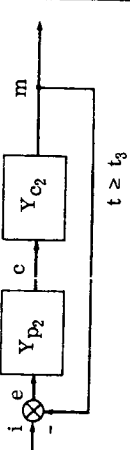
The effect of forcing function may be important. The model is derived from response data for a low-frequency random input. Higher frequency inputs could modify the results; however, they are unlikely to be encountered in a closed-loop vehicle analysis.

The forcing function may lead to analytical difficulties in the optimal control phase in predictive applications of the complex model. Inclusion of the input effect in a phase-plane analysis is laborious, and analog or digital computation may simplify this aspect of response prediction.

As proposed, the model will explain or predict operator response during any unstable complex transitions among controlled elements of the forms  $K$ ,  $K/s$ , and  $K/s^2$ . The model has been verified for transitions using only one other controlled-element form (see ref. 1), and additional data are required to sustain its more general applicability.

Existing data for some pure-gain transitions alone do not agree with the results observed for the same transition occurring in a complex transition sequence. In the complex sequence,

TABLE 4. -- COMPLEX TRANSITION MODE-SWITCHING MODEL SUMMARY

Response phase	Mode-switching	Duration and timing		Description
0 Pretransition steady state	 $-\infty < t < t_0$			Quasi-linear compensatory tracking
1 Pretransition retention	 $t_0 \leq t \leq t_1$	Posttransition controlled element	Approximate duration, sec 0.2 0.5 1.0	Transition occurs at $t = t_0$ . The operator continues tracking with the pretransition adaptation. An incorrect stick deflection and error buildup occur as functions of $i(t)$ and $Y_{c2}$ . At time $t_1$ the operator has detected the transition and ceased retention behavior.
2 Time-optimal nonlinear control	 $t_1 < t < t_3$	The switching time $t_2$ is determined by time-optimal control logic.		Just after $t_1$ the operator adopts either an optimal or suboptimal mode of control. The simplest hypothesis is the use of a nonlinear optimal controller. Variation of parameters such as control amplitude, $M$ , provides one suboptimal form. Quasi-linear control with lead and time delay provides another.
Posttransition steady state	 $t \geq t_3$	When the error and error rate are within allowable threshold levels, the operator adopts his post-transition quasi-linear describing function form.		Quasi-linear compensatory tracking



reversal errors are observed. These are probably due to the fact that higher order controlled elements with sign changes at transition were included in the experimental sequence leading to the adoption of the reversal strategy by the operator. This probabilistic effect is not included in the model, but should be considered in applications where such a mixture of transitions may occur.

Experimental results obtained by Sadoff (ref. 4) in a moving-cab simulator with a center stick controller do not agree with extant fixed-base data, or with moving-cab data with a side-stick controller. Consequently derived models based on these data are apparently not applicable to the moving-cab, center-stick, controlled-element transition problem. This may limit the applicability of the derived model to the in-flight transition problems which are of prime interest.

## CONCLUSIONS

Operator response and adaptation to step changes in the controlled element occur quickly and in most cases are completed within a few seconds. This is true even for transitions involving only a small reduction in the controlled-element gain, which are not consciously detected by the operator until long after his adaptation is completed. The only known exceptions are the results obtained in the moving cab with center-stick controller.

The pure-gain transition data indicate that the operator is responding in a way that is closed-loop with the visual modality.

The mode-switching models are the most appropriate with which to characterize operator transition response. Models which vary continuously with time, for example learning servos, do not appear to be valid. This is particularly evident in the light of Sadoff's error data which show that the control technique changes do occur suddenly.

There are sufficient data which demonstrate time-optimal control characteristics to say that this form of control is a valid intermediate phase in the transition model. Conversely, this is the only form of model which will explain time-optimal response data.

The model describes the transition data in the simplest way and in a minimum number of steps. It ties in directly with the known pretransition and posttransition steady-state characteristics of the operator.

## REFERENCES

1. Weir, D. H.; and Phatak, A. V.: Model of Human Operator Response to Step Transitions in Controlled Element Dynamics. Tech. Rep. 151-1, Systems Technology, Inc., June 1965.
2. Sheridan, T. B.: Time-Variable Dynamics of Human Operator Systems. AFCRC-TN-60-169 (ASTIA AD-237045), Mar. 1960.
3. Sheridan, T. B.: Studies of Adaptive Characteristics of the Human Controller. ESD-TDR-62-351, Dec. 1962.
4. Sadoff, Melvin: A Study of a Pilot's Ability to Control During Simulated Stability Augmentation System Failures. NASA TN D-1552, 1962.

5. Young, L. R.; Green, D. M.; Elkind, J. I.; and Kelly, J. A.: The Adaptive Dynamic Response Characteristics of the Human Operator in Simple Manual Control. NASA TN D-2255, 1964.
6. Elkind, J. I.; Kelly, J. A.; and Payne, R. A.: Adaptive Control Characteristics of the Human Operator in Systems Having Complex Dynamics. IEEE Proc. Fifth Nat. Symp. on Human Factors in Electronics (San Diego, Calif.), May 1964.
7. Elkind, J. I.: Human Operator Response to Changing Controlled Element Dynamics. Bolt Beranek and Newman, Inc., May 1963.
8. Kelly, J. A.; and Elkind, J. I.: Adaptation of the Human Operator to Changes in Control Dynamics. Rep. MR-10124-1. Bolt Beranek and Newman, Inc., Mar. 1964.
9. McRuer, Duane; Graham, Dunstan; Ezra, Krendel; and Reisener, William, Jr.: Human Pilot Dynamics in Compensatory Systems—Theory Models and Experiments with Controlled Element and Forcing Function Variations. AFFDL-TR-65-15, Jan. 1965.
10. McRuer, D. T.; and Krendel, E. S.: Dynamic Response of Human Operators. WADC-TR-56-524 (ASTIA AD-110693), Oct. 1957.
11. Wolkovitch, J.; Magdaleno, R., et al.: Performance Criteria for Linear Constant-Coefficient Systems With Deterministic Inputs. ASD-TR-61-501 (ASTIA AD-275515), Feb. 1962.
12. Graham, Dunstan; and McRuer, Duane: Analysis of Nonlinear Control Systems. John Wiley & Sons, Inc., 1961.
13. Smith, Otto J. M.: Nonlinear Computations in the Human Controller. IRE Trans., vol. BME-9, no. 2, Apr. 1962, pp. 125-128.
14. Platzer, H. L.: Nonlinear Approach to Human Tracking. Interim Tech. Rep. I-2490-1. Franklin Inst., Dec. 1955.
15. Pew, R. W.: A Model of Human Controller Performance in a Relay Control System. IEEE Proc. Fifth Nat. Symp. on Human Factors in Electronics (San Diego, Calif.), May 1964.
16. Miller, D. C.: A Model for the Adaptive Response of the Human Controller to Sudden Changes in Controlled Process Dynamics. B.S. and M.S. Theses, MIT, 1965.

## 6. ADAPTATIVE MODEL OF THE HUMAN OPERATOR IN A TIME-VARYING CONTROL TASK

*E.E. Gould and K.S. Fu*  
*Purdue University*

This paper presents a model for the human operator engaged in one-dimensional, compensatory, visual-manual tracking. Instead of a lumped input-output model, the human operator is considered as a system consisting of an input device (visual stimulus), an adaptive controller (central nervous system), and an actuator (arm and muscle mechanism). The main concern of this paper is modeling the strategy of the adaptive controller section. Pattern recognition techniques, which usually attempt to mimic human behavior, are used in the model to identify the type of plant being controlled. This basis for a model is then augmented by more conventional techniques to more closely approximate human behavior. The model has been simulated and is presently undergoing extensive tests.

The development of mathematical models which approximate the performance of the human operator engaged in a visual-manual control task has stimulated a great deal of research in the last decade. The models used to describe the input-output characteristics of such an operator have progressed from the linear continuous models (ref. 1) to sophisticated nonlinear and sampled-data models (refs. 2 to 5). Some of these models use schemes which account for the adaptive nature of the human operator. At least three solutions to human adaptation have been proposed. The first method involves estimation of parameters within specified confidence limits by time averages of data (ref. 6). From this information a slowly time varying characterization is possible. A second approach to time-varying dynamics is the formulation of a model with adjustable parameters which are used to minimize some criterion of error between the model output and the output of a human operator (ref. 7). A third approach has been to isolate the performance index used by the human operator and form this function within the model itself (ref. 4). This performance index is then minimized to adjust the model parameters. Since the performance index is supposed to be the same as the human performance index, the resulting model should follow human adaptation. Furthermore, since the performance index is generated internally, this is truly a self-contained adaptive model.

### PROBLEM AND APPROACH

The physical task chosen for this investigation was one-dimensional visual-manual compensatory tracking. The display device was an oscilloscope mounted at eye level and masked by a gray background so that only the CRT face was visible. A classroom desktop chair with an arm which was pivoted at the rear beneath the elbow and rode on a hard rubber wheel beneath the hand was used as the control lever. The output of a potentiometer whose shaft was connected to the rubber wheel was used as an input to an analog computer which simulated the

controlled plant dynamics. A block diagram of the experimental setup is shown in figure 1.

The external plant dynamics were of the form

$$G(S) = K_1 + K_2/S + K_3S \quad (1)$$

where  $K_1$ ,  $K_2$ , and  $K_3$  were parameters whose values were changed by an external environment. The inputs were step functions and white noise was band limited to 0.2 cps. The step functions had an unpredictable frequency and a magnitude which was one of four fixed magnitudes chosen in an unpredictable manner at each input time. By making the frequency and magnitude unpredictable, the step function input is an unpredictable signal and precognitive tracking was avoided. The period between step inputs varied between 1 and 15 seconds.

For the sake of clarity the distinction used in this report between the different parts of the human control loop should be noted. The model of a human operator is divided into three separate parts: an error estimator, an adaptive controller, and a physical actuator. While the properties of the visual error estimation system and the muscular activation system are interesting and important fields, they were not the primary area of interest in this investigation. The strategy employed by a human controller in tracking random-appearing step functions and random noise inputs with a plant of the type given in equation (1) was the area of primary concern for this investigation. A block diagram with these three parts of the human controller separated is shown in figure 2.

The strategy used in the adaptive controller is based on more than the input-output data obtained in tracking. Attention was given to answers given by subjects to a standard set of questions about their tracking performance. Considerable research has been accomplished to establish control models for the human-arm dynamics and eye-tracking system. Simple models for these systems were used so that the adaptive controller inputs and outputs could be dealt with directly. With this as a guide an attempt has been made to generate the same

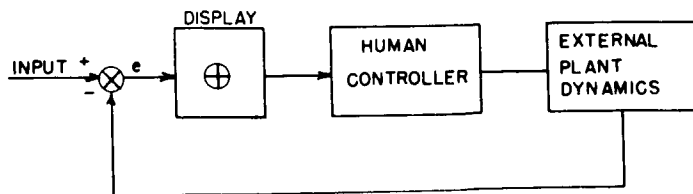


Figure 1. — Experimental setup.

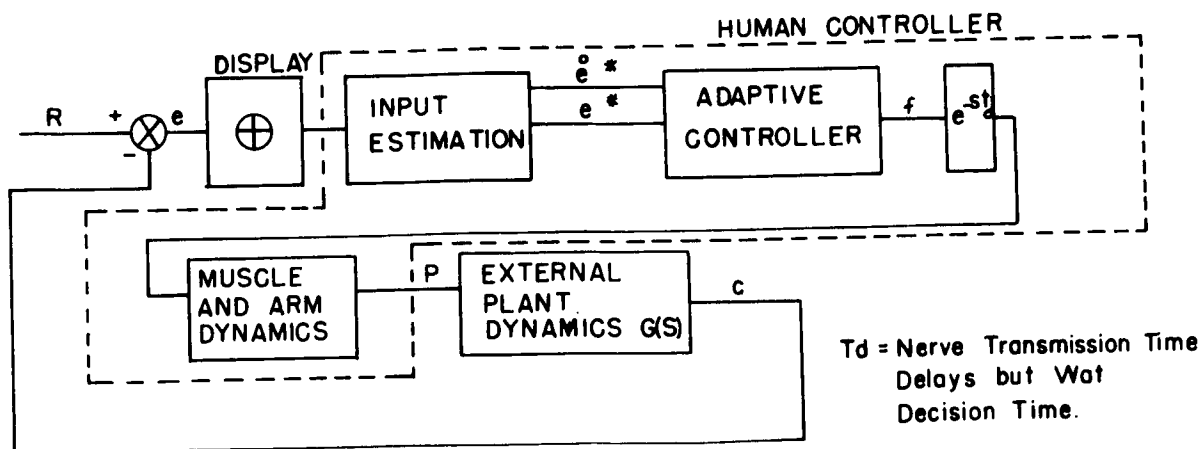


Figure 2. —Human controller functions.

force program as the human does, to adapt the same parameters of this force program, and to duplicate the human output to a given input by running this force program through an approximation to the arm dynamics and the same external plant dynamics. It was expected that in trying to formulate the problem in the same terms as the human does, the model might not be the simplest model for a given set of test conditions, but it was felt that if the basic functional form of the human conception of tracking and what he is doing could be the basis for the model, a one-to-one correspondence between model and human output was more likely. While the authors are confident that this goal has not been attained in its entirety, it has been the philosophy of the approach to the problem and it is hoped that some measure of success has been achieved.

## DEVELOPMENT OF A PATTERN-RECOGNIZING ADAPTIVE MODEL

DYNAMICS AND ERROR MEASUREMENTS. —For the purposes of this research it was decided that a purely inertial plant was a close enough approximation to the dynamics of the human arm muscle system.

$$\frac{X(S)}{F(S)} = \frac{1}{M} \frac{1}{S^2} \quad (2)$$

where

$X(S)$  distance moved by the arm

$F(S)$  force program transmitted to muscle system

$M$  mass of arm

Since the subject gripped the control lever so that there was no relative motion between the control arm and the human arm,  $M$  is really the sum of the human-arm and control-lever masses.

The model for the input system or error-measurement device is explained now. The following four questions arose in this choice:

- (1) Should the input  $e^*$  to the adaptive computer be considered as a continuous or a sampled data quantity?
- (2) Should the physical capability of the human controller to estimate zero error be included in the model?
- (3) How accurately can the human controller estimate oscilloscope deflections without using the scale?
- (4) Is velocity perception a direct sensory experience or an averaged value of displacement divided by time?

It was assumed that higher order derivatives were not formed at the visual level if at all. These four questions were treated in reference 7 for this very application and so only the conclusions are stated here. The detailed justification of each assumption can be found in reference 7.

(1) There is evidence that supports continuous error perception and a continuous control channel. Although the model does use a sample and hold device to generate the control function, this device was not included in the input section so that the continuous control channel could be provided for.

(2) The subjects had no difficulty in centering the dot on the zero reference line to within 0.01 inch. However, during tracking tests, errors of 10 times this magnitude were often ignored. This would indicate that the error threshold device is dominant and is located in the adaptive controller decision area rather than in the error estimation function and need not be considered in the estimation block.

(3) Noise values of 5 to 10 percent were introduced to simulate errors in estimation of displacement.

(4) The ability of the human operator to perceive velocity is well established and the exact nature of how this perception is arrived at was beyond the scope of this study. For convenience velocity will be assumed to be a direct sensory experience.

The resulting model for the input estimator is shown in figure 3.

**DESIRED CHARACTERISTICS.**—In various attempts to develop a suitable model of the human operator from an engineering standpoint many properties of the human operator have become known. These properties have either been observed from experimental data or are necessarily present because of physiological considerations. Although tracking performance is certainly affected by psychological factors, it is doubtful that an engineering approach would have much success at mechanizing and adapting to psychological factors. Psychological factors were most likely of secondary importance since only the characteristics which were common to all subjects were incorporated into the model. A list of the characteristics that are considered essential to the human model is given below. This list actually constitutes the authors definition of the necessary conditions for a suitable model and while they certainly are not all inclusive any model which satisfies all of them was deemed satisfactory.

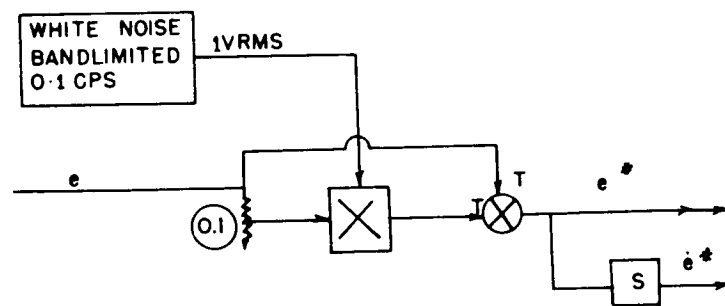


Figure 3.—Input estimation mechanization.

(1) Visual perception: The human visual system performs transduction of position and motion into electro-chemical signals which can be processed by the brain. The eye tracking mechanism has been the subject of much study by Young (ref. 8).

(2) Prediction: The human operator is able to extrapolate error and error rate to predict future values of error. In this manner the subject adds lead compensation to the system in an attempt to minimize error due to the large phase lags of the system.

(3) Rejection threshold: It is apparent from tracking data that the human operator is not willing to reduce small steady-state errors to zero. For each task a threshold is established which probably depends on the difficulty of the task, the amount of time for which no control is required, the estimated complexity of the task, and the instructions given. Therefore, the rejection threshold was empirically determined from tracking data.

(4) Reaction time: The time from the occurrence of a visual stimulus to the initiation of a response at the output of the control actuator is termed reaction time. It varies from subject to subject, but it is in the range of 50 to 500 milliseconds.

(5) Neuromuscular activation: The transmission and transduction of neural-force information to arm motion is a very complex and interesting subject. However, only a simple approximation of the dynamics of the arm system was included in the model.

(6) Optimization: It has been the contention of many investigators (ref. 9) and it is an intuitive feeling that the human controller optimizes some primary goal associated with the tracking instructions.

(7) Subgoals: The human operator also sets forth subgoals and attempts to satisfy these goals while tracking. The subgoals are usually more easily interpreted in terms of the variables of error and error rate than is the primary goal.

(8) Adaptation: Experimental evidence shows that the human operator is able to adjust his tracking performance to changes in the dynamics of the external plant, input, and many other factors. This ability is termed adaptation.

(9) Pattern recognition: If the plant dynamics are suddenly switched from one type to another type previously encountered, the human operator changes his strategy approach and possibly his subgoals. Sometimes this occurs after only one or two trials at nulling the error. The ability to divide tracking problems into classes and rapidly recognize these classes is closer to the area of pattern recognition than adaptation and is so termed. Also, it is more easily simulated by feature extraction and decision than hill climbing.

These nine characteristics are considered to be some of the most important features that characterize the human operator as an adaptive-pattern recognizing controller, and it was the object of this research to include these characteristics in a model.

PLANT MEASUREMENTS. — As has been previously stated the estimated values of error and error rate are available for the brain or adaptive computer. However, there are two other inputs that are used by humans during tracking. Arm position and velocity are sensed by the nervous system from the position and change of position of the various points in the arm. This gives the brain (adaptive controller) two inputs to the external plant and two outputs from it. The inputs

$P$  = Arm position

$\dot{P}$  = Arm velocity

(3)

and

can be compared with the outputs

$e^* =$  Estimated error

and

$\dot{e}^* =$  Estimated error rate

(4)

to give a direct measurement of certain external plant parameters (see fig. 4). The ability of the human to judge ratios is well established; in fact, it is generally thought to be easier and more accurate to tell that a 3-pound object is twice as heavy as a 1 1/2-pound object than to judge the two weights separately and divide. It is therefore proposed that ratios are formed in the brain from the variables in equations (3) and (4) to give at least partial identification of the external plant. Recalling equation (1), the external plants used were of the form

$$G(S) = K_1 + K_2/S + K_3S \quad (5)$$

Referring to figure 2, if  $K_2$  and  $K_3$  are zero

$$G(S) = K_1 = C/P \quad (6)$$

where

P output position of the human arm

C external plant output

but

$$e = R - C \quad (7)$$

and if  $\dot{R}$  is small with respect to  $\dot{C}$  (it is zero for a step function)

$$K_1 \doteq \dot{e}/\dot{p} \quad (9)$$

This is a quantity that is readily measured by the human operator and can be used to estimate the plant gain.

By the same reasoning when  $\dot{P} = 0$

$$K_2 P_1 = \dot{e}_1 - \dot{R}_1 \quad (10)$$

and if the arm is moved to a new position,

$$K_2 P_2 = \dot{e}_2 - \dot{R}_2 \quad (11)$$

Now if  $R$  is small with respect to  $\dot{C}$ ,

$$K_2 \doteq \frac{\dot{e}}{p} \quad (12)$$



Thus by noting the change in  $\dot{e}$  and the distance the arm moved  $p$ , the subject can estimate  $K_2$ . In similar manner

$$\frac{e}{p} = K_3 \quad (13)$$

Figure 5 shows the constants that can be estimated by comparing the variables connected by the arrows.

**PATTERN CLASSIFICATION.** —From the remarks of the subjects and the tracking data records it was evident that the human controller makes one of three classifications for the different plants possible in equation (1). Depending on the relative values of  $K_1$ ,  $K_2$ , and  $K_3$ , the plants are treated as

- (1)  $K_2 = K_3 = 0$  position track
- (2)  $K_3 = K_1 = 0$  integral track
- (3)  $K_1 = K_2 = 0$  derivative track

Even, for example, if  $K_1 = K_2 = 1.0$  and  $K_3 = 0$ , the resulting strategy by the human controller is the same as that for  $K_2 = K_3 = 0$ ,  $K_1 = 1.2$  where the higher value for  $K_1$  compensates somewhat for the erroneous consideration of  $K_2$ . The schemes employed by the human controller for conditions 1, 2, and 3 are apparently different in their subgoals, and the data records exhibit a definite switching characteristic. That is, one set of conditions for  $K_1$ ,  $K_2$ , and  $K_3$  will perhaps show position track with velocity errors while for just slightly different conditions, recordings show that an integral track scheme was used with errors caused by  $K_1 \neq 0$ . Behavior such as this on the part of the human controller suggested a pattern-recognizing model to determine the structure of the controller. In fact, the conception and development of pattern recognition was accomplished by attempts to describe behavior

such as this on the part of humans (ref. 10). Figure 4 is an example of position tracking with  $K_1 = 1.0$ ,  $K_2 = 0.5$ ,  $K_3 = 0.0$ . Position tracking is evident from the step-like output of the arm. The assumption that the  $K_2$  term is not considered in the tracking strategy for this case was strengthened by making  $K_2 = -0.5$ .

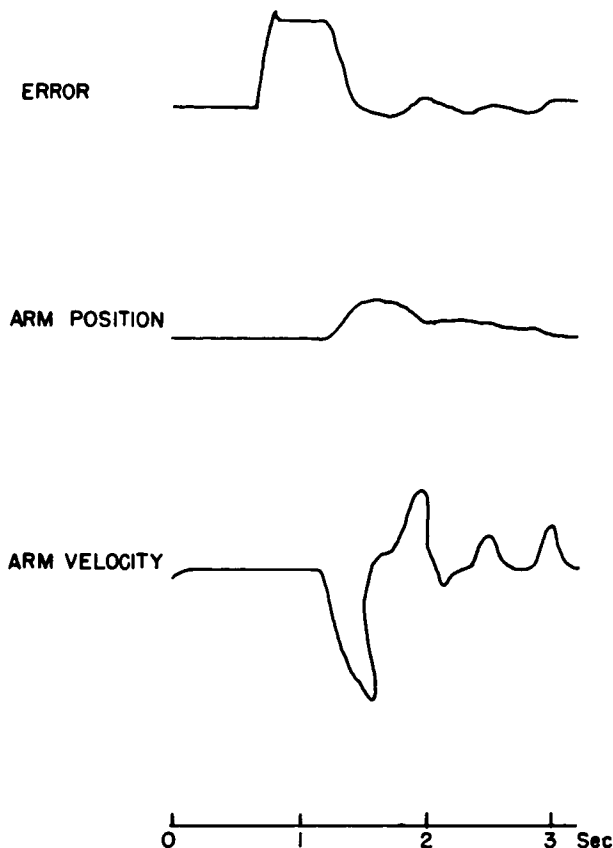


Figure 4. —Typical tracking performance  
 $K_1 = 1.0$ ,  $K_2 = 0.5$ ,  $K_3 = 0.0$

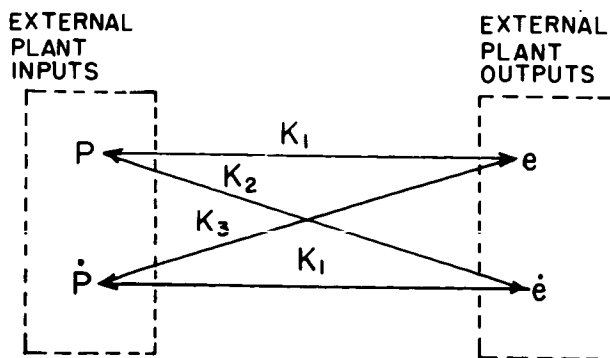


Figure 5.—Plant identification comparisons.

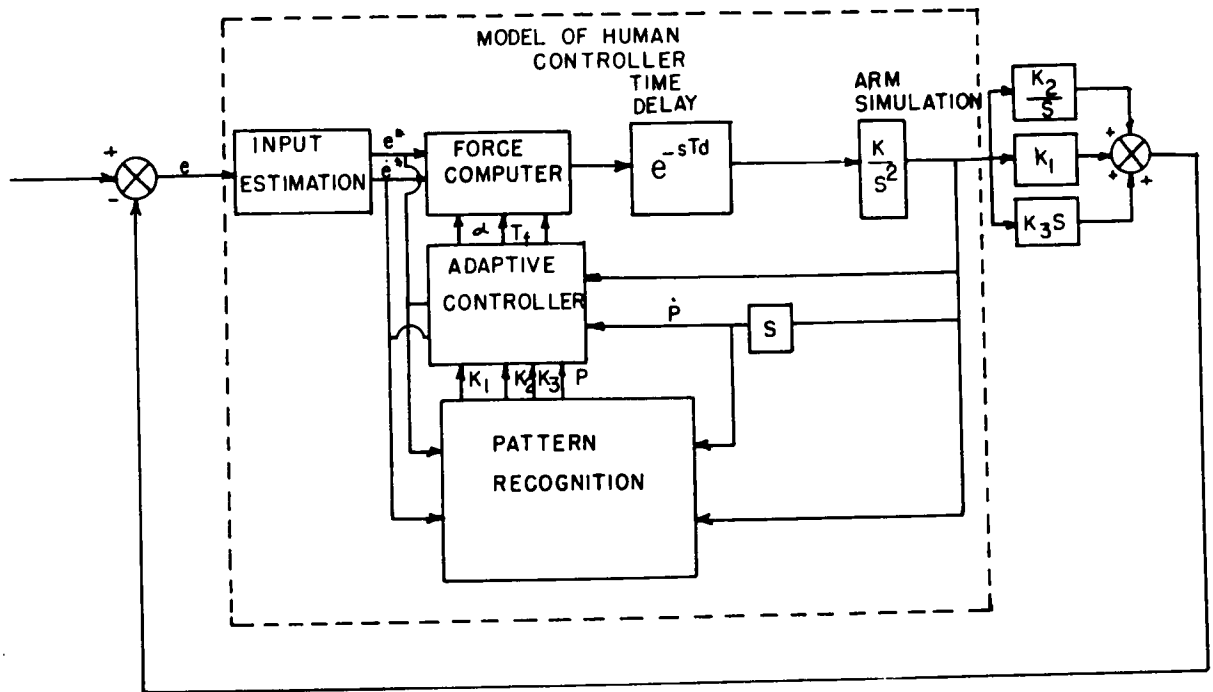


Figure 6.—Block diagram of pattern recognizing model.

This condition was uncontrollable for all subjects tested, because the error rate increases as the position is changed to compensate for the errors built up in the integrator. A block diagram of the pattern-recognizing model is shown in figure 6. The pattern-recognizing device shown in figure 6 performs two functions. The first is feature extraction. The inputs  $e^*$ ,  $\dot{e}^*$ ,  $P$ ,  $\dot{P}$  are used to calculate values for  $K_1$ ,  $K_2$ , and  $K_3$  which are the pattern features. The second function, decision, uses the values of  $K_1$ ,  $K_2$ , and  $K_3$  to determine whether case 1, 2, or 3 of equations (13) exists and thereby chooses the tracking strategy. Figure 7 shows a set of sample decision surfaces (which are lines in two dimensions) for the case where only  $K_1$  and  $K_2$  are considered. Note that the decision lines in figure 7 are linear switching surfaces. Whether or not the human uses a linear-decision boundary is a valid question and one that requires answering. If the boundary is linear, the decision function can be performed by threshold logic devices (ADALINE) whose characteristics have been investigated by Widrow (ref. 11). Very sketchy preliminary information indicates that a linear boundary may be approximately correct except around the origin. Further data are being taken to determine more accurately the location of the human decision boundaries. However, for the present simulation studies a linear weighting rule was used. Since the tracking data showed little difference with the sign of  $K_i$ , absolute values were used to simplify the mechanization of the decision rule. The decision is made in the following manner. First three quantities are formed

$$\sum_{i=1}^3 a_i \times |K_i| = D_1 \quad \sum_{i=1}^3 b_i \times |K_i| = D_2 \quad \sum_{i=1}^3 c_i \times |K_i| = D_3 \quad (15)$$

if

Preliminary tracking studies have resulted in the following set of values for the decision parameters  $a_i$ ,  $b_i$ , and  $c_i$

$$\left. \begin{aligned} |K_1| - 0.45 |K_2| - 0.40 |K_3| &= D_1 \\ -2.2 |K_1| + |K_2| - .45 |K_3| &= D_2 \\ -2.5 |K_1| - 2.2 |K_2| + |K_3| &= D_3 \end{aligned} \right\} (16)$$

Of course, it is realized that the decision boundaries vary slightly from subject to subject and with other factors so that the performance of the model is either an average performance or the parameters can be adjusted for a particular subject.

**CONTROL STRATEGY.**—Before the adaptive portion of the model can be discussed, it is necessary to describe the basic control strategy of the model for a simple position-tracking system that is not adaptive. Many of these features can be found in reference 7. Tracking records show that if an inertial plant is assumed for the arm model, the input to this double integrator is closely approximated by step functions with a basic form as shown in figure 8. The time  $T_f$  is the active control time for a step displacement in position. However, the effect of this control is only observable at the output after a time delay of  $T_d$  seconds due to nerve transmission time. The entire time for one control action to be executed and observed,  $T_d + T_f$ , is termed a control interval (CI). This distinction is important since certain functions are performed only every control interval while others are performed continuously. The magnitude  $F$  of these step functions is dependent upon the error at the beginning of each CI. The initial conditions and the final desired conditions form a two-point boundary-value problem over one CI. The form of the solution for the force  $f(t)$  is determined from tracking data as shown in figure 8. The problem can be stated as follows:

$$\left. \begin{aligned} K_1 e &= X_1 \\ X_2 &= \dot{X}_1 \\ \dot{X}_2 &= f(t) \end{aligned} \right\} (17)$$

with boundary conditions

$$\left. \begin{aligned} X_1(0) &= e(0) \\ X_2(0) &= 0 \\ X_1(T_f + T_d) &= 0 \\ X_2(T_f + T_d) &= 0 \end{aligned} \right\} (18)$$

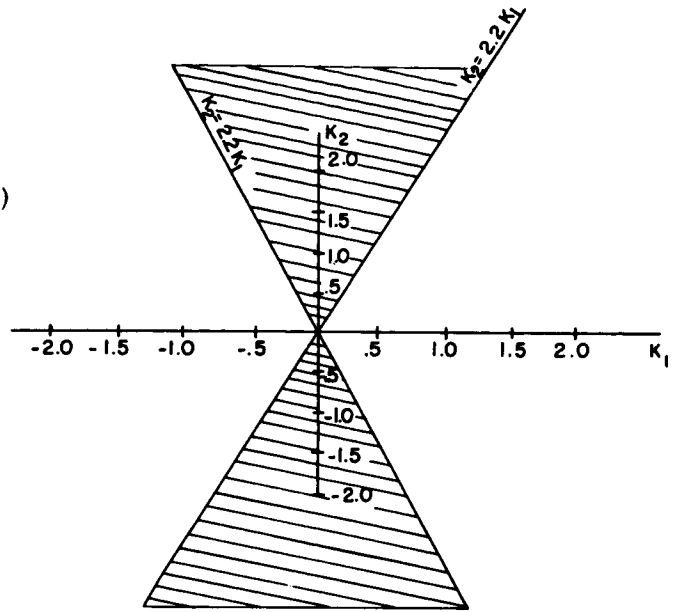


Figure 7.—Decision surfaces. Shaded area shows values for integral track. Unshaded areas result in position tracking.

where  $f(t)$  is of the form shown in figure 8(a). Solving this problem for  $F$  and  $T_s$ ,

$$\left. \begin{aligned} F &= \alpha e(0) \\ \alpha &= K_1/T_f^2 \\ T_s &= T_f/2 \end{aligned} \right\} \quad (19)$$

The adapted model then must generate the control functions of figure 8. For position tracking the control function is generated according to equation (19). For integral control the human controller attempts to establish an error rate which the operators usually describe as "comfortable to work with." It would

seem that this rate would vary with display, tracking instructions, and possibly other variables. However, since only one display was used in this study and the instructions were uniform, the rates established by the different subjects varied by less than 10 percent and had an average value of 8 arc-deg/sec. This rate was then held constant (no arm movement), until the error extrapolated ahead in time by  $T_f + T_d$  was zero, when the second control shown in figure 8(b) was initiated. At the end of each control interval a new sample of  $e(0)$  was taken and a new control interval was initiated. However, this does not mean that the model is strictly a sampled data model since some of the pattern recognizing functions and adaptive functions use continuous inputs of  $e$  and  $\dot{e}$ . The proposed model has both a sampled-data channel and a continuous channel.

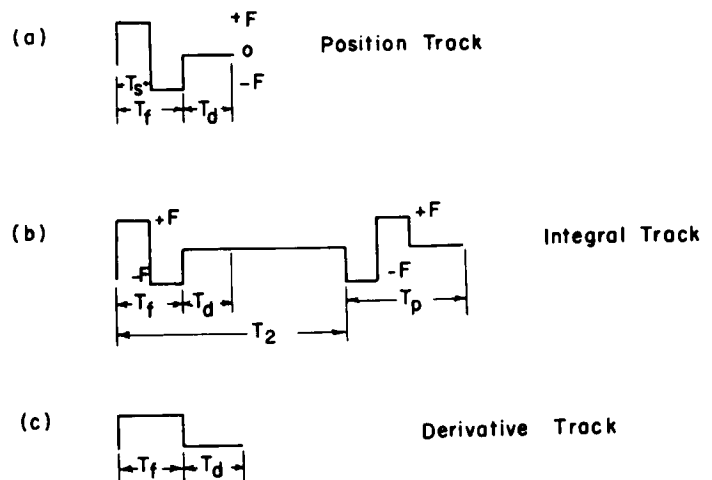


Figure 8. —Basic form of force computer outputs.

**ADAPTATION.** —In order to discuss meaningfully an adaptive model of the human operator, a definition of an adaptive control system is vital since this term has been defined in different ways by many engineers (refs. 12 to 14). Gibson (ref. 15) provides an operational definition which was used in this study. An adaptive control system is a system which is able entirely by itself to accomplish in a closed-loop fashion the functions of identification, decision, and modification. Identification is the complete or partial determination of the plant dynamics. Decision is the determination of an optimum controller based on measurement of an index of performance. Modification is the method of implementing the desired controller.

The identification of this model is done by the pattern recognizer previously described. A coarse estimate for the values of  $K_1$ ,  $K_2$ , and  $K_3$  is obtained from equations (9), (12), and (13), respectively. However, tracking data indicate that fine adjustments are made to these values at the end of each CI. This adjustment of  $K_1$ ,  $K_2$ , and  $K_3$  is a minimization of the index of performance  $e(T_f + T_d)$  for position and derivative track and  $\dot{e}(T_f + T_d)$  for integral track. Thus the adaptation equations can be expressed as

Case 1

$$K_1(n+1) = K_1(n) + K_d \frac{e(T_f + T_d)}{e(0)} \quad (20)$$

where

$e(T_f + T_d)$  error at end of CI

$e(0)$  error at beginning of CI

$K_d$  adaptive constant  $\doteq 0.45$

$T_f$  control time for particular subject

$T_d$  reaction time for subject

Case 2

$$K_2(n+1) = K_2(n) + K_d \frac{\dot{e}(T_f + T_d)}{\dot{e}(T_2)} \quad (21)$$

where

$T_2$  reaction time shown in figure 8(b)

Case 3

$$K_3(n+1) = K_3(n) + K_d \frac{e(T_f + T_d)}{e(0)} \quad (22)$$

Referring to figure 6, the operation of the model will now be outlined for position tracking. When an estimated error  $e^*$  greater than the threshold value appears in the adaptive controller, control is initiated. Position tracking is assumed and the initial value of  $K_1$  is assumed in order to compute  $\alpha$  by equation (19). During the first CI the pattern recognizer estimates  $K_1$  by equation (9), and at the end of the first control interval  $K_2$  and  $K_3$  are estimated with equations (12) and (13). The pattern recognizer then identifies (or actually recognizes) the mode. If the error  $e^*$  is still greater than the threshold, another control interval is initiated, and at the end of this CI the value for  $K_1$  is updated by equation (20). When the error is reduced to a value less than the threshold at the end of a CI, control ceases. The control strategy is similar for cases 2 and 3 except that the control functions of figure 8(b) and 8(c) are used, and  $K_2$  and  $K_3$  are the adapted variables.

## CONCLUDING REMARKS

An adaptive model for the human controller has been proposed. The model uses pattern recognition, which has long been known as a human characteristic, to identify the nature of the control task, and more conventional gradient methods are used for a fine adjustment of the adaptive parameters. The model proposed in this paper is presently being simulated and perfected.

## REFERENCES

1. Tustin, A.: The Nature of the Operators Response in Manual Control and its Implications for Controller Design. J. Inst. Elec. Engrs. vol. 94 (London), 1947, pp. 190-202.
2. Bekey, G. A.: Sampled Data Models of the Human Operator in a Control System. Ph.D. Dissertation, Univ. of Calif., Los Angeles, 1962.
3. Elkind, J. I.; Kelly, J. A.; and Payne, R. A.: Adaptive Characteristics of the Human Controller in Systems Having Complex Dynamics. IEEE Proc. Sym. on Human Factors in Electronics, 1964, pp. 143-159.
4. Knoop, E. E.; and Fu, K. S.: An Adaptive Model of the Human Operator in a Control System. IEEE Proc. Sym. on Human Factors in Electronics, 1964, pp. 252-265.
5. Kreifeldt, J. G.: A Sampled-Data Pursuit Tracking Model. IEEE Trans. on Human Factors in Electronics, vol. HFE-6, no. 1, Sept. 1965.
6. Elkind, J. I.; and Starr, E. A.: Evaluation of a Technique for Determining Time-Invariant and Time-Variant Dynamic Characteristics of Human Pilots. NASA TN D-1897, 1963.
7. Knoop, D. E.: An Adaptive Model of Human Operator in a Control System. Ph.D. Thesis, Purdue Univ., 1965.
8. Young, L. K.; Stark, L.; and Vossius, G.: Predictive Control of Eye Tracking Movements. IRE Trans. on Human Factors in Electronics, vol. HFE-3, Sept. 1962, pp. 52-57.
9. Roig, R. W.: Non-Linear Adaptation in Manual Control Systems. TR 7420-R4, MIT Servo Lab., June 1959.
10. Minsky, M.: Steps Toward Artificial Intelligence. Proc. IRE, vol. 49, no. 1, Jan. 1961.
11. Widrow, B.: Generalization and Information Storage in Networks of ADALINE Neurons. Self Organizing Systems, Spartan Press (Washington, D.C.), 1962.
12. Aseltine, J. A.; Mancini, A. R.; et al.: A Survey of Adaptive Control Systems. IRE Trans. on Automatic Control, vol. AC-6, Dec. 1958, pp. 102-108.

13. Truxal, J. G.: Computers in Automatic Control Systems. Proc. IRE, vol. 49, 1961, pp. 305-312.
14. Zadeh, L. A.: On the Definition of Adaptivity. Proc. IRE, March 1963, p. 469.
15. Gibson, J. E.: Introduction to Adaptive Control Systems in Nonlinear Automatic Control. McGraw-Hill Book Co., Inc., 1963.

N67-15858

## 7. MAN IN AN ADAPTIVE AND MULTILoop CONTROL SYSTEM

Y.T. Li

Massachusetts Institute of Technology

### CLASSIFICATION OF CONTINUOUS AUTOMATIC ADAPTIVE CONTROL SYSTEMS

At a previous symposium (International Symposium on Theory of Self-Adaptive Control Systems sponsored by the International Federation of Automatic Control, Sept. 14-17, 1965, in Teddington, England) a paper was presented to discuss the adaptive functions of man in man-machine control systems. In that paper the principles of operation of continuous automatic adaptive control systems were classified into the following four types:

- (1) Open-loop adaptive control system
- (2) Passive adaptive control system
- (3) Active adaptive control with precisely defined performance indices
- (4) Active adaptive control with inferred performance indices

This classification helps to draw a parallel between the inherent instinct of man and the machine logic created by him for adaptive control. In general, in adaptive control, the phenomenon of the nonstandard situation of the operation is recognized, and the appropriate remedy is made by some suitable adjustment of the controller as shown in figure 1.

In an active adaptive control system with precisely defined performance indices (type (3)), a rather elaborate computer is used to recognize the phenomena of the nonstandard situation of the operation in terms of the system performance function. The deviation of the performance function is then interpreted as a set of performance indices which are to be minimized by suitable adjustments of the controller. In general, the controller is designed following conventional engineering practice and subject to various constraints both in the configuration and in the level of the drive, so that even with the

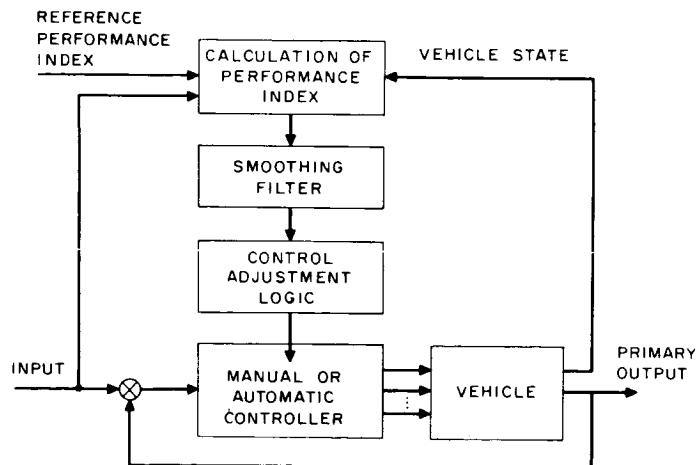


Figure 1.—Active adaptive control with precise performance indices.



best process identification scheme there is some limit in the adaptability. Furthermore, a thorough coverage of the process identification would require a considerable length of time compared with the characteristic time of the system and the bandwidth of the signal. To hasten the speed of adaption and at the same time simplify the complexity of the control system, an inferred performance index may be used. For instance in a model reference adaptive system as originated by Whitaker and modified by Osborn and Hagen, the performance index is essentially generated from the "error" between the output of the system and a reference "model" and weighted by a factor of  $\delta e / \delta a$  where  $a$  is the controller adjustment. The value of  $\delta e / \delta a$  is taken as if the system is operating near the adapted condition, thus hypothetically  $e(\delta e / \delta a)$  is a measure of the partial derivative of the error square with respect to the controller adjustment. It can therefore be used to guide the controller adjustment through a suitable smoothing filter which determines the response speed of the adaption.

Although the factor  $\delta e / \delta a$  is based upon the performance of the normal plant instead of the actual plant, the modified model reference system has amazingly good adaptive performance and a response speed of the same order of magnitude as the response speed of the primary loop. After seeing this result, a tempting question for the practitioner of human engineering is whether a human can accomplish the adaption himself, or at least some part of it. Of course, the next question is whether there is any advantage in having man do the fast adaption himself.

## MAN IN A CONTINUOUS ADAPTIVE CONTROL LOOP

Generally speaking, man is endowed with a phenomenal visual perception for the detection of various modes of motion with far greater accuracy and ease than many man-made devices. Human visual perception also provides man with some estimation of the rate of motion, even though this particular faculty is not as specialized as that of the frog, the cat, or even the monkey. However, with this ability to detect motion and motion rate he is able to play the role of the controller for systems with a fair amount of dynamic delay, such as double integration plus a first-order lag of the order of a second. In vehicle-control or moving-base simulator, his visual motion rate perceptor is augmented by his vestibular system as shown in figure 2 to allow him to perform better than by using visual observation alone.

However, on-line computation of a performance index, even in simple addition or multiplication of two signals with response of a good fraction of a second, is beyond the capacity of a normal person. For this reason, even for a simple adaptive control system such as the model reference system, it is difficult to expect a man to operate well by providing him only with the basic error signal of the system and the model. On the other hand, if the simple computation is provided for him, he should not have any difficulty in performing the adaption. This type of human adaption has been demonstrated in another type of active adaptive control with inferred performance indices such as one with limiting-cycle amplitude as the performance index. Since man can recognize the limiting-cycle pattern, it is a more effective input to him than a set of uncomputed multi-inputs. Another possible display to a human operator for adaptive control purposes is to show on a scope the transient response of the plant. With training and prior knowledge he is capable of correlating the needed controller adjustment with the observed response pattern.

In principle, of course, when a computer is used to reduce the state-variable signals of the system to a simple deviation from a reference value, there is actually very little of

the task left for the man to do. He certainly can do it, but the question is why not let the machine perform the whole job.

## MULTILOOP IN VEHICLE CONTROL SYSTEMS

This question in fact applies to all phases of a control system. The consideration of the adaption problem is only equivalent to the introduction of a second control loop over the primary control loop. This second loop introduces the basic multidecision problem in addition to the problems concerned with the control of each loop. For instance, if the problem is to avoid overloading the pilot with too many control functions, it is possible to have a flight engineer assigned to perform the adaption loop while the pilot is responsible for the primary loops. As appears in common practice, the adjustment of the propulsion system of an airplane in flight is often a routine adaptive control function carried out by the flight engineer. Similarly, he certainly can also perform the fast adaptation of the handling quality of the airplane if the handling quality is displayed to him. In this way the pilot and the flight engineer each have one loop to control for each mode of operation. By combining the adaptive loop with the primary loop, the task is no different from the controlling of two different outputs to which a pilot is constantly exposed. In fact, even in the simple situation of driving a car, the steering and the accelerator are controlled by two different loops. However, in the case of a space vehicle and a helicopter, there can be six primary loops for the control of the motion of the vehicle in space, and each may face the problem of the addition of one or more adaptive control loops.

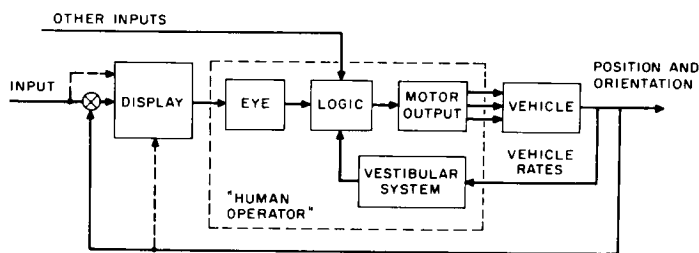


Figure 2. —The human sensors in vehicle control.

## CONTROL PROBLEMS OF HIGHER ORDER SYSTEMS

As in the case of adaptive control, where computation might be needed to generate the performance index for the human to close the loop easily, in the case of the primary control loop, a computer may also be needed to reduce various state variables into a simple deviation display for the operator to perform a simple pursuit type of control. For instance, with a high order system such as one with five cascading integrations, a human has no chance to close the loop and maintain stability with his visual deviation detection and his limited rate estimation of the primary output. However, if the signals from the various stages of integration were fed back as if each loop were performing the function of the feedback of a corresponding inner loop and the combined signal is displayed to the operator, he has no trouble in closing the loop with adequate stability.

As a typical example, the operation of backing up a trailer involves the control of five cascading integrations starting from steering rate to steering angle of the front wheel of the cab, to the angle of the cab and the trailer, and then to the position of the trailer. A trained operator may formulate a mental image of an inner loop aiming at controlling the angle between the cab and the trailer, which is then used to control the trailer position. Thus, a higher order system may be reduced to the control of two outputs with one slave to the other.

Another example is to control the position of a bicycle with the use of steering. In this problem, the steering is primarily used to maintain the balance of the bicycle in its roll mode and the controlled steering is then used to control the path of the bicycle. The two primary outputs are thus controlled by two separate loops, with one slaved to the other.

### INTERCOUPLED MULTILOOP SYSTEM

In the case of bicycle control, the inner loop for the roll stability has a fast response to make it stand out from the slower position-control loop. The fast response of the vestibular system helps to make this possible. In the case of a system in which the multioutputs are "intercoupled," such that their relationships with the control drives are expressed by a matrix, the corresponding loops are not distinguishable enough from each other to allow each loop to be controlled separately. To make an effective control of this system, it would be desirable to decouple the outputs to make each loop independent of the others. This scheme (fig. 3) of using a decoupling matrix to separate the dynamic behavior of the two dominating control inputs and two dominating control outputs of a jet engine is a classic example of reducing an intercoupled system into two separate independent loops. Here, in the original plant the two inputs such as the throttle and the blade angle control the temperature and thrust in an intercoupled manner. The decoupling matrix is used to make the temperature respond directly to the setting "b" and the thrust directly to the setting "a." Feedback loops, either with or without a human operator in the system, are then used to improve the performance of the control system to minimize the disturbance and nonlinear effects.

Ingenious displays are often essential for the decoupling of the various modes of motion. For instance, the motions of an airplane, such as roll and yaw in space, relative to the outside surroundings are highly coupled. With the use of a bank and roll indicator it is then possible to display the proper bank angle as a decoupled indication which is dominated by the aileron control and thus make it possible to separate the aileron-bank loop from the others and thereby reduce the control task.

In another simple example illustrating the geometrical decoupling of displays we might consider the popular toy "Etch A Sketch" which provides two knobs, each controlled by one hand to move a marker along the x- and y-axis (fig. 4). Without training it is quite difficult to draw a simple pattern such as a circle with the marker. In the first place, the operator has to form a mental picture of the circle and then create a deviation of the marker position from the imaginary circle. But the deviation of the marker relating to the circle is coupled by a varying sine and cosine angle on the circle. The nonintercoupling relationship of the x and y positions of the marker with respect to the control of the two knobs may be accomplished by first providing the reference circle marked clearly on the display glass and then providing a reference line following the motion of one knob and then letting the marker controlled by the second knob pursue the intersecting point between the reference line and the circle. Then, of course, the challenge is eliminated, and the value as a toy is lost.

### CHANNEL CAPACITY OF MAN FOR HANDLING MULTILOOP SYSTEM

Having thus established that the proper condition for a human to control several loops simultaneously, whether for the primary motion control loops or for the adaptive control loops, is through the use of decoupling techniques or making one loop a slave to the other, the total capacity of a man to control a multiloop system remains to be investigated. Of course, without limitation of time, there is practically no upper limit on his capacity. For fast, continuous vehicle-motion control, however, he is definitely limited by his input signal receiving channel capacity and the number of motoring modes that he can execute.

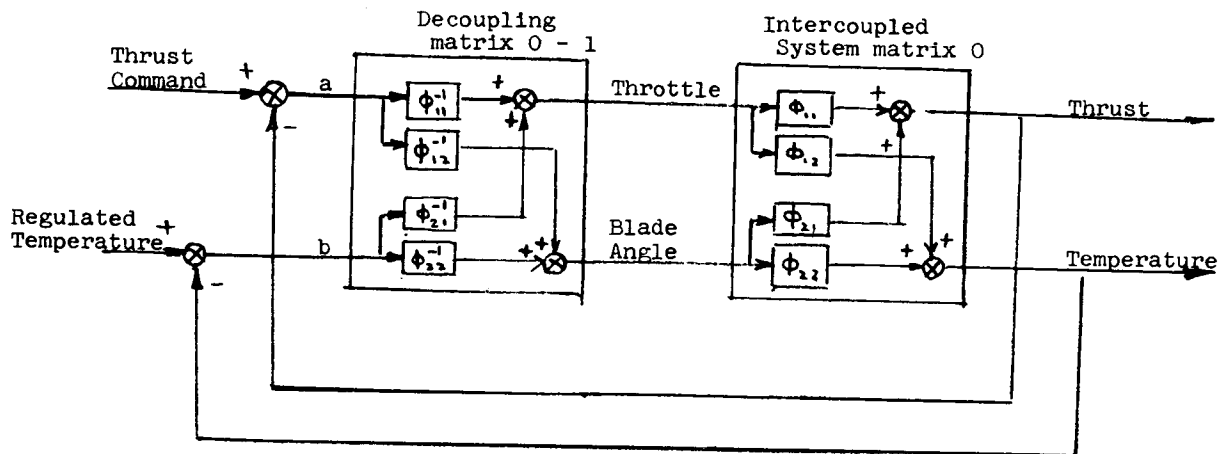


Figure 3. —Decoupling matrix used in conjunction with intercoupled system.

As shown in figure 2, the commonly recognized input signal sensors of man are the visual display augmented by the vestibular system for motion rate and acceleration. In natural environment, visual display can provide motion cues in all three dimensions simultaneously. But a good cockpit display of all three dimensions of motion with the same confidence as in the natural environment is still lacking. Various types of audio display have been attempted but only a few such as those used for tracking radio beacons by the pilot of an airplane seem to have achieved practical application. The usefulness of the vestibular system for vehicle control on the other hand is constantly a controversial subject. It definitely can provide useful information on vehicle motion, but because of the bizarre effects of the vestibular system in association with the three-dimensional vehicle motion, known as "disorientation," pilots are often taught to disregard the "seat of the pants" sensation as an unreliable input. As a result, visual display with its crowded channel capacity and imperfect display apparatus remains the primary contact between man and machine.

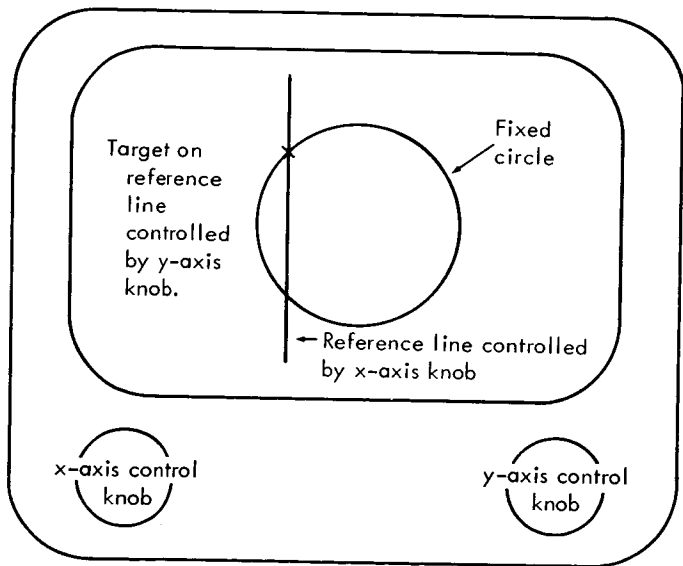


Figure 4. —Decoupling display arrangement.

Three courses may have to be taken to improve the man-machine total capacity. They are the following:

- (1) Improvement of the visual display methods
- (2) Introduction of other input channels

### (3) Development of a logical plan of loading the human operator with multiloop controls

As of now, visual display schemes are in dials and scopes. Dials are ideal for single channel display and scopes or the equivalent provide for the display of more complicated patterns and are therefore more suitable for simultaneous display of multichannelled inputs. A typical example is the use of phase plane display of the motion and rate of motion along a specified axis. Another example is the use of two straight lines to simulate the two sides of a runway and to convey the information on distance and orientation. Other patterns such as the size and shape of a circle, illumination, flashing rate, etc., can also be used for additional information in multiloop system operation.

The vestibular system is a naturally endowed instrument for the detection of motion. Even if it is not used as a feedback input, it provides an indication of comfort, and in extreme situations it causes motion sickness. As for the disorientation effect, it is not inconceivable that a movable chair may be incorporated on the vehicle to offset the turning motion of the vehicle which produces the disorientation. However, this tends to be quite complicated even though it might be possible. Along this same direction of thought, the utilization of the "seat of the pants" effect as a possible input may actually provide a sense of touch to the various parts of the body to indicate the condition of the system outputs.

This feedback information may be used to indicate the direct value or the rate of certain outputs to be controlled, or it may be used to indicate some other state variables which might effect the desirable sensitivity of the control loop. For instance, in the pitch control of an airplane, the stick motion is constrained by the force of a bob weight which provides a regulation of the sensitivity of the control loop as a function of the forward speed.

To illustrate the use of the sense of touch for feedback, one may try the simple task of balancing a broom stick on the palm of one's hand. The primary feedback for this operation is the visual observation which is quite sensitive for the detection of the deviation and the estimation of the rate. With some practice one can do this trick quite convincingly. Now if four little wires are attached to the end of the stick as shown in figure 5 to provide additional information to the operator, performance can be improved considerably. These wire whiskers serve as additional rate indicators and therefore are useful in providing additional damping to the inversed pendulum.

## CONCLUSION

In considering difficulties involved in the control of a multiloop system—such as that of providing effective visual

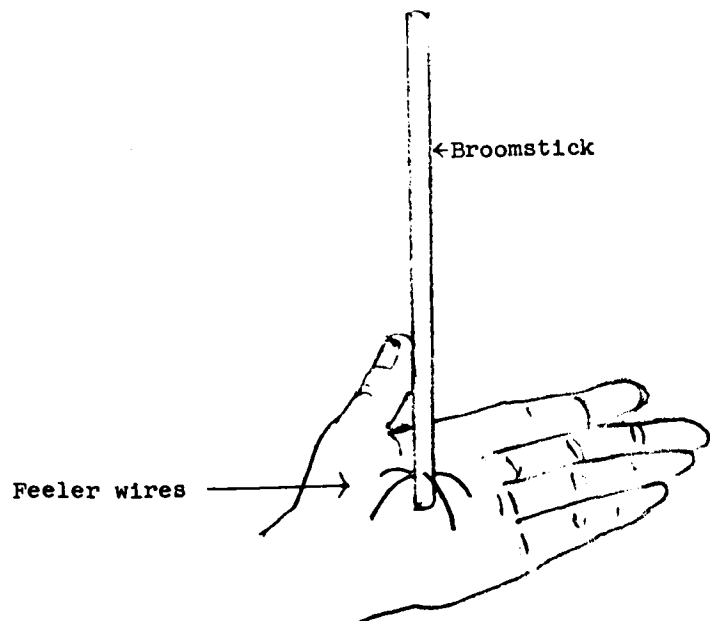


Figure 5.—Balancing a broomstick with feeler wires.

contact displays, the complications involved in providing other forms of displays, all the computation needed to decouple the intercoupled output-input relationships of a multiloop system, the compensation of the higher order dynamics, and the computation of the performance index for the adaptive control loop—it would appear that humans have very little place in the control of this type of system. Indeed, one primary advantage of the human is his visual perception of natural surroundings. But the other equally important aspect of the human operator is his ability to make impromptu adaptive control under situations which were unexpected by the systems designer or too complicated to be included in the system design. The importance of the human operator is illustrated by the numerous accident aversions handled by experienced pilots or drivers. In such a situation, he is powerless unless he has the primary control. For this reason manual operation should be employed in a primary control loop of the dominating vehicle output for the critical phase of operation. Automatic devices may be used to bypass the pilot for load relieving purposes. By this reasoning, in a multilooped vehicle control system, man should be burdened only with those functions for which his attention is needed under adverse operating conditions. For this purpose, both the system design and operator training should put emphasis on the effectiveness of the operator's function of facing all unforeseeable emergencies in the control loop. This type of impromptu adaption with the handling of the primary control loop should therefore play a much more important role than the operator's possible function in the on-line fast adaption of the handling quality of the primary control loops.

N67-15859

PRECEDING PAGE BLANK NOT FILMED.

## 8. TIME VARYING AND NONLINEAR MODELS OF HUMAN OPERATOR DYNAMICS\*

W. W. Wierwille and G. A. Gagné  
Cornell Aeronautical Laboratory of Cornell University

The application of a deterministic theory for characterizing or modeling the dynamics of a human operator in a manual control system was described in an informal presentation. In the study, linear time-varying, nonlinear time-varying, and nonlinear constant-coefficient models of the human operator's dynamics were obtained for one- and two-axis tracking tasks. The displays in the experiment included one- and two-axis compensatory (single spot) displays, an artificial horizon, separate panel meters, and separate panel meters with workload meter. The accuracy for these new models for the various tracking tasks was discussed in detail. In addition, new information about time variability and nonlinearity of the human operator, obtained by studying the models and the manual control system signals, was presented.

This study has shown that important gains in accuracy can be attained by using nonlinear and time-varying models. These models are still largely in the research stage and therefore are not yet ready for use in system design as is the linear constant-coefficient describing-function model. Time-varying linear models will generally possess errors of approximately 10 percent (normalized integral squared error between stick output and model output) for a smoothing time of approximately 5 seconds, nonlinear time-varying models will possess errors of 6 percent, and nonlinear constant-coefficient models will possess errors of 20 percent.

Several rules which explain, to some degree, the ways in which the human operator responds have been obtained by this study. First, the human operator's dynamics often exhibit a nonminimum phase characteristic when characterized by the deterministic theory. This characteristic is apparently the result of reaction time and corresponds to the pure delay factor often included in describing-function models. Secondly, it was found that time-variability of the linear models generally increases as task complexity is increased. This rule seems to corroborate the results of other investigators, in which remnant power increases with task complexity.

Another interesting phenomenon studied in detail was the "flat-topping" that appears in the trace of the human operator's stick output. This characteristic was found to be a highly individualistic nonlinear effect with very little intersubject correlation, since its appearance in ensemble data was almost nonexistent. Nonlinear time-varying characterization models can account for a significant portion of the flat-topping phenomenon, since these models can assume new nonlinear characteristics in a relatively short period of time.

\*This work was sponsored by Langley Research Center of the National Aeronautics and Space Administration under Contract NAS1-4920.

There appears to be no simple relationship between the time variations of the linear time-varying transfer characteristics and the signals of the corresponding manual control system. It now appears that the individual time variations are a function of the biological mechanism of the human operator and are caused by such phenomena as fluctuations in attention and general random drifting of biological characteristics. As supporting evidence that the above conclusion is correct, the example is cited that the human operator does not identically repeat his performance in any particular tracking experiment. Thus, his fluctuations are random functions of time and do not appear to be deterministic functions of the system signals.

Nonlinear constant-coefficient models of a highly complex nature were used to place a bound on the accuracy of logic models. The reasoning in this case is that a logic model is really a nonlinear constant-coefficient filter of a special type. Therefore, the optimal filter in a general class of nonlinear constant-coefficient filters will possess approximately the same accuracy as the best logic model. The results for a 68-element nonlinear filter show that optimal logic models will probably possess errors on the order of 20 percent.

This study describes the first application of any type of nonlinear synthesis models to manual control problems.



# INFORMATION THEORY

N67-15860

## 9. USEFULNESS OF TRANSFORMATION AS A MEASURE OF HUMAN TRACKING PERFORMANCE

*T. Wempe and D. Baty*  
*Ames Research Center, NASA*

This study was conducted to determine the applicability of information theory concepts to human tracking tasks. Data for one subject's tracking performance were analyzed for various bandwidths of the forcing function. The task was to track a filtered gaussian input, displayed on a cathode ray tube, by operating a controller with fixed-gain dynamics. This paper first examines different ways of applying information theory concepts to this tracking task as related to definitions of signal and noise. Then, describing functions and measures of information processing rates were determined for the experimental data. This provided material to examine measures of transformation rates along with relative tracking error for the same task. Finally, the concept of human capacity as related to this simple tracking task was investigated.

For the purpose of analyzing human performance and capability in tasks that include a requirement for tracking performance, such as piloting aircraft on various missions, the attractiveness of the concepts introduced in the field of information theory is obvious. An extrapolation of the theorems of this field of communications to the human suggests that there may be a human channel capacity and that this capacity places an achievable upper limit on the sum of the information processed while performing multiple concurrent subtasks. The benefits to be derived from the validity of this supposition are manifold—the design engineer of aircraft or spacecraft could obtain a measure of human capacity in the standardized units of bits per second; he could arrive at a standardized measure for each subtask required of the pilot, also in bits per second; these measures divided by the measure of human capacity would yield a dimensionless weight for each subtask; the sum of these derived weights could never exceed unity to allow successful human performance at any combination of concurrent subtasks; a method would be inferred for the evaluation of emergency conditions; etc.

Unfortunately, the extrapolation to human performance is not without special problems, and most control tasks are not directly equatable to a communications analogy. Since the pilot's principal task, when engaged in tracking, is one of error reduction, he must not only reproduce a linear function of the input signal or forcing function, he must also reproduce this signal with appropriate amplitudes and phase shifts relative to the forcing function and controlled dynamics at all frequencies. On the other hand, the function of the electronic device usually considered in communication problems is only to reproduce the information content of the input signal with a minimum of noise, thus allowing time delays, phase shifts, and amplitude variations in the output signal relative to the input signal.

Even with this large apparent discrepancy in a description of human performance as compared to the class of problems amenable to analysis by the techniques suggested by information

theory, the possible value of such an approach seemed great enough to provide the impetus for this investigation.

Since very little has been accomplished in the area of applying information theory to piloting tasks, it was deemed advisable to restrict the current investigation to the most elementary aspect of the problem, namely, what is a useful measure of the quantity of information processed in a single, pure-gain, closed-loop tracking task and how does this measure relate to the concept of maximum capacity? It is doubtful that much progress will be made toward the goal of being able to define human capacity to perform complex tasks involving some form of tracking until this innocuous-appearing question is answered with assurance and clarity.

The approach made in this investigation was first to examine the various ways of applying information theory concepts to a simple tracking task. This resulted in several formulas for measuring transinformation<sup>1</sup> rates occurring during the task, depending upon how signal and noise were defined. Then, experimental tracking data were analyzed by controls engineering techniques, to obtain approximate describing functions, as well as by the derived measures of transinformation rates.

This provided material to examine measures of transinformation rates concurrent with the measure of relative tracking error as they were related to the describing function model.

Finally, a search was made for evidence that would support the concept of human capacity as related to the tracking task.

## BRIEF LITERATURE REVIEW

The purpose of this review was twofold: first it was to find what applications of information theory had been made toward describing human behavior, and second, to determine which of these were directly applicable to the current investigation. There were many studies in the first category and only a handful in the second. To indicate the scope of the literature covered several of the categories of use will be mentioned.

Soon after the publication of reference 2 investigators began measuring human transinformation capabilities for various discretely definable tasks, such as typing, piano playing, reading, and mental arithmetic (refs. 3 to 7).

Bricker (ref. 8) summarized the work relating the magnitude of reaction time to the information value of the stimulus; he found, in general, that they are linearly related. Szafran (ref. 9) reports a practical application for this finding. Man's ability to discriminate among stimuli has also been expressed in information theory language (refs. 10 to 14). Although not always expressed in information theory terms, several studies have been prompted by Shannon's sampling theorem (ref. 2). Tracking performance has been measured under several experimental conditions limiting human sampling behavior. (refs. 15 to 23).

---

<sup>1</sup>The term "transinformation" used in this paper is the same as that defined in many texts on information theory, for example, reference 1.

On three studies were found that focused attention on the problem of measuring the transformation of a subject performing a simple tracking task (refs. 24 to 26). It is difficult to compare the results of these three studies since each used a different experimental procedure, different methods of data analysis, and different forcing functions. Each study measured a different aspect of performance, so it is not surprising that each one reported different information processing rates, ranging from 0.5 to over 7 bits/second.

It was shown (refs. 27 and 28) that performance depends not only upon the task input stimulus but also upon the imposed difficulty of the response required.

## APPARATUS, PROCEDURE, AND ANALYSIS

A one-dimensional pursuit tracking task was performed with target and cursor moving vertically. The subject (operator) sat in a dimly lighted room with his eyes 30 inches from, and level with, the display. The display was a dual-beam cathode ray tube with a usable diameter of approximately 4 inches. The target was a finely focused, horizontal line 3 mm long and the cursor was doughnut shaped with an outside diameter of 3 mm and an inside hole of 3/4 mm. Control of the cursor was through a hand operated sidearm controller with support for the forearm. The output of the controller was connected directly to the scope, that is, dynamics equal to  $K$ .

The filtered output of a low frequency gaussian noise generator was used to move the target. The specifications of the noise generator were gaussian amplitude probability distribution within  $\pm 1$  percent and output spectrum uniform to  $\pm 0.1$  dB from 0 to 35 cps.

The noise input was shaped by a second-order filter having the transfer function  $G/(S^2 + 2\xi\omega_n S + \omega_n^2)$ , providing a -80 dB/decade power spectrum for the input signal or forcing function. The filter gain was always adjusted so that the standard deviation of the input signal amplitude at the scope was 15 mm for each value of the filter natural frequency. The relationship between gain  $G$  and the natural frequency  $\omega_n$  was derived as follows, where  $K^2$  was the noise power amplitude.

Variance of the output  $\varphi(\omega)$  is

$$\varphi(\omega) = \frac{1}{2\pi} \int_{-\infty}^{\infty} \frac{K^2 G^2}{\omega^4 + 2(2\xi^2 - 1)\omega_n^2 \omega^2 + \omega_n^4} d\omega$$

Since the filter damping was set at  $\xi = \sqrt{1/2}$ , then

$$\begin{aligned} \varphi(\omega) &= \frac{K^2 G^2}{2\pi} \int_{-\infty}^{\infty} \frac{d\omega}{\omega^4 + \omega_n^4} \\ &= \frac{K^2 G^2}{2\pi} \frac{\sqrt{2\pi}}{2\omega_n^3} = \frac{CG^2}{\omega_n^3} \end{aligned}$$

It was desired that this variance be constant so that

$$G^2 = C_1 \omega_n^3$$

or

$$G = C_2 \omega_n^{3/2}$$

The values of natural frequency used were 1/8, 1/4, 1/2, 1, 2, 4, 8, and 16 radians/second.

One of the coauthors served as the subject in this experiment. He had participated in a prior experiment in which a similar tracking task was used. The runs for that experiment, together with the practice runs for this experiment, resulted in a total of more than 8 hours of practice distributed over 300 separate runs. For this experiment each recorded tracking run lasted 5 minutes.

The filter and subject outputs were recorded on FM magnetic tape for future spectral analysis. In addition to this the following values were directly computed during the first 100 seconds of each run: mean-square filter output, mean-square subject output, mean product of filter and subject output, mean filter output, and mean subject output. These data were later subjected to calibration corrections and then used to estimate means, standard deviations, and correlation coefficients to cross check the spectral data analysis.

The spectral analysis was accomplished with an analog low-frequency spectrum analyzer. Each tracking run was re-recorded on a separate magnetic loop tape. The analyzer compared the power contained in the data run with a different, preset frequency each time the tape cycled. The resulting data were values for input power (to subject), subjects output power, in-phase power (i.e., output to input), and quadrature power at each tested frequency. The spectral analysis was replicated at each frequency by obtaining values from an analysis using filter-filter, filter-subject, subject-filter, and subject-subject data as inputs to the two spectrum analyzer channels. This provided a means for correcting the spectral data assuming a linear model for the analyzer errors. For verification of the analog spectral analysis, one-tracking trial was digitized by two methods (automatic machine A-D conversion and hand-scored record) and a digital spectral analysis was done for both resulting sets of data on an IBM 7094. The results of this digital analysis compared favorably with the analog analysis and no further reference to this method will be made.

## RESULTS AND DISCUSSION

MEASURES OF TRANSINFORMATION.—Transinformation can be described as a measure of the reduction in uncertainty of the information content of the input signal (or signal transmitted) when only the output signal (or received signal) is known. When this concept is applied to a time function, the measure becomes a rate, usually expressed in bits/second. In the derivation of transinformation for a continuous input signal by Shannon (ref. 2), the signal and noise were assumed constant across  $W$ , the bandwidth considered.

$$I = W \log_2 \left( 1 + \frac{S}{N} \right), \text{ bits/sec} \quad (1)$$

When the signal and the noise are not constant across frequency, it directly follows, due to the additive property of transinformation, that equation (2) is the correct expression to use:

$$I = \int_0^\infty \log_2 \left[ 1 + \frac{S(f)}{N(f)} \right] df \quad (2)$$

$\rho(f) = \frac{|\phi_{io}|}{\sqrt{\phi_{ii} \phi_{oo}}} = \cos \alpha$  LINEAR CORRELATION: INPUT VS OUTPUT POWER

$r(f) = \frac{\text{Re } \phi_{io}}{\sqrt{\phi_{ii} \phi_{oo}}} = \cos \beta$  LINEAR CORRELATION: INPUT VS IN-PHASE OUTPUT POWER

$$1 + \frac{S_1 d}{N_1} = 1 + \frac{|G|^2 \phi_{ii}}{\phi_{nn}} = \frac{\phi_{oo}}{\phi_{nn}} = \frac{1}{\sin^2 \alpha} = \frac{1}{1 - \rho^2(f)}$$

$$1 + \frac{S_2 d}{N_2} = 1 + \frac{a^2 \phi_{ii}}{b \phi_{ii} + \phi_{nn}} = \frac{\phi_{oo}}{b^2 \phi_{ii} + \phi_{nn}} = \frac{1}{\sin^2 \beta} = \frac{1}{1 - r^2(f)}$$

the signal (or power of the coherent part of the output) figure that the value for  $1 + (S/N)$  by this definition [1], which is consistent with the usual relationship relation. Thus,  $I_t$ , the rate of transinformation in the channel, can be expressed as follows:

$$I_1 = \int_0^{\infty} \log_2 \left[ \frac{1}{1 - \rho^2(f)} \right] df, \text{ bits/sec} \quad (3)$$

$$I_2 = \int_0^\infty \log_2 \left[ \frac{1}{1 - r^2(f)} \right] df, \text{ bits/sec} \quad (4)$$

Note that  $I_2$  would always be less than  $I_1$  except when there were no phase lags in the system; then they would be equal. This agrees with the notion that a system that has phase lags is transmitting less information relative to the tracking task at hand.

At this point the authors sidestep the slippery discussion of what is signal and what is noise (even the remnant would not be noise in one sense if a nonlinear function could be found to account for it in terms of the input signal) and point out that all of the above reasoning has been pertinent only to the frequency domain, whereas the tracking task is actually time-domain oriented.

In the time domain, a practical measure of transinformation for a tracking task should express the reduction in uncertainty regarding the input signal at time  $t_0$ , with no knowledge of the output at  $(t_0 + \Delta t)$  (since the time machine has yet to be proved practical). Thus if any transport delays (reaction time effects) appear in the closed-loop transfer function  $G$ , then  $I_1$  is a measure of the transinformation that has not yet occurred at  $t_0$ . The quantity  $I_2$  (and incidentally any other measure between  $I_2$  and  $I_1$  that allows for phase shifts in the output due to filter lags but not transport delays) is a valid measure of the transinformation up to  $t_0$  but requires complete knowledge of the output in the time interval  $(0, t_0)$ . These observations are implicit in the transformation to the time domain of the expressions defining signal in the  $I_1$  and  $I_2$  quantities.

Thus, the  $I_2$  type of measure is indicative of what a good unscrambler could have done at any point  $t_i$  (assuming perfect knowledge of the operator's transfer function and knowledge of the output signal up to  $t_i$ ) to reduce the uncertainty in reproducing the input signal; however, the amount of information processing that was actually applied to the tracking task by the operator should express only what was done at any  $t_i$ . This, in essence, defines the problem as finding an expression for the transinformation in a memoryless system where the signal is continuous.

Since the input amplitude distribution for this study was a normal distribution function with a mean that was approximately zero, the amount of transinformation per independent sample point is equal to  $1/2 \log_2 [1/(1 - r^2)]$  where  $r$  is the correlation between input and output amplitudes at each point. Elkind (ref. 29), after Blackman and Tukey (ref. 30), has noted that  $2W_{\text{eff}}$  provides a measure of the number of independent samples per second occurring in a continuous signal. This leads to the final definition of transinformation to be discussed in this paper:

$$I_3 = W_{\text{eff}} \log_2 \left( \frac{1}{1 - r^2} \right) \quad (5)$$

In subsequent sections of this paper,  $I_3$  is used as a measure of the rate that information was processed by the operator and applied to the tracking task.

**TRANSFER FUNCTION APPROXIMATION.**—In this investigation of measures of performance the analytic technique of the controls engineer—namely, the method of determining quasi-linear transfer functions, descriptive of human behavior in tracking tasks—was used. This approach was made because of the success achieved by other investigators using this technique to describe human behavior and because of the implicit relationship between the transfer function and performance measures (without a random or nonlinear component).

Although this study used a pursuit tracking task, analysis of the obtained data indicated that the quasi-linear describing function usually associated with compensatory tracking tasks

seemed to account for the subject's performance very well for input effective bandwidths<sup>2</sup> above 0.24 cps. For input effective bandwidths below this frequency, the fit was not so good and the spectral data became increasingly unreliable as effective bandwidths were lowered. An example of the Bode plots used for determining the approximate transfer functions is given in figure 2. All the open-loop transfer function approximations for the various input effective bandwidths were of the following form:<sup>3</sup>

$$H(j\omega) = \frac{\omega_{XO} e^{-j\omega\tau}}{j\omega + (1/T_I)} \quad (6)$$

In this expression,  $\omega_{XO}$  is the zero dB crossover frequency in radians/second,  $\tau$  is the reaction time delay in seconds, and  $1/T_I$  is the lag constant in radians/second. The system gain  $K$  is equal to  $\omega_{XO}$  multiplied by  $T_I$ . Table 1 presents the parameters determined for the above expression (converted to cps where appropriate) along with other results of the analysis for each of the data runs. It is noted that variability between parameter estimates for the pairs of data runs having the same input signal spectrum was small for forcing functions above 0.24 cps effective bandwidth. The other data of this table will be discussed in subsequent sections as appropriate.

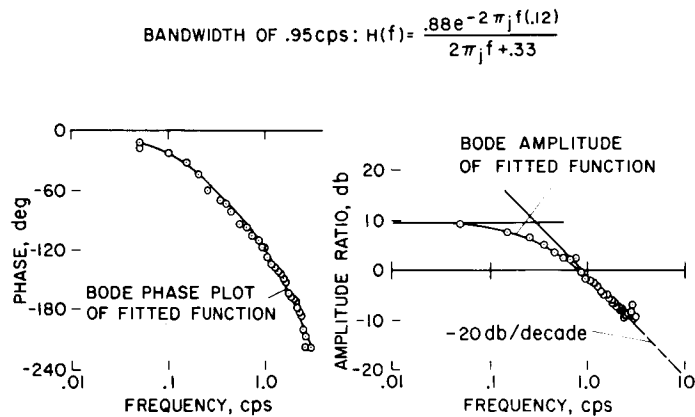


Figure 2.—Sample of Bode plot fitted to subject's tracking results.

Figure 3, a plot of the relative error (rms error/rms input) and what the relative error would have been with the remnant removed, suggests that the remnant made only a small contribution to the tracking error. This is an important point inasmuch as one of the concepts of the amount of information processed is based primarily on the magnitude of the remnant component. The other curve on this figure was derived by numerical solutions of equation (7)—the relative error of a noiseless closed-loop system with unity gain dynamics where the open-loop transfer function is given by equation (6). The parameters were obtained from the subject's performance data of table 1.

<sup>2</sup>Effective bandwidth is defined as the bandwidth of a rectangular power spectral density that has the same area and variance as the power spectral density being described. This definition has been used by other authors in similar applications (refs. 29 and 31):

$$W_{\text{eff}} = \frac{\left[ \int_0^\infty \varphi_{ii}(f) df \right]^2}{\int_0^\infty \left[ \varphi_{ii}(f) \right]^2 df}, \text{ cps}$$

<sup>3</sup>Though frequency measures were generally given in cps throughout this paper, some of the formulas were stated in radians/second for simplicity.



TABLE 1.—SUMMARY OF SUBJECT'S TRACKING RESULTS

[Blanks indicate that parameters were poorly defined by Bode plots and were discarded]

Task	Input, $W_{\text{eff}}$ , cps	Rel- ative error (1)	Rel- ative rem- nant (2)	Rel- ative noise- less error (3)	$1/T_I$ , cps	$f_{XO}$ , cps	$\tau$ , sec	$I_1$ , bits/sec	$I_3$ , bits/sec
12	0.03	0.10	0.30	---	---	---	---	1.8	0.20
11	.06	.05	.16	---	---	---	---	1.9	.52
10	.12	.09	.09	---	0.15	1.15	0.11	4.7	.82
1	.24	.18	.18	---	.10	1.0	---	3.3	1.17
9	.24	.18	.11	.14	.09	.98	.07	4.7	1.17
2	.47	.32	.19	.26	.08	1.2	.12	5.4	1.57
8	.47	.36	.19	.31	.068	1.1	.15	5.7	1.40
3	.95	.65	.27	.59	.22	.8	.12	6.0	1.10
7	.95	.69	.33	.61	.30	.88	.12	6.1	1.04
4	1.88	.98	.34	.92	.62	.55	.14	5.0	.32
6	1.88	.98	.38	.90	.54	.54	.13	4.9	.34
5	3.77	1.14	.45	1.04	.32	.25	.15	2.3	0

$$^1\text{Relative error} = \sqrt{\frac{\frac{1}{\pi} \int_0^\infty \varphi_{ee}(\omega) d\omega}{\frac{1}{\pi} \int_0^\infty \varphi_{ii}(\omega) d\omega}}$$

$$^2\text{Relative remnant} = \sqrt{\frac{\frac{1}{\pi} \int_0^\infty \varphi_{nn}(\omega) d\omega}{\frac{1}{\pi} \int_0^\infty \varphi_{ii}(\omega) d\omega}}$$

$$^3\text{Relative noiseless error} = \sqrt{\frac{\frac{1}{\pi} \int_0^\infty \varphi_{ee}(\omega) d\omega - \frac{1}{\pi} \int_0^\infty \varphi_{nn}(\omega) d\omega}{\frac{1}{\pi} \int_0^\infty \varphi_{ii}(\omega) d\omega}}$$

$$\text{Relative error} = \frac{\sqrt{\frac{1}{\pi} \int_0^{\infty} \varphi_{ee}(\omega) d\omega}}{\sqrt{\frac{1}{\pi} \int_0^{\infty} \varphi_{ii}(\omega) d\omega}} = \sqrt{\frac{1}{\pi} \int_0^{\infty} \frac{[(1/T_I)^2 + \omega^2] \varphi_{ii}(\omega) d\omega}{\omega_{XO}^2 + (1/T_I)^2 + 2\omega_{XO}(1/T_I) \cos \omega T - 2\omega_{XO} \omega \sin \omega T + \omega^2}} \quad (7)$$

where

$$\varphi_{ii}(\omega) = \frac{2\sqrt{2} \omega_n^3}{\omega_n^4 + \omega^4}$$

Since this curve includes no remnant component, it is to be compared with the subject's performance with remnant removed. The agreement between these two curves is very good above the input effective bandwidth of 0.24 cps, indicating the validity of the model for describing performance without the random part of the output. The source of the remnant was not investigated, though it was noted that the noise spectra for all of the data runs could be fitted fairly well by the following equation:

$$\varphi_{nn}(f) = ae^{-bf} \quad (8)$$

#### TRANSFORMATION CONCEPTS APPLIED TO DATA.—

Values for  $I_1$  and  $I_3$ , both for the data of this study and some of the results for pursuit tracking presented in Elkind's study (ref. 32), are presented in figure 4 for comparison. (The  $I_1$  curve for Elkind's rectangular data first appeared in ref. 25). Thus, this figure invites comparisons between the two measures of transformation for various shapes of input spectra. Curves are shown for rectangular input spectra, and for filtered input spectra having a slope of -80 dB/decade beyond the natural frequency of the filter. Also shown are isolated points for "filtered" input

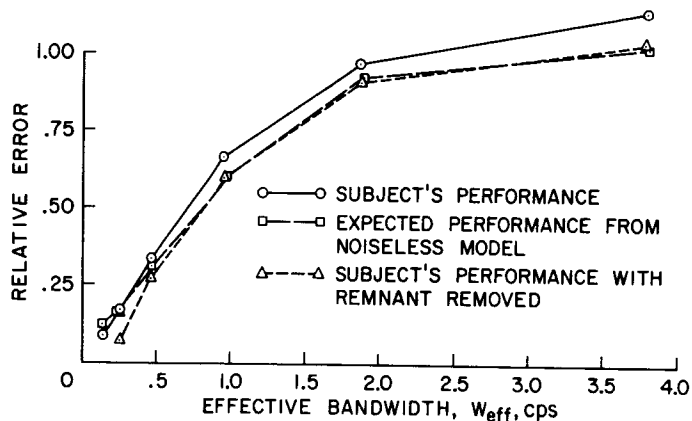


Figure 3.—Comparison of relative error data—subject's performance with and without remnant and predicted performance from noiseless model.

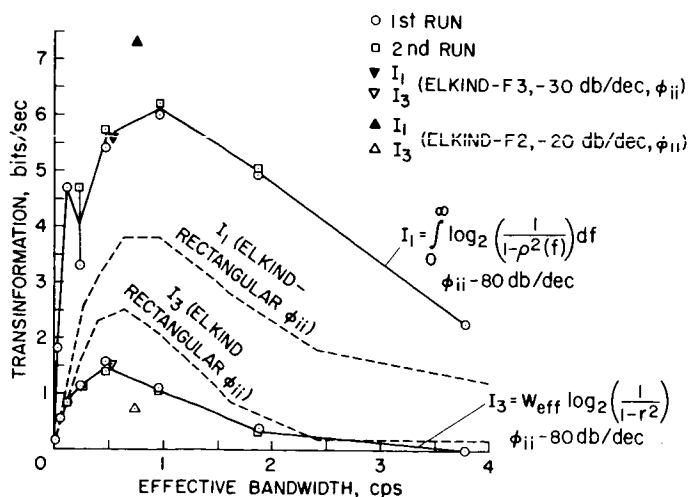


Figure 4.—Comparisons of  $I_1$  and  $I_3$  for various input signals.

spectra having slopes of -20 dB/decade and -30 dB/decade beyond the corner frequency of 0.24 cps. In the following discussion, the variation of the input spectral characteristics from a slope of  $-\infty$  dB/decade at the cutoff frequency for the rectangular input, through -80 dB/decade, -30 dB/decade and to a slope of -20 dB/decade beyond the corner or natural frequency of the filters is referred to as a "flattening" of the input spectra. The following comments are made regarding figure 4.

(1) The curves for  $I_1$  are similar in shape to the curves for  $I_3$ , with the  $I_1$  curves being above (higher  $I$ ) and to the right of (higher  $W_{eff}$ ) the  $I_3$  curves. Though it is obvious that  $I_3$  must be less than  $I_1$  and that  $I_3$  can be predicted fairly accurately from knowledge of the transfer function, it is not obvious why  $I_1$  has the same configuration as  $I_3$  since it is strictly a function of the remnant. The implications here are left for future research.

(2) The  $I_1$  curves (and points) appear to be members of a family of curves increasing in magnitude as the input spectrum flattens to -20 dB/decade.<sup>4</sup> The maximum  $I_1$  curve probably occurs for input spectra attenuated at about -20 or -10 dB/decade. Elkind's data for a -10 dB/decade

<sup>4</sup>That the data for Elkind's results with an input spectra of -30 dB/decade beyond the corner frequency fall almost on both  $I$  curves of this study where the input was -80 dB/decade beyond the natural frequency of the filter caused little concern, since different controllers, presentations, subjects, and analyzers were used.

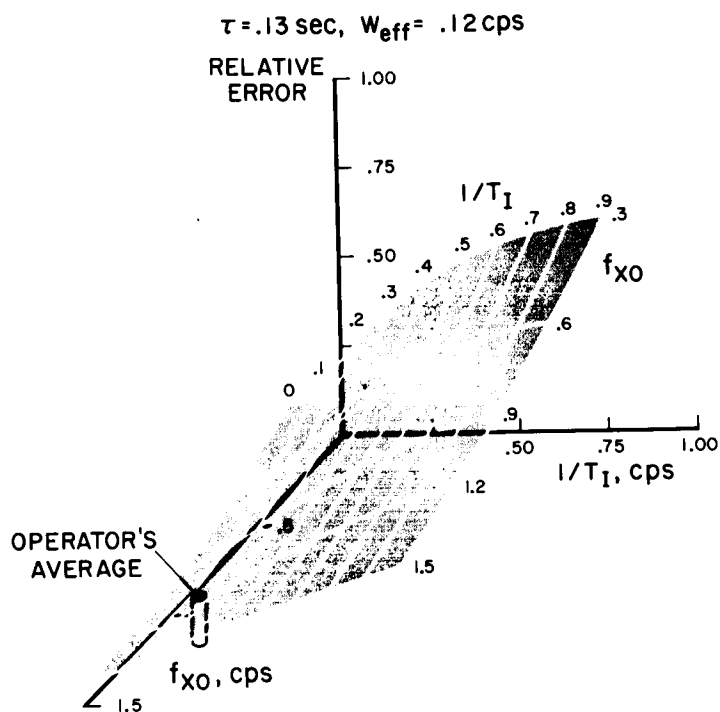


Figure 5.—Relative error versus parameter variations for noiseless model with operator's average performance shown for  $W_{eff} = 0.12$  cps.

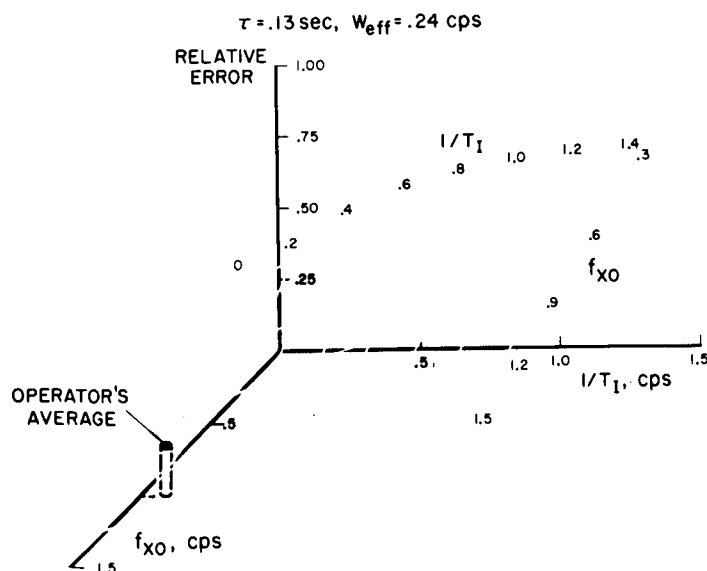


Figure 6.—Relative error versus parameter variations for noiseless model with operator's average performance shown for  $W_{eff} = 0.24$  cps.

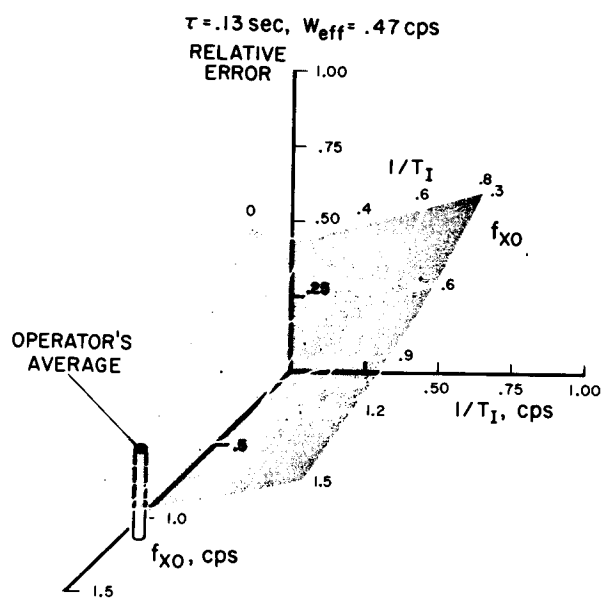


Figure 7. —Relative error versus parameter variations for noiseless model with operator's average performance shown for  $W_{eff} = 0.47$  cps.

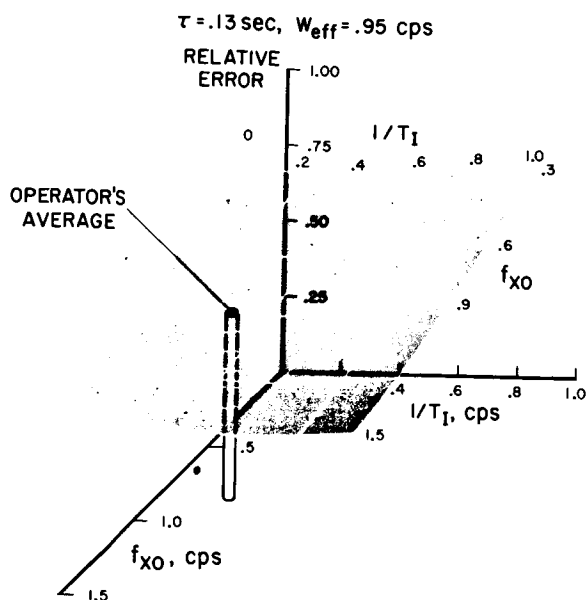


Figure 8. —Relative error versus parameter variations for noiseless model with operator's average performance shown for  $W_{eff} = 0.95$  cps.

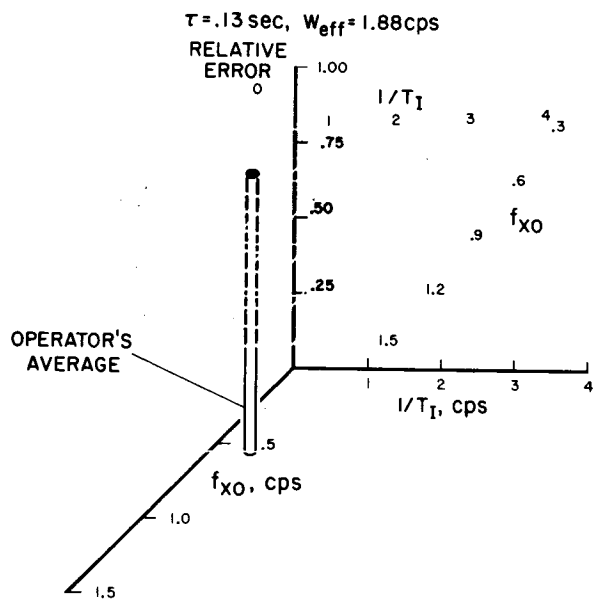


Figure 9. —Relative error versus parameter variations for noiseless model with operator's average performance shown for  $W_{eff} = 1.88$  cps.

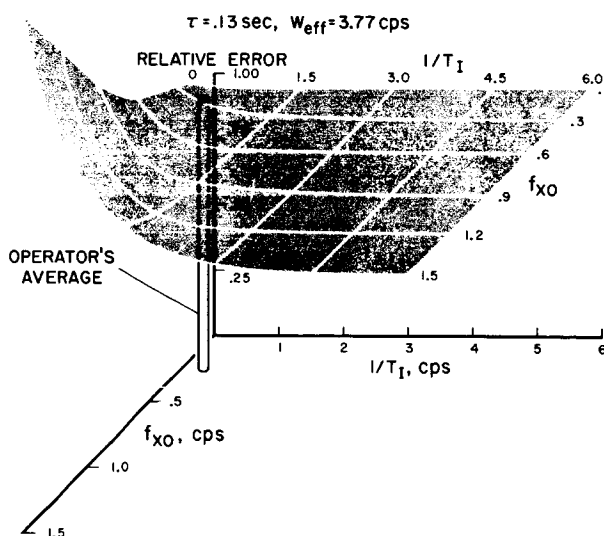


Figure 10. —Relative error versus parameter variations for noiseless model with operator's average performance shown for  $W_{eff} = 3.77$  cps.

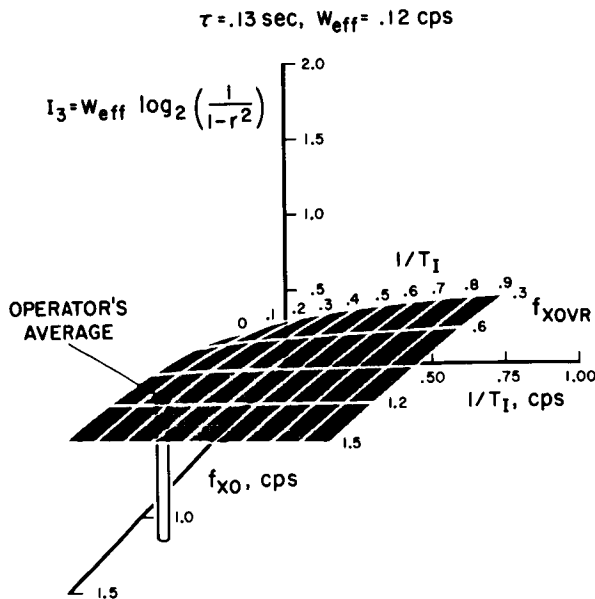


Figure 11.  $-I_3$  versus parameter variations for noiseless model with operator's average performance shown for  $W_{\text{eff}} = 0.12 \text{ cps}$ .

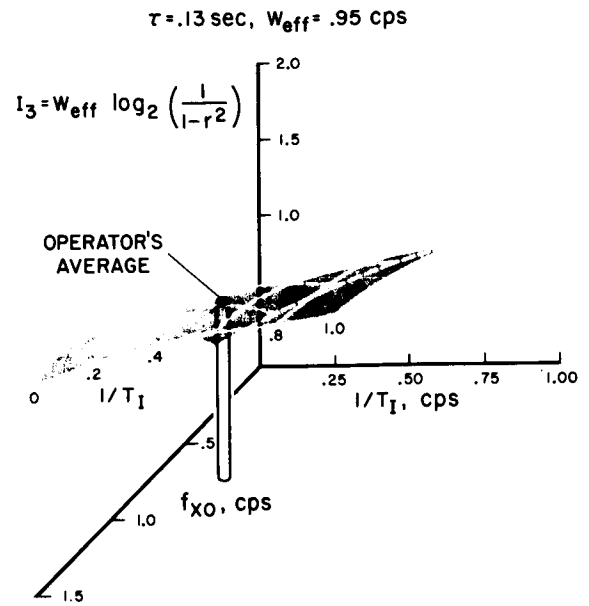


Figure 12.  $-I_3$  versus parameter variations for noiseless model with operator's average performance shown for  $W_{\text{eff}} = 0.95 \text{ cps}$ .

input (not plotted) had about the same value for  $I_1$  as his data for a  $-20 \text{ dB/decade}$  input. And since the input spectrum would be rapidly approaching a rectangular input with infinite bandwidth if it were made flatter than  $-10 \text{ dB/decade}$ , and  $I_1$  would be approaching a value of zero, it is believed that the maximum for this curve is in the region of  $-20 \text{ dB/decade}$ .

Elkind (ref. 25) recognized the phenomenon stated in item (2) and attributed the low transinformation for the rectangular input data to high-frequency components affecting the signal-to-noise ratio at low frequencies and attributed the high transinformation for the filtered inputs to an increase in bandwidth concurrent with high-frequency components of small amplitude having less effect on the low frequency signal-to-noise ratio.

(3) The  $I_3$  curves also appear to be members of a family of curves decreasing in magnitude as the input spectrum flattens to  $-20 \text{ dB/decade}$ . This is principally due to the transport delay in the system. As higher frequency components are introduced by flattening the input spectrum, the system becomes more out of phase and less effective.

(4) There is a large difference between the  $I_1$  and the  $I_3$  curves for each input spectrum, and this difference increases as the input spectrum flattens. The causes for this are discussed in items (2) and (3), but the implication is that human operators are very poorly suited to tracking tasks and must process large quantities of information to realize small benefits.

Finally, the measure  $I_3$  appeared more related to operator subjective opinion of effort and accomplishment relative to the tracking task than either  $I_1$  or relative error. As the

bandwidth of the input was increased over the range where the slope of  $I_3$  was positive, the operator stated that he felt the task was becoming more difficult but that he could keep up with it. Beyond the point where the slope of  $I_3$  became negative, the operator felt the task was getting out of hand and that he was falling behind. At the point where  $I_3$  became zero, the operator stated he could no longer track the signal although the  $I_1$  measure indicated he was processing over 2 bits/second of information at that point. Since the relative error is a monotonically increasing function of  $W_{\text{eff}}$ , it has no hand holds on which to hang labels; hence, it is not easily related to subjective opinion.

**EFFECTIVE TRANSFORMATION,  $I_3$ , AND RELATIVE ERROR.**—At this point an answer to the following question seems pertinent, "Does the operator adapt to the task to maximize  $I_3$ , or does he adapt to minimize relative error?" Figures 5 to 10 present relative error performance contours for variations of  $1/T_I$  and  $f_{XO}$ , assuming the noiseless model of equation (6) with the reaction time  $\tau$  given as 0.13 second (the average reaction time for the operator of this study - table 1). These contours were obtained by numerical solutions of equation (7) for each of the input spectra used in this study. Also located on each of these contours is a pylon representing the average of the subject's transfer function parameters from table 1.

In every case (except for  $W_{\text{eff}} = 0.12$  cps, where the operator's lag was a little on the high side) the operator adjusted the parameters that he could (namely,  $f_{XO}$  and  $1/T_I$ ) out from zero values until only a small negative gradient

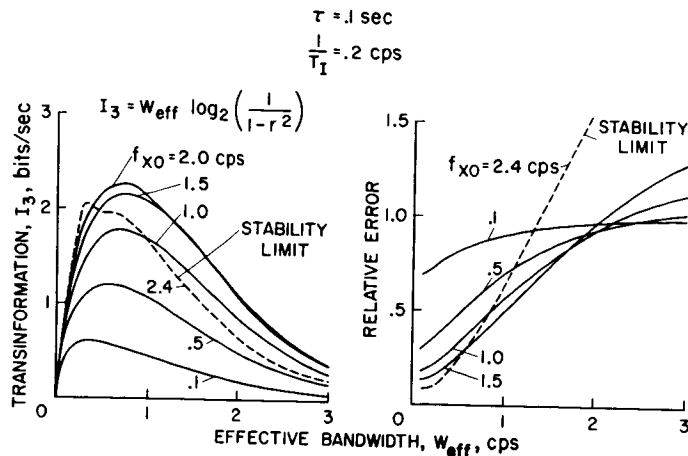


Figure 13.—Dependence of  $I_3$  and relative error on  $W_{\text{eff}}$  and  $f_{XO}$ .

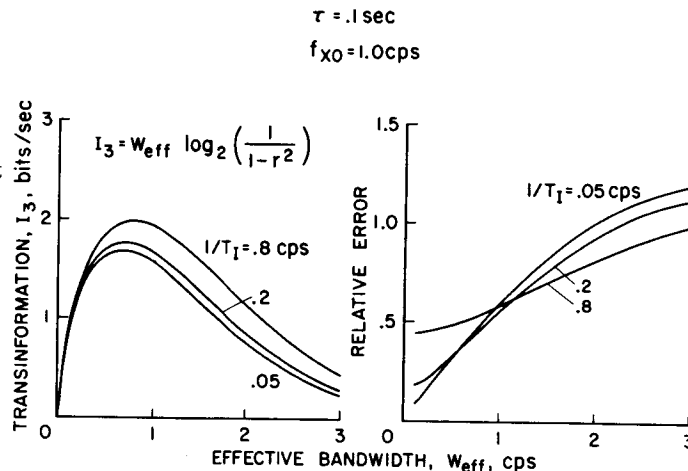


Figure 14.—Dependence of  $I_3$  and relative error on  $W_{\text{eff}}$  and  $1/T_I$ .

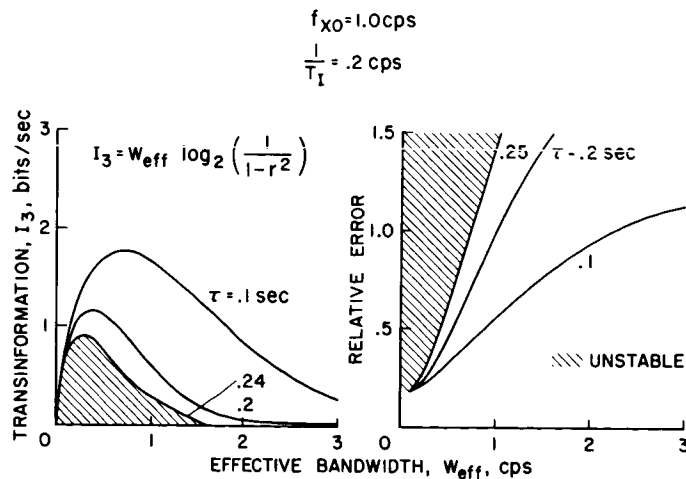


Figure 15.—Dependence of  $I_3$  and relative error on  $W_{\text{eff}}$  and  $\tau$ .

in relative error would be obtained by further effort in increasing these parameters. This is clear evidence that the operator was doing an excellent job of obtaining a reasonably low relative error for the task and his reaction time.

For selected input spectra  $I_3$  sheets were determined by numerical methods for variations of  $1/T_I$  and  $f_{XO}$  using the model of equation (6) and the definition of  $I_3$ , equation (5), and presented in figures 11 and 12. For application in equation (5),  $r$  was determined by:

$$r = \frac{\frac{1}{\pi} \int_0^{\infty} \text{Re} \varphi_{iO}(\omega) d\omega}{\sqrt{\left[ \frac{1}{\pi} \int_0^{\infty} \varphi_{ii}(\omega) d\omega \right] \left[ \frac{1}{\pi} \int_0^{\infty} \varphi_{oo}(\omega) d\omega \right]}} \quad (9)$$

This value for  $r$  is expressed in the notation of this discussion in equation (10).

$$r = \frac{\frac{1}{\pi} \int_0^{\infty} \frac{\omega_{XO} [(1/T_I) \cos \omega\tau - \omega \sin \omega\tau + \omega_{XO}] \varphi_{ii}(\omega) d\omega}{\omega_{XO}^2 + (1/T_I)^2 + 2\omega_{XO} (1/T_I) \cos \omega\tau - 2\omega_{XO} \omega \sin \omega\tau + \omega^2}}{\sqrt{\frac{1}{\pi} \int_0^{\infty} \frac{\omega_{XO}^2 \varphi_{ii}(\omega) d\omega}{\omega_{XO}^2 + (1/T_I)^2 + 2\omega_{XO} (1/T_I) \cos \omega\tau - 2\omega_{XO} \omega \sin \omega\tau + \omega^2}}} \quad (10)$$

where

$$\varphi_{ii}(\omega) = \frac{2\sqrt{2} \omega_n^3}{\omega^4 + \omega_n^4}$$

Though figure 11 ( $W_{\text{eff}} = 0.12$  cps) shows an insensitivity of  $I_3$  in the same region where the variables  $f_{XO}$  and  $1/T_I$  produced a low value for relative error, figure 12 ( $W_{\text{eff}} = 0.95$  cps) clearly shows that the operator was not obtaining a maximum  $I_3$ . For the same task, figure 8 ( $W_{\text{eff}} = 0.95$  cps) shows that he was reasonably near the optimum in reducing the relative error. These figures, in conjunction with the foregoing figures and discussion, suggest that the operator concentrated on reducing his relative error and at the same time was indifferent to maximizing the value  $I_3$ .

Figures 13 to 15 depict another set of numerical solutions for equations (7) and (5) that reinforce the idea of independence between maximum  $I_3$  and minimum relative error. Whereas  $W_{\text{eff}}$  was held constant in figures 5 to 12, these last three figures show that performance varies with different sets of parameters when  $W_{\text{eff}}$  is varied. Figure 15 is of particular interest because it shows the large effect of  $\tau$  on performance.

THE CONCEPT OF HUMAN CAPACITY FOR INFORMATION PROCESSING.—Up to this point in this paper no evidence has supported the concept that for a given task, a highly motivated operator will process information at a rate approaching some constant representative of his maximum ability. With this thought in mind, figure 4 presents a bewildering set of curves where different rates of transinformation resulted only from variations in the shape of the input spectrum. This certainly does not support any notion of fixed capacity.

$$I_3 + I_1 = I_{\text{total}} \quad (11)$$

The diagram illustrates a human control system model for a tracking task. The process begins with an **INPUT** signal entering a summing junction ( $\Sigma$ ). The summing junction also receives a feedback signal from the **CONTROLLER** block. The output of the summing junction is the **PURSUIT ELEMENT**, which is added to the **INPUT** to produce the **ERROR** signal. The **ERROR** signal is fed into the **VISUAL RECEPTOR AND INTERPRETOR** block. This block also receives **ACUITY NOISE** and sends a signal to the **RESPONSE ORGANIZER** block. The **RESPONSE ORGANIZER** block sends a signal to the **RESPONSE MODEL** block, which also receives **NOISE**. The **RESPONSE MODEL** block sends a signal to the **PSEUDO-SERVO** block. The **PSEUDO-SERVO** block sends a signal to the **CONTROLLER** block. The **CONTROLLER** block sends the **OUTPUT** signal. Feedback loops are shown with dashed lines: one from the **PSEUDO-SERVO** block to the **VISUAL RECEPTOR AND INTERPRETOR** block (labeled  $I_1$ ), and another from the **CONTROLLER** block to the **VISUAL RECEPTOR AND INTERPRETOR** block (labeled  $I_3$ ).

TOTAL I =  $I_1 + I_3$

Y-axis: TOTAL I, bits/sec

X-axis: EFFECTIVE BANDWIDTH -  $W_{eff}$ , cps

Curves shown:

- MAXIMUM ACHIEVABLE TOTAL I
- ELKIND-F3, -30 db/dec,  $\phi_{ii}$
- ELKIND-F2, -20 db/dec,  $\phi_{ii}$
- $\phi_{ii}$ : -80 db/dec
- ELKIND-RECTANGULAR  $\phi_{ii}$

Included in figure 17 is a line channel model. representing the maximum achievable rate of transinformation for the sum of two parallel channels receiving inputs from the same visual receptor under certain assumptions.<sup>6</sup>

<sup>5</sup>For expedience the remnant effect was not removed from  $I_3$  measures in these results since its effect was small; however, this may have accounted for the lower values for the  $-\infty$  dB/decade results for  $I_{\text{total}}$  since the remnant effect was greatest for that data.

<sup>6</sup>It was assumed that the operator's visual acuity resulted in a rms error of 1 minute of arc (0.15 mm at a viewing distance of 20 in.). With the rms of the signal amplitude held constant at 15 mm on the CRT,  $S/N = (15)^2/(0.15)^2$ . From reference 2, the maximum rate of transinformation with a fixed error is  $R = W \log_2 S/N$ , which yielded the line on figure 17 when  $W_{\text{eff}}$  was substituted for  $W$  and the resulting value of  $R$  doubled to account for the sum of parallel channels.



This figure suggests that the human operator does have an information-processing capacity independent of the shape of the input spectrum. As the input bandwidth increases from zero, the operator progressively processes almost all of the information available from his visual receptors until he reaches a maximum limit of about 7 bits/second in the vicinity of 1/2 cps (input effective bandwidth), beyond which his rate gradually tapers off as he realizes the futility of the task.

## CONCLUDING REMARKS

Since this study was exploratory, conclusions are more or less a collection of observations rather than the results of testing hypotheses. The following conclusions were relative to the application of information theory to a closed-loop pursuit tracking task.

Measures of transinformation rates determined in the frequency domain can have unusual interpretations in the time domain, for example,

(1) Measures such as  $I_2$  (eq. (4)) require a decoder which has perfect memory of the output over the time interval  $(0, t_0)$  in order to reduce the uncertainty regarding the input at  $t_0$  to the extent indicated in that measure.

(2) Measures such as  $I_1$  (eq. (3)) also require a similar decoder over  $(0, t_0)$  but can only reduce uncertainty regarding the input up to  $(t_0 - \tau)$  to the degree indicated if the input-output relationship includes a transport delay  $(\tau)$ .

The quantity  $I_3$  (eq. (5)) is a measure of the rate of transinformation effectively applied to the tracking task.

There was some evidence that the human operator performs as a dual-signal processor with one capacity for the sum of both channels. That is, if one channel were considered to be an organizing channel measured by  $I_1$  and the other a task-performing channel measured by  $I_3$ , the measure of  $I_1$  plus  $I_3$  tended to be constant for a given  $W_{\text{eff}}$  for variations in the input spectrum.

Other observations were made regarding human tracking performance in a simple pursuit task:

(1) The human operator is poorly suited for tracking tasks primarily because of his inherent reaction time. This statement is based on the observation that he processes much more information than he can apply to the task.

(2) Within his reaction-time limitations, the human operator is reasonably optimum in reducing relative error by adjusting  $f_{XO}$  and  $1/T_I$ .

(3) The operator apparently does not attempt to maximize his rate of effective transinformation,  $I_3$ .

(4) Of the performance measures considered,  $I_3$  was the best indicator of the operator's subjective opinion relative to task difficulty and his accomplishment.

(5) Assuming the dual channel mentioned above, the human operator has a capacity of about 7 bits/second.

## REFERENCES

1. Reza, M.: Introduction to Information Theory. McGraw-Hill Book Co., Inc., 1961.
2. Shannon, C. E.; and Weaver, W.: The Mathematical Theory of Communication. The University of Illinois Press, 1949.
3. Augenstine, L.; Blank, A. A.; Quastler, H.; and Wayner, M.: Human Performance in Information Transmission. Part IV - Flash Recognition of Familiar Displays. Rep. R-69, Control Systems Lab., Univ. of Illinois, 1956.
4. Augenstine, L. G.: Human Performance in Information Processing. Part VI - Evidence of Periodicity in Information Processing. Rep. R-75, Control Systems Lab., Univ. of Illinois, Dec. 1958.
5. Staff and Consultants, Biosystems Group: Human Performance in Information Transmission. Part III - Flash Recognition-Scale Reading. Rep. R-68, Control Systems Lab., Univ. of Illinois, 1955.
6. Quastler, H.; and Wulff, V. J.: Human Performance in Information Transmission. Part I - General Remarks; Part II - Sequential Tasks (Over-learned Activities). Rep. R-62, Coordinated Science Lab., Univ. of Illinois, 1955.
7. Quastler, H.; and Brabb, B.: Human Performance in Information Transmission. Part V - The Force of Habit. Rep. R-70, Control Systems Lab., Univ. of Illinois, 1956.
8. Bricker, Peter D.: Information Measurement and Reaction Time: A Review. Information Theory in Psychology; Problems and Methods, H. Quastler, ed., Free Press Publishers (Glencoe, Ill.), 1955, pp. 350-359.
9. Szafran, Jacek: Age Differences in Choice Reaction Time and Cardiovascular Status Among Pilots. Nature, vol. 200, no. 4909, 1963, pp. 904-906.
10. Eriksen, C. W.; and Hake, H. W.: Multidimensional Stimulus Differences and Accuracy of Discrimination. J. Exp. Psychol., vol. 50, no. 3, 1955, pp. 153-160.
11. Hake, H. W.; and Garner, W. R.: The Effect of Presenting Various Numbers of Discrete Steps on Scale Reading Accuracy. J. Exp. Psychol., vol. 42, no. 5, 1951, pp. 358-366.
12. Klemmer, E. T.; and Frick, F. C.: Assimilation of Information From Dot and Matrix Patterns. J. Exp. Psychol., vol. 45, no. 1, 1953, pp. 15-19.
13. Nickerson, R. S.; and Duva, J. S.: Target Position as a Coding Dimension. AFCCDD-TR60-41, Operational Applications Office, Air Force Command and Control Development Division, Nov. 1960.

14. Pollack, Irwin; and Ficks, Laurence: Information of Elementary Multi-Dimensional Auditory Displays. *J. Acoust. Soc. Am.*, vol. 26, no. 2, 1954, pp. 155-158.
15. Battig, W. F.; Gregg, L. W.; et al.: Tracking and Frequency of Target Intermittence. *J. Exp. Psychol.*, vol. 47, no. 5, May 1954, pp. 309-314.
16. Battig, W. F.; Voss, J. F.; and Brogden, W. J.: Effect of Frequency of Target Intermittence Upon Tracking. *J. Exp. Psychol.*, vol. 49, no. 4, Apr. 1955, pp. 244-248.
17. Bennett, C. A.: Sampled-Data Tracking: Sampling of the Operator's Output. *J. Exp. Psychol.*, vol. 51, no. 6, June 1956, pp. 429-438.
18. Hunt, D. P.: Effects of Nonlinear and Discrete Transformations of Feedback Information on Human Tracking Performance. *J. Exp. Psychol.*, vol. 67, no. 5, May 1964, pp. 486-494.
19. Katz, M. S.; and Spragg, S. D. S.: Tracking Performance as a Function of Frequency of Course Illumination. *J. Exp. Psychol.*, vol. 40, 1955, pp. 181-191.
20. McConnell, D.; and Shelly, M. W.: Tracking Performance on a Sequence of Step Functions Which Approaches a Continuous Function as a Limit. *J. Exp. Psychol.*, vol. 59, no. 5, May 1960, pp. 312-320.
21. Poulton, E. C.: On the Stimulus and Response in Pursuit Tracking. *J. Exp. Psychol.*, vol. 53, no. 3, Mar. 1957, pp. 189-194.
22. Senders, John W.: Tracking With Intermittent, Illuminated Stimuli. Tech. Rep. 55-378, WADC, Oct. 1955.
23. Senders, John W.: The Human Operator as a Monitor and Controller of Multi-Degree-of-Freedom Systems. National Symposium on Human Factors in Electronics, Washington, D. C., May 2, 1963. (Also in *IEEE Trans. on Human Factors in Electronics*, vol. HFE-5, Sept. 1964, pp. 2-5.)
24. Crossman, E. R. F. W.: The Information-Capacity of the Human Motor System in Pursuit Tracking. *Quart. J. Exp. Psychol.*, vol. 12, 1960, pp. 1-16.
25. Elkind, J. I.; and Sprague, L. T.: Transmission of Information in Simple Manual Control Systems. *IRE Trans. on Human Factors in Electronics*, vol. HFE-2, no. 1, Mar. 1961, pp. 58-60.
26. Holding, D. H.: Rates of Handling Continuous Information. FPRC-1068, Flying Personnel Res. Comm., Air Ministry, 1959.
27. Fitts, P. M.; and Peterson, J. R.: Information Capacity of Discrete Motor Responses. *J. Exp. Psychol.*, vol. 67, no. 2, Feb. 1964, pp. 103-112.
28. Fitts, P. M.: The Information Capacity of the Human Motor System in Controlling the Amplitude of Movement. *J. Exp. Psychol.*, vol. 47, no. 6, June 1954, pp. 381-391.

29. Elkind, J. I.: A Survey of the Development of Models for the Human Controller. Progress in Astronautics and Aeronautics, vol. 13, R. C. Langford and C. J. Mundo, eds., Academic Press, 1964, pp. 623-643.
30. Blackman, R. B.; and Tukey, J. W.: The Measurement of Power Spectra, From the Point of View of Communications Engineering. Dover Publ., Inc., 1959.
31. McRuer, Duane; Graham, Dunstan; Krendal, Ezra; and Reisener, William, Jr.: Human Pilot Dynamics in Compensatory Systems: Theory, Models, and Experiments with Controlled Element and Forcing Function Variations. AFFDL-TR-65-15, Systems Technology, Inc., July 1965.
32. Elkind, Jerome I.: Characteristics of Simple Manual Control Systems. Tech. Rep. 111, Lincoln Lab., MIT, Apr. 1956.

## 10. MEASURED INFORMATION CAPACITY AS A PERFORMANCE INDEX IN MANUAL TRACKING TASKS

*Patrick A. Gainer*

*Langley Research Center, NASA*

Two applications of the concepts of information theory to the assessment of human performance in compensatory tracking tasks are presented. One analyzes the input and output of the whole system, treating as noise any part of the output that is not correlated to the input through a linear dynamic system. The second application considers only the tracking error signal and the filtering operations that must be performed on it. Although the second approach is rather crudely approximated, it shows that the human operator may logically use his information capacity in ways which are not made apparent by linear analysis of throughput. Until more is learned of the internal dynamics of the human operator, there is little hope for the discovery of a single performance index for evaluation of control and display systems.

The evaluation of display and control systems by experiment is frequently indecisive because of intersubject variability. It is especially confusing when subjective ratings do not correlate with objective performance measures, or when the designer of the system can make it perform better than can experienced pilots. It is sometimes said that the pilot is biased against new devices and adjusts his performance to back him up. The designer, of course, is completely unbiased.

One of the roots of the problem is that there is no certainty about what criterion the man uses to optimize his performance. This being the case, there is no certain way of evaluating the correlation, or lack of correlation, between subjective and objective tests.

Considering the man-machine system as a communication channel, it is certain that any mismatch between different components in the system will reduce the capacity of the system. Measurements of the rate of transmission of information through the system may conceivably furnish indices that correlate more strongly with subjective evaluations.

This paper begins by reviewing those basic concepts of information theory which are pertinent. These concepts are contained in reference 1. Next, a method of computing information rate from the input and output signals of the overall system is derived. Then a method of estimating an upper limit of the human operator's information capacity from the tracking error alone is described. This latter approach deals with the irremovable errors of filtering random signals. It is concluded that no single linear performance measure can show whether a human operator is using his information capacity efficiently.

### BASIC CONCEPTS

The truly fundamental concept of information theory is that of entropy as a measure of disorder of the state of a time-varying quantity. The greater the entropy of a variable, the

more difficult it is to observe or to transmit. Entropy is defined, for a continuous variable, in terms of its probability density function. The entropy  $H(x)$  of signal  $x$  with density function  $p(x)$  is

$$H(x) = - \int_{-\infty}^{\infty} p(x) \log p(x) dx \quad (1)$$

If the density function is gaussian,

$$H(x) = \frac{1}{2} \log 2\pi e \sigma_x^2 \quad (2)$$

where  $\sigma_x^2$  is the variance of  $x$ . The gaussian density function has greater entropy than any other distribution of the same variance. If the spectrum of the signal is not flat, the geometric mean variance should be used, according to reference 1. The geometric mean variance is defined by

$$\sigma_{x,m}^2 = \exp \frac{1}{W_x} \int_0^{W_x} \log \phi_{xx}(f) df \quad (2a)$$

where  $W_x$  is the frequency above which there is no significant signal power, and  $\phi_{xx}(f)$  is the power spectral density of the signal.

The conditional entropy between two signals is a measure of the uncertainty of one when the other is known. The conditional entropy,  $H_y(x)$ , of signal  $x$  when signal  $y$  is known is expressed in terms of the joint probability density function  $p(x, y)$  and the conditional probability density function  $p(x/y)$  as:

$$H_y(x) = - \int_{-\infty}^{\infty} \int_{-\infty}^{\infty} p(x, y) \log p(x/y) dx dy \quad (3)$$

The maximum of  $H_y(x)$  occurs when one signal gives no information about the other, in which case

$$H_y(x) = H(x) \quad (4)$$

The conditional entropy between a gaussian random signal at time  $t$  and the same signal at time  $t + \tau$  is

$$H(t) [x(t + \tau)] = \frac{1}{2} \log \left\{ 2\pi e \frac{[\phi_{xx}^2(0) - \phi_{xx}^2(\tau)]}{\phi_{xx}(0)} \right\} \quad (5)$$

where  $\phi_{xx}(\tau)$  is the autocorrelation function of signal  $x$ . (Eq. (5) is not given in ref. 1 but was derived from probability density functions given in ref. 2.)

The rate of transmission through a channel is defined as the entropy per symbol or per second of the entering signal less the conditional entropy rate of the entering signal when the received signal is known. Thus, for input  $x$  and output  $y$ ,

$$R_{xy} = H(x) - H_y(x) \quad (6)$$

Alternatively,

$$R_{xy} = H(y) - H_x(y) \quad (7)$$

If  $H(x)$  is the entropy per symbol, it may be multiplied by the rate at which independent symbols enter the channel to obtain entropy per second. The independent symbol rate for a continuous signal is the Nyquist sampling rate, which is twice the signal bandwidth.

The capacity of a channel is defined as the maximum of the information rate when all possible sources are considered for the input signal.

In determining the conditional entropy, one may allow the possibility that the signal  $y$  is not intended to be a one-to-one replica of  $x$ , but may be some consistent transformation of it. A noise-free transport delay, for example, may or may not be considered as impairing the certainty of the transmitted signal, depending upon the use to which the signal is to be put. Any other linear or nonlinear transformation may be treated in similar fashion. Only that part of the signal  $y$  which does not correlate with  $x$  through the allowable transformation or set of transformations is treated as error.

## POSSIBLE APPLICATIONS TO ANALYSIS OF HUMAN PERFORMANCE

The present concern is with manual compensatory, or null-seeking, tracking tasks. As shown in figure 1 the net motion  $E$  of the controlled plant is the sum of an unknown external input, detoned  $M$ , and output  $M'$  generated by the human operator. The information rate of the operator is then

$$R_{MM'} = 2W_{M'}H(M') - H_M(M')2W_{M'} \quad (8)$$

The input  $M$  is usually a gaussian random variable in order to get maximum entropy for a given power. The signal  $M'$  is then usually not significantly different from gaussian, and its entropy per second maybe expressed in terms of its power spectrum as

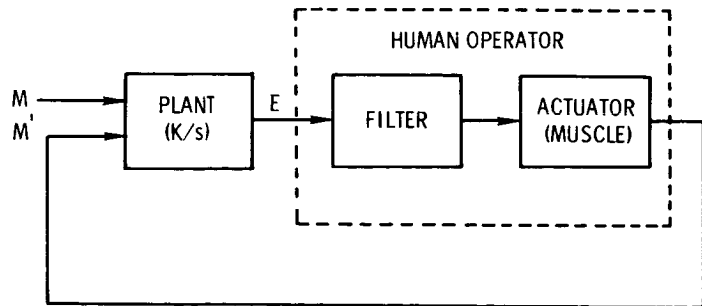


Figure 1. —Block diagram of compensatory tracking task.

$$2W_{M'}H(M') = \int_0^{W_{M'}} \log \Phi_{M'M'}(f) df \quad (9)$$

In determining the conditional entropy  $H_M(M')$  it must be allowed that the human controller may be trying to generate  $M'$  which is not an exact replica of  $M$ , perhaps because he wants some visible information about the input  $M$ . Given only input and output functions, the most general transformation that can be analyzed is a linear dynamic system. In that case, the linearly uncorrelated part of the output spectrum is used in calculating the conditional entropy rate  $2W_{M'}H_M(M')$ . Thus,

$$2W_{M'}H_M(M') = \int_0^{W_{M'}} \log \left\{ [1 - \gamma^2(f)] \Phi_{M'M'}(f) \right\} df \quad (10)$$

where  $\gamma(f)$  is the coherency function defined by

$$\gamma^2(f) = \frac{|\hat{\Phi}_{MM'}|^2}{\hat{\Phi}_{MM}\hat{\Phi}_{M'M'}} \quad (11)$$

Combining equations (8), (9), and (10) the information rate becomes

$$R_{MM'} = \int_0^{W_{M'}} \log \hat{\Phi}_{M'M'}(f) df - \int_0^{W_{M'}} \log \left\{ [1 - \gamma^2(f)] \hat{\Phi}_{M'M'}(f) \right\} df \quad (12)$$

Equation (12) may also be written

$$\begin{aligned} R_{MM'} &= \int_0^{W_{M'}} \log \hat{\Phi}_{M'M'}(f) df - \int_0^{W_{M'}} \log [1 - \gamma^2(f)] df \\ &\quad - \int_0^{W_{M'}} \log \hat{\Phi}_{M'M'}(f) df \end{aligned} \quad (13)$$

$$= - \int_0^{W_{M'}} \log [1 - \gamma^2(f)] df \quad (14)$$

$$= \int_0^{W_{M'}} \log \left[ \frac{1}{1 - \gamma^2(f)} \right] df \quad (15)$$

Equation (15) gives the true information rate only if the whole system, including the man, is a linear dynamic system. An estimate of the human operator's information capacity may be obtained by considering how certain necessary filtering operations are influenced by the characteristics of the tracking error.

The tracking error signal is the source of the operator's information and is also, at least in part, the result of his operations. This information must be extracted by the operator by some filtering process which must produce as an output a command to his muscular system (denoted "actuator" in the diagram). There is a delay in this filter-actuator as is evidenced by the fact that some time elapses before the operator begins to respond to an unpredictable stimulus. In continuous tracking, the delay is counteracted by anticipation. The filter, then, must predict the proper command. Prediction of random signals cannot be done without error, which therefore places an upper limit on the information capacity of the operator. Other operations of the filter, which include deduction of time derivatives and combining them into proper commands, may further limit the capacity, but these operations will not be considered in this paper.



The errors of a prediction filter can be calculated if the impulse response of the filter and the autocorrelation function of the input to the filter are known. The theory and methods for calculating these errors are given in reference 2. Generally speaking, these methods would be difficult to use when the autocorrelation function is known only through numerical analysis, and not as an equation. The simplest prediction filter is one which computes the future value as a constant times the present signal. In terms of the normalized autocorrelation function of the tracking error  $\rho_{EE}(\tau)$  this prediction takes the form

$$\hat{E}(t) = \rho_{EE}(\tau)E(t - \tau) \quad (16)$$

and the mean-square error of prediction is

$$\sigma_{\hat{E}}^2(t) = \varphi_{EE}(0) \left[ 1 - \rho_{EE}^2(\tau) \right] \quad (17)$$

where  $\varphi_{EE}(0)$  is the mean-square tracking error.

The information rate through the prediction filter is considered to be the limiting factor in defining the information rate of the controller, and so is designated  $R_{EM'}$ . This rate, in bits per independent sample, is

$$R_{EM'} = H[E(t)] - H_E(t - \tau) [E(t)] \quad (18)$$

where  $H_E(t - \tau) [E(t)]$  is the entropy of the prediction error.

Using previously given definitions of entropy and assuming that both the tracking error and the prediction error have gaussian probability density functions, equation (18) may be written as

$$R_{EM'} = \frac{1}{2} \log_2 \varphi_{EE}(0) - \frac{1}{2} \log_2 \left\{ \varphi_{EE}(0) \left[ 1 - \rho_{EE}^2(\tau) \right] \right\} \quad (19)$$

or simply

$$R_{EM'} = \frac{1}{2} \log_2 \left[ \frac{1}{1 - \rho_{EE}^2(\tau)} \right] \quad (20)$$

An estimate of the information rate in bits per second can be made if the time between independent samples of the tracking error is known. This sampling period is, of course, related to the signal bandwidth, which is difficult to define even when the power spectrum of the signal is known. For the sake of obtaining a reasonable relative estimate of sampling period, it is suggested that the value of  $\tau$  at the point where the normalized autocorrelation function is 0.50 be used. (It is not the intention here to say that the human operator is sampling, but that the results of his operations could be represented by discrete samples with  $R_{EM'}$  binary digits taken  $1/\tau_s$  seconds apart.)

The primary purpose of this simplified analysis of prediction errors has been to obtain an expression that illustrates certain trends, rather than a true expression for information rate or capacity. Whatever might be the nature of the tracking error autocorrelation before the operator begins controlling, it will change afterward. Therefore, the operator has, to some degree, control over his own information capacity. The usual result of attempts to reduce the amplitude of the tracking error is a decrease in the value of  $R_{EM'}$  (bits per sample).

While the sampling rate may increase to keep the information rate per second constant or nearly so, the usefulness of the information changes. For example, if the operator must attend to several tasks, it would be to his advantage to control so as to keep the value of  $R_{EM}'$  high. In such a case, the operator probably does sample each task, and his output may be discontinuous as well. The information rate  $R_{EM}'$  will also be relatively high when the operator desires to minimize the physical effort of control. Experienced pilots often respond to the velocity of the tracking error in order to minimize effort. When peak displacement has been reached, the control is relaxed with the expectation that the external disturbance will move the tracking error toward zero. In both cases, the operator's output may be very nonlinear. The uncorrelated remnant may make up a large percentage of the tracking error.

The operator's information capacity  $R_{EM}'/\tau_s$  may be used in a number of ways which may seem to be inefficient if judged by the linear measure  $R_{MM}'$ . The operator's use of his capacity should be judged according to how well his weighting of several indices, including tracking error amplitude,  $R_{EM}'$ , and physical effort, satisfies the mission objectives.

### EXPERIMENTAL DATA

A few runs of a more comprehensive tracking experiment have been analyzed to date. These runs were single-axis tasks, two of roll and one of pitch control. The controlled plant was a single integrator (K/s). Two subjects, one an experienced test pilot and the other an engineer with laboratory tracking experience, performed the three tasks. Figure 2 shows the displays used and the normalized root-mean-square tracking errors.

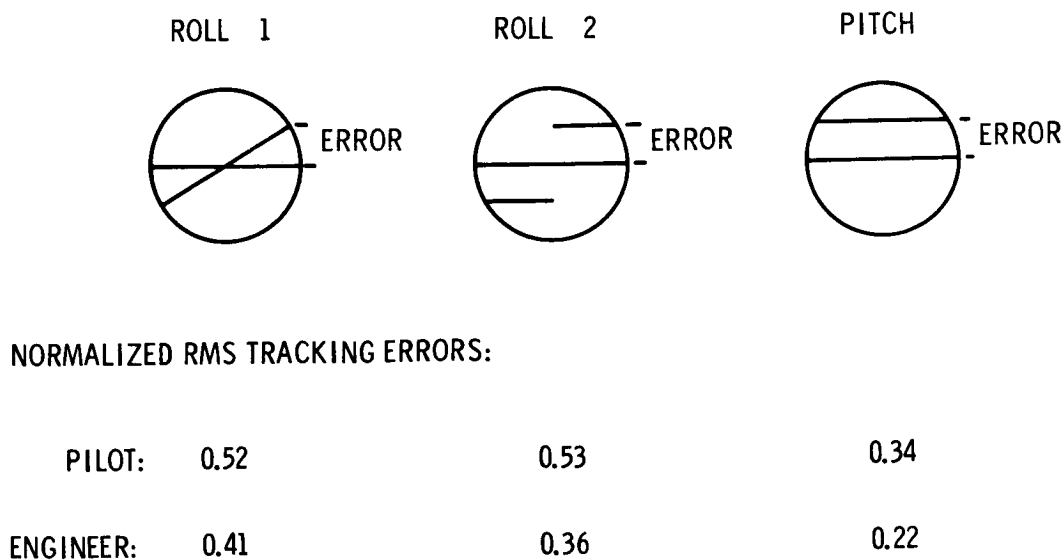


Figure 2. —Displays used and typical results of tracking experiments.

Perhaps the differences in performance should not be disturbing; however, they are consistent and favor the engineer. Figure 3 shows plots of  $\log_2 [1/(1 - \sqrt{2}(f))]$  against frequency. Areas under these plots are the information rates by the first approach. Again, the results are in favor of the engineer. If the pilot is doing his best, he is doing it either very "noisily" or in a very nonlinear manner.

The pilot commented that he used a rate control technique to reduce his effort. In his opinion, the peak error was little or no greater than would have occurred had he responded to each displacement, and he did not get the feeling that he was fighting himself. His control output was pulse-like, with periods of no output separating the pulses.

Normalized autocorrelation functions of the tracking error signals are shown in figure 4. The value of  $R_{EM}'$  (bits per sample) is shown in each plot, and the sampling period  $\tau_s$  is indicated by the dashed line. A reaction time of 0.2 second was used in calculating  $R_{EM}'$ .

All the indices referred to thus far are listed in table 1.

The capacities  $R_{EM}'/\tau_s$  are about the same throughout. (These capacities are only relative, of course, because of the assumptions made in defining them.) Comparing  $R_{MM}'$  with  $R_{EM}'/\tau_s$  would seem to show that the pilot is making less efficient use of his information capacity than the engineer. Actually, there is not sufficient information to justify this conclusion. The engineer subject had a preconceived notion of best control as being minimization of error by working at the highest possible frequency. The pilot sensed a diminishing return with regard to error amplitude as he worked harder. If the sampling frequency  $1/\tau_s$  is considered as an indication of physical effort, the pilot would have had to work about twice as

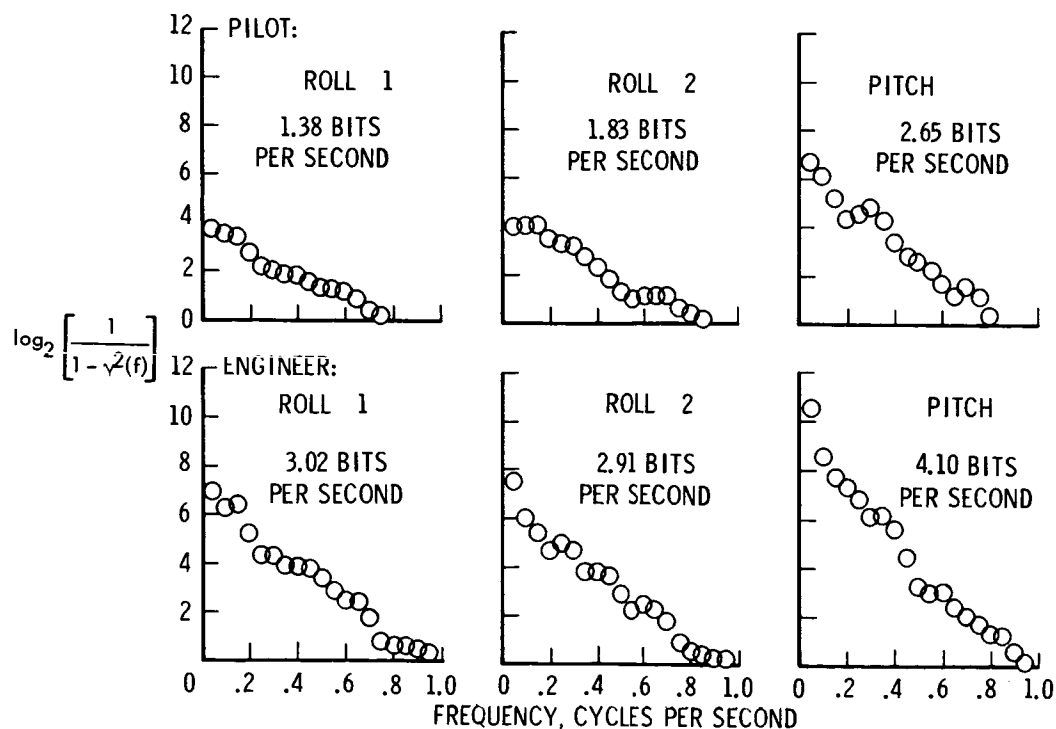


Figure 3. —Logarithm of ratio of signal-plus-noise to noise versus frequency.

hard to get a 50-percent improvement in tracking error. If the pilot had reduced his effort by adopting a low-gain linear control technique rather than the nonlinear pulse-like technique, his values of  $RMM'$  might have been as high as those of the engineer. While the pulse-like control reduces the long-term linear correlation between input and tracking error, during the time when no control is exerted the correlation is perfect, so that the pilot probably knew more about the characteristics of the input  $M$  than did the engineer. It is quite likely, then, that the pilot was making efficient use of his information capacity.

Obviously the pilot considered himself to be holding attitude in level flight through turbulent air, a task in which returning to correct attitude in minimum time is not the objective. Had he been practicing a gunnery run or a landing maneuver, his criteria would have been different.

It might be possible to design a control-display system that forces the pilot to minimize the tracking error, without regard for effort or predictability. If that kind of performance is not essential to mission success, the pilot should, and probably would, complain.

In conclusion, it may be seen that there is no single index by which the performance of different subjects, or the performance of the same subject on different missions may be compared. A consideration of several indices and the comments of the subjects may allow an estimate as to whether each subject is making best use of his information capacity. Further studies of the human operator as an information channel which performs receiving, decoding, encoding, and transmitting functions may yield more definite answers in the future.

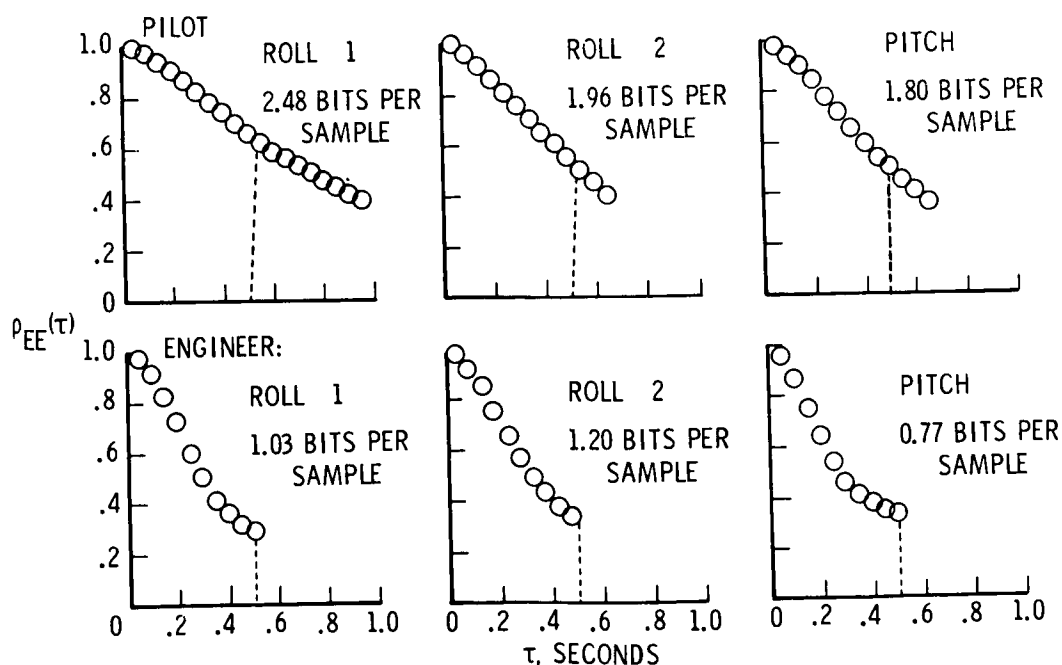


Figure 4. —Normalized autocorrelation functions of tracking error.

TABLE 1.—VARIOUS PERFORMANCE INDICES

	$R_{MM}'$ , bits/sec	$\sigma_E/\sigma_M$	$R_{EM}'$ , bits/sample	$\tau_s$ , sec/sample	$R_{EM}'/\tau_s$
Pilot					
Roll 1	1.38	0.52	2.48	0.74	3.35
Roll 2	1.83	.53	1.96	.55	3.68
Pitch	2.65	.34	1.80	.49	3.56
Engineer					
Roll 1	3.02	0.41	1.03	0.30	3.50
Roll 2	2.91	.36	1.20	.34	3.49
Pitch	4.10	.22	.77	.27	2.84

## REFERENCES

1. Shannon, C. E.: A Mathematical Theory of Communication. The Bell System Technical Journal, vol. 27, no. 3, July 1948, pp. 379-423.
2. Lee, Y. W.: Statistical Theory of Communication. John Wiley & Sons, Inc., 1960.

# MULTIVARIABLE CONTROL

67-15862

## 11. HUMAN PERFORMANCE IN SINGLE- AND TWO-AXIS TRACKING SYSTEMS\*

*E.P. Todosiev, R.E. Rose, and L.G. Summers*  
*TRW Systems*

A compensatory tracking experiment was performed on single and uncoupled two-axis tracking systems to determine the effects of training and task difficulty on the parameters of a describing function model of the human operator. The plant dynamics were identical in both the single-axis system and the symmetrical two-axis system. Second-order dynamics consisting of a pure integration and first-order lag were used. Task difficulty was varied by changing the magnitude of the lag time constant and the frequency bandwidth of the input disturbance. Linear second-order describing functions, obtained by a model matching technique, were used to model the operator's performance.

Analysis of system tracking error showed that the rate at which error decreased with training was dependent upon task difficulty. The amplitude ratio and phase lead of the model describing function increased with training, indicating an increase in open-loop bandwidth and a decrease in phase margin. Increasing the plant lag time constant resulted in an increase in the model lead time constant and a decrease in the zero frequency gain. No significant difference was found to exist in the tracking error per axis between the two-axis tasks and the single-axis tasks. However, the model lead time constant was significantly greater in two-axis tracking.

Human tracking performance in compensatory tracking systems has commonly been described by linear dynamic mathematical models. The model parameters obtained can be related to the dynamic characteristics of the tracking system and are consequently of value in the design and analysis of such systems. Primarily, the model parameters are dependent on the plant dynamics and the nature of the forcing function. However, the model parameters also depend on the training level of the human operator. Determination of this latter dependence was the primary consideration in the study as no knowledge of this relationship was available. The effect of task difficulty on training was also evaluated. A secondary consideration in the study was the effect of plant dynamics and the forcing function on the model parameters. A comprehensive analysis of this effect may be found in reference 1.

Both single and uncoupled two-axis tracking systems with symmetrical plant dynamics were analyzed. Linear second-order describing functions, obtained by a model matching technique, were used to model the operator's performance. Task difficulty was varied by changing the plant dynamics and the frequency bandwidth of the input disturbance.

---

\* This work was supported by the National Aeronautics and Space Administration under Contract NAS 1-4419.

## EXPERIMENTAL DESIGN

Training and performance experiments were conducted on two manual control systems in which the human operator performed compensatory tracking of a spot on a CRT using a finger-tip controller. One system was restricted to single-axis control and the other to two-axis control with symmetrical uncoupled plant dynamics. Figure 1 illustrates the configuration of the single-axis tracking system used. This system was a simulation of the roll attitude control system typical of fighter-type aircraft and consequently represents a realistic control task. The plant dynamics used had the following form:

$$G(s) = \frac{\phi}{\delta_a}(s) = \frac{K}{s(T_s + 1)}$$

Specifically

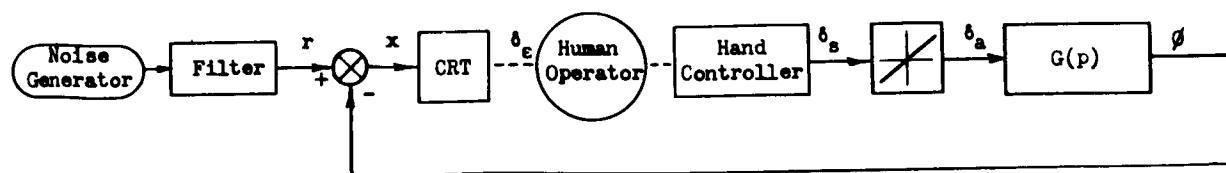
$$K = TL_{\delta_a} = 5.15 \left( \frac{\text{roll deg/sec}}{\text{aileron deg}} \right)$$

where  $L_{\delta_a}$  is the roll angular acceleration per unit aileron angular deflection and  $T$  is the lag time constant. For a maximum stick deflection of  $20^\circ$ , two plant dynamics were chosen according to reference 2 to give both satisfactory and unsatisfactory control tasks. With a time constant of 0.3 second, the control is satisfactory (Cooper rating = 3) while with a 3-second time constant the control is unsatisfactory (Cooper rating = 5).

TABLE 1. — CONTROL-TASK PARAMETERS

Task	$\omega_b$ , rad/sec	T, sec
1	0.2	0.3
2	.2	3.0
3	1.0	.3
4	1.0	3.0

In the two-axis experiment, two channels identical to the system shown in figure 1 were used. Four control tasks exhibiting a progressive increase in control difficulty were formulated for the experiment and were common to both the single- and two-axis phases. Specifically, the tasks were defined as shown in table 1.



- $r$  = input roll angular disturbance (roll degrees)
- $x$  = tracking error (roll degrees)
- $\phi$  = roll angle (roll degrees)
- $\delta_e$  = visual angle (eye degrees)
- $\delta_s$  = angular stick deflection (stick degrees)
- $\delta_a$  = angular aileron deflection (aileron degrees)

Figure 1. —Single-axis tracking system.



The variable  $\omega_b$  represents the break frequency of the third-order input filter while  $T$  represents the time constant of the plant dynamics. In two-axis tracking, a separate gaussian noise generator was used for each axis to insure that the correlation between the two inputs would be zero.

The experimental design was a split plot factorial with single-axis versus two-axis tracking as the between-group variable. The within-group variables were task difficulty and number of sessions. There were four replications within each session. A random sample of three subjects was used within each group. The a priori reasons for the choice of number of axes as the between group variable was that there might be a transfer of training effect when a subject goes from a single to a two-axis task or vice versa. Subjects with former tracking experience were used. Experimental runs were of 3 minutes duration, and only the central 2 minutes were scored.

The run schedule for the single-axis group was divided into eight sessions, where the first six sessions constituted the training period and the last two sessions were the performance sessions. In half of the training and performance periods, the single-axis experiment was performed with the system error ( $x$ ) displayed vertically on the CRT display, while in the other half the error was displayed horizontally. A vertical error required that the operator manipulate his fingertip controller in a vertical plane while a horizontal error required a horizontal response.

Each session consisted of 48 runs in which each of the two subjects performed four replications of each of the four control tasks. The order of presentation of the tasks was randomized for each subject and each session. Subject fatigue was kept at a minimum by using a rest period of approximately 3 minutes after each replication. Since training was a major variable in the experiment, each subject was given a performance score upon the completion of each replication. The normalized mean-square tracking error was used as the performance measure.

The run schedule for the two-axis phase differed from the schedule given above for the single-axis phase only in that five sessions were used for training instead of six.

The human response data obtained in the performance sessions were analyzed using a continuous model matching technique as described in reference 3. This technique models the human operator's performance by the describing function:

$$H(s) = \frac{\delta_s(s)}{x(s)} = \frac{K(T_1 s + 1)}{(T_2 s + 1)(T_3 s + 1)}$$

where  $s$  is the Laplace operator,  $K$  is the zero frequency gain, and  $T_1$ ,  $T_2$ ,  $T_3$  are the describing-function time constants. An open-loop formulation of the model matching technique was used in obtaining the describing function parameters. Reference 4 gives details of a previous study in which a continuous model matching technique was used to obtain similar human operator models. For tasks 3 and 4, the models obtained accounted for 70 to 80 percent of the human operator's response. In task 2 only 50 to 60 percent of the response was modeled. Task 1 data could not be modeled due to the instability in the parameter adjustment loop caused by the very low frequencies in the human operator's response.

## EFFECT OF TRAINING AND TASK DIFFICULTY ON SYSTEM TRACKING ERROR

In order to analyze the system tracking error, the normalized mean square error was used as a performance measure. Specifically, this measure is defined by

$$\overline{x_N^2} \triangleq \frac{\int_0^2 x^2 dt}{\int_0^2 r^2 dt}$$

which indicates that the integral square error is normalized by the integral square input signal over the 2-minute scoring period. Two analyses of variance tests were conducted to determine significant differences between the variables. The first analysis tested differences during the learning period while the second analysis tested differences during the performance period.

TABLE 2.—ANALYSIS OF VARIANCE ON SYSTEM TRACKING ERROR

Source	Significance level
Training period:	
Tasks	0.01
Training	.001
Task-Training Interaction	.001
Performance period:	
Tasks	.001

In the first analysis the variables were training, number of axes, and task difficulty. For this test the second replicate of the normalized tracking error for each of the first seven training sessions was used as the test score. A score was chosen alternately from the horizontal or the vertical axis of the two-axis tracking scores for testing against the single-axis score. A summary of the significant variables is shown in table 2. This table indicates that task difficulty, training, and training-task difficulty interaction were significant. There was no significant difference between one- and two-axis tracking. To evaluate further the effect of training, the error scores were determined for each task and training session by averaging across subjects. These scores are shown in figure 2 and indicate that the task difficulty varies directly with the task code number; that is, task 4 was the most difficult, and task 2 the least difficult. Figure 2 also indicates that the amount of learning that occurred varied directly with task difficulty; that is, for the more difficult tasks, the amount of learning was greater. This relationship would explain the significant interaction.

The variables of the second analysis were replicates of the performance period, number of axes, and task difficulty. For this test the four replicates of each of the last two sessions were used as test scores. Table 2 shows that for this test the only significant difference was due to task difficulty. The levels of task difficulty, averaged across subjects and replicates, are apparent for the performance sessions shown in figure 2. It should be noted that in this test as in the previous training analysis there was no significant difference between single- and two-axis tracking.

## EFFECT OF TRAINING ON DESCRIBING-FUNCTION PARAMETERS

Human describing-function parameters were examined to determine which parameters a human operator alters when learning a control task. Both single- and two-axis control tasks were analyzed, and emphasis was placed on describing the operator's performance in the frequency domain.

Human describing-function parameters were obtained for the single-axis control tasks 2, 3, and 4 using the model matching technique. In the training phase, only the second replicate in each training session was used while every replicate was evaluated in the two performance sessions of the experiment. The parameters obtained were plotted versus replication R to determine if any correlation existed between the parameters and training. The method of least squares was used to obtain the best linear fit to the variation of the data points with replication. The linear trends obtained for each task were averaged over the three subjects to obtain the average parameter trends as a function of training and are shown in figures 3 and 4. The trends evident in the single-axis system (fig. 3) were an increase in the gain K for task 3 and an increase in the time constant  $T_1$  for task 4. In two-axis tracking (fig. 4) the trends were an increase in the gain K for task 3 and an increase in the time constant  $T_1$  for both tasks 3 and 4. In addition, the lag time constant  $T_3$  increased for task 3 and decreased for task 2.

Further insight into the variation of parameters with training may be obtained by plotting Bode diagrams for the average untrained subject ( $R=4$ ) and the average trained subject ( $R=32$ ). Bode diagrams were used because they give a complete picture of the describing function in the frequency domain and hence provide an overall view of the interactions among the parameters.

In single-axis tracking the Bode diagrams were typically of the form shown in figure 5 for task 4. Examination of the Bode diagrams revealed that over a large frequency range, the amplitude ratio and phase lead increased with training for tasks 2 and 4. Task 4 exhibited the greatest increase in gain and phase lead while task 3 showed relatively little change. Task 3 did exhibit an increase in the zero frequency gain. The system open-loop Bode diagram (human operator plus plant) for task 4

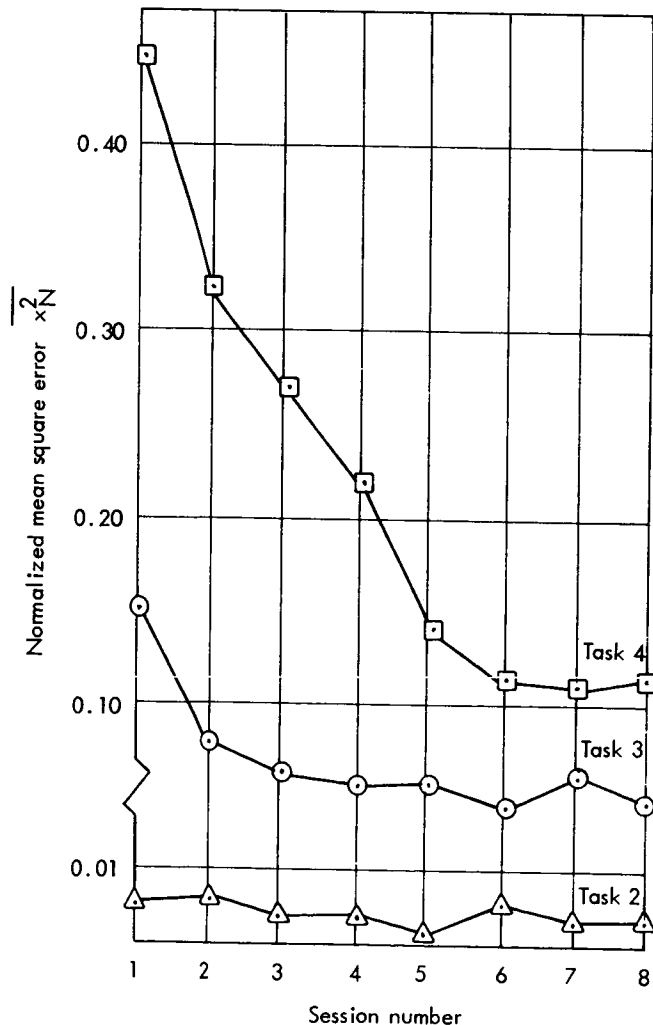


Figure 2.—Learning curves for tasks 2, 3, and 4.

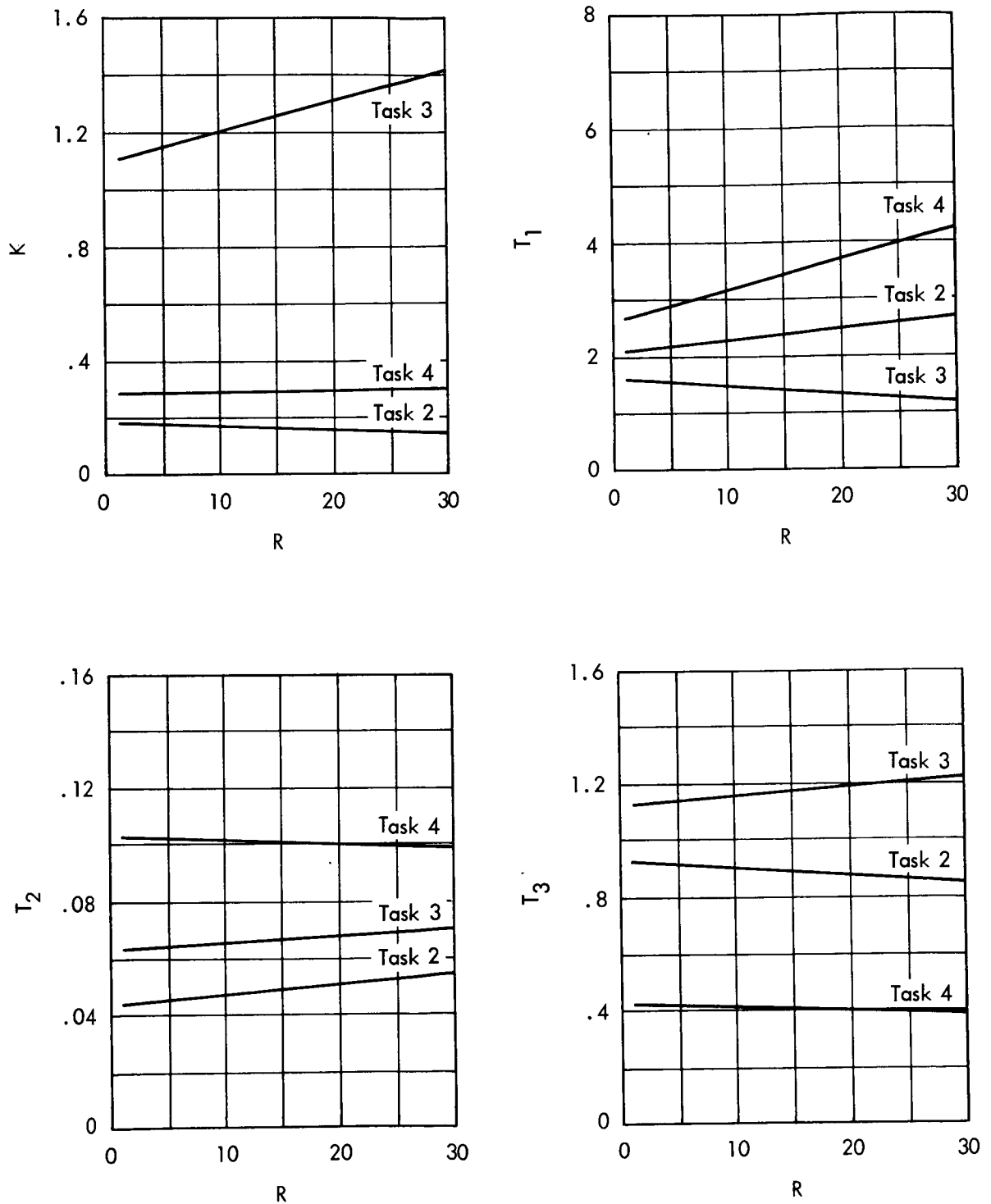


Figure 3.—Average parameter trends for single-axis tracking.

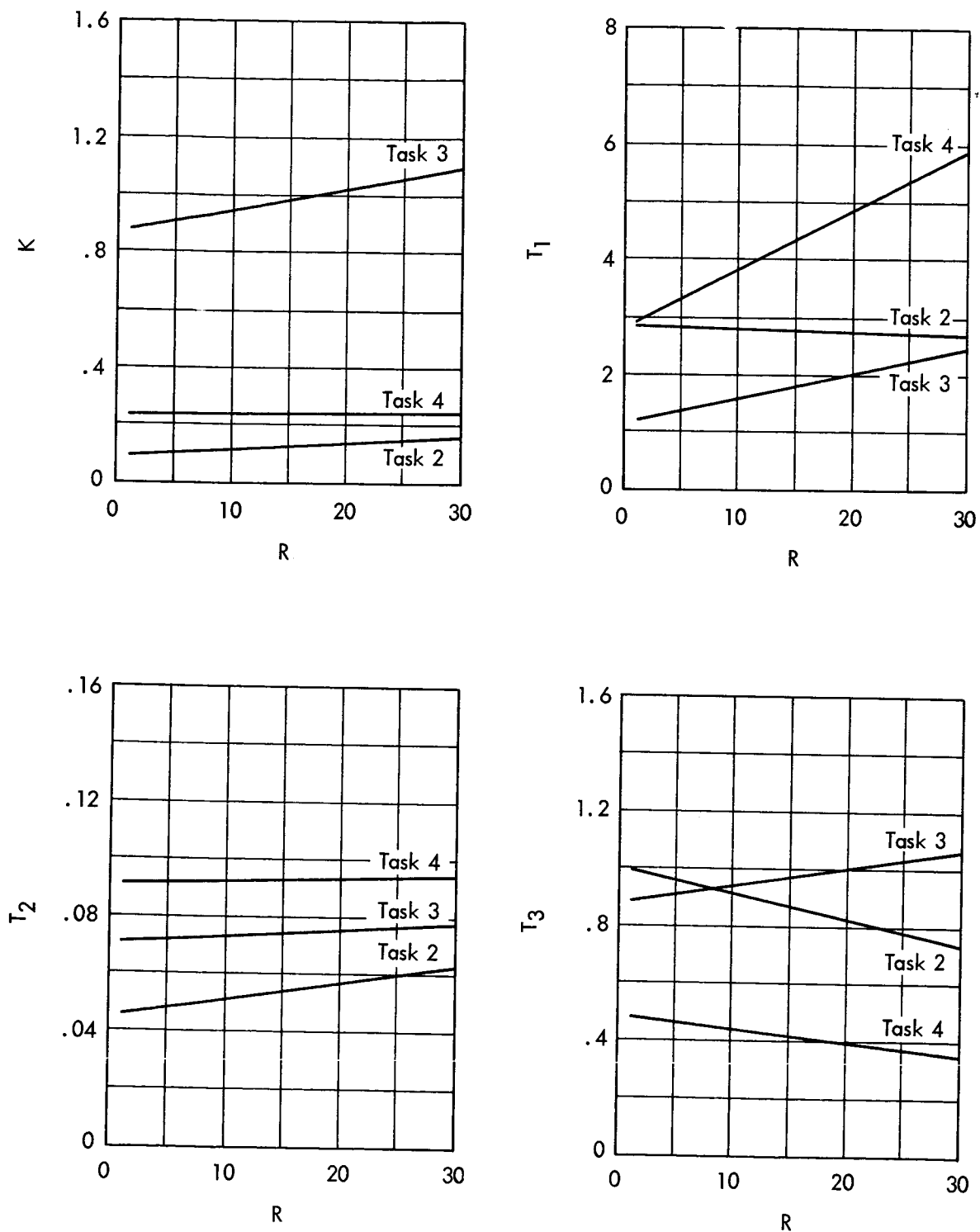


Figure 4.—Average parameter trends for two-axis tracking.

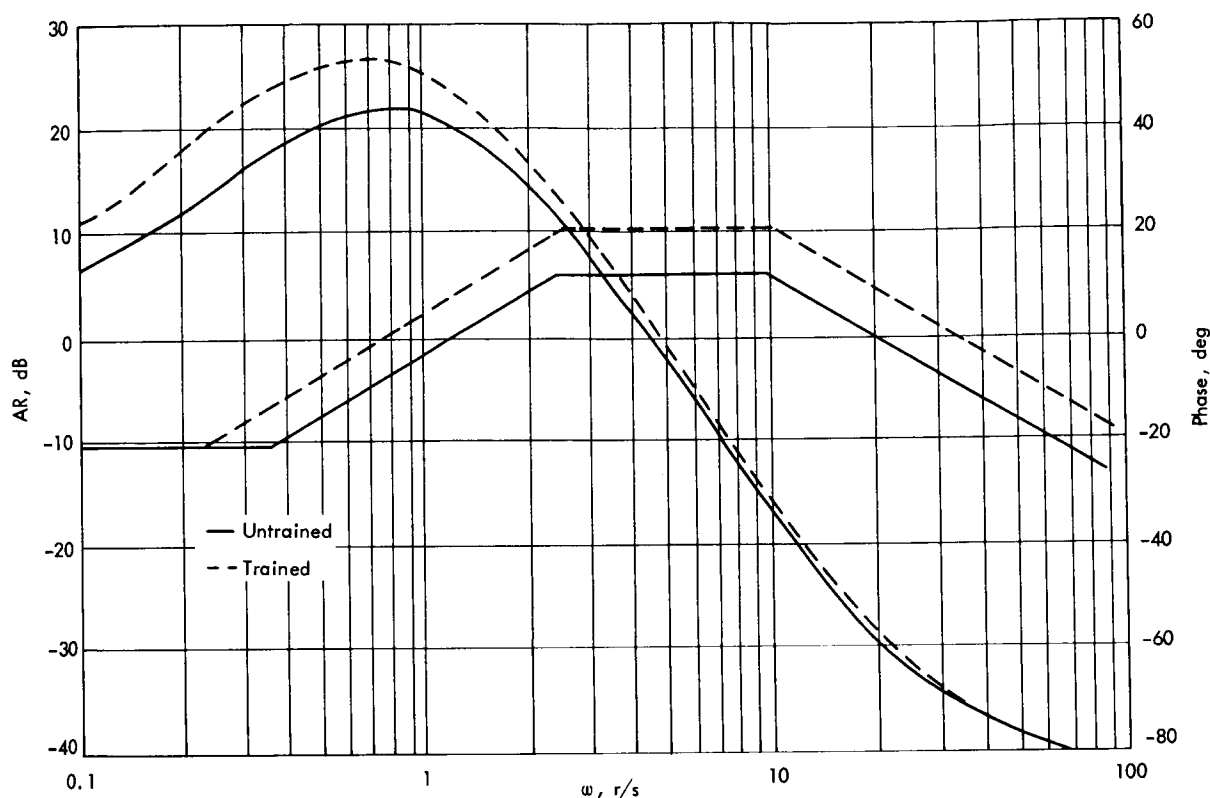


Figure 5.—Average Bode diagrams for task 4 (single-axis).

is shown in figure 6 and clearly indicates an increase in amplitude ratio and phase lead with training. As a result the open-loop bandwidth (i.e., the frequency range over which the amplitude ratio is greater than -3 dB) also increases with training. The phase margin  $\gamma$  shows little change with training and has a value of approximately  $50^\circ$ .

In two-axis tracking, the Bode diagrams obtained for tasks 2, 3, and 4 consistently indicated an increase in the amplitude ratio and bandwidth with training. Figure 7 shows the Bode diagram obtained for task 4. The system open-loop Bode diagram for task 4 is shown in figure 8 and indicates that an increase in amplitude ratio, phase lead, and bandwidth was obtained with training. In addition the phase margin decreased from  $52^\circ$  to  $40^\circ$ .

In the analysis of variance on  $K$  and  $T_1$ , discussed in the following section, training was one of the variables. However, the variation in  $K$  and  $T_1$  due to learning was found to be insignificant. This factor may be due to subject differences, the small sample size, or the internal accuracy limitations of the modeling technique used. Since subjects were treated as a random sample from a population, differences between subjects could not be tested.

### EFFECT OF TASK DIFFICULTY ON DESCRIBING-FUNCTION PARAMETERS

The analysis in the section entitled "Effect of Training and Task Difficulty on System Tracking Error" was concerned with the relative difficulty of the four tasks of the experiment.

This section deals with the correlations obtained between task difficulty and the frequency response of the human operator. Both single- and two-axis tracking data were analyzed.

Bode diagrams obtained for all tasks of the performance period in the single- and two-axis tracking systems were averaged over subjects. The mean amplitude and phase diagrams are shown in figures 9 to 12. An analysis of variance was performed on the describing function parameters  $K$  and  $T_1$  to obtain their significance level. The design of the analysis was identical to that used in the section entitled "Effect of Training and Task Difficulty on System Tracking Error." Tables 3 and 4 summarize the analysis of variance and indicate that the dependencies of both  $K$  and  $T_1$  on tasks were significant at the 0.1-percent level. Examination of the Bode diagrams led to the following conclusions on the correlations obtained between task difficulty and the describing-function parameters:

- (1) The task difficulty (as measured by tracking error) was found to increase significantly with the task code number.
- (2) The rate of decrease of system tracking error with training was dependent upon task difficulty. The more difficult tasks showed a greater degree of learning.
- (3) The human operator model showed a significantly higher zero frequency gain in task 3 than either tasks 2 or 4 because task 3 was more stable as the lag time constant in the plant dynamics was smaller by a factor of 10. For the same reason, the human operator's model lead time constant was significantly greater in tasks 2 and 4.

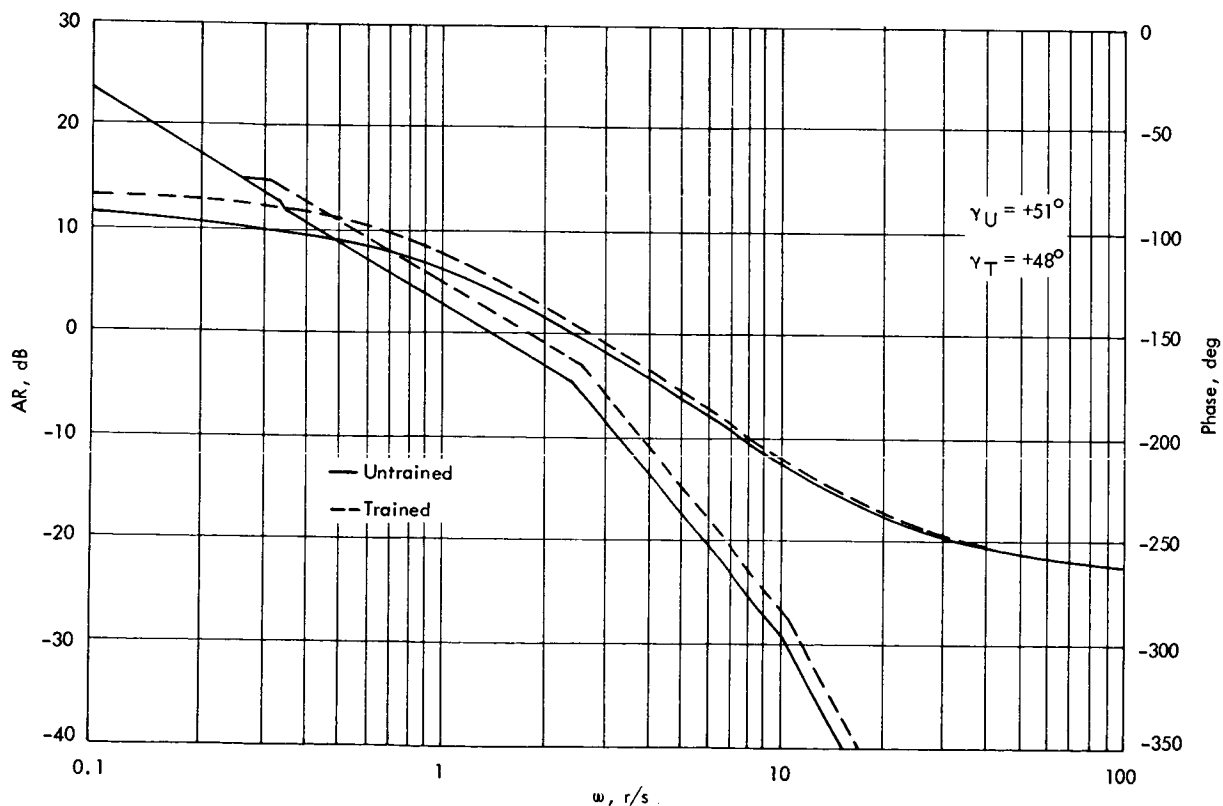


Figure 6.—Average open loop Bode diagrams for task 4 (single-axis).

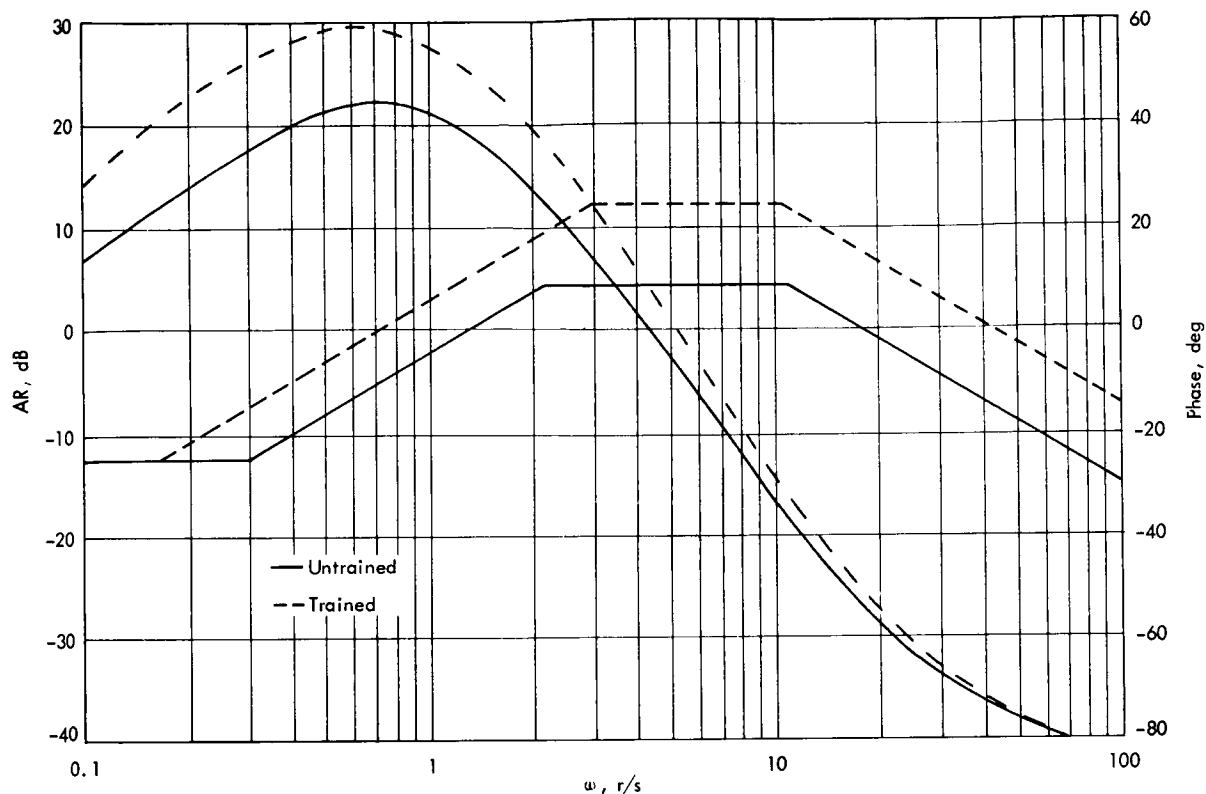


Figure 7. —Average Bode diagrams for task 4 (two-axis).

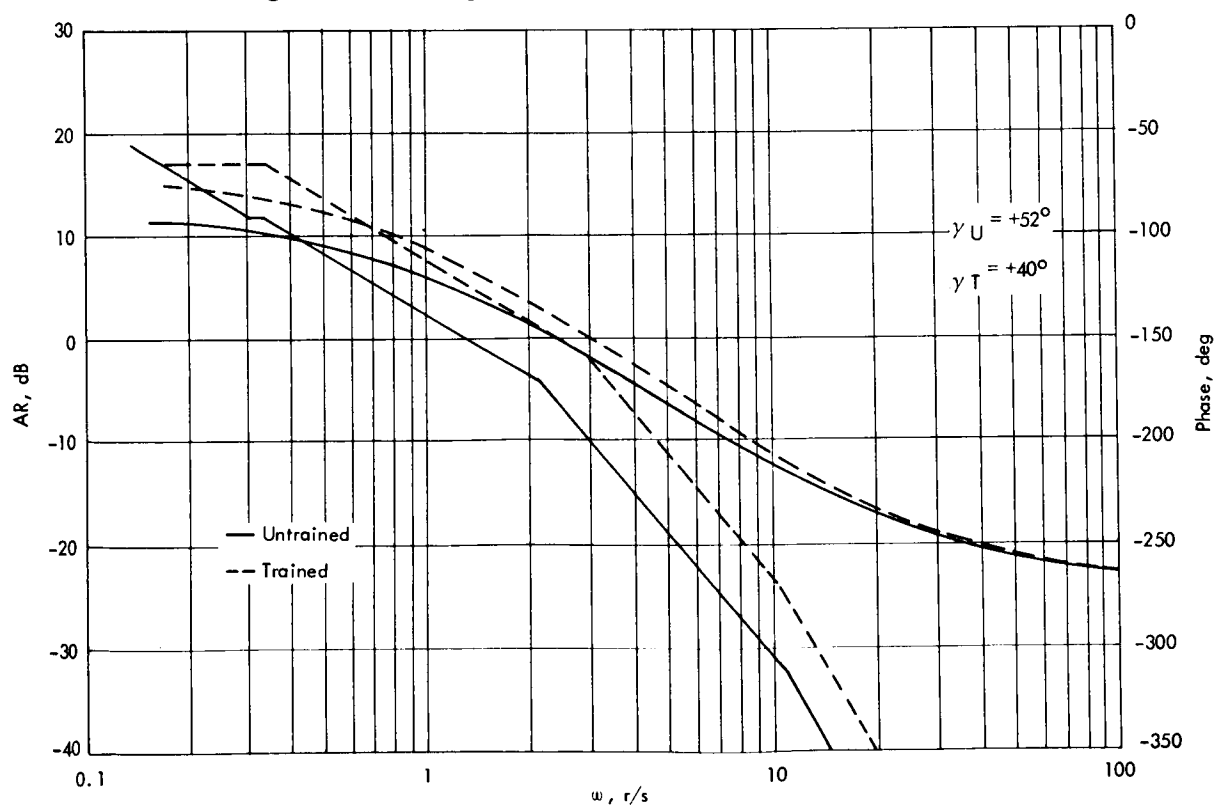


Figure 8. —Average open loop Bode diagrams for task 4 (two-axis).



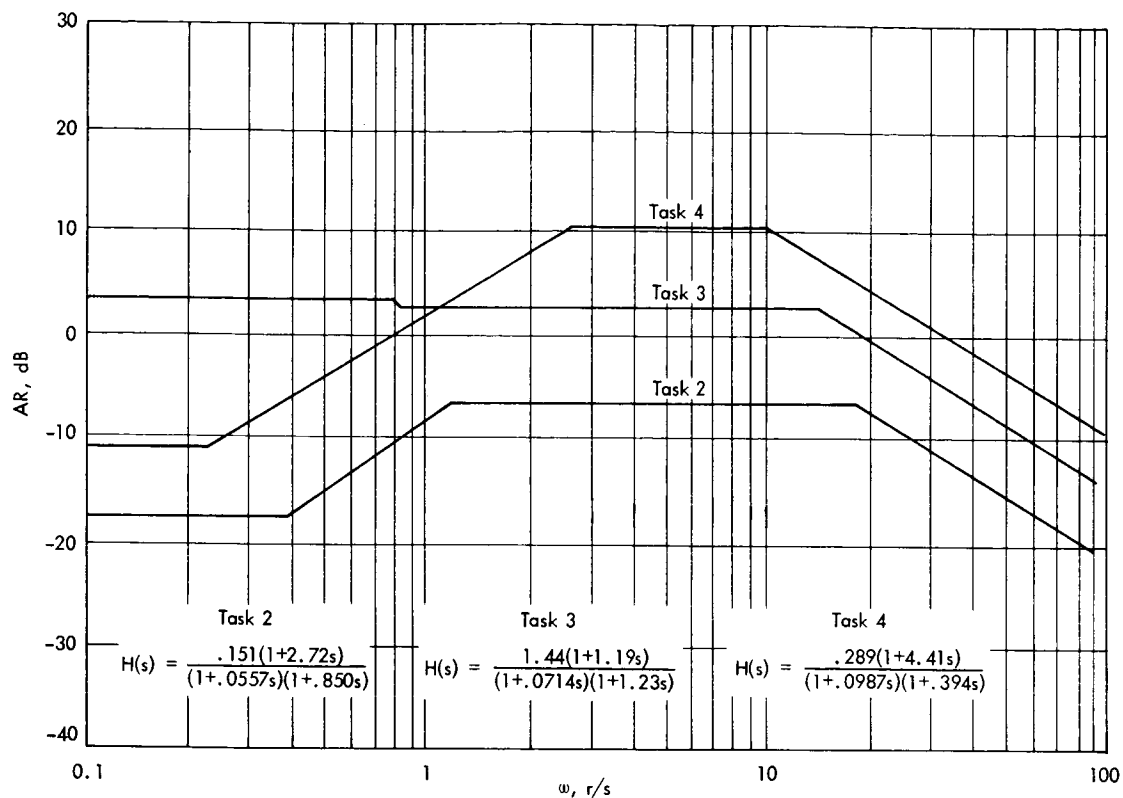


Figure 9.—Mean amplitude ratio diagrams for single-axis tracking.

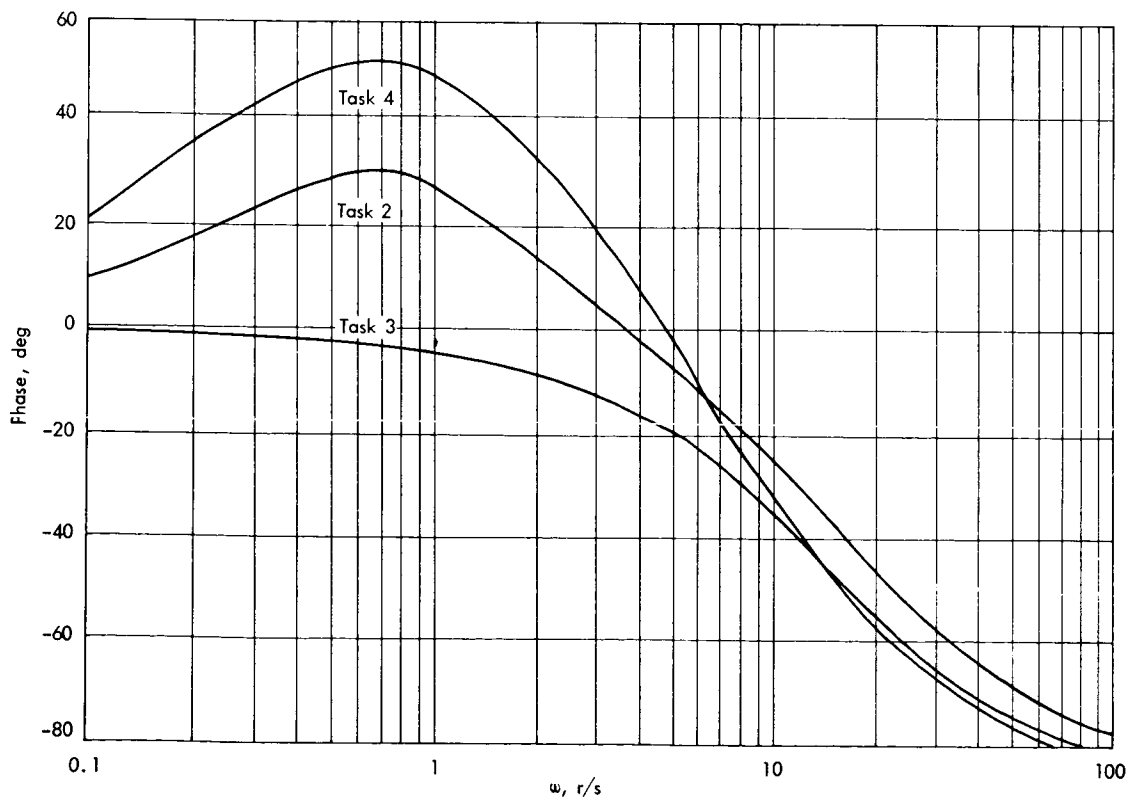


Figure 10.—Mean phase diagrams for single-axis tracking.

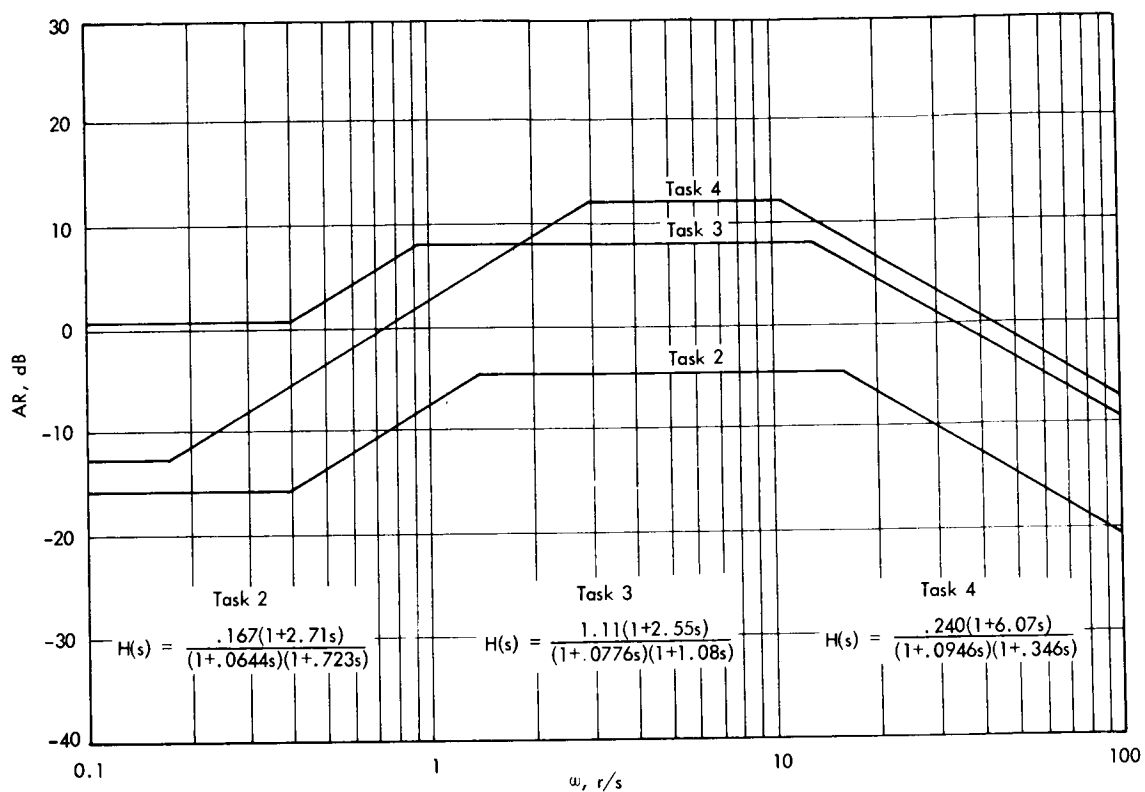


Figure 11. —Mean amplitude ratio diagrams for two-axis tracking.

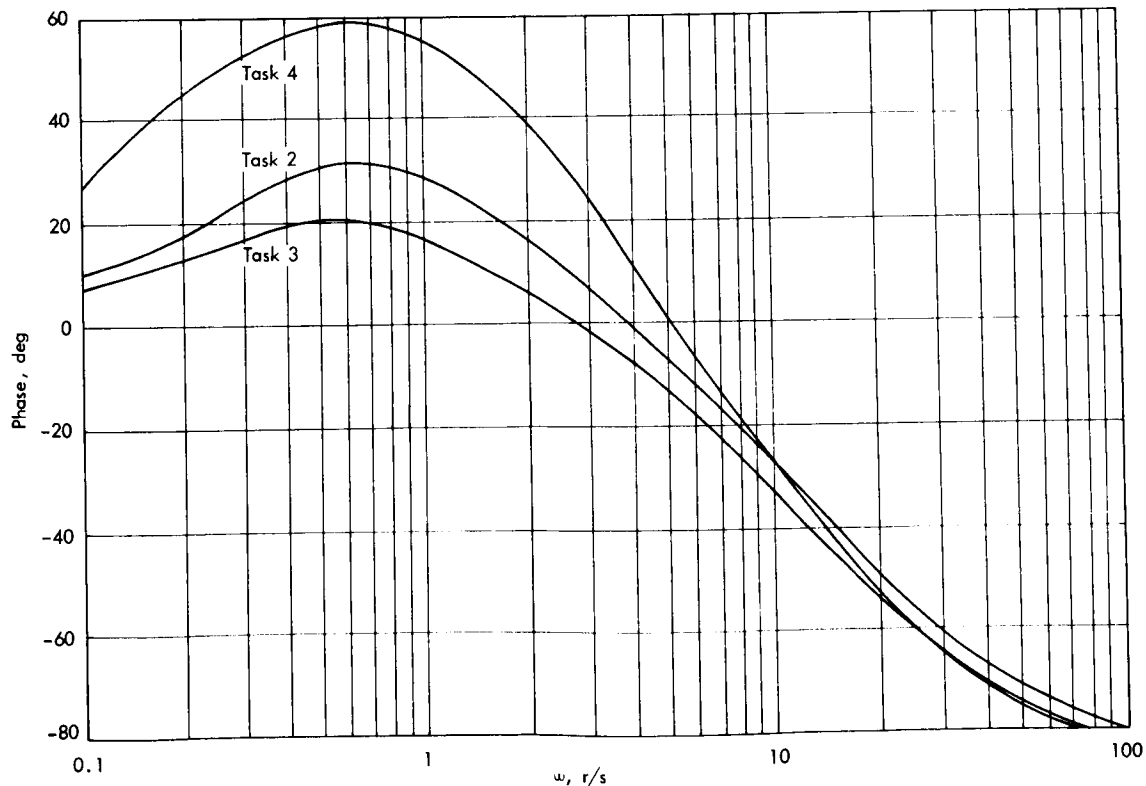


Figure 12. —Mean phase diagrams for two-axis tracking.

TABLE 3.—ANALYSIS OF VARIANCE ON K

Source	Significance level
Training period:	
Tasks	0.001
Performance period:	
Tasks	.001

TABLE 4.—ANALYSIS OF VARIANCE ON  $T_1$ 

Source	Significance level
Training period:	
Tasks	0.001
Performance period:	
Tasks	.001
Task-axis interaction	.05

(4) The operator's model lead time constant was greater in task 4 than task 2 because task 4 was a more difficult task due to the larger input frequency bandwidth.

### COMPARISON OF SINGLE- AND TWO-AXIS TRACKING

A comparison was made between single- and two-axis tracking to determine what differences existed between these two types of control tasks. An analysis of variance performed on the system tracking error for both types of control tasks showed that no significant difference existed between single- and two-axis tracking for all control tasks as far as the system tracking error was concerned (cf. section entitled "Effect of Training and Task Difficulty on System Tracking Error"). However, the analysis of variance for the  $T_1$  data obtained in the performance period (cf. section entitled "Effect of Task Difficulty on Describing-Function Parameters"), showed that the interaction between tasks and single- versus two-axis tracking was significant at the 5 percent level. This interaction is shown explicitly in the values for  $T_1$  averaged across subjects and replicates in table 5 where only tasks 3 and 4 show a difference. For both tasks  $T_1$  was significantly larger in the two-axis tracking system. Bode diagrams obtained from the performance data of the section entitled "Effect of Training on Describing-Function Parameters" are shown in figures 13 to 15. The Bode diagrams in general confirm the analysis of variance data, in that the only large difference between single- and two-axis tracking appears to be the phase angle of tasks 3 and 4.

The fact that system tracking error in either axis of the two-axis group was no greater than that for the single-axis group is not contradictory of earlier results. In reviewing the literature, very few studies have directly tested this difference. In analyzing the results of a study of Chernikoff et al. (ref. 5), there appears to be no difference between one- and two-axis tracking for tasks with controlled elements of position, rate, and acceleration. Recently in results reported in reference 6, no difference was shown between single- and two-axis tracking.

TABLE 5.—AVERAGE  $T_1$  FOR SINGLE- AND TWO-AXIS TRACKING

Task	$T_1$ , sec, for —	
	Single axis	Two axis
2	2.69	2.83
3	1.32	2.09
4	4.13	5.12

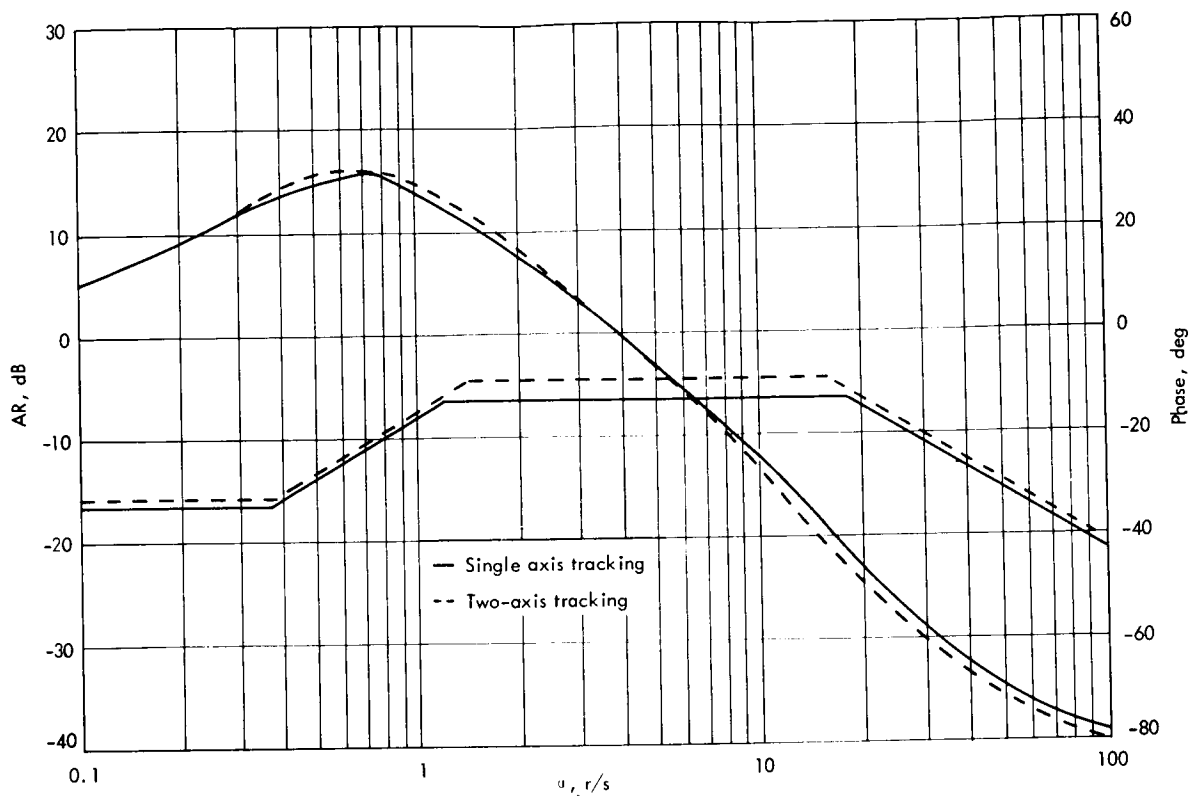


Figure 13. —Bode diagrams of task 2.

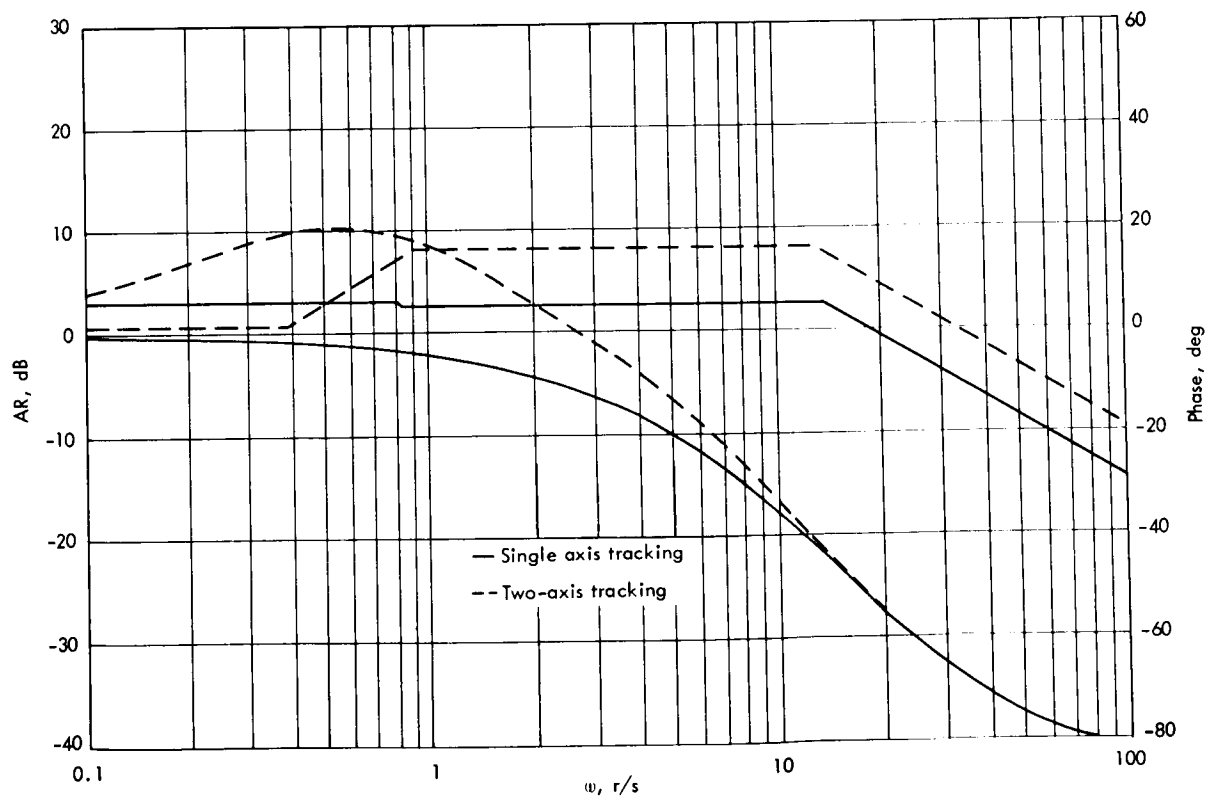


Figure 14. —Bode diagrams of task 3.

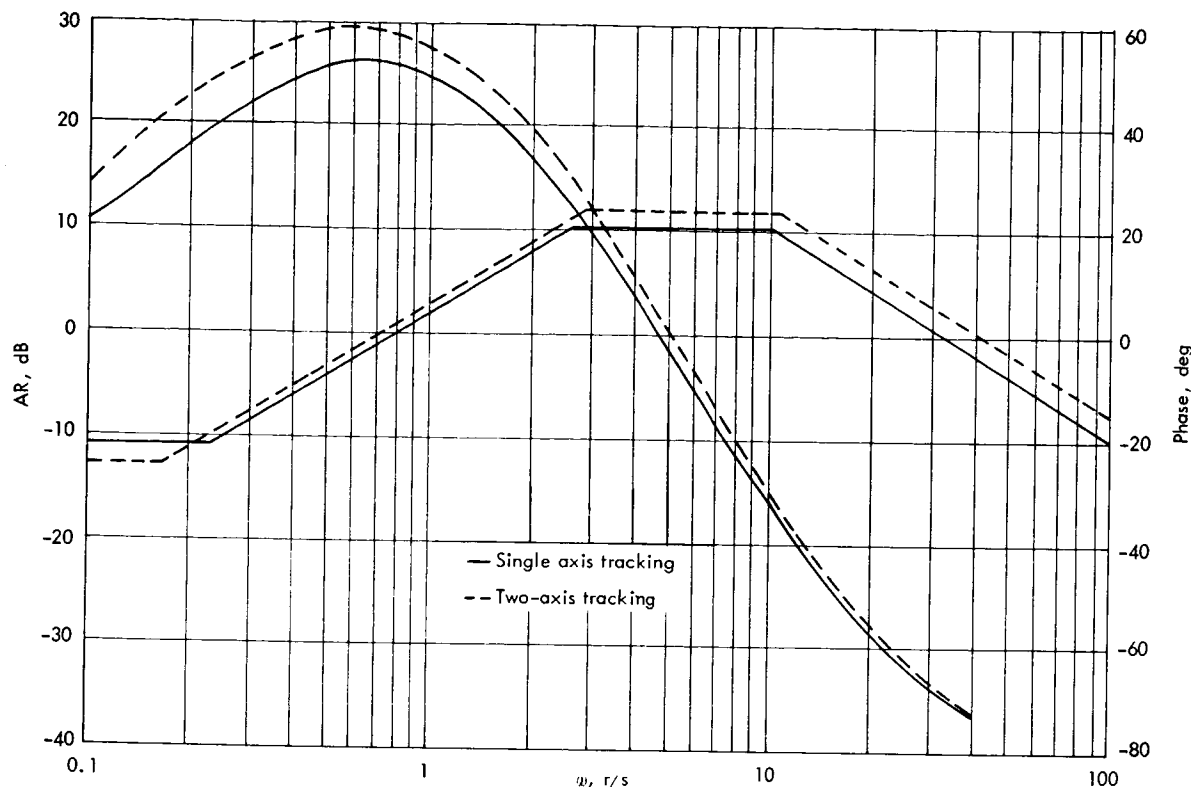


Figure 15.— Bode diagrams of task 4.

## CONCLUSIONS

Experimental data obtained from single- and two-axis tracking experiments were analyzed using continuous matching techniques and conventional control system theory. An analysis of variance was performed on the results obtained to determine their significance level. Conclusions were drawn from the analysis of the human performance data. The following conclusions were reached on the effects of training:

(1) System tracking error decreased significantly for all control tasks in both single- and two-axis tracking during training.

(2) For both single- and two-axis tracking, the average human operator increased his amplitude ratio and phase lead with training as measured from model Bode diagrams. These changes resulted in an increased open-loop bandwidth and a decreased phase margin.

(3) An analysis of variance showed no significant trend to exist in the variation of the parameters  $K$  and  $T_1$  (zero frequency gain and lead time constant) with level of training. Parameters  $T_2$  and  $T_3$  were not tested.

The following conclusions were reached on the results of single- versus two-axis tracking performance:

(1) The system tracking errors in the two-axis tasks were not significantly different from the single-axis tasks. If it is assumed that the subject's information processing

capability is not fully loaded the results of this experiment are plausible. The latter hypothesis could be tested by the addition of more axes with the same input function and dynamics until the subject's performance starts to degrade due to task loading.

(2) For tasks 3 and 4 only, the lead time constant  $T_1$  was significantly larger in models of two-axis tracking than in models of single-axis tracking. Since this difference did not appear in task 2, it can be concluded that  $T_1$  is a measure of difference in operator performance between single- and two-axis tracking only when the input signal bandwidth is sufficiently high.

## REFERENCES

1. McRuer, D.; Graham, D.; Krendel, E.; and Reisener, Wm., Jr.: Human Pilot Dynamics in Compensatory Systems. Tech. Rep. NR AFFDL-TR-65-15, July 1965.
2. Creer, B. Y.; Stewart, J. D.; Merrick, R. B.; and Drinkwater, F.J., III: A Pilot Opinion Study of Lateral Control Requirements for Fighter Type Aircraft. NASA MEMO 1-29-59A, Mar. 1959.
3. Todosiev, E. P.; Rose, R. E.; Bekey, G. A.; and Williams, H. L.: Human Tracking Performance in Uncoupled and Coupled Two-Axis Systems. TRW Systems 4380-6003-R0000, Dec. 1965.
4. Bekey, G. A.; Meissinger, H. F.; and Rose, R. E.: Mathematical Models of Human Operators in Simple Two-Axis Manual Control Systems. IEEE Trans. on Human Factors in Electronics, vol. HFE-6, no. 1, Sept. 1965.
5. Chernikoff, R.; Duey, J. W.; and Taylor, F. V.: Two-Dimensional Tracking with Identical and Different Control Dynamics in Each Coordinate. J. Exp. Psychol., vol. 60, 1960.
6. Bolt Beranek and Newman, Inc.: Studies of Manual Control Systems. Prog. rep. no. 7, May 1965.

183  
N67-15863

## 12. TWO-DIMENSIONAL MANUAL CONTROL SYSTEMS

*William H. Levison  
Bolt Beranek and Newman, Inc.*

Experiments were conducted to determine what modifications to the current models of the human controller of single-variable systems are necessary for them to be good representations of the controller in two-variable situations. These experiments were performed with a single compensatory display and a single two-axis control. Two descriptors of performance were obtained for each axis: the normalized mean squared error, and the describing function. Of prime interest was the extent to which performance on a given axis was modified by the requirement of simultaneously tracking a second axis. Three two-axis control situations were investigated: (1) homogeneous control situation, in which the input power spectra and controlled elements were identical on X and Y; (2) heterogeneous inputs, in which the input bandwidths were different but the controlled elements were identical; and (3) heterogeneous dynamics, in which the controlled-element dynamics were different but the input bandwidths were identical.

Two-axis performance degradation was small when the tracking conditions were homogeneous and when the inputs (but not the dynamics) were heterogeneous. Large and significant performance differences were seen when the dynamics were heterogeneous. In this situation the increase in normalized mean squared error ranged from 15 percent to 125 percent, depending on the subject and the axis under consideration. In addition, there were important changes in the controller's equalization.

Three factors that affect human controller characteristics in two-axis control situations are identified. They are: (1) visual-motor interaction, (2) differential allocation of attention, and (3) nonhomogeneity of required equalization when the controlled-element dynamics are nonhomogeneous.

A simple model has been developed for predicting visual-motor interference effects. Models for the prediction of attention and equalization effects have not yet been developed. Single-axis describing-function models for the human controller should be modified to include the effects of these factors in order to obtain accurate predictions of human-controller characteristics in two-axis situations and probably also in higher dimensional control situations.

Most of the laboratory research on manual control systems directed toward the development of mathematical models for the human controller has dealt with single-loop, single-axis systems (refs. 1 to 3). Mathematical models for the human controller that provide accurate predictions of his behavior over a wide range of single-axis control situations have resulted from these studies. However, most systems of practical importance are multi-variable

systems, and therefore it is important to develop models for the human controller that are applicable to situations in which he is controlling several variables simultaneously.

The research summarized in this report was the first phase of a continuing theoretical and experimental study of multivariable manual control systems. The purpose of this research was to investigate in detail the extent to which the current single-variable models for the human controller apply to two-axis control situations and to determine what modifications to these models are necessary for them to be good representations of human-controller behavior in two-axis situations. A more complete documentation of this research is provided in reference 4.

## BACKGROUND

SINGLE-VARIABLE MODELS.—The most comprehensive discussion of single-variable models of the human controller appears in reference 3 which offers models of varying degrees of complexity to describe human-control behavior in a wide variety of tracking tasks. A simple describing-function model derived from reference 3 that illustrates explicitly the adaptive capabilities of the human controller is:

$$H(s) = K_h \frac{(T_L s + 1)}{(T_I s + 1)} \cdot \frac{e^{-\tau s}}{(T_N s + 1)} \quad (1)$$

The lead-lag term  $(T_L s + 1)/(T_I s + 1)$  is an equalizer which together with the gain  $K_h$  is adjusted by the human controller to achieve a good system performance. The delay  $\tau$  and the lag  $1/(T_N s + 1)$  approximate the dynamic characteristics of the neuromuscular system. Experimentally obtained estimates of  $\tau$  are in the neighborhood of 0.09 second. When tracking with controlled-element dynamics of  $K$  (which is one of the controlled elements used in our experiments), the controller generates a small lead time constant  $T_L$  of about 0.11 second which has the effect of cancelling the effects of the neuromuscular lag. He also employs a lag time constant of  $T_I$  and a gain  $K_h$  such that the gain crossover frequency is in the neighborhood of 8 rad/sec. When tracking with  $K/s^2$  dynamics (the other dynamics used in our experiments) the controller generates a lead time constant of about 5 seconds, has a neuromuscular time constant  $T_N$  of about 0.11 second, and has essentially no equalizer lag  $T_I$ . He adjusts the gain  $K_h$  to achieve a gain crossover frequency of about 4 rad/sec.

TWO-AXIS TRACKING.—A number of investigators have found one-axis two-axis differences in error scores or in describing function parameters (refs. 5 to 8). Todosiev et al. (ref. 5) found that the lead time constant of the human controller's describing function was significantly greater in the two-axis situation than in the single-axis situation for some of the tracking tasks studied. On the other hand, they did not find a significant difference between the two-axis mean squared error performance and the single-axis performance.

Chernikoff et al. (ref. 6) investigated two-axis tracking performance using various pairs of controlled-element dynamics. The controlled dynamics were either  $K$ ,  $K/s$ , or  $K/s^2$ . The subjects were presented with integrated control and display configurations. For a given set of dynamics, they found that performance was best when the dynamics in the two axes were the same. The performance degradation increased as the difference between the X and Y dynamics increased. Duey and Chernikoff (ref. 7) compared single- and two-axis performance when the controlled-element dynamics were either pure acceleration or quickened acceleration.



Statistically significant differences in average absolute error were found when the dynamics were pure acceleration in both axes or more acceleration in one axis and quickened acceleration in the other.

Verdi et al. (ref. 8) also investigated single-axis and two-axis tracking behavior with controlled dynamics of quickened and unquickened accelerations. They found a significant one-axis, two-axis change in the describing function only when one axis was quickened and the other axis was unquickened.

Since these investigators have demonstrated that human controller behavior in a two-axis control situation is different from that in a single-axis system, it is evident that modifications of single-axis human-controller models are necessary to make them applicable to multivariable control situations.

**PRE-EXPERIMENT MODEL OF A TWO-VARIABLE HUMAN CONTROLLER.**—Figure 1 is a block diagram of a two-axis compensatory manual control system which contains integrated control and display configurations. The human controller monitors an integrated two-dimensional display of the error and responds by manipulating a control device in two orthogonal dimensions. Each of the two orthogonal components of effector output is fed to a controlled element. A linear flow diagram of the system is given in figure 2. There is assumed to be no linear coupling between axes.

The human controller is represented as a modified parallel processor in the block diagram of figure 3. The sensory processor (visual system) monitors the error display and resolves the error into X and Y components. The central processor determines the appropriate strategies (equalizer characteristics) for the two axes. Commands are sent to the motor (neuromuscular) systems corresponding to each axis of control. The X and Y components of hand motion are summed vectorially to yield a two-dimensional response.

If the human is truly a parallel controller, there will be no interaction between signals processed on the two axes, and the performance on one axis will be unaffected by the presence or absence of a simultaneous task on the other. The arrows between corresponding X- and Y-axis functions indicate the possibility of one or more sources of interference, or interaction, between axes. Peripheral sampling, either visual or motor, has been eliminated by consideration of an integrated two-dimensional display and control configuration. Other potential sources of interference are perceptual interference (or masking), information processing limitations, a single-channel central processor, a single strategy processor, increased variability, differential allocation of attention, and motor interference.

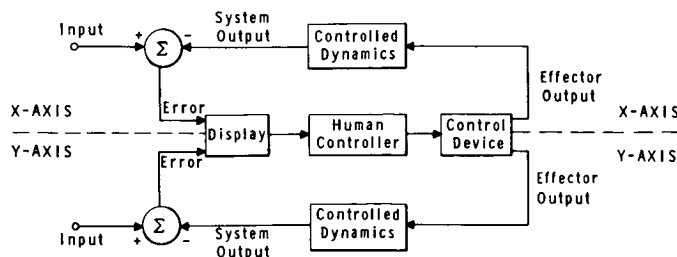


Figure 1.—Block diagram of a two-axis manual control system with integrated control and display configuration.

## DESCRIPTION OF EXPERIMENTS

**EXPERIMENTAL PROGRAM.**—Three formal experiments were performed in which there were two main variables, the plant dynamics which were either  $K/s^2$  or  $K$ , and the input forcing function bandwidth which was 3.5 rad/sec, 2.5 rad/sec, or 1.5 rad/sec.

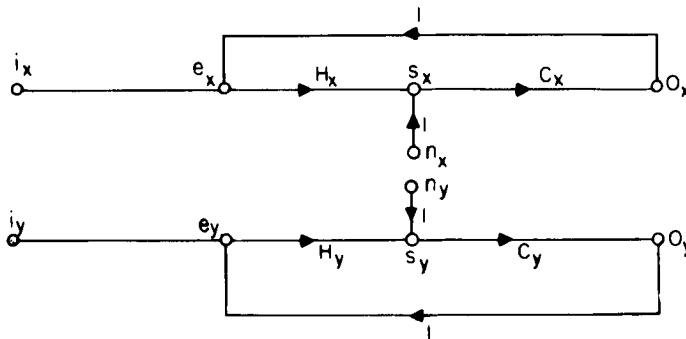


Figure 2.—Linear flow diagram of the two-axis compensatory tracking system.

$i_x$  = x-component of the input forcing function.

$e_x$  = x-component of the error displayed to the human operator.

$s_x$  = x-component of the stick deflection (operator's response).

$o_x$  = x-component of the system output.

$n_x$  = x-component of the operator's response that is not linearly correlated with  $i_x$  or  $i_y$ .

$H_x$  = linear relation between x-component of operator's response and x-component of error.

$C_x$  = controlled element relating x-component of system output to x-component of stick deflection.

Signals and system functions in the Y axis correspond to those defined above for the X axis.

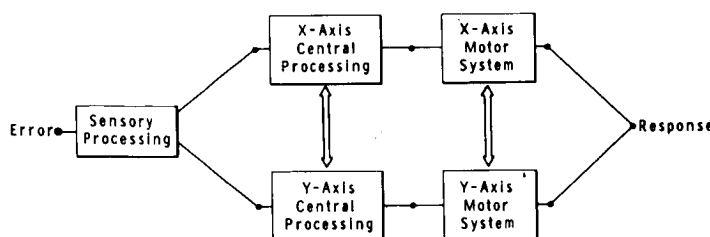


Figure 3.—Block diagram of the human controller when presented with integrated two-dimensional control and display configuration.

**Experiment 1: Homogeneous Control Situation.**—In the first experiment the dynamics in the two axes were the same and the input forcing functions were the same. The principal variable of this experiment, in addition to the one-axis, two-axis primary variable, was the input bandwidth. The purpose of this experiment was to test the hypothesis that the human controller could have two parallel channels in a two-axis homogeneous situation with each channel operating as well as in a single axis control situation.

Forcing functions having rectangular spectra with cutoff frequencies of 3.5, 2.5, and 1.5 radians were investigated in that order. The corresponding controlled-element dynamics relating stick displacement in centimeters to error dot displacement in centimeters were  $64/s^2$ ,  $32/s^2$ , and  $16/s^2$ . The forcing-function spectra and the controlled-element dynamics were the same in both axes for all experiments.

**Experiment 2: Heterogeneous Inputs and Homogeneous Dynamics.**—

This experiment was performed to show whether or not the parallel processing capabilities of the controller depended upon the bandwidth of the movements. Forcing functions of different cutoff frequencies were employed—the low-bandwidth input (1.5 rad/sec) on the X-axis and the high-bandwidth input (3.5 rad/sec) on the Y-axis. The waveforms were identical to those used in the homogeneous-tracking experiment. In order to provide maximum control-display compatibility, the controlled-element dynamics were  $64/s^2$  on both axes.

Two variations of this experiment were performed. The mean square of the forcing functions for both axes were equal during the first variation. A second variation was conducted with the mean square of the forcing functions readjusted to produce approximately equal mean-squared tracking errors on the two axes.

Experiment 3: Heterogeneous Dynamics and Homogeneous Inputs.—Homogeneous inputs were used in the third experiment, but the controlled-element dynamics in the two axes were different. One axis had acceleration dynamics of  $64/s^2$ , whereas the other had proportional dynamics of 4. The forcing functions on both axes had cutoff frequencies of 3.5 rad/sec, their mean-squared amplitudes were equal, and the waveforms were identical to those employed in the first experiment. The purpose of this experiment was to confirm the findings of others that heterogeneous dynamics lead to a degradation in the operator's ability to behave as a two-channel controller. In addition, we wanted to determine the extent and nature of the one-axis two-axis differences in human controller describing functions in order to develop a model for the controller that would be applicable to this kind of heterogeneous situation.

APPARATUS.—The human controller was presented with a two-axis compensatory oscillographic display consisting of a single error dot and a stationary reference circle. The controller attempted to keep the dot in the center of the circle by manipulating a two-axis control stick with his right hand. The stick was attached to a force-sensitive hand control (Measurement Systems Hand Control, Model 435) which provided two independent electrical outputs, one proportional to the X- and the other to the Y-component of deflection. The response of the error dot to a deflection of the stick was in the same direction as the stick deflection. The stick was allowed to move freely in both axes in all experiments. In the single-axis experiments the error dot in the inactive axis was clamped electronically at zero displacement.

The input signals were pseudo-gaussian with augmented rectangular power spectra. Each input signal contained a primary and a secondary component. Both components were constructed by summing 40 or more sinusoids of equal amplitudes spaced linearly in frequency. Therefore, they had essentially flat power spectral densities extending from slightly above 0 rad/sec to their respective cutoff frequencies. The cutoff frequency of the primary signal  $\omega_1$  was either 1.5, 2.5, or 3.5 rad/sec. The cutoff frequency of the secondary component was 9 rad/sec in all cases. The power level of the secondary component was 26 dB below that of the primary component. Preliminary experiments indicated that a secondary signal would permit valid measurements beyond the frequency range of the primary signal without seriously affecting the low-frequency behavior of the human controller. The X and Y input signals were linearly uncorrelated in all cases.

In experiments 1 and 3 and in the first variation of experiment 2 the mean-square deviation of the forcing function was  $4.0 \text{ cm}^2$  on each axis. Thus, the total (that is, X plus Y) mean squared amplitude was  $4 \text{ cm}^2$  for either single-axis task and  $8 \text{ cm}^2$  for the two-axis task. In the second variation of experiment 2, in which we adjusted the input magnitude to produce approximately equal errors in the two axes, mean-squared input levels were 6.9 and  $1.1 \text{ cm}^2$ , on the X- and Y-axes, respectively. The two-axis total input level was thereby maintained at  $8 \text{ cm}^2$ .

The subjects were instructed to minimize the mean-squared tracking error. In order to encourage the subjects to adopt this criterion, they were given knowledge of their performance in two ways. A delayed indication was provided in terms of the performance scores, which were available for inspection after each block of trials. Continuous feedback of the subject's performance was also provided by variations in the diameter of the reference circle.

Three subjects participated in the first experiment, two in the second, and three in the third. All subjects were college students without flight experience who received extensive

training in the tracking situations tested in these experiments. Data were taken when the performance appeared to become stable.

Data taking required a total of nine 4-minute trials per subject per experimental condition. The trials were presented in a balanced order as shown by the experimental plan outlined in table 1. The trials were grouped into three sessions, each of which contained an X-axis, a Y-axis and a two-axis trial. The sessions were separated by 15-minute rest periods, and the trials within a session were separated by 1-minute rest periods. Each axis condition was included in each session to allow the pairing of performance scores and thereby reduce the influence of learning and fatigue on the experimental results. Three performance scores were obtained during each 4-minute trial. The same 4-minute input signal was presented repeatedly to a subject via an analog tape system in order to minimize experimental variation and to determine the dependence of the operator's behavior on the particular waveshape of the forcing function. Thus, only one pair of input waveforms (one for X and the other for Y) was used for each experimental condition.

**DESCRIPTIVE MEASURES.**—Normalized mean-squared errors (NMSE) were computed for each axis individually and for the two-axis task as a whole. The NMSE for an individual axis was obtained by dividing the mean-squared tracking error on that axis by the corresponding mean-squared input deviation. When two axes were tracked simultaneously, two such independent measurements were obtained, one for each axis. The error scores obtained during two-axis tracking were also combined to yield a single, total-task NMSE. This measure was computed by dividing the total squared error by the total squared input. In order to have a combined-axis measurement relating to single-axis performance, the sum of the mean-squared errors obtained from the X and Y axes tracked singly was divided by the sum of the X and Y mean-squared inputs.

Human-controller describing functions relating centimeters of stick displacement to centimeters of error displacement were obtained using a multiple regression analysis technique described in references 9 and 10.

TABLE 1.—FORMAL EXPERIMENTAL PLAN

Session	Run number	Task
1	1	X-axis
	2	Y-axis
	3	2-axis
2	4	Y-axis
	5	2-axis
	6	X-axis
3	7	2-axis
	8	X-axis
	9	Y-axis

## EXPERIMENTAL RESULTS

**EXPERIMENT 1: HOMOGENEOUS CONTROL SITUATION.**—Average performance levels for experiment 1 are shown in table 2, and the percent difference between the one- and two-axis scores for each subject under each bandwidth-axis condition is given in table 3. Each entry represents the percent change in NMSE on a given axis caused by the addition of a simultaneous tracking task on the other axis. The percent change is defined as

$$\Delta \text{NMSE} = \frac{(2\text{-axis NMSE}) - (1\text{-axis NMSE})}{(1\text{-axis NMSE})} \times 100 \quad (2)$$

A positive change indicates that one-axis performance was superior.

TABLE 2.—PERFORMANCE LEVELS FOR EXPERIMENT 1  
(HOMOGENEOUS CONTROL SITUATION)

Subject	Normalized mean-squared error for —					
	X-axis		Y-axis		Total task	
	1 axis	2 axes	1 axis	2 axes	1 axis	2 axes
Input bandwidth = 3.5 rad/sec						
RL	0.22	0.24	0.24	0.27	0.23	0.26
CP	0.26	0.23	0.21	0.26	0.24	0.25
BL	0.24	0.27	0.20	0.27	0.22	0.27
3 subjects	0.24	0.25	0.22	0.27	0.23	0.26
Input bandwidth = 2.5 rad/sec						
RL	0.11	0.11	0.08	0.09	0.10	0.10
CP	0.12	0.11	0.08	0.10	0.10	0.11
BL	0.17	0.16	0.10	0.13	0.13	0.14
3 subjects	0.13	0.13	0.09	0.10	0.11	0.12
Input bandwidth = 1.5 rad/sec						
RL	0.032	0.032	0.025	0.029	0.029	0.030
CP	0.051	0.045	0.026	0.035	0.039	0.040
BL	0.061	0.067	0.030	0.043	0.046	0.054
3 subjects	0.048	0.048	0.027	0.036	0.038	0.042

TABLE 3.—DIFFERENTIAL PERFORMANCE LEVELS FOR EXPERIMENT 1  
(HOMOGENEOUS CONTROL SITUATION)

Subject	Change in normalized mean-squared error, percent, for —		
	X-axis	Y-axis	Total task
Input bandwidth = 3.5 rad/sec			
RL	9	13	12
CP	-10	<sup>a</sup> <sub>20</sub>	4
BL	12	<sup>b</sup> <sub>35</sub>	<sup>a</sup> <sub>22</sub>
3 subjects	4	<sup>c</sup> <sub>23</sub>	<sup>b</sup> <sub>13</sub>
Input bandwidth = 2.5 rad/sec			
RL	1	3	1
CP	-8	<sup>b</sup> <sub>25</sub>	5
BL	-8	<sup>b</sup> <sub>30</sub>	6
3 subjects	5	20	4
Input bandwidth = 1.5 rad/sec			
RL	0	13	5
CP	-12	<sup>b</sup> <sub>34</sub>	3
BL	8	<sup>a</sup> <sub>43</sub>	<sup>b</sup> <sub>19</sub>
3 subjects	-1	<sup>c</sup> <sub>30</sub>	<sup>a</sup> <sub>10</sub>

<sup>a</sup>Significant at the 0.05 level<sup>b</sup>Significant at the 0.01 level<sup>c</sup>Significant at the 0.001 level

The experimental conditions which yielded significant one-axis two-axis differences in NMSE are indicated in table 2. The significance of the results for each subject individually was computed as follows: (1) Each NMSE score obtained from a single-axis trial was subtracted from the corresponding score obtained during two-axis tracking; nine such paired-difference scores were computed for each subject-axis-bandwidth condition; (2) the hypothesis that the mean of the paired differences was zero was tested by a two-tailed Student's t-test. The sensitivity of the experimental procedure was such that an average fractional change of about 15 percent would be significant at the 0.05 level.

The average  $\Delta$ NMSE of the three subjects for each bandwidth-axis condition are also indicated in the table. Each entry is the average of 27 scores. The significance of these entries was determined by an analysis of variance.

Table 3 shows that the percent changes in total task NMSE were small and did not increase with input bandwidth. For bandwidths of 1.5, 2.5, and 3.5 rad/sec, respectively, the average changes were 10 percent (significant at the 0.05 level), 4 percent (not significant), and 13 percent (significant at the 0.01 level).

The percent changes were not the same on the two axes. The performance degradation was consistently greater on the Y axis. One-axis two-axis differences ranged from 3 percent to over 40 percent on the Y axis and were consistently significant for two of the subjects. On the other hand, changes on the X axis were less than 15 percent for all subject-bandwidth conditions and were not statistically significant.

Average human-controller describing functions are shown for the 3.5 rad/sec bandwidth condition in figure 4. Each describing function is the average of three Y-axis describing functions, one for each subject. Figure 4(a) shows the average one-axis and two-axis<sup>1</sup> describing functions. The difference between these two describing functions is shown in figure 4(b). A t-test revealed no significant differences between corresponding one-axis and two-axis describing functions. In general, the differences between one- and two-axis amplitude ratios were about 1 dB, and the phase differences were about 5°. These small differences are in accord with the small one-axis two-axis percent differences in NMSE. Similar describing function differences were obtained with the 2.5- and 1.5-rad/sec inputs.

EXPERIMENT 2: HETEROGENEOUS INPUTS, HOMOGENEOUS DYNAMICS. — The average performance levels and percent changes are shown in table 4. Neither subject showed a significant change in normalized mean-squared error for the total-task measurement. Subject CP showed no significant changes on either the X- or Y-axis. Subject RL showed a performance degradation of almost 100 percent on the low-bandwidth axis that was effectively offset by a 16 percent improvement in performance on the other axis. Both changes were statistically significant. This same subject showed no significant changes on either axis when the forcing-function amplitudes were readjusted to yield the same mean squared errors in X and Y.

EXPERIMENT 3: HETEROGENEOUS DYNAMICS, HOMOGENEOUS INPUTS. — Table 5 shows the performance levels and percent changes for the three subjects individually and collectively for the axis with proportional control (the "K-axis"), or the axis with acceleration control (the " $K/s^2$ -axis"), and for the total task. The average increases in NMSE were 98 percent, 62 percent, and 69 percent for the K-axis,  $K/s^2$ -axis, and total-task measurements, respectively, for the subjects collectively. Because of the differences between subjects, only the K-axis performance difference was statistically significant.

One-axis two-axis differences were statistically significant for the subjects individually for each axis condition. There were, however, large differences in strategies among the individual subjects. Subject EK, who showed the smallest total-task degradation (38 percent), showed the least change on the  $K/s^2$ -axis (13 percent) and the greatest change on the K-axis (124 percent). The subject showing the greatest total-task change of 87 percent, RL, performed in a similar way on the two axes. His NMSE increased 110 percent on the K-axis and

---

<sup>1</sup>The term "two-axis describing function" refers to a describing function measured under two-axis tracking conditions. The describing function is a one-dimensional descriptor which relates a single input variable to a single output variable.

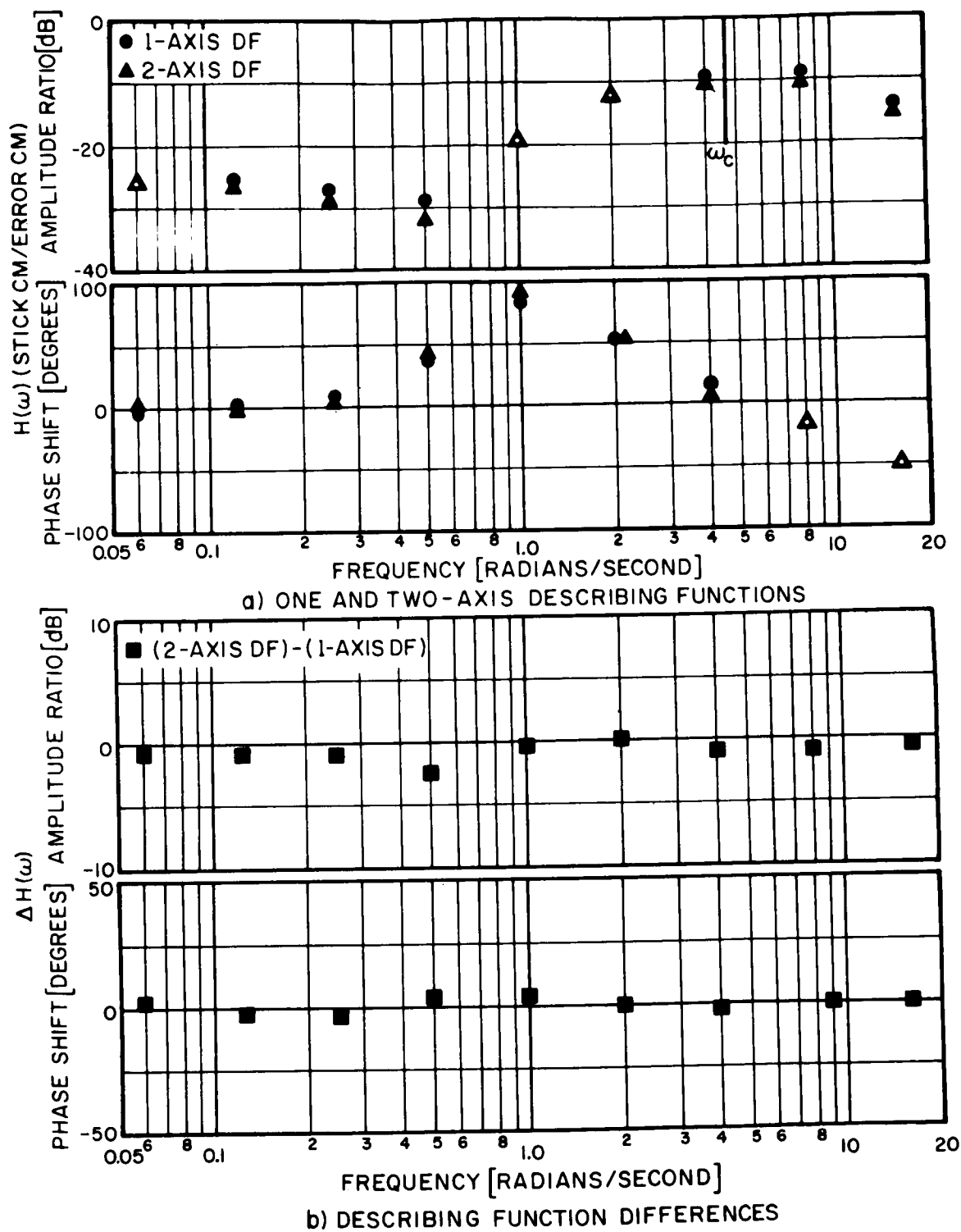


Figure 4.—Human controller describing functions for experiment 1 (homogeneous control situation); input BW=3.5 rad/sec, 3 subjects (3 runs).



TABLE 4. — PERFORMANCE LEVELS FOR EXPERIMENT 2  
(HETEROGENEOUS INPUTS, HOMOGENEOUS DYNAMICS)

[The mean squared input was  $4.0 \text{ cm}^2$  for the X- and Y-axis conditions for subjects CP and RL(1). Mean squared X and Y inputs were  $6.9$  and  $1.1 \text{ cm}^2$ , respectively, for subject RL(2).]

Normalized mean squared error for						
Subject	X-axis ( $w_i=1.5$ )		Y-axis ( $w_i=3.5$ )		Total task	
	1 axis	2 axes	1 axis	2 axes	1 axis	2 axes
CP	0.031	0.034	0.13	0.13	0.079	0.082
RL(1)	0.017	0.034	0.12	0.10	0.067	0.066
RL(2)	0.022	0.024	0.15	0.14	0.040	0.041
Change in Normalized mean squared error, percent, for						
Subject	X-axis ( $w_i=1.5$ )		Y-axis ( $w_i=3.5$ )		Total task	
CP	9		-2		4	
RL(1)	<sup>a</sup> 96		<sup>b</sup> -16		-2	
RL(2)	8		-5		1	

<sup>a</sup>Significant at the 0.001 level

<sup>b</sup>Significant at the 0.01 level

TABLE 5. — PERFORMANCE LEVELS FOR EXPERIMENT 3  
(HETEROGENEOUS DYNAMICS, HOMOGENEOUS INPUTS)

Normalized mean squared error for						
Subject	K-axis		K/s <sup>2</sup> -axis		Total task	
	1 axis	2 axes	1 axis	2 axes	1 axis	2 axes
RL	0.049	0.103	0.14	0.25	0.094	0.18
CP	.039	.062	.11	.22	.075	.14
EK	.037	.083	.13	.14	.082	.11
3 subjects	.042	.083	.13	.21	.083	.14
Change in normalized mean squared error, percent, for						
Subject	K-axis		K/s <sup>2</sup> -axis		Total task	
RL	<sup>a</sup> 110		<sup>a</sup> 79		<sup>a</sup> 87	
CP	<sup>a</sup> 59		<sup>a</sup> 91		<sup>a</sup> 81	
EK	<sup>a</sup> 124		<sup>b</sup> 13		<sup>a</sup> 38	
3 subjects	<sup>a</sup> 98		62		69	

<sup>a</sup>Significant at the 0.001 level

<sup>b</sup>Significant at the 0.05 level

about 80 percent on the  $K/s^2$ -axis. Subject CP showed a smaller percent change on the K-axis (59 percent) than on the  $K/s^2$ -axis (91 percent), while suffering a total-task degradation of 81 percent.

Describing functions for proportional and acceleration tracking are shown in figures 5 to 9. Figures 5 and 9 show the behavior of the subjects collectively, whereas the remainder of the Bode plots show the behavior of the subjects individually. The individual-subject describing functions are the average results of three replications. The resulting average describing functions, one per axis per subject, were used to compute the average collective behavior. Amplitude ratio and phase differences significant at the 0.05 level, as determined by a t-test, are indicated by asterisks beside the points plotted in part (b) of the figures. Standard deviations of the amplitude ratio and phase shift at selected frequencies are indicated in the figures by brackets.

Open-loop describing functions (human controller cascaded with the controlled element) are presented for data obtained from proportional tracking so that the gain crossover frequencies and phase margins may be determined by inspection. The human controller's describing function has the same critical frequencies and time delay as the open-loop describing function and may be derived from the latter by subtracting 12 dB from the amplitude ratio at all frequencies. Human controller describing functions are presented for acceleration tracking.

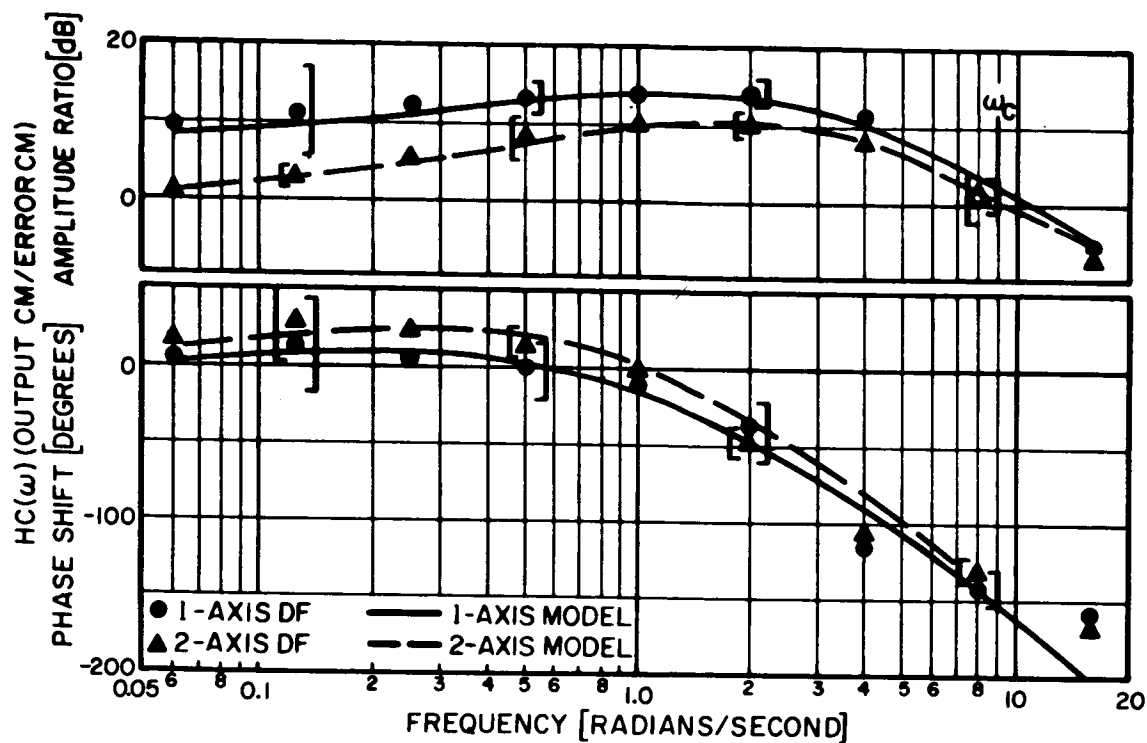
The describing functions were approximated by transfer functions of the following form:

$$H(s) = \frac{(T_L s + 1) e^{-\tau s}}{(T_{I'} s + 1)(T_I s + 1)(T_N s + 1)} \quad (3)$$

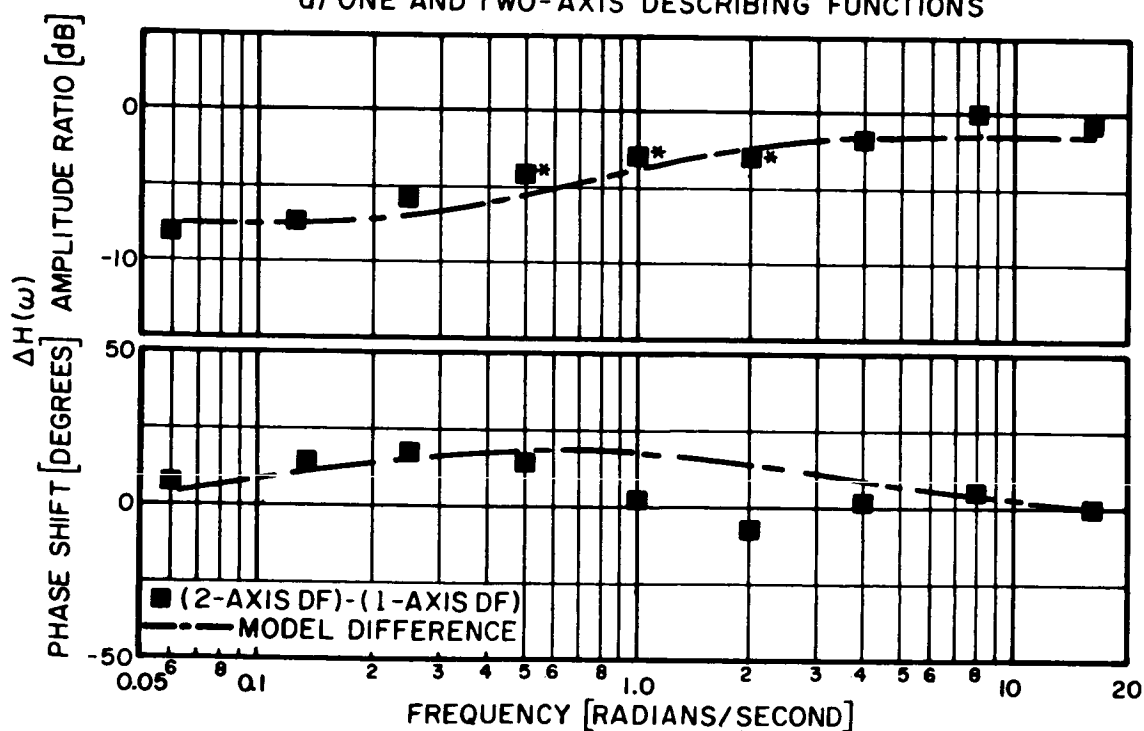
where  $\tau$  and  $T_N$  represent the time delay and neuromuscular lag discussed by McRuer et al. (ref. 3). The remainder of the model is a departure from that of equation (1), which was derived from reference 3, in that we have added a second lag term  $(T_{I'} s + 1)$ . This lag affects only the low-frequency response, and  $1/T_{I'}$  was always 1.0 rad/sec or less. This modification is necessary to provide an adequate approximation to our describing functions, some of which exhibit a low-frequency lead-lag behavior. The parameters of the approximations are tabulated in table 6.

Figure 5 shows the describing functions averaged for the three subjects for the K-axis. Low-frequency lead appeared in both the one-axis and two-axis describing functions. Two-axis tracking caused a decrease in amplitude ratio at all frequencies below 8 rad/sec. These differences ranged from 8 dB at 1/16 rad/sec to 2 dB at 4 rad/sec and were statistically significant between 1 and 4 rad/sec. Over this frequency range, the differences were approximately 3 dB, which is what we would expect from the doubling of the NMSE. The two-axis situation also caused an increase in phase shift of up to 20 degrees at frequencies below 2 rad/sec, but these differences were not statistically significant.

There is a corresponding difference in the analytic approximations. Whereas  $1/T_L$  remains constant at 0.25 rad/sec,  $1/T_{I'}$  increases from 0.5 rad/sec for one-axis tracking to 1 rad/sec for two-axis tracking. This increase in  $1/T_{I'}$ , coupled with a lowering of the gain  $K_h$ , accounts for much of the difference between the one- and two-axis describing functions.

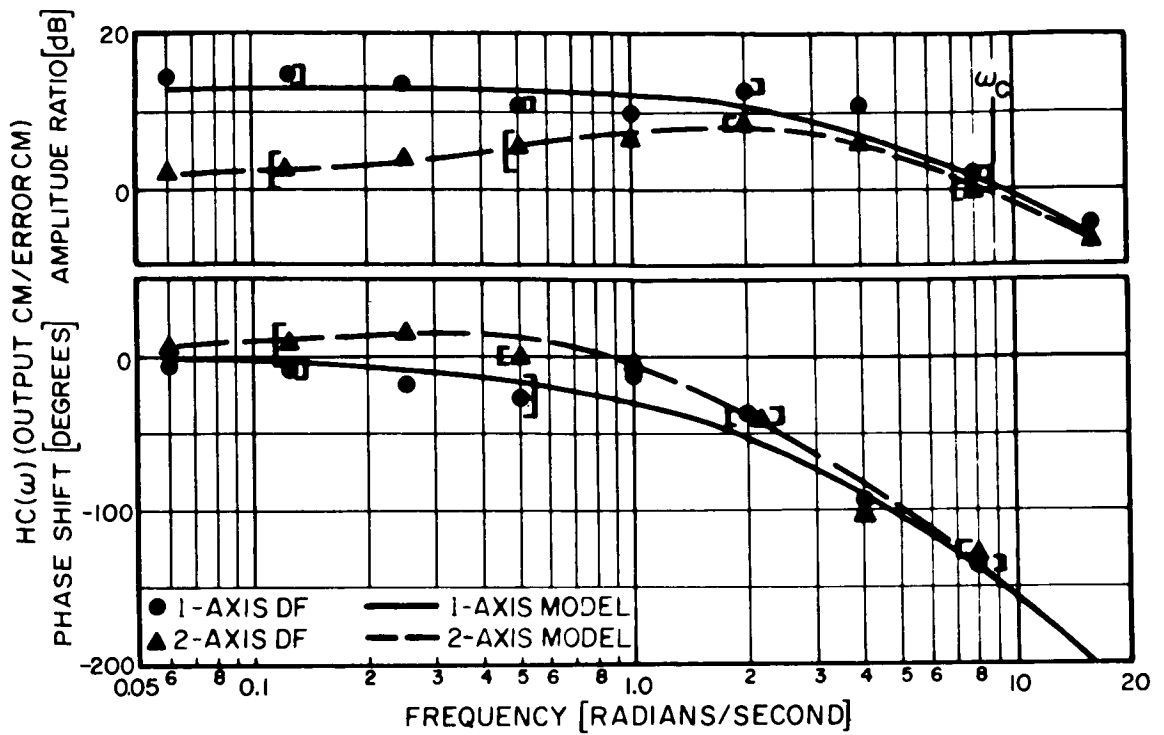


a) ONE AND TWO-AXIS DESCRIBING FUNCTIONS

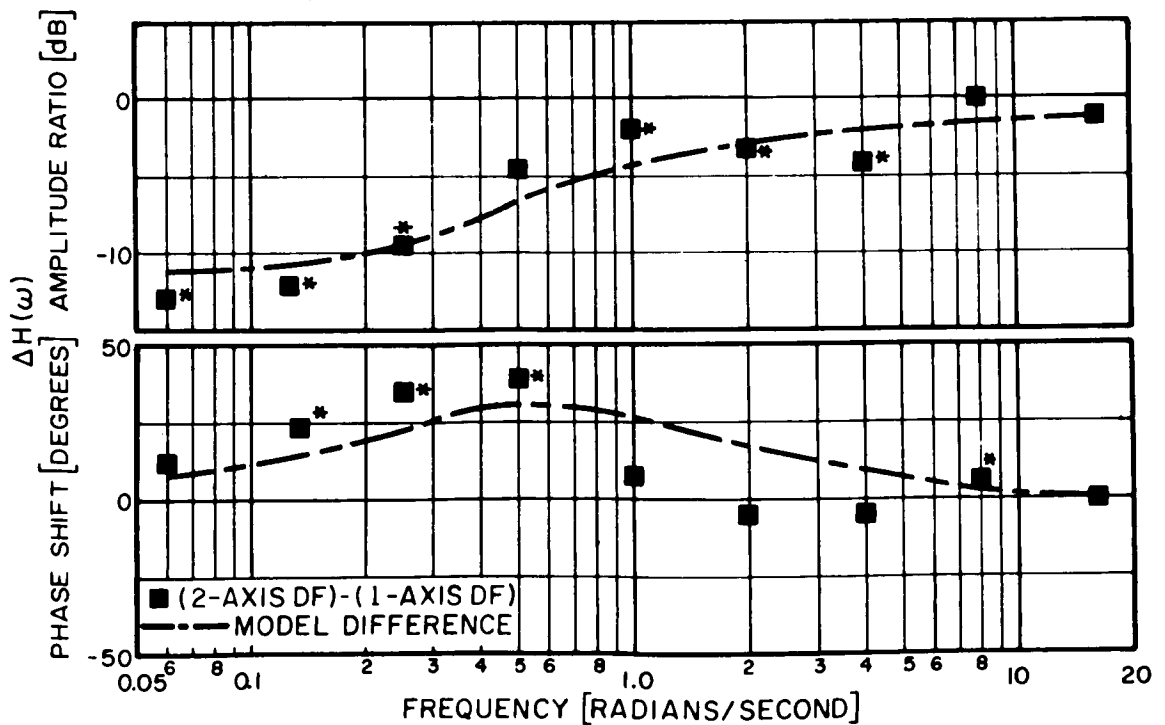


b) DESCRIBING FUNCTION DIFFERENCES

Figure 5. — Open loop describing functions for experiment 3 (heterogeneous dynamics);  $C=4$ , 3 subjects (9 runs).

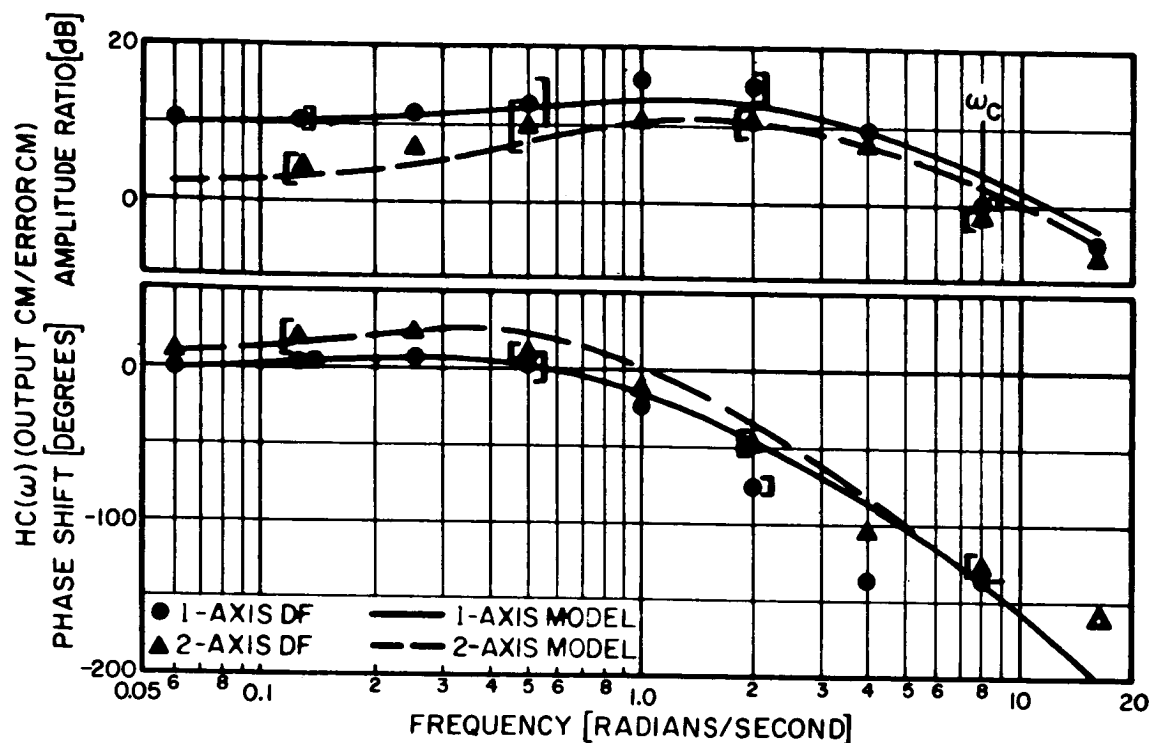


a) ONE AND TWO-AXIS DESCRIBING FUNCTIONS

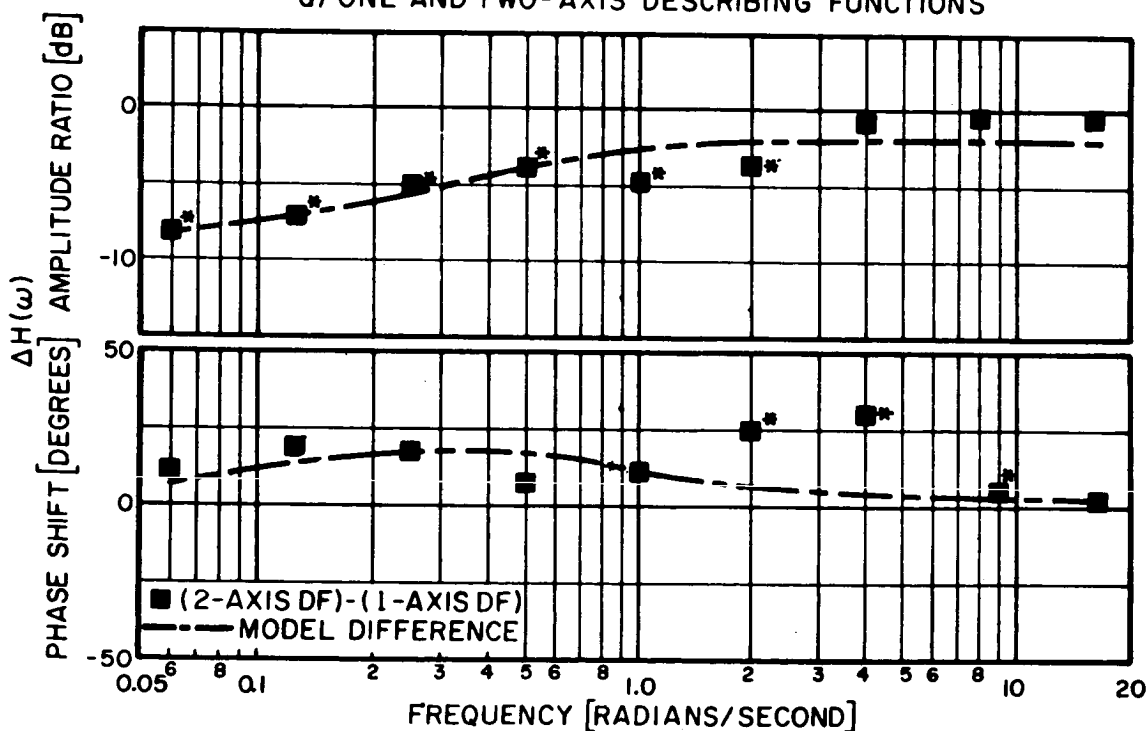


b) DESCRIBING FUNCTION DIFFERENCES

Figure 6. — Open loop describing functions for experiment 3 (heterogeneous dynamics);  $C=4$ , subject RL (3 runs).

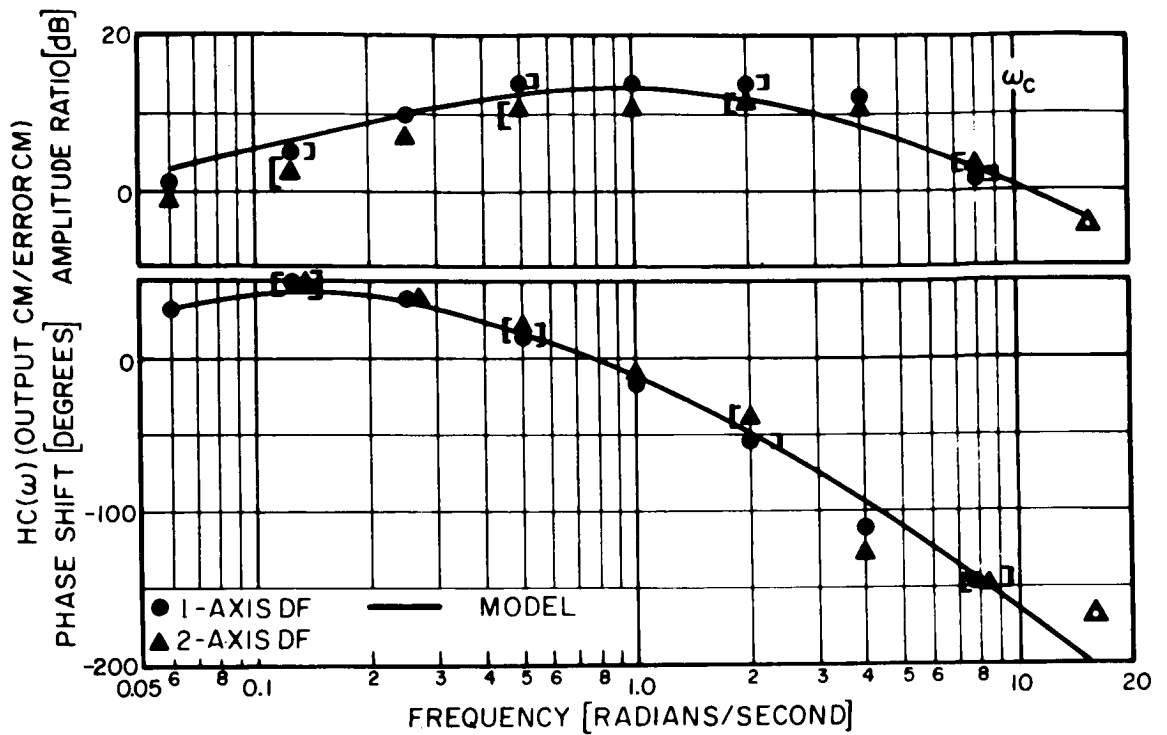


a) ONE AND TWO-AXIS DESCRIBING FUNCTIONS

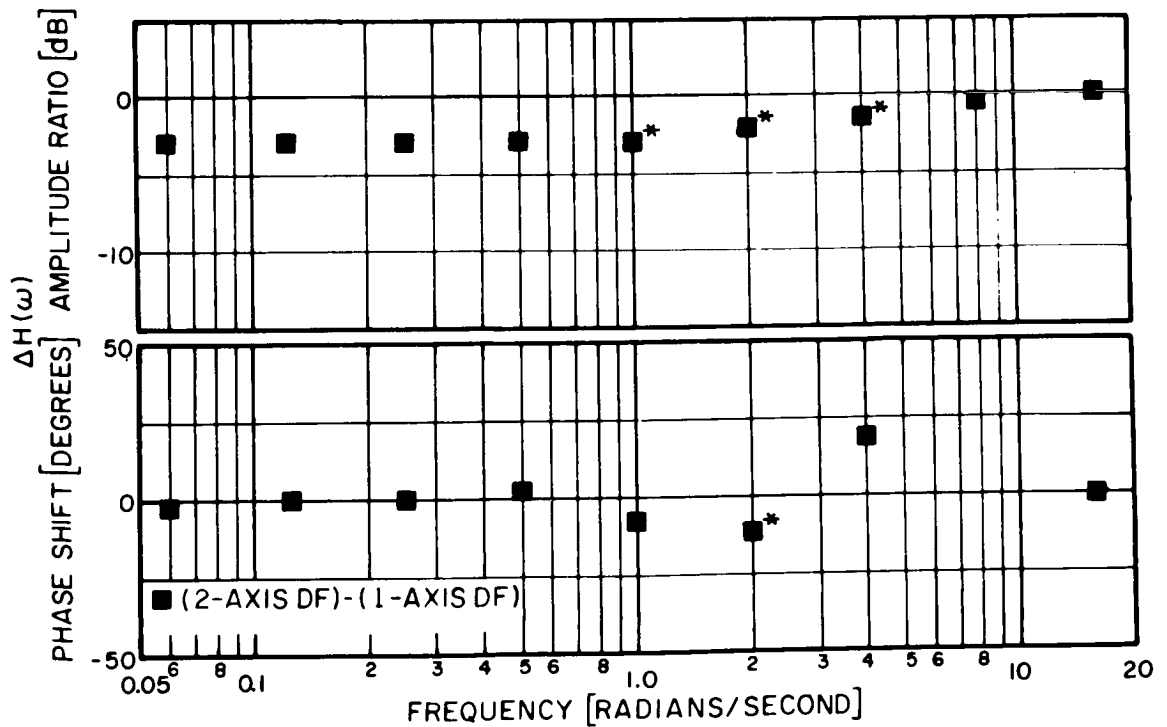


b) DESCRIBING FUNCTION DIFFERENCES

Figure 7.—Open loop describing functions for experiment 3 (heterogeneous dynamics);  $C=4$ , subject EK (3 runs).



a) ONE AND TWO-AXIS DESCRIBING FUNCTIONS



b) DESCRIBING FUNCTION DIFFERENCES

Figure 8. —Open loop describing functions for experiment 3 (heterogeneous dynamics); C=4, subject CP.

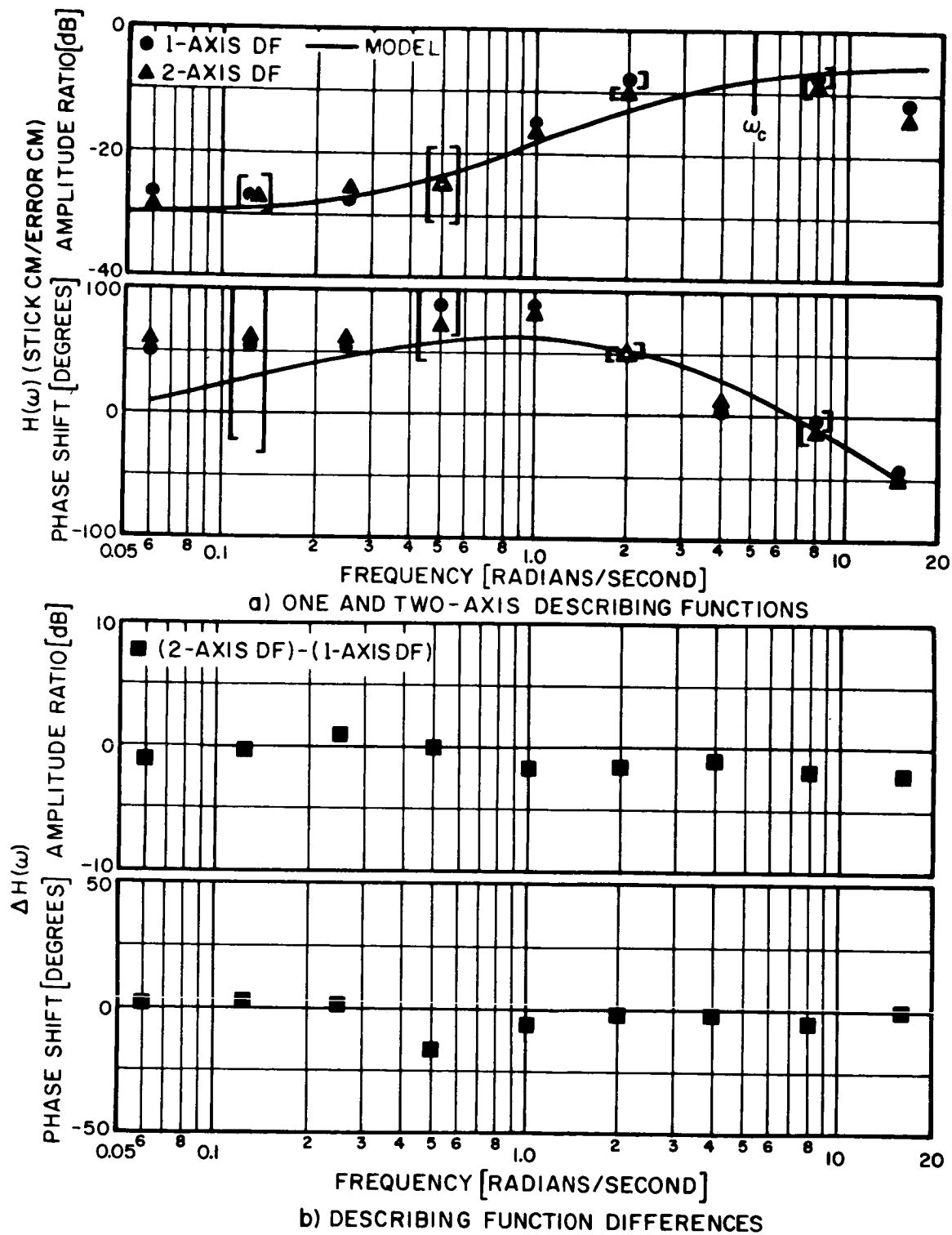


Figure 9. — Human controller describing functions for experiment 3 (heterogeneous dynamics);  $C=64/s^2$ , 3 subjects (9 runs).

Figures 6 to 8 contain the K-axis describing functions for the individual subjects. Each subject showed a statistically significant decrease in amplitude ratio over part of the spectrum under two-axis conditions. In addition, two of the subjects changed their low-frequency equalization by increasing the separation between  $1/T_L$  and  $1/T_{I'}$ .

The average  $K/s^2$  describing functions are shown in figure 9. Two-axis tracking caused a decrease in amplitude ratio at all but two measurement frequencies. The amplitude ratio decreased between 1 and 2 dB over the frequency range of significant error power (1-4 rad/sec). Phase differences were generally less than  $10^\circ$ . None of the gain or phase differences were statistically significant.

Since there was no change in equalization, a single analytical approximation has been derived for the pair of describing functions. A good approximation is obtained with a zero ( $1/T_L$ ) at 0.25 rad/sec, a pole ( $1/T_N$ ) at 4 rad/sec, and a time delay of 0.07 sec. The lag constants  $T_I$  and  $T_{I'}$  are zero.

None of the subjects individually showed a one-axis two-axis difference in equalization. The primary change in the describing functions was a lowering of the amplitude ratio from 1 to 3 dB in the two-axis situation.

TABLE 6.—ANALYTIC APPROXIMATIONS TO THE DESCRIBING FUNCTIONS OF EXPERIMENT 3 (HETEROGENEOUS DYNAMICS, HOMOGENEOUS INPUTS)

$$\left[ \text{The analytic approximations were of the form: } K_h \frac{(T_L s + 1) e^{-\tau s}}{(T_{I'} s + 1)(T_I s + 1)(T_N s + 1)} \right]$$

Parameter	3 subjects K-axis		RL K-axis		EK K-axis		CP K-axis	3 subjects K/s <sup>2</sup> -axis
	1 axis	2 axes	1 axis	2 axes	1 axis	2 axes	1 & 2 axes	1 & 2 axes
$\tau$ , sec.....	0.09	0.09	0.09	0.09	0.09	0.09	0.09	0.07
$1/T_N$ , rad/sec...	16	16	16	16	16	16	16	4
$K_h$ , dB.....	9	1.5	13	2	10	2	0	-18
$1/T_L$ , rad/sec...	0.25	0.25	0	0.33	0.5	0.25	0.06	4
$1/T_{I'}$ , rad/sec...	0.5	1	0	1	1	1	0.33	0
$1/T_I$ , rad/sec....	2.5	2.5	2.5	2.5	2.5	2.5	2.5	0



## DISCUSSION

FACTORS AFFECTING TWO AXIS PERFORMANCE.—Of the many factors tested in this series of experiments, only three appeared to have had an important effect on the performance of the human controller in a two-axis task relative to that in a one-axis task. They are: (1) visual-motor interference effects; (2) attentional effects; and (3) the requirement of generating simultaneously two different equalizations. The last one of these had the greatest effect on system and human controller performance.

Visual-Motor Interference.—When the human controller is controlling simultaneously in two axes and is using an integrated display and control, we would expect a certain amount of cross-coupling or interference between the stick movements intended for the two axes. This interference may be introduced in the visual system where the presence of an error or error velocity in one axis may interfere with the ability of the human controller to estimate error displacement and velocity in the other axis. The interference may also occur in the motor system where a movement intended for one axis inadvertently leads to a movement in the other. In addition, random cross-coupling introduced at the central processing level may produce interference effects similar to those introduced in the visual and motor systems. In our experiments we cannot distinguish among interference introduced at the visual, motor, or central processing level, and we shall lump all three types of interference together under the designation visual-motor interference.

It is reasonable to assume that the components of the error on one axis resulting from visual-motor interference effects will be uncorrelated with the input forcing function on that axis and will therefore be a source of remnant. A sampling of remnant data indicates that for the homogeneous control situation almost all of the increase in NMSE is accounted for by the increase in the uncorrelated portion of the normalized mean-squared error. If we assume that the increase in the uncorrelated error observed in going from one- to two-axis tracking is entirely due to visual-motor interference, we can account for almost all of the degradation in performance observed with homogeneous dynamics. On the other hand, less than half of the increase in NMSE observed when the controlled element dynamics were heterogeneous can be attributed to this type of interference.

Allocation of Attention.—Allocation of attention is the extent to which a subject concentrates on or gives preference to one axis of the control task at the expense of the other when tracking two axes simultaneously. Attentional effects of this kind are evident in the results of all three of the experiments performed. They are most clearly seen, however, in the behavior of subject RL in experiment 2. As indicated in table 4, when the mean-squared inputs in the two axes were equal, the NMSE of subject RL on the low-bandwidth axis showed a large increase in going from one to two axes, whereas the NMSE on the high-bandwidth axes actually decreased slightly. When controlling two axes simultaneously, the subject apparently attended more to the high-bandwidth axis, which was the source of most of the mean-squared error in the two-axis task, than he did to the low-bandwidth axis. This behavior was reasonable if the subject's objective was to minimize the total mean-squared error, and if by attending differentially to the more difficult task, he could actually improve his performance on that axis.

When the input amplitudes were adjusted so that the single-axis, mean-squared errors on the two axes were approximately equal, the one-axis, two-axis performance differences were about the same for the high-and the low-bandwidth axes. In this situation each axis contributed

about equally to the total mean-squared error and it was important for the subject to attend to each about equally.

This same kind of concentration on the axis contributing most to the total error is seen in the results of experiment 3 in table 5. When tracking two axes simultaneously with dissimilar controlled-element dynamics, subject EK managed to hold the increase total-task performance NMSE to less than 40 percent even though the K-axis NMSE increased over 100 percent. The NMSE in the K axis was much smaller than in the  $K/s^2$  axis, and minimization of the total mean squared error was more critically dependent on minimization of the errors on the  $K/s^2$  axis.

Heterogeneity of Required Equalization.—It is clear from the results of the three experiments that the heterogeneity of the controlled-element dynamics is responsible for the large changes in performance and in human-controller describing function. Experiment 1 demonstrated that two-axis operation was possible without important performance changes when the dynamics were homogeneous. Experiment 2 demonstrated that differences in spectral characteristics of the error signal and stick movements did not lead to important changes in total task performance. Remnant data indicated that visual-motor interference effects can account for at most 40 percent of the increase in NMSE observed in experiment 3. The source of the large changes in experiment 3, particularly on the K axis, is thus fairly well pinpointed to the heterogeneity of the controlled-element dynamics. This result is consistent with the results obtained by Chernikoff (ref. 6) and Verdi (ref. 8).

When the controlled-element dynamics in the two axes are different, the human controller must provide different kinds of equalization in the two axes in order to stabilize the system and to achieve good performance. It appears that in this situation the subjects cannot maintain the appropriate difference between the X- and Y-axis describing functions when they must be generated simultaneously. Table 6 shows that subject RL adopted a lead-lag characteristic in the K axis in the two-axis situation. Subject EK decreased the lead break frequency, thereby producing a more important lead-lag effect in two-axis tracking. Subject CP did not show important changes in lead-lag frequencies, but he already had an important lead-lag in single axis tracking. Moreover, the one-axis, two-axis differences in his K-axis NMSE were the smallest of the three subjects.

The important lead-lag observed in the one-axis K-axis describing function of subject CP and to a lesser extent with subject EK was unexpected. Such an effect was not found by Elkind (ref. 1) in his study of K-axis tracking. One possible explanation for the presence of this effect in the describing functions of subject CP is that he was trained first with  $K/s^2$  dynamics and had extensive practice with this type of controlled-element before he started training with K dynamics. Moreover, much of the K training for both subjects was in a two-axis situation in which the other axis had a  $K/s^2$  controlled-element. They may have simply continued the strategy of providing a lead-lag that was appropriate to  $K/s^2$  tracking when controlling K dynamics. Figure 10 of reference 11, which contains describing functions obtained in our preliminary experiments, shows that the describing function of subject EK did not exhibit a low-frequency lead-lag before that subject was trained with heterogeneous dynamics.

It should be noted that the large one-axis, two-axis differences observed in experiment 3 were obtained after all subjects had received extensive training in this control situation. Subjects CP and RL had about 6 hours of experience in this situation with heterogeneous dynamics.

Subject EK had 8 hours. There is no indication that further training would have eliminated or reduced the differences in performance materially.

MODIFICATION OF THE SINGLE-AXIS MODELS.—The single-axis human controller models provide predictions of two-axis behavior that are reasonably good in control situations in which the controlled-element dynamics are homogeneous. These predictions will, however, be subject to errors from two sources—visual-motor interference and differential attention. The single-axis models should be modified to include these factors if accurate predictions are to be achieved.

The amount of visual-motor interference will depend upon the controlled-element dynamics and upon the design of the control device. A simple proportional cross-coupling model can be derived to provide a reasonably good prediction of interference effects once the coupling coefficient is determined. The coupling coefficient, however, will have to be determined in a separate experiment.

Differential allocation of attention can have an important effect on system performance in an axis which is receiving little attention. The allocation of attention appears to depend upon subject training and preferences, signal amplitude, and no doubt upon other factors such as display sensitivity and instructions. We do not yet know how to measure attention or to predict its effect on performance.

The most important changes to the one-axis models are required when the controlled-element dynamics are heterogeneous. In this situation major changes in the form of the human controller's describing function are observed. It appears that when different equalizer characteristics are required of the subject for the two axes, his two-axis describing functions tend to resemble each other more than they do in a one-axis tracking situation. We have not yet been able to develop methods for predicting the extent of the changes in describing functions that occur in this kind of heterogeneous situation. This is one of the important problems in manual control that requires solution.

## CONCLUSIONS

Three factors that affect human controller characteristics in two-axis control situations have been identified. They are (1) visual-motor interaction, (2) differential allocation of attention, and (3) nonhomogeneity of required equalization when the controlled dynamics are not homogeneous. Single-axis describing function models for the human controller must be modified to include the effects of these factors in order to obtain accurate predictions of human controller characteristics in two-axis situations. These factors are also likely to have important effects on performance in higher-dimensional control situations.

A simple model has been developed for predicting visual-motor interference effects. Models for the prediction of attention and equalization effects have not yet been developed. Further work is required to develop such models and to determine how to apply them to higher dimensional systems.

## REFERENCES

1. Elkind, J. I.: Characteristics of Simple Manual Control Systems. TR-111. MIT Lincoln Laboratory, Apr. 1956.
2. McRuer, D. T.; and Krendel, E. S.: Dynamic Response of Human Operators. WADC-TR-56-524, Oct. 1957.
3. McRuer, D. T.; Graham, D.; Krendel, E. S.; and Reisener, W., Jr.: Human Pilot Dynamics in Compensatory Systems, Theory, Models, and Experiments with Controlled Element and Forcing Function Variations. AFFDL-TR-65-15, July 1965.
4. Levison, W. H.; and Elkind, J. I.: Studies of Multi-Variable Manual Control Systems: Two Axis Compensatory Systems with Compatible Integrated Display and Control. Rep. no. 1339. Bolt Beranek and Newman, Inc., Jan. 1966.
5. Todosiev, E. P.; Rose, R. E.; Bekey, G. A.; and Williams, H. L.: Human Tracking Performance in Uncoupled and Coupled Two-Axis Systems. Rep. 4380-6003-R0000. TRW Systems, Dec. 1965.
6. Chernikoff, R.; et al.: Two-Dimensional Tracking with Identical and Different Control Dynamics in Each Coordinate. NRL rep. 5424, Nov. 1959.
7. Duey, J. W.; and Chernikoff, R.: The Use of Quickening in One Coordinate of a Two-Dimensional Tracking System. IEEE Trans., vol. HFE-1, Mar. 1960, pp. 21-24.
8. Verdi, A. P.; et al.: Effects of Display Quickening on Human Transfer Functions During a Dual-Axis Compensatory Tracking Task. ASD-TDR-65, BSL, WPAFB, Mar. 1965.
9. Elkind, J. I.; Starr, E. A.; Green, D. M.; and Darley, L.: Evaluation of a Technique for Determining Time-Invariant Dynamic Characteristics of Human Pilots. NASA TN D-1897, 1963.
10. Elkind, J. I.; and Green, D. M.: Measurement of Time-Varying and Nonlinear Dynamic Characteristics of Human Pilots. ASD-TR-61-225, Dec. 1961.
11. Bolt Beranek and Newman, Inc.: Studies of Manual Control Systems. Prog. rep. no. 5, Dec. 1964.

67-15864

# 13. PILOT DESCRIBING FUNCTION MEASUREMENTS IN A MULTILoop TASK\*

R.L. Stapleford, D.T. McRuer, and R. Magdaleno  
Systems Technology, Inc.

As an element in a control system the human pilot operates, in general, in a nonlinear and time-varying manner. In many situations, however, his on-the-average responses can be represented by a quasi-linear model such as that shown in figure 1. The describing function component of the quasi-linear model gives that portion of the pilot response which is linearly related to the system input. The remnant is then the remainder of his response, that is, that portion which is not correlated linearly with the command input.

For single-loop compensatory tracking situations the quasi-linear model is well developed; the most detailed recent treatment is provided in reference 1. Current research activities are directed at expanding the model in several areas—pursuit tracking, multiloop control tasks, and multimodal pilot inputs. The work reported in this paper deals with the expansion to multiloop situations.

At the outset of this program there had been several investigations in which human-operator describing-function measurements had been made in multi-axis situations (refs. 2 to 4). In these studies the assumed (for data analysis purposes) and appropriate (based on data results) block diagram structure of the pilot/vehicle system was that shown in figure 2. Such a system can be termed "multiple single-loop," and the determination of the operator's describing function for each of the loops is quite simple, that is,

$$Y_{p_1} = \frac{\Phi_{i_1 c_1}}{\Phi_{i_1 e_1}} \quad (1)$$

$$Y_{p_2} = \frac{\Phi_{i_2 c_2}}{\Phi_{i_2 e_2}} \quad (2)$$

where  $\Phi_{i_1 c_1}$  is the cross-spectral density between  $i_1$  and  $c_1$ , etc.

Multiloop systems differ considerably from multiple single-loop systems, and represent a higher level of pilot/vehicle complexity. Examples of multiloop systems, with a classification based on the degree of coupling in the human controller, are shown in figure 3. The

\*The results of the work presented in this paper was supported by the National Aeronautics and Space Administration under Contract NAS 2-1868-3.

fundamental distinction between these and the multiple single-loop systems mentioned is in the interaxis coupling inherent in the controlled-element dynamics. It is this kind of system which is of central interest here. Until the present experimental series there were no human-operator describing-function data available for such situations.

In spite of the data deficiency, pilot models for multiloop situations, based on a rational extension of single-loop results, have been in use for several years. Some of these have been quite successful in a number of applications (for example, refs. 5 to 9). Nonetheless, questions and uncertainties uncovered in these application studies have provided both incentive and context for experimental measurements of pilot dynamics in multiloop manual control systems. As a result, the experimental program described here was undertaken to provide data essential for the development of detailed adjustment rules, loop-closure criteria, and other aspects of model refinement.

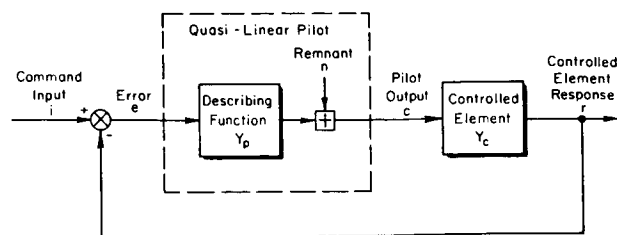


Figure 1. —Quasi-linear model for a single-loop compensatory system.

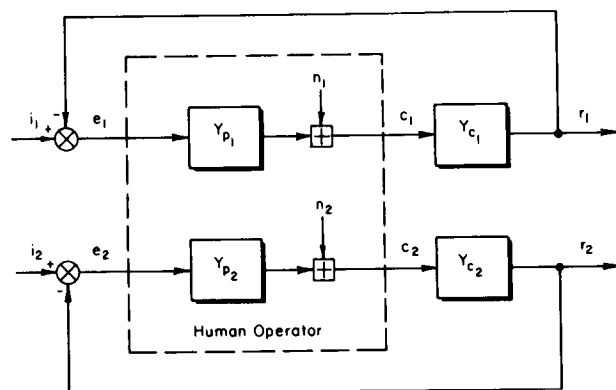


Figure 2. —Multiple single-loop manual control system.

The authors wish to thank W. C. Reisener, Jr., of the Franklin Institute who provided invaluable contributions to the experiments and data reduction.

## DESCRIBING FUNCTION MEASUREMENTS FOR MULTILoop SYSTEMS

It can be shown that, in general, the number of measurable pilot describing functions is equal to the number of uncorrelated inputs times the number of pilot outputs or controls. For example, with the two inputs and two pilot outputs of the cross-fed multipoint controller (fig. 3(c)) the equations for the pilot outputs are:

$$c_1 = Y_{p_{11}} e_1 + Y_{p_{12}} e_2 + n_1 \quad (3)$$

$$c_2 = Y_{p_{21}} e_1 + Y_{p_{22}} e_2 + n_2 \quad (4)$$

By taking the cross-spectra of the quantities in equations (3) and (4) with each input, one obtains four equations of the form:

$$\Phi_{i_j c_j} = Y_{p_{j1}} \Phi_{i_1 e_1} + Y_{p_{j2}} \Phi_{i_2 e_2} \quad (i, j = 1, 2) \quad (5)$$

These equations can, in principle, be solved for the four (two uncorrelated inputs times two pilot outputs) describing functions  $Y_{p_{11}}$ ,  $Y_{p_{12}}$ , etc.

Two of the four equations involve cross-spectra with the first input and the other two equations contain cross-spectra based on the second input. When the inputs are composed of sums of sine waves, they are uncorrelated only if their components are at different frequencies. Consequently, the four cross-spectral equations cannot be evaluated at the same frequencies. To solve the four equations simultaneously, it would be necessary to perform one of the following operations:

- (1) Interpolate the cross-spectral measurements to obtain values of the cross-spectra at the same frequencies for all four equations
- (2) Interchange the frequencies of the inputs and rerun the experiment so that data are available at the same frequencies for all the cross-spectra

If, on the other hand, the pilot crossfeeds,  $Y_{p_{12}}$  and  $Y_{p_{21}}$ , were not present, this problem would be eliminated. In fact, because each "pilot box" in this direct multipoint controller is characterized by one input and one output, only one system input would be needed to determine the two pilot describing functions. These would be given by the simple relationships

$$Y_{p_{11}} = \frac{\Phi_{ic_1}}{\Phi_{ie_1}} \quad (6)$$

$$Y_{p_{22}} = \frac{\Phi_{ic_2}}{\Phi_{ie_2}} \quad (7)$$

Intermediate between the direct multipoint and cross-fed multipoint controllers is a system in which only one crossfeed is present. This is shown in figure 4 with the crossfeed  $Y_{cf}$  shifted to the output of the series pilot box. In terms of the cross-fed multipoint controller quantities,  $Y_{cf}$  is  $Y_{p_{21}}/Y_{p_{11}}$ . With only one input,  $Y_{p_{11}}$  can still be determined explicitly because equation (6) still holds. The cross-spectral ratio of equation (7), however, no longer gives  $Y_{p_{22}}$  explicitly; instead, this cross-spectral ratio contains both  $Y_{p_{22}}$  and  $Y_{p_{cf}}$ , that is,

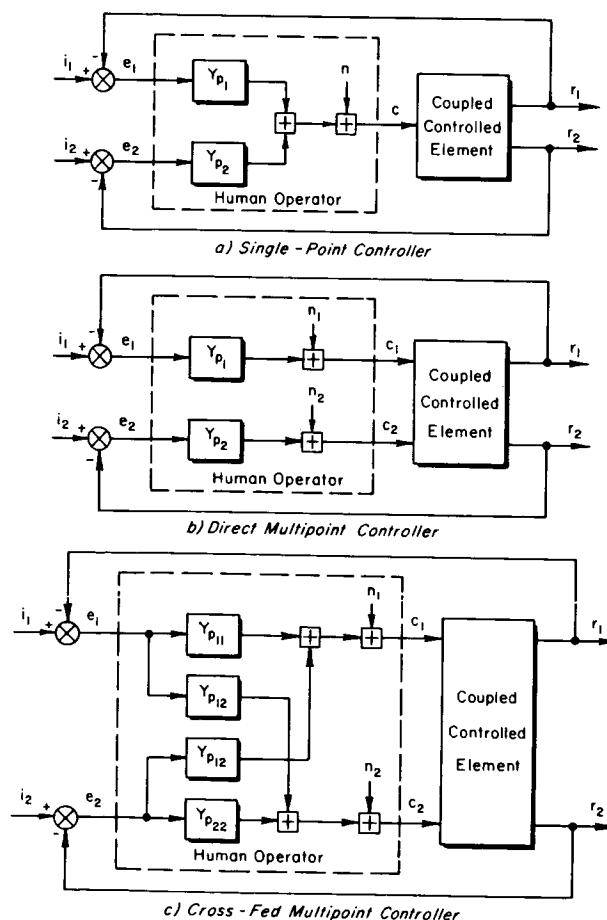


Figure 3.—Examples of multiloop manual control system.

$$\frac{\Phi_{ic_2}}{\Phi_{ie_2}} = \frac{Y_{p22} \left( \frac{r_2}{c_1} \right) + Y_{pcf}}{\left( \frac{r_2}{c_1} \right) + Y_{pcf} \left( \frac{r_2}{c_2} \right)} \quad (8)$$

where  $r_2/c_1$  and  $r_2/c_2$  are vehicle open-loop transfer functions. Consequently, the effect of the crossfeed cannot be separated from that of the loop closure, except implicitly, if the task involves but one forcing function.

From the standpoint of evolutionary development of pilot describing-function data, the ideal experimental situation at this pioneering stage would be the direct multipoint controller with one forcing function. This would constitute a net advance over previous studies without the necessity of a complicating and perhaps unrealistic secondary input. On a more tangible and practical level, any multiloop experiments are fundamentally restricted in scope by the equipment and data-reduction apparatus available. In our particular situation, this consideration made single-input tasks most desirable. Thus, an important implicit criterion in our control-task selection was to avoid controlled elements which demanded  $Y_{p12}$  and  $Y_{p21}$  crossfeeds for their control. Ideally, neither crossfeed should be present, although this was recognized as perhaps too drastic a departure from realism. Even with just one command input the presence of crossfeed can be detected readily from the cross-spectral measurements when they are compared with analytical predictions, and some insight can be gained into the nature of the likely crossfeed by implicit techniques. Consequently, our consideration of measurement and analysis limitations suggested that the control task selected involve a single forcing function, or a controlled element which ideally would be controlled as a direct multipoint controller, or which, at worst, required no more than one crossfeed in the human pilot.

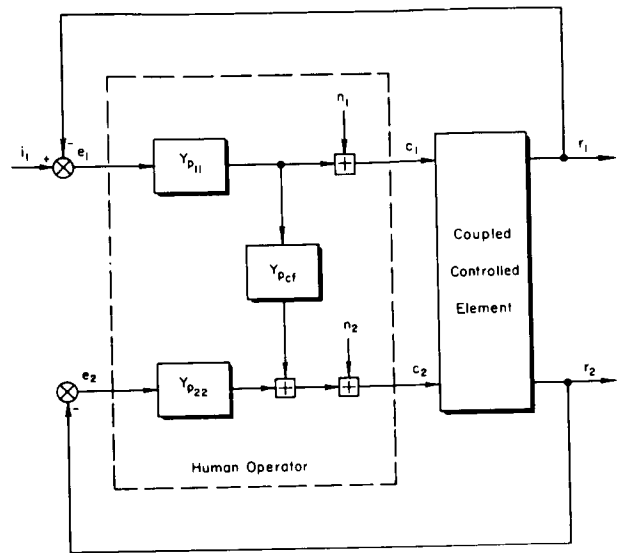


Figure 4.—Multipoint control system with one crossfeed.

## CONTROL TASK DESCRIPTION

**SELECTION CRITERIA.**—As a first step in experimental planning several criteria were established to guide the selection of the specific control tasks to be used in the experiments. The first two criteria were presented in the preceding paragraph. Others are as follows:

(1) At least two versions of controlled-element dynamics are needed, corresponding to single-loop and multiloop control, respectively.

- (a) For the single-loop task the controlled-element dynamics should be similar to those of the outer loop in the multiloop situation so that the two conditions can be compared. The dynamics should also be similar to those of previous single-loop experiments (e.g., ref. 1) to allow a tie-in with previous data.

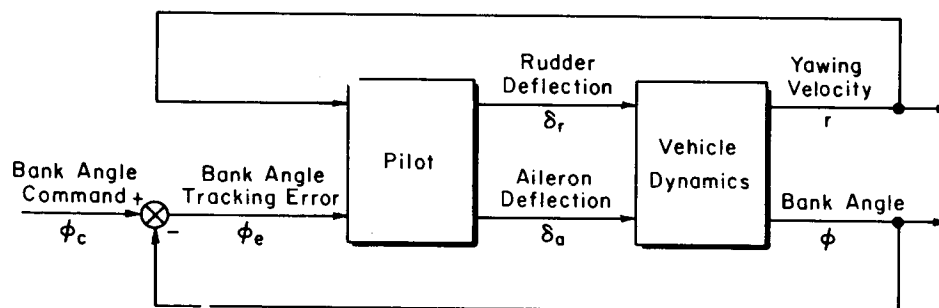


- (b) The multiloop configuration should be so designed that direct control of the command input is impossible without the addition of a secondary or inner loop. Ideally, the dynamics should be such that with these loops closed by the pilot the resulting outer loop characteristics are similar to those of the single-loop version.

(2) For the multiloop task there should be at least two inner-loop closure possibilities available to the pilot so that the feedback selection hypothesis (ref. 10) can be tested. This hypothesis states that given a number of inputs and possible outputs, the pilot will select those feedbacks which give him the best dynamic performance with least pilot effort. This can be demonstrated by having two inner loop possibilities which differ markedly in their performance potential.

(3) To the extent possible, the controlled-element dynamics should impose a moderate constraint on the form of the pilot describing functions in each of the two channels. This serves to reduce the variability in the measurements and the number of runs required to obtain accurate data (ref. 1).

**CONTROLLED-ELEMENT DESCRIPTION.**—After an extensive investigation of several possible vehicle control tasks, an aircraft control situation consisting of a bank-angle tracking task was selected. Figure 5 shows the control situation and the vehicle dynamic equations.



(a) Block Diagram of Bank Angle Tracking Multiloop Control Task

$$\text{Side Acceleration: } s\beta - \frac{g}{U_0}\phi + r = 0 + 0$$

$$\text{Rolling Acceleration: } -L'_\beta\beta + s(s-L'_p)\phi - L'_r r = 0 + L'_{\delta_a}\delta_a$$

$$\text{Yawing Acceleration: } -N'_\beta\beta - N'_p s\phi + (s-N'_r)r = N'_{\delta_r}\delta_r + N'_{\delta_a}\delta_a$$

(b) Vehicle Equations of Motion (Ref. 11)

Figure 5.—Multiloop control task.

A bank-angle command was the system input, and the difference between that command and the actual bank angle of the airplane was displayed to the pilot along with the aircraft yaw rate. The pilot could then use the ailerons and the rudders to control the vehicle dynamics, which were simulated on an analog computer.

Now, conventionally, bank-angle tracking is a single-loop task for aircraft with good characteristics. Any configuration which exhibits such good handling qualities, and which also has dynamics in the crossover region which are similar to some set previously tested (ref. 1), would be suitable for the single-loop baseline condition. For the multiloop configuration, the pilot can be forced into multiloop behavior by making the dutch-roll mode dynamically unstable. This can be done in such a way that there is no equalization which the pilot can adopt to allow him to stabilize the dutch-roll mode with only a bank-angle-to-aileron closure. In fact, by judicious selection of the unstable vehicle characteristics, the dutch-roll mode can be made slightly more unstable by the pilot closure of this loop. This is clearly seen in the root-locus sketch of figure 6, which shows the closed-loop roots resulting from a bank-angle-to-aileron loop closure with pilot behavior approximated by a gain and transport lag describing function.<sup>1</sup>

One piloting technique for control of this vehicle is the use of a yaw-rate-to-rudder loop to stabilize the dutch-roll mode and then a bank-angle-to-aileron closure to perform the tracking task. The effects of this inner and outer loop are shown in the root-locus sketches of figure 7, again with gain and transport lag pilot elements. The inner loop yaw-rate-to-rudder feedback has the effect not only of stabilizing the dutch-roll mode but also of shifting the bank angle zero. The outer loop closure (fig. 7(b)) is therefore very simple to achieve. (In fact, the outer open-loop characteristics illustrated here are approximately those desired for the single-loop configuration.)

An alternate possibility to control the dutch-roll instability is for the pilot to use bank angle and yaw rate closures with ailerons alone. This second technique is quite inferior to the first as regards performance. The nature of these closures is shown in the root locus sketches of figure 8. The yaw-rate-to-aileron closure can stabilize the dutch-roll mode, but the bank-angle closure destabilizes it such that attainable system bandwidth is

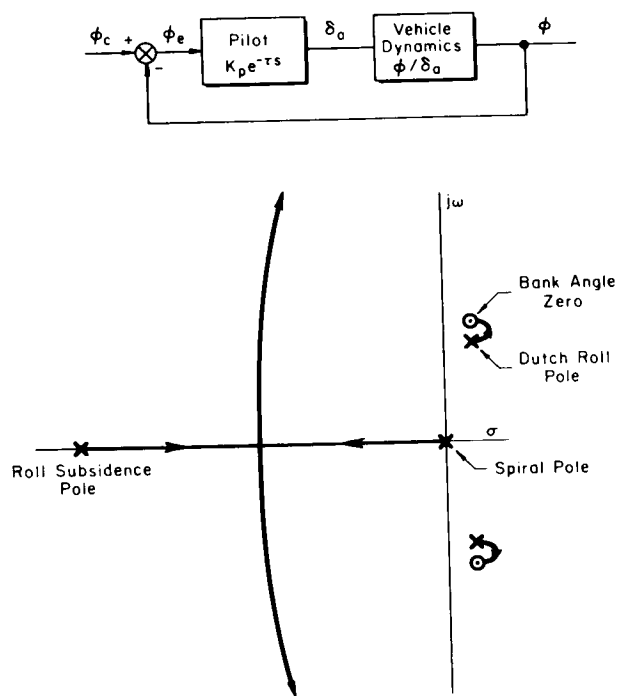


Figure 6. —Root locus of bank-angle-to-aileron closure for unstable dutch-roll mode.

<sup>1</sup>The actual preexperiment analyses, conducted to guide the selection of controlled-element details, were performed using the more complex human pilot mathematical models of reference 1. The gain and transport lag models are suitable only for oversimplified qualitative descriptions. These are all that are required at this point.

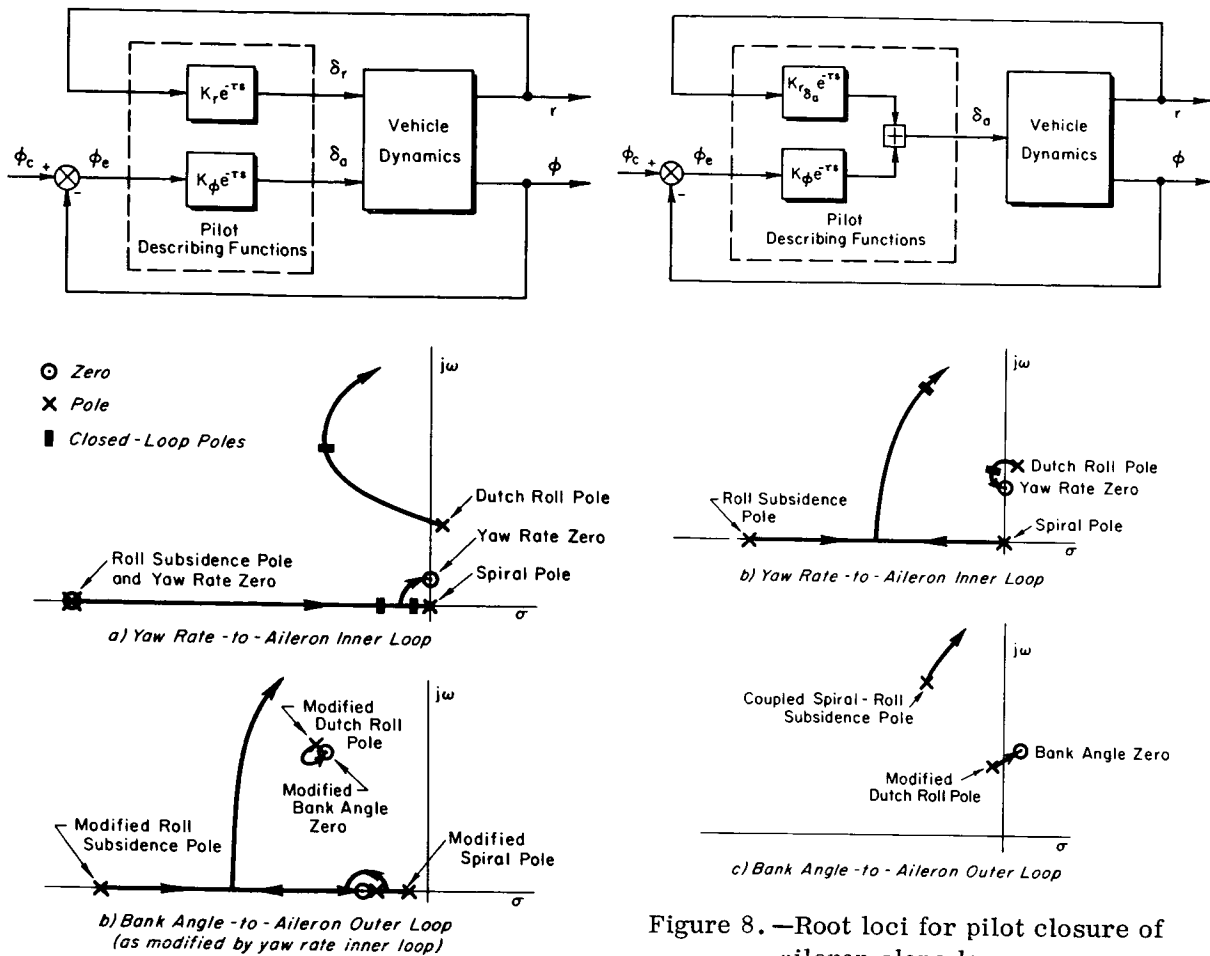


Figure 8. —Root loci for pilot closure of aileron alone loops.

Figure 7. —Root loci for pilot closures of rudder and aileron loops.

severely limited. Consequently, tracking performance using the second technique is very inferior to that with the yaw-rate-to-rudder inner loop.

The performance obtainable by the yaw-rate-to-aileron plus bank-angle-to-aileron control technique can be altered considerably by varying the stability derivative  $N_p^1$ , which is the amount of yaw acceleration produced by a unit rolling velocity. This is shown in the root-locus sketches of figure 9. When  $N_p^1$  is increased, the complex zeros of the yaw-rate-to-aileron transfer function are reduced in frequency so that more damping of the dutch roll can be obtained with the bank-angle-to-aileron closure.  $N_p^1$  is also an important cause of cross-coupling between the rolling and yawing degrees of freedom and, as discussed in a subsequent section, this consideration was also important in setting up the final configurations.

## PRELIMINARY EXPERIMENTS

Although the criteria and considerations previously outlined were sufficient to establish the general characteristics of the controlled elements in some detail, there were still several

loose ends and specifics which required resolution before the final experimental configurations could be established. To this end some preliminary experiments, in which no measurements of pilot describing functions were taken, were performed in the simulator facility at Systems Technology, Inc. The objectives of these experiments were the following:

- (1) To finalize the specific details of the configurations to be used in the main experimental program (e.g.,  $N_p'$  and dutch-roll damping ratio)
- (2) To verify the general qualitative nature of the preexperimental analyses and verify that pilot behavior would be of the type postulated
- (3) To check the scaling and the gains for both the display and the controls
- (4) To check the possibility of display sampling

The experimental setup consisted of a fixed-base cockpit, an analog computer to simulate the equations of motion, and a cathode-ray tube for the display. The displayed quantities were bank-angle error, which was represented by the difference between a fixed and a rotating line, and yaw rate, which was represented by the horizontal displacement of a small spot (see fig. 10). In terms of a real-flight situation the moving line in figure 10 represents the horizon, and this part of the display is essentially an inside-out bank-angle attitude indicator. The yaw-rate display was scaled so that the motion of the spot corresponded to that of the top of the turn needle in a conventional bank-and-turn indicator.

For both the preliminary and main experiments the instructions to the pilots were to minimize the bank-angle error by using whatever control technique they chose. When initially confronted with an unstable configuration, the pilots found that they could control the bank-angle error very well for a few seconds using only the ailerons. Then, as time advanced, they would notice that the yaw-rate spot oscillated with an ever-increasing amplitude, although this did not seriously affect the bank-angle tracking until the yaw rate got

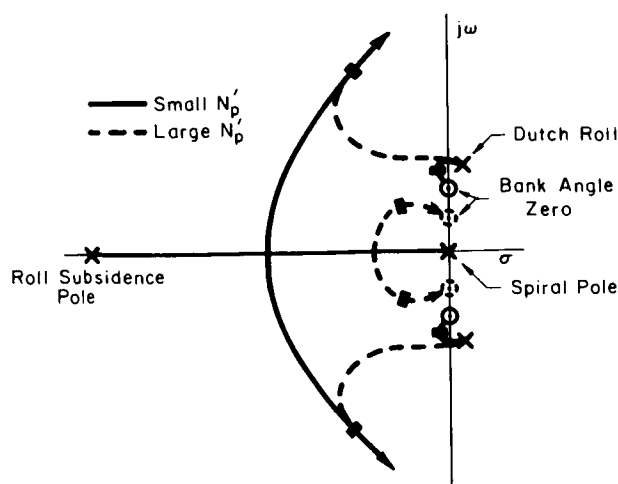


Figure 9. —Effects of  $N_p'$  on yaw-rate-to-aileron closure.

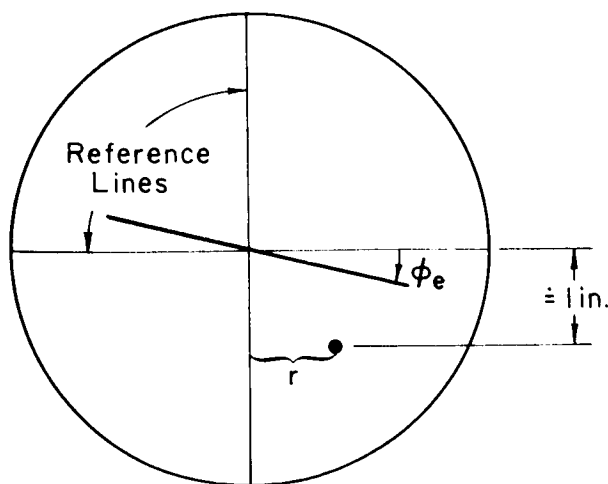


Figure 10. —Display.

rather large. At this point the bank-angle tracking would rapidly deteriorate so as to make recovery almost impossible. All subjects soon learned that the best technique was to track yaw rate simultaneously with rudder and bank angle with aileron, and they would attempt to keep the yaw rate very small to avoid the problem of trying to recover once it got very large.

The yaw rate seen by the pilot is primarily a result of the excitation of the dutch-roll mode, which is more or less a nuisance mode in that the pilot is not trying to use it to control his bank angle although he is, inadvertently, exciting it in the process of trying to track the bank-angle command. This excitation comes primarily from two aerodynamic cross-coupling sources—the yaw acceleration produced by the ailerons and the yaw acceleration produced by roll rate as the aircraft is rolled back and forth to follow the command. These correspond to  $N'_{\delta_a}$  and  $N'_{p_p}$ , respectively, in the vehicle equations of motion (fig. 5). As already noted, an increase in  $N'_p$  increases the excitation of the dutch-roll mode and at the same time improves the performance potential of aileron-alone control. It was, accordingly, a major variable in the preliminary experiments in the evolution of final configurations which were qualitatively adequate in terms of the criteria set forth in the last section.

The preliminary experiments served all their purposes in the resolution of fine points. They also provided more important and general results, which can be summarized as follows:

(1) The roll control task had clear primacy, with inner-loop stabilization being a necessity to accomplish the outer-loop task. There was no apparent tendency, or need, to crossfeed rudder to aileron.

(2) No evidences of display sampling were noted. This is based on the reports of the subjects and from visual observations of eye movements. The display was such that both bank angle and yaw rate could be observed simultaneously through the use of parafoveal vision.

(3) The bank-angle- and yaw-rate-to-aileron technique was found to be possible but very inferior to the yaw-rate-to-rudder and bank-angle-to-aileron technique. Consequently, the subjects would use the former only if instructed not to use the rudder pedals. Given a choice, the subjects would always adopt the yaw-rate-to-rudder and bank-angle-to-aileron technique regardless of the value of  $N'_p$ .

(4) A small value of  $N'_p$  was desirable to avoid yaw-rate scaling problems in the display and computer. Small values of  $N'_p$  were also desirable to minimize the possibilities of control crossfeed. With large values of  $N'_p$  the subjects tended to use an aileron-to-rudder crossfeed to reduce the excitation of the dutch-roll mode produced by the bank angle tracking.

On the basis of these preliminary experiments, three controlled-element configurations were selected to be run in the main set of experiments. The only variable between configurations was the derivative  $N'_r$ , which could be set to give the several levels of dutch-roll damping required. The complete set of vehicle dynamic parameters is given in the appendix.

A low value of  $0.02 \text{ sec}^{-1}$  was set on  $N'_p$  for all configurations. In anticipation of some of the later results, it is worth noting that with this value in the preliminary experiments the impressions of the subjects regarding control crossfeed were divided. One subject claimed to be using some aileron-to-rudder crossfeed, whereas the other was sure that he was not.

## MAIN EXPERIMENTS

**TASK VARIABLES.**—As a result of the preliminary experiments, three basic sets of controlled-element dynamics were evolved. These corresponded to three different levels of dutch-roll damping, listed in table 1 as configurations A, B (D, E), and C. The roll subsidence mode is the same for all configurations, and was selected to be compatible with good rolling characteristics, as indicated by reference 12. The spiral-mode and dutch-roll undamped natural frequency are slightly different for the three configurations. These are incidental consequences of the changes in  $N_T'$  used to create the variation in dutch-roll damping ratio.

Configuration A has a stable dutch-roll, so an inner-loop closure is not necessary. The characteristics of this configuration in the region of system crossover approximate the properties of other simpler systems already tested and reported in reference 1. Thus, the configuration can be used to provide a tie-in with these previous data. It also provides a reference for comparison with the cases in which the pilot was forced to use an inner loop. Configuration B (D and E) is just unstable enough to force the pilot to adopt multiloop control, whereas configuration C has an instability level near the maximum controllable by the pilot. In fact, several practice runs were required before this configuration could be controlled at all for the 4-minute run length used. These three controlled-element variations therefore provide a rather large range of variation of dutch-roll damping and of required multiloop control activity.

The forcing-function task variable was made up of a sum of 10 sine waves with frequencies which were more or less equally spaced logarithmically across the measurement bandwidth. The vast majority of the input power was of a low-frequency nature, achieved by setting the lower frequencies at one amplitude and the higher frequencies at an amplitude one-tenth that of the lower frequency waves. The total effect of all was a root mean square forcing function amplitude of  $11^\circ$ . The bandwidth of the input refers to the highest frequency of the large amplitude waves. For the controlled-element variations tested in configurations A, B,

TABLE 1.—TESTED CONFIGURATIONS

Configuration	Input bandwidth, rad/sec	Inverse time constants (sec <sup>-1</sup> )		Dutch-roll mode	
		Spiral mode	Roll subsidence mode	Damping ratio	Undamped natural frequency
A	1.6	0.20	5.0	0.75	0.87
B	1.6	0	5.0	.075	1.03
C	1.6	.054	5.0	.35	1.01
D	1.2	0	5.0	.075	1.03
E	2.4	0	5.0	.075	1.03

and C this was set at 1.6 rad/sec, which corresponds approximately to the  $\omega_1 = 1.5$  augmented rectangular forcing function used in the reference 1 experiments.

In addition to the controlled-element variations with fixed forcing function bandwidth, a complementary series was set forth using a fixed controlled element and three controlled-element bandwidths. This series is obtained from configurations D, B, and E. The objective of this series was to determine whether the variations of describing function with input bandwidth observed in reference 1 for single-loop tasks had their analog in multiloop situations.

Measurements taken during the experiments consisted of average performance measures, pilot ratings, and cross-spectral data. The performance measures included mean-squared bank angle tracking error,  $\overline{\varphi_e^2}$ , and mean-squared yawing velocity,  $\overline{r^2}$ . The cross-spectral data were obtained using much of the equipment and techniques previously employed in the single-loop experiments of reference 1. To make the cross-spectral measurements, advantage was taken of the sum-of-sinusoid forcing function. Component sinusoids were used as references in conjunction with pilot outputs or other system parameters as signals into a watt-hour-meter analyzer. In this equipment the real and imaginary parts at a particular input frequency are obtained by using a component of the input, and this component shifted  $90^\circ$  in phase as reference signals to two watt-hour meters. The signal being cross-correlated with the input (e.g., the pilot output and system error) makes up the other input to the meters. The watt-hour meters then perform the cross-spectral analysis functions of multiplication and integration, resulting in measurements proportional to the real and imaginary parts of the cross-spectrum, respectively, on the two meters (ref. 13).

The subject for the experiments was a Navy test pilot stationed at the Naval Air Test Center, Patuxent River, Maryland. He was thoroughly trained on each of the dynamic configurations to achieve a nearly stationary level of performance. For the data runs the conditions were presented several times in a randomized order to minimize any effects due to order of presentation. The actual order used is apparent in figure 17. Although only one subject was used for the entire series, two efforts were made to enhance the generality of the results. The first was to use spot checks on certain configurations performed by two other Navy test pilots. The results obtained from these checks were in general agreement with the data for the first subject. The second was a careful tie-in of the data with previous single-loop results. These two efforts were intended to be accomplished only with configuration A; however, the outer loop measurements in the other configurations also showed remarkably good agreement with some of the single-loop experimental data. This will be discussed in the subsection on outer loop control behavior.

INNER LOOP CONTROL BEHAVIOR.—As noted earlier, if the crossfeed is absent the pilot describing functions in the yaw-rate loop,  $Y_r$ , can be measured directly from the simple ratio of cross-spectra,

$$Y_r = \frac{\overline{\Phi_{\varphi_c \delta r}}}{\overline{\Phi_{\varphi_c r}}} \quad (9)$$

whereas with cross-control the same cross-spectral ratio contains two pilot describing functions which cannot be separated, that is,

$$\frac{\Phi_{\varphi_C \delta_r}}{\Phi_{\varphi_C r}} = \frac{Y_r \left( \frac{r}{\delta_a} \right) + Y_{cf}}{\left( \frac{r}{\delta_a} \right) + Y_{cf} \left( \frac{r}{\delta_r} \right)} \quad (10)$$

An examination of the data on this cross-spectral ratio clearly indicated that the pilot was cross-controlling in the multiloop configurations. For instance, the data for configuration B, shown in figure 11<sup>2</sup> cannot be fitted by the simple describing-function form which would be estimated to represent pilot closure of a yaw-rate-to-rudder loop on a single-loop basis. We therefore used a composite of three different methods to find values for the pilot crossfeed and yaw-rate-to-rudder describing functions which were both physically reasonable and compatible with the data.

The first technique was to assume for either the crossfeed,  $Y_{cf}$ , or yaw-rate-to-rudder,  $Y_r$ , describing function and to solve for the other describing function from the equation

$$\Phi_{\varphi_C \delta_r} = Y_r \Phi_{\varphi_C r} + Y_{cf} \Phi_{\varphi_C \delta_a} \quad (11)$$

The second method used was to assume that the crossfeed and yaw-rate-to-rudder describing functions were constant between adjacent frequency points. Then by taking the cross-spectral data for these frequency points, we effectively had two equations in two unknowns. This unfortunately was not completely successful because it required that the cross-spectra change significantly between frequency points while the pilot describing functions did not change significantly. The third technique used was to attempt to locate frequency regions for the various cross-spectra or ratios of cross-spectra in which the effects of either the cross-feed or the yaw-rate-to-rudder closure would dominate.

Combining the results obtained from all three approaches, the following can be stated:

- (1) The magnitude of the yaw-rate-to-rudder describing function in the region of cross-over appears to be about that required to maximize the damping of the closed-loop dutch-roll mode
- (2) There definitely was an aileron-to-rudder crossfeed
- (3) The magnitude of this crossfeed near the crossover frequency was roughly that required to cancel the yaw acceleration produced by the ailerons,  $N'_{\delta_a}$

<sup>2</sup>The small circles indicate the means of several runs, the short horizontal lines indicate the means plus or minus one standard deviation, and the small numbers at the top of the figure indicate the number of runs which were averaged for each frequency point. The number of runs is not the same for all frequencies because each run generally consisted of recording bank angle data at five frequencies and yaw rate data at the other five frequencies. Simultaneous recording of bank angle and yaw rate data at all 10 frequencies was not possible because of the limited number of watt-hour meters available.



(4) The crossfeed describing function included a low frequency lag-lead which would reduce the cross-coupling effects of  $N'_p$

To reinforce the plausibility of these assumptions, consider figure 12.

One curve in figure 12 is the preexperimental estimate made using the single-loop model and adjustment rules to form a yaw-rate loop closure with no crossfeed. The experimental data have trends similar to the estimate in certain frequency regions, although the amplitude ratio departs drastically in the frequency region of 0.3 to 1.0 rad/sec and the phase is generally translated to the right. While it is theoretically possible to "resolve" these differences by assigning more equalization to the yaw-rate closure, the result would demand an exceedingly complex pilot equalizing capacity which has no precedence. On the other hand, the provision of an aileron-to-rudder crossfeed which tends to cancel the  $N'_p$  and  $N'_{\delta_a}$  aerodynamic cross-coupling has the basic effect of modifying the amplitude ratio and phase in precisely those regions where the preexperimental estimates depart most drastically from the experimental results. This is shown in figure 12, where the crossfeed is the simple lag-lead noted there. As can be seen, the amplitude fit in the region 0.3 to 1.0 rad/sec is improved considerably, as is the phase fit in the region 1 to 2 rad/sec. The amplitude fit near 4 rad/sec is not as good with the crossfeed in, but that could probably be improved by additional modifications to  $Y_r$  and  $Y_{cf}$ . Additional rationales for this explanation are provided by the pilot's volunteered subjective impression that this was precisely what he was

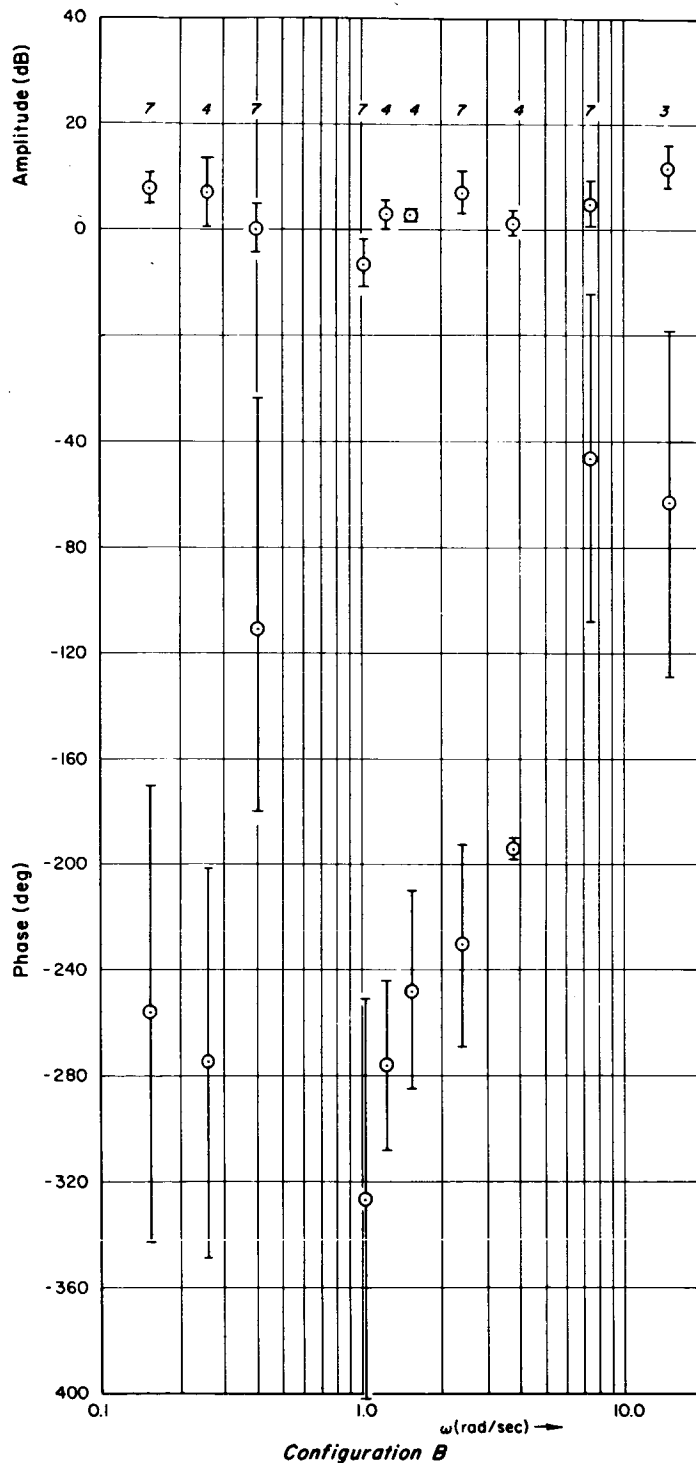


Figure 11.—Measured cross-spectral ratio

$$\frac{\Phi_{\omega_c \delta_r}}{\Phi_{\omega_c r}}$$

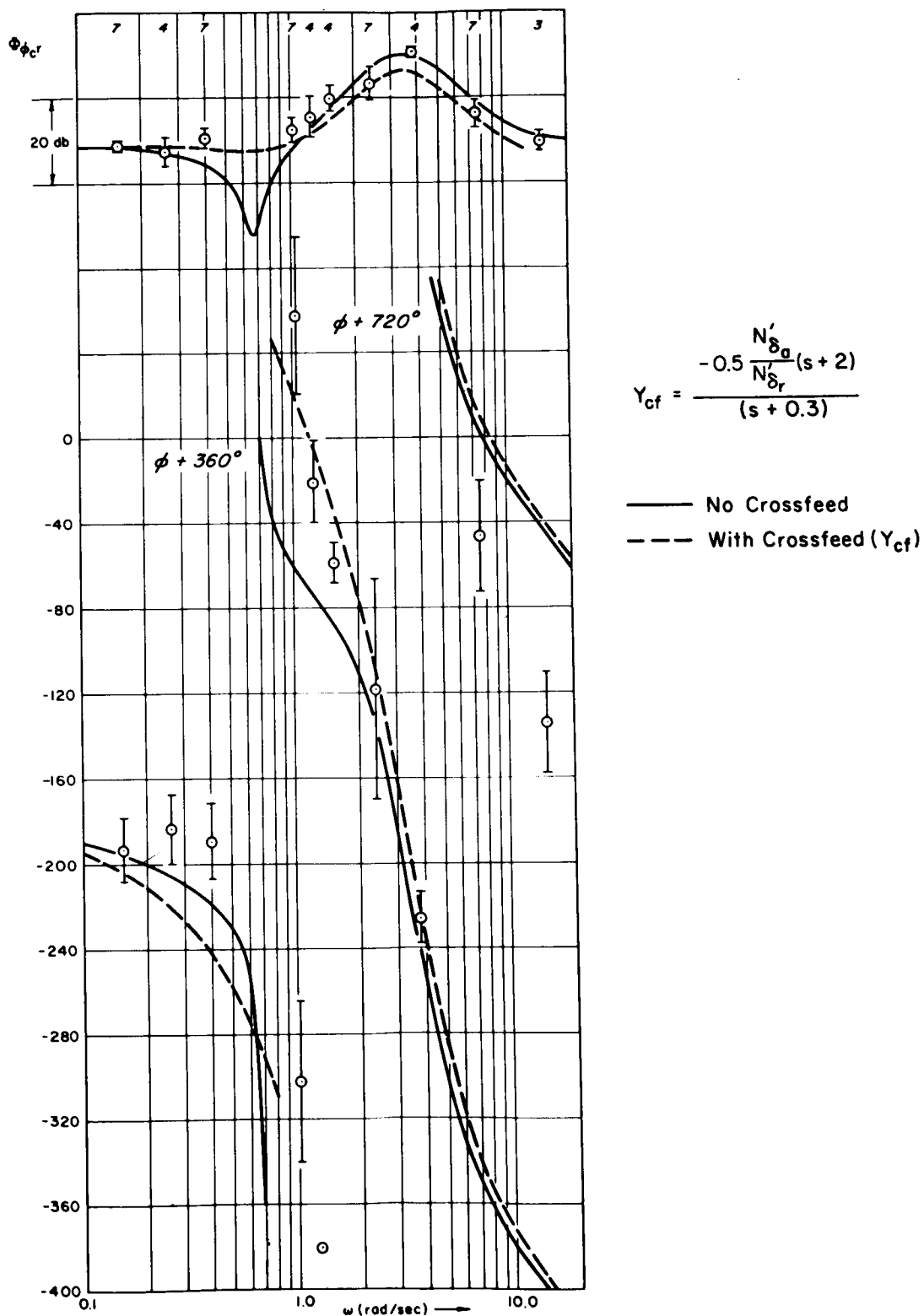


Figure 12. —Effect of crossfeed on yaw-rate response.

attempting to do, and by the similarity between pilot action and that often used in automatic flight controls to achieve the same purposes.

**OUTER LOOP CONTROL BEHAVIOR.**—While some difficulty was encountered in the interpretation of the inner loop data, the results for the command (bank angle) loop were quite clear and conclusive. The measured bank-angle-to-aileron describing functions are shown in figures 13 and 14. Also shown in the figures are the analytic curve fits made for the describing function data. Values of the describing function parameters for all five configurations are listed in table 2, along with similar parameters for the  $K/s$  and  $K/s^2$  controlled elements from reference 1.

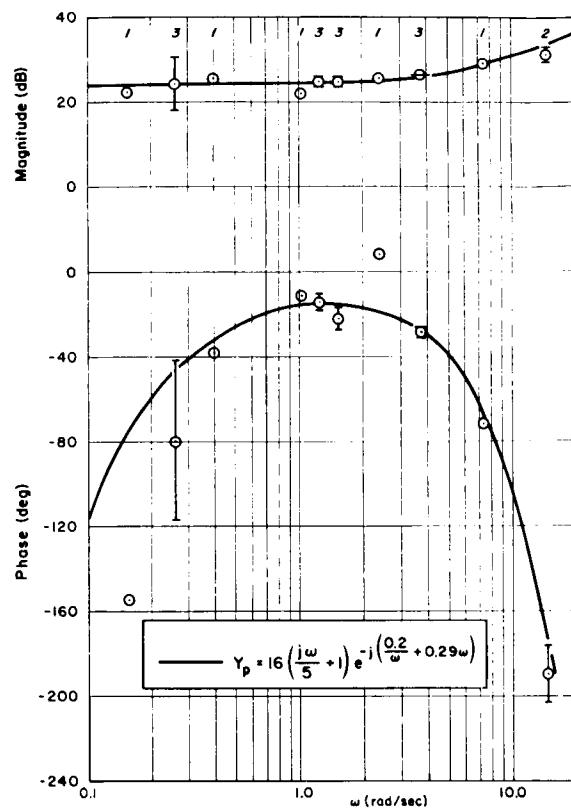
Comparisons of the entries in table 2 show the surprising result that the pilot characteristics in the command loop were independent of his behavior in the inner loops, that is, the pilot describing functions were the same for the stable, slightly unstable, and highly unstable configurations, A, B, and C, respectively. In addition, the outer loop measurements were in very good agreement with the single-loop experiments of reference 1. The identical control element was not tested in reference 1, but the bank-angle tracking task with a stable dutch roll<sup>3</sup> should fall somewhere between the  $K/s$  and  $K/s^2$  experiments of

TABLE 2.—COMMAND LOOP CHARACTERISTICS

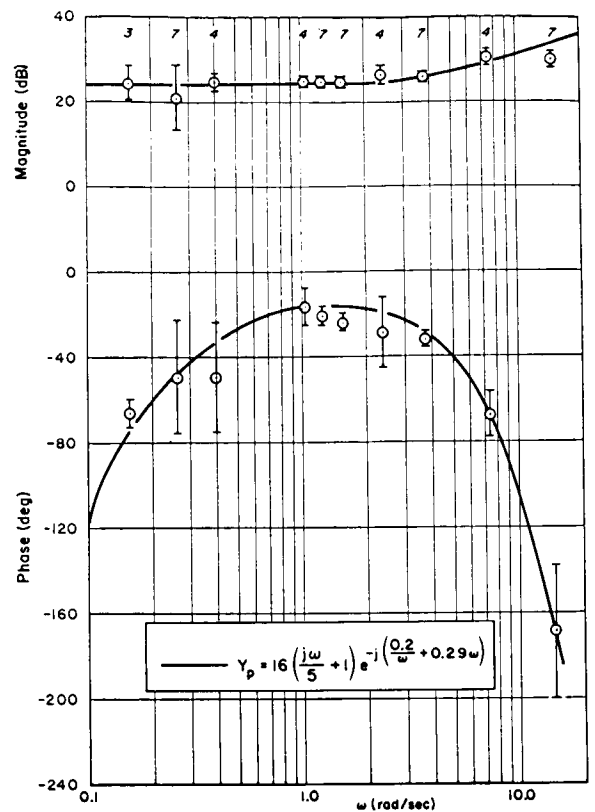
$$\left[ \text{Pilot describing function} = K_p(j\omega T_L + 1)e^{-j(\alpha/\omega + \omega\tau_e)} \right]$$

Configuration	Input bandwidth, rad/sec	$\alpha$ , rad/sec	$\tau_e$ , sec	$T_L$ sec	Crossover frequency, rad/sec	Phase margin, deg
A (stable)	1.6	0.20	0.29	0.20	3.2	20
B (slightly unstable)	1.6	.20	.29	.20	3.2	20
C (highly unstable)	1.6	.20	.29	.20	3.2	20
D (slightly unstable)	1.2	.20	.29	.20	3.2	20
E (slightly unstable)	2.4	.20	.29	.31	3.2	34
$K/s$ (ref. 1)	1.5	.14	.24	0	4.6	24
$K/s$ (ref. 1)	2.5	.11	.18	0	4.7	42
$K/s^2$ (ref. 1)	1.5	.20	.39	5	3.2	16
$K/s^2$ (ref. 4)	2.5	.33	.34	5	3.3	26

<sup>3</sup>Bank-angle-to-aileron response is closely approximated by  $K/s(T_R s + 1)$ , where  $T_R = 0.2$  sec.

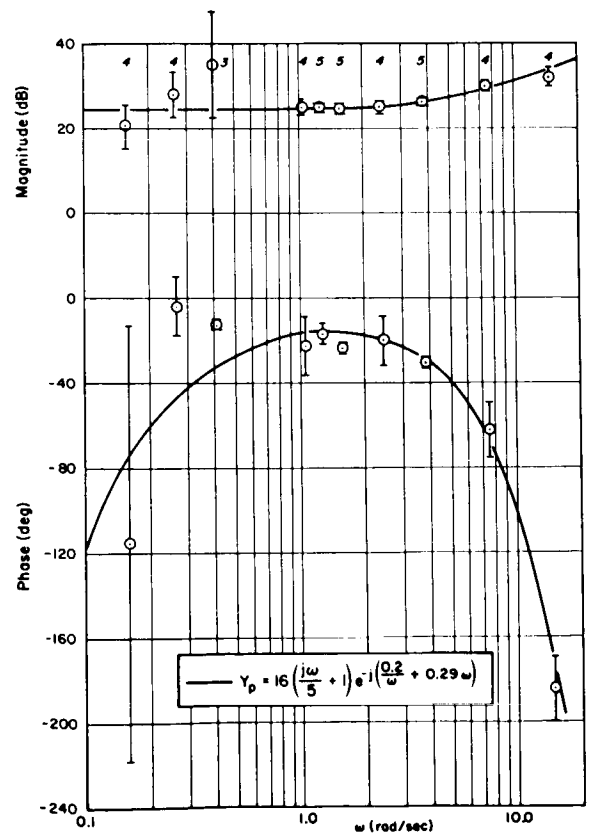


(a) Configuration A

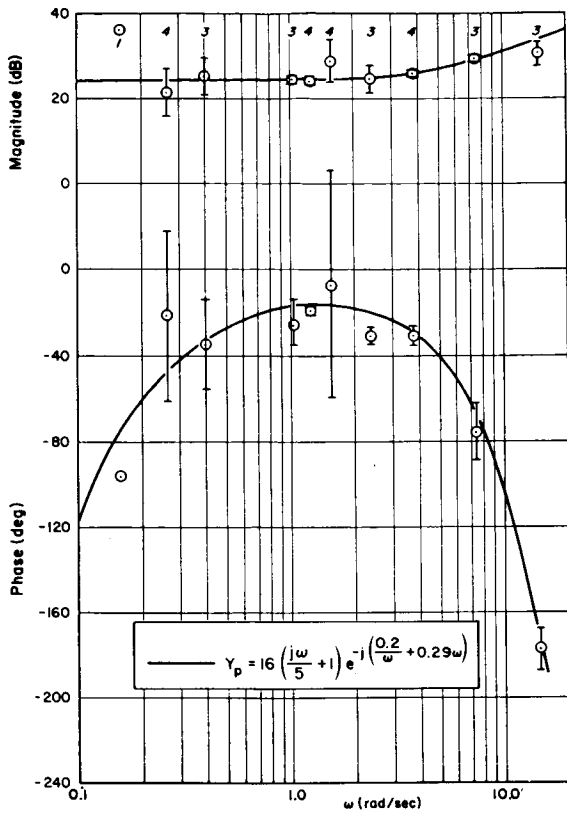


(b) Configuration B

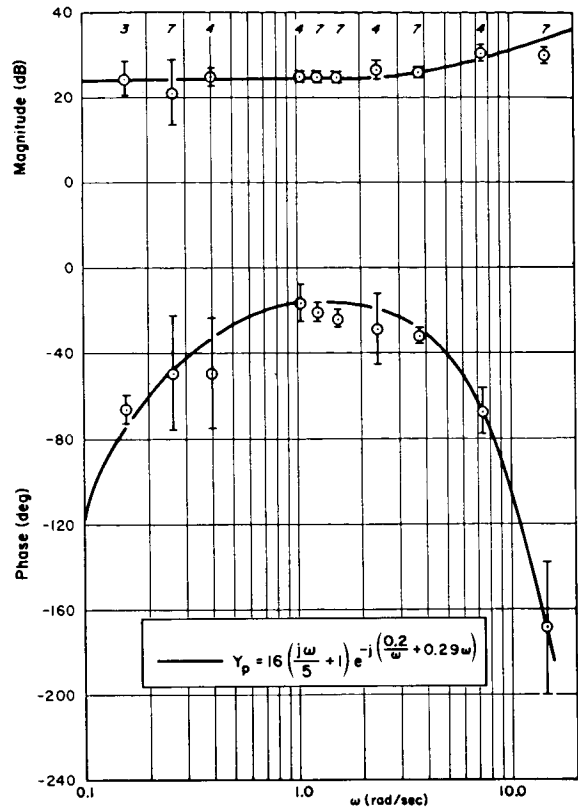
Figure 13. —Pilot command-loop describing functions.



(c) Configuration C

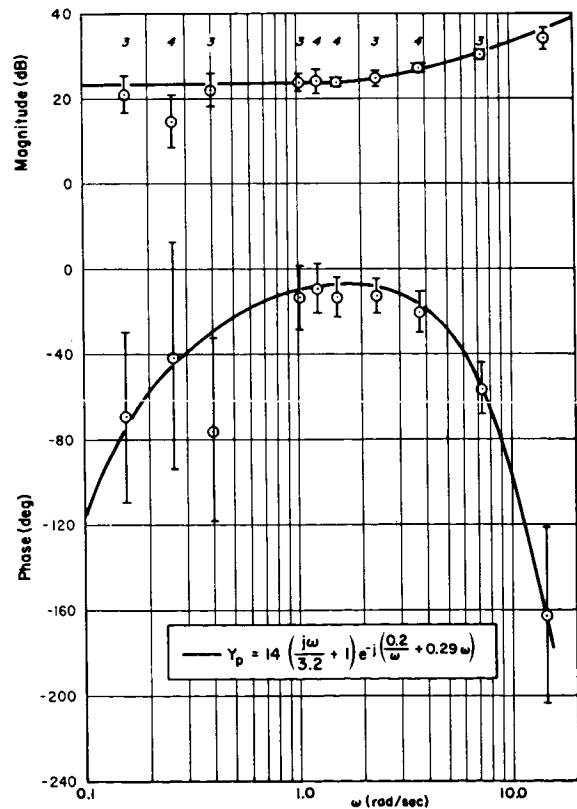


a) Configuration D



b) Configuration B

Figure 14. —Pilot-command loop describing functions.



c) Configuration E

reference 1. Not only are the command-loop data and the single-loop data of reference 1 very similar, but it is, in fact, apparent that the pilot describing function model and adjustment rules of reference 1 can be carried over directly to the control of command loops in multiloop systems.

Particularly noteworthy in table 2 are the values of the pilot lead time constant,  $T_L$ , for all the configurations with input bandwidth of 1.6 rad/sec or below (A through D). This is set almost exactly to cancel the roll subsidence time constant,  $T_R$ . For the larger bandwidth situation,  $T_L$  is increased. Because the crossover frequency is unchanged, this has the effect of increasing the phase margin, which in turn results in a decrease in tracking error under that which would be present if the change was not made. This effect coincides with its single-loop equivalent described in reference 1.

The values for crossover frequency and phase margin were obtained from the measured cross-spectra of input and bank-angle error. These cross-spectra can be written

$$\Phi_{\varphi_c \varphi_e} = \frac{1}{1 + Y_{\varphi(\varphi/\delta_a)_{\text{eff}}} A_c} \quad (12)$$

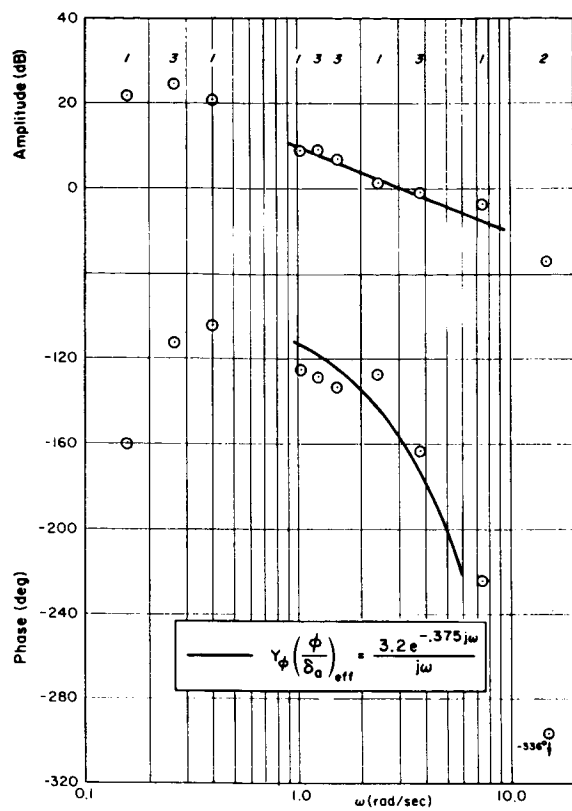
where  $(\varphi/\delta_a)_{\text{eff}}$  is the effective bank-angle-to-aileron transfer function, that is, the  $\varphi/\delta_a$  response with all pilot inner loops closed, and  $A_c$  is the amplitude of an input wave. The effective open-loop describing function,  $Y_{\varphi(\varphi/\delta_a)_{\text{eff}}}$ , was computed from equation (12) using the measured command bank angle error cross-spectra  $\Phi_{\varphi_c \varphi_e}$ . These are shown in figures 15 and 16. These figures show that the pilot was able to use the inner loops to keep the effective bank-angle-to-aileron response invariant with changes in dutch-roll stability.

The curves superimposed on the data of figures 15 and 16 illustrate the application of the simple crossover model to these situations. This most simple of human pilot models, which was evolved originally for very simple controlled elements, is seen to be reasonably valid in these far more complicated multiloop situations.

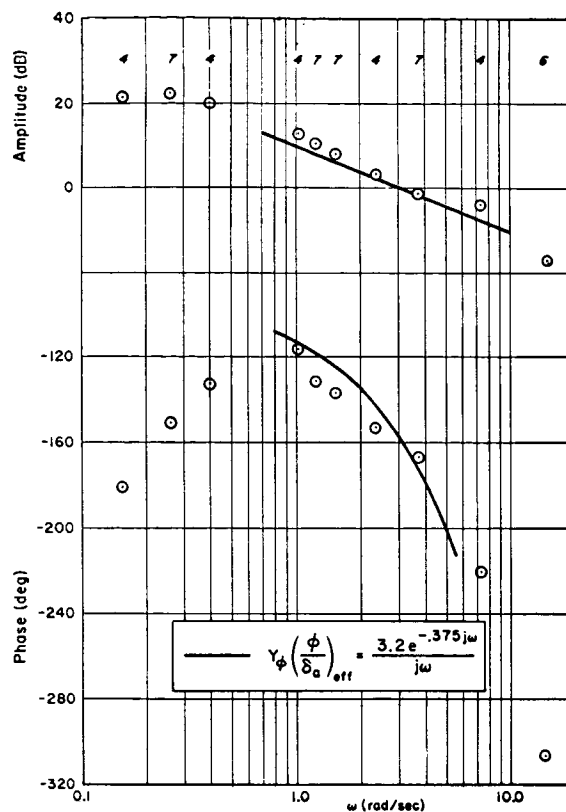
**PERFORMANCE MEASURES AND PILOT RATINGS.**—The describing function results discussed above also correlate with the measured tracking performance. Figure 17 shows the rms tracking errors for all the data runs (practice runs made the first day of the tests are not shown). The tracking performance for configurations A (stable) and B (slightly unstable) are essentially the same, while the errors for configuration C (highly unstable) appear slightly less. Thus, of these three the pilot did the best tracking when he was working the hardest in the inner loops. The error trend with input bandwidth is as expected: increasing input bandwidth (configurations D, B, and E) increased tracking errors.

The rms error data also correlate fairly well with the one-third law (ref. 1), that is,  $\sigma_{\varphi_e}/\sigma_{\varphi_c} \doteq (1/\sqrt{3})(\omega_i/\omega_c)$ . The one-third law predicts

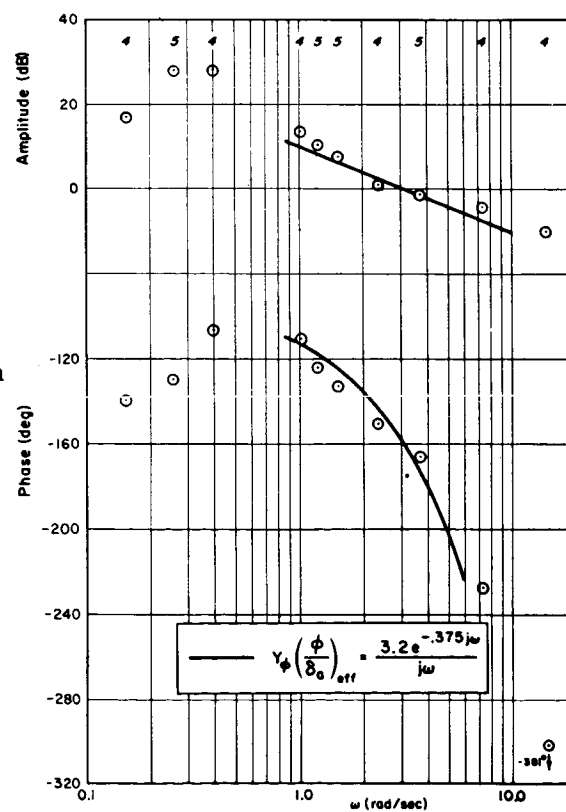
$$\frac{\sigma_{\varphi_e}}{\sigma_{\varphi_c}} \doteq \begin{cases} -11 \text{ dB for configurations A, B, and C} \\ -13 \text{ dB for configuration D} \\ -7 \text{ dB for configuration E} \end{cases}$$



a) Configuration A



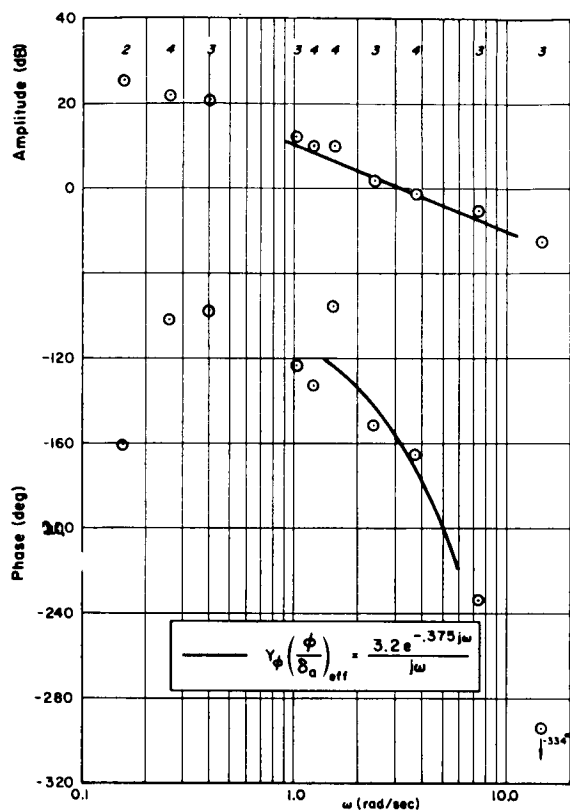
b) Configuration B



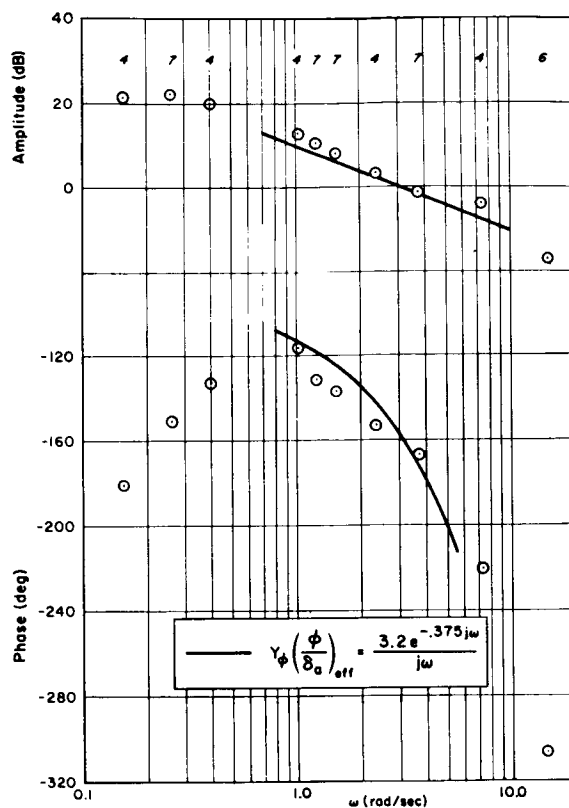
c) Configuration C

Figure 15. —Effective open-loop transfer function

$$Y_{\phi} \left( \frac{\phi}{\delta_a} \right)_{\text{eff}}$$



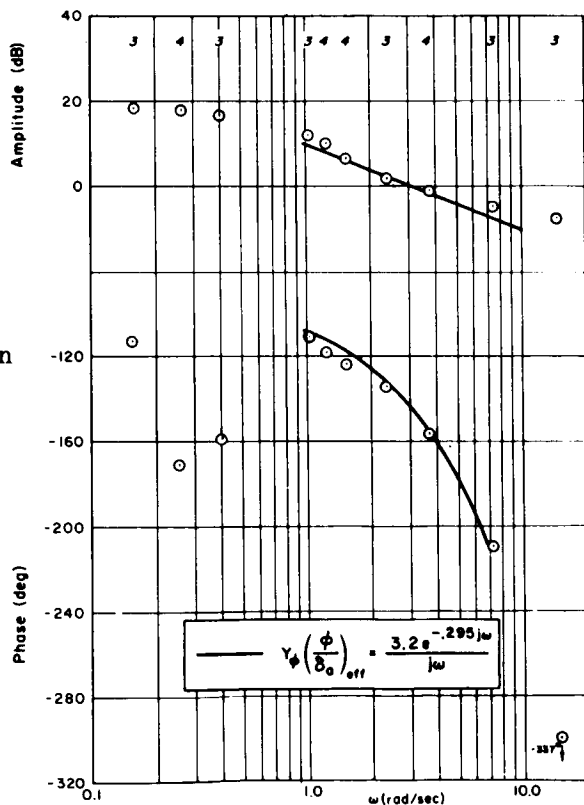
a) Configuration D



b) Configuration B

Figure 16. —Effective open-loop transfer function

$$Y_{\phi}(\frac{\phi}{\delta_a})_{\text{eff}}$$



c) Configuration E



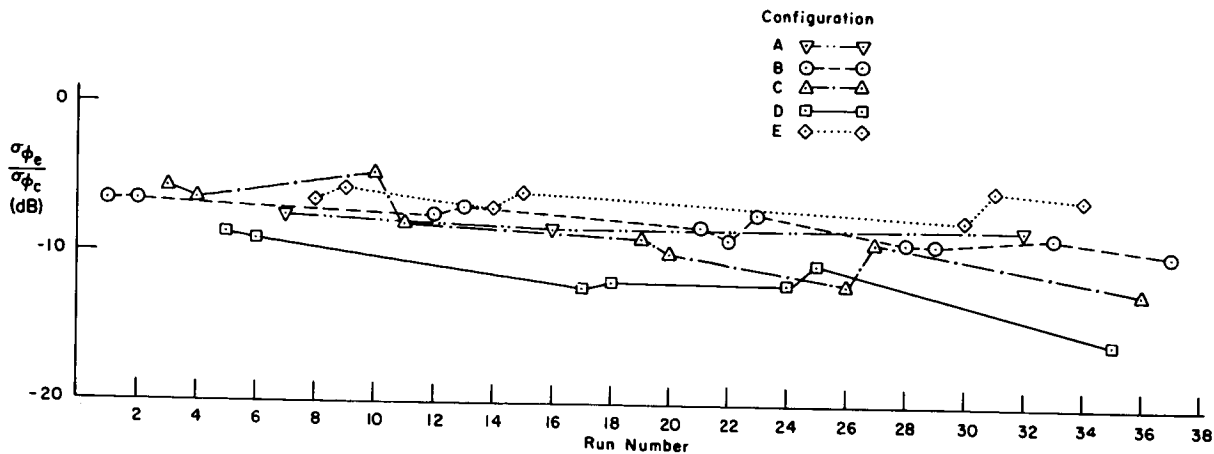


Figure 17.—Relative rms tracking errors,  $\sigma_i = 11^\circ$ .

The rms yaw rate is shown in figure 18. The variation with dutch-roll mode stability is as would be expected—yaw rate increases as the dutch-roll instability is increased. The variation with input bandwidth is somewhat peculiar, as the yaw rates for configurations D and E are both larger than that for configuration B.

One final bit of data worthy of note is the pilot ratings. The severe degradation in pilot rating as the dutch-roll instability was increased is shown in the following table:

Configuration	Pilot rating (Cooper scale)
A (stable)	4
B (slightly unstable)	6
C (highly unstable)	8

The less severe effects of input bandwidth are shown by:

Configuration	Input bandwidth, rad/sec	Pilot rating (Cooper scale)
D	1.2	5.5
B	1.6	6
E	2.4	7

The pilot rating for configuration A can be compared with the roll control experiments of reference 12. In those experiments a configuration of  $T_R = 0.2$  second was rated 1 to 2.5 when the control sensitivity was optimum (in our experiments the pilot was allowed to select

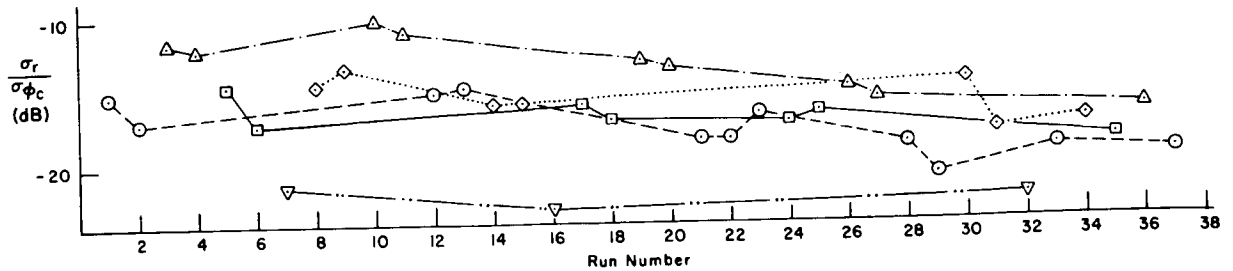


Figure 18.—Relative rms yaw rate,  $\sigma_i = 11^\circ$ .

the control sensitivity). The poorer rating for configuration A is apparently due to the magnitude and frequency content of the command input (the ref. 12 experiments did not include an input).

## CONCLUSIONS

Both general and specific conclusions can be drawn from the data and analyses presented here. The specific conclusions are given in the individual sections, so only the general conclusions are summarized as follows:

- (1) For multiloop control situations with an integrated display, the quasi-linear pilot model and adjustment rules evolved for single-loop systems are applicable to the multiloop system command loop.
- (2) The single-loop pilot model is also applicable, with reservations, to inner loop closures.
- (3) When it is advantageous to do so, a pilot will adopt a control crossfeed to reduce the inadvertent excitations of a subsidiary or nuisance mode.
- (4) Even while providing both crossfeed and inner-loop damping, pilot performance in the command loop—as measured by his describing function and rms errors—can be as good as that in a single-loop task. His subjective opinion, however, will be severely degraded.
- (5) When several feedback possibilities are present in a multiloop situation, the pilot will select those which permit the best dynamic performance with least pilot effort.

## APPENDIX

The numerical values of the stability derivatives used in the main experiments are as follows:

$$L'_{\beta} = -10 \text{ sec}^{-2}$$

$$N'_{\beta} = 1.0 \text{ sec}^{-2}$$

$$g/U_0 = 0.046 \text{ sec}^{-1}$$

$$L'_p = -5.0 \text{ sec}^{-1}$$

$$N'_p = 0.02 \text{ sec}^{-1}$$

$$L'_r = -1.5 \text{ sec}^{-1}$$

$$N'_r = \begin{cases} -1.5 \text{ sec}^{-1} & \text{for configuration A} \\ 0.15 \text{ sec}^{-1} & \text{for configurations B, D, and E} \\ 0.75 \text{ sec}^{-1} & \text{for configuration C} \end{cases}$$

$$N'_{\delta_a}/L'_{\delta_a} = 0.02$$

$$L'_{\delta_a}, N'_{\delta_r} \quad (\text{pilot selected the control gains})$$

The pertinent open-loop transfer functions can be written in the following form:

$$\frac{\varphi}{\delta_a} = \frac{L'_{\delta_a} (s^2 + 2\zeta_{\varphi} \omega_{\varphi} s + \omega_{\varphi}^2)}{\Delta}$$

$$\frac{\varphi}{\delta_r} = \frac{N'_{\delta_r} L'_r (s + 1/T_{\varphi})}{\Delta}$$

$$\frac{r}{\delta_a} = \frac{N'_{\delta_a} (s + 1/T_{r_a}) (s^2 + 2\zeta_{r_a} \omega_{r_a} s + \omega_{r_a}^2)}{\Delta}$$

$$\frac{r}{\delta_r} = \frac{N'_{\delta_r} (s + 1/T_{r_r}) (s^2 + 2\zeta_{r_r} \omega_{r_r} s + \omega_{r_r}^2)}{\Delta}$$

where

$$\Delta = (s + 1/T_s) (s + 1/T_R) (s^2 + 2\zeta_d \omega_d s + \omega_d^2)$$

Numerical values of the transfer-function factors are as follows:

Factor	Configuration			Factor	Configuration		
	A	B, D, E	C		A	B, D, E	C
$1/T_s, \text{ sec}^{-1}$	0.199	0	-0.054	$1/T_{r_a}, \text{ sec}^{-1}$	←	6.07	→
$1/T_R, \text{ sec}^{-1}$	5.00	5.00	5.01	$\zeta_{r_a}$	←	-0.055	→
$\zeta_d$	0.746	-0.075	-0.347	$\omega_{r_a}, \text{ rad/sec}$	←	0.674	→
$\omega_d, \text{ rad/sec}$	0.873	1.025	1.012	$1/T_{r_r}, \text{ sec}^{-1}$	←	5.02	→
$\zeta_{\varphi}$	0.671	-0.082	-0.356	$\zeta_{r_r}$	←	-0.030	→
$\omega_{\varphi}, \text{ rad/sec}$	1.095	1.095	1.095	$\omega_{r_r}, \text{ rad/sec}$	←	0.303	→
$1/T_{\varphi}, \text{ sec}^{-1}$	←	-6.67	→				

## REFERENCES

1. McRuer, Duane; Graham, Dunstan; Krendel, Ezra; and Reisener, William, Jr.: Human Pilot Dynamics in Compensatory Systems—Theory, Models, and Experiments with Controlled Element and Forcing Function Variations. AFFDL-TR-65-15, Jan. 1965.
2. Hall, I. A. M.: Effects of Controlled Element on the Human Pilot. WADC-TR-57-509, Aug. 1958.
3. McRuer, D. T.; and Krendel, E. S.: Dynamic Response of Human Operators. WADC-TR-56-524, Oct. 1957.
4. Seckel, E.; Hall, I. A. M.; McRuer, D. T.; and Weir, D. H.: Human Pilot Dynamic Response in Flight and Simulator. WADC-TR-57-520, Oct. 1957.
5. Cromwell, C. H.; and Ashkenas, I. L.: A Systems Analysis of Longitudinal Piloted Control in Carrier Approach. Tech. Rep. 124-1, Systems Technology, Inc., June 1962.
6. Ashkenas, I. L.; and Durand, T. S.: Simulator and Analytical Studies of Fundamental Longitudinal Control Problems in Carrier Approach. AIAA Simulation for Aerospace Flight Conference, Aug. 1963, pp. 16-34.
7. Durand, T. S.: Theory and Simulation of Piloted Longitudinal Control in Carrier Approach. Tech. Rep. 130-1, Systems Technology, Inc., Sept. 1963.
8. Stapleford, R. L.; Johnston, D. E.; Teper, G. L.; and Weir, D. H.: Development of Satisfactory Lateral-Directional Handling Qualities in the Landing Approach. NASA CR-239, 1965.
9. Stapleford, R. L.; Wolkovitch, J.; Magdaleno, R. E.; Shortwell, C. P.; and Johnson, W. A.: An Analytical Study of V/STOL Handling Qualities in Hover and Transition. AFFDL-TR-65-73, May 1965.
10. McRuer, D. T.; and Graham, D.: Pilot Models for Single- and Multi-Loop Systems with Random Forcing Functions. Tech. Rep. 134-1 (The Franklin Institute Rep. STI-FIL 5), Systems Technology, Inc., Nov. 1964.
11. Ashkenas, I. L.; and McRuer, D. T.: Approximate Airframe Transfer Functions and Application to Single Sensor Control Systems. WADC-TR-58-82, June 1958.
12. Creer, B. Y.; Stewart, J. D.; Merrick, R. B.; and Drinkwater, F. J., III: A Pilot Opinion of Lateral Control Requirements for Fighter-Type Aircraft. NASA Memo 1-29-59A, Mar. 1959.
13. Seltzer, L. J.; and McRuer, D. T.: Survey of Analog Cross Spectral Analyzers. WADC-TR-59-241, Dec. 1959.

N67-15865

## 14. PILOT RESPONSE IN MULTILoop TRACKING TASKS IN COMBINATION WITH SIDE TASKS

James J. Adams  
Langley Research Center, NASA

During the past year at Langley Research Center, testing with multiloop tasks has continued. At a previous conference on manual control<sup>1</sup> we presented figure 1 which shows the response of a human controller in a simplified multiloop task—one based on the horizontal translation control of an Apollo lunar excursion module—and the reproduction of this response that was obtained with linear, constant-coefficient models placed in the control loop instead of the pilot. The system that is controlled in this case consists of a vehicle supported by a rocket engine which is aligned with the vertical body axis of the vehicle. Horizontal translation is performed by tilting the vehicle until the desired horizontal acceleration is achieved. In this simulation which was used to obtain figure 1 this operation was displayed to the pilot with an X-Y plotter and a small dial meter. The attitude of the vehicle was displayed using the meter, which was mounted on the moving carriage of the X-Y plotter. The horizontal movement of the plotter carriage displayed the horizontal movement of the vehicle. The task was to start from a given horizontal position, move a represented 1000 feet, stop, and hover.

During the last year response records of human control of the same system in more complex control situations have been obtained. These situations which were studied are based on a lunar letdown maneuver. Six degrees of freedom were represented in the simulation. The pilot had control of main engine thrust and vehicle attitude, and thrust was controlled proportionally from 100 percent down to 10 percent. Attitude rate was controlled with a first-order response having a time constant of 1 second in a proportional manner except that a small dead band, large enough to cover the friction in the control stick, was included. Attitude was presented to the pilot with a three-axis 8-ball instrument. Altitude and horizontal velocity were presented on dial-type instruments.

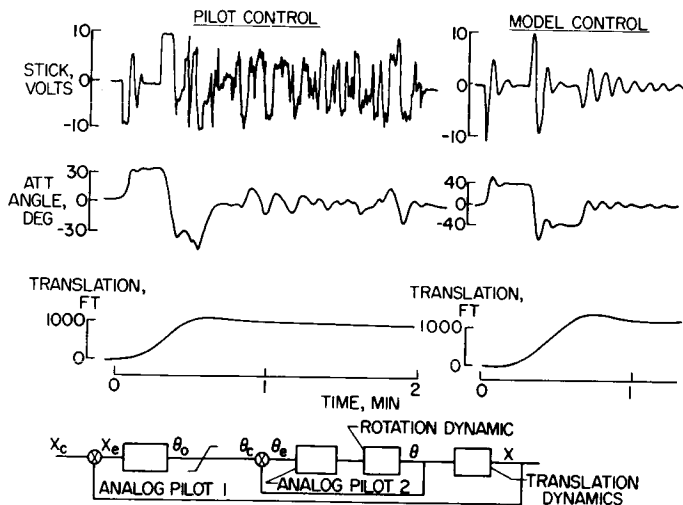


Figure 1.—Comparison of response obtained in a multiloop simulation with a human controller and with analog models for the pilot.

<sup>1</sup>First Annual NASA-University Conference on Manual Control, Ann Arbor, Mich., 1964.

The task presented to the pilot was to follow a predetermined pitch program which was designed to bring the vehicle from a 50 000-foot orbit to a condition of zero vertical velocity and low horizontal velocity at an altitude of approximately 1500 feet. At this point the pilot must depart from the pitch program, adjust pitch attitude and thrust to establish a stable hovering condition, and reduce the horizontal velocity to zero. This was the terminal condition for the simulation. The pilots were able to perform this maneuver in a very smooth manner, as shown in figure 2(a).

This type of test was also conducted with side tasks added to the pilot's work load. These side tasks were presented using the simulator known as the Mercury Procedures Trainer. They consisted of such items as coping with stopping the suit ventilation fan. In this example situation the pilot had to consider whether the fan failure was due to a fuse failure, in which case he would switch to the alternate fuse, or due to a fan motor failure, in which case he would select one of two alternate motor switch positions. The fan would also stop, in combination with other events, if a battery or an inverter failure occurred. A total of 26 such failures could be caused to occur, each with its own indication, or combination of indications, of failure, and its own procedure for correction. These failures were presented to the pilot in random succession. As soon as the pilot corrected one failure, he would be presented with another.

The effect of such side tasks on the maneuver response is shown in figure 2(b). During the first 5 minutes of the run, when the pilot was following the pitch program, there was no effect. However, in that portion of the run when the pilot was attempting to establish a stable hovering condition, the response was no longer as smooth and precise as it was when no side tasks were present. No dangerous condition, such as going below zero altitude, resulted. A longer time was required to establish the desired terminal altitude, and then there was a noticeable oscillation in this altitude, with a period of about 30 seconds.

No reproduction of this human control for this complex maneuver was attempted with the use of models. However, the simpler multiloop tests involving only the horizontal translation response were performed with the addition of side tasks also, and the same sort of random response noted in the lunar-letdown task was also noted in the simpler simulation. Reproductions of the human response were obtained using models for the simpler task. These results will now be presented.

A research pilot performed the horizontal translation multiloop task very smoothly, and the linear, constant-coefficient models gave a very good reproduction of this maneuver, as shown in figure 3. When the side task was added, the maneuver was done in a less precise manner, as shown in figure 4. The translation mode of motion shows a very noticeable oscillatory response which consistently had a period of about 30 seconds. One way of arranging the model so that it would reproduce this characteristic was

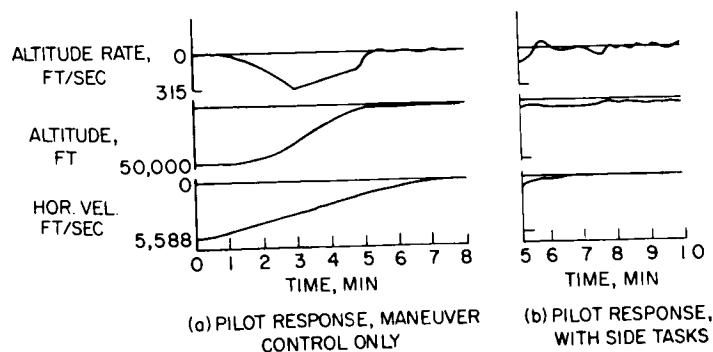


Figure 2. —Pilot controlled response in a lunar letdown maneuver with and without side tasks.

to switch the lead gain of the outer-loop human transfer function on and off. This switching was done as a function of the translation being within a selected band around the desired value for the length of time required for three control motion peaks. When the translation entered this band, the model lead would be switched off for a selected length of time. At the end of the time, the translation would again be tested, and the switch on the lead again cycled. This arrangement

gives the time history shown in figure 4(b). We feel that this arrangement for switching gives a good reproduction of the human pilot in this type of control task.

The side tasks used in these tests were either the subsystem monitoring that was generated with the Mercury Procedures Trainer or a dot-making task. In this dot-making task the subject made as many dots as possible alternately in two separated, restricted areas. The same effect on the tracking task could be produced with either of these two side tasks.

Another response characteristic which was noted in these tests was one which occurred when engineer subjects performed the task with no side tasks. The attitude mode of motion was often quite random appearing although the translation mode of motion was well regulated. Engineer subjects were more prone to this type of response than were pilot subjects. This type of characteristic was reproduced by incorporating a duty cycle in the inner-loop pilot model. In this case the switching was applied to the static gain of the model, which would reduce the output of the inner-loop pilot model to zero when the switch was in the off position. The results of including this type of switching are shown in figure 5.

In addition to the work done on time-varying model representation of the human, linear, constant-coefficient models have been used to examine the system instability that can occur in a multiloop task when an unexpected damper failure occurs in the inner loop. An example of this instability which was obtained with an engineer subject is shown in figure 6. After the damper failure two cycles of a divergent oscillation occur, after which the response becomes that which is normally obtained with an undamped vehicle. The corresponding characteristics obtained with linear models are presented in table 1, which presents the closed-loop characteristics for the complete system. It is shown that the normal system has an attitude mode of motion with a positive damping ratio.

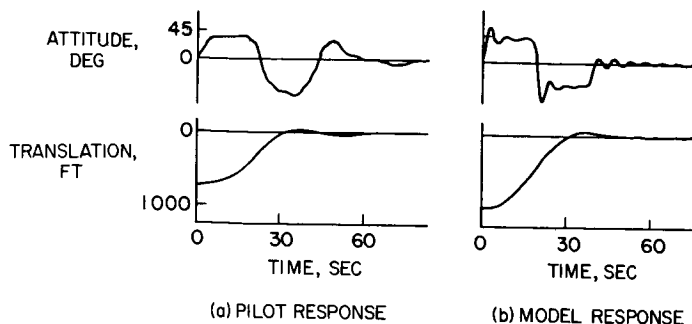


Figure 3.—Comparison of test-pilot control and model control in a multiloop simulation.

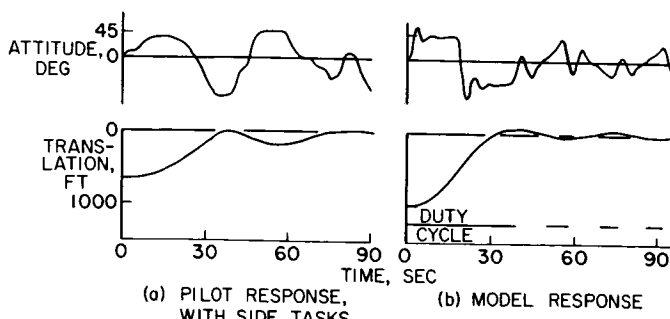


Figure 4.—Comparison of test-pilot control of a multiloop task with side task added, and model control. Model contains a duty cycle on the lead gain in the outer-loop analog pilot.

TABLE 1. —CLOSED-LOOP CHARACTERISTICS BEFORE AND AFTER A DAMPER FAILURE

$\omega$ , rad/sec	$\zeta$	Real roots
<p>Normal system</p> <p>Inner-loop pilot model, <math>\frac{\delta}{\epsilon} = \frac{K_1\tau + K_1K_2s}{(\tau + s)^2}</math></p> <p>where <math>K_1 = 5.0</math>, <math>K_2 = 3.0</math>, <math>\tau = 5.0</math></p> <p>Dynamics <math>\frac{\theta}{\delta} = \frac{2}{s(s+1)}</math></p> <p>Outer loop: <math>K_1 = 0.09</math>, <math>K_2 = 92.0</math>, <math>\tau = 10.0</math></p> <p>Dynamics <math>\frac{x}{\theta} = \frac{5.36}{s^2}</math></p>		
1.40 10.2	0.33 .99	-0.16, -0.41, -2.82, -6.40
<p>After damper failure</p> <p>Inner-loop dynamics changed to <math>\frac{2}{s^2}</math></p>		
1.54 10.2	-0.077 .99	-0.18, -0.27, -3.21, -6.31
<p>After pilot adaption to <math>\frac{2}{s^2}</math> dynamics</p> <p>Inner-loop pilot gains: <math>K_1 = 5.0</math>, <math>K_2 = 5.0</math>, <math>\tau = 7.0</math></p>		
1.33 10.5	0.029 .99	-0.18, -0.26, -4.77, -7.53



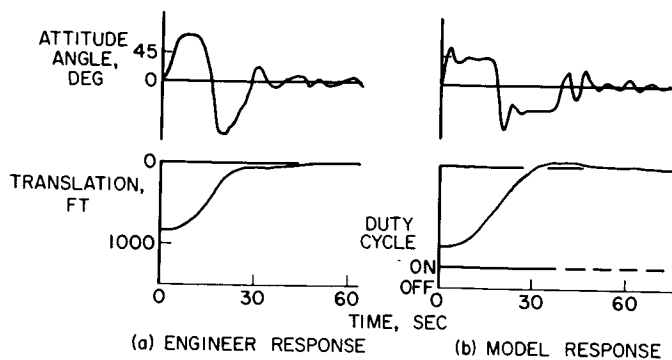


Figure 5. —Comparison of engineer test subject control of a multiloop task and model control. Model contains a duty cycle on the static gain in the inner-loop analog pilot.

When the vehicle damping is removed, this damping ratio becomes negative. Further, when an analog model which represents the response of a human controlling an undamped vehicle is substituted in the system, the system characteristics again become stable.

It is felt that these calculations of system characteristics illustrate that linear pilot models can contribute to a quantitative understanding of the damper failure problem. This understanding should aid in the further determination of the exact nature of the human adaptation to a damper failure, and perhaps lead to some improvement in this potentially dangerous control situation. It has also been shown that including switching in the model of human controllers can contribute to a better representation of a human in a complex control task.

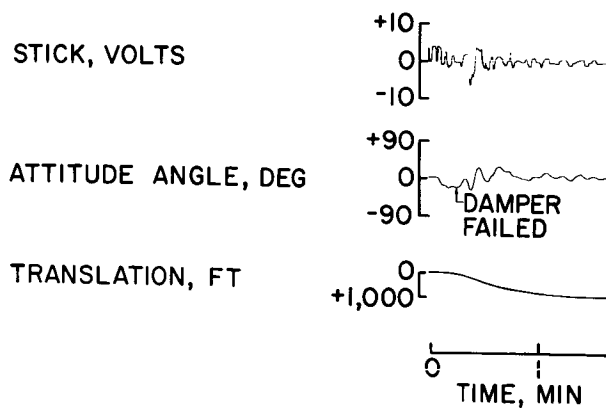


Figure 6. —Examples of manual control with unexpected damper failures.

**DISPLAY**

N67-15866

## 15. SYMBOLIC AND PICTORIAL DISPLAYS FOR SUBMARINE CONTROL\*

*Robert C. McLane and James D. Wolf  
Honeywell, Inc.*

The Navy has given extensive support to the development of several different integrated display concepts for nuclear submarines. This paper describes a research program through which comparative, empirical analyses of these concepts were accomplished.

The experiments established guidelines for use of these integrated displays in vehicle control including monitoring and mission plan revision as a function of external constraints such as attacking weapons systems. The displays evaluated can be classed in two general categories — symbolic and pictorial. The pictorial contact analog format was tested with symbolic and with pictorial or perspective-quicken tracking techniques. The symbolic depth-azimuth format was tested with symbolic quickened tracking and with a pictorial presentation of a predictor tracking device.

The experimental approach employed tests which were designed to reveal differences between the displays that have practical significance to the Navy. The tests were: measurement of tracking performance with forced sampling or blanking; recording reaction, judgment, and decision times in response to the presence of a homing torpedo; and determination of the correctness of the decision on collision imminence.

There was no appreciable degradation in tracking performance due to periodic blanking of the display for as long as 75 percent of a 10-second period. The pictorial or contact analog format produced lower tracking error scores than those with the symbolic depth-azimuth format. This result was a general trend, rather than a statistically significant difference in all cases, and may be attributable to their perceptual differences and differences in their quickening equations. The predictor display yielded a significantly smaller number of collisions than any of the other display configurations. There were no significant differences between the displays in the recordings of reaction, judgment, and decision times.

This paper describes a research effort directed at understanding the significance of differences in four integrated steering and diving display concepts for contemporary submarines. The stimulus for this effort was a display feasibility study for the tandem-propeller submarine (refs. 1 to 3) in which quickened tracking was introduced to a pictorial display in a perceptually integrated, perspective manner.

---

\*This study was sponsored by the Office of Naval Research under Contract Nonr 3675(00)(FBM).

The question was raised of whether this technique of introducing quickened tracking—or of monitoring automatic controller performance—into a pictorial display would offer advantages over the conventional technique of a symbolic tracking overlay, as embodied in the Norden contact analog display system described in reference 4. Furthermore, while comparing these two display concepts, it seemed appropriate to include two other display concepts which were of active interest to the Navy—the symbolic depth-azimuth Electric Boat SQUIRE (ref. 5) system; and the Kelley predictor display (ref. 6).

The objective of the study was not to establish whether a man should be assigned to the tracking task, but rather to discern the sensitivity of the man-display combination to effective utilization of information presented in the display space which required use of his tracking and decision skills.

## EXPERIMENTAL APPARATUS

The experimental equipment for this study consisted primarily of an analog computer facility with a fixed-base, single-operator, control-display station designed for rapid change-over between all four display systems under study. Thus it was possible to generate all four displays in such a manner that the same group of subjects could be used on all displays in a balanced design.

Two of the four systems incorporated a contact analog display generator with a 17-inch commercial television monitor. The monitor exhibited the contact analog cues which were mixed via closed-circuit TV with externally generated display symbols as required. Standard laboratory function generators, analog computer techniques, and electronic switches were used to form these symbols. This closed-circuit TV system was also employed in generation and display of the symbolic display formats which did not embody the contact analog cues.

Acronyms have been assigned to each display, not to conceal the developer and/or inventor identity but to emphasize that these display systems were simulated representations, rather than production systems. Furthermore, with the knowledge and technical cooperation of Norden and Electric Boat, certain minor modifications of format were required in order to have comparable displays to test. These factors are discussed in the description of each display.

**DEPTH-AZIMUTH DISPLAY WITH SYMBOLIC QUICKENED TRACKING (DepAzSymb).—** This display placed four shape-coded symbols upon a depth-azimuth coordinate frame. These symbols indicate ordered position, actual position, obstacle or target position, and a quickened tracking reticle. The general characteristics of this display are shown in figure 1. In this study, an auxiliary digital range display was added immediately above the display screen to aid in obstacle or target judgment. The DepAzSymb display represented the Electric Boat SQUIRE system (ref. 5), with the azimuth dimension reduced from a full  $+180^\circ$  to a sector of  $\pm 37\frac{1}{2}^\circ$  to correspond to the scaling of the contact analog which could not feasibly be expanded. This required a proportional reduction of the rudder term in the quickening equations. A photograph of this display appears as figure 2. The azimuth-depth scale was placed on a bezel about the face of the TV monitor and, therefore, was subject to parallax errors in reading display dimensions. However, this scale was used only in a qualitative sense rather than providing a primary element of the display, and this effect was not felt to be serious. Its principal use was in noting depth clearances in the torpedo avoidance task. The quickening equations are a function of many variables and involve several products-of-motion variables

including absolute values. This made it difficult to equate the sensitivity, or gain, of the display with that of the other three displays, which were essentially of simpler form. For example, one could say that a given pitch or trim rate caused each display to displace a specific amount and that they were not scaled equally. However, the contribution of pitch rate was seen in two terms in the SQUIRE equation: one linear, and another proportional to depth error magnitude. This is only one example, but it shows the problem of scaling on a comparison of this type, since it is clear that scaling, or gain, has so significant an effect upon performance.

It was necessary to provide limiters on the displacement of the quickened element of the DepAzSymb display so that the operator did not lose the symbol if he developed large errors and then was unable to determine his proper recovery action. These limits were a firm requirement but tended to cause critical overcontrol during restoration of normal performance. The operators learned of this tendency and tended to undercontrol, thus keeping the errors larger than desired.

#### CONTACT ANALOG DISPLAY WITH SYMBOLIC QUICKENED TRACKING (ConAnSymb).—

This is a pictorial inside-out "window" display with a superimposed symbolic compensatory tracking task. This concept represents real world geometry consistent with available sensors and on-board navigational computation, on a two-dimensional perspective plane. The symbolic tracking task permits the introduction of quickened information without loss of vehicle status information with respect to the earth coordinate reference frame. In figure 3, the operator is shown a horizon, a grid structure representative of the surface of the sea, and a parallel structure representative of the sea floor or test depth of his vehicle. Between these surfaces, a command path is displayed which is earth stabilized and offers cues of depth and azimuth errors.

Figure 4 shows the display as employed in the experiment. Here, the ship is below the path, and the operator has to bring his bow reference cross up into the quickened tracking square. For purposes of illustrating display gain similarities in the depth and azimuth rate axes, this figure has initial conditions in these axes, and so the operator must steer right

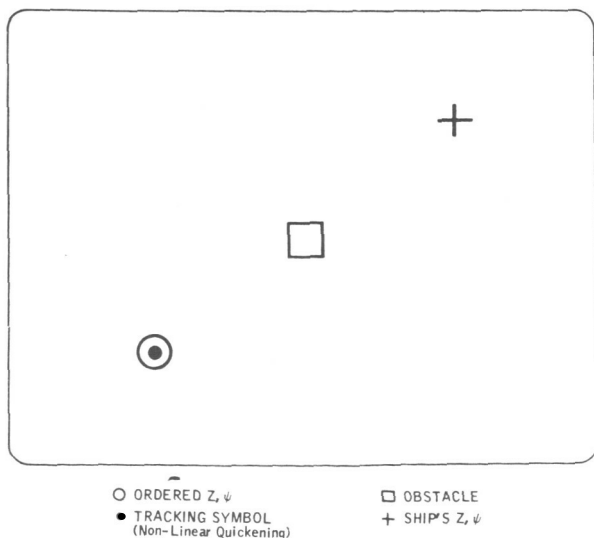


Figure 1.—Symbolic depth-azimuth quickened display.

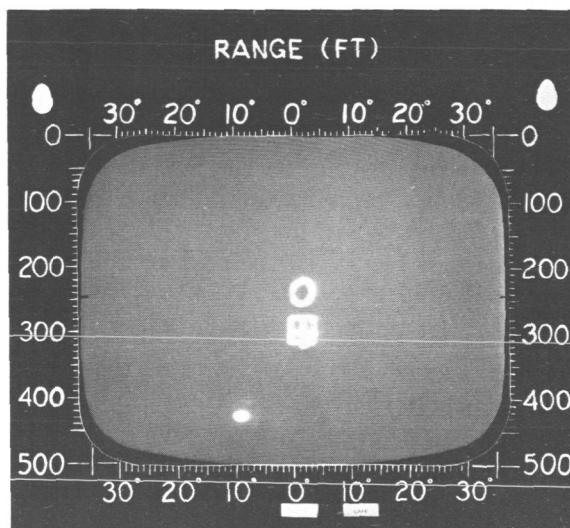


Figure 2.—DepAzSymb simulation of the SQUIRE display.

or his path will drift off the screen when the simulator is turned on. Comparison of figures 2 and 4 show relative sensitivities to identical initial conditions for these displays.

It is clear that in the ConAn-Symb display, the operator need not use the display cues offered by the path in the tracking process, since it consists of merely nulling the bow reference marker into the quickened compensatory tracking symbol. It was mandatory, however, that he use these cues in the obstacle judgment task. In addition, these cues were useful in controlling when the quickened symbol was subjected to the required displacement limits.

The ConAnSymb display represented the Norden contact analog system (ref. 4), utilizing the display generation equipment provided for the tandem propeller submarine study of references 1 to 3. In this display, the obstacle appears as a pole between the grid structures with a short horizontal bar to indicate obstacle depth. Range is determined by perspective cues.

CONTACT ANALOG DISPLAY WITH PERSPECTIVE TRACKING SYMBOL (ConAnPers).—By introducing the quickened tracking information in the three-dimensional perspective of the contact-analog space, the operator is given a consistent display rooted in real-world geometry. This concept is described as consistent because vehicle situation and tracking functions are perceptually integrated. The operator forces the tracking symbol to conform to the perspective of the pathway element in the contact analog by appropriate control column deflections in a pursuit tracking task. This action brings his vehicle to the

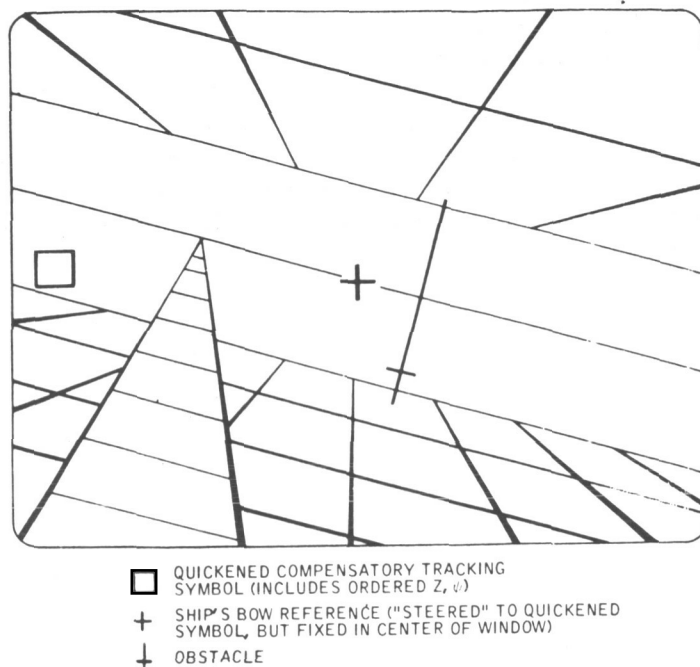


Figure 3.—Contact analog display with symbolic quickened tracking.

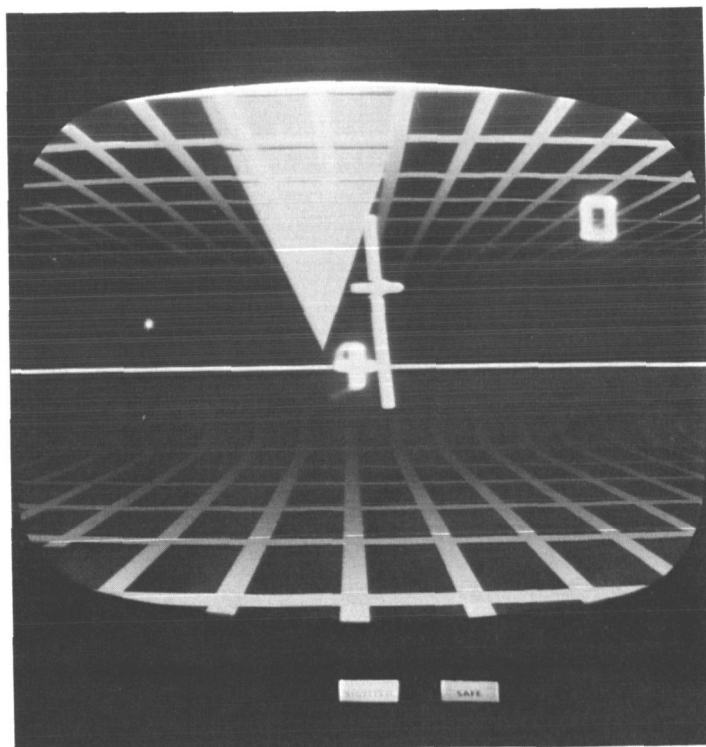


Figure 4.—ConAnSymb simulation of the Norden contact analog symbolically quickened display.

ordered depth and azimuth of the pathway. The quickened tracking symbol is made up of an element of the horizon and elements of the left and right curbstones of the pathway. As shown in figure 5, the tracking symbol is matched, in a pursuit tracking manner, with the appropriate elements of the real-world analog. This figure represents the quiescent state of error-free vehicle status, with the pathway tangent to own ship keel. The elements of the display format are defined in figure 6. Display sensitivity is illustrated in figure 7 for comparison with figures 2 and 4 for the same initial conditions of vehicle-motion variables.

#### SYMBOLIC DEPTH-AZIMUTH PREDICTOR DISPLAY (DepAzPred).—

The predictor concept is clearly compatible with a wide variety of display formats and could have been employed as an element in a pictorial contact analog display.

However, in this research study, limitations of the particular equipments available for the program required the symbolic depth-azimuth format. This technique utilized the two-time-scale computer method of prediction, where a model of the vehicle in a fast-time simulation is employed to determine future trajectories of the vehicle with prevailing initial conditions, and various control input programs.

The operator selects a desired future time to rendezvous with the ordered depth-azimuth position, and within the known programed system dynamics, he can apply appropriate control column deflection to effect this solution. The particular mechanization of this concept tested is shown in figure 8. As in the first display discussed, the range to the target or obstacle is given to the subject on an adjacent digital voltmeter readout. This display concept was originated by C. R. Kelley of Dunlap Associates (ref. 6). The simulation of this display is shown in figure 9, with the same initial conditions of depth and azimuth rate as used in figures 2, 4, and 7.

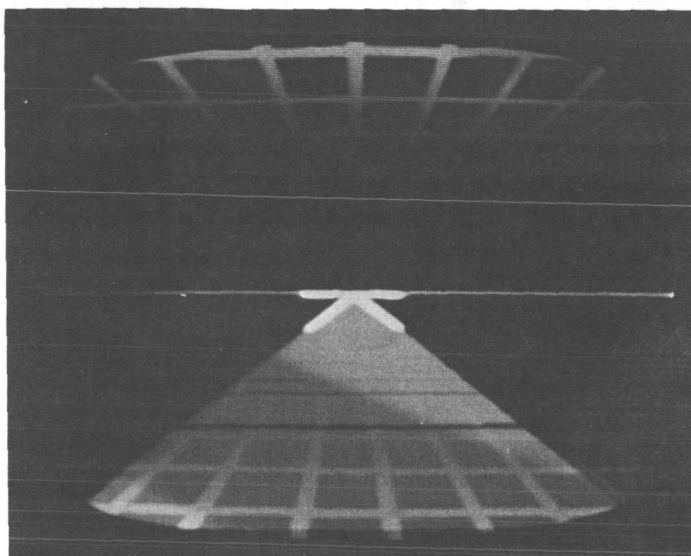
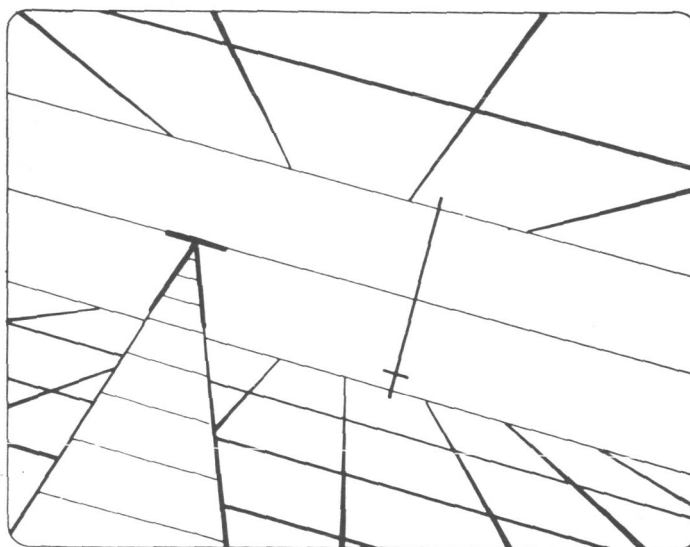


Figure 5.— ConAnPers simulation of the Norden contact analog perspective quickened display.



△ ORDERED Z,  $\psi$   
 TRACKING SYMBOL  
 (Perspective Tracking Symbol)

+ OBSTACLE  
 SHIP'S Z,  $\psi$  GIVEN BY TOTAL WINDOW  
 VIEW, GRIDS, PATH, HORIZON

Figure 6.— Contact analog display with perspective quickened tracking.

Since the predictor display had not been reduced to a system mechanization for sea tests, as both the ConAnSymb and DepAzSymb displays have been, and because of the promising performance in torpedo avoidance noted in the first experiment, it was decided to conduct an additional study on variations of this display. One of the variables selected was predictor span.

COMPARATIVE SENSITIVITY OF THE FOUR DISPLAYS.—In table 1, the displacement of each display for single initial conditions in each of the motion variables is given. While this is indicative of the sensitivity of each display to that single variable, it may change with simultaneous excitation of initial conditions, depending on the quickening equations.

THE CONTROL COLUMN AND SUBJECT RESPONSE DEVICES.—The manual-control input device was a handle bar-type helm wheel for rudder control, with a deck-pivoted fore-aft column motion for stern plane control. The force levels provided an average of 1/6 lb/deg of wheel rotation, with a 6 pound maximum force corresponding to full command rudder deflection. Maximum command stern plane deflection required about 10 pounds of push or pull force, with an average gradient of 2/3 lb/deg, or 1/3 lb/in. of column deflection.

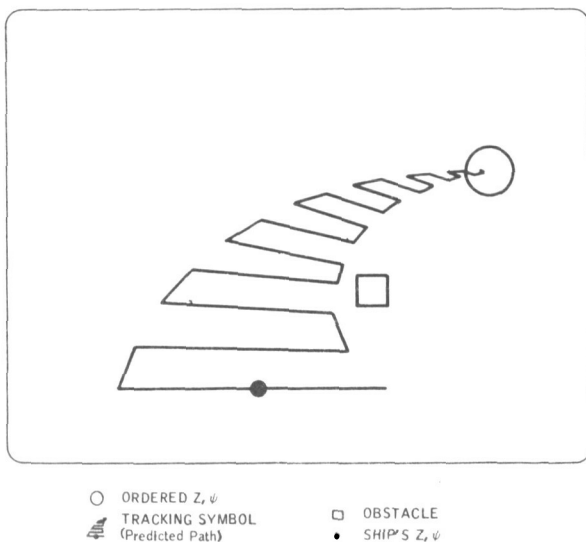


Figure 8. — Symbolic depth-azimuth predictor display.

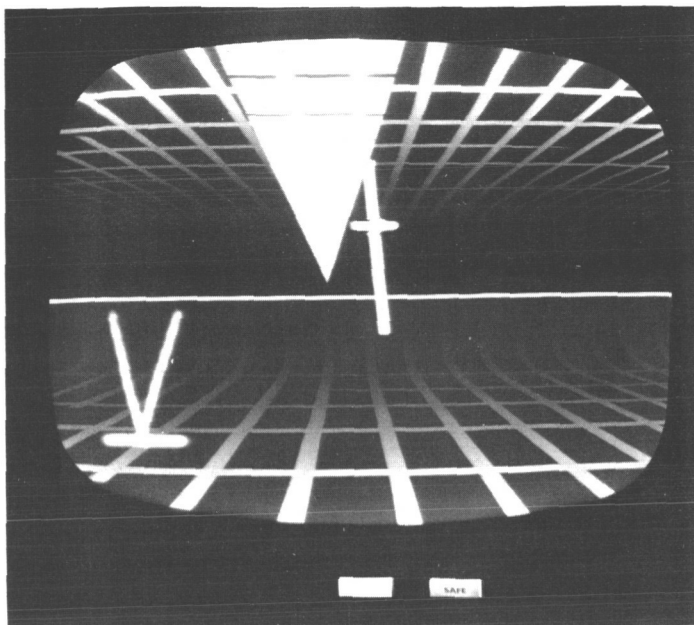


Figure 7.— ConAnPers simulation of the Norden contact analog perspective quickened display.

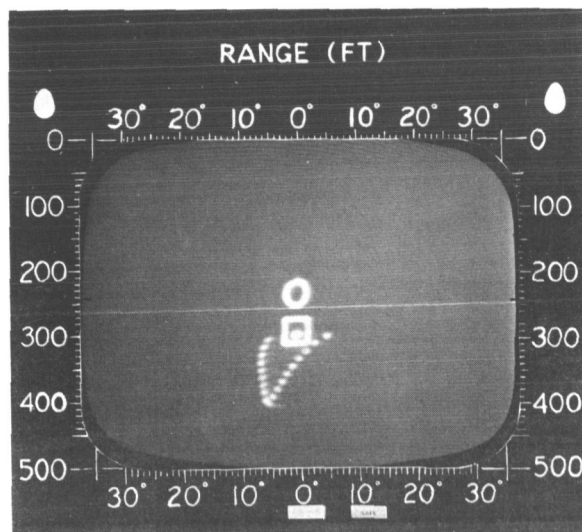


Figure 9. —DepAzPred simulation of the Kelley predictor instrument.



TABLE 1. — SINGLE PARAMETER SENSITIVITY OF DISPLAYS

Motion parameter	DepAzSymb	ConAnSymb	ConAnPers	DepAzPred
	Displacement, in.			
Depth rate ( $\pm 5$ ft/sec)	$\pm 2.6$	--	--	--
Pitch or trim ( $\pm 3^\circ$ )	$\pm 1.0$	$\pm 2.7$	$\pm 2.7$	$\pm 1.4$
Pitch rate ( $\pm 2$ deg/sec)	$\pm 1.3$	$\pm 2.7$	$\pm 2.7$	$\pm 1.4$
Yaw rate ( $\pm 0.7$ deg/sec)	$\pm 1.2$	$\pm 3.0$	$\pm 3.0$	$\pm 0.7$

A thumb-actuated push-button switch was placed on the right grip of the wheel, for the subject to indicate his awareness of the presentation of the obstacle. Foot switches were secured to the deck for the subject's use in recording his arrival at a judgment of collision imminence or safe passage with respect to the obstacle. Suitably inscribed light-panel indicators below the television display latched and stored these switch actuations. Thus, an unintended switch actuation could be verbally addressed to the experimenter by the subject. A small panel of lights was placed at the side of the booth to announce trial run and rest cycles, as well as torpedo obstacle collisions.

**THE VEHICLE SIMULATION.**—Complexity in simulation of vehicle equations of motion had to be avoided because of the large demand upon computer capacity for display generation, scoring error criteria, and task generation. Pitch, roll, and yaw body rotations, together with transverse and normal translations, were simulated with the following assumptions: neutral buoyancy, constant forward speed, no hydrodynamic or inertial coupling, and linearized trigonometric functions. Previous work (ref. 7) supports the validity of such simplifications in simulation of vehicle dynamics for applications and studies of this type. Stability derivatives were obtained from reference 8. These equations were programed in both real time and fast time, the latter being required for the predictor display concept.

The homing-torpedo barrier was generated by assuming that the torpedo carried sufficient sensing and control capability to maintain constant relative azimuthal bearing to the submarine and that it could follow the depth of the submarine within a first order time lag. This configuration presented a sufficiently difficult task that the subject was compelled to devote considerable attention to displayed cues and to execute carefully contemplated maneuvers to avoid a collision while minimizing departures from command azimuth and depth. The task evolved from simpler configurations which offered little challenge, and showed less likelihood of exhibiting differences between the display concepts.

## EXPERIMENTS

The experimental method was developed to test for the significance of differences between the four display configurations in their utility in judgment and decision functions as well as in tracking performance.

The experimental study was conducted in two parts. The first part was the major effort, comparing all display formats, while the second part was concerned with further study of just one of the displays.

## EXPERIMENTS—PART I

**SUBJECTS.**—Subjects were selected at random from a list of University of Minnesota NROTC midshipmen who had volunteered for this study. Although none of the subjects were previously experienced at controlling either real or simulated submarines or large surface vehicles, all were familiar with the meaning of such terms as "course" and "relative bearing" which were used in instructions to describe the experimental task. Each subject was paid on an hourly basis for his time, with an additional bonus payable upon completion of the 12 sessions required by the experimental design. Apparently due to their participation in the NROTC program the subjects were very highly motivated and cooperated very well throughout the study.

**EXPERIMENTAL DESIGN.**—The design used was essentially a fractional replication of a  $p \times p \times q$  factorial experiment (refs. 9 and 10) in which the four displays (D) and four orders (O) of display presentation represented the two dimensions of a Latin square. The third design dimension represented trial sets (means of each set of three consecutive trials) within sessions. A parallelepiped of this design is shown in figure 10. In this figure it can be seen that for each level of T (trial sets), the design is exactly the same. Two subjects were randomly assigned to each of four groups (G), with each group receiving a different order of display presentation.

This design was repeated for each of three phases of data collection, with the same subjects serving in each phase. In phase I, basic tracking performance was determined. In phase II, tracking performance was measured for different levels of display blanking forced sampling. During phase III, the displayed information was continuously available, but an additional judgment, decision, and maneuver task was added.

Each subject was required to participate in 12 experimental sessions. The first session began with the phase I task utilizing the display designated by the experimental design. Phases II and III on the same display were then completed during the two subsequent sessions. Thus, each subject completed all three phases on a given display before continuing with the succeeding display.

All sessions consisted of eighteen 3-minute trials with a 1-minute rest period after every first and second trial and a 3-minute rest after every third trial. During all but the last 10 seconds of each rest period, the display was blanked out while the computers were automatically cycled to "hold" mode and data were recorded by the experimenter. The computers then cycled to "reset"

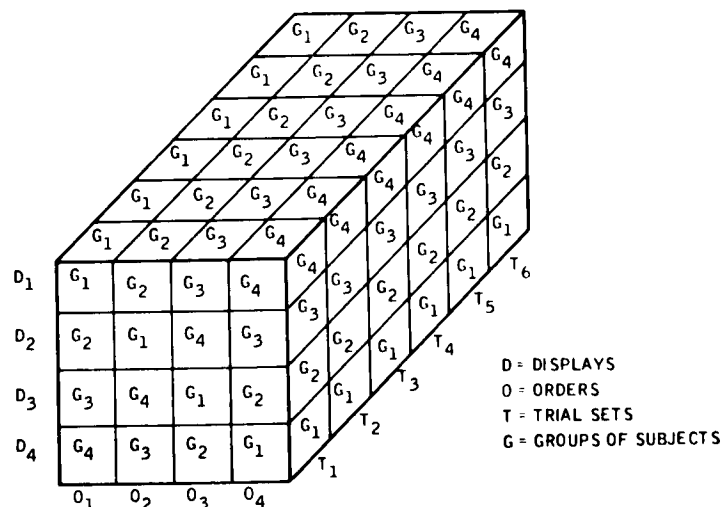


Figure 10.—A parallelepiped representative of the experimental design.

mode, and the symbols again appeared on the display, indicating to the subject that he had 10 seconds to prepare for the onset of the next trial.

Instructions specific to display type and experiment phase were read by the experimenter to the subject at the beginning of every session. Included in each reading was a demonstration trial in which the experimenter maneuvered the submarine under conditions specified in the instructions. This procedure clarified each phase task requirement for the subject and assured the experimenter that the simulator was operating correctly.

VEHICLE CONTROL AND DECISION TASKS.—As previously noted, data collection was partitioned into three phases. Phase I required the subject to bring the submarine to a series of discrete depth and azimuth commands. Each trial involved two command changes, with one command at the onset of each trial and another after 80 seconds had elapsed. The required sequence of 36 commands was selected at random from an 81-cell depth versus azimuth matrix of nine depth changes ranging between 0 and  $\pm 180$  feet, and nine azimuth changes between 0 and  $\pm 27^\circ$ .

Phase II was identical to phase I, with the exception that the display was blanked out periodically to simulate three levels of operator work load. The three levels of blanking used were light-dark ratios of 25/75, 62.5/37.5, and 100/0, the first two being presented at 10-second periods and the third representing continuous visual feedback.

In addition to the phase I tracking task, phase III required that the subject avoid colliding with a simulated homing torpedo. The torpedo was programed to move only on an east-west vertical plane and its fire-control computer was able to hold a constant relative bearing to the submarine. Thus, a collision in azimuth was inevitable as the submarine proceeded in a nominally north direction at a constant 20 knots. It was possible, however, to avoid the torpedo obstacle by judicious maneuvering of the submarine in depth.

In the instructions which the experimenter read, the subject was told that, on some trials, the rate of depth change achieved in bringing the submarine to the command depth would be sufficient to avoid collision as the submarine passed through the plane of the torpedo barrier. During their trials, depth-change rates concomitant to following the command depth would not be sufficient and evasive action would be necessary. After the evasive maneuver, the subject returned to the command azimuth and depth. The subject was required to decide, as quickly as possible, which condition of the two existed each time the obstacle appeared. He was asked to record his decision by depressing one of two foot switches, designated "SAFE" and "COLLIDE," which were located on the deck at each side of the control column. Before making his decision, the subject indicated awareness of the torpedo by depressing the "SIGHTED" thumb switch on the control column. The subject was instructed to accomplish the appropriate evasive maneuver with the submarine if his decision was indicative of a collision imminence. No immediate feedback concerning the correctness of the decision was given to the subject, although yellow indicator lights in the control booth and on the experimenter's console did come on if a collision occurred as the submarine passed through the torpedo barrier plane.

The discrete commands of depth and azimuth were chosen because the emphasis of the study was upon the determination of differences in operational utility between the displays. Random forcing functions would have yielded data appropriate to study of the fine structure of human operator performance. The use of discrete commands contributed a significant

component to the results from trial-to-trial. A set of base line data for each sequence of discrete commands was generated with a 0.1-second first-order lag for the human operator in the control loop. The rms error scores in azimuth and depth obtained for each trial by this means were subtracted from the human operator's raw scores for the same trials. Although this procedure eliminated a large portion of the trial-to-trial differences in error scores which necessarily occurred due to varying azimuth and depth command magnitudes, it had no effect on the analysis of differences between displays. All references made to rms error scores in this paper are to those normalized in this manner.

## RESULTS AND DISCUSSION—PART I

**TRACKING ERROR IN  $rms_{\downarrow}$ .**—A breakdown of the significant main effect for displays was accomplished by the use of Duncan's multiple range test (ref. 11). Summaries of all multiple comparison tests applied in the analysis of  $rms_{\downarrow}$  error results are found in table 2. Mean  $rms_{\downarrow}$  errors for each display and phase indicated that performance decrement due to display blanking on phase II is minimal, with no large differential effect between displays due to this factor. The DepAzPred display indicated the smallest increase in error of the four displays on phase II. Performance on phase III continued at approximately the same level as that on phases I and II, with only the DepAzPred deviating from this trend. Since the subjects were instructed on phase III to continue to track the command azimuth as accurately as possible while evading the torpedo in depth, little, if any, degradation of performance would be expected.

TABLE 2.—SUMMARY OF DUNCAN'S MULTIPLE RANGE TESTS  
FOR  $rms_{\downarrow}$  ERROR

[Means in all summaries are ranked from left to right in order of increasingly better performance on the criterion measures which they represent. Comparisons underscored by the same line are not significant at the 0.01 level of confidence.]

Corrected $rms_{\downarrow}$ error (phase I), deg				
Displays	DepAzPred	DepAzSymb	ConAnSymb	ConAnPers
Means	5.79	3.17	<u>1.93</u>	<u>1.79</u>
Corrected $rms_{\downarrow}$ error (phase II), deg				
Displays	DepAzPred	DepAzSymb	ConAnPers	ConAnSymb
Means	5.93	3.65	<u>2.62</u>	<u>2.55</u>
Corrected $rms_{\downarrow}$ error (phase III), deg				
Displays	DepAzPred	DepAzSymb	ConAnPers	ConAnSymb
Means	7.48	<u>3.63</u>	<u>2.49</u>	<u>2.29</u>

As a measure of system performance in the present study, rms error represents, essentially, the total deviation of the submarine from a series of two commands averaged over a trial period of 180 seconds. Since almost all of the error is accumulated during brief periods after new course commands are given, the total error averaged over an entire trial period results in an rms error score which is considerably lower than if it were averaged over a period approximating only the interval during which most of the error occurred. While the scores based on  $\tau=180$  seconds are valid for analytical purposes, the mean differences between displays in terms of degrees of error over this entire trial interval are not representative of the true magnitude of differences between displays which existed during the relatively brief intervals following command inputs. Estimates of these maximum error periods were made by measuring intervals on the strip chart recorder-output data samples of integrated error corresponding to the acquisition time for each command.

From table 2, it may be seen that mean differences in rms<sub>ψ</sub> error range from the insignificant level of only 0.07° between ConAnPers and ConAnSymb on phase II to a significant difference of 5.19° between the ConAnSymb and DepAzPred displays on phase III.

**TRACKING ERROR IN rms<sub>Z</sub>.**—The multiple comparisons tests of rms<sub>Z</sub> error scores (see table 3) indicated fewer significant differences between individual displays than did the tests of rms<sub>ψ</sub> tracking error. The only significant difference occurring consistently on all phases was between the DepAzSymb and ConAnPers displays, with the latter yielding lower error scores.

TABLE 3.—SUMMARY OF DUNCAN'S MULTIPLE RANGE TESTS  
FOR CORRECTED rms<sub>Z</sub> ERROR

[Means in all summaries are ranked from left to right in order of increasingly better performance on the criterion measures which they represent. Comparisons underscored by the same line are not significant at the 0.01 level of confidence.]

rms <sub>Z</sub> error (phase I), ft				
Displays	DepAzSymb	DepAzPred	ConAnSymb	ConAnPers
Means	<u>13.88</u>	<u>12.65</u>	<u>10.61</u>	<u>5.30</u>
rms <sub>Z</sub> error (phase II), ft				
Displays	DepAzSymb	DepAzPred	ConAnSymb	ConAnPers
Means	<u>14.29</u>	<u>8.57</u>	<u>7.75</u>	<u>7.34</u>
rms <sub>Z</sub> error (phase III), ft				
Displays	DepAzSymb	ConAnSymb	DepAzPred	ConAnPers
Means	<u>45.24</u>	<u>32.87</u>	<u>28.28</u>	<u>16.61</u>

Table 3 indicates a range of between-displays differences from an insignificant 0.41-foot between the ConAnSymb and ConAnPers during phase II to a highly significant average difference of 28.63 feet between the DepAzSymb and ConAnPers displays during phase III.

Mean  $rms_z$  error scores for each display and phase suggested varying degrees of tracking-error increase between phases II and III on the four displays. Error score increments occurring between these phases for each display indicated that the largest performance decrement resulted on the DepAzSymb display, with the ConAnPers yielding the smallest increase in error during torpedo avoidance in phase III.

Phase II display blanking results were similar to those obtained in azimuth tracking, with no significant change in  $rms_z$  error due to blanking. Mean phase II error scores did, in fact, decrease from the phase I levels on the ConAnSymb and DepAzPred displays; this decrease is probably attributable to relatively greater learning effects on these two displays across phases I and II.

"SIGHTED" REACTION TIME.—All reaction-time data were transformed before analysis to reciprocals ( $1/X$ ), in order to stabilize variances. The "sighted" reaction time measure, that is, the simple reaction time to presentations of the torpedo symbol on the display, did not yield significant differences between displays. Only the main effect for orders was significant, with means of 0.73, 0.60, 0.56, and 0.58 second indicating a general decrease in reaction time on all displays across orders. Mean reaction time for the DepAzSymb, DepAzPred, ConAnPers, and ConAnSymb displays were 0.57, 0.61, 0.62, and 0.65 second, respectively.

"DECISION" REACTION TIME.—The measure of time required by the subject to decide whether he would or would not collide with the torpedo did indicate a significant difference between displays at the 0.05 confidence level. A multiple comparisons test of these data resulted in a significant difference between the ConAnSymb and DepAzSymb displays, with the latter producing shorter decision times. The between-subjects portion of the displays by orders interaction [ $D \times O(b)$ ] was highly significant, with an F-ratio of 102.07. This interaction is, in fact, the between-groups sum of squares, and represents differences between groups (pairs of subjects) in time required to make the torpedo avoidance decision.

NUMBER OF CORRECT DECISIONS.—The mean percentages of the total number of trials in which decisions were correct were 95, 93, 86, and 85 percent for ConAnPers, DepAzPred, DepAzSymb, and ConAnSymb display formats. Although these mean differences range up to 10 percent, none were significant. The primary sources of data variance on this performance measure are differences between trial-sets and between groups of subjects.

NUMBER OF COLLISIONS.—The multiple comparisons between displays on the number of actual collisions with the torpedo are shown in table 4. The predictor display, as noted in table 4 gave significantly fewer collisions than did either of the contact-analog displays but was not significantly better than the other symbolic display at the 0.01 level. Although not noted in table 4, the difference between symbolic display formats (DepAzSymb and DepAzPred) was significant at the 0.05 level of confidence.

TABLE 4.—SUMMARY OF DUNCAN'S MULTIPLE RANGE TESTS FOR DECISION REACTION TIMES AND NUMBER OF COLLISIONS

Means in all summaries are ranked from left to right in order of increasingly better performance on the criterion measures which they represent. Comparisons underscored by the same line are not significant at the 0.01 level of confidence.

Decision reaction time, sec				
Displays	ConAnSymb	DepAzPred	ConAnPers	DepAzSymb
Means	<u>1.00</u>	<u>0.83</u>	<u>0.76</u>	<u>0.60</u>
Trials on which collisions occurred, percent				
Displays	ConAnSymb	ConAnPers	DepAzSymb	DepAzPred
Means	<u>18</u>	<u>13</u>	<u>11</u>	<u>4</u>

## EXPERIMENTS—PART II

In establishing a common basis for the comparison of the four displays in part I of the experimental program, one of the necessary conditions was to standardize the command tracking procedures employed with all displays. With the quickened displays, the subject was required to track the quickened symbol onto the command symbol, except that with the ConAnSymb, compensatory tracking was employed in a sense compatible with the "window" display concept and required the subject to steer the "fixed" bow reference cross into the moving quickened square display element. With the predictor display, the subject was instructed to track the path tip into the command circle. Although this error technique is common with quickened displays, it was demonstrated in this study not to be the most suitable for use with the more recently developed predictor display format.

One of the objectives in the part II experimental study was to evaluate what is designated in this paper as the "forced solution procedure," an alternative approach to tracking with the predictor.

A second goal was to evaluate operator performance as a function of displayed predictor span. Data were collected on each of three prediction spans: 20, 30, and 40 seconds.

**SUBJECTS.**—Twenty male university-student volunteers served as subjects during part II of the study. All were considered naive with respect to relevant elements of the experimental task. Each subject was paid on an hourly basis after the completion of the required three sessions.

**EXPERIMENTAL DESIGN.**—Five subjects were assigned at random to each of the four groups, with each group performing on one of the predictor variations. Thus, the display's main effect was a "between-subjects" effect as shown on the following page.

	$T_1$	$T_2$	$T_3$	$T_4$	$T_5$	$T_6$	
$D_1$							Group 1
$D_2$							Group 2
$D_3$							Group 3
$D_4$							Group 4

As before, the design was repeated for each phase of data collection.

The general procedure was identical to that of part I with the exception that the inter-trial interval after every third trial was reduced from 3 minutes to 1 minute.

**PERFORMANCE MEASURES.**—With the exception of "sighted" reaction time and number of correct decisions, all performance measures recorded in part I were employed again in part II of the study. The above two indices were not repeated since neither was significant in part I, and no a priori reason could be determined for their potential significance in part II.

Three additional measures which a pilot study indicated as relevant to the display comparison of part II (magnitude of depth command overshoot, time on command course, and time on command depth) were also recorded and analyzed.

**VEHICLE CONTROL AND DECISION TASKS.**—Sessions 1 and 2, representing data-collection phases IV and V, required only that the subject bring the submarine to a series of discrete depth and azimuth commands, as in phase I. Obstacle-avoidance data were collected on the third and final session (phase VI) under conditions identical to those of phase III of part I. Also, the command sequence was the same as that which was used in part I of the study.

## RESULTS AND DISCUSSION—PART II

Since the primary purposes of session 1 were to acquaint the subjects with the experimental environment and to establish a reasonable level of skill in control of the vehicle, data from the session (phase IV) were not analyzed. Results obtained from phase V and VI data for each performance index are described below.

**TRACKING ERRORS IN  $rms_{\psi}$  AND  $rms_z$ .**—Multiple range tests of these data resulted in no significant differences between the 20-, 30-, and 40-second predictors.

**TIME ON COMMAND COURSE AND DEPTH.**—Since analyses of the data from these two performance indices produced results which were, in almost all instances, equivalent to those for rms error scores, they are not included in this paper.

**DECISION REACTION TIME AND NUMBER OF COLLISIONS.**—Neither performance index yielded significant difference between displays.



MAGNITUDE OF DEPTH COMMAND OVERSHOOT.—Overshoot magnitudes on the 40-second predictor were significantly greater than on the other variations. Except for these larger overshoots with the 40-second predictor, no differences were observed between the three displays. This fact can be attributed to the equalizing tendency of the forced-solution tracking procedure. Had the path-tip-in-the-circle procedure also been used with these three displays, rms errors would necessarily have increased with an increase in prediction span.

The additional operator-judgment element involved in the forced-tracking procedure allows the operator to become more familiar with the response characteristics of the vehicle itself. An end result of this familiarity is a higher degree of control accuracy during maneuvers as exemplified by the torpedo avoidance task. This was supported by the trend toward fewer collisions on the displays where forced solution tracking was utilized (ref. 12).

Also, it is hypothesized that an operator skilled in the use of forced-solution tracking on a predictor display could more efficiently transfer this skill to the use of backup control instrumentation than could an operator experienced only with the more programed or stereotyped responses called for on quickened and predictor path-tip-tracking displays.

## REFERENCES

1. Anon.: Phase II Final Report on the Stability and Manual Controllability of the Tandem Propeller Submarine. Aero rep. 1936-TR3, Honeywell, Inc., Oct. 1963.
2. Sperling, H. G.; McLane, R. C.; and Anderson, D. A.: Peripheral Augmentation of Range Perception in Pictorial Displays. 1964 IEEE International Convention Record, vol. 12, part 7, pp. 226-232.
3. McLane, R. C.; Sperling, H. G.; Anderson, D. A.; and Senders, J. W.: Manual Control and Display in Six-Degrees-of-Freedom. Proceedings of the 5th National Symposium on Human Factors in Electronics, IEEE, 1964.
4. Anon.: Technical Manual for CONALOG Control and Display Set. NAVSHIPS 365-2898, vol. I, Norden Div., United Aircraft Corp., June 1964.
5. Anon.: SQUIRE, A Unified Display for Submarine Ship Control. Tech. rep. U-411-61-094, Electric Boat Div., General Dynamics Corp., Aug. 1961.
6. Anon.: Developing and Testing the Effectiveness of the Predictor Instrument. Tech. rep. 252-60-1, Dunlap and Associates, Inc., Mar. 1960.
7. Anon.: Training Effectiveness as a Function of Simulator Complexity. Tech. rep. NAVTRADEVCEEN 458-1, U.S. Naval Training Devices Center, Sept. 1959.
8. Anon.: Military Specification CONALOG System for Submarine Steering and Diving Instrumentation and Control. MIL-C-22940, Aug. 1961.
9. Winer, B. J.: Statistical Principles in Experimental Design. McGraw-Hill Book Co., Inc., 1962.

10. Lindquist, E. F.: Design and Analysis of Experiments. Houghton Mifflin, 1953.
11. Duncan, D. B.: Multiple Range and Multiple F Tests. Biometrics, vol. 11, 1955, pp. 1-42.
12. Anon.: Final Research Report on the Experimental Evaluation of Symbolic and Pictorial Displays for Submarine Control. Res. rep. 1550-FR1, Honeywell, Inc., Sept. 1965.

# **MOTION AND STRESS**

N67-15867

PRECEDING PAGES BLANK NOT FILMED.

## 16. SOME EFFECTS OF MOTION CUES ON MANUAL TRACKING

*Laurence R. Young*  
*Massachusetts Institute of Technology*

It has been adequately demonstrated that sustained high acceleration or vibration can have a deleterious effect on tracking ability. This paper, however, considers some situations in which the motion cues, as felt in flight or moving base simulation, yield a significant improvement in pilot performance.

The first of these situations is in a control task requiring more lead compensation than is easily developed from visual displays. The vestibular and tactile sensations contribute velocity and acceleration information which is used in stabilization. Experiments on control of inverted pendulums and VTOL's, with and without motion cues, demonstrate the extent to which this lead is used in certain tasks. Tests of labyrinthine-defective patients on similar tasks demonstrated the critical importance of vestibular inputs.

The importance of motion cues in rapid adaptation to controlled element failures was investigated in a simulated blind landing experiment. Motion effects were found to be important in a class of flexible booster control experiments. These results were combined with many comparisons of fixed-base, moving-base, and flight experiments in the literature to arrive at some general conclusions regarding the effects of motion cues on tracking.

The effect of motion cues on a piloting task is a question of considerable practical importance for which no general answer currently exists.

A number of specific studies on a wide variety of vehicles have compared fixed and moving base simulations with flight results. These comparisons, yielding performance measures, pilot-opinion ratings, limits of controllability, and pilot transfer functions, contribute valuable data sets to be used in assessing the importance of motion cues. The goal of a theory covering the effects of motion would be a guide for the vehicle control designer, indicating at which stage fixed-base simulation is sufficient, how the results of fixed-base simulation would be expected to be modified in flight, and when the predicted effects of motion cues would justify the expense and time of motion-base simulation.

This paper reports some results of four recent fixed-base, moving-base experiments at the MIT Man-Vehicle Control Laboratory which add to the data base on this subject. It also presents a tentative set of hypotheses to incorporate much of these data.

## INVERTED PENDULUM.

We have previously demonstrated the importance of motion cues in extending the limits of controllability for a single-axis compensatory task of stabilizing an undamped simulated inverted pendulum (refs. 1 and 2). The difficulty of this task increases as the static stability ( $\omega^2$ ) becomes more negative—corresponding to a shorter inverted pendulum, and requiring more lead compensation or shorter time delay on the part of the human operator to maintain stability. Figure 1 shows the crucial role of motion cues in this task, where the subject is required to maintain the orientation

of the simulator vertical. The three conditions refer to tracking situations in which (1) the operator is seated outside the simulator and performs fixed base control using the simulator cab as a display (visual), (2) the operator is seated in the moving simulator with a full view of the surrounding laboratory (combined), and (3) the operator is seated in the moving simulator with a hood eliminating visual cues and no instruments in the cab (vestibular). At low divergence frequencies where the instability is easily controlled, the advantage of visual information in reducing the rms error is apparently attributable to the accuracy with which an accurate alinement to the vertical can be achieved visually. As the instability becomes more severe ( $\omega > 2$ ), how-

ever, the stabilization task required more lead compensation, and rapid detection of changes in orientation becomes more important than accuracy in alinement. At these frequencies the helpful effect of the roll motion cues becomes obvious. At still higher divergence frequencies, which are uncontrollable on the basis of visual information alone, the presence of motion cues alone or in conjunction with visual cues permits the operator to stabilize the system.

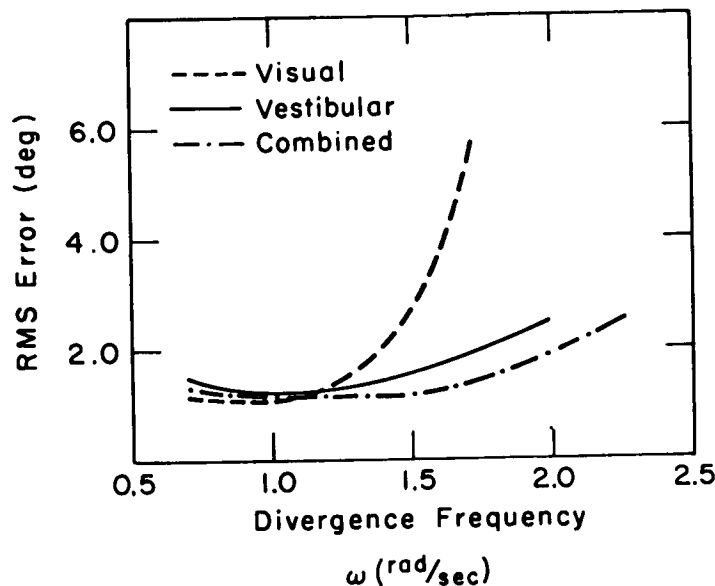


Figure 1.—Rms error for control of inverted pendulum.

We have postulated the importance of the vestibular system as effective angular and linear rate transducers in furnishing the lead information required for closed-loop stabilization. In a series of recent experiments performed in collaboration with Ashton Graybiel of the U. S. Naval School of Aviation Medicine, we have repeated some of these experiments on labyrinthine-defective subjects with various vestibular disorders. Preliminary results indicate that although tactile and other nonvestibular cues are of some value in conjunction with visual cues, it is primarily vestibular-system contributions which allow motion cues to aid pilot performance.

## ROLL RECOVERY IN BLIND LANDING

A more realistic situation in which motion cues were found to aid pilot performance significantly occurred during our experiments on man's ability to take over control following a failure or disturbance in an automatic blind-landing system. Simulating the landing of a

Caravelle with both fixed base and moving base, Vuorikari introduced step disturbances in pitch rate and roll rate at various points on the glide path and determined the interval required for the pilot to recover from the disturbance (ref. 3). Figure 2 shows a set of lateral control recovery times versus disturbance magnitude and indicates a nearly 100 percent increase in recovery interval when motion cues were eliminated. Even though stability is not a major problem in this case, the motion cues are important because they rapidly alert the pilot to sudden changes in attitude rates.

### HELICOPTER HOVERING

Helicopter stabilization and VTOL landing and transition have been recognized as tasks in which motion cues play an important role. To investigate the importance of visual and motion cues in single axis lateral control of an uncompensated helicopter, Benjamin experimented with fixed- and moving-base helicopter simulations in which he always showed lateral position but did not always indicate roll angle (ref. 4). Since the roll (inner) loop must be stabilized before the position (outer) loop can be closed, some roll feedback was necessary. The extent to which attitude motion cues were used for roll loop stabilization depended very strongly on the experience of the subject in correctly interpreting the motions. The relative

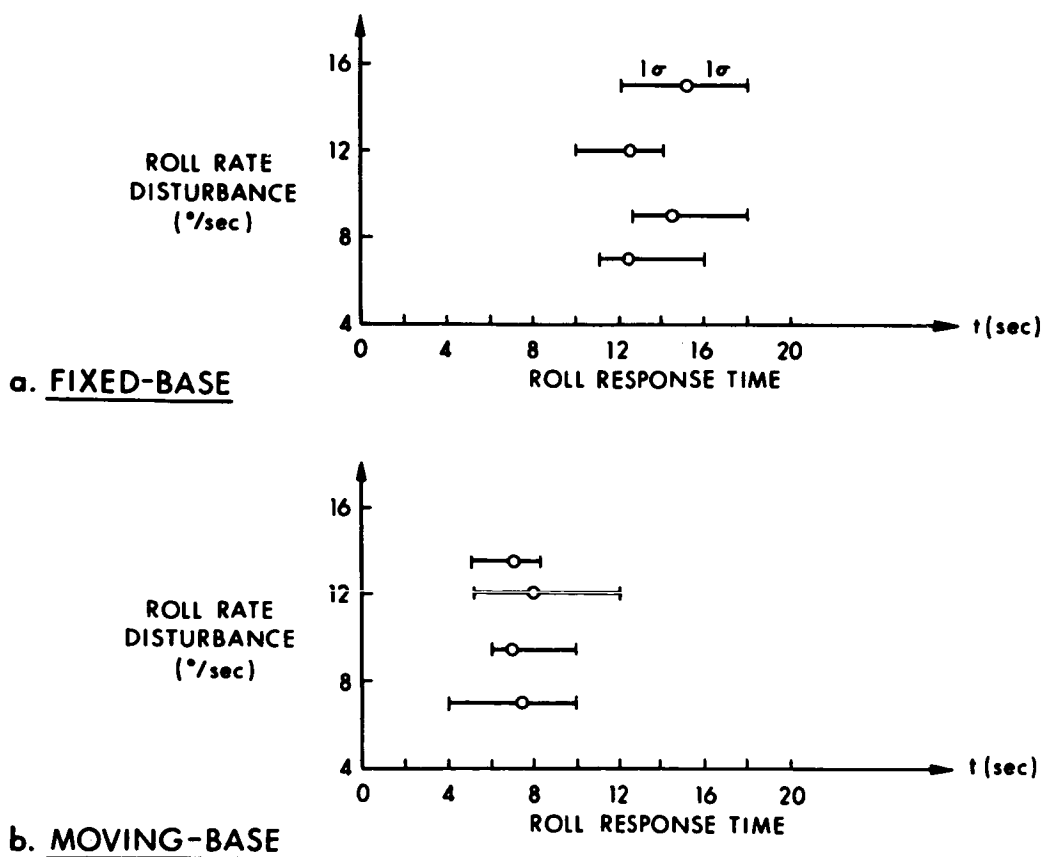


Figure 2. —Median roll-response time to step roll-rate disturbance in simulated landing.

lateral position error in hovering is indicated in figure 3 for the five subjects tested under the conditions of (1) fixed-base simulation with roll angle as well as position displayed, (2) roll angle motion-base simulation with the same display, and (3) motion-base simulation with the visual roll display removed. The experienced helicopter pilots had difficulty with the fixed-base simulation but performed well when the motion was added. One of the pilots did nearly as well when the visual roll cue was removed, indicating that the experienced helicopter pilot does rely heavily on motion cues for attitude stabilization. By way of contrast, the moderately trained nonpilots at first found the motion of the simulator to be disturbing and less controllable than in the fixed-base simulation. Since the position control task required stabilizing the cab to some orientation other than vertical, the motion cues may have been less beneficial to the new subject than in the case of the inverted pendulum stabilization discussed above. This explanation seemed to be borne out by the one nonpilot subject who had considerable experience in the moving-base simulation. In time, he began to use the motion cues to provide roll information and performed better than in the fixed-base simulation.

### FLEXIBLE BOOSTER CONTROL

A final set of experiments recently performed in our laboratory and bearing on the subject of motion effects on pilot control concerned the influence of bending mode accelerations

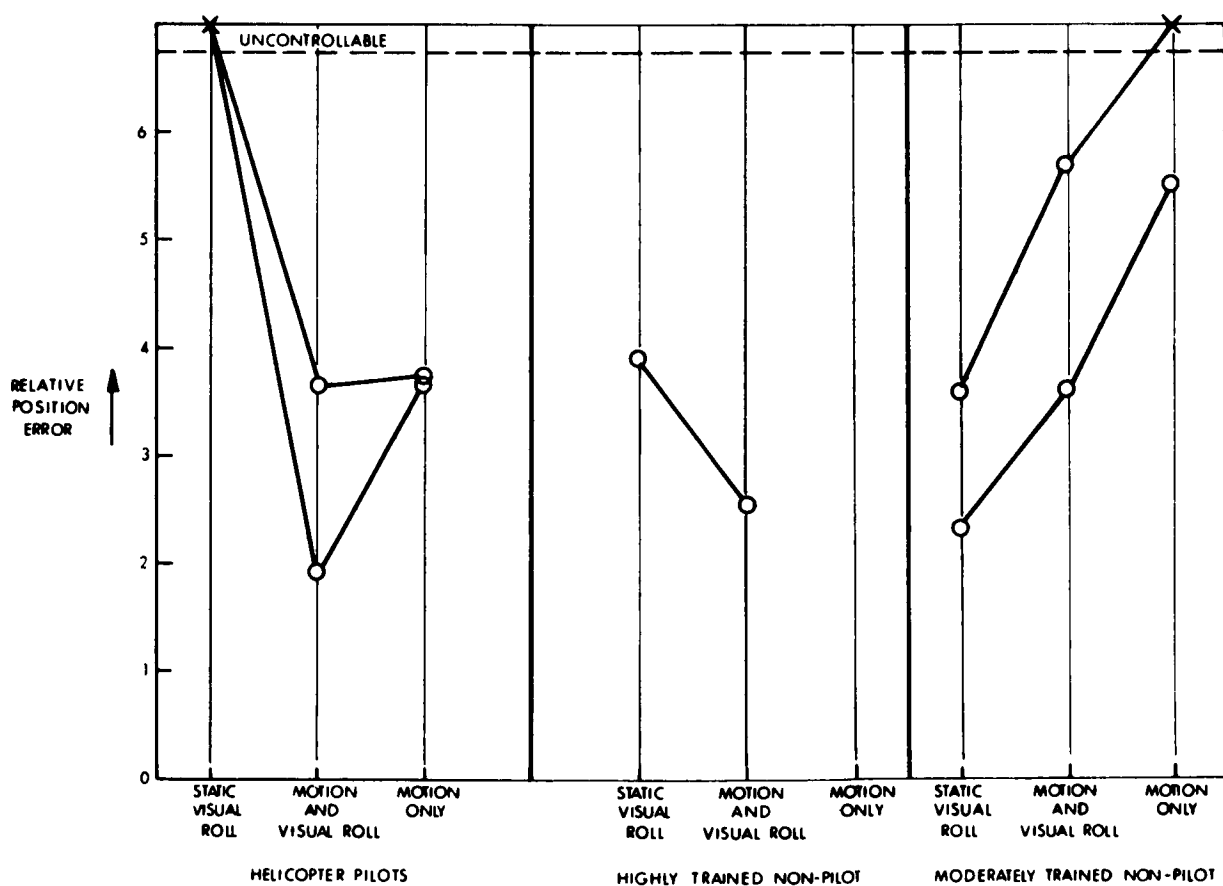


Figure 3.—Effect of motion and visual roll cues on helicopter lateral hovering.

on manual control of flexible launch vehicles. To accentuate the bending-mode influence Kilpatrick (ref. 5) simulated single-axis control of the Saturn V launch vehicle using the rate feedback recommended by Hardy et al. (ref. 6) but permitting pilot commands to go directly to the engine gimbals without being smoothed by a stick filter. Since the rigid-body poles fell in a region where control was quite easy (divergent pole at  $\omega = -0.15$  rad/sec), and yet the first bending-mode poles were not widely separated from the rigid body (bending frequencies of 5 and 7 rad/sec were studied), it was not known whether the motion cues would aid or hinder performance. Previous studies, using stick filters to reduce bending-mode amplitudes, showed no important dependence of performance on motion. Measured pilot-transfer functions and normalized error found by Kilpatrick show a deleterious effect of the motion in all cases. Figure 4, for example, compares the subject amplitude ratio for several bending mode amplitudes in fixed- and moving-base simulation. At all bending-mode amplitudes the subjects showed lower gains (by approximately one-half) and generally greater delay times in moving-base than in fixed-base simulation. These results are in general agreement with the type of findings reported by Seckel et al. in 1958 (ref. 7). The consistent decrease in subject's gain with bending-mode amplitude is ascribed to his avoidance of large sudden control movements when they might excite the large bending modes. The resulting variation in performance is shown in figure 5, where it is seen that the normalized altitude errors are approximately 50 percent greater with motion-base simulation than with fixed-base simulation, and for both simulation

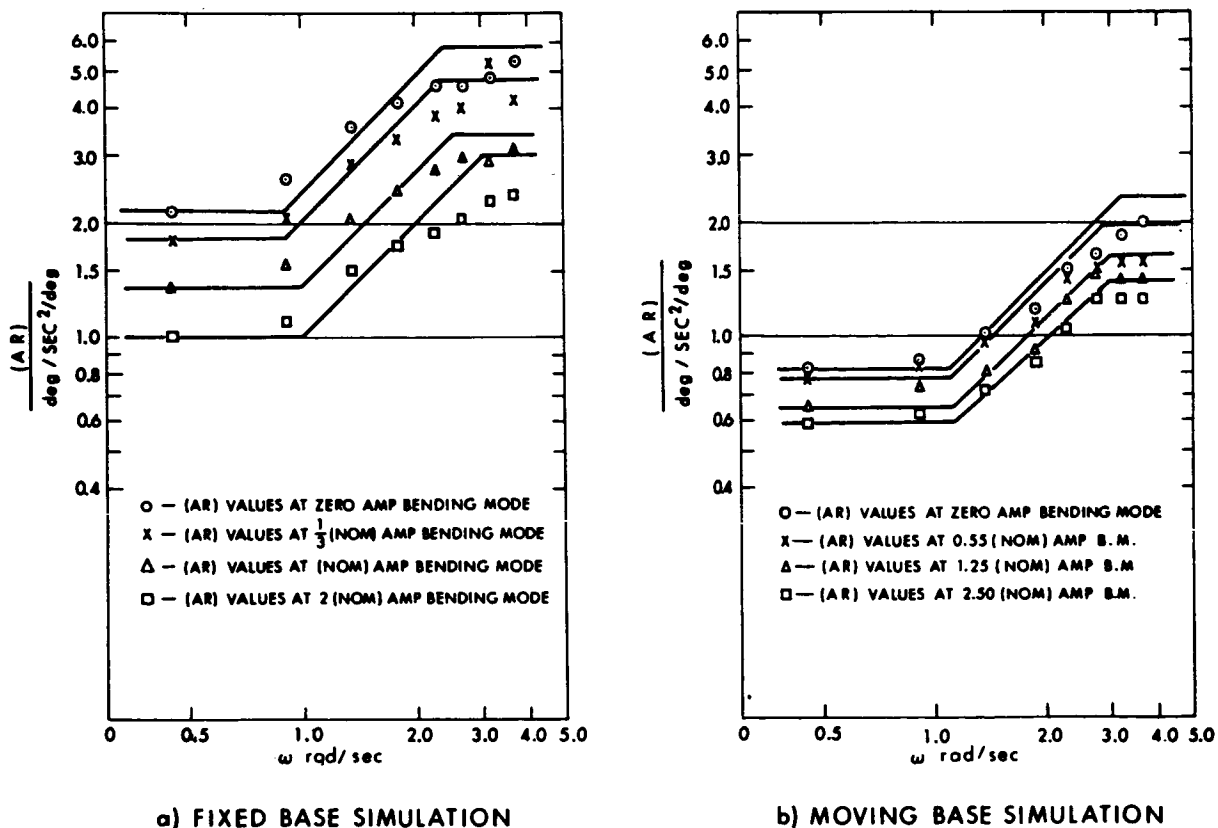


Figure 4.—Human operator amplitude ratio, flexible launch-vehicle control  
( $\omega_{nbd} = 7$  rad/sec).



modes the errors increase markedly with unfiltered bending-mode amplitude. It should be noted that the subjects had considerable training but were not pilots, which may account for the disturbing effect of the motion.

## DATA COMPARISON AND DISCUSSION

The isolated experimental results reported above may be added to a number of other contributions in an attempt to map out the conditions under which motion-base simulation or flight tests may be expected to yield a significantly different performance than the fixed-base simulation. The diagrams in figure 6 show the results of a number of such comparisons by many investigators plotted on a map of handling qualities representing the position of the dominant poles of the system (the sources of the data of figure 6 are given in table 1). Only some vehicles, whose handling qualities are characterized by second-order systems, are represented in this composite.

The loci of handling qualities were based on pilot-opinion studies and were deliberately taken from a number of sources. The limits of control were selected from fixed-base and centrifuge experimental data by Holleman et al. (ref. 8) for longitudinal launch-vehicle control and, for comparison, fixed-base simulator studies by Taylor and Day for longitudinal control of a Mach 3 aircraft (ref. 9). The locus of handling qualities, which are just unacceptable (Cooper rating 6.5), was determined by Sadoff et al. (ref. 10) for longitudinal vehicles control on a centrifuge study. The region of acceptable dynamics is from flight evaluations of longitudinal handling qualities by Harper (ref. 11).

All of the data points shown as filled or mostly filled circles represent comparisons in which motion cues proved helpful in terms of pilot opinion, performance, or pilot-describing function. The filled circles represent more significant motion effects. Other examples of helpful motion cues reviewed by Sadoff and Belsley include VTOL hover and transition and reacting to engine failure in a supersonic transport (refs. 12 and 13).

Those data points, which are open or slightly filled, represent comparisons in which the effect of motion cues or other aspects of motion simulation or flight degraded the performance found with fixed-base simulation. Examples of performance degradation through high levels of constant acceleration or high vibration beyond the frequencies of pilot control are specifically

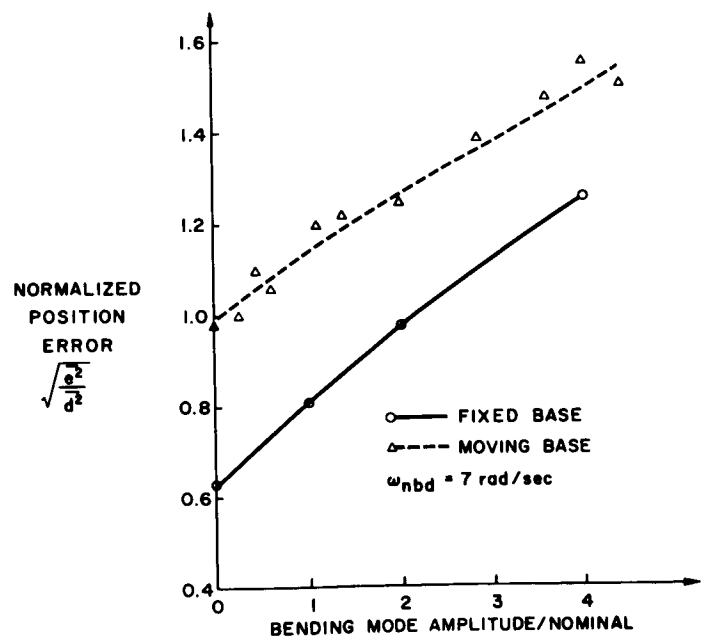


Figure 5.—Normalized error versus bending mode amplitude flexible booster control.

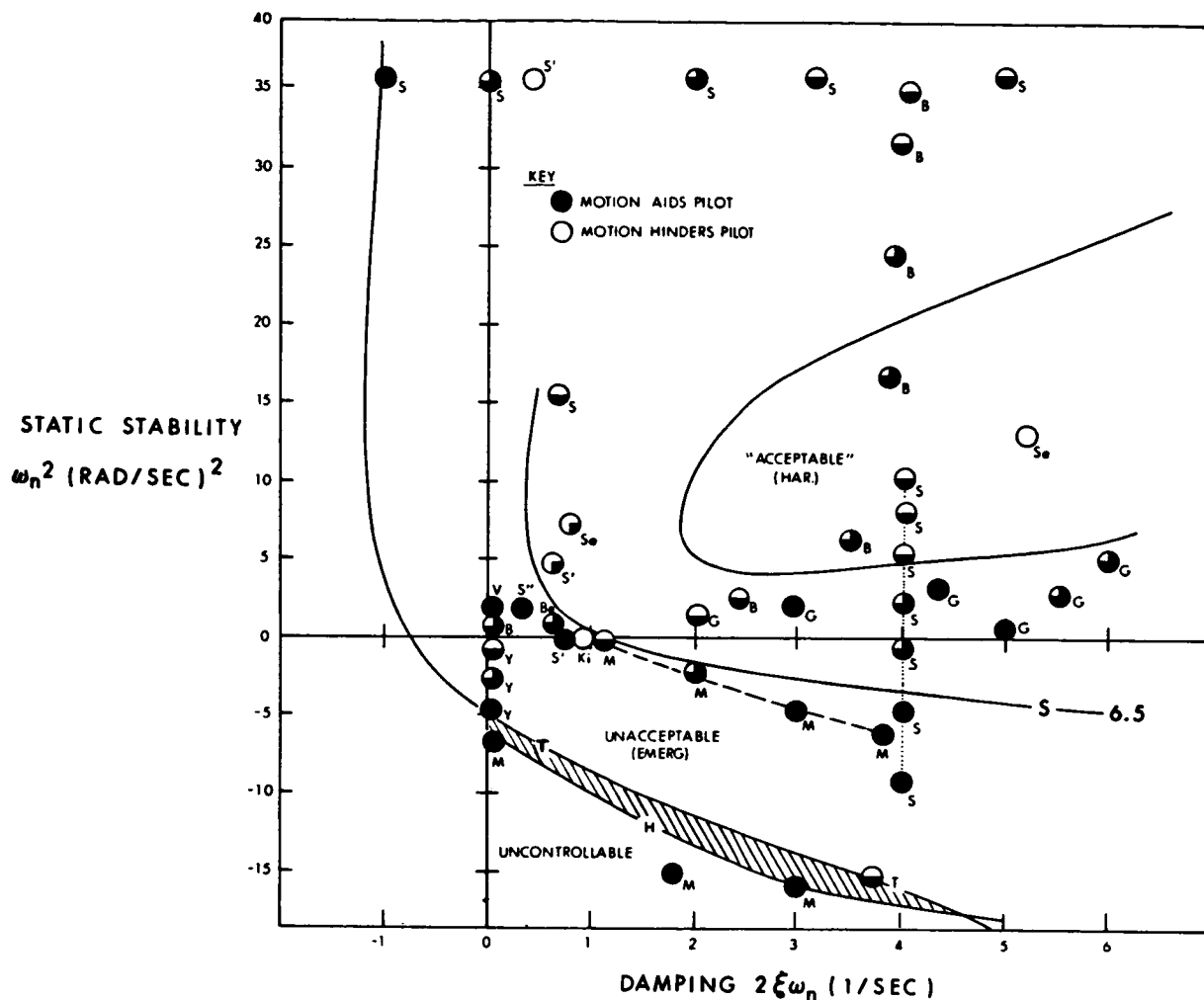


Figure 6.—Effect of motion cues.

TABLE 1.—SOURCES OF DATA FOR COMPILATION

Key		
MB = Moving base	●	Motion aids pilot significantly
FB = Fixed base	◐	Motion aids pilot slightly
FLT = Flight test	○	Motion does not effect performance
Cent = Centrifuge	◑	Motion hinders pilot slightly
	◒	Motion hinders pilot significantly
Se	Seckel et al.	A/C long., lat. FB and FLT (7)
G	Gerdes	VTOL height FB and MB (vert.) (17)
Y	Young, Meiry	Inv. pend. FB and MB (roll) (1,2)
S	Sadoff et al.	A/C long. FB, MB (pitch-roll), cent., FLT (10)
S'	Sadoff	A/C long. failures, FB, cent. (18)
S''	Sadoff and Harper	A/C (SST) failure FB, MB (12)
Be	Benjamin	VTOL lat. FB, MB (roll) (4)
Ki	Kilpatrick	Booster long. FB, MB (pitch) (5)
V	Vuorikari	A/C lat., long. FB, MB (roll) (3)
K	Kuehnel	A/C long. FB, FLT (19)
T	Taylor and Day	A/C long. FB, MB, cent., FLT (9)
M	McFadden et al.	A/C long. FLT (20)
H	Holleman et al.	Booster long. FB, cent. (8)
B	Brown et al.	A/C long. FB, MB (pitch, vert.) (21)
Har	Harper	A/C long. FLT (11)

excluded from this compilation since they depend upon a nonlinear effect rather than the vehicle dynamics. Dolkas and Stewart (ref. 14), Sadoff (ref. 15), and Summers and Burrows (ref. 16) have recently written on this subject.

The following general conclusions can be drawn from the data compilation:

(1) When vehicle dynamics are removed from the acceptable region, motion cues become more helpful to the pilot. Easily controlled vehicles do not require additional cues. Marginally stable or unstable vehicles, however, may require more lead compensation than is comfortably generated by pilots on the basis of instruments and consequently the rate sensing elements of the vestibular system prove valuable in giving early indications of attitude changes.

(2) Motion cues are more helpful with unstable dynamics than with lightly damped oscillatory vehicles. As noted by others, the motion accompanying high-frequency vehicle oscillations may shake the pilot about in the cockpit making precise control and accurate reading of instruments difficult.

(3) Moving-base simulation yields closer agreement with flight experience than fixed-base simulation, especially in marginally stable or difficult vehicles. For most applications, simulation of vehicle angular motions is more important than translation simulation. Stabilization requires attitude control prior to control of position, thus emphasizing rotational motions. Normal accelerations, from centrifuge simulations, do not appear as important as angular cues except under high g conditions, and the spurious motions associated with closed-loop centrifuge simulation often cloud the pilot stabilization picture.

## REFERENCES

1. Young, L. R.; and Meiry, J. L.: Manual Control of an Unstable System with Visual and Motion Cues. IEEE International Convention Record, vol. 13, part 6, 1965, pp. 123-127.
2. Meiry, J. L.: The Vestibular System and Human Dynamic Space Orientation. MIT Man-Vehicle Control Lab Rep. T-65-1, June 1965 (Sc. D. Thesis, MIT).
3. Vuorikari, V. O.: Human Role in the Control Loop of the Automatic Landing Aircraft (S.M. Thesis, MIT, 1965).
4. Benjamin, P.: Visual and Motion Cues in Helicopter Flight. MIT Man-Vehicle Control Lab Rep. T-66-1, Jan. 1966.
5. Kilpatrick, P. S.: Bending Mode Acceleration Influence on Pilot Control of Flexible Booster Dynamics. MIT Man-Vehicle Control Lab Rep. T-65-2, Sept. 1965.
6. Hardy, G. H.; West, J. V.; and Gunderson, R. W.: Evaluation of Pilot's Ability to Stabilize a Flexible Launch Vehicle During First-Stage Boost. NASA TN D-2807, May 1965.

7. Seckel, E.; Hall, I. A. M.; McRuer, D. T.; and Weir, D. H.: Human Pilot Dynamic Response in Flight and Simulator. WADC Tech. Rep. 57-520, 1958.
8. Holleman, E. C.; Armstrong, N. A.; and Andrews, W. H.: Utilization of the Pilot in the Launch and Injection of a Multistage Orbital Vehicle. IAS paper no. 60-16, 1960.
9. Taylor, L. W.; and Day, R. E.: Flight Controllability Limits and Related Human Transfer Functions as Determined from Simulator and Flight Tests. NASA TN D-746, 1961.
10. Sadoff, M.; McFadden, N. M.; and Heinle, D. R.: A Study of Longitudinal Control Problems at Low and Negative Damping and Stability with Emphasis on Effects of Motion Cues. NASA TN D-348, 1961.
11. Harper, R. P., Jr.: Flight Evaluations of Various Longitudinal Handling Qualities in a Variable-Stability Jet Fighter. WADC Tech. Rep. 55-299, 1955.
12. Sadoff, M.; and Harper, C. W.: Piloted Flight-Simulator Research: A Critical Review. Aerospace Eng., vol. 21, no. 9, pp. 50-63, 1962.
13. Belsley, S. E.: Man-Machine System Simulation for Flight Vehicles. IEEE Trans. on Human Factor in Electronics, vol. HFE-4, no. 1, pp. 4-14, 1963.
14. Dolkas, C. B.; and Stewart, J. D.: Effect of Combined Linear and Oscillatory Acceleration on Pilot Attitude-Control Capabilities. NASA TN D-2710, 1965.
15. Sadoff, M.: Effects of High Sustained Acceleration on Pilot's Performance and Dynamic Response. NASA TN D-2067, 1964.
16. Sommers, L. G.; and Burrows, A. A.: Human Tracking Performance Under Transverse Acceleration. NASA CR-21, 1964.
17. Gerdes, R. M.: A Piloted Motion Simulator Investigation of VTOL Height-Control Requirements. NASA TN D-2451, 1964.
18. Sadoff, M.: A Study of Pilot's Ability to Control During Simulated Stability Augmentation System Failures. NASA TN D-1552, 1962.
19. Kuehnel, H. A.: Human Pilot's Dynamic Response Characteristics Measured in Flight and on a Nonmoving Simulator. NASA TN D-1229, 1962.
20. McFadden, N. M.; Vomaske, R. F.; and Heinle, D. R.: Flight Investigation Using Variable-Stability Airplanes of Minimum Stability Requirements for High-Speed, High-Altitude Vehicles. NASA TN D-779, 1961.
21. Brown, P. B.; Johnson, H. I.; and Murgall, R. G.: Simulator Motion Effects on a Pilot's Ability to Perform a Precise Longitudinal Flying Task. NASA TN D-367, 1960.

N67-15868

PRECEDING PAGE BLANK NOT FILMED.

## 17. ACCELERATION STRESS EFFECTS ON PILOT PERFORMANCE AND DYNAMIC RESPONSE

*Melvin Sadoff and C.B. Dolkas*  
*Ames Research Center, NASA*

Several brief studies were conducted to assess the effects of a wide range of acceleration environments, varying from zero gravity to high sustained accelerations, on pilot performance and dynamic response. The results indicated that the control-performance decrements observed at high sustained accelerations were attributable to decreased pilot gains and corresponding reductions in open-loop system crossover frequency. Limited results for extreme vibratory accelerations suggested that performance deterioration was associated with a reduction in pilot lead equalization (and a corresponding reduction in open-loop crossover). Under short-term weightless conditions, performance in a simulated control task was appreciably poorer than under comparable 1 g conditions for one of two sets of simulated vehicle dynamics investigated. The reason was attributed primarily to increased pilot excitation of the vehicle's lightly damped short-period mode. Russian data, available from Voskhod flights, indicated that cosmonauts did not perform as well in a simulated control system as during ground training sessions.

Research on manual control systems during the past decade or so has focussed considerable attention on the problem of describing human pilot dynamics in terms consistent with flight-control engineering practice. This description is an essential prerequisite to the analytical treatment of manned flight control systems. However, versatility and adaptability, which characterize the human pilot, have made such descriptions difficult to obtain, to generalize, and to apply. Recently, however, some inroads have been made; currently, control system analysis techniques and pilot models are used in the study and optimization of man-vehicle systems.

Although these studies have provided considerable knowledge on pilot performance and dynamic response for a wide range of simulated tasks (refs. 1 to 5), relatively little is known about how these characteristics may vary with the environmental extremes imposed on the crew of advanced aircraft or spacecraft. Such data would provide a more realistic basis for the prediction of man's performance in these advanced systems.

During the past 5 years, a considerable research effort (refs. 6 and 7) has been devoted to studying the effects of acceleration stress on human physiological responses, on control-task performance, and on associated pilot dynamics. Portions of these programs, relevant to the present paper, are outlined in table 1. These studies provided basic information on (1) pilot tolerance to and performance under high sustained accelerations (conducted on the Navy centrifuge at Johnsville, Pa.), (2) pilot performance during combined steady and vibratory accelerations (conducted on the Ames centrifuge), and (3) pilot performance in a simulated control task during short-term zero-g flights (in an Air Force, two place F-104B airplane).

TABLE 1.—ACCELERATION ENVIRONMENTS STUDIED

Environment	Vehicle dynamics	Facility	Pilot	Source
<u>Sustained acceleration:</u> 10 g (EBO) 10 g (EBI) 7 g (EBD)	$Y_c = \frac{13.4 (1 + 2.3S)}{S \left( \frac{S^2}{11.3} + \frac{2(0.53)}{3.35} S + 1 \right)}$	NADC Johnsville centrifuge	A B C	Ref. 6
<u>Combined stress:</u> Sustained acceleration, 3.5 g (EBI) Vibration, <sup>a</sup> 0 g ±1.5 ±2.0 ±3.0	$Y_c = \frac{1.3}{\frac{S^2}{0.92} + \frac{2(0.64)}{0.96} S + 1}$	Ames five-degree-of-freedom simulator (with vibration chair)	D	Ref. 7
<u>Zero acceleration:</u> 1 g (ground) 1 g (flight) 0 g (flight)	$Y_c = \frac{13.0 (1 + S)}{S \left( \frac{S^2}{16} + \frac{2(0.06)}{4} S + 1 \right)}$ (Dynamics "A")	F-104B aircraft	E	Unpublished
1 g (ground) 1 g (flight) 0 g (flight)	$Y_c = \frac{13.0 (1 + S)}{S \left( \frac{S^2}{36} + \frac{2(0.04)}{6} S + 1 \right)}$ (Dynamics "B")			

<sup>a</sup>Vibration frequency, 11 cps

The purpose of the present paper is to review briefly pertinent results from the first two studies and to summarize available results from the third program. Where data are available, possible ties between physiological, control-task-performance, and describing-function measures will be indicated.

### SYMBOLS

- AR    amplitude ratio, dB
- $A_x$     longitudinal acceleration, g
- $A_y$     lateral acceleration, g
- $A_z$     normal acceleration, g
- f      frequency, cps
- g      acceleration of gravity; 1 g = 32.2 ft/sec<sup>2</sup>

$h_p$	pressure altitude, ft
$M$	Mach number
$S$	Laplace transform variable
$Y_c$	vehicle pitch transfer function
$Y_p$	pilot describing function
$\delta_H$	pilot controller deflection
$\theta$	vehicle pitch attitude, deg
$\theta_e$	pitch tracking error, deg
$\theta_i$	system forcing function, deg
$\tau$	pilot reaction time, sec
$\Phi_{ee}$	tracking error power spectrum
$\varphi$	phase angle, deg
$\omega$	angular frequency, radians/sec

### SUSTAINED ACCELERATION

This section provides a brief review of the effects of high sustained acceleration on pilot performance and dynamic response. Most of the results discussed are taken from reference 6. Figures 1 to 6 illustrate the range of results obtained during the Ames programs. In figure 1, averaged pilot tolerance boundaries for high sustained accelerations (taken from ref. 8) are shown for eyeballs-in, eyeballs-out, and eyeballs-down directions of the applied accelerations. Also spotted on these curves are individual points representing the results for pilots A, B, and C. (These points pertain to the task performance, pilot describing function, and physiological measures discussed subsequently for these pilots.) The results in figure 4 represent the longest periods of time a test pilot, preconditioned to the effects of acceleration and suitably restrained, would voluntarily endure a given sustained g-level and perform the control task (see refs. 6 and 9 for task description). These results do not necessarily reflect physiological-tolerance limits.

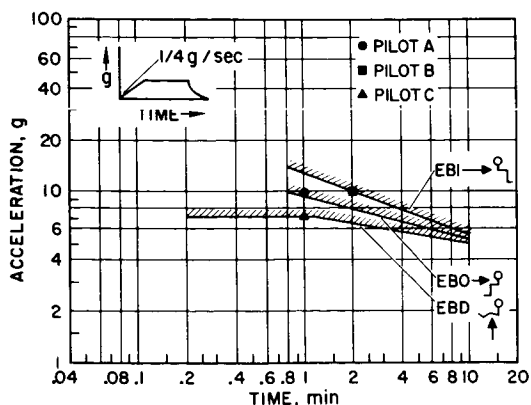


Figure 1.—Pilots' tolerance boundaries for sustained accelerations.

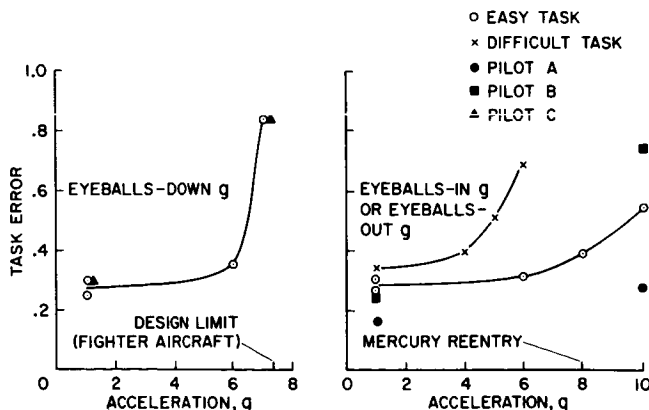


Figure 2.—Effects of sustained accelerations on task performance.

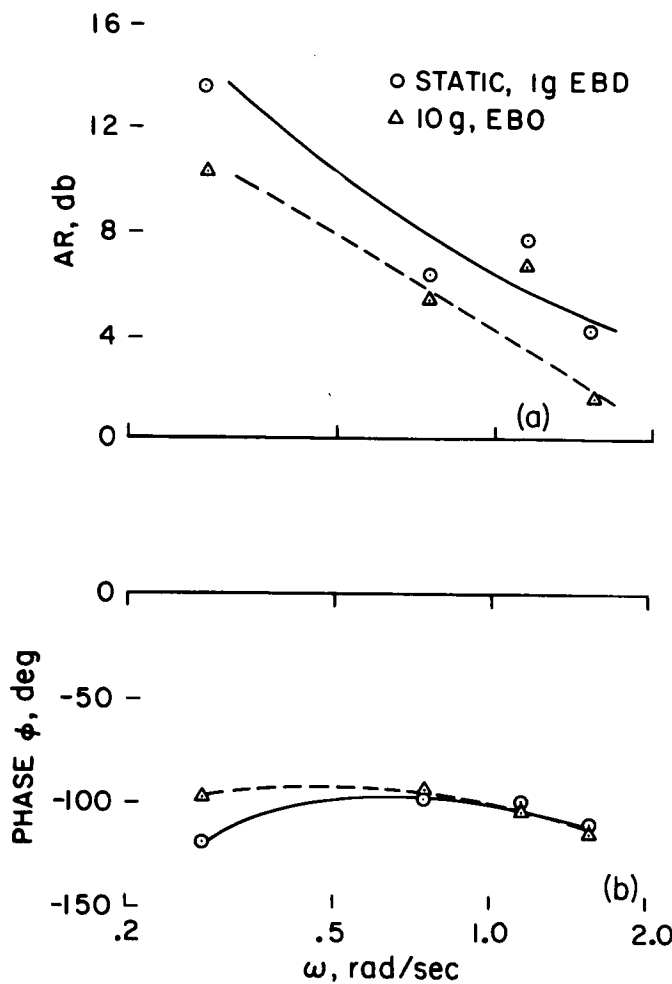


Figure 3.—Effects of acceleration on open-loop system response (pilot A). (a) Amplitude ratio; (b) Phase.

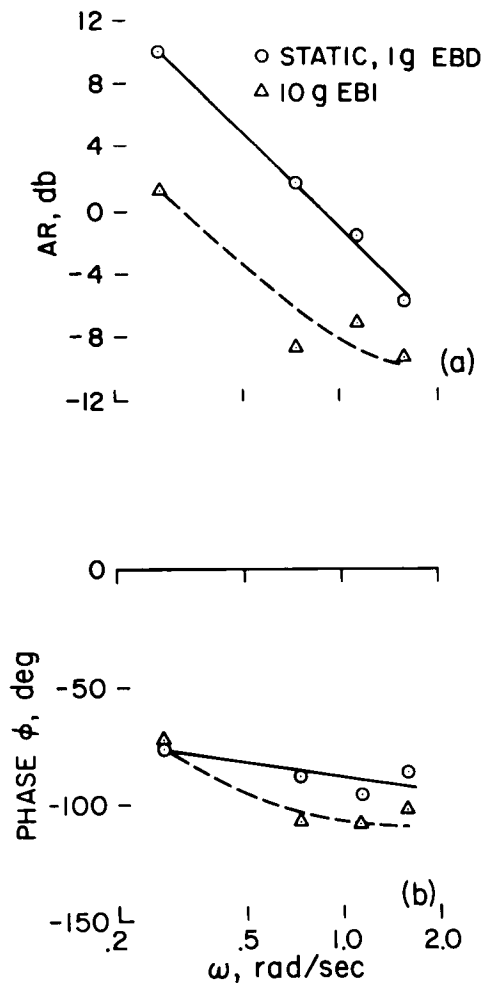


Figure 4.—Effects of acceleration on open-loop system response (pilot B). (a) Amplitude ratio; (b) Phase.

Figure 2 provides a summary of averaged data showing the effects of acceleration on pilots' normalized mean-square error in the assigned control task. This task, described in detail in reference 6, consisted of tracking a target whose random-appearing motion was generated by the sum of four sinusoids with the amplitude-frequency characteristics shown in the following table:

	Sine wave component			
	1	2	3	4
Amplitude, mean square, $\text{deg}^2$ . . . .	14.4	6.3	2.0	1.0
Frequency, rad/sec . . . . .	.28	.74	1.15	1.60



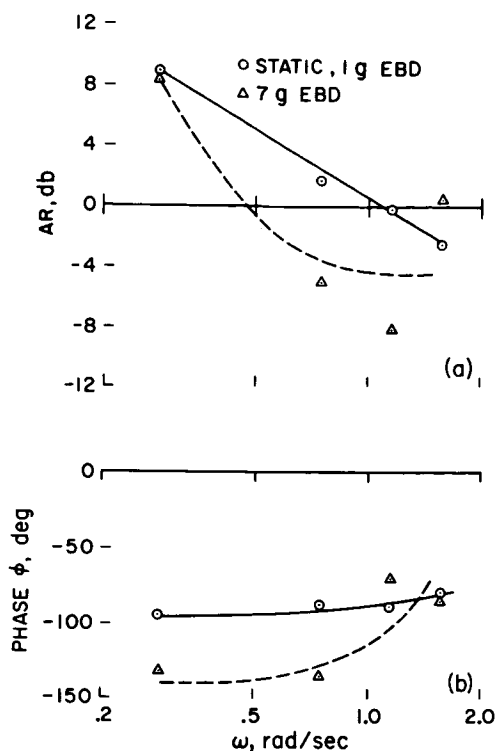


Figure 5.—Effects of acceleration on open-loop system response (pilot C). (a) Amplitude ratio; (b) Phase.

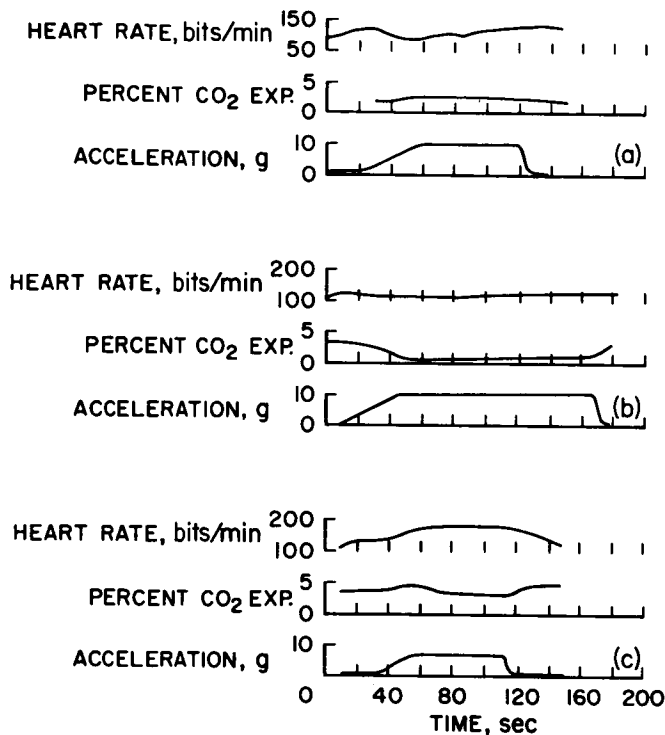


Figure 6.—Physiological performance measures during high sustained accelerations. (a) Pilot A (10 g, EBO); (b) pilot B (10 g, EBI); (c) pilot C (7 g, EBD).

This task was essentially the same for all studies described in table 1. Shown also in figure 2 are the individual results for three pilots for both the 1 g static case and for the maximum-acceleration runs discussed in this paper. Pilot C's rapid deterioration of performance above about 6 g EBD is of particular interest and is undoubtedly associated with impending blackout. Also of interest is the significant difference in the acceleration levels (EBI or EBO) at which performance deteriorates rapidly for two different tasks. For a difficult task (poorly damped vehicle), performance deteriorates rapidly above 4 g; for the easy task (well-damped vehicle), performance deteriorates moderately above about 6 g. Unfortunately, data on which to base pilot describing functions are not available for the "difficult" task, so that reasons for the observed difference are not obvious. It may be desirable to investigate this problem in a later study.

In figures 3 to 5, the effects of acceleration on open-loop system responses for pilots A, B, and C are presented. The results in figure 3 for pilot A show relatively little effect of acceleration on pilot-vehicle system response. Although not too well defined, open-loop crossover (fig. 3 (a)) decreases from about 3.3 rad/sec (1 g EBD) to about 2.4 rad/sec (10 g EBO). This observation is consistent with the small increase in normalized error shown for pilot A in figure 2. The 6 dB/octave attenuation in the region near crossover is compatible with other results (e.g., ref. 1) which indicate that the optimal control strategy for minimizing mean square error is (1) to insure system crossover at frequencies beyond those at which

significant forcing function power exists, and (2) to equalize the system to provide a 6 dB/octave attenuation near crossover frequencies. The associated phase margins for pilot A (fig. 3(b)) vary from roughly  $35^\circ$  (1 g EBD) to about  $55^\circ$  (10 g EBO).

The results for pilot B (fig. 4) are a bit more interesting and varied. The amplitude-ratio data for the open-loop system (fig. 4(a)) show that crossover varied from about 0.9 rad/sec to 0.35 rad/sec as the acceleration level was changed from 1 g EBD to 10 g EBI. The crossover frequencies shown are both below those at which appreciable forcing function power exists, and they reflect the relatively poor performance of pilot B shown in figure 2. Despite these low crossovers, the pilot again adapted so that the attenuation of system response in the region of crossover was about 6 dB/octave. The associated phase margins for this case were about  $90^\circ$  for both the static and high-g runs (see fig. 4(b)).

The results for pilot C are given in figure 5. The amplitude-ratio data (fig. 5(a)) again show that the primary effect of acceleration on pilot-vehicle response was an appreciable reduction in system crossover from 1.1 to 0.47 rad/sec. The variability of the high-g data (i.e., lack of smooth trends at the higher frequencies) is of interest and may reflect increasing variability in pilot-control function. Some support for this observation is provided in reference 6, where it is shown that the pilot's average linear coherence decreased from 0.86 to 0.68 (mainly due to increased time variability in the pilot's response). The system phase response (fig. 5(b)) for pilot C indicates phase margins of the order of  $85^\circ$  (1 g EBD) and  $35^\circ$  (7 g EBD).

Limited results on the physiological response of the three test pilots are provided in time-history form in figure 6. (Additional information in this area is given in ref. 9.) This figure presents some relatively simple physiological measures obtained during the same tests covered in the preceding discussion. The intent here is to speculate on how these results may be related to the observed changes in pilot performance and pilot-vehicle dynamic-response measures previously discussed. Shown in figure 6 are time histories of heart rate and the percent of carbon dioxide contained in the expiratory air for the various levels and direction of the applied acceleration vector. The heart rate is a standard and familiar measure; the percent of  $\text{CO}_2$  expired is important because it is related here to the respiratory efficiency of the pilot, particularly to his ability to maintain proper oxygen and carbon dioxide levels in the blood. Results in figure 6(a) show a relatively small, steady increase in heart rate during 10 g EBO accelerations and practically no change in percent of  $\text{CO}_2$  expired. Results in reference 10 show that, while no respiratory embarrassment was observed for high EBO accelerations, visual symptoms, such as tearing and blurred vision, were noted which may account for the somewhat poorer performance of pilot A. The results in figure 6(b) show that 10 g EBI acceleration had relatively little effect on heart rate, but significantly decreased the  $\text{CO}_2$  expired. Results in reference 10 indicate that this reduction reflects a serious respiratory problem at high EBI accelerations. The problem results from a reduction in tidal volume to little more than the pulmonary dead space; consequently, alveolar ventilation is seriously diminished and the pilots may suffer from "acceleration-hypoxia," not unlike the normal environmental hypoxia. One could speculate that this effect may be the basic reason for the deterioration of pilot performance at high EBI accelerations as illustrated in figures 2 to 5. The results in figure 6(c) show a significant increase in heart rate and relatively small changes in  $\text{CO}_2$  expired as the acceleration attained a 7 g EBD level. The increase in heart rate is usual for high eyeballs-down accelerations and is due to reflex action of the cardiovascular system, which attempts to maintain blood flow rates at normal, unstressed levels. In the present case, this regulatory mechanism was not equal to the task, and the pilot reported symptoms of partial blackout.

## COMBINED SUSTAINED ACCELERATION AND VIBRATION

Results from references 7 and 11 are shown in figures 7 and 8. As indicated in reference 7, these studies were conducted to investigate the effects of combined sustained and vibrational stresses on pilot control and monitoring capabilities. These stresses are typical of a class of large, liquid-fueled launch vehicles. The specific conditions discussed here are sustained accelerations of about 3.5 g (EBI) combined with vibration of 11 cps up to about  $\pm 3g$ .

Figure 7(a) is a typical time history of a tracking run for a relatively unstressed condition (sustained accelerations, 3.5 g). Pertinent quantities shown are task errors, vehicle pitch angle, pilot controller deflections, input forcing function, and the acceleration time

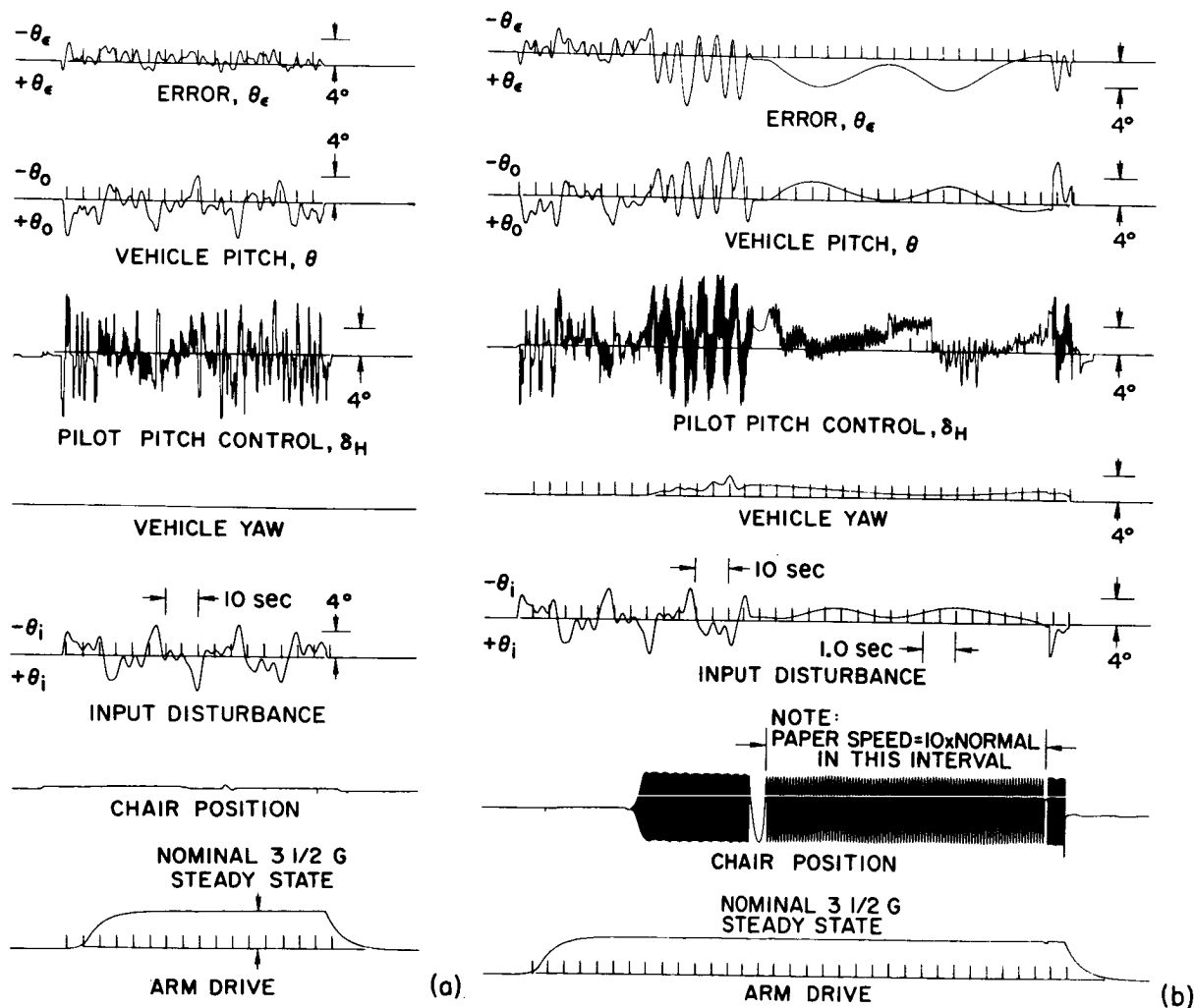


Figure 7.—Typical time histories of tracking runs. (a) Bias acceleration, 3.5 g;  
(b) Bias acceleration, 3.5 g vibration,  $\pm 3g$ .

history. The considerable pilot control activity is typical of that associated with pilots attempting to cope with relatively high-frequency disturbances with "sluggish" vehicle dynamics (see table 1). The high-frequency controller motions may be due to centrifuge track rumble and the type of controller used (ref. 7).

The results in figure 7(b) are for sustained accelerations of 3.5 g combined with severe vehicle vibrations of  $\pm 3$  g. The time scale for a portion of the time history has been expanded to show more clearly the pilot's vibration environment and the associated vibrations in his control output. Because of the relatively low bandwidth vehicle dynamics, these vibrations are not reflected in either the vehicle output or in the error traces. A comparison of portions of the record (without and with vibration) of vehicle output, error, and controller traces shows a large buildup of task errors, coincident with a regular oscillation at about the natural period of the vehicle (about 6 sec) during vibration. No explanation is available for this control behavior on the part of the pilot, but his introducing lag-lead equalization, rather than lead-lag, may account for it; however, good describing-function data are not presently available. (This point is briefly elaborated upon later in this section.)

Figure 8 provides averaged results for two pilots for normalized task errors (fig. 8(a)) and for dial reading errors (fig. 8(b)) as a function of vibration level. The dial reading errors were taken from reference 11. Also given in figure 8(a) are the individual points for pilot D associated with the results in figure 7. The effects of vibration on control-task performance are quite apparent, with a rapid deterioration occurring above about  $\pm 1.5$  g. Describing-function data, which are not presented because of their inconsistency, do suggest, however, that the pilot's ability to generate lead (which is required to compensate for vehicle dynamics attenuation above 0.9 rad/sec) is impaired. This "result" is not incompatible with pilots' comments during the test program. With no vibration, the pilots were able to follow the target motion in the display and easily follow error reversals and error rate. As vibration was introduced, the actual display indications became a blur<sup>1</sup>, particularly at the higher vibration levels, and the pilots presumably lost their ability to extract error rate information from the display. This observation, if verified, may have important applications to display design for vehicles susceptible to appreciable vibrations in the crew compartment (e.g., launch vehicles, helicopters, current and projected transports, low-level, high-speed flight vehicles, etc.).

The results in figure 8(b) show an increase in gross dial reading errors which parallel, roughly, the increase in control-task error shown in figure 8(a). Again a rapid increase in error is observed as the vibration level exceeded approximately  $\pm 1.5$  g.

## ZERO-GRAVITY EFFECTS

The results discussed in this section were obtained in a study conducted some time ago by Ames Research Center on an F-104B airplane. Currently, where orbital flights of 7 to 14 days appear commonplace, it may be presumptuous to present results obtained during zero-g flights of less than a minute. However, it is believed the results are of interest, since very little quantitative data are available from the manned space flights to indicate whether manual control functions are influenced significantly under weightless conditions.

<sup>1</sup>This was referred to as diplopia, or "double vision," by one of the subjects of the study who was a medical doctor, as well as pilot.

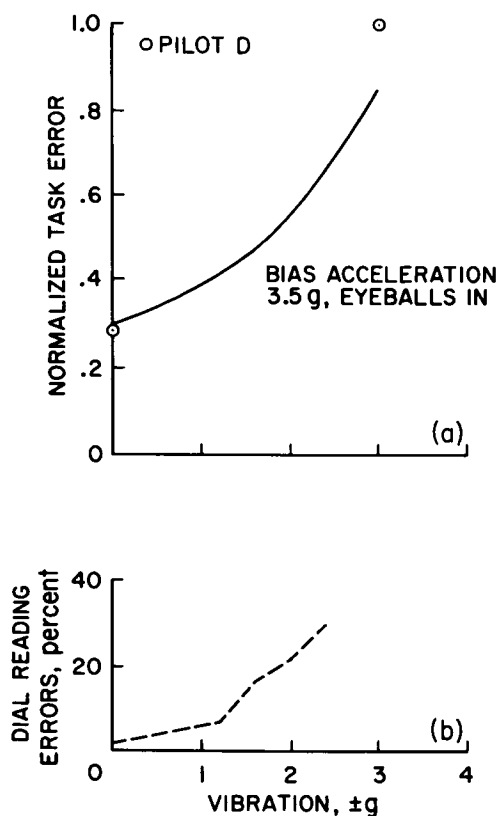


Figure 8.—Effects of combined acceleration stress on task performance. (a) Control task errors; (b) Dial reading errors.

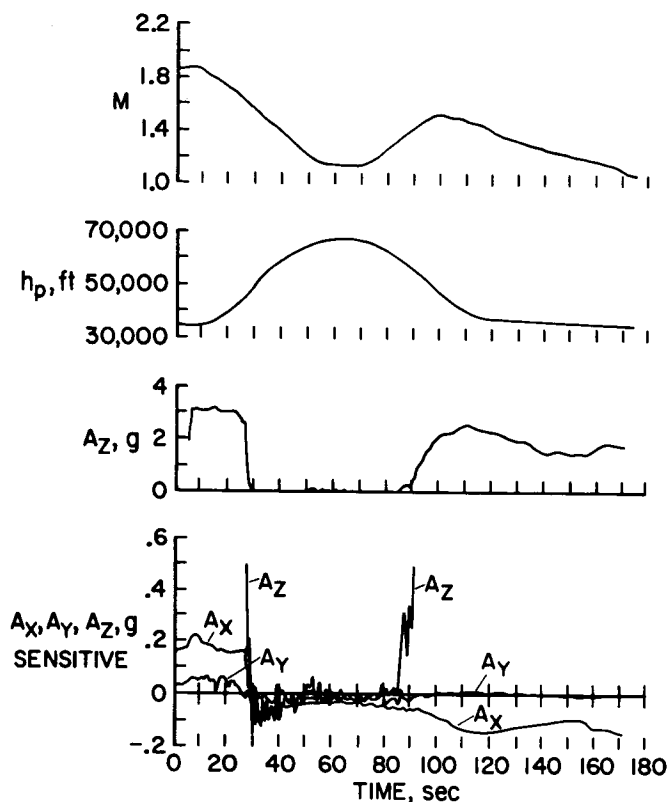


Figure 9.—Typical time history of zero-gravity maneuver (F-104B).

The primary results of this study are provided in figures 9 to 16. (Figure 17 provides available pertinent data from Russian Voskhod flights.) During a preliminary series of tests, pilot reaction times, both simple and complex, and percentage of control reversals during the complex reaction-time trials were obtained. For these tests, a scope display and controller with unit gain dynamics to the display were used. The pilot's task was to follow random-step, unidirectional inputs to the display (simple reaction time) and random, dual-directional steps (complex reaction time). In later tests, the pilot was given control tasks similar to those imposed during the sustained acceleration and combined acceleration-stress studies. The results selected for discussion are for a fairly difficult task, for example, a very lightly damped vehicle (see table 1).

To provide some indication of the actual acceleration levels imposed on the pilot and the type maneuvers performed to produce the "weightless" environment, a typical time history is given in figure 9. Accelerations of about 0.02 to 0.05 g are observed for the zero-g portion of the time history.

### REACTION-TIME AND CONTROL REVERSALS.—

Results from the preliminary study on reaction time are illustrated in figure 10. Very little effect of zero gravity on simple reaction time is shown (fig. 10(a)). The complex reaction-time data show significant increases at both 0 and 3 g relative to the 1 g flight value. It should be noted that these results are mean values for about 15 to 20 runs. Although these results are relatively meager, the trends appear to indicate an appreciable effect of 0 g (and 3 g) on the central nervous system. It would be of interest to verify these trends under space-flight conditions.

The increase in the percentage of control reversals at 0 and 3 g, relative to the 1 g case (fig. 10(b)), parallels the increase in complex reaction time, lending additional support to the possibility of "central-data-processor" changes due to weightlessness.

**CONTROL TASK PERFORMANCE.**—In figure 11, results show the effects of varying the acceleration environment on normalized mean-square error (fig. 11(a)), normalized error spectra (fig. 11(b)), and on the error spectrum (fig. 11(c)). The relatively large increase in mean-square error between 1 and 0 g flight shown in figure 11(a) (vehicle dynamics "A") is due to (1) a moderate increase in normalized error spectra at forcing-function frequencies shown in figure 11(b), and (2) a large increase in the error peak near the vehicle short-period frequency. Although the pilot's performance (ref. 12) of this difficult task varies considerably, the observed increase in mean-square error in the present example is significantly greater than the variability noted for the same pilot (and for the same vehicle dynamics) in the study of reference 12.

Similar results for vehicle dynamics "B," which is also a fairly difficult task, are presented in figure 12. For these dynamics, there does not appear to be a significant effect of zero gravity on pilot performance. The results in figure 12(c), as well as those in figure 11(c), may be slightly misleading because of the difference in computed input spectrums between the 1 g flight and 0 g runs. However, these data, combined with those in figure 12(b), are generally indicative of the relative contributions to the overall mean-square error of component errors at forcing-function frequencies and those occurring due to excitation of the vehicle short period.

**SYSTEM RESPONSE MEASURES.**—Figures 13 and 14 present pilot describing-function data for vehicle dynamics "A" and "B," respectively. In the former case, neither the amplitude-ratio response (fig. 13(a)) nor the phase response (fig. 13(b)) reveals any startling effects of 0 g on pilot response. Actually, the most significant difference is noted between the 1 g ground and the 1 g and 0 g flight data. Data provided in figures 14(a) and 14(b) show

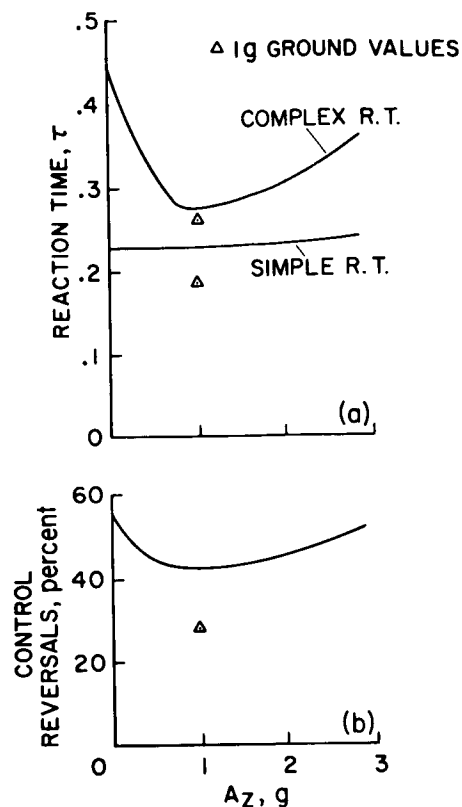


Figure 10.—Reaction time and control reversal results. (a) Reactions; (b) Control reversals.

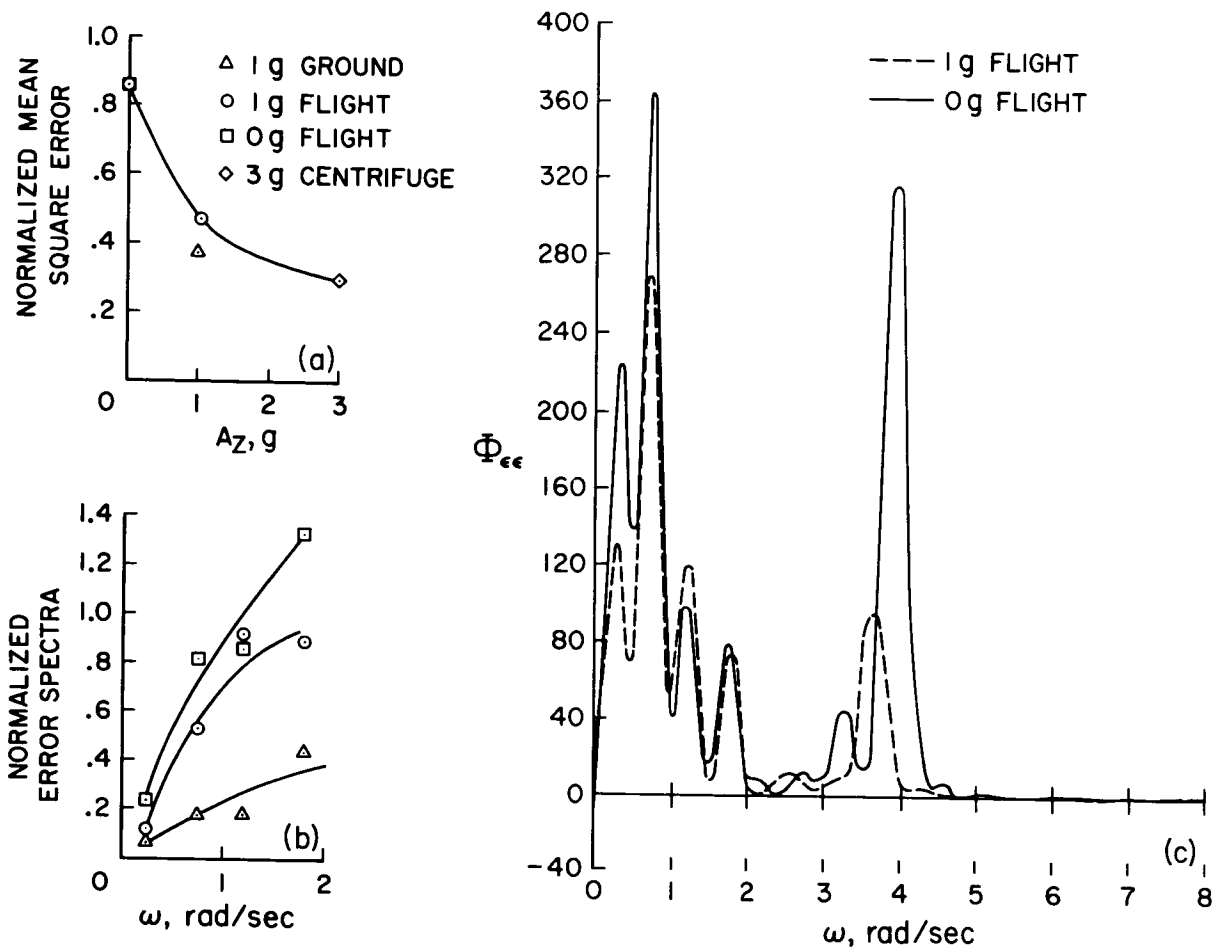


Figure 11.—Effects of short-term weightlessness on task performance (dynamics "A").  
 (a) Normalized mean square error; (b) Normalized error spectra; (c) Error spectra.

again the trend toward reduced gains and increased phase shifts between the ground and flight environments. No significant effect of 0 g on pilot dynamics at forcing function frequencies is apparent. This observation is compatible with the relatively small performance variations shown in figure 12(a).

Open-loop pilot-vehicle system responses are presented in figures 15 and 16. Several observations of interest may be made regarding the results in figure 15 for vehicle dynamics "A":

- (1) Open-loop system crossover decreased from about 1.5 to 0.8 rad/sec between the ground and flight situations.
- (2) The attenuation at crossover is about 6 dB/octave which, as noted earlier, satisfies one of the two "optimal-control" strategies required for minimizing mean-square error.
- (3) Phase margins for all three cases considered are roughly  $75^\circ$  to  $80^\circ$ .

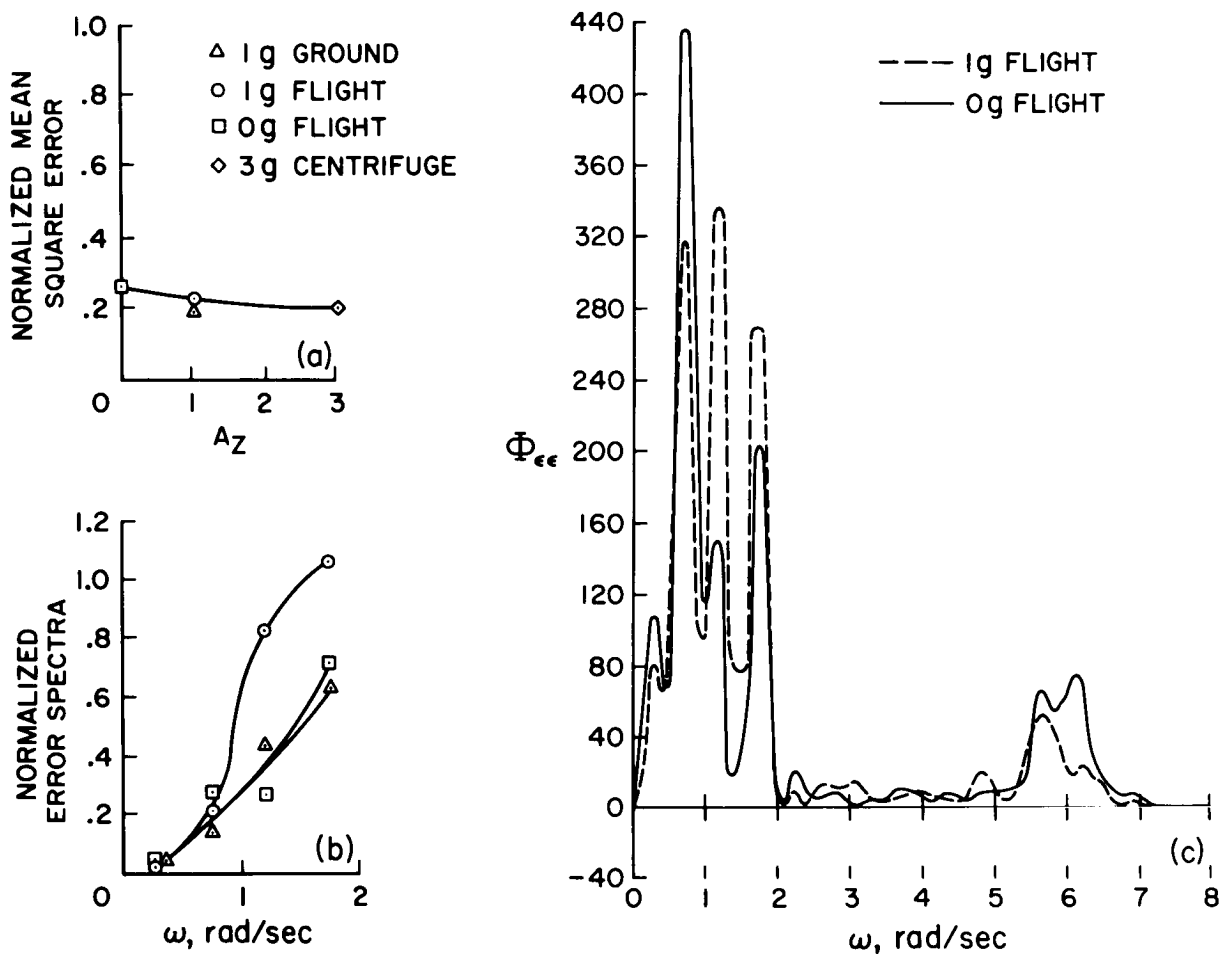


Figure 12.—Effects of short-term weightlessness on task performance (dynamics "B"). (a) Normalized mean square error; (b) Normalized error spectra; (c) Error spectra.

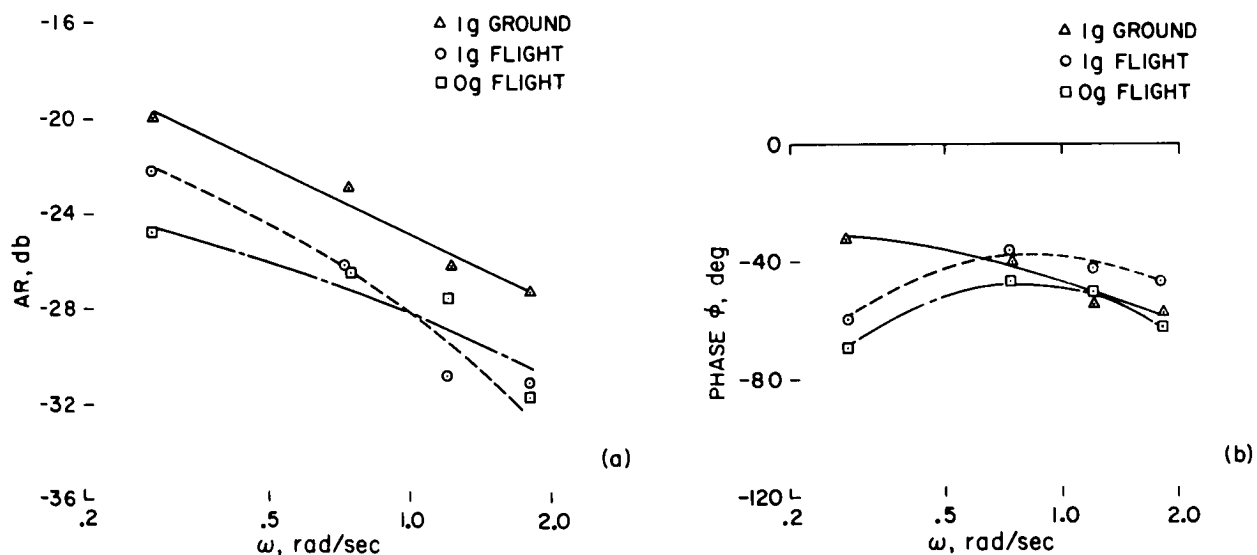


Figure 13.—Comparative describing function data (dynamics "A"). (a) Amplitude ratio; (b) Phase.



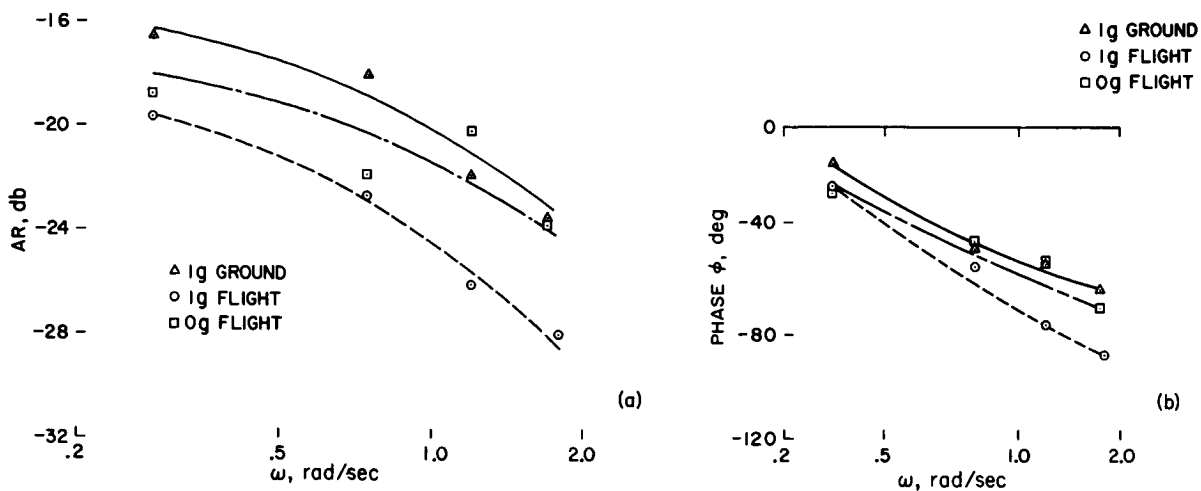


Figure 14.—Comparative describing function data (dynamics "B"). (a) Amplitude ratio; (b) Phase.

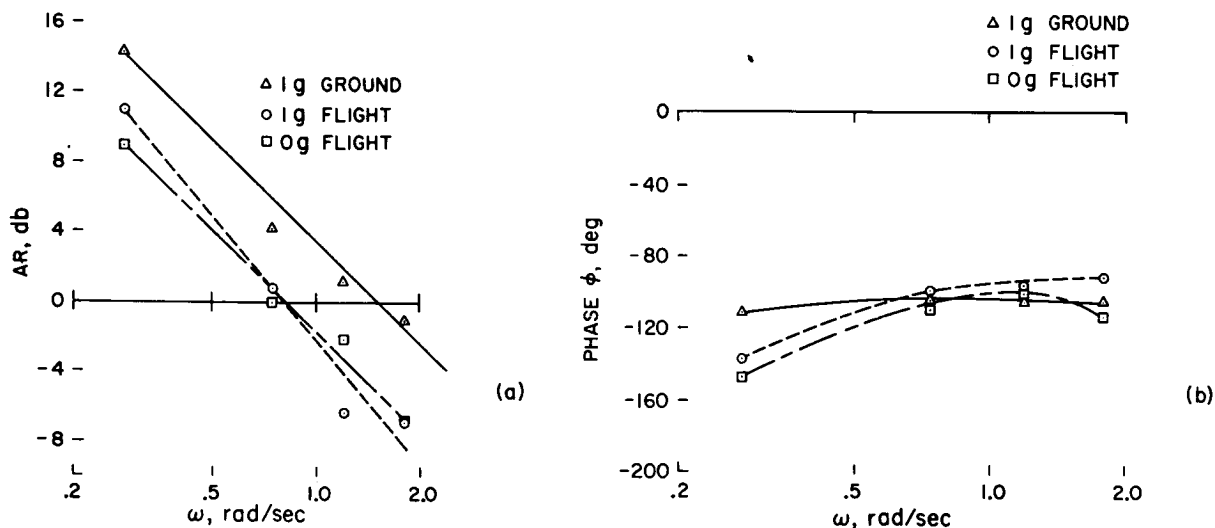


Figure 15.—Open-loop system response (dynamics "A"). (a) Amplitude ratio; (b) Phase.

(4) The crossover frequencies in all cases are relatively low and below those for which appreciable forcing function power exists; this accounts for most of the relatively large normalized error shown in figure 11(a) for the 1 g ground and 1 g flight runs. Most of the increased error at 0 g resulted from the pilot "chasing" the lightly damped, short-period motions.

Results for vehicle dynamics "B" in figure 16 indicate clearly that the pilot was using the proper control strategy to minimize his errors; that is, he employed equalization which resulted in system attenuation of 6 dB/octave at crossover, and he used sufficient gain to insure crossover at frequencies generally higher than those containing power in the input. The associated phase margins indicated by the results in figure 16 are about 60° to 70°.

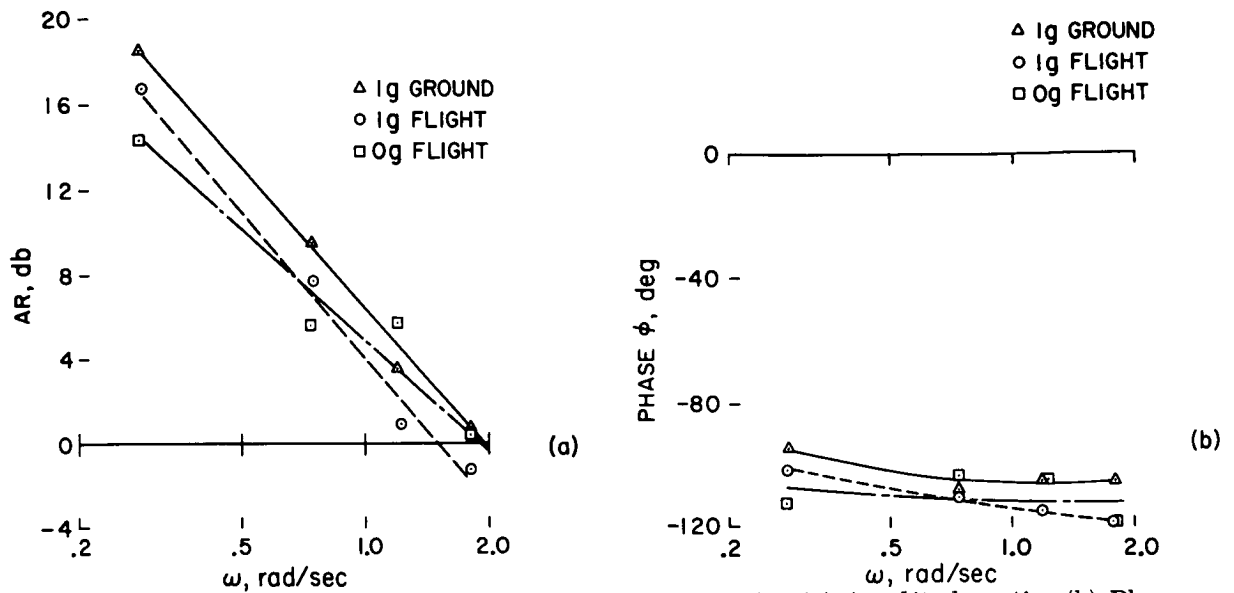


Figure 16.—Open-loop system response (dynamics "B"). (a) Amplitude ratio; (b) Phase.

### PHYSIOLOGICAL DATA

During the short-term weightlessness tests in the F-104B, heart rate, blood pressure (diastolic and systolic), and respiratory rate were measured on the pilot performing the simulated control tasks. The results (not shown) indicated that short-term weightlessness had a significant effect on the cardiovascular response and little effect on respiratory response. Pulse rates decreased appreciably and pulse pressures (difference between systolic and diastolic values) increased somewhat under zero gravity. Comparison of these limited results with subsequent mean results obtained during the first manned orbital Mercury flight (MA-6) showed substantial agreement in the observed trends in cardiovascular response. Although these are meager results, they do suggest that short-term weightless flights in high-performance aircraft may provide results on human performance and behavior related to those observed in orbital flight.

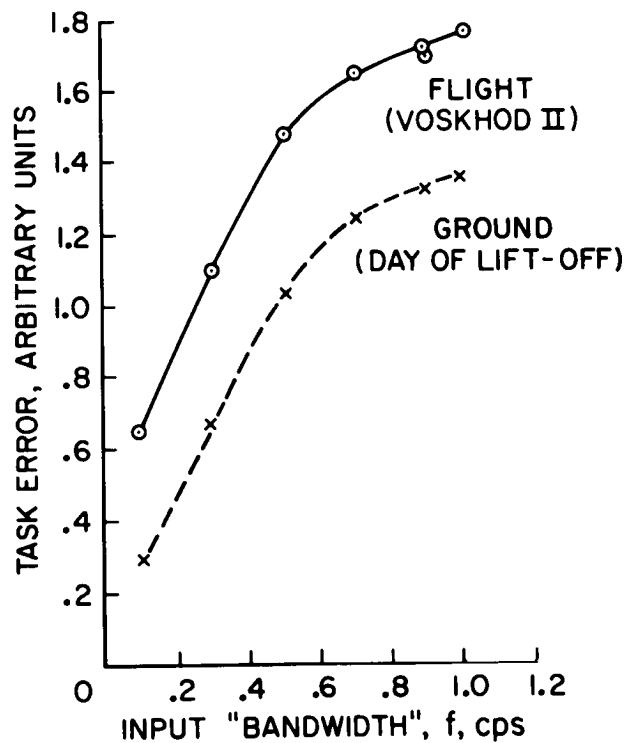


Figure 17.—Model control system results in Voskhod flights.

## RUSSIAN VOSKHOD II RESULTS

In reference 13, a brief description was provided of results obtained during the Voskhod II flight which indicated that performance of the cosmonaut in a model control system deteriorated during flight relative to his performance during training in a mock-up of the spacecraft. Additional available details of the experiment and results, provided in reference 14<sup>2</sup>, are considered pertinent to the present discussion. In this experiment the dynamic characteristics of human subjects, operating a model control system, with immediate and delayed feedback, were investigated.

The input signals used were graduated, of random type, and were sinusoidal signals with nonmultiple frequency characteristics. It was observed in reference 14 that "the operator was able to accomplish control with immediate and delayed feedback in the system. The results show that, in actual space flight as compared with the data obtained in simulators of the capsule and in training, the mean-square error of the operator increases (up to 25 percent), showing a steeper rise at the higher frequencies of the signal" (fig. 17). It was also noted that "the reliability margins of the operator under the influence of space flight factors likewise declined with respect to the phase and modulus of the amplitude-frequency characteristics." These descriptions of results, taken from reference 14, are somewhat confusing. However, it is clear that control performance deteriorated appreciably during the Voskhod flights, relative to performance of the same control task on the ground.

## CONCLUDING REMARKS

Several programs were carried out to determine the effects of various acceleration fields (ranging from high sustained levels to short-term weightlessness) on several pilot performance measures. Based on the results of these studies, several general observations are indicated:

(1) High, sustained accelerations generally resulted in—

(a) Appreciable decrements in control-task performance at accelerations above about 6 g

(b) Reduced open-loop system crossover frequencies

(c) Physiological responses, indicating, or suggesting, embarrassment of the cardiovascular, respiratory, and visual systems during eyeballs-down, eyeballs-in, and eyeballs-out accelerations, respectively

(2) Combined sustained accelerations and vibration resulted in a rapid deterioration of task performance as the vibration level (at 11 cps) exceeded about  $\pm 1.5$  g. Pilots' observations, supported by some describing-function data (not presented), suggest that required lead equalization disappeared during severe vibration.

(3) Test results obtained during short-term weightless flights in an F-104B, two-place airplane showed that—

---

<sup>2</sup>In addition to the model control system study, information is provided on (1) time required to perform manual control of vehicle as a function of the number of orbits, (2) time required to perform various medical checks at various flight stages, visual efficiency, etc.

(a) Complex reaction time and control reversals increased under 0 g, relative to 1 g flight conditions.

(b) Control task performance decreased significantly for one of the two sets of simulated vehicle dynamics studied and very little for the other set. (This decrement was attributed mainly to pilot excitation of the vehicle short-period mode beyond forcing function frequencies.)

(c) Pilot describing function and open-loop system response revealed no significant effects of short-term weightlessness on these measures for the control tasks considered here.

(4) Russian data indicated that operator performance in a model control system was significantly degraded during Voskhod flights, relative to levels measured on the ground during training.

## REFERENCES

1. McRuer, Duane; Graham, Dunstan; Krendel, Ezra; and Reisener, William, Jr.: Human Pilot Dynamics in Compensatory Systems - Theory, Models and Experiments with Controlled Element and Forcing Function Variations. Tech. Rep. AFFDL-TR-65-15, July 1965.
2. Young, Laurence R.; Green, David M.; Elkind, Jerome I.; and Kelly, Jennifer A.: The Adaptive Dynamics Response Characteristics of the Human Operator in Simple Manual Control. NASA TN D-2255, 1964.
3. Todosiev, E. P.; Rose, R. E.; Bekey, G. A.; and Williams, H. L.: Human Tracking Performance in Uncoupled and Coupled Two-Axis Systems. 4380-6003-R0000, Dec. 8, 1965.
4. Hall, Ian A. M.: Effect of Controlled Element of the Human Pilot. WADC Tech. Rep. 57-509, Wright Patterson Air Force Base, Dayton, Ohio, Aug. 1958.
5. Adams, J. J.: A Simplified Method for Measuring Human Transfer Functions. NASA TN D-1782, 1963.
6. Sadoff, Melvin: Effects of High Sustained Acceleration on Pilots' Performance and Dynamic Response. NASA TN D-2067, 1964.
7. Dolkas, Constantine B.; and Stewart, John D.: Effect of Combined Linear and Oscillatory Acceleration on Pilot Attitude-Control Capabilities. NASA TN D-2710, 1965.
8. Creer, Brent Y.; Smedal, Harald A.; and Wingrove, Rodney C.: Centrifuge Study of Pilot Tolerance to Acceleration and the Effects of Acceleration on Pilot Performance. NASA TN D-337, 1960.

9. Creer, Brent Y. ; Smedal, Harald A. ; and Stewart, John D. : A Summary on the Influence of Sustained Acceleration on Pilot Performance and Pilot Physiology. Paper presented at the Aerospace Medical Panel Meeting, Advisory Group for Aeronautical Research and Development, NATO, Paris, France, July 6-10, 1962.
10. Smedal, Harald A. ; Rogers, T. A. ; and Duane, T. D. : Physiological Factors Affecting the Pilot Under High Sustained Accelerations. Paper presented at the 33rd Annual Meeting of the Aerospace Medical Association, Atlantic City, N.J., Apr. 1962.
11. Clarke, Neville P. ; Taub, Harvey ; Scherer, Harris F. ; Temple, William E. ; Vykukal, Hubert C. ; and Matter, Milton : Preliminary Study of Dial Reading Performance During Sustained Acceleration and Vibration. AMRL-TR-65-110, Aug. 1965.
12. Sadoff, Melvin ; McFadden, Norman, M. ; and Heinle, Donovan R. : A Study of Longitudinal Control Problems at Low and Negative Damping and Stability With Emphasis on Effects of Motion Cues. NASA TN D-348, 1961.
13. Anon. : Gzenko Discusses Soviet Space Medicine. Aviation Week and Space Technology, vol. 82, no. 23, June 7, 1965, pp. 40-45.
14. Isakov, P. I. ; Popov, V. A. ; and Khachatur'yants, L. S. : Problems in Evaluating the Physical Fitness of Cosmonauts. NASA TT F-9593, 1965.

## 18. THE EFFECT OF MINOR ALCOHOL STRESS ON TRACKING SKILL

C. B. Gibbs

*Defense Research Laboratories*

Twenty men were tested in step-input tracking. Minor stress was imposed by moderate alcohol dosage and an incompatible directional relation between control and display. Some target movements demanded a response in an improbable direction and posed a choice between long delay in response and a movement in the wrong direction. The duration of response latency and the number of directional errors revealed a subject's preference for accuracy or speed and his ability to estimate probabilities. Directional errors stem from wrong decisions and may be more relevant to accidents than lack of precision in tracking which has been the main measure used in previous studies of alcohol effects.

Directional errors, response latencies, and eye movements were recorded before and after drinking, when breathalyzer readings were zero, and at 0.05-percent and 0.1-percent breathalyzer levels which may be produced in a man weighing 160 pounds by drinking two and four 12-ounce bottles of beer, respectively.

Alcohol caused a progressive increase in response latencies in and errors ( $p < 0.01$ ); there was no evidence for a threshold below which alcohol has no adverse effect. The test emphasized the markedly different effects of the same alcohol dosage on the skill of different subjects, but habitual drinkers obtained no undue advantage on the test. The task was learned quickly, and extensive practice did not reduce the discriminatory power of the test. The effects of a dose producing a 0.05-percent breathalyzer reading were not significantly different in an ascending or descending series of levels of intoxication. The alcohol dosages tested had no significant effect on simple reaction time.

Considerable success has been achieved in measuring physiological changes due to alcohol consumption and other causes of stress, but there is a serious lack of simple, reliable measures of the effects of minor stress on actual behavior. For example, drivers suspected of impairment may be required to walk a line, touch their nose with eyes shut, and perform other actions that are not used in driving. In some individuals, the accuracy of these movements is not noticeably affected by heavy drinking. Breathalyzer readings only indicate physiological states and not the very different effects of the same state upon the behavior of individuals. More sensitive and relevant measures are needed for behavioral studies of individuals' tolerance of alcohol, its more immediate and delayed effects, and the relative importance of different forms of stress.

In a previous study of learning and proprioceptive functions (ref. 1), subjects were tested in a task of step-input tracking that demanded occasional responses in an improbable direction. These steps posed a choice between a long response latency or a movement which was initially in the wrong direction (error). Errors usually occurred because the subject responded too rapidly, on the mistaken assumption that an improbable response would not be required. The frequency of error and the latency of responses therefore revealed the subject's preference for speed or accuracy and his tendency to confuse improbable with impossible

events. Most studies of impaired driving ability have measured tracking errors which reflect the speed and accuracy of movement (refs. 2 to 4). In contrast, directional mistakes are errors of decision, and these, together with response latency, can give some indication of the number of correct decisions that a person can make in a given time.

This decision rate and speed or accuracy preferences may well prove to be useful measures in personnel selection and in studying stress. In the main, the present experiment on intoxication effects is a preliminary investigation of promising new measures of performance although the test was also designed to provide additional data on several problems where existing findings are conflicting. For example, some studies (refs. 5 to 9) indicate that the degree of impairment at a given alcohol level is greater on an ascending than a descending series of degrees of intoxication, but there was no difference in another experiment (ref. 4). Heavy drinkers develop a higher tolerance than others to alcohol but there is some conflict of evidence whether habituation is general or applies only to specific activities (refs. 4 and 9 to 12). Data conflict on the effects of alcohol on simple reaction time (ref. 13). There is some evidence that complex, recently acquired skills are more vulnerable than others to the effects of alcohol (ref. 13). More data are needed, however, on the relative effects of alcohol on different skills and capacities.

## METHOD

Twenty subjects used a joystick to position a cursor on an oscilloscope and track a target spot of light. The subjects were instructed to respond as rapidly and accurately as possible. Joystick movement was limited to the horizontal plane. The target appeared for 1 second in any one of five different positions 1.125 inches apart, disappeared for 1 second, and reappeared in a new position. Each position and each possible pair of successive positions were presented with equal frequency in a complete run of 100 steps. There was a three-to-one probability that a target at position 2 would next move to the right rather than outward to position 1; a target at position 4 was more likely to move left than right. Steps are termed "probable" when the movement actually demanded conformed to the higher probability; steps outward from position 2 or 4 are termed "improbable." Responses beginning at position 3 are called "equiprobable" because the two possible directions of movement were equally probable. Movements from positions 1 or 5 were "unequivocal" with respect to direction.

The electro-oculographic method was used for recording eye movement. Breathalyzer readings were taken when needed.

The subjects had ten 100-step runs but no alcohol on day 1. On day 2, the subjects began with four nondrinking runs and then drank whiskey, gin, or rum diluted to their taste until their breathalyzer readings were about 0.05 percent. The subjects had four runs at this level and another four runs when further drinking raised their breathalyzer level to about 0.1 percent. The subjects then stopped drinking for the day, but they had four more runs when their breathalyzer readings fell to 0.05 percent and another four runs on return to the zero level. The same routine was followed on day 3. On day 4 four runs were given without alcohol.

Tests with eight subjects (group A) showed that the most sensitive measures of alcohol effects were (1) the total number of directional errors, and (2) the response latency of correct responses on improbable steps. It was noted that during the 1 second of target disappearance, the eye often made an anticipatory (lead) movement toward the center of the display. The

movements reduced the maximum possible separation between a reappearing target and clear foveal vision from four positions to two. In terms of angular eye movement, the reduction was from  $8^\circ$  to  $4^\circ$ , and in terms of linear separation at the display from 4.5 inches to 2.25 inches. The lead movements reduced the chances of missing a target, and the total movement per run was measured together with manual response latency and error. The tests with group A strongly suggested that the highly sensitive measures were detecting adverse effects of overnight drinking although breathalyzer readings were zero when morning testing began. Group B (12 subjects) therefore slept in the laboratory for 3 nights to permit close control of drinking.

Subjects were also tested for simple reaction time in pressing a hand switch in response to a light that appeared at irregular intervals ranging from 2 to 4 seconds. Each subject made ten responses at the zero, 0.05-percent and 0.10-percent breathalyzer levels.

## RESULTS

Simple reaction times at the zero, 0.05-percent and 0.1-percent breathalyzer levels were 0.29, 0.29 and 0.31 second, respectively. There was no significant difference between these results nor close agreement between the ranking of subjects' simple reaction time results and their response latencies in the tracking task.

Figure 1 shows the mean response latency for correct and incorrect responses as circles and crosses, respectively. The triangles indicate the sums of the mean times taken to respond incorrectly and to amend the error. It appears that the speed and accuracy requirements are incompatible on improbable steps but not on the others.

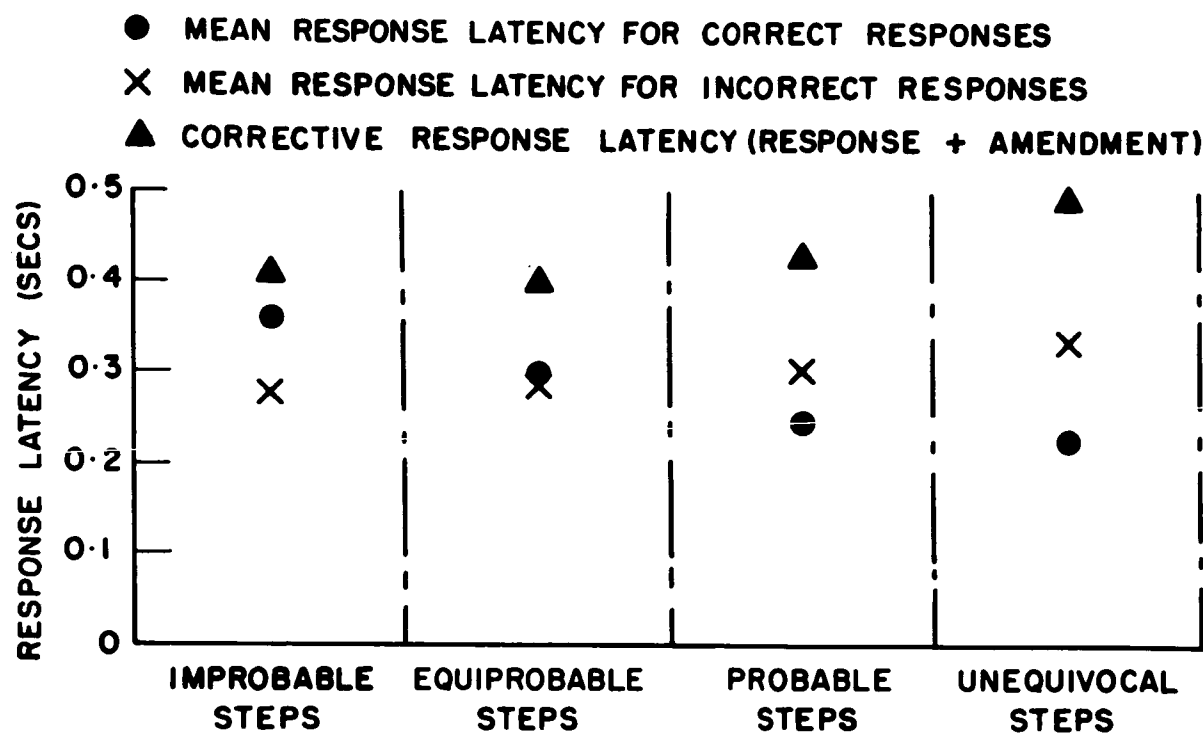


Figure 1.—Mean response latency for correct and incorrect responses and the sum of response latency and amendment time when errors were made on steps of different probability.



Figures 2 and 3 show the mean response latency on improbable steps (circles) and the total number of errors (triangles). Squares indicate the total anticipatory eye movements per run expressed as inches traced over at the display.

The data of the third and fourth runs in each series of four runs were analyzed. There was no significant difference between the third and fourth runs at any breathalyzer level, nor between the scores at the 0.05-percent breathalyzer level on ascending and descending series. The data relating to the same breathalyzer level were pooled and means were computed. The plotted points of figures 2 and 3 show the means of subjects in group B, except that the scores for day 1 are for the final run (no. 10) on that day.

Open symbols denote results with zero breathalyzer reading and closed symbols show scores at the approximate 0.05-percent and 0.1-percent breathalyzer levels. The actual breathalyzer readings of each subject are shown opposite the letters B.A. at the foot of the figures. The letters L, M, H and V.H. at the top of the figure refer to light, moderate, heavy and very heavy drinkers, respectively. Their respective consumptions, in terms of 12-ounce bottles of beer, or the alcoholic equivalent were under 21, 21 to 42, 43 to 64, and over 64 bottles per week.

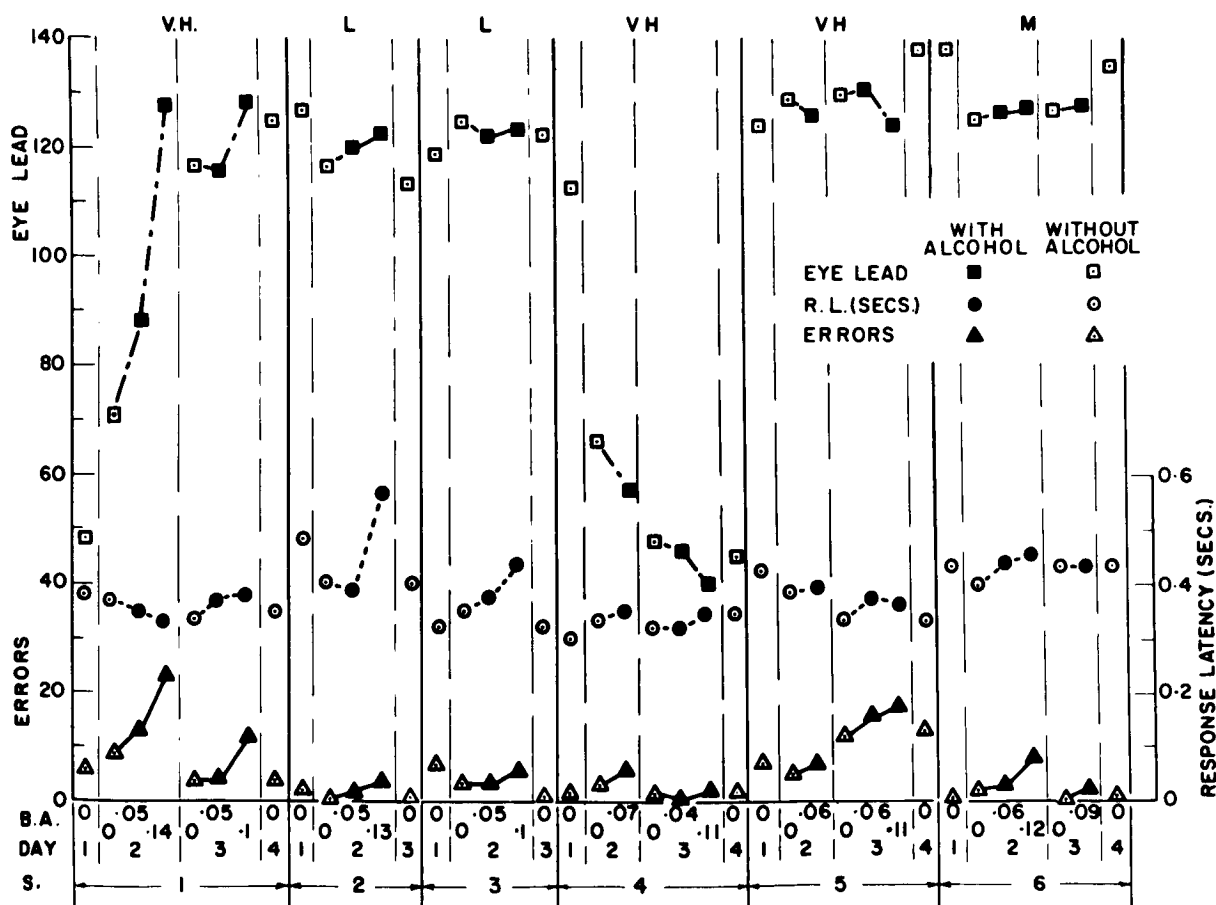


Figure 2.—Test results for subjects 1 to 6.

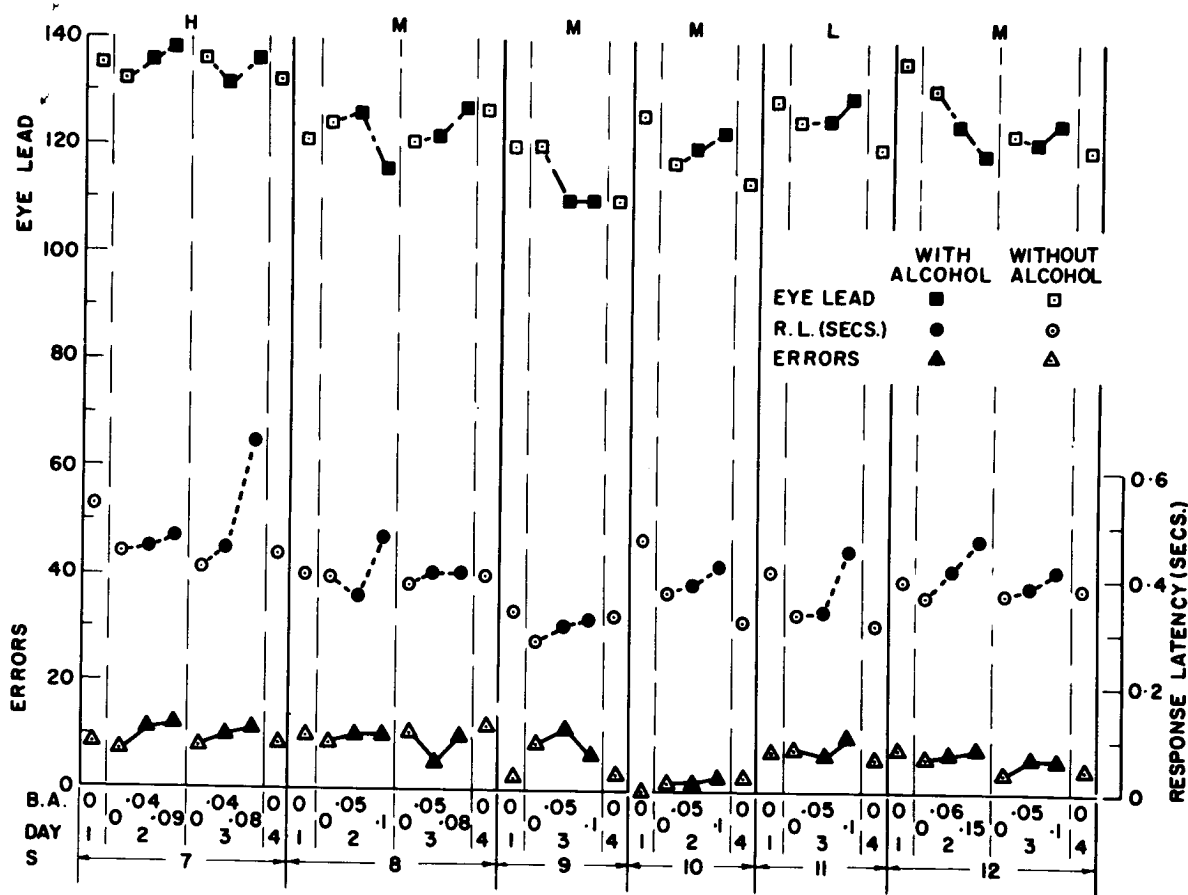


Figure 3. —Test results for subjects 6 to 12.

Paired comparisons were made between each subject's errors and response latencies at the zero and 0.05-percent breathalyzer levels and between the 0.05-percent and 0.1-percent levels on each of 2 days. In a total of 80 comparisons of errors and response latencies at the 0.05-percent breathalyzer level, 63 showed increases with alcohol and only 17 showed decreases or no change — a significant difference ( $p < 0.01$ ). Similar comparison of 68 and 12 positive and negative cases showed a significant ( $p < 0.01$ ) increase of impairment following an increase of breathalyzer level from 0.05 percent to 0.1 percent.

Forty-six percent and 40 percent of all errors occurred on the improbable and equiprobable steps forming 10 percent and 20 percent, respectively, of the total number. Only 14 percent of the errors were made on probable and unequivocal steps which were 70 percent of the total number of steps.

Practice effects were negligible after run 3 and were outweighed by the adverse effects of the lowest alcohol dose that was tested.

Alcohol dosage had no consistent effects on anticipatory eye movements in the group as a whole. Subjects 1 and 4 represent opposite extremes. The former tended to increase lead movements with increased dosages, and the movements increased over the 4 days' trials on nondrinking runs. Subject 4 showed the opposite tendency.

## DISCUSSION

In this study, at the 0.05-percent breathalyzer level, errors were slightly, but not significantly more numerous, on an ascending than a descending series of degrees of intoxication. The finding is opposed to results reported in references 5 to 9.

Figures 2 and 3 show that habitual drinking gave no undue advantage in the present test. Subjects 1 and 4 were very heavy drinkers, but they made more errors than subjects 2 and 3 who were light drinkers. The incompatible control/display relation caused many errors in early practice, particularly on improbable steps, but after run 3, the effects of the lowest alcohol dosage outweighed the effects of further practice. The results support the hypothesis that alcohol has particularly adverse effects when events are improbable and when the skill is recently acquired. Apparently, habituation applies mainly to long established skills and probable events.

Tests of reaction time, walking a straight line, touching the nose etc., are extremely crude and insensitive compared with the present test, and disputes on the validity of earlier behavioral measures (ref. 13) are now redundant.

In agreement with reference 4 no threshold was found below which alcohol had no adverse effects.

ANTICIPATORY MOVEMENTS.—During the 1-second period of target absence, many anticipatory movements of eyes and display cursor travelled inward toward position 3 from other positions; their frequency varied greatly between subjects. Anticipatory manual movements predisposed the subjects to error in improbable steps where the target moved outward from position 3. Subjects with high manual anticipation made frequent errors, in a previous study (ref. 1) and in the present test. In contrast, anticipatory eye movements did not produce a bias for cursor movements in the same direction, and they were usually beneficial in maximizing acuity and minimizing the movement needed to acquire a new target. Predictions of a subject's errors could therefore be based on anticipatory movement of the hand but not of the eyes.

Figure 2 shows that on day 2 increase of the dosage of subject 1 was accompanied by an increase in visual anticipation and manual errors together with a decrease in response latency. The subject also made frequent manual anticipatory movements. Subject 4 adopted an opposite strategy on day 3 by reducing visual anticipation and increasing response latency with a negligible increase in errors. Apparently, subject 4 relied upon good peripheral vision and rapid responses rather than visual anticipation to minimize the number of missed targets and manual errors. He made few movements of anticipation with the eye and virtually none with the hand. The performance of subjects 1 and 4 represent opposite extremes in the strategies adopted under increasing alcohol stress. Subject 1 became more dependent on probabilities and expectancies than real events, and his actions were based on diminishing periods of sampling. In contrast, subject 4 materially reduced anticipatory behavior, became increasingly dependent on real events, and increased his sampling period. Figure 3 shows that, with increasing dosage, subject 10 increased visual anticipation but also increased response latency to minimize errors. Subject 9 produced an interesting variant in behavior. He showed truly remarkable consistency in the last 10 runs that were analyzed (including all the dosages tested) in making anticipatory eye movements of identical total extent.

The large individual differences in anticipatory activity under alcohol stress probably reflect the use of different strategies by subjects of different temperaments. The differences bring into question the widely quoted view that alcohol is a depressant or inhibitor of activity and the consequent implication that the effect on individual subjects will be uniform. This "explanation" would apply directly to those (e.g., subjects 4 and 12) whose visual anticipation diminished with increased dosage. The opposite effect appeared, however, in subjects 1 and 11. To account for this finding, the inhibition hypothesis requires the ad hoc assumption that in special cases, alcohol inhibits the neural centers that normally inhibit activity. This type of argument may be extended, ad nauseum, to the nth generation of inhibitory pseudo-mechanisms, but it cannot account for the varied effects of alcohol on different individuals.

**SPEED VERSUS ACCURACY.**—While measures of latency have little value in studies of stress when considered alone, they can be combined with directional errors to reveal differences in temperament and in individual preferences for accuracy and speed. A tendency to prefer speed to accuracy is a well-known personal characteristic that has been studied extensively as a part of so-called risk-taking behavior. A concise review of the literature is available (ref. 14). The correlation of risk-taking behavior with accidents has been studied (refs. 15 and 16). Speed or accuracy preference appears quite consistently in the same subject in different tasks (refs. 17 and 18). It is important to test the possibility that the present method can predict the risk-taking behavior of subjects under stress in practical situations (e.g., driving and flying).

The interaction of speed and accuracy appears clearly in the results of subjects 9 and 10 (fig. 3) who had virtually equal scores in nondrinking runs on day 4 and in the simple reaction test and presumably had similar basic ability. The latter apparently chose to increase his reaction latencies in order to minimize errors while drinking; the former chose a different strategy and reacted more rapidly but made more errors than subject 10. Figure 2 shows the consistent trend of subject 5 over the 4 days of practice, in reducing reaction latencies and increasing errors on nondrinking runs. This subject actually learned to make more errors in order to save a little time—a common characteristic of poor performers in many different skills. This observation, and the change in the strategy of subject 1 between days 2 and 3, suggests that the preference of speed over accuracy can be modified by experience.

**ERRORS OF DECISION AND PRECISION.**—An error of direction is an error of decision which could have catastrophic effects in driving and flying. A slight increase in reaction latency is of comparatively minor importance. Error of undershoot and overshoot (precision) in tracking has often been used as a criterion of alcohol effects (refs. 2 to 4) but error of decision may be a more important criterion of ability and impairment in many practical skills.

The use of error of decision as the major criterion permits ranking of the subjects. Five subjects (2, 3, 4, 9, and 10) limited their errors to about 5 percent at their highest dosage level. A second group of five subjects (6, 7, 8, 11, and 12) had lower ability, with about 10 percent of errors per run at their highest dosage. Both groups limited their errors on drinking runs by increasing reaction latency as required. In contrast subjects 1 and 5 had about 10 errors on nondrinking runs on days 2 and 3, respectively, but unlike the other subjects, they tolerated a large increase in error frequency after drinking. With breathalyzer readings ranging from 0.1 percent to 0.13 percent, subjects 2, 4, and 10 made fewer errors than most other subjects at the zero breathalyzer level. Subject 5 made more errors on nondrinking runs on day 4 than most other subjects at the highest dosage tested. Comparisons of the subjects' scores (e.g., subjects 4 and 5) show that differences in individual ability had a

far greater effect on errors than the consumption of alcohol to the highest level that was tested. This confirms findings reported in references 3 and 4 where individual differences also far exceeded the changes produced by the dosages that were tested.

**PRACTICAL IMPLICATIONS.**—There is an urgent need for a good test of the impairment of skill caused by either the direct effects or the aftereffects of alcohol consumption. Habitual drinkers should not have an undue advantage and extensive practice should not reduce the discriminatory power of the test. The present test meets these requirements, and it may therefore be a useful supplement to breathalyzer tests. The latter cannot recognize the large differences in the effect of the same alcohol dosage in different individuals, nor detect the after-effects of heavy drinking, which caused serious deterioration in the performance of some subjects in group A.

There can be no doubt that many accidents occur because of a preference for speed rather than accuracy, or because an improbable contingency is confused with an impossible event, for example, at road or rail crossings that are normally deserted.

It is better to avoid accidents by effective selection techniques than to punish the person at fault after an accident has occurred. The data suggest that a major cause of accidents is a failure to eliminate persons with marginal ability from potentially dangerous activities. In such cases, minor stress from alcohol, lack of sleep, frustration, improbable events, etc., may be sufficient to cause an accident. In view of the disproportionate importance of individual differences and those produced by moderate stress, the most effective application of new measures or instruments probably lies in the field of selection.

## REFERENCES

1. Gibbs, C. B.: Probability Learning in Step-Input Tracking. *Brit. J. Psychol.*, vol. 56, nos. 2 and 3, 1965, pp. 233-242.
2. Bjerver, E. K.; and Goldberg, L.: Effect of Alcohol Ingestion on Driving Ability; Results of Practical Road Tests and Laboratory Experiments. *Quart. J. Stud. Alc.*, vol. 11, 1950, pp. 1-30.
3. Coldwell, B. B., ed.: Report on Impaired Driving Tests. Edmond Cloutier, Queens's Printer (Ottawa), 1957.
4. Drew, G. C.; Colquhoun, W. P.; and Long, H. A.: Effect of Small Doses of Alcohol on a Task Resembling Driving. *Med. Res. Council (G. Britain) Memo. No. 38*, H. M. Stationery Office (London), 1959.
5. Mellanby, E.: Alcohol—Its Absorption Into and Disappearance From the Blood Under Different Conditions. *Spec. Rep. Ser. Med. Res. Council*, no. 31, H. M. Stationery Office (London), 1919.
6. Miles, W. R.: Alcohol and Human Efficiency. *Carnegie Inst. No. 333*, 1924.
7. Schmidt, M.: Alcohol Studies II—Concentration of Alcohol in the Blood. *J. Industr. Hyg.*, vol. 16, 1934, pp. 355-365.

8. Eggleton, M. G.: The Effect of Alcohol on the Central Nervous System. *Brit. J. Psychol.*, vol. 32, 1941, pp. 52-61.
9. Goldberg, L.: Tolerance to Alcohol in Moderate and Heavy Drinkers and Its Significance to Alcohol and Traffic. *Proc. First Intl. Conf. Alcohol and Road Traffic*, Kugelberg, Stockholm, 1951, pp. 85-106.
10. Jetter, W. W.: Studies in Alcohol—I. The Diagnosis of Acute Alcohol Intoxication by a Correlation of Clinical and Chemical Findings. *Amer. J. Med. Sci.*, vol. 196, 1938, pp. 475-487.
11. Goldberg, L.: Quantitative Studies on Alcohol Tolerance in Man. The Influence of Ethyl Alcohol on Sensory, Motor and Psychological Functions, Referred to Blood Alcohol in Normal and Habituated Individuals. *Acta Physiol. Scand.*, vol. 5, Suppl. 16, 1943, pp. 1-128.
12. Newman, H. W.: Some Factors Affecting the Rate of Metabolism of Ethyl Alcohol. *Quart. J. Stud. Alc.*, vol. 8, 1947, pp. 377-383.
13. Jellinek, E. M.; and McFarland, R. A.: Analysis of Psychological Experiments on the Effects of Alcohol. *Quart. J. Stud. Alc.*, vol. 1, 1940, pp. 272-371.
14. Slovic, P.: Assessment of Risk Taking Behaviour. *Psychol. Bull.*, vol. 3, no. 61, 1964, pp. 220-233.
15. Dunlop, J. M.; Orlansky, J.; et al.: An Analysis of Risk and Exposure to Automobile Accidents. Report Dunlop and Associates, Contract DA 49-007-MD-239, Office of the Surgeon General Dept. of the Army, 1953.
16. Suchman, E. A.; and Schetzer, A. L.: Current Research in Childhood Accidents. Association for the Aid of Crippled Children, 1960.
17. Johnson, L. C.: Speed and Confidence of Judgment as Psychological Variables. Report Stanford Univ. Dept. of Psychol., Contract Nonr. 225-01, Office of Naval Research, 1954.
18. Block, J.; and Peterson, P.: Some Personality Correlates of Confidence, Caution and Speed in a Decision Situation. *J. Abnorm. Soc. Psychol.*, vol. 51, 1955, pp. 34-41.

N67-15870

## 19. AN EVALUATION OF THREE TYPES OF HAND CONTROLLERS UNDER RANDOM VERTICAL VIBRATION

A.Z. Weisz, R.W. Allen, and C.J. Goddard  
Hughes Aircraft Company

Man-machine interface design in a manual control system can have significant effect on the performance of a demanding task. For continuous control tasks, interface configuration is critical in the face of high-frequency, random forcing functions which require rapid decision making and response output, and when other factors (e.g., environmental conditions, side tasks) increase the task loading of the human operator. The present study investigates the effect of hand-control design on continuous manual control performance in a vibration environment.

Conventional hand-control designs range from freely moving types that offer no appreciable resistance to movement to rigid controllers that displace very little under large forces and whose output is directly related to applied force. Gibbs and Baker (ref. 1) have shown a force stick to yield better performance on a random-appearing manual tracking task than a free-moving control. Briggs et al. (ref. 2) suggest that the superiority of force-type sticks in continuous positioning control is due to the greater accuracy of force proprioceptive feedback. On the basis of theoretical analyses Knoop (ref. 3) has concluded that a force stick is superior to a viscously damped position stick in terms of (1) speed of response, (2) lack of coupling between channels in a two-dimensional task, (3) linearity of stick response, (4) resistance to environmental noise (vibration), and (5) minimum energy required for actuation. In a subsequent simulation Knoop (ref. 4) found a force stick to yield better performance than viscously damped position controls in the simulated task of tracking an aircraft at high angular rates.

### EXPERIMENTS

The present experiment was conceived to determine degradations in manual tracking performance due to whole-body vertical vibration for different controller designs. Also of interest were measures of operator-controller response for the controller designs to be obtained through correlation and transfer-function analyses.

The controllers compared in this study consisted of (1) a standard free-moving hand control (fig. 1) with no spring centering and negligible friction or viscous damping, (2) a viscously damped low-inertia pencil stick (fig. 2) with no spring centering, and (3) a torque stick (fig. 3) with negligible motion response to applied torques about the center of the hand grip. The gain of the displacement controllers was set at 0.14-in./sec steady-state display deflection per degree of hand-control deflection. The gain of the torque stick was set at 0.75-in./sec steady-state display deflection per pound-inch of applied torque about the centroid of the hand grip.

The manual control problem was a continuous, two-dimensional, compensatory tracking task with a random-appearing input. Error was presented to the subject on an oscilloscope

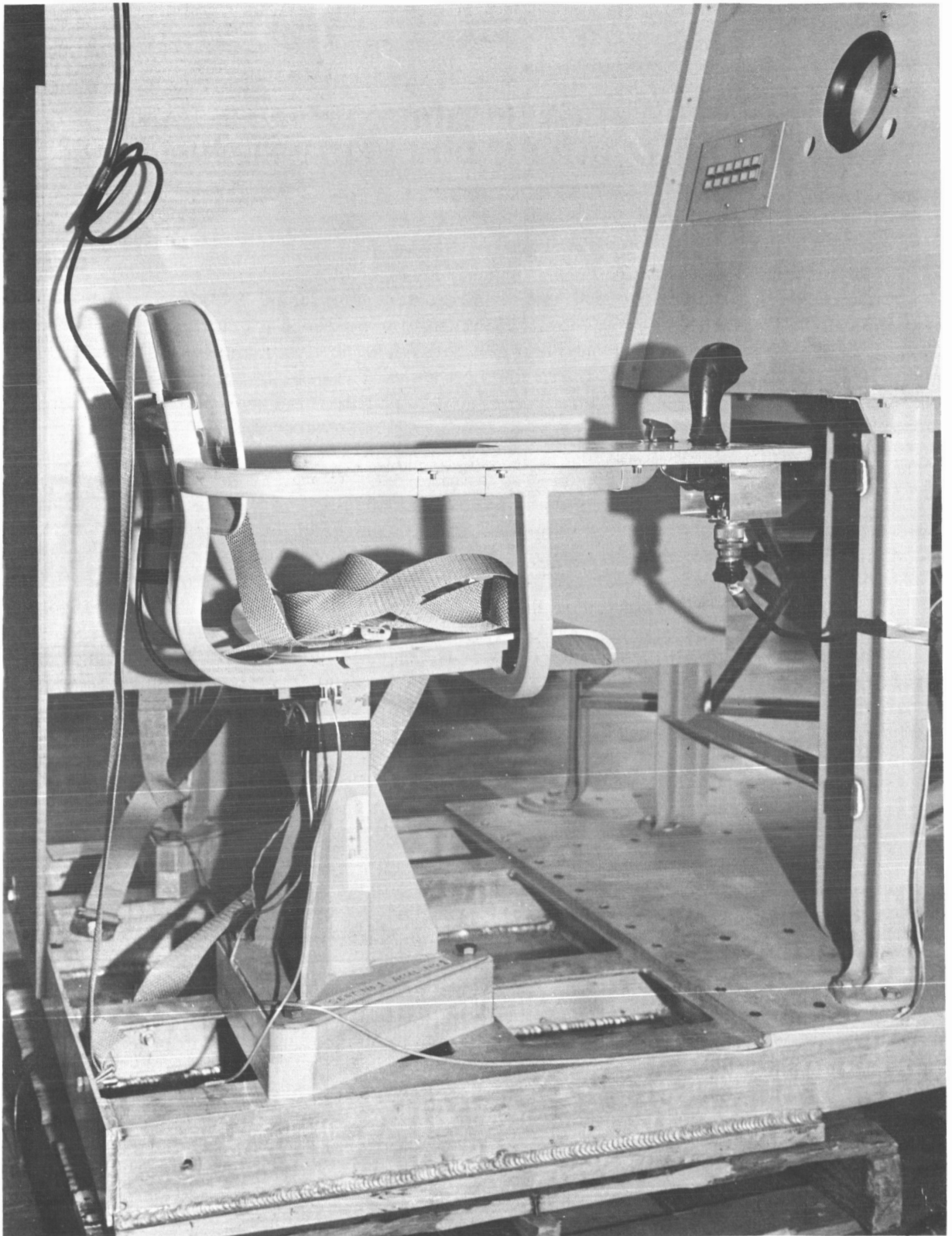


Figure 1.—Station of dual vibration apparatus.



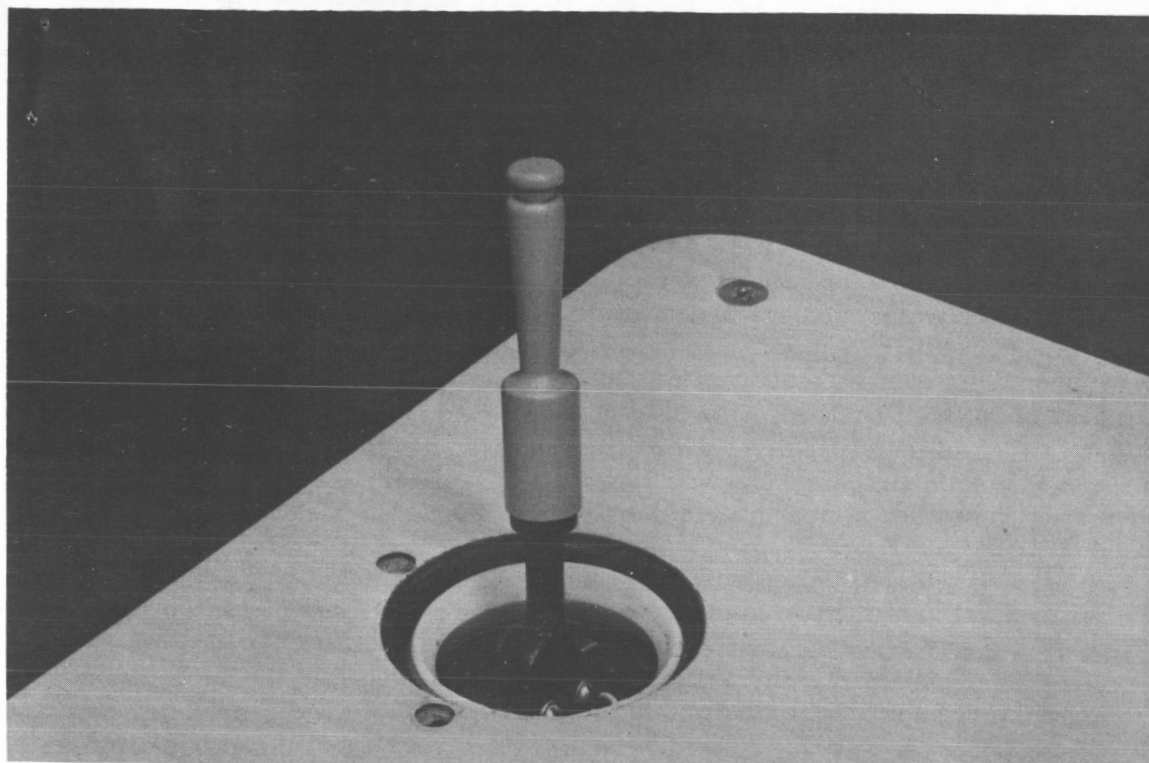


Figure 2.—Pencil controller.

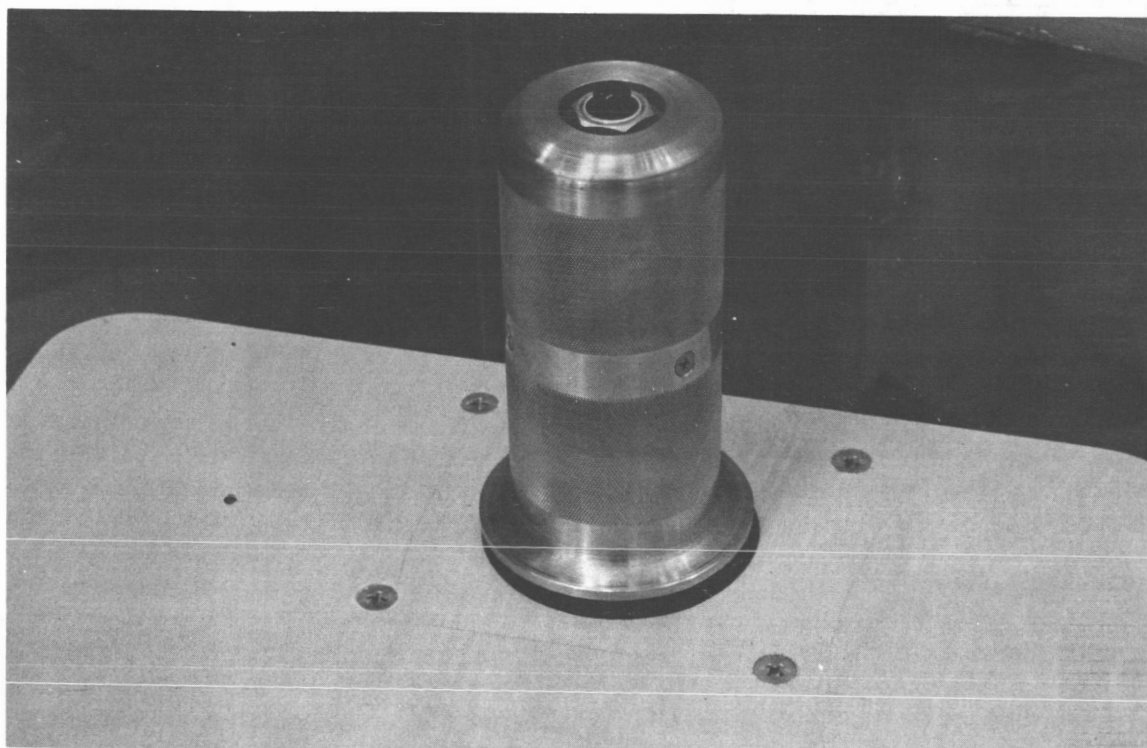


Figure 3.—Torque controller.

as the difference in position between an error dot and the center of a 1/8-inch reference circle which remained fixed in the center of the cathode ray tube (CRT). The dynamics consisted of pure integration in the horizontal (X) dimension and pure integration plus a second-order filter ( $\omega_n = 1.1$  Hz (cps),  $\xi = 0.7$ ) in the vertical (Y) dimension.

The forcing function in each dimension of the tracking task was composed of the sum of 30 sine waves. About 95 percent of the power in the forcing function was contained in 15 sine waves equally spaced in frequency between 0.012 Hz and 0.12 Hz. A high frequency shelf containing 15 equally spaced sine waves between 0.12 Hz and 1.2 Hz containing the remaining power was included to give good transfer-function measurement at higher frequencies. The relative amplitudes of the 15 sine waves in either group were originally set equal, with the total power of the shelf being set at 10 percent of the main function. The sum of the shelf and main function had to be attenuated, however, with a second order filter ( $\omega_n = 0.62$  Hz,  $\xi = 1.2$ ) in order to set the difficulty of the task at a reasonable level. The displayed magnitude of the forcing function was set at an average absolute value of 0.3 inch in each dimension of the task.

Two types of vibration signals were used: One was a 5-Hz signal with random amplitude; the other was random noise between 4 Hz and 12 Hz. In addition, a nonvibration control condition was employed. The acceleration level for the two vibration conditions was 0.248 rms g, equivalent to 35 percent of the 1-minute human tolerance level for 5-Hz sinusoidal vibration.

Two subjects were tested simultaneously on a dual vibration fixture mounted on the shaker head of a Ling L249 electrodynamic test facility. Subjects were seated on unpadded tablet-arm school chairs shown in figure 1. The hand controls were mounted on the tablet arm. The CRT displays were positioned directly before the subjects at a viewing distance of approximately 30 inches.

Six engineers, all with previous tracking experience, served as subjects for the experiment. Each received approximately 1 hour of practice on each hand controller under nonvibration conditions. During the practice sessions, subjects were informed of their horizontal and vertical error scores following each trial.

**EXPERIMENTAL DESIGN.**—The three hand controllers were each tested under the control and the two vibration conditions, resulting in a total of nine treatment combinations. Subjects received all three vibration conditions during each of three experimental sessions, with each subject using a different hand controller for each session. The order of presentation of the vibration conditions was balanced among pairs of subjects, with the same order retained throughout the study. The order of presentation of hand controllers was balanced among subjects with two subjects (in different pairs) assigned to the same controller for each experimental session.

**EXPERIMENTAL PROCEDURE.**—The subjects were instructed to keep the error dot in the center of the reference circle as much of the time as possible. To insure standardized posture and seat position, seat belts and harnesses were employed.

Prior to a testing period the subjects were given a 2-minute practice exposure to each of the vibration conditions using the appropriate hand controller for the session. During this practice, an acceleration level of 0.177 rms g was used for the two vibration conditions.

Each experimental trial lasted 6 minutes with a scoring period of 4.5 minutes. The scoring period commenced 30 seconds after the trial began and ended 1 minute before the end of the trial. In an effort to reduce fatigue effects, a 5-minute rest was given between trials. Information regarding performance measures was discontinued during the experimental session.

**DATA ANALYSIS.**—The experiment was treated as a  $6 \times 3 \times 3$  balanced, factorial design with one observation per cell. Subjects, hand controllers, and vibration conditions were the experimental variables.

Integrated absolute errors for the horizontal and vertical dimensions of the tracking task were used as performance measures for statistical analyses. Separate analyses of variance were performed on the horizontal and vertical error scores. The techniques suggested by Winer (ref. 5) were utilized, with subjects and vibration conditions treated as random factors and hand controllers treated as a fixed factor. When necessary, quasi-F ratios of the F form (ref. 6) were employed.

Time records of the error input to the subject and the hand-control output were tape recorded and digitized for use in cross covariance and linear-gain and phase-frequency response analyses. Thirty-second segments of the records were digitized at a rate of 10 samples per second. The actual calculations were performed using a computer program developed at the Health Sciences Computing Facility, UCLA (ref. 7). The program computes auto- and cross-covariance functions and, through Fourier transformation, calculates the corresponding linear transfer function.

## RESULTS

The results of the analyses of variance carried out on the tracking error scores are summarized in table 1. Of primary interest are the significant variations in performance due to hand controllers for both horizontal and vertical dimensions. The only additional significant effects are those for differences in horizontal tracking performance among subjects, and an indication of differential horizontal performance with the various controllers among subjects (subjects by hand-controller interaction).

Inspection of figures 4 and 5, in which results are plotted for each controller-vibration condition combination, indicates that the torque controller gave rise to superior performance under both static and vibration test conditions.

The Duncan new multiple range test was used to evaluate the statistical significance of these differences. These results, presented in table 2, demonstrate that performance with the torque stick was significantly better than that for the pencil and standard controller in all instances except the horizontal-error comparison with the pencil stick under vibration of 4 to 12 Hz. Thus, no differences were found between the pencil and standard controllers, and the torque stick was significantly better in 11 of the 12 cases tested.

The same data are plotted in figures 6 and 7 in terms of an efficiency index expressing mean tracking performance as the proportion of the forcing-function error dot motion removed by the subject. Using tracking efficiency as a performance measure, the results indicate that the use of the torque stick enabled subjects to remove 4 to 8 percent more error in the horizontal dimension and 10 to 17 percent more error in vertical dimension than with the other two manual controllers.

TABLE 1.—ANALYSIS OF VARIANCE SUMMARIES FOR HORIZONTAL AND VERTICAL TRACKING ERROR  
[n = 1]

Source of variation	df	Horizontal error		Vertical error	
		MS	F	MS	F
Subjects - A	5	1.619	<sup>a</sup> 3.67	1.374	0.75
Hand controllers - B	2	6.929	<sup>a</sup> 5.50	28.173	<sup>b</sup> 13.38
Vibration conditions - C	2	.023	.05	5.728	3.15
AB	10	1.179	<sup>a</sup> 2.56	1.728	1.58
AC	10	.441	.96	1.821	1.67
BC	4	.164	.36	.459	.42
Residual error	20	.461		1.092	

<sup>a</sup>Significant at the 0.05 level

<sup>b</sup>Significant at the 0.01 level

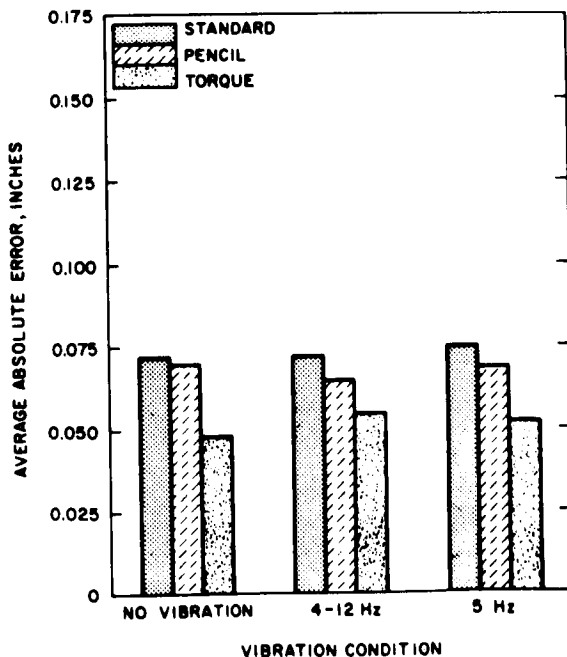


Figure 4.—Horizontal tracking error scores as a function of vibration condition and hand controller.

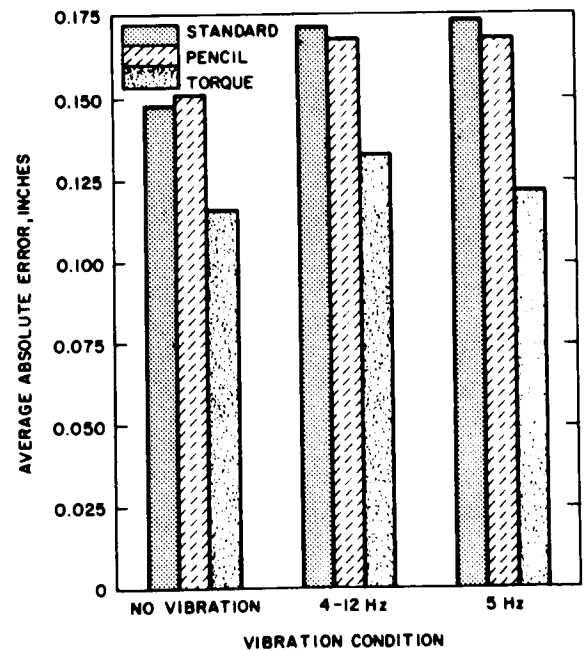


Figure 5.—Vertical tracking error scores as a function of vibration condition and hand controller.

These tracking efficiency measures show that the superiority of the torque stick was most pronounced in vertical performance, which is the more difficult dimension of the tracking task because of the second order lag employed.

\*TABLE 2.—AVERAGE ABSOLUTE TRACKING ERROR IN INCHES FOR THE HAND CONTROLLER AND VIBRATION CONDITION INTERACTION

[Values not underlined by the same line differ significantly ( $p < 0.05$ ) as determined by the Duncan multiple range test]

	Horizontal error			Vertical error		
	Torque	Pencil	Standard	Torque	Pencil	Standard
Nonvibration	0.048	<u>0.071</u>	<u>0.073</u>	0.117	<u>0.152</u>	<u>0.148</u>
5-Hz random amplitude	.052	<u>.069</u>	<u>.075</u>	.122	<u>.169</u>	<u>.173</u>
4- to 12-Hz random amplitude	<u>.055</u>	<u>.065</u>	<u>.073</u>	.134	<u>.169</u>	<u>.173</u>

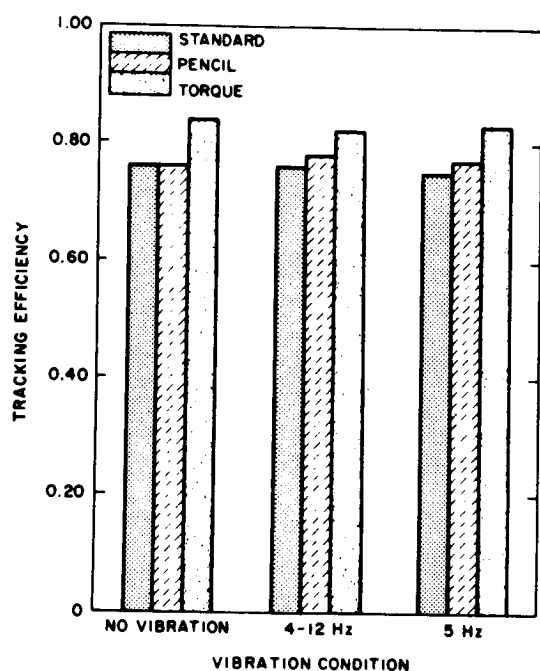


Figure 6.—Horizontal tracking efficiency as a function of vibration condition and hand controller.

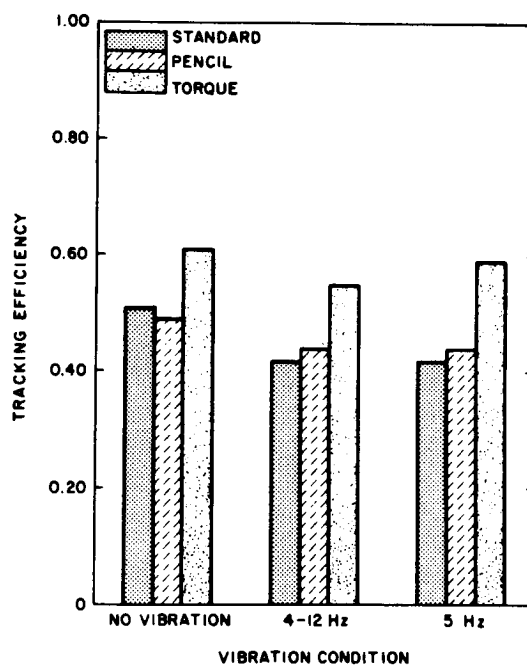


Figure 7.—Vertical tracking efficiency as a function of vibration condition and hand controller.

Further analyses were undertaken to investigate the bases for the superior performance found with the torque controller under static and vibration conditions. Normalized cross-covariance functions  $\rho(\tau)$  between error input and hand controller output for one subject's data are shown in figures 8 and 9. The peak of the curve for the torque controller has about 0.1 second less lag than the pencil stick controller, indicating that the superiority of the torque stick is due to the quicker response it allows. The same conclusion is reached from the transfer-function curves plotted in figures 10 and 11. The phase lag of the subject's response with the torque controller is generally less than that yielded with the pencil stick. In addition, the gain afforded by the torque stick for frequencies above 1 Hz is significantly greater than that with the pencil controller.

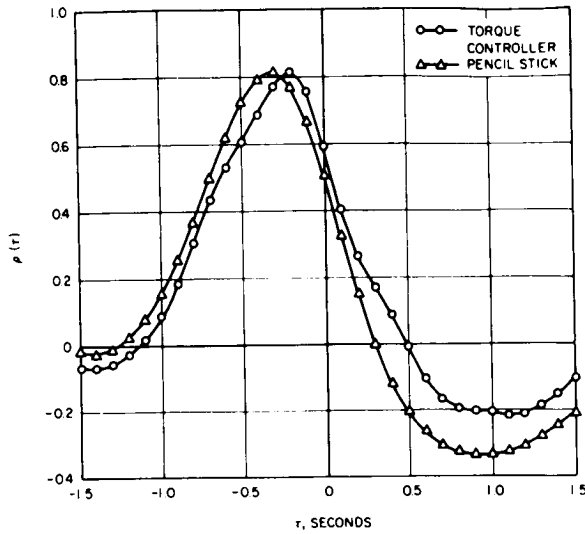


Figure 8.—Normalized cross-covariance function between error and controller output in the horizontal dimension.

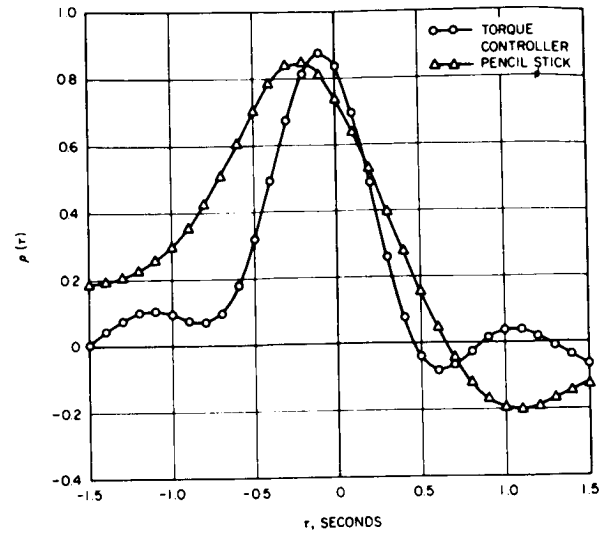


Figure 9.—Normalized cross-covariance function between error and controller output in the vertical dimension.

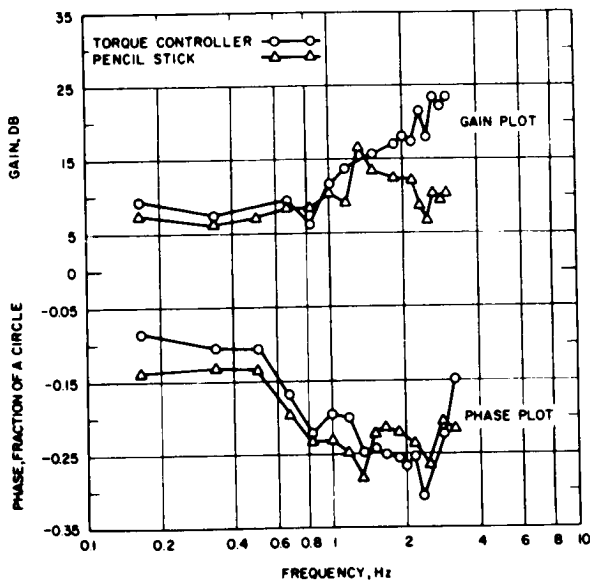


Figure 10.—Linear gain and phase relationships between error function and controller output for the horizontal dimension.

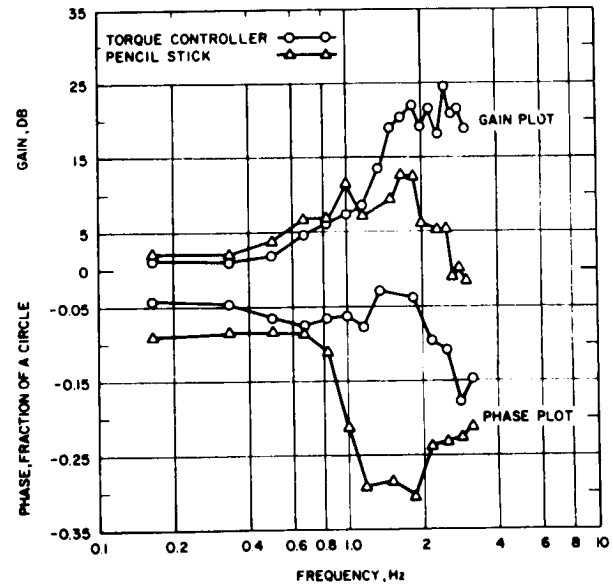


Figure 11.—Linear gain and phase relationships between error function and controller output for the vertical dimension.

The effects of cross coupling between hand-control axes was also investigated. These results are illustrated in figure 12, where it can be seen that the cross-covariance between the horizontal error function and vertical response is significantly less for the torque controller at all lag and lead values of interest.

## DISCUSSION

The experimental torque controller tested in this study was designed for use in vibration environments. The principle of construction employed makes it insensitive to translational forces in both dimensions with maximal sensitivity to rotational forces applied about the center of the hand grip. The pairs of strain-gage sensors utilized in this design were not miniaturized, so that the prototype was somewhat difficult to use because of its ungainly size. It can be expected that further development would result in a torque controller yielding improved performance.

The results of this study indicate that the speed of response possible with a rigid controller leads to improved tracking performance in both static and vibration environments. Further tests should be undertaken to determine whether this advantage is found under vibration conditions for other combinations of tracking task and controller dynamics, including zero order (target designation) and rate-aided applications.

## REFERENCES

1. Gibbs, C. B.; and Baker, J. C.: Free-Moving Versus Fixed Control Levers in a Manual Tracking Task. *Automatic and Manual Control*, A. Tustin, ed., Academic Press, 1964.
2. Briggs, G. E.; Fitts, P. M.; and Bahrick, H. P.: Effects of Force and Amplitude Cues on Learning and Performance in a Complex Tracking Task. *J. Exp. Psychol.*, vol. 54, 1957, pp. 262-268.
3. Knoop, D. E.: Preliminary Study of Various Types of Control Sticks for TOW Helicopter. IDC 2147.3/62, Hughes Aircraft Co., Nov. 1964.
4. Knoop, D. E.: A Study of Human Operator in a High Speed Track Loop. IDC 2147.3/80, Hughes Aircraft Co., Jan. 1965.

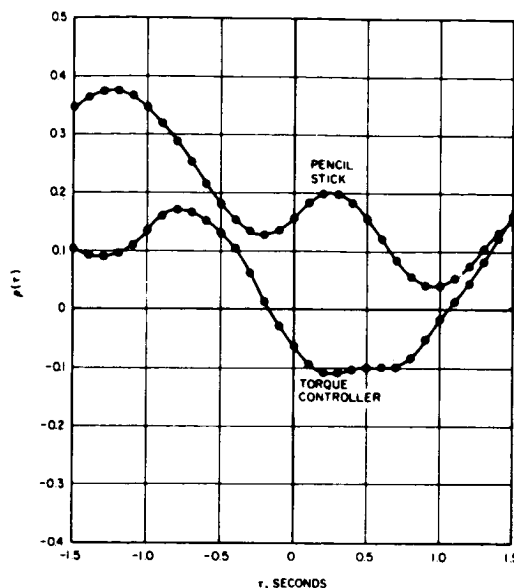


Figure 12.—Normalized cross-covariance function between horizontal error function and vertical dimension controller output.

5. Winer, B. J.: Statistical Principles in Experimental Design. McGraw-Hill Book Co., Inc., 1962.
6. Satterthwaite, F. E.: An Approximate Distribution of Estimates of Variance Components Biometric Bull., vol. 2, 1946, pp. 110-114.
7. Dixon, W. J., ed.: BMD02T, Autocovariance and Power Spectral Analysis. Biomedical Computer Programs, Health Sciences Computing Facility, UCLA, 1964, pp. 459-481.



N67-15871

## 20. HUMAN DESCRIBING FUNCTIONS MEASURED IN FLIGHT AND ON SIMULATORS

*Harriet J. Smith*  
*Flight Research Center, NASA*

Comparisons have been made between human describing functions measured in flight and on the ground using two different types of ground simulation. A T-33 variable-stability airplane was used for the in-flight measurements. The ground tests were conducted in the T-33 airplane on the ground with simulated instrument flight and also on a general-purpose analog computer in conjunction with a contact analog display. For this study a multiple-degree-of-freedom controlled element was used in a single-loop compensatory tracking task. The input disturbance in each case consisted of the sum of 10 sine waves with a cutoff frequency of 1.5 radians per second.

A digital computer was used to analyze the data, which were stored on magnetic tape. The power spectra and cross spectra used to compute the describing functions were determined from Fourier transforms of the time histories. By eliminating the need to store all the data in the computer, as is required when computing autocorrelation functions, it was possible to process considerably more data points per run, thereby increasing the accuracy of the results.

The results of this investigation indicate no significant difference between the average describing functions measured in flight and those measured in a fixed-base simulator. However, the variance was found to be considerably higher in the flight data. The system open-loop describing functions measured in the fixed-base simulator agreed well with the results of an investigation by McRuer in which the tracking task was similar, although the controlled-element dynamics were different. The average linear coherence was also close to the values found in this same investigation. Although contrary to the results of previous investigations, the linear-correlation function  $\rho$  was always equal to 1.

Considerable effort has been devoted to finding a suitable mathematical model of the pilot in man-machine systems. As a part of this effort, several experimental investigations have been made to measure pilot dynamic behavior in single-loop compensatory tracking situations. However, most of the experiments conducted in the past used rather simple controlled-element characteristics in fixed-base simulators. Reference 1 reported the results of an investigation to determine the differences in pilot behavior in flight and in ground-based simulators. A Navion aircraft was used for these tests, which involved simulated air-to-air gunnery tracking. It was found from these experiments that significant differences resulted both in gain and phase in the longitudinal mode and in the phase in the lateral mode.

To study further the effect of flight on pilot behavior, the NASA Flight Research Center, the U.S. Air Force, and Cornell Aeronautical Laboratory are conducting a program to analyze human-response data obtained both in flight and in ground-based simulators, using a realistic airplane-type controlled element. However, it was also considered desirable to tie in these results with some of the previous research in this area. Thus, the design of these experiments was largely influenced by the work of McRuer (ref. 2) and others in this field.

## SYMBOLS

$c$	pilot output time function
$\bar{c}^2$	square of the pilot's mean output
$\overline{c^2}$	mean squared pilot output
$e$	error time function
$F( )$	Fourier transform
$F^*( )$	conjugate of Fourier transform
$i$	input (tracking task) time function
$i^*$	input (control-stick deflection) time function
$j = \sqrt{-1}$	
$K_c$	controlled-element gain
$m$	system output time function
$T$	record length
$Y_c$	controlled-element transfer function
$Y_p$	pilot describing function
$Y_p Y_c$	system open-loop describing function
$\Delta t$	time increment
$\delta_a$	aileron deflection
$\delta_{as}$	control-stick deflection
$\rho$	linear-correlation coefficient
$\rho_a$	average linear coherence coefficient
$\Phi_{cc}$	power-spectral density of pilot output
$\Phi_{ic}$	cross-spectral density between $i$ and $c$
$\Phi_{ie}$	cross-spectral density between $i$ and $e$
$\Phi_{ii}$	power-spectral density of input
$\Phi_{im}$	cross-spectral density between $i$ and $m$
$\varphi$	bank angle
$\omega$	frequency
Subscript:	
auto	autopilot

## DESCRIPTION OF THE PROGRAM

The following three methods of simulation were used to obtain the human-response data:

- (1) Ground based — contact analog display
- (2) Ground based — T-33 variable-stability airplane with conventional IFR cockpit display
- (3) In flight — T-33 variable-stability airplane

The equation used for the controlled-element dynamics was:

$$\frac{\varphi}{\delta_a}(s) = \frac{0.782(s^2 + 0.502s + 5.29)}{\left(s + \frac{1}{270}\right)\left(s + \frac{1}{0.389}\right)(s^2 + 0.474s + 5.29)} \approx \frac{0.782}{s\left(s + \frac{1}{0.389}\right)}$$

As nearly as possible, both the controlled-element dynamics and the tracking task were the same in each case. The tracking task was the sum of 10 sine waves with a frequency range from 0.16 to 14 radians per second, which was the same task as that used in reference 2. The bandwidth chosen for these tests was 1.5 radians per second. Six of the 10 input frequencies were included in this bandwidth, and the amplitude of the remaining four was one-tenth of the low-frequency amplitudes. Run lengths were 4 minutes each, which also conformed to the tests in reference 2.

Figure 1 shows the block diagram for the fixed-base analog simulation. For this method of simulation, a general-purpose analog computer was used in conjunction with a contact analog display. A high-speed digital computer was used to generate the tracking task, which was converted to an analog signal for the simulation. The tracking task as well as the simulator outputs which were converted to a digital format were stored on magnetic tape for later analysis. The quantities that were recorded consisted of the output of the simulated aircraft, the tracking task, and the error — all in terms of bank angle — and the aileron-deflection output of the pilot.

For the T-33 simulations, a T-33 variable-stability airplane was used to simulate the desired aircraft characteristics. A simplified block diagram of the system is shown in figure 2. These tests differed somewhat from the tests in reference 1. As can be seen in

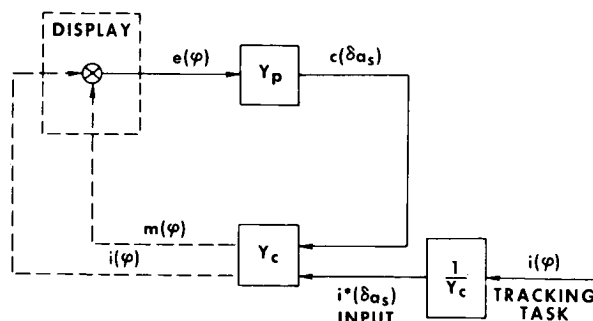
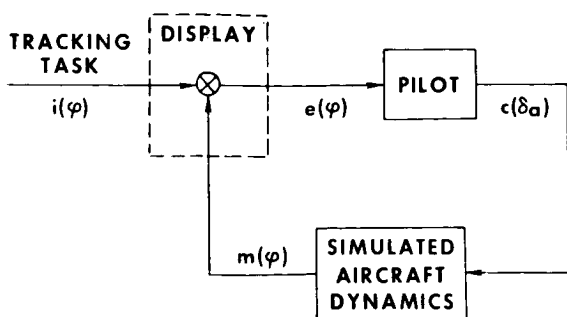


Figure 1.— Fixed-base analog simulation.

Figure 2.— T-33 simulation.

this figure, the input was in the form of a control input, which resulted in disturbing the aircraft. The desired tracking task was obtained by modifying the sum of 10 sine waves by using the inverse transfer function of the simulated airplane. In reference 1, a random noise input was added to the display and the aircraft itself was not disturbed. The pilot's task was to keep the error in the display zero, rather than to keep the aircraft's wings level as in the present tests.

For the ground simulation, the variable-stability system was used to simulate the desired aircraft characteristics the same as it was in flight. The essential difference was that the six-degree-of-freedom equations of motion of the normal T-33 airplane were mechanized on an analog computer and connected to the control-surface actuators to replace the aerodynamic and mass effects of flight. The cockpit canopy was covered, and the only cues available were those displayed on the cockpit instruments. Pitch and roll angles were presented by means of a two-axes ball, and sideslip angle was presented as the horizontal translation of a vertical bar. Other quantities displayed were airspeed and altitude, rate of climb, angle of attack, heading angle, normal acceleration, and yaw rate. All the outputs in both the flight simulation and ground simulation were recorded on FM tape. The pertinent quantities recorded were the input and pilot output in inches of stick deflection and the error in degrees of bank angle. The FM tapes were later converted to a digital format for analysis on a digital computer.

The technique used in analyzing these data was slightly different from that generally used, in that the power spectra and cross spectra used to compute the describing functions and linearity parameters were obtained by taking the Fourier transforms of the time histories directly rather than first computing the autocorrelation functions (see paper 28). The following equations were used:

$$Y_p = \frac{\Phi_{ic}}{\Phi_{ie}} = \frac{F^*(i) F(c)}{F^*(i) F(e)} \quad (1)$$

$$Y_c = \frac{\Phi_{im}}{\Phi_{ic}} = \frac{F^*(i) F(m)}{F^*(i) F(c)} \quad (2)$$

$$\rho = \frac{|\Phi_{ic}|}{\sqrt{|\Phi_{ii}| |\Phi_{cc}|}} \quad (3)$$

$$\rho_a = \sqrt{\frac{\frac{2}{T^2} \sum_{1}^{10} \rho^2 F^*(c) F(c)}{c^2 - \bar{c}^2}} \quad (4)$$

## RESULTS

Some of the results obtained to date from this program are shown in figures 3 to 9. Standard deviations are indicated by the vertical lines. Where none is shown, the deviation was within the size of the symbol. Figure 3 shows the aircraft transfer function that was determined from the experiments on the analog computer. The curve is the actual transfer function used on the computer. This figure is shown only to give an indication of the accuracy that can be expected from the method of analysis used.

Figure 4 shows the pilot describing functions that were obtained from the analog study for each of the three pilots. These are the means of all the runs that were analyzed in each case. Ten runs were analyzed for pilot A, and three runs each for pilots B and C. The only apparent difference in the gains of the three pilots occurred at the higher frequencies where pilot A decreased his gain. At the lower frequencies, all three pilots showed some run-to-run variability, as can be seen from the standard deviations shown; therefore, no significant differences could be noted among the three pilots. Phase angles were also in good agreement throughout the middle frequency range.

Figure 5 shows the open-loop describing functions obtained from the analog study. As expected, the same differences are seen here. The crossover frequency occurs at approximately 2.8 radians per second for all three pilots, and it is noted that, in the region of crossover, the behavior of all three pilots is virtually identical. It was pointed out in reference 2 that the pilot in a compensatory tracking situation adjusts his behavior in such a way that the

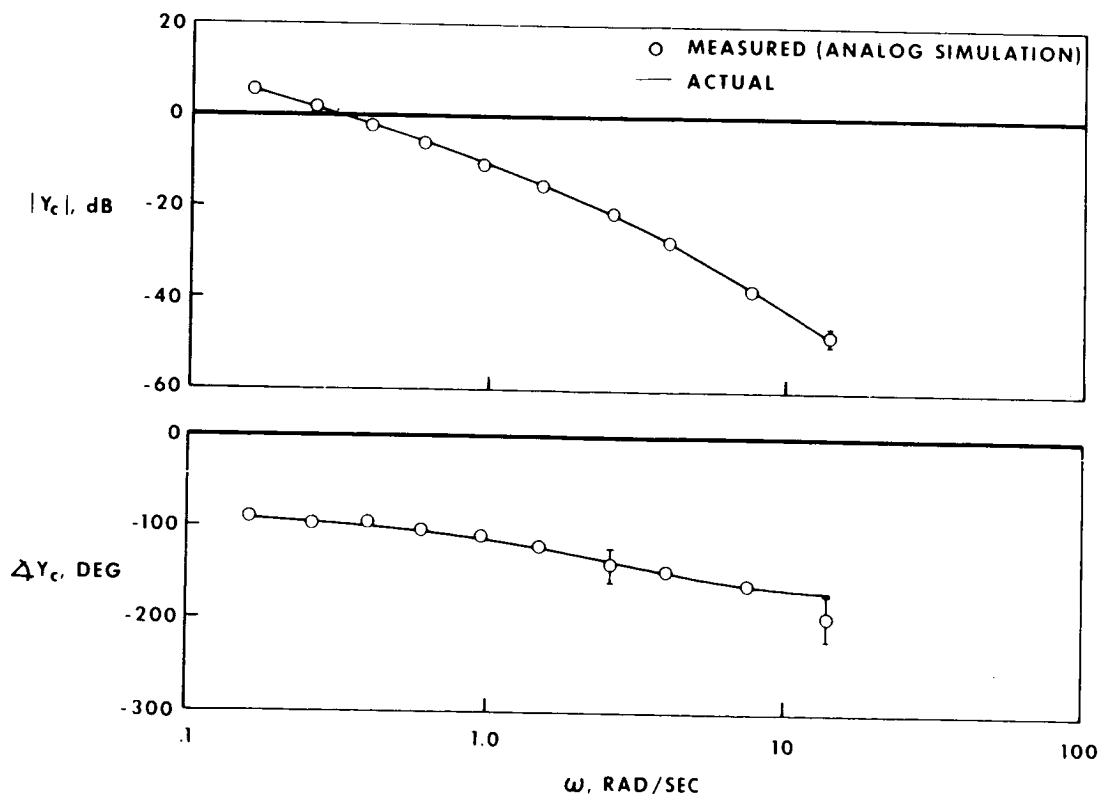


Figure 3.—Controlled element.

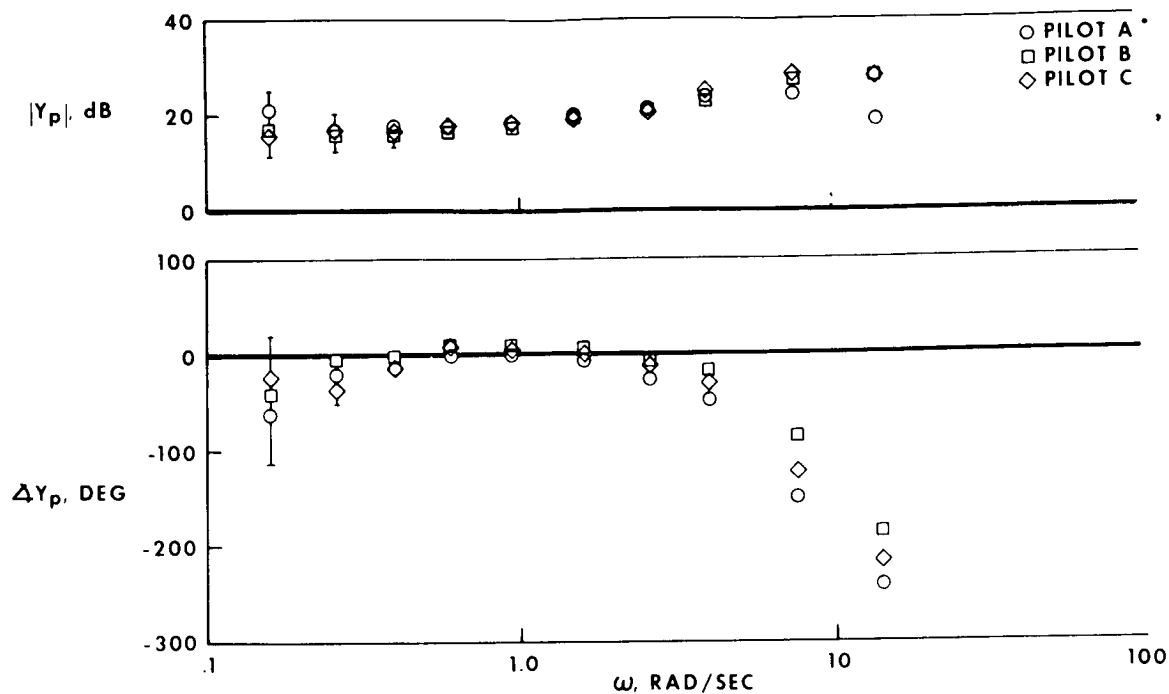


Figure 4. —Pilot-to-pilot variability in human describing functions from analog simulation.

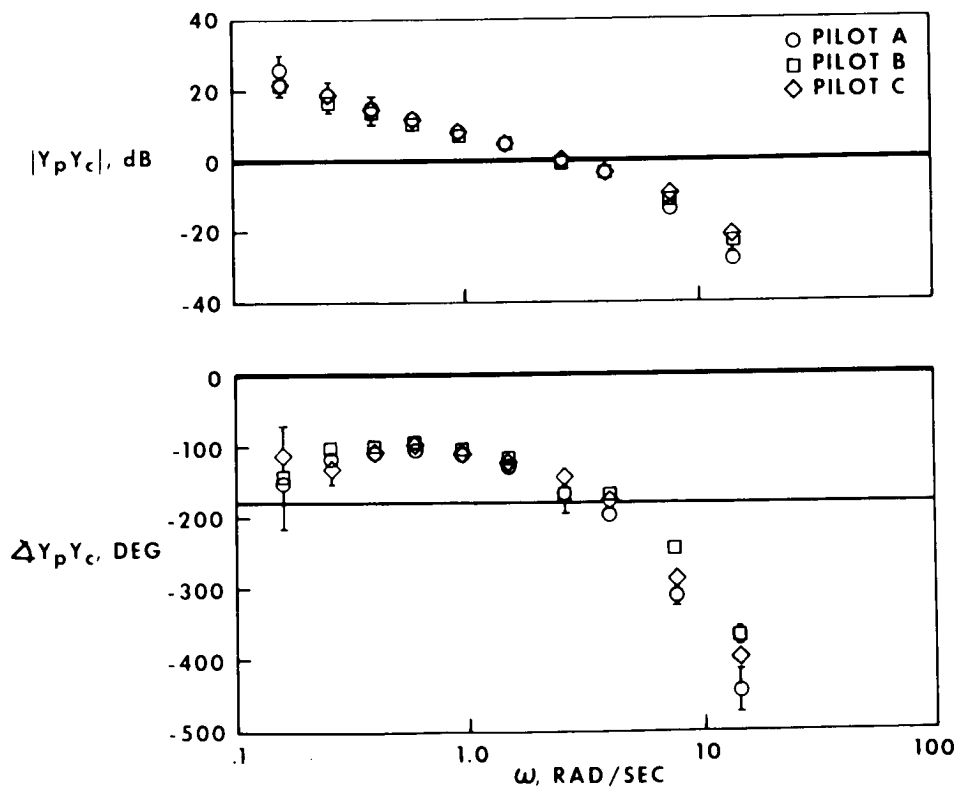


Figure 5. —Pilot-to-pilot variability in open-loop describing functions from analog simulation.

system open-loop characteristics remain essentially the same in the crossover region. It was also noted that the slope of  $|Y_p Y_c|$  at the crossover frequency is usually about 20 dB per decade and the phase angle is between approximately  $-140^\circ$  and  $-180^\circ$ . The data shown here generally agree with this. The phase margins are approximately  $20^\circ$ .

In figure 6, the averaged open-loop describing functions for all three pilots are compared with some of the results of reference 2. Although the controlled-element dynamics are different, it can be seen that the system's open-loop describing functions correlate well, particularly around the crossover frequency. It is encouraging to see that results using simple controlled elements are applicable to actual aircraft transfer functions.

The differences between the pilot describing functions obtained in flight and those obtained in the analog simulation are shown in figure 7. The aircraft transfer functions and therefore the system open-loop describing functions are not available at this time for the tests made on the T-33.

Figure 7(a) shows the comparison between flight and analog for pilot A. Seven flights were analyzed, compared to 10 analog runs. Although the mean data differ somewhat, the only really significant difference appears to be that the run-to-run variability is considerably higher in the flight data, which is evident from the large variances shown. This is particularly true for the phase angles; however, there was general agreement throughout most of the frequency range.

The comparison between flight and analog simulation for pilot B is shown in figure 7(b). This appears to be very similar to the comparison for pilot A except that pilot B appears to be increasing his gain even more at the higher frequencies in flight than in the analog simulations. However, only four flight runs were analyzed and, because of the large variance, it is not certain that this observation is really significant.

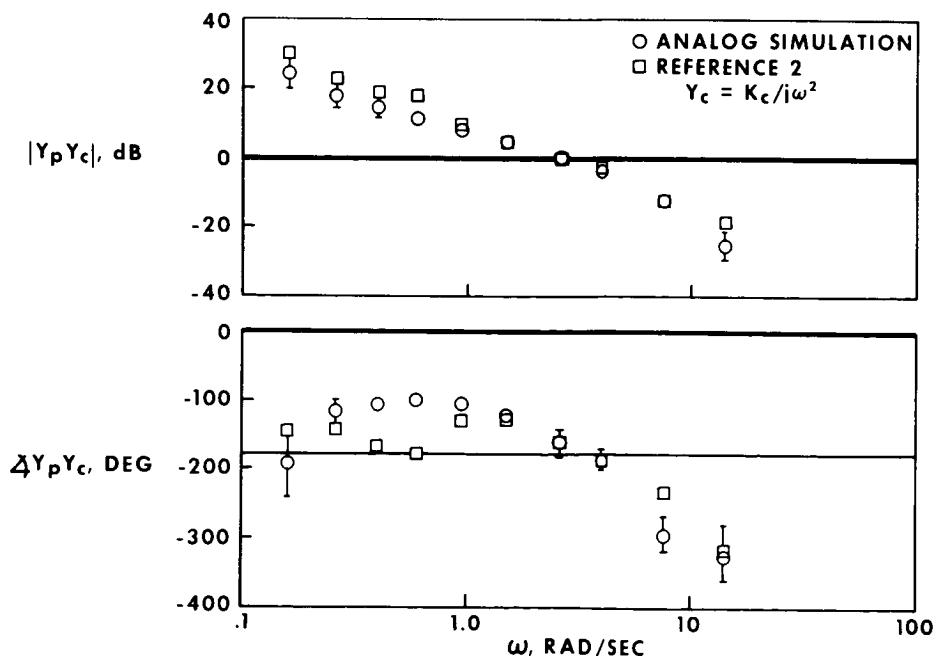
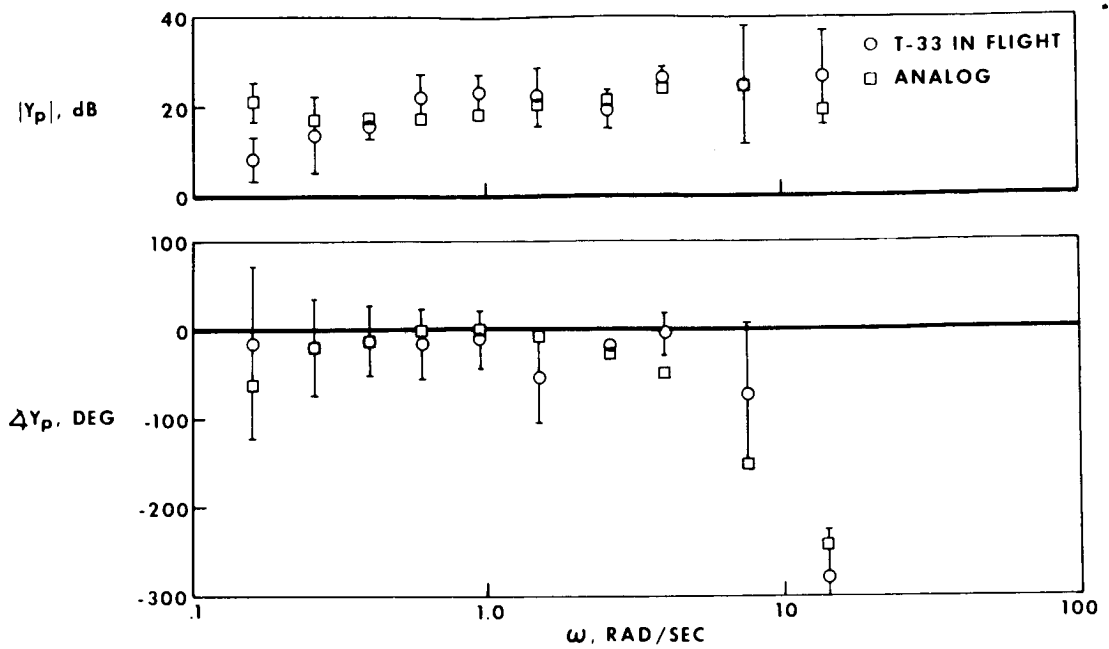
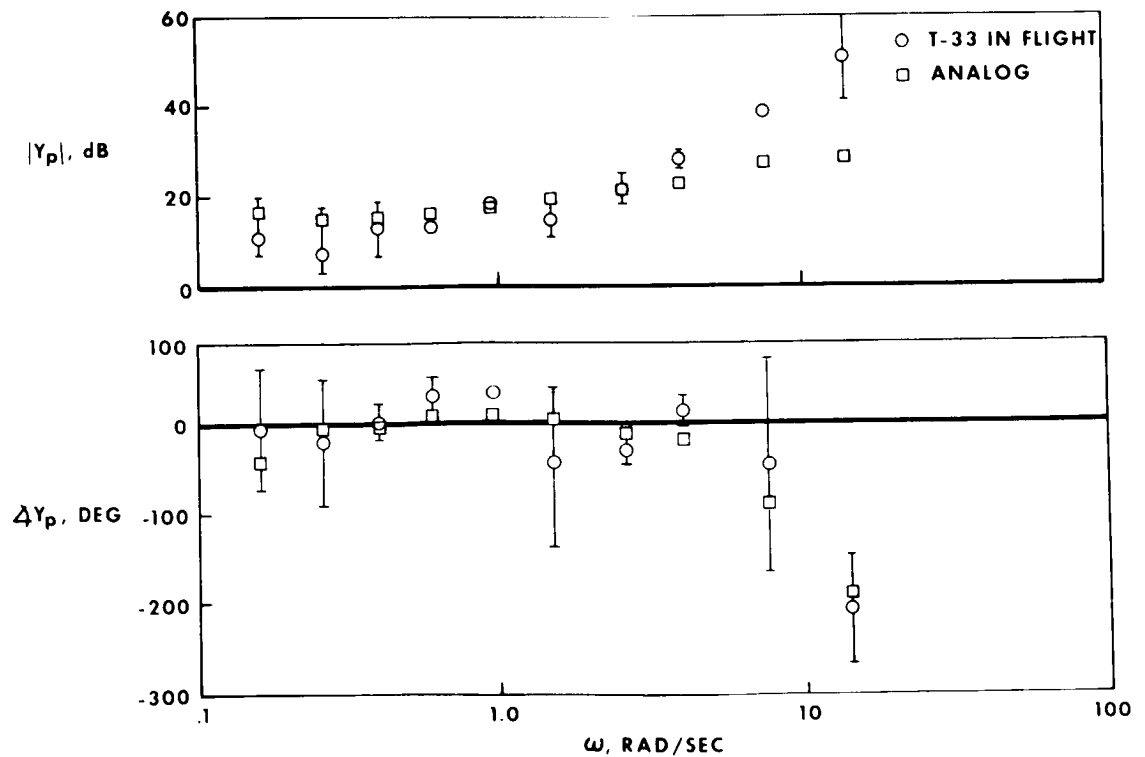


Figure 6. —Averaged open-loop describing functions.



(a) Pilot A

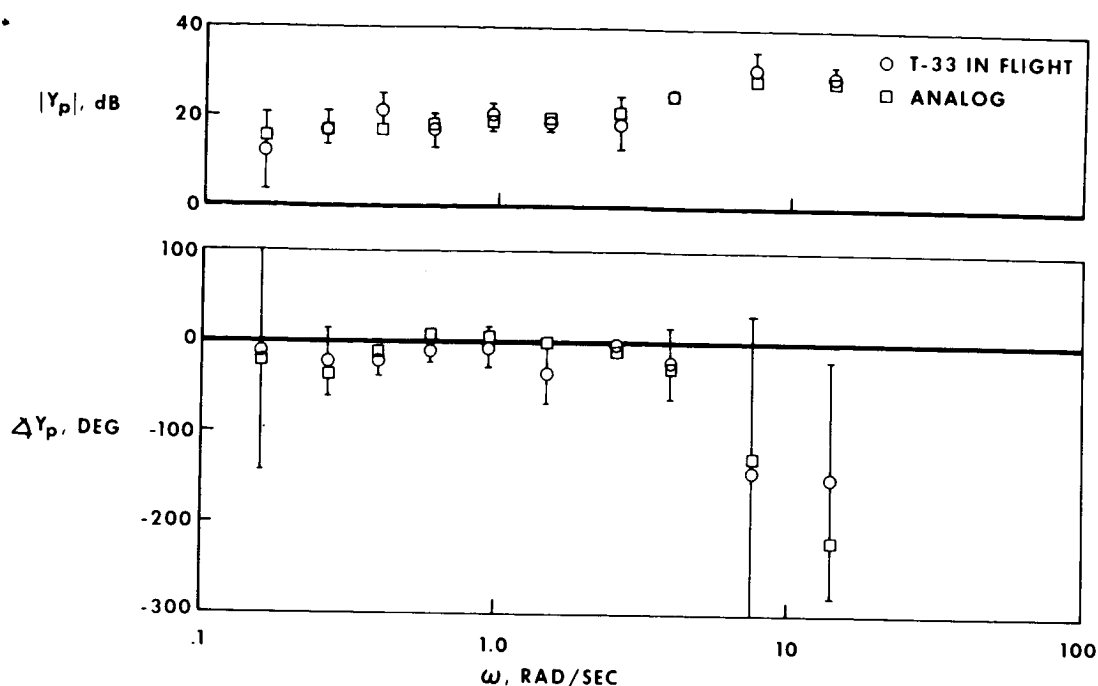
Figure 7. — Comparison of in-flight human describing functions with analog simulation.



(b) Pilot B

Figure 7. — Continued.





(c) Pilot C  
Figure 7. — Concluded.

For pilot C, three flight runs were analyzed; this comparison is shown in figure 7(c). The behavior of pilot C in flight differs very little from that in the fixed-base simulation. Very good agreement is shown for both gain and phase. Although the variances are larger in flight, they appear to be smaller than those of the other two pilots.

Figure 8 shows the comparison between the pilot describing functions obtained from the T-33 ground simulation with those obtained from the analog simulation. The comparison is shown only for pilot A, for whom five runs were analyzed. Here, there appears to be a significant difference in the pilot gain at the lower frequencies, and it is noted that, in this region, there is comparatively little run-to-run variability. Although the gains differed appreciably, the phase angles agreed reasonably well at most frequencies.

Averaged pilot describing functions for all three methods of simulation are shown in figure 9. It can be seen here that there are no significant differences between the flight and the analog data. At the middle frequencies, the data agree well, and at the higher and lower frequencies the variance is large enough to make any differences that occur insignificant. Although the T-33 ground data are for only one pilot, they are shown for comparison with the averaged results from the flight and analog simulations. Here it is seen that the gains are consistently lower at the lower frequencies than those obtained from either of the other two methods of simulation. One T-33 ground run was analyzed for pilot C also and, although not shown, the results indicated the same difference: the gain was appreciably lower at all frequencies. One possible explanation for this difference is the better display in flight and in the contact analog. The attitude ball was somewhat "sticky" and also the error displayed in inches was considerably smaller.

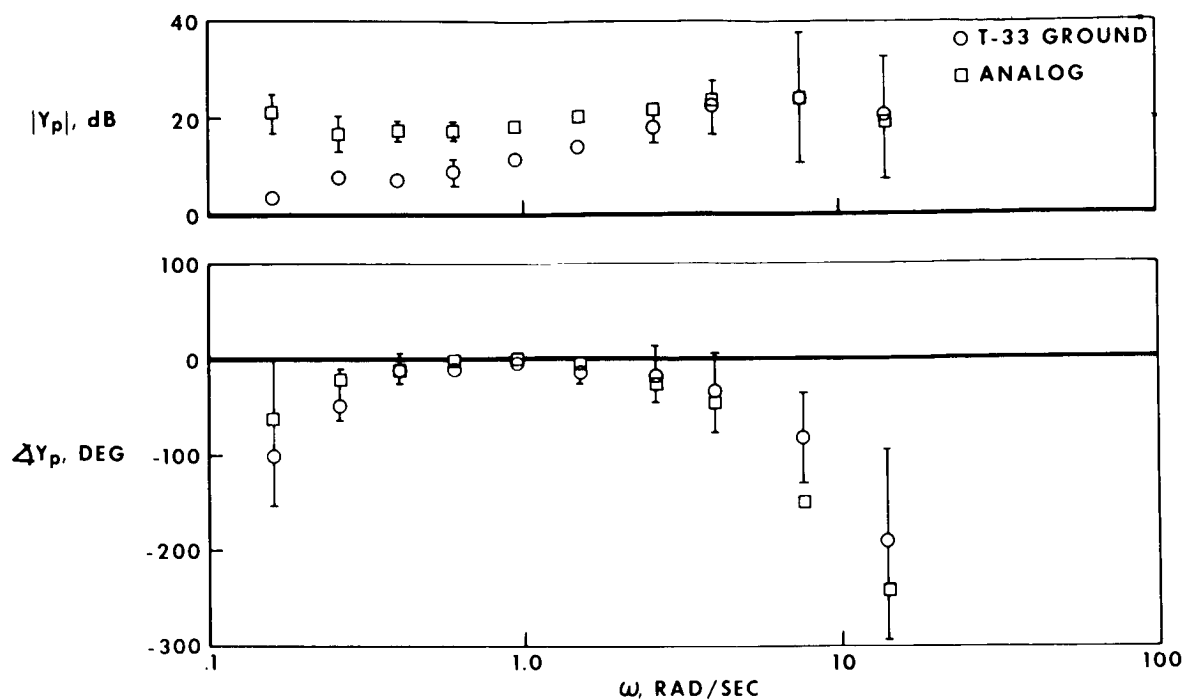


Figure 8.—Comparison of ground-based T-33 human describing functions with analog simulation for pilot A.

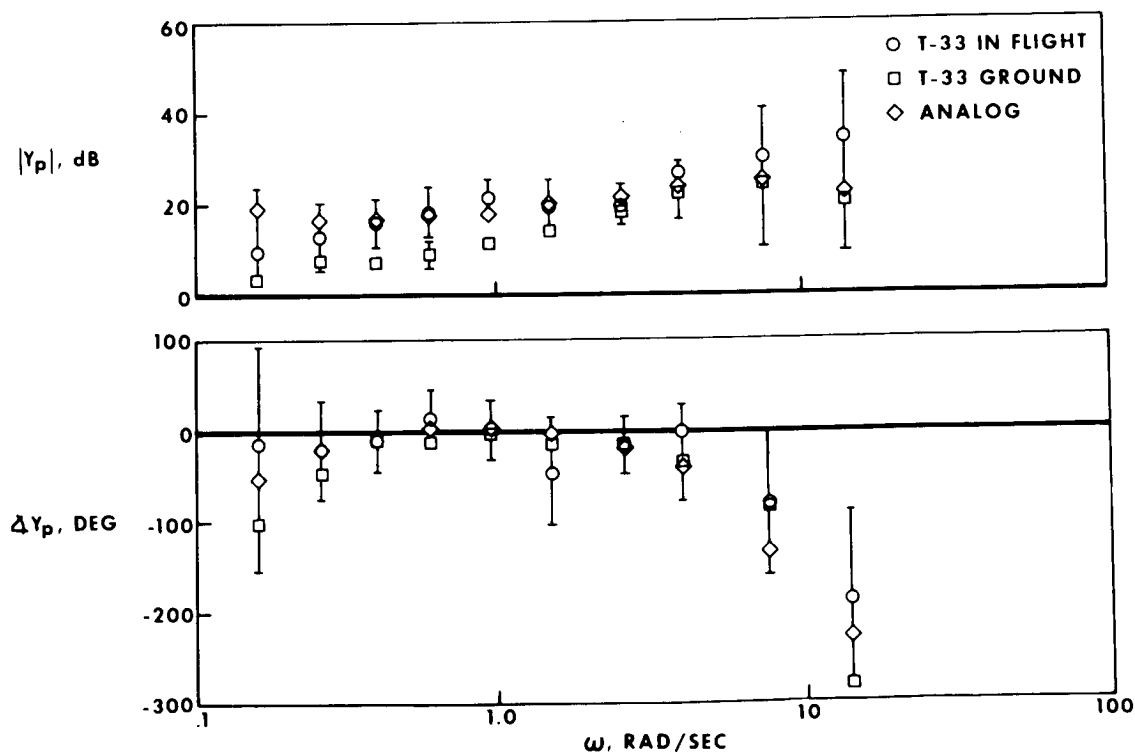


Figure 9.—Averaged human describing functions.

One of the parameters commonly used by human-response analysts to indicate a measure of linearity or stationarity is the parameter  $\rho$ . However, in this study,  $\rho$  was always found to equal 1.0 (see paper 28). The average linear coherence  $\rho_a$  was also measured. It was assumed that  $\bar{c}^2$  was zero (see eq.(4)); however, when the FM tapes were digitized, it was observed that in a number of cases there were large zero shifts. Rather than changing the program, this was accounted for by adding a constant voltage before digitizing the tapes. This was only approximate; however, it is estimated that the resulting error in  $\rho_a$  is no greater than 15 percent, and the error in the describing-function results should be negligible. For the analog runs the average value of  $\rho_a$  was about 0.69, which was very close to the values reported in reference 2 for  $Y_c = K_c/j\omega^2$ . (The average value for six pilots was about 0.63.) For the T-33 simulations, this parameter was considerably lower. For the flight data the average was 0.2 and for the ground data it was 0.37. The controller used in the T-33 variable-stability airplane had a sizable friction band. This caused the pilot's output to be more step-like than it would have been otherwise, which might account for these lower values of  $\rho_a$ .

Because the results of this study always showed the linearity coefficient  $\rho$  to be 1.0, an attempt was made to test one of the programs used where power-spectral densities were obtained from the autocorrelation functions. A simple model using an autopilot was used in the fixed-base simulator to obtain the data for this test, and the program used was the same one used in reference 3. Some of the results from this program are shown in figure 10. This figure shows the autopilot gains that were measured using both methods of analysis, and the actual curve for comparison. The circle symbols are the measured values that were obtained from the program used in the present study at the 10 input frequencies. Nearly perfect

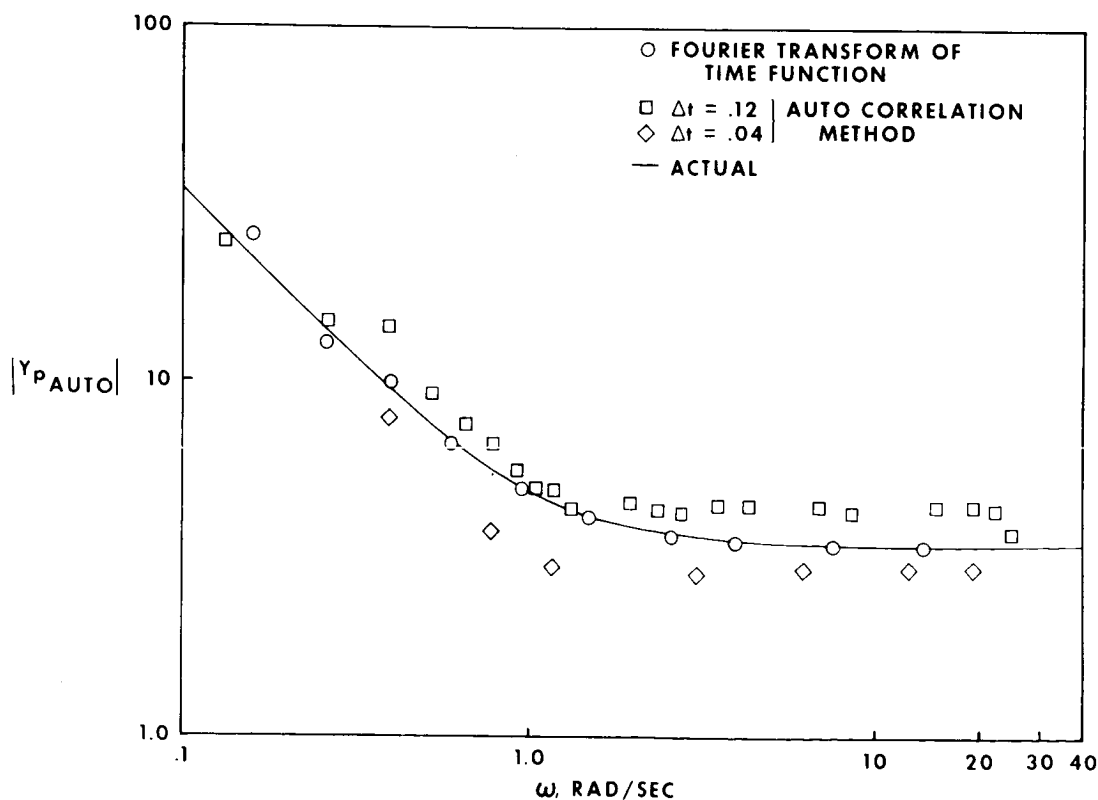


Figure 10.—Comparisons of measured and actual autopilot gain.

agreement is shown at these frequencies. In the autocorrelation program the data were computed at constant frequency intervals where this frequency interval is determined by the time increment and the number of lags chosen. The program was run twice with the same data, and the maximum number of lags permitted in the program was used both times. In the first instance, the time increment was 0.04 second, which resulted in a fairly large frequency interval so that the lowest frequency at which data were obtained was larger than some of the input frequencies. These results are shown by the diamond symbols. To obtain a smaller frequency interval, the time increment had to be increased, so the program was run a second time with a time increment of 0.12 second. These results are shown by the square symbols. The two sets of results bracket the correct values, but it can be seen that neither gives the agreement that is possible by computing the power-spectral densities directly from the time histories. The linear-correlation coefficient  $\rho$  was also computed; however, at most frequencies either  $\rho$  was greater than 1.0 or it could not be computed because of zero or negative power spectra, which makes one suspect the validity of the method of analysis.

### CONCLUDING REMARKS

A follow-on program is planned to begin soon. At that time, additional data will be obtained and a more thorough analysis will be made of human describing functions measured in flight. The data that have been analyzed to date are limited and the results are therefore still inconclusive. The results show a marked increase in the variance of the data obtained in flight; however, it would be premature to attribute all of this to variability in pilot behavior. It is possible that there were some variations in  $Y_C$  which might account for some of this variability. The differences found in reference 1 between the phase angles measured in flight and those measured in ground-based simulators are not evident in the results of this study; however, as noted earlier, the tests did differ. Because of the large variance of the flight data it appears now that any differences that occurred between the data obtained in flight and those obtained in the fixed-base simulators are insignificant and no greater than the differences among pilots or even the run-to-run variability of one pilot. Where the open-loop describing functions were measured, the results were in good agreement with the results of a previous study (McRuer et al.) where the tracking task was similar even though the controlled-element dynamics differed. The values of  $\rho_a$  obtained from the analog study were also in good agreement with previous results; however, the values resulting from the T-33 simulations were considerably lower. Contrary to the results of past investigations, the linear-correlation coefficient  $\rho$  was always equal to 1.0.

### REFERENCES

1. Seckel, Edward; Hall, Ian A. M.; McRuer, Duane T.; Weir, David H.: Human Pilot Dynamic Response in Flight and Simulator. Tech. Rep. 57-520 (ASTIA No. AD130988), Wright Air Dev. Center, U.S. Air Force, Aug. 1958.
2. McRuer, Duane; Graham, Dunstan; Krendel, Ezra; Reisener, William, Jr.: Human Pilot Dynamics in Compensatory Systems. Tech. Rep. AFFDL TR-65-15, U.S. Air Force, July 1965.
3. Sadoff, Melvin: Effects of High Sustained Acceleration on Pilot's Performance and Dynamic Response. NASA TN D-2067, 1964.

**OPTIMAL CONTROL**

N67-15872

## 21. PREVIEW CONTROL BEHAVIOR AND OPTIMAL CONTROL NORMS\*

*T.B. Sheridan, B.F. Fabis, and R.D. Roland*  
*Massachusetts Institute of Technology*

A model, based upon the theory of optimal control, is presented for characterizing the human operator in a preview control task, that is, where he can observe the input targets and their importance prior to the time he must initiate a response to them. While in need of much further development from the behavioral science point of view, the model provides a frame of reference for investigation of performance value and learning in manual control. Two exploratory experiments are reported which may illustrate some relevant experimental variables and provide a rough comparison of the human operator to an optimal preview controller.

In most manual control tasks that humans are called upon to perform, the inputs may be previewed (i.e., the input is available to the human controller a short time before it is appropriate that he initiate a response), and sequential segments of input are of nonuniform importance (i.e., the penalty for a given error at one time is typically different from the penalty for the same size error at some later time). Such tasks may be continuous, such as driving an automobile on the highway, or discrete, such as maneuvering the car into a parking place.

A major constraint of the transfer function as a norm or model of the human controller has been that it is valid only for random-appearing inputs. Even here, it is presumed that the human is attempting to "minimize error" in some "natural" way, based upon some constant implicit error criterion. Whether he should minimize mean-square error, root mean-squared error, averaged absolute error, etc., is usually not specified; nor is the penalty criterion for expended effort (control stick motion) specified. However, it has been shown (ref. 1) that simple instructions to "try harder" (i.e., increase the penalty he associates with error relative to the penalty he associates with effort) significantly reduce error. The fact that instruction to "minimize error" is by no means a unique criterion of performance has been discussed over the years by various writers (ref. 2). A recent experiment (ref. 3) has illustrated that the transfer function may be manipulated by feedback of a good-bad signal based upon a sum of smoothed error and stick motion where different relative weights of error and stick motion result in decidedly different behavior. When the input is previewed, the lack of a specific error-effort penalty tradeoff makes the measured dynamic-response characteristics even more ill-defined than for random appearing inputs, since the human controller now has time in which to anticipate and plan ahead.

\*This research was supported by the National Aeronautics and Space Administration under Grant NsG 107-61.

In a previous paper (ref. 4) one of the authors suggested that there are three sets of models appropriate to the preview control situation:

(1) The first model is an extension of simple linear convolution where the impulse response or weighting function extends into the future as well as into the past (or alternatively where the "present" input value is the farthest point the operator can see ahead and all the weighting function extends into the past).

(2) The second model presumes that the human operator incorporates a fast-time dynamic analog of himself, plus the controlled process, and has the ability to set repetitively his present position, velocity, and acceleration into the analog, "try it out" (with various assumptions about control strategy) over the preview span, and take similar or different actions in forcing the real-time controlled process based upon the relative success of these fast-time trials.

(3) The third model similarly presumes that the human operator incorporates a fast-time dynamic analog of himself plus the controlled process. But rather than use the fast-time thought experiments in trial and error fashion, this model of the human operator presumes an ability to plan optimal trajectories over the preview span of input.

The first two models do not directly treat the problem of the error-effort penalty trade-off, while the third does. In fact the third, based upon the notion of optimal control, suggests the penalty or cost function to be the primitive to the transfer function. The present paper further discusses some aspects of optimal control with respect to modeling the human operator in previewed input situations.

## DETERMINING THE OPTIMAL TRAJECTORY

Consider the human operator plus controlled process as a cascade of an active measurement-and-computation element plus a passive fixed-parameter filter (fig. 1). The hypothetical active element performs the following three functions: (1) reads the sequence of input or "command course" position values  $y(t)$ , together with a corresponding importance value  $I(t)$  at each  $t$ ; (2) stores these values; (3) computes an optimal control policy by means of a procedure such as a dynamic programming algorithm; and (4) meters out a control signal  $f^*(t)$ . This control signal forces the passive element, which is presumed to include both the irreducible dynamic constraints or the human (reaction time plus neuromuscular lag) as well as the dynamics of the given controlled process.

The optimal trajectory computation is based upon two equations:

Dynamics of the fixed reaction time  $T_r$  and neuromuscular lag of man  $T_n$  plus the given controlled process  $Y_p$  is given as

(1)

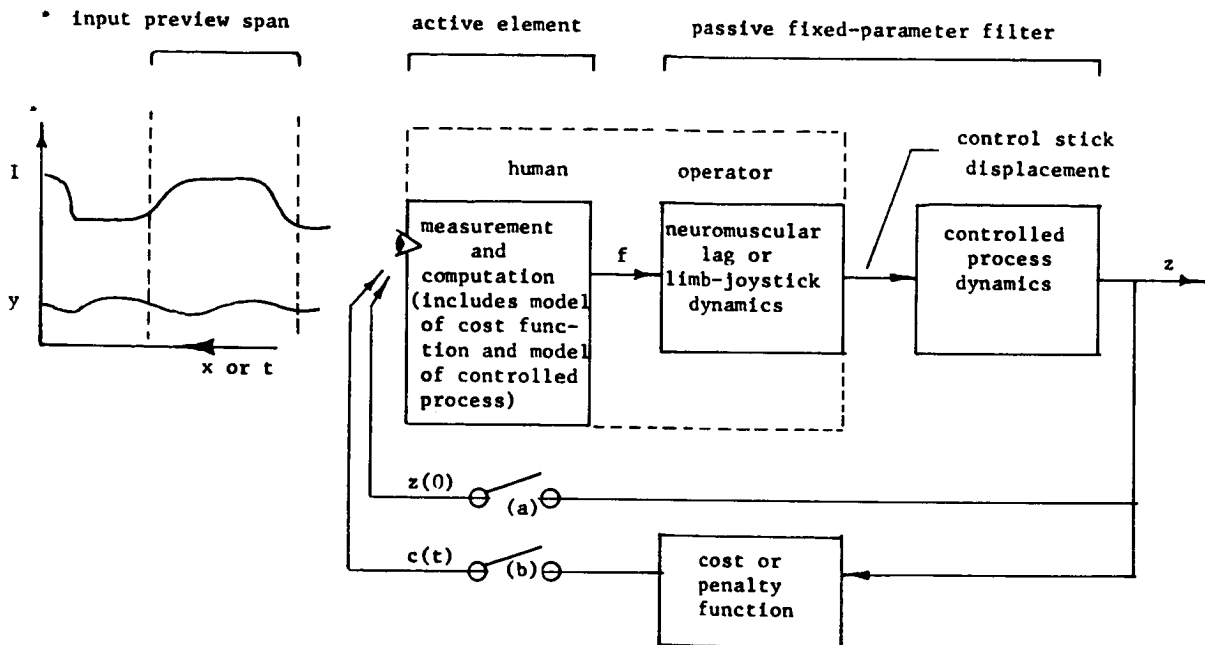


Figure 1.—Hypothetical model of human operator in preview control task. Switch (a) is presumed to close momentarily whenever there is need for updating of initial conditions and a control strategy for an updated preview. Both (a) and (b) are presumed to close during learning of the controlled process and cost function.

where  $z$  is the controlled process output and  $f$  is a neuromuscular forcing function. If reaction time were considered elsewhere and "neuromuscular lag" could instead be "visco-inertance of the arm," then  $f$  would simply be muscle force.

An incremental cost or penalty function or performance criterion appropriate to conditions at each  $t$  is

$$c(t) = c_e [y(t) - z(t)] + c_f [f(t)] + c_t(t) \quad (2)$$

The first term indicates the "error cost," the penalty function of the difference between "ideal" and actual states of system output. The second term indicates "effort cost," the penalty function of using effort (fuel, etc.). The third term indicates "time cost," the penalty function for expenditure of time to reach some goal or subgoal. These functions may take any form and may involve powers of their arguments of two or more. The total cost is typically a linear sum as indicated, but may be a more complex function of  $y$ ,  $z$ ,  $f$ , and  $t$ .

It is usually assumed that the total or cumulative cost over an interval  $0 < t < T$  is the sum of the incremental costs:



Then the optimal  $z^*(t)$  trajectory over  $T$ , given also the initial conditions  $z(0)$ ,  $\dot{z}(0)$ , etc., and the terminal conditions  $z(T)$ ,  $\dot{z}(T)$ , etc., may be determined by minimizing equation (3), under conditions given by equations (1) and (2), by a procedure such as that outlined in the appendix. Given the optimal  $z^*(t)$  trajectory, the optimal control policy  $f^*(t)$  is specified by equation (1). However, it will be seen that since  $f^*(t)$  is not an observable variable, it is expedient to work directly with  $z^*(t)$ .

Equation (1) is the human operator's knowledge of the dynamic constraints; equation (2) is his own implicit performance criterion, which may or may not agree with some given performance criterion explicit in the task or instructions.

The above solution may be determined analytically by variational calculus under special conditions of equation (2) such as when the arguments of  $c_e$  and  $c_f$  are squared. It may be done numerically under almost any conditions provided enough computer memory is available, using an optimizing algorithm such as dynamic programming (ref. 5). For the reader not familiar with dynamic programming, two examples are given in the appendix.

If the manual control task is discrete, that is, if the human operator can preview all the "inputs" which must be encountered through to some final or terminal condition, only one optimal trajectory need be computed and followed. If the task is continuous, some repetitive updating or recomputation of the optimal trajectory  $z^*(t)$  must take place, and the control signal  $f^*(t)$  simply consists of that segment of optimal policy after one updating and prior to the next updating, with rate of updating inverse to length of preview.

## THE COST FUNCTION AS A NORM FOR HUMAN RESPONSE

The cost function provides a norm with respect to which the active element may be characterized. This may be done in two ways:

(1) Active element which is suboptimal with respect to an explicit cost function.—In a particular preview control task, that is, a given ideal response (reference input), a given controlled process (including saturation constraints and initial conditions), and a given function of error, effort, and time to be minimized (scoring criterion given as part of the instructions to subject), there is a unique optimal trajectory. The actual trajectory made by the human will, in general, be different and this difference will serve as a description of the active element. The optimal trajectory, and consequently the discrepancy from optimal, will be different depending upon whether the known passive dynamics of the human are lumped in the controlled process (passive element).

(2) Active element which is optimal with respect to an implicit cost function.—Alternatively to the above, one may say that in a particular preview control task, the active element is optimal with respect to some implicit (unknown) cost function, part of which is determined by the externally imposed scoring criterion and part of which is determined by internal criterion constraints. To discover this cost function, one may compare empirical trajectory data with optimal trajectories based on various cost functions until a satisfactory fit is found, implying that the human optimizes with respect to the associated cost function. Clearly, for trajectories which are far from optimal for any "simple" or "sensible" cost function the investigator cares to try, this second or "inverse" norm breaks down. Noisy, erratic response trajectories would require complex and arbitrary interactions of error, effort, and time in the cost function in order to "appear optimal."

• From either of the above points of view the transfer equation, as conventionally utilized as a model for human control behavior, is secondary to the performance or cost or penalty function. If for a given tracking course the human is near optimal for an explicit criterion, or if a criterion is found with respect to which he is near optimal, then specification of the transfer equation is determined and therefore redundant as a model of the human in that particular course.

The closeness with which the human response approximates optimal for an explicit cost function, or the cost function according to which a given human response trajectory is optimal, may and probably will vary from course to course—due to changes in the "true" criterion function. The linear transfer function which is a "best fit" to empirical response data will similarly and necessarily suffer variations from course to course if the control criterion changes, as we have indicated earlier. But the best fit linear transfer function will vary from course to course for a second very important reason unrelated to a changing criterion—the human transfer equation is, in all probability, quite nonlinear with respect to different previewed courses. The optimal norm, on the other hand, is in no sense constrained to be a linear transfer equation.

## EXPERIMENTAL PROBLEMS

We are concerned with how well the human operator can optimize with respect to arbitrarily given cost functions, process dynamics, and input courses. We are also concerned as to whether he uses some implicit cost function only partly related to the explicit and apparent penalties. These questions, in turn, raise fundamental questions about practice and learning.

A human subject with no experience in tracking or in mathematics could hardly be expected to be optimal if told to sit down and minimize the sum of error squared and absolute value of joystick displacement cubed. Conversely, if he were continually informed of his score he would, after months of constant practice with the same input, controlled process, and cost function, be relatively close to optimal. The latter, however, would be a result of brute force operant conditioning; though the final behavior would approximate optimal, one might question whether the method of getting there was optimal. Thus, how quickly or with how little practice the human converges on optimal behavior is of primary interest.

There are really three different aspects of the task which the human controller must learn:

- (1) The controlled process dynamics, that is, the relation between muscle forcing  $f$  and controlled process response  $z$
- (2) The explicit cost function, that is, the relation between muscle forcing  $f$ , trajectory error, and incremental cost  $c$
- (3) The optimal  $f(t)$  program for some particular input (target position  $y$  and importance  $I$ ) given the process dynamics and cost function

The process dynamics and cost function can be presented to the human in equation form. The human, however, cannot assimilate these as symbolic statements; to understand them he must experience them dynamically in a control task. Given such experience for a particular

controlled process and cost function, one might hypothesize that the human operator can select, on the first try with a new input or target configuration, a near-optimal  $f^*(t)$ . One might also hypothesize that he can "understand" simple symbolically presented modifications in the cost function (e.g., let the error penalty be ten times what it was before, relative to the effort penalty) or simple modifications to the controlled process (e.g., let the time constants be doubled) by cognitive extrapolation from the experientially established baseline.

## EXPERIMENT I: EFFECT OF SPEED AND EXPLICIT COST FUNCTION

**METHOD.**—A small digital computer (PDP-8) was programed with a second-order un-damped system in difference equation form

$$z(x) - 2z(x-1) + z(x-2) = f(x) \quad \begin{array}{l} x = 1, 2 \text{ --- } 15 \text{ intervals} \\ z = 1, 2 \text{ --- } 15 \text{ intervals} \end{array} \quad (4)$$

where  $f$  was forced from outside by a human operator manually selecting states  $-2, -1, 0, 1, 2$  on a rotary five-position control switch. The human operator viewed a scope display on which  $z(x)$  was the lateral displacement of an illuminated spot having constant vertical velocity  $dx/dt$ . Thus,  $f(t)$  was sampled at even discrete intervals of  $x$ . By pressing a switch the operator initiated a trial which started the spot moving vertically from the lower edge of the square display ( $x = 1$ ) with zero lateral velocity. The operator's task was to control  $f(x)$  so as to make  $z(x)$  have an optimal trajectory relative to two target spots, continuously displayed at lateral displacement  $y_a$ , and vertical displacement  $x_a$  and at  $y_b, x_b$ , respectively. The explicit cost function given the subject and with respect to which he was to optimize his trajectory was

$$c = K_I \cdot |z(x) - y(x)| \cdot I(x) + |f(x)| \quad I(x_a) = I(x_b) = 1; \text{ otherwise } I(x) = 0 \quad (5)$$

The coefficient  $K_I$  took on values 1, 10, and 100 for different runs. There were four configurations of the two targets,  $(y_a, x_a)$  and  $(y_b, x_b)$ , and the starting point  $y(1)$  used in different runs. Typical target configurations are illustrated in figure 2. (The combination of this second order system, these cost functions, and these target configurations meant that the optimal trajectory usually hit the targets, but sometimes it did not.) Three vertical velocities  $dx/dt$  were used in different runs: 1.2, 1.6, and 2.3 intervals per second. Thus there were three cost functions by three velocities by four target configurations, or 36 combinations. These were presented to the first subject in pseudorandom order, for 360 runs, or 10 iterations on each combination. A second subject underwent the same except for the  $K_I = 100$  conditions.

Both of the subjects had several hours of practice on the various combinations of conditions employed, with knowledge of results (total cost scores evaluated by the computer for each run). Before each test run the subject was given a "preview run" in which he was allowed to observe the control spot move vertically past the targets with no control on his part. He thereupon pressed a switch to initiate the test run.

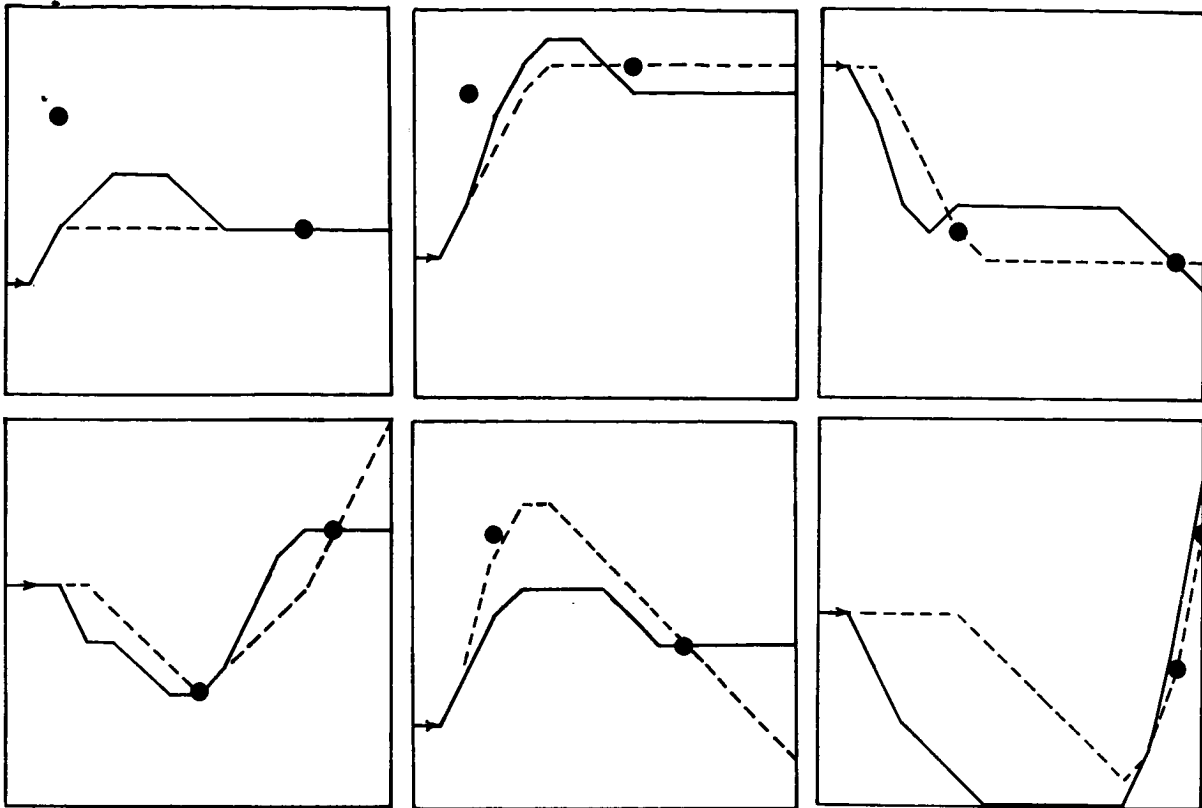


Figure 2.—Sample trajectories used in experiments I and II. Solid lines indicate human trajectories; dotted lines indicate optimal trajectories; the heavy dots are the targets. The starting positions are on the left; actually the subject saw the display oriented so that the arrows pointed up.

The human's trajectories were typed out by the computer for each run. These were compared with optimal trajectories determined by dynamic programming for the identical controlled process, cost functions, starting positions, and target configurations used in the experiment. The computer memory size (4096 words) and the order of the system [2] constrained the problem to a  $15 \times 15$  array. This is the reason the experiment with the human operator was constrained to a  $15 \times 15$  interval array. Indeed, comparing results of a spatially continuous human control task with a coarsely reticulated optimal trajectory would have made no sense.

**RESULTS.**—Experimental results are presented in table 1 and figure 3. Each point for  $K_I$  of 1 or 10 in figure 3 represents an average of 10 runs times 4 patterns times 2 subjects, while for  $K_I$  of 100 only 1 subject was employed.

Figure 3(a) shows the effort costs (number of acceleration units) to be 20 to 30 percent above the optimal for the low and middle speed and about 50 percent or more above optimal at the higher speed. The optimal trajectories were independent of sampling speed. The discrepancy between human and optimal was not surprising in view of the critically stable process dynamics and the need to time movements of the control knob just to precede sampling levels

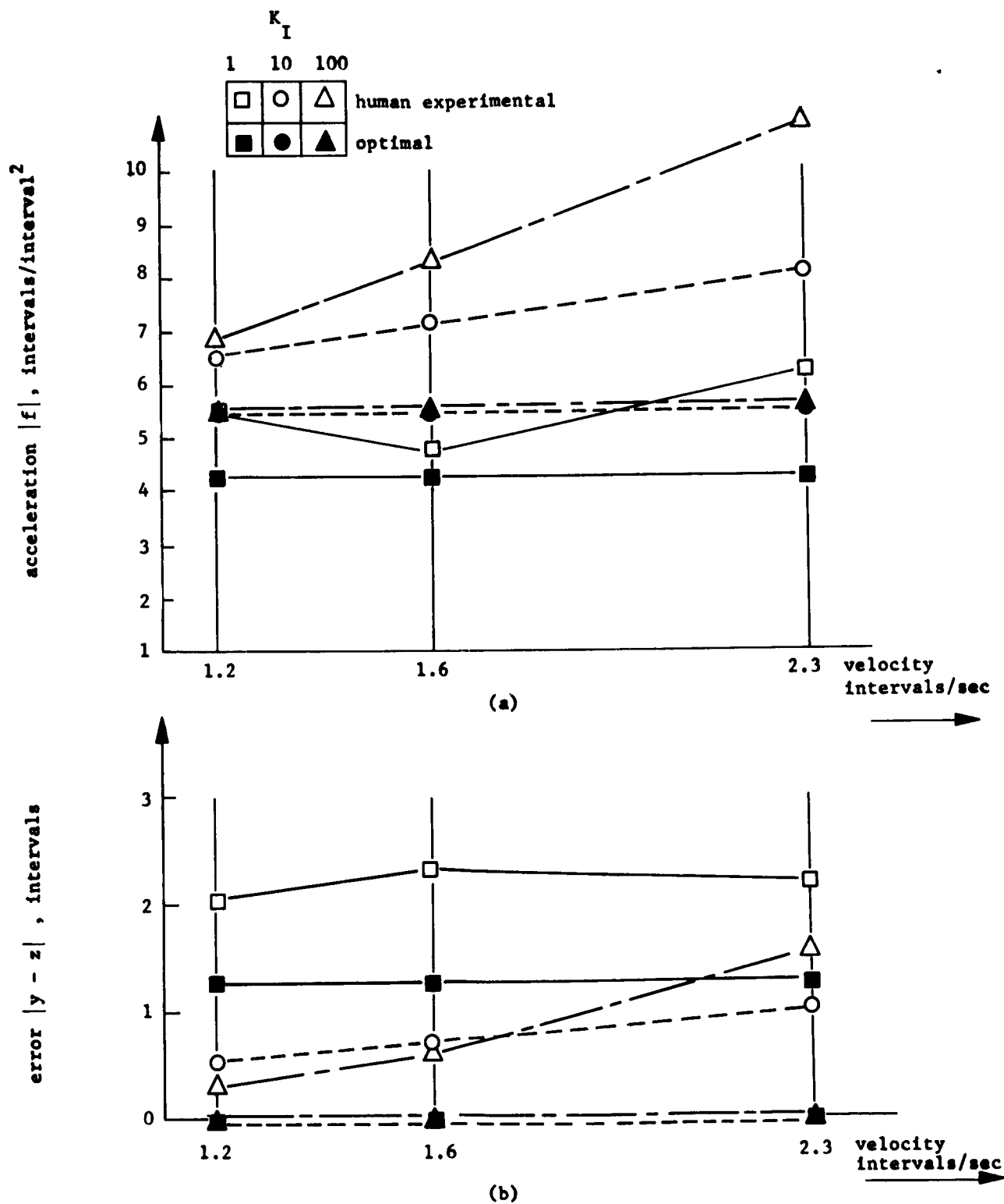


Figure 3.—Acceleration and error results from experiment I. (a) For  $K_I = 1$  and 10 each experimental data point is an average of 2 subjects by 4 target configurations by 10 iterations, or 80 trials; (b) For  $K_I = 100$  one subject was used so that data points are for 40 trials.

TABLE 1.—SUMMARY RESULTS FROM EXPERIMENT I. ALL VALUES ARE AVERAGES. TOTAL COST SCORES ARE DETERMINED BY  $c = f + K_I |y(x) - z(x)|$ ,  $C = \sum c$ , INDICATED SCORE IS  $\bar{C}$

	dx/dt intervals per sec	1.2			1.6			2.3		
	$K_I$	1	10	100	1	10	100	1	10	100
Subject SM	f, intervals per interval <sup>2</sup>	5.8	5.8	5.9	5.1	5.9	7.2	6.5	7.1	9.8
	$ y(x) - z(x) $ intervals	1.56	0.79	0.3	1.68	0.79	0.6	1.73	1.17	1.55
Subject RR	f, intervals per interval <sup>2</sup>	3.1	5.2	-	2.37	6.3	-	3.99	7.1	-
	$ y(x) - z(x) $ intervals	2.6	0.28	-	2.94	0.58	-	2.7	0.9	-
Optimum	f intervals per interval <sup>2</sup>	3.25	4.50	4.50	3.25	4.50	4.50	3.25	4.50	4.50
	$ y(x) - z(x) $ intervals	1.25	0	0	1.25	0	0	1.25	0	0

of  $x$ . The greater the value of  $K_I$  the greater the number of acceleration units, in approximate proportion to the optimal behavior. This would be rational behavior if it served to decrease error. Note that the optimal trajectory included no errors for  $K_I = 10$  or 100, and thus the optimal acceleration program was the same for both  $K_I$  values.

Looking to the error costs (fig. 3(b)) one notices that error decreased with increasing  $K_I$  as it should. It is also evident that there was an average of about one error above optimal for all  $K_I$ , dx/dt combinations, except for a tendency for errors to increase with dx/dt at the higher  $K_I$  values, possibly a perceptual stress effect. For the highest  $K_I$ , it is apparent that increased  $f$  brought about no compensating decrease in error relative to the scores for intermediate  $K_I$ .

The total cost scores (fig. 4) reveal the high penalties brought about by errors at higher values of  $K_I$ , in spite of the increased expenditure of  $f$ .

Comparison of the two subjects' results in table 1 shows that while at the higher speed their acceleration-error tradeoffs were similar, at the lower speed the subjects had somewhat different strategies in trading error with acceleration, even though their total scores were similar in the latter case. One might hypothesize an increasing manifestation of individual differences when there is more time to plan.

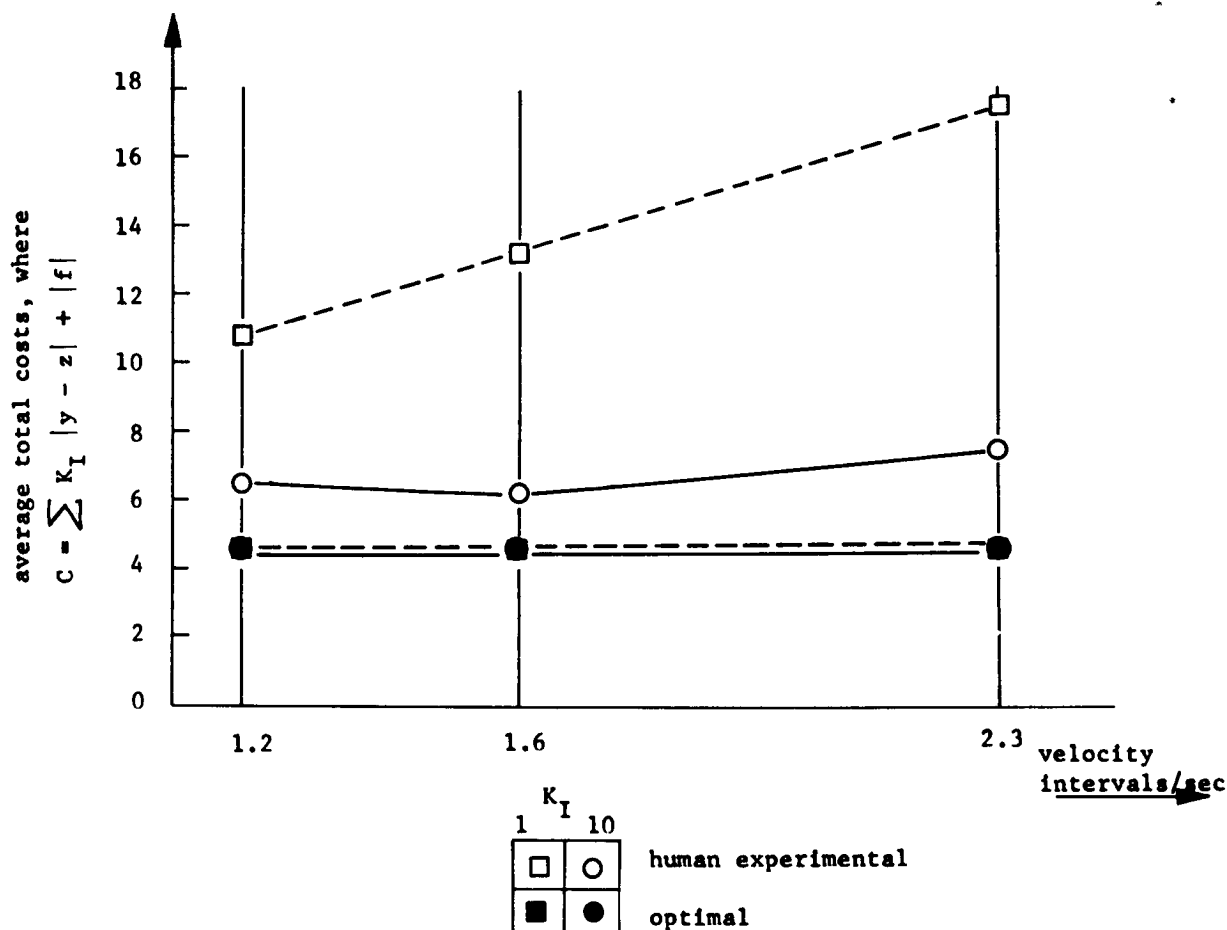


Figure 4.— Total cost score results from experiment I. For  $K_I = 1$  and 10 each experimental data point is an average of 2 subjects by 4 target configurations by 10 iterations, or 80 trials. For  $K_I = 100$  one subject was used so that data points are for 40 trials.

## EXPERIMENT II: EFFECT OF TARGET CONFIGURATION

**METHOD.**—In experiment I four target and starting position configurations were used repeatedly, so that the subjects could easily recognize them and employ their prelearned strategies. This experiment used the same task, same process dynamics, lowest velocity in the preceding set ( $dx/dt = 1.2$  intervals per second) from experiment I. In this experiment  $K_I$  was held at a compromise value of 4; one of the previous subjects was used.

There were two changes in experimental conditions: First, each new run had a randomly assigned starting position and targets randomly placed on the  $15 \times 15$  grid. Second, each of 3 sets of 15 runs had a different display procedure: the first 15 incorporated a preview run before each test run as before, the next 15 simply did away with the preview run, and the third 15 also omitted the illuminated grid on the oscilloscope which coincided with the  $15 \times 15$  array and which was used throughout the first experiment.

**RESULTS.**—Results from the 44 runs (one was aborted) were categorized by difficulty into three groups, where the difficulty criterion was the cost for the optimal trajectory. Categories were: scores of 2 or 3, 4 to 8, 12 or more. These three categories represented approximately equal contributions to the sum of cost scores even though there were more runs in the easiest category than in the most difficult. Then, for each category the sum of error costs and sum of effort (acceleration) costs were separately normalized as percentages of the sum of the total costs (i.e., error plus effort) for the optimal trajectories in that category. These normalized cost contributions are plotted in figure 5.

It is evident that the sum of the human's total costs (normalized with respect to the sum of optimal total costs) diminished as the target configuration became more difficult. The

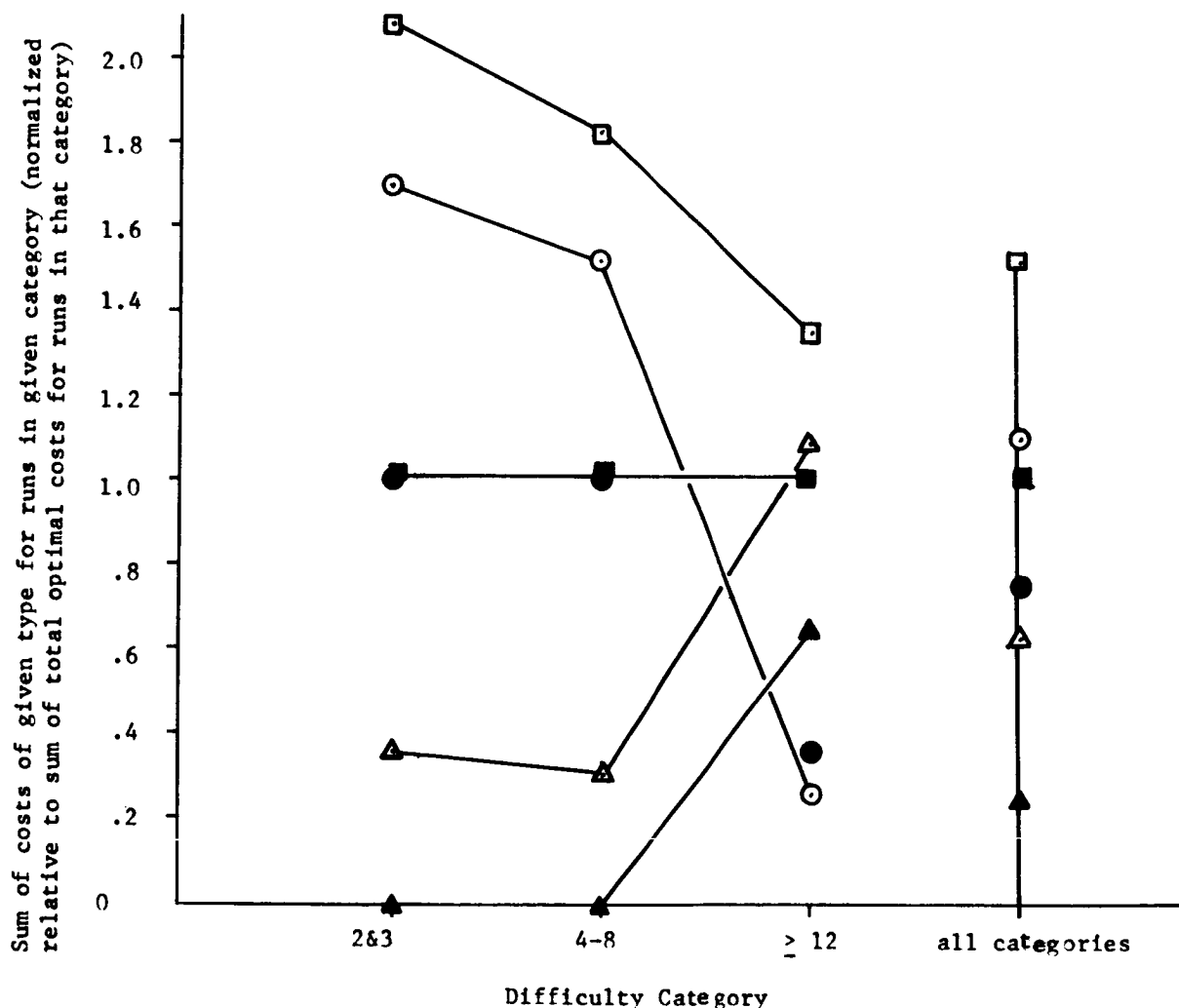


Figure 5.—Results of experiment II, effect of target configurations. (Note that there were no optimal scores of 9-11.)

- |                                    |                             |
|------------------------------------|-----------------------------|
| □ Total, human experimental        | ● Acceleration, optimal     |
| ■ Total, optimal                   | △ Error, human experimental |
| ○ Acceleration, human experimental | ▲ Error, optimal            |



normalized human acceleration cost sum decreased relative to the normalized optimal acceleration cost sum as target difficulty increased, while the normalized human error cost sum remained at a constant level above the normalized optimal error cost sum at all difficulty levels. The tradeoffs between optimal acceleration and error costs (note the latter were zero for the less difficult targets) are artifacts of the coarseness of the grid and the particular target configurations used.

Most of the errors were made on the second of the two targets to be passed on each run. While the optimal trajectories committed errors only on the first target and for the most difficult target category, the human trajectories showed a total of 5, 4, and 20 errors on the first target and 1, 1, and 2 errors on the second target in the three categories from easy to difficult. The tendency to compromise the first target and hit the second resulted from the fact that the starting position and velocity was not under the subject's control.

## DISCUSSION AND CONCLUSIONS

A norm has been described against which the behavior of a human operator in a preview control task may be quantified and predicted. The optimal control norm will hopefully bring into better focus questions of what is learned in a motor skill task and provide an operational definition of good and bad in this context.

Two exploratory experiments have been presented which suggest, for a relatively difficult control task, that the human operator is reasonably close to optimal and trades off error with effort in a rational fashion. The discrete nature of control required in these experiments proved somewhat unnatural; similar experiments ought to be repeated, with finer reticulation approaching continuous control. Sharply nonlinear cost functions should be added to the experiment.

The human control may be suboptimal in a preview control task for at least five reasons:

- (1) He cannot adequately see and remember the previewed input positions and importances
- (2) He has had insufficient experience with the given controlled process and/or explicit cost function
- (3) He utilizes an implicit cost function which differs from that which he is given
- (4) He is incapable of computing an optimal control strategy even though he understands the controlled process and explicit cost function
- (5) He is incapable of implementing an otherwise sound control program

# APPENDIX

## EXAMPLE I: A SIMPLE NUMERICAL EXAMPLE OF DYNAMIC PROGRAMING

Assume at each of four stages in time after the initial stage there are three possible states of a system, represented by circles in figure 6, and that from each state at a given stage, the cost to get to any state at the next stage is directly a function of the two states. These costs are represented by the numbers along the lines connecting the states.

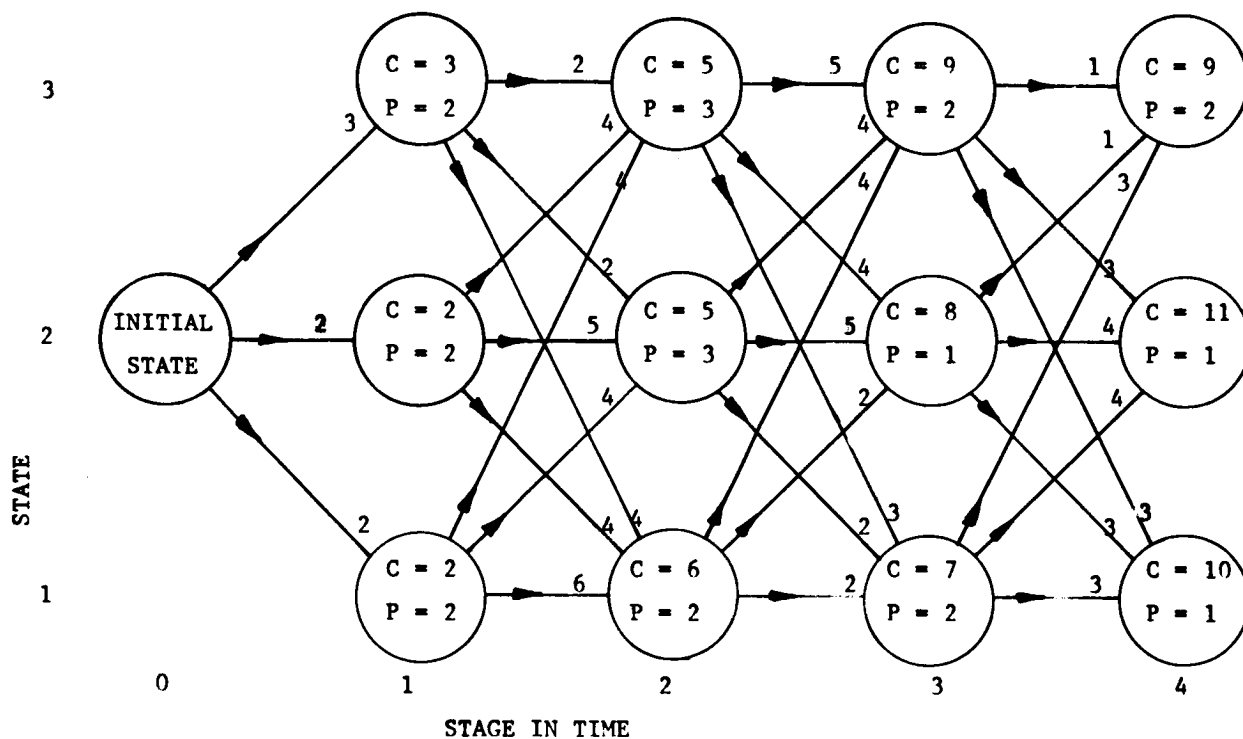


Figure 6.—A simple numerical example of dynamic programming.

Starting with stage 1, the cost, C, indicated within each circle at stage 1 is simply given by the number along the line from the initial state; the least-cost path, P, is 2 in every case since this is the only previous state available.

At stage 2, the cost to state 1 is the least of path 1 (cost =  $2+6=8$ ), path 2 (cost =  $2+4=6$ ), and path 3 (cost =  $3+4=7$ ). The state 1 circle is thus marked with this least cost and best path. Similarly, the cost to state 2 is the least of path 1 ( $2+4$ ), path 2 ( $2+5$ ), and path 3 ( $3+2$ ) and is thus marked as cost 5 and path 3, and similarly for state 3 at stage 2.

Having completed the least-cost and best path determination for stage 2 we can throw away all cost information about stage 1, since in determining costs at stage 3 we need know only the costs to the states at the previous stage. But the best path information must be retained.

At stage 3 we similarly obtain the least cost and corresponding path to reach each of the three states, and so with stage 4.

Now, assuming stage 4 is the terminal stage we could require that state 2 be the terminal state. We observe from our stored path information that we should have come there via state 1 at stage 3; and at state 1 at stage 3 we observe that we should have come via state 2 at stage 2, thence via state 3 at stage 1, and finally back to the initial state. This is the optimal trajectory, the least-cost way of reaching state 2 at stage 4.

On the other hand, we could have looked for the least-cost state at stage 4, which is found to be state 3. The optimal trajectory to reach this state is found to be entirely different: state 2 at stage 3, state 1 at stage 2, state 2 at stage 1, and back to the initial state.

All trajectories need not be different. The optimal trajectory to state 1 at stage 4 is seen to be the same as that to state 2 except for the last step.

The reader should note that in determining the least-cost paths from any one stage to the next the number of trial comparisons was 9, the square of the number of states, and only the three best path values were stored. Both the total number of comparisons and the total number of stored path values were linear with the number of time stages traversed. Accordingly, for  $T$  stages and  $N$  states at each stage, the dynamic programming algorithm requires at most  $TN^2$  comparisons and  $TN$  stored "best path" values to determine the optimal trajectory. Compare this to trying all possible  $N^T$  paths of  $M$  points each.

## EXAMPLE II: DETERMINING AN OPTIMAL TRAJECTORY FOR A SECOND ORDER CONTROLLED PROCESS

On an  $xy$  plane (fig. 7) the controlled vehicle or device is at initial state  $S_0$  with certain initial conditions; and the aim is to get to the terminal state  $S_T$  with least cost or penalty. This cost is, and must be, an explicit function both of error,  $e(t)$ , and of control effort,  $m(t)$ , the effort expended in controlling the system. (Assume  $dx/dt$  is constant and unity so that arguments  $x$  and  $t$  are equivalent.) We assume that the vehicle obeys some given differential equation relating to the control signal forcing function  $m(t)$  to the position  $y(t)$ , such as

$$m(t) = M \frac{d^2 z}{dt^2} + B \frac{dz}{dt} \quad (A1)$$

where  $M$  is the mass and  $B$  is the viscosity coefficient describing the controlled vehicle. The space between  $S_0$  and  $S_T$  may be strewn with obstacles, the hitting of which poses a high error cost. The aim might be to find the one of an infinity of possible paths from  $S_0$  to  $S_T$  which minimizes the system's effort given that it also hits no obstacle. Alternatively, there may be a single "ideal" path  $y(t)$  shown dotted in figure 7 (i.e., ideal if control effort made no difference) with non-uniform error importance  $I(t)$  as we considered earlier. In either case, one can say we want to minimize some cost function of both error and effort, where in the former case the requirement that we hit no obstacle means the cost of collision is very large. For the sake of our example let us assume the latter type of control task, but the reader will appreciate that the method applies equally well to both types of task. Let the

given cost function be a sum of effort cost  $c_e$  and effort cost  $c_f$  of a form such as

$$\begin{aligned} c(t) &= c_e(e) + c_f(m) \\ &= |y(t) - z(t)|^{K_e} I(t) + |m(t)|^{K_f} \end{aligned} \quad (A2)$$

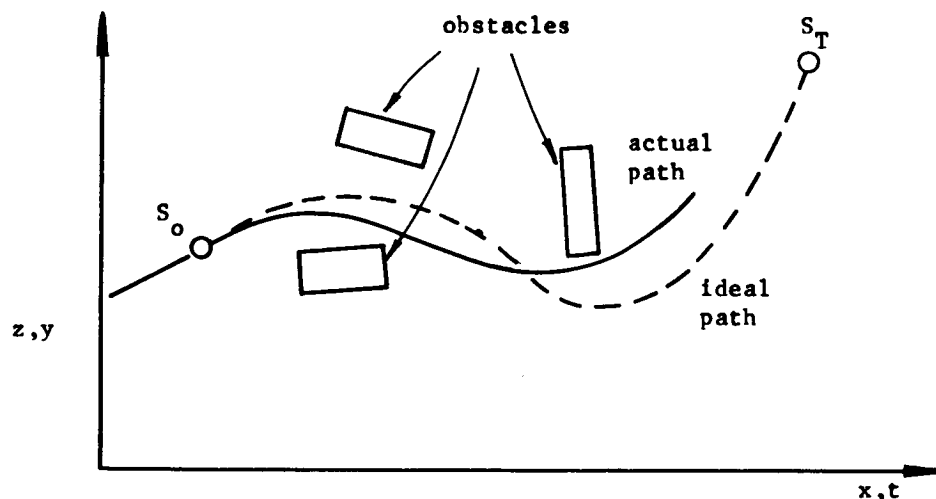


Figure 7.—The physical space of the preview control problem, example II.

In order to facilitate the computation of the minimum cost trajectory or control strategy over the given interval, the  $xy$  of  $ty$  space is reticulated into  $T$  discrete stages ( $t = 1, 2, 3 \dots T$ ) along the time dimension and  $N$  states ( $z = 1, 2, 3 \dots N$ ) along the control dimension as shown in figure 8. The minimum cost path to get from  $S_0$  to  $S_T$  can now be found by the same dynamic programming algorithm as described in the previous example. In the present problem, namely, the control of a vehicle described by (A1) to minimize a cost specified by (A2) over a given interval, the solution proceeds as follows:

The differential equation (A1) is changed into a difference equation

$$m(t) = M \left\{ [z(t) - z(t-1)] - [z(t-1) - z(t-2)] \right\} + B \left\{ z(t) - z(t-1) \right\} \dots \quad (A3)$$

and the penalty function (eq. (A2)) becomes

$$c(t, i, j, k) = |y(t) - z(t)|^{K_e} I(t) + |m(t, i, j, k)|^{K_f} \quad (A4)$$

where the two quantities in large brackets represent acceleration and velocity defined with respect to the present and preceding points in time. In figure 8 the initial state at  $S_0$  is specified by  $z(0)$  plus the initial velocity by  $[z(0)-z(-1)]$ . Thus the pair of points (open circles),  $z(0)$  and  $z(-1)$ , is equivalent to specification of  $z(0)$  and  $dz/dt(0)$ . For any point such as that shown (solid dot) for  $z(1)$ , equation (A3) may be evaluated to obtain  $m(t)$  and then equation (A4) may be evaluated to determine  $c(t)$ .

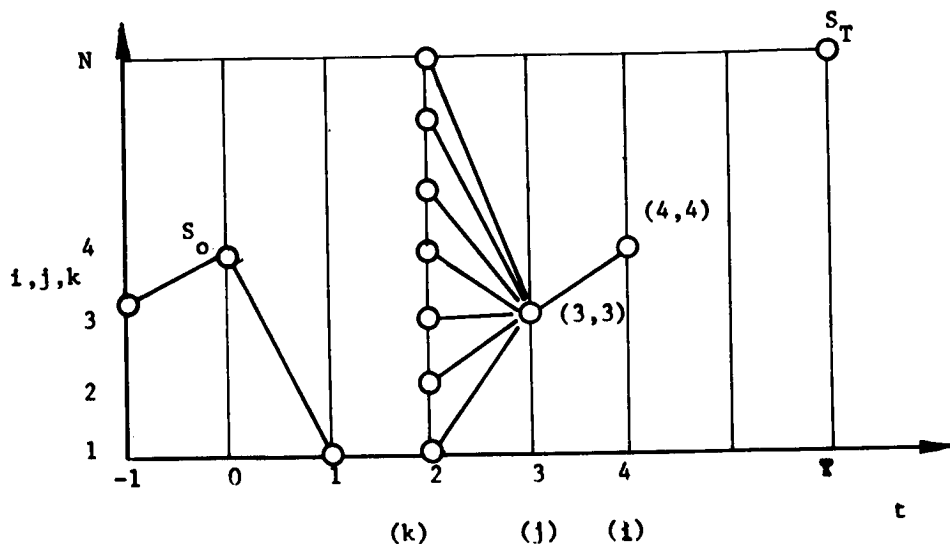


Figure 8. —The discrete computational space of the dynamic programming solution, example II.

The dynamic programming algorithm proceeds by determining, for any given pair of points,  $(t, i)$  and  $(t-1, j)$ , representing position and velocity at  $t$ , which of the  $N$  points  $(t-2, k)$  produces the least cumulative cost  $C$ . This is determined from the recursive relation

$$C(t, i, j) = \min_k [C(t-1, j, k) + c(t, i, j, k)] \quad (A5)$$

For example the cost to arrive at  $(4, 4)$  from  $(3, 3)$  in figure 8 is minimized over all possible combination of  $(3, 3)$  and  $(2, k)$  shown on the figure arbitrarily at time stages 2, 3, and 4. This least cumulative cost  $C(t, i, j)$  is stored for use in the next stage (it becomes  $C(t-1, j, k)$ ), and the corresponding value of  $k$  at  $(t-2)$  is stored as the best path value  $P(t, i, j)$ ,  $k^*$ .

The above process is carried out for every  $ij$  position and velocity combination, that is, every  $z(t)$  and  $z(t-1)$  pair at stage  $t$ . The whole process is then iterated at the next time stage, and so on, just as in the earlier example. When the last stage  $T$  is reached, either some predetermined position-velocity state  $S_T = I, J$  is of interest, or the least cost state at this stage is selected. Then the stored  $P(T, I, J)$  gives the optimal  $k$ ,  $k^*$ , to have come from. The stored  $P(T-1, J, k^*)$  gives the next previous optimal path value, and thus the optimal path is traced back to the starting point. A computer flow diagram for this algorithm is given in figure 9.

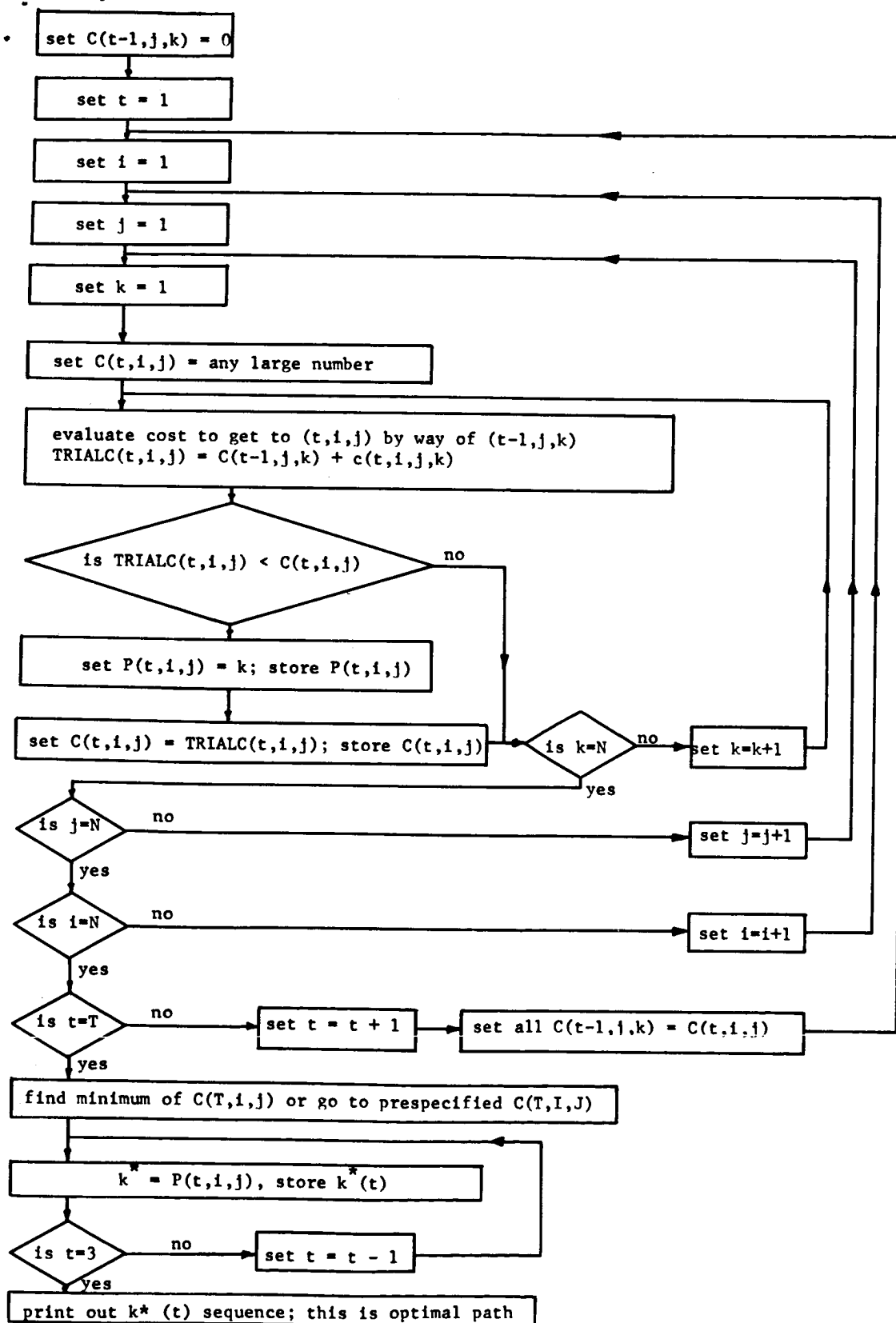


Figure 9.—Computation flow chart for dynamic programming solution, example II.

## REFERENCES

1. Russel, L.: Characteristics of the Human Operator as a Linear Servo-Element. M.S. Thesis, MIT, May 1951. (See also description of Russel experiment in McRuer and Krendel: Dynamic Response of Human Operators, WADC-TR-56-524, Oct. 1957.)
2. Sheridan, T.: Time Variable Dynamics of Human Operator Systems. AFCRC-TN-60-169, Mar. 1960, p. 7.
3. Miller, D.: The Effects of Performance-Scoring Criteria on Compensatory Tracking Behavior. IEEE Transactions HFEG, vol. HFE-6, no. 1, Sept. 1965.
4. Sheridan, T.: Three Models of Preview Control. Presented at the 1965 Symposium on Human Factors in Electronics, IEEE, May 1965.
5. Bellman, R.; and Dreyfus, S.: Applied Dynamic Programming. Princeton University Press, 1962.

N67-15873

## 22. STUDIES IN OPTIMAL BEHAVIOR IN MANUAL CONTROL SYSTEMS: THE EFFECT OF FOUR PERFORMANCE CRITERIA IN COMPENSATORY RATE-CONTROL TRACKING\*

*Richard W. Obermayer, Raymond B. Webster, and Frederick A. Muckler  
The Bunker-Ramo Corporation*

Twelve college students performed compensatory tracking with rate control dynamics ( $1/s$ ) and a low-frequency forcing function composed of the sum of six sinusoidal components. After two practice sessions, the subjects performed the basic task with four performance criteria: (1) keep the display bar in the center, (2) only keep the display bar from exceeding 1-centimeter boundaries on the display face, (3) minimize a total score which is the sum of mean-squared display deviation and mean-squared control deflection, and (4) minimize mean-squared display deviation. The following kinds of information were collected: learning curves; display, control, and total scores; amplitude ratio and phase at each forcing function frequency; centimeter tolerance-band counts; correlation coefficients; reversals; oscillograph recordings; control and display amplitude distribution; and average control response as a function of display deviation. These data show different levels of human control behavior and nonamplifier-type behavior, and yield methodological implications.

In recent years new techniques under the heading of modern optimal control theory have been fruitfully applied to automatic systems and a new insight into control problems has been gained. In particular the concept of optimal control is developed in terms of the specific criteria one wishes to optimize. When one views the problems of manual control systems in this way, there appears the possibility that if one can specify the manner in which these systems are optimal, new insight may be gained into the techniques and strategies that the human controller applies to his task. This approach is taken in this study of rate-control tracking.

### MODERN CONTROL THEORY AND HUMAN OPTIMAL CONTROL BEHAVIOR

Modern optimal control theory generally requires that one specify the criteria which a control system is expected to optimize and then derive the system configuration and parameters which will yield performance which is optimal in the defined way. It is important to note that this theory does not attempt to derive a universal optimal system. That is, any system may be optimal if the criteria are defined appropriately (if we may include some trivial criteria). Under some conditions one may reverse the optimal-control design problem (ref. 1) and attempt to find the performance criteria under which a given system is optimal. In the context of manual control systems, we may ask (ref. 2) in what ways are the human behavior and the overall system optimal?

---

\*This paper reports research conducted under National Aeronautics and Space Administration Contract NAS2-3113.



The question of human optimal control behavior has not passed without comment in the literature. Frequently models of the human controller are found to have characteristics which the servo-engineer would desire. Further, the human controller tends to perform in an "optimal" fashion over a wide range of control environments. McRuer and Krendel (ref. 3) comment, "In fact, the human operator is the very prototype of an adaptive optimizing servo system." Roig (ref. 4) compared the performance of a human operator against a linear controller which minimized root-mean-square error and noted similarities in overall performance. The task was one-dimensional compensatory tracking with two types of stochastic non-gaussian inputs, and with controlled element dynamics approximating a rate control with large delay. Under these conditions, it appeared that the human operator performed about as well as a highly constrained optimal linear controller. Leonard (ref. 5) evaluated two cases of human-operator mathematical models against a minimum mean-square-error criterion. In each case the parameters of the math model were varied and the mean-square-error score was computed until the minimum mean-square-error condition was found. Leonard concluded that "the trained human often adopts dynamics that nearly minimize the mean-square tracking error (subject to the human's inherent limitations)." Thus, a case has been established that the human controller may tend to control in a fashion which will minimize mean-square tracking error.

## EXPERIMENTAL APPROACH

The human operator, however, is characteristically an adaptive and flexible controller, and perhaps may be capable of optimizing with respect to a range of performance criteria. For example, a number of investigators (e.g., refs. 3, 6, and 7) have noted that their subject's performance or performance level could be changed by simply giving them different verbal instructions. Miller (ref. 8) found that his subjects changed tracking behavior as the nature of a continuous scoring criterion feedback was changed. The criteria investigated consisted of various weighted sums of mean-squared error and mean-squared stick movement.

The current study, therefore, investigated human performance over four conditions of performance criteria, but in all cases the basic display, control, controlled element, and forcing function remained the same. With a view to identifying changes in performance criteria and control technique the following four conditions were studied:

CONDITION 1. "KEEP THE DISPLAY BAR IN THE CENTER."—In many reports of experimental investigations, the detailed instructions are not included; and in many cases, since the subjects are skilled pilots or servo-engineers they are assumed to employ more sophisticated criteria than those given to them in basic instructions. However, where the task is compensatory tracking, the instructions are generally of the form, "keep the display bar in the center of the display as well as you can." No instruction is given as to what to do when the display bar is not in the center, whether to treat large or small deviations differently, whether the number of hits on the exact center is more important than the amount of time spent at the exact center, etc.

CONDITION 2. "KEEP THE DISPLAY BAR BETWEEN BOUNDARIES ON THE DISPLAY."—Some practical control criteria appear to be different from condition 1. For some systems performance must only be maintained within given boundaries, and either loose control or no control is exerted when system parameters are within bounds. Condition 2 defines performance within boundaries (1 cm) on the display screen to be equivalent to keeping the display bar precisely in the center, and requires that the boundaries never be exceeded.

• CONDITION 3. "MINIMIZE A QUADRATIC PERFORMANCE INDEX."—A general quadratic performance index may be expressed in the following form for rate-control tracking:

$$J = \int (Qe^2 + Ru^2)dt = Qe^2 + Ru^2$$

where

e        displayed error  
u        control stick deflection

To minimize the quadratic performance index, a compromise between display deviations and the amount of control used must be made. Condition 3 incorporates feedback of knowledge of results at the end of each tracking trial. Three knowledge-of-results meters were used: Display score ( $e^2$ ), Control score ( $u^2$ ), and a total score ( $J$ ). The display score and control score were weighted equally to produce the indication on the total score meter ( $J = e^2 + u^2$ ). The basic instruction to the subjects was, "minimize the indication on the total score meter."

CONDITION 4. "MINIMIZE A MEAN-SQUARED-ERROR CRITERION."—A mean-squared-error criterion is a special case of condition 3 ( $R = 0$ ). Under condition 4 only the subject's display score meter indicated at the end of each trial; the basic instruction was, "minimize the indication on the display-score meter."

## APPARATUS

SUBJECT'S STATION.—A cathode ray tube (CRT) display was located directly in front of the subject at approximately 28 inches viewing distance; the subject's chair was located between marks on the floor to maintain a constant chair-display relationship for all subjects. The display face was inclined  $5^\circ$  from the vertical, and the desktop was inclined  $15^\circ$  from the horizontal. When the subject was seated with his forearm resting on the inclined surface, the pencil-type control stick was located approximately at his hand position. A neon lamp was located directly above the display to warn the subject to get ready. Three meter displays were located on the inclined desk surface to present knowledge of results for some of the experimental conditions.

The ambient incident illumination was maintained at approximately 4 foot-candles through the use of controlled-intensity fluorescent lighting. Curtains and partitions were used to screen the subjects from distractions, and all of this equipment was contained within another larger closed room. Medium-gray color tones were used throughout in the attempt to produce a restful environment.

CRT DISPLAY.—All but a 4- by 10-centimeter rectangular area of the display was masked with black paper. The oscilloscope graticule was illuminated to approximately the same brightness as the horizontal bright green line produced on the CRT phosphor. The bright green line was the only movable element of the display, the horizontal green line could only move up and down. The center horizontal line was used as a command reference, and the horizontal lines 1 centimeter above and below the center were also used in one of the experimental tasks. The display presented a compensatory task, with the distance between the bright green line and the central reference line proportional to the difference between the subject's control and the input forcing function.

**CONTROL STICK.**—The subject's controller was a spring-centered pencil-type control stick 4 inches long and movable through an arc of  $57^\circ$ . The arc traced by the top of the control stick between extreme deflections was about 4 inches. Potentiometers mechanically coupled to the control stick produced voltages proportional to the angle at which the control stick was deflected from the neutral position. While the control stick was free to move left and right, as well as forward and back, only forward and back motions contributed to the output voltage. The subjects deflected the control stick with their finger tips; a sand-blasted region was provided to prevent finger slippage.

**FORCING FUNCTION.**—If the subjects were to make no response, the only movement on the CRT display face would be due to the input forcing function. The forcing function was identical to that reported by McRuer, et al. (ref. 9). The forcing function was constructed from the sum of six sinusoidal components of equal amplitudes, random phase relationships, and with the angular frequencies given in table 1. This forcing function has the property that its amplitude is approximately normally distributed; in terms of deviations from the center of the forcing function, the mean and standard deviation were 0.0 inch and 1/2 inch, respectively.

**ANALOG COMPUTER.**—An EAI TR-20 analog computer was used to simulate the controlled element ( $1/s$ ), to generate the quadratic performance scores, and to scale and provide marker signals for magnetic tape recording. The scaling for the control stick (2.5 volts/inch displacement measured along the arc of the top of the control stick) was equal to the display screen scaling (2.5 volts/inch on display face). Thus, if the ( $1/s$ ) were replaced with a unity-gain amplifier, a 1 to 1 relationship would exist between display and control displacements.

**KNOWLEDGE-OF-RESULTS DISPLAYS.**—The analog computer circuitry included means for generating signals for a display score proportional to the mean-square display deviation, a control score proportional to the mean-square control deflection, and a total score proportional to the sum of the display and control scores. Each of these signals was displayed on each of the three 2-1/2 inch voltmeters on the inclined desktop in front of the subject. Appropriate scaling changes were made with different trial lengths so that equivalent performances yielded the same meter indications. However, under condition 4, the scaling of display score meter was changed to yield readings four times those for other conditions. Relay circuitry was provided so that scores were displayed on the voltmeters only during the rest period after each trial.

**PROGRAM CONTROL.**—A motor-gear-cam-microswitch unit was used to program experimental events. The subjects rested for 12 percent of a cam revolution and tracked for the remaining 88 percent however, only the last 80 percent of the tracking time was scored. Prior to the tracking trial, a warning light was illuminated for approximately 2 percent of a cam revolution. Two gear systems were available for cam revolution times of 300 seconds and 120 seconds, that is, providing for scoring periods of 4 minutes and 96 seconds, respectively. The program was stopped manually for longer rest periods, and a hand-set bell timer was used to time these break periods.

TABLE 1.—FORCING FUNCTION FREQUENCIES

Component	Angular frequency, rad/sec
1	0.157
2	.262
3	.393
4	.602
5	.969
6	1.490

**MEASUREMENT EQUIPMENT.**—All measurements other than the display, control, and total scores were derived from signals recorded on a Sanborn seven-channel FM instrumentation magnetic tape recorder. From these magnetic tapes the display signal and the subject's control stick response were converted to digital punched paper tape using a DYMEC 2010B data acquisition system. The analog-digital conversion sampled both signals each 1/2 second, but sampled the control signal 0.1 second after the display signal. All subsequent measurement and data analysis were performed on the Bunker-Ramo 130 digital computer. These measures included:

- (1) Fourier analysis for each of the forcing function frequencies. Due to the 0.1-second sampling delay, a reaction-time delay must be accounted for in these data.
- (2) Amplitude distributions of display and control signals. Computer counts were made of signal amplitudes for intervals of 0.1 inch.
- (3) Average response for a given display deviation. The average control-stick deflection was computed for each display deviation amplitude distribution interval.
- (4) Centimeter tolerance band counts. A count was made of the number of times the display deviation exceeded 1 centimeter in a given trial.
- (5) Correlation coefficient. The product-moment correlation coefficient was computed for the display deviation and control deflection pairs of a given trial.
- (6) Reversal score. This score is a count of the number of times a subject moved the control stick in the wrong (error-increasing) direction in a given trial. For a specified tolerance band, a reversal was counted only if (a) both the display deviation and control deviation of a given 1/2-second sample exceeded the tolerance band, (b) both the display deviation and control deviation had increased since the last 1/2-second sample, and (c) the display deviation and control deflection were the same sign (they should be opposite sign to reduce error).

## EXPERIMENTAL DESIGN

In this study all subjects received all experimental conditions (table 2). However, it was considered necessary to counterbalance the effects of the order of presentation, therefore an equal number of subjects were administered the four experimental conditions in the four orders of presentation listed in table 2. It will be noted that each of the conditions was administered first, second, third, and last an equal number of times, and that each condition was administered following all other conditions an equal number of times.

Due to measurement requirements, two different lengths of measurement trials were used during the course of the investigation, one with a 96-second scoring period, and one with a 4-minute scoring period. Thus the experimental design was chosen for the analysis of three

TABLE 2.—ORDER OF PRESENTATION OF EXPERIMENTAL CONDITIONS

Order	Presentation of conditions
1	1 2 3 4
2	2 4 1 3
3	3 1 4 2
4	4 3 2 1

experimental factors: four experimental conditions, four orders of presentation, and two trial length times. Since an equal number of subjects received each order of presentation (subjects were tested in orders of presentation) but otherwise all subjects received all combinations of the remaining two factors, the data collection procedure satisfied the requirements dictated by Winer (ref. 10, p. 319) for a three-factor experiment with repeated measures (case 1).

## SUBJECTS

Twelve male college students served as subjects in this experiment. All were right-handed, only two wore glasses, and none had ever served in a similar study before. Their ages ranged from 18 to 23, with a mean age of 20.

## PROCEDURE

Each subject performed for two sessions of approximately 3-1/2 hours each, one session per day for a total of 2 days; half the group performed on Tuesdays and Thursdays, the other half performed on Wednesdays and Fridays. Over the 2 days of data collection, the subjects performed in two practice sessions and four experimental condition sessions: practice 1, practice 2, condition 1, condition 2, condition 3, and condition 4. The practice sessions were always administered first, but the conditions were administered according to the order of presentation designated for a particular subject group. Practice session 1, practice session 2, and one of the experimental conditions were administered on the first day, while the three remaining experimental conditions were administered on the second day.

The sequence of events for the subjects were similar for both the practice sessions and the experimental sessions with minor exceptions. A warning light was illuminated for a brief period indicating to the subject that the trial was about to start at which time the subject grasped the control stick as instructed and was prepared to initiate controlling action when the display started to move. The warning light was automatically extinguished when the display started to move. During the two practice sessions, the subject tracked for 20 trials each with a 3-minute rest period after the 5th and 15th trials and a 10-minute rest period after the 10th trial. During the experimental session the subjects had a 3-minute break after the 5th trial and a 10-minute break after the 10th trial prior to engaging in the four 4-minute trials. At the end of each block of 5 trials during the second practice session and conditions 3 and 4, the subjects were presented a card summarizing his scores obtained for those trials.

## STATISTICAL ANALYSIS

DISPLAY, CONTROL, AND TOTAL SCORES.—Display, control, and total scores were generated at the end of all trials (ten 96-sec and four 4-min measurement intervals for each experimental condition). In the attempt to avoid warm-up effects, and end effects, only the last five short trials (96 sec) and the second and third long trials (4 min) were analyzed. The means for these trials are entered in tables 3 to 5 for the display, control, and total scores. Analysis of variance showed that the effect of the four conditions of performance criteria is statistically significant for the display, control, and total scores, but the effects of order of presentation and trial length were not sufficient.

AVERAGE GAIN.—For each experimental condition, five short trials and two long trials, as indicated above, utilized as samples of display signal and control deflection signal (at 2 samples/sec) were converted to punched-paper tape form for digital computer analyses.

TABLE 3.—DISPLAY SCORES

Subject	Condition 1		Condition 2		Condition 3		Condition 4	
	Short <sup>a</sup> trials	Long <sup>b</sup> trials	Short <sup>a</sup> trials	Long <sup>b</sup> trials	Short <sup>a</sup> trials	Long <sup>b</sup> trials	Short <sup>a</sup> trials	Long <sup>b</sup> trials
1	0.56	0.49	0.77	0.54	2.40	3.20	0.33	0.23
2	1.07	.82	.96	1.22	6.13	3.67	.59	.61
3	.75	.64	.33	.32	1.71	1.79	.20	.31
4	1.21	1.45	2.50	1.76	3.42	4.31	1.05	1.84
5	.37	.37	.45	.66	1.79	1.34	.28	.28
6	1.19	1.72	1.29	1.67	1.60	3.20	.42	.71
7	.21	.33	.52	.58	1.06	.92	.12	.27
8	.72	.77	.88	1.04	3.50	3.38	.47	.55
9	.89	.97	.67	.94	2.99	2.80	.49	.63
10	.84	.88	.84	.82	3.33	3.50	.28	.31
11	.27	.36	.42	.40	1.70	2.39	.26	.45
12	.27	.43	.82	.77	.28	.29	.27	.39
Means	0.695	0.771	0.871	0.895	2.492	2.568	0.397	0.549
	0.733		0.883		2.530		0.473	

<sup>a</sup>Averaged over five 96-second measurement intervals.<sup>b</sup>Averaged over two 4-minute measurement intervals.

TABLE 4.—CONTROL SCORES

Subject	Condition 1		Condition 2		Condition 3		Condition 4	
	Short <sup>a</sup> trials	Long <sup>b</sup> trials	Short <sup>a</sup> trials	Long <sup>b</sup> trials	Short <sup>a</sup> trials	Long <sup>b</sup> trials	Short <sup>a</sup> trials	Long <sup>b</sup> trials
1	12.31	11.12	8.46	8.65	4.47	3.31	9.43	8.70
2	8.89	8.72	8.77	11.04	1.77	4.97	9.80	9.86
3	10.88	11.09	7.73	7.94	5.09	5.91	9.33	9.19
4	7.71	7.55	10.58	11.58	3.21	2.78	4.61	5.18
5	7.16	7.08	7.21	8.32	4.82	5.50	7.52	7.36
6	11.77	11.64	9.05	8.30	8.46	7.14	10.24	11.88
7	8.07	8.01	10.10	10.01	6.04	7.57	7.32	8.47
8	7.63	8.43	12.38	13.82	3.18	3.33	10.19	9.07
9	7.43	8.09	8.26	8.79	5.51	5.79	8.58	8.65
10	9.06	8.37	6.66	7.57	3.17	3.22	7.84	7.98
11	8.42	8.53	7.03	7.60	4.48	4.22	10.00	8.44
12	8.51	8.45	11.56	9.99	9.12	8.73	9.88	9.65
Means	8.986	8.924	8.981	9.469	4.944	5.208	8.728	8.704
	8.955		9.225		5.076		8.716	

<sup>a</sup>Averaged over five 96-second measurement intervals.<sup>b</sup>Averaged over two 4-minute measurement intervals.

TABLE 5.—TOTAL SCORES

Subject	Condition 1		Condition 2		Condition 3		Condition 4	
	Short <sup>a</sup> trials	Long <sup>b</sup> trials	Short <sup>a</sup> trials	Long <sup>b</sup> trials	Short <sup>a</sup> trials	Long <sup>b</sup> trials	Short <sup>a</sup> trials	Long <sup>b</sup> trials
1	7.72	6.97	5.54	5.52	4.12	3.91	6.44	5.78
2	5.97	5.73	5.84	7.36	4.74	5.19	7.30	7.37
3	6.98	7.04	4.84	4.96	4.08	4.62	6.08	6.26
4	5.35	5.40	7.85	8.01	3.97	4.26	5.30	7.52
5	4.52	4.47	4.59	5.39	3.97	4.11	5.18	5.10
6	7.78	8.02	6.20	5.99	6.04	6.20	7.14	8.83
7	4.97	5.01	6.37	6.35	4.26	5.10	4.69	5.73
8	5.01	5.52	7.96	8.91	4.01	4.03	7.24	6.77
9	4.99	5.44	5.36	5.84	5.10	5.16	6.32	6.70
10	5.94	5.55	4.50	5.03	3.90	4.03	5.39	5.55
11	5.21	5.34	4.47	4.81	3.71	3.97	6.62	6.15
12	5.27	5.33	7.43	6.46	5.64	5.41	6.57	6.72
Means	5.809	5.817	5.911	6.219	4.462	4.666	6.189	6.540
	5.813		6.065		4.564		6.364	

<sup>a</sup>Averaged over five 96-second measurement intervals.

<sup>b</sup>Averaged over two 4-minute measurement intervals.

From these data, a Fourier analysis was conducted, and amplitude ratio and phase were computed for the subject's input/output, at each of the six forcing function frequencies.

The predominant differences found in the data are the measured gains. For each trial analyzed, therefore, the amplitude ratios for each forcing function frequency were averaged. Further averages were taken over the five short trials and two long trials, and these data were entered in table 6. An analysis of variance showed the only significant effect to be that of the four conditions of performance criteria.

**CENTIMETER TOLERANCE BAND COUNTS.**—Since in one of the experimental conditions the subjects were requested not to allow the display bar to deviate more than 1 centimeter from the center, it is of interest to determine how often this tolerance band was exceeded for each experimental condition. Therefore, the digital computer was programmed to test each 1/2-second sample for five short trials and two long trials for each experimental condition for display deviations exceeding 1 centimeter. The number of counts thus made were converted by dividing by the total number of samples and multiplying by 100 percent. The percent centimeter tolerance band counts for each trial analyzed are entered in table 7. An analysis of variance showed only the effect of performance criteria to be statistically significant.

**CORRELATION COEFFICIENT.**—As a possible test of the degree of linearity of the human operator's transfer characteristic, a product-moment correlation coefficient was computed. For each trial for which data were converted to digital form, a list of input data

TABLE 6.—AVERAGE GAIN

Subject	Condition 1		Condition 2		Condition 3		Condition 4	
	Short <sup>a</sup> trials	Long <sup>b</sup> trials	Short <sup>a</sup> trials	Long <sup>b</sup> trials	Short <sup>a</sup> trials	Long <sup>b</sup> trials	Short <sup>a</sup> trials	Long <sup>b</sup> trials
1	4.785	10.000	3.509	5.740	1.150	1.255	7.481	12.030
2	3.098	3.203	2.400	6.208	0.327	0.720	2.940	4.521
3	8.207	1.784	6.652	4.867	2.641	1.607	10.510	6.439
4	2.280	2.251	1.931	2.823	0.993	0.989	1.717	1.781
5	3.906	3.317	3.691	4.010	4.018	3.491	4.343	4.735
6	2.329	4.221	1.731	4.298	1.602	1.834	3.554	5.627
7	6.893	4.677	4.381	4.444	2.262	4.728	7.630	6.991
8	3.466	3.534	4.484	5.723	1.040	1.103	4.655	4.132
9	2.364	2.726	3.409	2.485	1.412	1.108	8.243	2.505
10	3.731	5.857	2.696	3.589	0.949	1.250	5.409	10.210
11	6.117	6.063	5.698	4.842	2.582	1.660	12.890	4.152
12	9.909	3.029	6.900	2.551	11.230	4.266	11.050	5.414
Means	4.757	4.222	3.957	4.298	2.517	1.834	6.702	5.628
	4.490		4.128		2.176		6.165	

<sup>a</sup>Averaged over five 96-second measurement intervals.<sup>b</sup>Averaged over two 4-minute measurement intervals.TABLE 7.—CENTIMETER TOLERANCE BAND COUNTS  
(PERCENT OF TOTAL POSSIBLE COUNTS)

Subject	Condition 1		Condition 2		Condition 3		Condition 4	
	Short <sup>a</sup> trials	Long <sup>b</sup> trials	Short <sup>a</sup> trials	Long <sup>b</sup> trials	Short <sup>a</sup> trials	Long <sup>b</sup> trials	Short <sup>a</sup> trials	Long <sup>b</sup> trials
1	38.12	18.00	50.06	18.00	78.01	64.21	29.72	2.82
2	22.54	13.67	42.76	22.56	75.91	25.60	26.85	13.02
3	15.14	27.22	9.50	9.87	40.88	23.10	5.52	7.27
4	53.59	39.59	64.64	46.31	71.49	57.30	49.28	29.26
5	12.04	20.61	11.05	35.03	8.51	20.17	4.97	18.44
6	45.52	22.44	52.82	27.81	61.77	42.34	23.20	15.45
7	22.43	9.33	39.89	19.96	60.33	27.98	11.16	5.64
8	39.12	25.92	47.96	38.50	65.75	58.72	27.73	18.76
9	40.99	46.96	29.17	34.49	55.47	61.39	11.16	33.84
10	39.34	14.53	54.92	32.86	83.54	69.96	27.51	5.21
11	16.24	8.13	17.02	8.89	41.55	41.87	10.94	12.15
12	4.86	22.89	31.27	39.48	7.07	18.33	5.86	13.56
Means	29.16	22.44	37.59	27.81	54.19	42.42	19.49	15.45
	25.80		32.70		48.30		17.47	

<sup>a</sup>Averaged over five 96-second measurement intervals.<sup>b</sup>Averaged over two 4-minute measurement intervals.



TABLE 8.—CORRELATION COEFFICIENTS

Subject	Condition 1		Condition 2		Condition 3		Condition 4	
	Short <sup>a</sup> trials	Long <sup>b</sup> trials	Short <sup>a</sup> trials	Long <sup>b</sup> trials	Short <sup>a</sup> trials	Long <sup>b</sup> trials	Short <sup>a</sup> trials	Long <sup>b</sup> trials
1	0.755	0.657	0.796	0.749	0.676	0.666	0.742	0.609
2	.692	.493	.715	.443	.493	.347	.764	.596
3	.564	.362	.687	.604	.868	.487	.558	.517
4	.869	.851	.532	.706	.914	.921	.867	.891
5	.452	.639	.571	.578	.520	.696	.570	.641
6	.708	.658	.739	.652	.726	.726	.781	.691
7	.727	.667	.686	.660	.882	.824	.709	.654
8	.854	.820	.473	.420	.922	.929	.756	.761
9	.809	.640	.779	.746	.859	.809	.780	.796
10	.731	.753	.820	.746	.713	.719	.799	.656
11	.784	.724	.815	.820	.893	.890	.678	.784
12	.642	.632	.605	.703	.614	.698	.587	.698
Means	0.716	0.658	0.685	0.652	0.757	0.726	0.716	0.691
	0.687		0.668		0.742		0.704	

<sup>a</sup>Averaged over five 96-second measurement intervals.

<sup>b</sup>Averaged over two 4-minute measurement intervals.

sampled at 1/2-second intervals and a list of subject output data sampled at 1/2-second intervals were available to form the correlation coefficient between the two lists. These data were averaged over five short trials and two long trials; the results were entered in table 8. An analysis of variance found no statistically significant effects.

**REVERSAL SCORES.**—Reversal scores were computed for the five short trials only, for each experimental condition. The reversal scores were computed for three tolerance band levels (0.0 in., 0.1 in., and 0.2 in.); both the display and control deviations had to exceed the tolerance-band level before a reversal could be counted at a given 1/2-second sample. The totals over five short trials are entered in table 9. No statistically significant differences were found for the 0.0 inch and 0.1 inch tolerance bands. The data for the 0.2 inch tolerance band was not analyzed since very few counts were recorded.

**NEWMAN-KEULS TESTS.**—No inferences will be drawn about differences between experimental conditions where the previous analyses of variance have shown no statistical significance. However, where statistical significance was found, a further statistical test is possible regarding the difference between treatment means. Since the only statistical significance was on the effect of the experimental conditions of performance criteria, further tests were limited to the comparison of the differences between the means of conditions 1, 2, 3, and 4.

All possible Newman-Keuls tests (ref. 10) on the differences between the means of experimental conditions were computed. While the lowest display score occurred with

TABLE 9.—REVERSAL SCORES

[Each entry represents the sum for five 96-second measurement intervals]

Subject	Condition 1			Condition 2			Condition 3			Condition 4		
	0.0 in.	0.1 in.	0.2 in.	0.0 in.	0.1 in.	0.2 in.	0.0 in.	0.1 in.	0.2 in.	0.0 in.	0.1 in.	0.2 in.
1	37	5	0	46	7	1	41	1	1	49	2	0
2	59	3	1	52	2	0	199	10	0	60	1	1
3	86	3	1	77	0	0	24	0	0	86	1	0
4	39	2	0	97	33	13	5	0	0	34	3	1
5	80	4	0	62	0	0	54	1	1	74	0	0
6	69	6	0	71	10	0	92	20	2	64	1	1
7	48	2	0	47	3	3	21	1	0	57	1	0
8	28	0	0	114	25	4	10	0	0	56	2	0
9	55	2	1	51	1	0	19	0	0	31	1	1
10	45	8	4	32	1	0	42	0	0	36	1	0
11	51	0	0	38	0	0	15	0	0	66	0	0
12	79	1	0	89	8	1	64	0	0	86	0	0
Totals	676	36	7	776	90	22	577	33	4	663	13	4
Average per trial	11.27	0.60	0.12	12.93	1.50	0.37	9.62	0.55	0.07	11.05	0.22	0.07

condition 4, no statistical difference exists between condition 4 and conditions 1 and 2, but the display scores for this trio are significantly less than that for condition 3. Similarly, for the control and total scores, only those of condition 3 are significantly less than the remaining conditions. Of course, the total score has only explicit meaning for condition 3. For the average gain data, conditions 1 and 2 were not significantly different, but conditions 4 and 3 elicited significantly highest and lowest gain scores, respectively. Correspondingly, conditions 4 and 3 elicited the lowest and highest CM tolerance band counts, respectively, with condition 1 and 2 nonsignificantly different.

### TIME HISTORIES

Graphic time histories were collected during the eighth trial (middle of the second group of five short trials) to sample at a time when the subject was expecting to be controlling at a stable level of behavior. In viewing these recordings it is difficult to make statements which would hold for all subjects. However, it may be noted that many subjects tend to linger with the control stick in the neutral position whenever possible. For condition 2 the responses are somewhat square shaped, indicating a preference for particular levels of control deflection. Under condition 3, for which the subjects were instructed in amplifier-like control behavior, a few subjects did very well as instructed. However, a few subjects deviated widely from amplifier-like control to what amounts to occasional pulsing of the control stick.

## AMPLITUDE DISTRIBUTIONS

For five short trials, the digital sampled data were analyzed for the frequency with which the display and control signals were within 0.1-inch bands across the range of each signal. The amplitude distribution plots verify many of the observations of the time histories; the control deflection distributions have pronounced peaks, particularly for condition 3. For condition 2 there is a suggestion that the distribution is trimodal. The display distributions appear uniform in shape, with condition 4 most centrally distributed and condition 3 being the most broadly distributed. The plots of average control deflection as a function of display deviation show a linear response for midrange control deflections (although many time histories are suggestive of high nonlinearity), but show a distinct aversion by the subjects to respond proportionately to large display deviations (although questionnaire data show otherwise).

## OPTIMAL HUMAN CONTROL BEHAVIOR

QUADRATIC PERFORMANCE CRITERIA.—In condition 3 of this study the subjects were given instruction in appropriate amplifier-type control response, and they were also given knowledge of results with regard to the full nature of the applicable performance index. If the subject produced a control response proportional to the display deviation, on an instant-by-instant basis, the task was primarily one of finding the appropriate gain. The appropriate gain was approximately 1 to 1.2, although the region of the minimum is rather shallow. (Gain of 1.0 is defined as equal instantaneous amounts of displacement of the top of the control stick and display deviation).

The results of this study show a decided shift in control behavior for this task as compared with the other three. In particular, there is a distinct shift to lower gain than any other condition, and the resulting gain level is approximately that required by the task of minimizing the quadratic performance criterion. However, it must be noted that several subjects did not exhibit an appropriate shift in gain, or for that matter control in proportion to the display deviation, and only about half of the subjects performed the task well (i.e., approximately unity gain).

BOUNDARY CRITERIA.—In condition 2 of this study the subject's task was to keep the display bar between 1-centimeter boundaries on the display face. As the standard deviation of the forcing function was 1/2-inch, it was expected that the subject would have to do very little to meet the performance criterion. On the contrary, the subject's generated an average control score numerically greater than for any other condition (although not necessarily statistically significantly greater). Further, except for condition 3 where performance criteria required the subject to exceed the 1-centimeter tolerance band frequently, under condition 2 the subjects exceeded the 1-centimeter tolerance band more frequently on the average than any of the remaining conditions (although not statistically significant). These results are somewhat puzzling and require further investigation. However, subject's comments may offer a partial explanation: one-half of the subjects commented in the open-ended portion of a questionnaire that although the tolerance band was generous, they frequently found the display bar too close to the boundary to avoid exceeding the tolerance band.

MEAN-SQUARED-ERROR CRITERIA.—When tracking under condition 4 the subjects were given knowledge of results with regard to mean-squared error and were requested to minimize this score. The mean-squared-error score reduces with each increase in the subject's gain level, and under this condition the average gain was significantly greater than

any other condition. It is difficult to assess the degree of achievement since the required theoretical gain tends toward infinity; however, the shift in the subject's behavior was distinctly in the correct direction. There is no direct evidence as to the factors limiting the subject's gain level, but it is clear that the subjects were operating at display deviations small enough to create a difficult visual task.

As previously mentioned, several investigators have offered evidence that in tasks like condition 1, the human controller pursues a criterion similar to mean-squared error, that is, like condition 4. A difference between condition 1 and condition 4 occurred in the statistical significant differences in gain. This does not, however, refute that the behavior under condition 1 and condition 4 was alike, for the subjects could have been pursuing similar goals but performing better under condition 4 due to motivational factors supplied by the presence of knowledge of results. However, the plots of control deflection as a function of display deviation show a tendency for the subjects to make token responses to large display deviations. This is, of course, inconsistent with a mean-squared-error criterion. Further, based on the results of the current study, it would appear that the scores for condition 2 most closely parallel those collected under condition 1 (no significant differences were found between condition 1 and condition 2).

## HUMAN AMPLIFIER CONTROL BEHAVIOR

The describing function data collected in this study supports the evidence of other investigators (ref. 9) that the human operator's response can be fitted well with a pure gain model (with a reaction time delay, and of course, this is generally only applicable to rate-control dynamics as in the present case). Nevertheless it must be noted that a number of differences from amplifier-type behavior existed in these data. It is evident in comparing display and control oscillograph records that these signals are not simply proportionally related. Many of the records show a pronounced tendency to linger with the control stick in the neutral position, and otherwise to use a pulsing control. The peaked control distributions verify the tendency to linger with the control in the neutral position. The plots of average control deflection as a function of display deviation show a deviation from a straight-line characteristic for large display deviations. This may be an indication of part of the subject's strategy or technique since it is clear that he knows that under the experimental conditions the display bar will eventually come back to the region of the center, and for large display deviations it is likely to return soon. Further, under condition 3 where the subjects were specifically instructed in amplifier-type control response, many subjects responded in a clearly proportional manner, but several subjects deviated grossly from a linear response.

## IMPLICATIONS TO EXPERIMENTAL METHODOLOGY

It is clear that while no changes in forcing function or controlled elements were made during the course of data collection, several distinct shifts in human operator control behavior took place. It is evident that the same subjects can perform the same basic task differently. It follows that if we have an explicit performance criterion in mind, but do not indicate this to our subjects, it is very possible they will do something other than what we wish. And it is possible that they will not all do the same task—in spite of the efforts taken in this study some subjects behaved quite differently from other subjects.

The determination of human controller criteria, techniques, and strategies presents a dilemma: although we might wish to find the strategy the human operator would prefer based

on his own criteria, unless a subject group is uniform, we are forced to structure the performance criteria for the subjects to collect consistent data. And, of course, we are limited in knowledge of techniques for clearly expressing our criteria in a form usable to the human operator. The latter problem has direct practical consequences to the design of manual control systems.

## REFERENCES

1. Kalman, R. E.: When Is a Linear Control System Optimal? J. Basic Eng., Apr. 1964, pp. 51-60.
2. Obermayer, R. W.; and Muckler, F. A.: On the Inverse Optimal Control Problem in Manual Control Systems. NASA CR-208, 1965.
3. McRuer, D. T.; and Krendel, E. S.: Dynamic Response of Human Operators. WADC TR56-524, USAF Wright Air Development Center, 1957.
4. Roig, R. W.: A Comparison Between Human Operator and Optimum Linear Controller RMS-Error Performance. IRE Trans. Hum. Factors Elect., vol. HFE-3, 1962, pp. 18-22.
5. Leonard, T.: Optimizing Linear Dynamics for Human-Operated Systems by Minimizing the Mean-Squared Tracking Error. vol. 4, part 4, WESCON, 1960, pp. 57-62.
6. Elkind, J. I.: Characteristics of Simple Manual Control Systems. Tech. Rep. 111, MIT Lincoln Laboratory, 1956.
7. Russell, L.: Characteristics of the Human as a Linear Servo-Element. M.A. Thesis, MIT, 1951.
8. Miller, D. C.: The Effects of Performance-Scoring Criteria on Compensator Tracking Behavior. Human Factors in Electronics, HFE-6(1), 1965, pp. 62-65.
9. McRuer, D.; Graham, D.; Krendel, E.; and Reisener, W., Jr: Human Pilot Dynamics in Compensatory Systems: Theory, Models, and Experiments With Controlled Element and Forcing Function Variations. AFFDL-TR-65-15, Air Force Flight Dynamics Laboratory, 1965.
10. Winer, B. J.: Statistical Principles in Experimental Design. McGraw-Hill Book Co., Inc., 1962.

33  
N67-15874

## 23. HUMAN DECISION-MAKING IN MANUAL CONTROL SYSTEMS

*R.E. Thomas and J.T. Tou*  
*Battelle Memorial Institute*

A model is proposed to describe human decision making in manual control systems. The human operator in the control loop is represented by a model which will generate an output consisting of (1) operational control actions as a result of sequential decision-making, and (2) verbal statements or heuristics of how to achieve optimal control. In the proposed model, the operational control actions are generated by a search algorithm, and the verbal statements are determined through the detection of invariance of variables associated with minimum incremental "cost." At high levels of generality the verbal prescriptions for obtaining optimal control are called heuristics. These heuristics are considered as the verbal equivalents of those mathematical statements expressed in terms of "characteristic numbers" which are often used in dimensional analysis. By making use of the heuristics, adaptive features can be introduced into the search algorithm.

The proposed model will carry out sequential evaluation of the validity of the heuristics which are derived on the basis of past experience. By associating a Bayesian probability with the derived heuristic, this model simulates the evolution of a heuristic to a high subjective probability of being valid, even though the controller may have difficulty in executing the heuristic as shown by control actions which do not optimize the criterion function. An experiment is suggested for testing the validity of the proposed model.

Early work in the study of manual control from the point of view of control engineering dates back to the late 1940's. In 1947, Tustin (ref. 1) proposed a description of the nature of the operator's response in manual control and its implications for controller design. In 1948, Ragazzini (ref. 2) discussed engineering aspects of the human being as a servomechanism. During the past decade, research interest in mathematical characterization of the human operator in a control system has been greatly intensified. Among the mathematical models proposed are the quasi-linear model, the sampled-data model, the nonlinear model, and the time-varying model. Papers and reports describing these human operator models exist in abundance. Practically all the proposed models appearing in the literature represent attempts to provide a mathematical description of certain major characteristics of the human operator in the form of a transfer function. The various models are developed to describe the compensatory tracking behavior and the pursuit tracking behavior. Little work has been done on the mathematical modeling of the decision-making behavior of the human operator in a control system, although both the tracking behavior and the decision-making behavior are regarded as the major characteristics of the human in a manual control system. The fact that research in mathematical modeling of the human decision-making has been lagging far behind that of the human-tracking behavior is primarily due to the complexity and difficulty in the mathematical description of the decision-making behavior of the human controller. Physical laws may be used to characterize the tracking task but not the decision-making behavior, since the latter involves a mental process which deals with such aspects as thinking, experience, extrapolation, judgment, inference, and generalization.

In 1961, a study on the decision-making aspects of a human controller was conducted at the Columbus Laboratories of Battelle Memorial Institute by R. E. Thomas (ref. 3). To the authors' knowledge, this might represent the earliest attempt to study the decision-making behavior of a human controller from the engineering viewpoint. It was suggested that dynamic programming (refs. 4 to 6) would serve as a useful tool in studying the characteristics of the human controller. His work consists of a proposed set of test problems which would be presented to a human controller. The problems can be solved for their optimal solutions using dynamic programming or maximum principle (ref. 7). It was proposed that human subjects be repeatedly allowed to generate solutions to one of these problems in order to determine whether or not human subjects can "learn" optimal control by repeated trial. The only information given to the subject consists of the values of the state variables and the value of the objective functional after the completion of a trajectory. By trial and error the subjects would learn how to alter their trajectories in order to minimize the objective function. The performance of the subject could be compared with the optimal performance obtained from the dynamic programming solution to the control problem.

In the dissertation of H. W. Ray (ref. 8), the proposed approach of Thomas was carried out for one of the control problems. In general, it was found that approximately half of the subjects tested achieved nearly optimal control in approximately 20 repetitions of the problem. As emphasized by Thomas and Ray, this approach does not make any assumptions about how the human learns optimal control. It merely furnishes a way of making concise comparisons between the human's performance and mathematical optimal performance. Similar remarks may be made concerning the work of A. Rapaport (ref. 9) who studied a stochastic control problem proposed by Thomas. Stated in different terms, these investigations did not generate any mathematical model of how the human organizes his previous experience in order to improve his performance. Consequently, these investigations did not yield results that could be used to simulate the decision-making behavior of a human controller by means of an algorithm.

In this paper, we study the problem of determining a mathematical model which describes the manner in which a human operator exhibits on-line adaptive behavior in a control system. No repeated trial is permitted in the human operator's decision-making process while solving the optimal control problem. In other words, the model of the human operator is concerned with on-line learning. It is hoped that our work will be applicable not only to on-line learning but also to on-line learning in real time. The theoretical model is believed to be closely related to real-time control problems of the trajectory type that are of interest to space navigation. In the earlier work on human decision-making processes, regular state variables were used in the dynamic programming formulation, and no investigation was made to study how a human controller applies his decision-making process to achieve optimal control. In this paper, we introduce the use of probabilistic state variables to describe levels of heuristics in the dynamic programming formulation of human decision making. We are primarily concerned with how the human controller organizes his experience, extrapolates his past and present information, and applies his judgment to the control of an on-going control process.

The primary difficulty centers around the question of the extent to which a human controller can be characterized as a Bayesian decision-maker. Edwards (ref. 10) has shown that the human may be regarded as Bayesian, but he is not "efficient." That is, the human requires more data to alter his probabilities than would be required by a strict application of Bayes' theorem. Much greater difficulties in mathematical formulations are apparently associated with quantitative characterization of concept evolution, generalization, and the judgments of the human controller. Some of these difficulties are made explicit by Watanabe

(ref. 11). Our attempts to circumvent these difficulties in modeling human decision-making in manual control systems are discussed in this paper.

## CONCEPTUAL FRAMEWORK FOR MODELING MANUAL CONTROL

In the on-line generation of a solution to a control problem it is not expected that the solutions generated by human controllers will agree with the mathematical solutions. In fact, these differences suggest that three possible configurations are associated with a manual control problem, as illustrated in figure 1. These three configurations yield the mathematical solution, the human solution, and the model solution which is mathematical in form but aims to describe human performance. The mathematical solutions are obtained using control theory (ref. 7). A human solution may be obtained by simply requiring a human subject to control the system. The model solution requires the synthesis of various aspects, represented in mathematical terms, which can be related to observed human performance. It should be emphasized that the model solutions need not agree with every aspect of human control behavior. At present it would be desirable to have model solutions which exhibit some degree of correspondence with human performance. In the model described in this paper, the human operator is modeled in two respects: the generation of control strategy and the characterization of verbal behavior. His selection of control actions is modeled by a search technique to determine the control sequence which minimizes the incremental "cost." The verbal behavior of the human operator is modeled in terms of heuristic statements which will be used as guidelines for achieving optimal control. The aim of this portion of the model is to produce evolving mathematical expressions which can be related to the verbal statements made by the human controller.

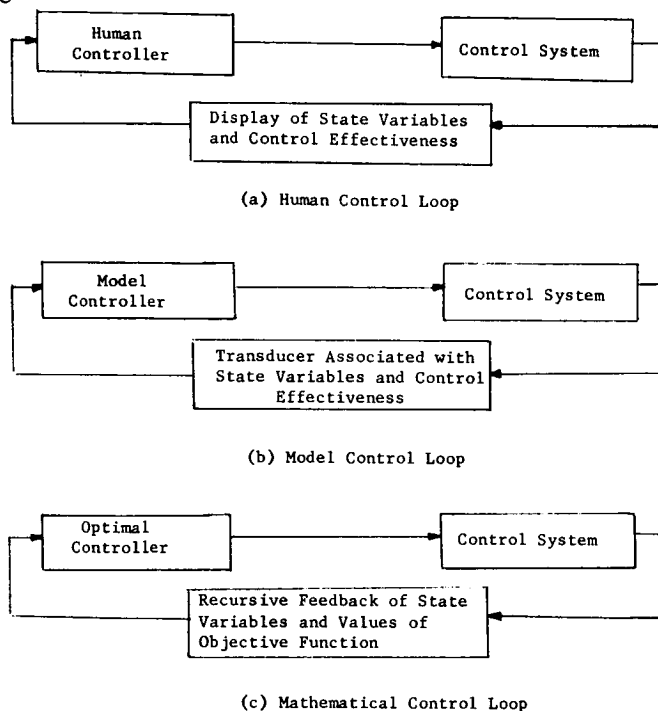


Figure 1.— Block diagrams describing three configurations of the control problem.

## SEARCH MODEL FOR HUMAN CONTROL OPERATIONS

Under the assumption that the human controller generates his solution to the control problem in an on-line fashion, it appears reasonable to suppose that the human will concern himself with "cost" increments. In an off-line, repeated-trial situation the human could be concerned with the accumulated total "cost" function. However, in the above context it is observed that, even though the human is instructed to minimize the cumulated total costs, he will attempt to do this by selecting control operations which minimize the cost increments between successive times. Thus, the human controller can be modeled by a search procedure that attempts to minimize successive cost increments. A simple search procedure is described as follows.



Let  $D$  denote a generalized "distance" to the goal so that  $\nabla D$  denotes the goal gradient. To minimize  $D$  one would like to go in the "direction" given by  $-\nabla D$ . Similarly, let  $\Delta F$  denote a cost increment, so that  $-\nabla(\Delta F)$  represents the "direction" of decreasing incremented costs. Initially, the human may not know the effect on  $D$  and  $\Delta F$  that would be produced by applying a particular control operation  $y \in M$  for  $\tau$  time units. As a result of selecting a control operation, one of the following would be obtained:

	D decreased	D increased
$\Delta F$ decreased	$[-\nabla D, -\nabla(\Delta F)]$	$[\nabla D, -\nabla(\Delta F)]$
$\Delta F$ increased	$[-\nabla D, \nabla(\Delta F)]$	$[\nabla D, \nabla(\Delta F)]$

The condition  $[-\nabla D, -\nabla(\Delta F)]$  would be regarded as desirable and the control value that leads to this result would be selected again and again until the goal is reached or one of the other conditions is encountered. If  $[-\nabla D, -\nabla(\Delta F)]$  is followed by  $[-\nabla D, \nabla(\Delta F)]$ , then a minimum in the incremental cost function has been crossed. As discussed later, the values of the state variables where such minimums occur would be stored for later processing. If the condition  $[-\nabla D, \nabla(\Delta F)]$  results from a control action, it would be assumed that the controller would select some other control action unless he is in the terminal stages of the control problem where the goal must be reached with whatever cost penalty is required. If the condition  $[\nabla D, -\nabla(\Delta F)]$  results from a control action, then the system is associated with a favorable cost increment, but there is an increase in the distance from the goal. If such an event occurs in the terminal stages, some other control action must be applied in an effort to obtain  $-\nabla D$ . If such an event occurs in an earlier stage, the controller could choose to continue this condition in order to arrive at a state from which the increased distance to the goal can be covered at a lower net cost. Unless the controller has learned that such a net decrease in cost would result, such a procedure would be a gamble. Consequently, in early stages of the control problem, we assume that if the condition  $[\nabla D, -\nabla(\Delta F)]$  occurs, the controller will choose some other control action. After the human controller has evolved heuristics for the control problem, the search algorithm must then be appropriately modified. The modification will be required because the controller must then search for those control actions which will accomplish the goal in accordance with his current heuristic. This kind of modification will depend on the generality of the heuristic used by the controller. If the condition  $[\nabla D, \nabla(\Delta F)]$  occurs, the system is receding from the goal with unfavorable cost increments. Clearly, in this case we assume that the controller chooses a different control value.

Based on the above procedure an algorithm could be written. By choosing the control actions in accordance with the prevailing condition, the controller would aim to maximize the number of occurrences of the condition  $[-\nabla D, -\nabla(\Delta F)]$ , and within these conditions he would seek those sequences of control values for which  $\Delta F$  is minimal so that  $-\nabla(\Delta F) = 0$ . It should be noted that if the  $\Delta F$  function has local minimums, the controller is assumed to ignore this feature and base his control actions on the first minimums encountered. It should also be noted that several different control operations may produce the desired condition. However, in most cases, only one of these is optimal. Thus, in implementing the search procedure, it would be necessary to select the optimal control action from a class of control actions. To obtain some correspondence with human behavior, a Bayesian method could be associated with these selections. In such an approach it would be assumed that the human would select that control operation which has the highest subjective probability of yielding the desired condition.

## MATHEMATICAL MODEL FOR VERBAL HEURISTICS

In this section an approach is proposed to obtain a mathematical model for the verbal heuristics of a human controller. In its simplest form the approach consists of a search for invariant "patterns" among "meter readings" presented as input data to the controller or among certain simple combinations of the "meter readings." Such input data are assumed to include the state variables and output variables of the control system, and the associated cost increments. The existence and complexity of the invariant patterns depend on both the dynamics of the control process and the form of the objective functional.

From experience, we have observed that a human controller often undergoes the evolution of his concepts through successive concern with numerical values, relevant variables, relevant combinations of variables, and possibly functional relations among combinations of relevant variables. The corresponding mathematical model should yield expressions which can serve as mathematical equivalents of the verbal heuristics generated by the human controller as he attempts to solve the control problem. The evolution of mathematical equivalents of the verbal heuristics may be carried out by making use of the concepts of dimensional analysis (ref. 12).

In brief, we assume that the human controller first makes an empirical analysis to discover which variables are relevant to the control problem. Following this he aims to express his discovery of invariant patterns with maximum generality. It is assumed that this will lead him to make verbal statements which correspond to the dimensionless ratios and products that may be obtained by dimensional analysis. Those verbal statements will identify the structure derivable from his initial search technique. These same statements will serve as a basis for generating the optimizing heuristics which constitute the controller's rules for how he believes the control can be optimized. As each heuristic is evolved, the controller is assumed to modify and adapt his search algorithm appropriately.

The mathematical basis of dimensional analysis is obtained from Buckingham's Pi-theorem (ref. 13). As stated by Brand (ref. 14) the theorem has the following form:

**Theorem.** Let  $x_1, \dots, x_n$  be positive measures of physical variables with a dimensional matrix of rank  $r = n-k$ :

$$\underline{A} = \begin{bmatrix} \underline{P} & \underline{R} \\ \underline{Q} & \underline{S} \end{bmatrix} \quad (1)$$

where  $\underline{P}$  is a nonsingular  $r \times r$  matrix. Then if  $f(x_1, \dots, x_n)$  is dimensionally homogeneous with respect to  $m$  reference units  $U_1, \dots, U_m$ , it follows that

$$f(x_1, \dots, x_n) = 0 \quad (2)$$

is equivalent to

$$f(1, \dots, 1, \pi_1, \dots, \pi_k) = 0 \quad (3)$$

in which the first  $r$  arguments are 1, and

$$\pi_i = x_1^{e_{i1}} \dots x_n^{e_{in}} \quad (i = 1, \dots, k) \quad (4)$$

are  $k$  independent and dimensionless quantities with the  $k \times n$  matrix of exponents given by

$$\underline{E} = (-\underline{Q}\underline{P}^{-1}, \underline{I}_k) \quad (5)$$

where  $\underline{I}_k$  is the  $k \times k$  unit matrix.

To apply this theorem to the modeling problem, let the matrix  $\underline{B}$  denote a subset of the new data obtained by the controller. The rows of  $\underline{B}$  contain the numerical values of the input variables at times when the incremental cost function is minimal. Thus, the rows of  $\underline{B}$  are generated sequentially as data accumulate. The columns of  $\underline{B}$  denote the input variables  $x_1, \dots, x_n$ . The matrix  $\underline{B}$  is examined for invariance as follows: If the control system is subject to certain control signal and the numerical values of the  $i$ th column of  $\underline{B}$  are approximately equal to a constant when  $\nabla(\Delta F) = 0$  but are fluctuating when  $\nabla(\Delta F) \neq 0$ , then the constant, for instance  $x_i^*$ , is called a "characteristic number" and the ratio  $(x_i/x_i^*)$  is taken to be a relevant variable. To supplement the above procedure dimensional analysis may be used to obtain dimensionless ratios and products. These dimensionless variables are examined in order to determine whether any of them are nearly constant when  $\Delta F$  is minimal, but are nonconstant when  $\Delta F$  is not minimal. If any such dimensionless variables are found, they are taken to be relevant dimensionless variables. These results are used to simulate human verbal performance. The characteristic numbers or the invariant patterns among dimensionless ratios and products obtained above may lead to some mathematical equivalent to the verbal form expressed by the human controller. It is observed that the associated relevant variables are equal to 1 when  $\Delta F$  is minimal. Thus, in this case the model controller would aim to maintain  $(x_i/x_i^*) = 1$  over the maximum possible time interval. The above results would be able to lead to a verbal equivalent of the following heuristic: Select those control actions which yield  $(x_i/x_i^*) = 1$  as early in the control process as possible and maintain this equality until either the terminal condition of the trajectory is reached or the attainment of this terminal condition requires that  $(x_i/x_i^*) \neq 1$ . These heuristics which are generated from observations, computations, and experience will serve as a guideline for the design of more efficient search algorithm through adaptation.

## VALIDITY MEASURE FOR VERBAL HEURISTICS

As the human controller evolves the heuristics described in the preceding section, it is asserted that his "confidence" in the validities of the verbal heuristics can be measured in terms of Bayesian probabilities. Depending on the human controller, varying levels of confidence would be expected when the heuristic is first generated, and these may be associated with prior subjective probabilities. As the controller gains further experience, these prior probabilities are assumed to be updated in accordance with the formalism given below. Because some verbalized heuristics may be incorrect, it is assumed that the associated Bayesian probabilities for these heuristics will decrease to such a level that the controller ultimately rejects the heuristic. On the other hand, if accumulated experience supports the validity of the heuristic, then the human controller will have high confidence in the heuristic, and the associated Bayesian probability will be approximately equal to 1. In contrast, however, the human controller may not have high confidence in his ability to carry out the

procedure prescribed by his own heuristic. That is, the human may know what to do but may not be able to do it. His inability to carry out the optimal solution is measurable in terms of the difference between the optimal total "cost" based on cost increments and his actual total "cost."

With these preliminaries we let

$$\mathcal{H} = \{H_\alpha\}, \alpha \in A, \quad (6)$$

be a class of heuristics indexed by the index set A. Let

$$X = \{p_\alpha\} \quad (7)$$

be a measure defined on  $\mathcal{H}$  with  $p_\alpha \in R$ , for every  $\alpha \in A$ , where  $R$  denotes the set of nonnegative rationals. Then  $p_\alpha$ ,  $\alpha \in A$ , may be written as  $n_\alpha/m_\alpha$  with  $n_\alpha, m_\alpha \in I$ , and  $I$  denoting the set of nonnegative integers. Now define the operation  $\oplus$  as follows:

$$p_\alpha \oplus p'_\alpha = \frac{n_\alpha + n'_\alpha}{m_\alpha + m'_\alpha} \quad (8)$$

Let

$$E = \{e_\alpha\} \quad (9)$$

where

$$e_\alpha = \begin{cases} 1/1 \\ 0/1 \\ 0/0 \end{cases}, \quad \alpha \in A \quad (10)$$

and the ratio assumed by  $e_\alpha$  depends on the objective functional. Let  $p_\alpha^0$  be the prior probabilities and update the probabilities by computing  $p_\alpha \oplus e_\alpha$  until convergence to 0 or 1 for each  $\alpha \in A$  is approximated. The value of  $e_\alpha$  is associated with the controller's judgment of whether the preceding period showed the heuristic  $H_\alpha$  to be supported (1/1), refuted (0/1), or irrelevant (0/0).

In some simple cases the human controller may have a prior subjective probability equal to 1 when he first "discovers" invariant relations among the state variables when the cost increment is minimal. However, such cases would be expected to be rare because, in general, the search for minimal cost increments can only yield approximations to the values of the associated state variables. These approximations, in turn, can only yield approximate invariant relations. Thus, the human controller will generally have some doubt about the suspected invariance of a relation. It is primarily for this reason that the preceding validity measure is needed.

## PROPOSED EXPERIMENTAL DESIGN

An experiment is designed to test the proposed model of human decision making in a manual control system. The human controller is required to generate an optimizing trajectory to pass through (or near) the levels  $V_0, \dots, V_n$  using the one-dimensional state variable called velocity, over a time interval  $[0, T]$ , as shown in figure 2. The transformation law is assumed to be

$$v_{k+1} = a v_k + y_{k+1} \quad (0 < a < 1) \quad (11)$$

with  $v_0 = V_0$  at  $t = 0$  and  $v_k = V_k$  at specified times  $t_k = m_k \tau$ ,  $t_0 = m_0 \tau = 0$ , and  $t_n = m_n \tau = T$ . The control variable  $y_{k+1}$  must satisfy

$$y_{k+1} = \begin{cases} -2 \\ -1 \\ 0 \\ 1 \\ 2 \end{cases} \quad (12)$$





for all  $k$ , and the optimal trajectory minimizes the objective functional:

$$I = \sum_{k=1}^n \left\{ \sum_{j=m_k \tau + 1}^{m_{k+1} \tau} \left[ (v_j - A_k)^2 + B y_j^2 \right] + C (v_k - V_k)^2 \right\} \quad (13)$$

The  $A_k$ ,  $k = 1, \dots, n$  are constant "coasting velocities" for each of the  $n$  subproblems defined by  $V_0, \dots, V_n$ . The term  $(v_j - A_k)^2$  shows that the contributions to the control functional by the state variable will be zero whenever  $v_j = A_k$ ,  $m_k \tau + 1 \leq j \leq m_{k+1} \tau$ . The constants  $B$  and  $C$  assign weights to the "power" contribution of  $y_j^2$  and the "miss-distance"  $(v_k - V_k)$  at the end of each subproblem.

The control subproblems may be classified into the four types listed in table 1.

TABLE 1. —A CLASSIFICATION OF THE SUBPROBLEMS FOR THE EXPERIMENT

Type I:		Final velocity exceeds initial velocity coasting level between initial and final velocity ( $V_k < A_k < V_{k+1}$ )
Type II:		Initial velocity exceeds final velocity coasting level between initial and final velocity ( $V_k < A_k < V_{k+1}$ )
Type III:		Coasting level exceeds initial and final velocity ( $V_k < A_k, V_{k+1} < A_k$ )
Type IV:		Initial and final velocity exceeds coasting level ( $V_k > A_k, V_{k+1} > A_k$ )

The human controller will not be informed of the existence of the coasting velocities. It is expected that his attempts to minimize the incremental costs will lead him to "discover" a coasting velocity. It is further expected that such a discovery would be verbalized and communicated to the second controller assumed to be starting a similar problem. If the subject controller verbalizes his discovery in terms of a numerical value for the coasting level for the current subproblems, this statement is called a "solution." If the subject asserts that the numerical value for the coasting velocity holds for all subproblems (and he acts accordingly),

this verbal statement will be called an incorrect "policy." The error of the policy must be discovered by the subject, however. After encountering a sequence of subproblems of types I and II, he is expected to discover that each subproblem has its own coasting velocity; it is expected that he will verbalize this discovery in a nonnumerical form. Such a verbalization will be called a heuristic and the expected form of the statement would be equivalent to the following:

"Go toward the terminal velocity until a coasting level is found which yields zero 'cost' increments. Stay at that level as long as possible."

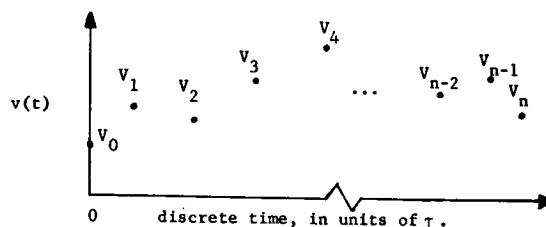


Figure 2.—Description of the test problem.

The above heuristic would not be correct for subproblems of types III and IV. Thus, after the subject has gained some confidence in the validity of the heuristic associated with subproblems of types I and II, he would be presented a mixture of types I, II, III, and IV. It is expected that he will downgrade the above heuristic and replace it by a statement equivalent to the following: "Go to the coasting level and stay there as long as possible."

It is expected that this sequence of problems will ultimately lead the human to assert high confidence in the validity of his final heuristic, although he may have great difficulty in determining the correct time at which the coasting velocity level should be abandoned in the terminal stages of each subproblem. By associating Bayesian probabilities with the verbal statements, it is expected that some measure of the human's confidence level can be obtained.

## CONCLUSIONS

This paper presents the conceptual framework which is being developed to obtain a model for human decision-making in control systems. The operational control actions are to be generated by a search algorithm which is based on choosing that control operation which minimizes "cost" increments. The verbal statements of the human controller may be used as guidelines or heuristic objective functions for achieving optimal control. At high levels of generality these verbal statements are called heuristics and are corresponding to the "characteristic numbers" or invariant patterns which are associated with minimum incremental "cost." Because the human controller can detect only approximate invariance among the variables, his "confidence" in the heuristics may be measured in terms of Bayesian probabilities. With the accumulation of experience these probabilities are updated and approach 1 or 0 as the associated heuristic is found to be valid or invalid.

Computational algorithms for the characterization of human decision-making in a control system based upon the above conceptual framework are in the process of development, and will be reported in a future paper.

## REFERENCES

1. Tustin, A.: The Nature of the Operator's Response in Manual Control and its Applications for Controller Design. J. Inst. of Elec. Eng. (London), vol. 94, 1947, pp. 190-202.
2. Ragazzini, J. R.: Engineering Aspects of the Human Being as a Servo-Mechanism. Presented at the American Psychological Association Meeting, 1948.

3. Thomas, R. E.: Development of New Techniques for Analysis of Human Controller Dynamics. MRL-TDR-62-65, Behavioral Sciences Laboratory, 1962.
4. Bellman, R. E.: Dynamic Programming. Princeton University Press, 1957.
5. Howard, R. A.: Dynamic Programming and Markov Processes. Technology Press and John Wiley & Sons, 1960.
6. Tou, J. T.: Optimum Design of Digital Control System. Academic Press, 1963.
7. Tou, J. T.: Modern Control Theory. McGraw-Hill Book Co., Inc., 1964.
8. Ray, H. W.: The Application of Dynamic Programming to the Study of Multistage Decision Processes in the Individual. Ph.D. Dissertation, Ohio State University, 1963.
9. Rapaport, A.: A Study of Human Control in a Stochastic Multistage Decision Task. Behavioral Sci., vol 11, 1966, pp. 18-32.
10. Edwards, W.: Optimal Strategies for Seeking Information: Models for Statistics, Choice Reaction Times, and Human Information Processing. Journal of Math. Psychol., vol. 2, 1965, pp. 312-329.
11. Watanabe, S.: Information-Theoretical Aspects of Inductive and Deductive Inference. IBM J. Res. and Devel., 1960, pp. 208-230.
12. Pankhurst, R. C.: Dimensional Analysis and Scale Factors. Reinhold Publishing Corp., 1964.
13. Buckingham, E.: On Physically Similar Systems. Phys. Rev., vol. 4, 1914, pp. 354-376.
14. Brand, L.: The Pi Theorem of Dimensional Analysis. Archive for Rational Mechanics and Analysis, vol. 1, 1957, p. 33.

N67-15875

## 24. DIFFERENTIAL GAMES AND MANUAL CONTROL

Sheldon Baron  
Electronics Research Center, NASA

Variational methods are used to solve a particular pursuit-evasion differential game. The problem involves the determination of optimal strategies for both the pursuer and evader. The performance measure is the miss distance at some fixed terminal time. Both pursuer and evader have limited control energy. The performance of a trained research pilot, for both single- and two-axis control tasks is compared with that of the optimal pursuer. State vector display and "quicken" display are discussed. A film showing typical pilot performance is presented. The results suggest that differential game problems could be quite useful in the study of manual control.

The theory of differential games was initiated by Isaacs in 1954 (ref. 1). It was later studied in greater detail by Fleming and Berkowitz (refs. 2 and 3). Recently, Ho, Bryson, and the author applied variational techniques to solve a class of differential games (ref. 4). In an effort to demonstrate the results of reference 4, a simulation of a simple pursuit-evasion differential game was conducted. As a matter of some interest, it was decided to compare the performance of a human pilot with that of an optimal pursuer. The results and some implications of this comparison are the subject of this paper. It should be emphasized that these results, from a manual control standpoint, are not extensive since the primary purpose of the research was the study of a class of differential games; nevertheless, they do suggest that differential game problems could be useful in the study of manual control.

### WHAT IS A DIFFERENTIAL GAME?

A differential game problem may be stated briefly, and roughly, as follows (a rigorous, precise formulation may be found in ref. 3):

Given the payoff

$$J(\underline{u}, \underline{v}) = \phi(\underline{x}(T), T) + \int_{t_0}^T L(\underline{x}, \underline{u}, \underline{v}, t) dt \quad (1)$$

and the constraints

$$\dot{\underline{x}} = f(\underline{x}, \underline{u}, \underline{v}, t) \quad \underline{x}(t_0) = \underline{x}_0 \quad (2)$$

$$\underline{u} \in U \quad \underline{v} \in V \quad (3)$$

determine the pair of feedback control laws



$$\underline{u}^0 = \underline{k}(\underline{x}(t), t) \in U \quad (4)$$

$$\underline{v}^0 = \underline{\bar{k}}(\underline{x}(t), t) \in V \quad (5)$$

satisfying the relation

$$J(\underline{u}^0, \underline{v}) \leq J(\underline{u}^0, \underline{v}^0) \leq J(\underline{u}, \underline{v}^0) \quad (6)$$

for arbitrary  $\underline{u} \in U$ ,  $\underline{v} \in V$ .

In the parlance of game theory,  $J$  is called the payoff,  $\underline{x}$  the (vector) state of the game and  $\underline{u}$  and  $\underline{v}$  are called (vector) strategies and are restricted to certain sets of admissible strategies,  $U$  and  $V$ , which depend in general, on the specific problem to be solved. If strategies  $\underline{u}^0$  and  $\underline{v}^0$  can be found such that equation (6) is true, they are called optimal pure strategies, and the pair  $(\underline{u}^0, \underline{v}^0)$  is called a saddle-point of  $J$ . The payoff evaluated at the saddle-point,  $J(\underline{u}^0, \underline{v}^0)$ , is called the value of the game.

The class of problems in which the differential equations (2) are linear and the payoff equation (1) is quadratic was solved using variational methods in reference 4. A special case is discussed in the next section.

### A SIMPLE PURSUIT-EVASION DIFFERENTIAL GAME

The kinematic equations of motion for an interceptor and target in space may be written as

$$\left. \begin{aligned} \ddot{\underline{r}}_p &= \underline{f}_p + \underline{a}_p ; \quad \underline{r}_p(t_0) = \underline{r}_{p_0}, \quad \dot{\underline{r}}_p(t_0) = \dot{\underline{r}}_{p_0} \\ \ddot{\underline{r}}_e &= \underline{f}_e + \underline{a}_e ; \quad \underline{r}_e(t_0) = \underline{r}_{e_0}, \quad \dot{\underline{r}}_e(t_0) = \dot{\underline{r}}_{e_0} \end{aligned} \right\} \quad (7)$$

where  $\underline{r}$  represents the position vector of the body in three-dimensional space,  $\underline{f}$  is the external force per unit mass,  $\underline{a}$  is the control acceleration of the body and the subscripts  $p$  and  $e$  refer to pursuer and evader, respectively. If it is assumed that the altitude difference between the two bodies is small and we consider their relative position, the effect of external forces may be neglected and we obtain

$$\ddot{\underline{r}} = \ddot{\underline{r}}_p - \ddot{\underline{r}}_e = \underline{a}_p - \underline{a}_e \quad (8)$$

We take as a payoff for this game

$$J = \frac{a^2}{2} (\underline{r}(T) \cdot \underline{r}(T)) \quad (9)$$

that is, a measure of the miss distance at some fixed terminal time,  $T$ . The objective of the pursuer is to minimize the miss distance while the evader attempts to maximize it. The controls of both pursuer and evader are assumed to be constrained by the following relations:

$$\int_{t_0}^T \vec{a}_{\rightarrow p} \cdot \vec{a}_{\rightarrow p} dt \leq E_p^2(t_0) \quad (10)$$

$$\int_{t_0}^T \vec{a}_{\rightarrow e} \cdot \vec{a}_{\rightarrow e} dt \leq E_e^2(t_0) \quad (11)$$

Equations (10) and (11) may be thought of as constraints on the control energy available to the two players. It is intuitively clear, and readily proven, that under optimal play the evader will use all his energy. Similarly, it can be shown that if the pursuer has less energy than is required for capture<sup>1</sup>, or just enough energy to capture, he too will use all his energy in an optimal play of the game. We shall only consider such cases so that equations (10) and (11) may be replaced by the corresponding equality constraints

$$\int_{t_0}^T \vec{a}_{\rightarrow p} \cdot \vec{a}_{\rightarrow p} dt = E_p^2(t_0) \quad (12)$$

$$\int_{t_0}^T \vec{a}_{\rightarrow e} \cdot \vec{a}_{\rightarrow e} dt = E_e^2(t_0) \quad (13)$$

Then the differential game problem is to determine a saddle-point  $(\vec{a}_{\rightarrow p}^0, \vec{a}_{\rightarrow e}^0)$  of equation (9) subject to the constraints of equations (8), (12) and (13).

This problem may be solved by considering the payoff

$$J = \frac{a^2}{2}(\vec{r}(T) \cdot \vec{r}(T)) + \int_{t_0}^T \left\{ \frac{\vec{a}_{\rightarrow p}(t) \cdot \vec{a}_{\rightarrow p}(t)}{2c_p} - \frac{\vec{a}_{\rightarrow e}(t) \cdot \vec{a}_{\rightarrow e}(t)}{2c_e} \right\} dt \quad (14)$$

where  $c_p^{-1}$  and  $c_e^{-1}$  are Lagrange multipliers to be determined such that equations (12) and (13) are satisfied. The results of reference 4 may now be applied and, upon evaluating  $c_p$  and

<sup>1</sup>Capture is defined here as  $\vec{r}(T) = 0$ .

$c_e$ , one finds that the optimal controls and the minimax miss distance are<sup>2</sup>

$$\vec{a}_{p(e)}(t) = - \frac{E_{p(e)}(t_0)(T-t) \hat{\vec{r}}(t_0)}{\sqrt{\frac{(T-t_0)^3}{3}} \|\hat{\vec{r}}(t_0)\|} \quad (15)$$

$$\|\vec{r}(T)\| = \|\hat{\vec{r}}(t_0)\| - (E_p(t_0) - E_e(t_0)) \sqrt{\frac{(T-t_0)^3}{3}} \quad (16)$$

where  $\hat{\vec{r}}(t)$  is defined by

$$\hat{\vec{r}}(t) \triangleq \vec{r}(t) + (T-t)\dot{\vec{r}}(t_0) \quad (17)$$

Optimal strategies (feedback control laws) may be obtained from equation (15) by letting  $t_0 = t$ . The result is

$$\vec{a}_{p(e)}(t) = - \frac{E_{p(e)}(t)}{\sqrt{\frac{T-t}{3}}} \frac{\hat{\vec{r}}(t)}{\|\hat{\vec{r}}(t)\|} \quad (18)$$

with a corresponding minimax miss distance

$$\|\vec{r}(T)\| = \|\hat{\vec{r}}(t)\| - (E_p(t) - E_e(t)) \sqrt{\frac{(T-t)^3}{3}} \quad (19)$$

$E_p(t)$  and  $E_e(t)$  are just the energies remaining at time  $t$  and are calculated from

$$E_{p(e)}^2(t) = E_{p(e)}^2(t_0) - \int_{t_0}^t \vec{a}_{p(e)}(t) \cdot \vec{a}_{p(e)}(t) dt \quad (20)$$

The vector  $\hat{\vec{r}}(t)$  will be called the predicted miss. Given a relative position and velocity,  $\vec{r}(t)$  and  $\dot{\vec{r}}(t)$ , at time  $t$ , then  $\hat{\vec{r}}(t)$  is the relative position which would be obtained at time  $T$  if no further control were applied by either pursuer or evader. The quantity  $\|\hat{\vec{r}}(t)\|$  in equation (18)

<sup>2</sup>Norm notation is used to denote the length of a vector, that is,  $\|\underline{y}\| = (\underline{y} \cdot \underline{y})^{1/2}$ .

is just a unit vector in the direction of the predicted miss. Hence, the minimax controls are applied in the opposite direction of the predicted miss and have magnitude depending only on the energy remaining and the time to go. (Note that as a result of the minus sign in equation (8), the evader's control is actually a positive feedback in the system, as one would expect.) From equation (19) we see that the minimum pursuit energy required for capture, under optimal play, is

$$E_p(t) = \frac{\|\hat{\mathbf{r}}(t)\|}{\sqrt{\frac{(T-t)^3}{3}}} + E_e(t) \quad (21)$$

An interesting special case of the above results is the following: let the pursuer and the target be on a nominal collision course with range  $R$  and closing velocity  $V_c = R/(T-t)$ . Let  $r_x$  represent the lateral deviation from the collision course (fig. 1) and let the pursuer have just enough energy to capture at time  $T$ . Then, for small lateral deviations  $r_x = R\sigma$  and the optimal pursuit strategy according to equation (15) is

$$a_{p_x}(t) = - \frac{E_p(t)}{\sqrt{\frac{(T-t)^3}{3}}} \frac{V_c \dot{\sigma} (T-t)^2}{\|\hat{\mathbf{r}}(t)\|} \quad (22)$$

Substituting for  $\|\hat{\mathbf{r}}(t)\|$  from equation (21) yields

$$a_{p_x}(t) = - \frac{3V_c \dot{\sigma}}{1 - \frac{E_e(t)}{E_p(t)}} \quad (23)$$

which is simply proportional navigation with an effective navigation constant which depends on the energies of both players.

Note that although the above problem has been interpreted as a pursuit-evasion game, one could also interpret it simply as a problem of controlling, in a specified manner, several externally disturbed double integrator plants. The disturbance in this case is not a random disturbance, but rather, the worst possible disturbance in a class of admissible disturbances. In this context it should be pointed out that by a relatively straightforward extension of the results and techniques of reference 4, one can obtain a solution to the problem with a payoff

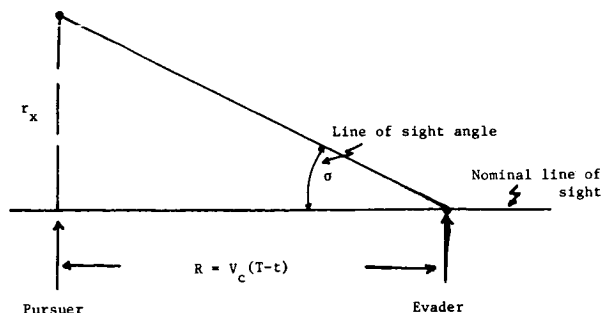


Figure 1.—Geometry of proportional navigation.

$$J = \frac{a^2}{2} (\vec{r}(T) \cdot \vec{r}(T)) + \int_{t_0}^T \left\{ \frac{\vec{r}(t) \cdot \vec{r}(t)}{2} + \frac{\vec{a}_p(t) \cdot \vec{a}_p(t)}{2c_p} - \frac{\vec{a}_e(t) \cdot \vec{a}_e(t)}{2c_e} \right\} dt \quad (24)$$

However, in the present investigation, the problem with payoff given by equation (24) is not considered, since this payoff did not seem to be consistent with the pursuit-evasion interpretation.

## SIMULATION

**ANALOG MECHANIZATION.**—Two particular cases of the above problem were simulated on an analog computer. Both cases involved planar motion. However, in the first case, two-axis control was required, whereas, in the second case, which corresponds to the proportional navigation situation described above, only single-axis control was necessary. The values for the initial conditions were selected for convenience and do not necessarily correspond to any realistic situation. The initial values along with the minimax miss distance, for each case, are given in table 1.

An interesting development occurred in attempting to mechanize the optimal solution on the analog computer. In the first attempt at accomplishing this task, equations (8), (18), and (20) were mechanized directly. The results of this mechanization deviated considerably from the analytically obtained optimal solution. The difficulty, from an analog mechanization standpoint, is apparent upon examination of table 1. If the y-component of the miss distance is considered, one sees that the analog computer will encounter resolution difficulties; when the computer is scaled to accommodate the initial miss distance of 2832 feet, the terminal miss distance, 2.4 feet, is represented by a voltage in the noise range of the computer. The effects of the limited resolution in this formulation were most pronounced in the terminal phase of the solution. While feedback control might normally be expected to reduce these errors, it must be remembered that the evader's control introduces a positive feedback loop. It was, in fact, demonstrated by generating the open-loop optimal trajectories that the feedback loop aggravated the problem.

Further examination of equations (8) and (18), along with table 1, indicates the means for overcoming the resolution difficulties. The procedure is to formulate the problem directly in terms of the predicted miss,<sup>3</sup> which for the y-component, has a much smaller dynamic range. The differential equation for the predicted miss is simply

$$\dot{\vec{r}} = (\vec{a}_p - \vec{a}_e)(T-t) \quad (23)$$

With the formulation the instantaneous position and velocity are calculated as open-loop outputs for display purposes only; the actual problem solution involves variables which present no resolution difficulties. The results of the analog mechanization for this formulation were in excellent agreement with the analytic results.

<sup>3</sup>It is interesting to note that parallel theoretical work associated with reference 4 led to the conclusion that the results for the general problem were most simply and meaningfully stated in terms of the predicted miss.

TABLE 1.—INITIAL CONDITIONS AND MINIMAX MISS DISTANCES  
FOR CASE 1 AND CASE 2

Case	$r_x(t_0)$ (ft)	$r_y(t_0)$ (ft)	$\dot{r}_x(t_0)$ ft/sec	$\dot{r}_y(t_0)$ ft/sec	$E_p^2(t_0)$ (ft) <sup>2</sup> /(sec) <sup>3</sup>	$E_e^2(t_0)$ (ft) <sup>2</sup> /(sec) <sup>3</sup>	$(T-t_0)$ sec	$\hat{r}_x(t_0)$ (ft)	$\hat{r}_y(t_0)$ (ft)	$r_x(T)$ (ft)	$r_y(T)$ (ft)	$\ r(T)\ $ (ft)
1	99	2832	0	-100	25	9	27	99	132	1.8	2.4	3
2	162	2700	0	-100	25	9	27	162	0	0	0	0

**INSTRUMENT DISPLAY.**—The prime consideration in designing the display for this study was that the pilot must be presented all the information necessary to generate the optimal pursuit strategy. Secondary considerations were that the display should be easy to read and reasonably realistic. The resulting display is shown in figure 2.

The scope at the top of the panel presented the relative position of the evader (the pursuer is located at the origin). A scale change was programed to improve resolution when the pursuer closed to within 50 feet in the y-direction and/or 20 feet in the x-direction. A light situated below the scope indicated the appropriate scale.

The vertical tape-instrument at the center of the panel displays predicted y-miss and instantaneous closing (relative) velocity (note that the instantaneous closing velocity and the predicted closing velocity are identical for this problem). The horizontal tapes present the same information for the x-components. The circular meters to the right and left of the tapes provide, respectively, pursuit energy remaining and time-to-go. The circular meter at the bottom of the panel indicates evasive energy remaining. The display of evasive energy was included in accordance with the ground rule, stated above, namely, that all information required for generation of the optimal pursuit strategy would be displayed. In the derivation of the optimal pursuit strategy, it was assumed that the evader's energy was known; thus, although the final expression for the pursuit strategy (eq. (18)) does not depend explicitly on  $E_e$ , it was decided to display this information.

If the information content of the display is examined, it is seen that the display may be interpreted as a state vector display and/or a "quickened" display. In the usual fashion, the quantities  $r_x$ ,  $r_y$ ,  $\dot{r}_x$  and  $\dot{r}_y$  may be considered the components of the "state" of the system and their display constitutes a "state vector display"; displaying the predicted miss, which is a linear combination of the state vector and constitutes a signal proportional to the desired control, corresponds to the so-called "quickened" display (ref. 5). However, the distinction between the two types of display, at least for this problem, seems somewhat arbitrary. As was seen in the above discussion, and in reference 4, the predicted miss may be taken as the state vector of the system, and then the distinction between state vector display and "quickened" display vanishes. In this regard, it is important to note that one can, and indeed should, include the energies remaining,  $E_p^2(t)$  and  $E_e^2(t)$ , and the time-to-go,  $(T-t)$ , in the state vector of the system. Hence, a display of acceleration command (i. e., eq. (18)) could also be considered a "quickened" display.

The above discussion is indicative of a more general point concerning "state vector" displays. Since the state representation of a system is, in general, not unique, there often exists considerable freedom in choosing a set of state variables. Different selections will

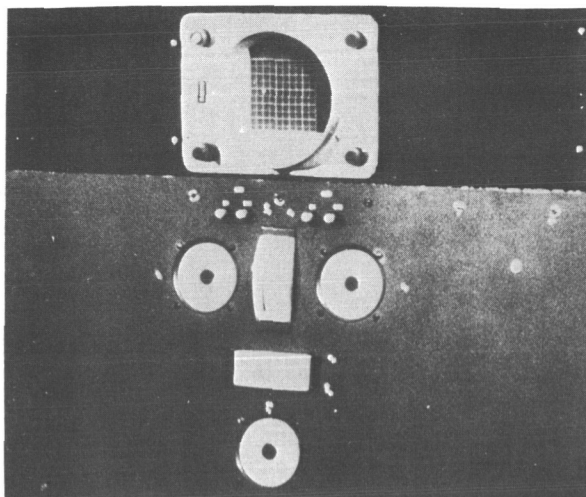


Figure 2.—Instrument display panel.

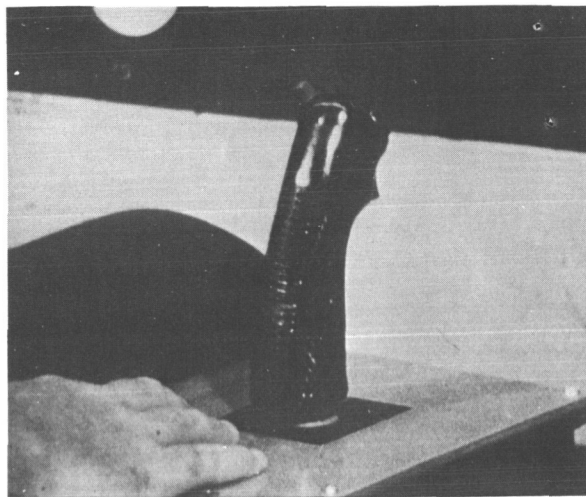


Figure 3.—Controller.

have different implications in terms of a state vector display and the proper choice of state variables could easily make the difference between a good and a poor display.

**CONTROLLER.**—The pilot's acceleration inputs were introduced through a grip-type two-axis side controller located at the end of the pilot's right arm rest. (Actually, the controller could have been used for three-axis inputs if such had been required.) A photograph of the controller is presented in figure 3. Acceleration inputs in the x-direction are actuated by rotating the grip laterally about pivot axis located slightly below the grip; y-acceleration inputs are actuated by motions of the hand about a pivot axis passing through the wrist.

The controller has physical stops which impose an amplitude constraint on the pilot's control inputs. However, no amplitude constraint was imposed in deriving the optimal pursuit strategy (to impose such a constraint complicates the problem considerably). To avoid the difficulties associated with the amplitude constraint, the full-scale deflection of the controller was initially scaled to correspond to twice the maximum acceleration ever used in the optimal pursuit strategy. After some preliminary runs the scaling was changed so that full deflection yielded an acceleration which was equal to the maximum optimal acceleration. The reason for this change will be discussed below.

## RESULTS AND DISCUSSION

A NASA research pilot served as a subject for the demonstrations of the pursuit-evasion game. His task was to minimize the miss distance at the terminal time, subject to the energy constraint; that is, he replaced the optimal pursuer. The evader's control remained an optimal evasive strategy. The corresponding runs for the first case are plotted in the  $\hat{r}_x$ - $\hat{r}_y$  plane in figure 4. The pilot's best performance was characterized by a miss distance of approximately 16 feet for the first case and a miss distance of approximately 15 feet for the second case. It should be noted that the pilot made about fifty runs during the course of one afternoon. The majority of these runs were for the first case. Some of the

more interesting qualitative results obtained from the study are discussed in the following paragraphs.

When the scope was used as a primary position information source for the pilot, his performance was quite poor. After learning to interpret the predicted miss quantities, the pilot improved his performance considerably. Part of this improvement may be due to reduced scan requirements. However, it seems clear that the major sources of improvement are improved resolution and the fact that the predicted miss represents information more pertinent to the required task than does the instantaneous relative position. It is interesting to note that the difficulties associated with the analog mechanization were indicative of the problems the pilot would encounter in trying to use instantaneous relative position information. Of more importance is the fact that the vector  $[\hat{r}_x, \hat{r}_y, E_p^2(t), E_e^2(t), (T-t)]$  is the minimal state representation of the system (if we insist on including the last three components as state variables), and therefore, excluding possible integrated displays, the minimal state vector display appears to be the best state vector display for this problem. The question of whether this is true in general seems worthy of further investigation.

The pilot tended to ignore the display of the evader's energy. This may have been due to the fact that he was not used to having this information available. Of course, as seen from equation (18), the pilot did not need the evader's energy to construct the optimal control.

The pilot's performance improved markedly after he was allowed to observe the optimal trajectory several times. He attributed this improvement to what he called a "pinball fix." In essence, this amounted to duplicating a correlation he noted between the energy remaining and the time-to-go for the optimal trajectory. This point is interesting from the standpoint of understanding, and possibly modeling, the pilot's learning process.

In the preliminary runs the pilot generally started by initially commanding zero acceleration. This placed him at a disadvantage since the initial acceleration for optimal pursuit is, in fact, the maximum commanded acceleration. The pilot was informed that optimal pursuit required commanding an initial acceleration. However, so long as he was required to judge the initial acceleration required, his performance did not substantially improve. In order to minimize the effects of the initial conditions, it was decided to scale full-scale deflections of the controller to correspond to the maximum commanded optimal accelerations. The pilot then started his pursuit with the controller against the stops and his performance improved considerably.

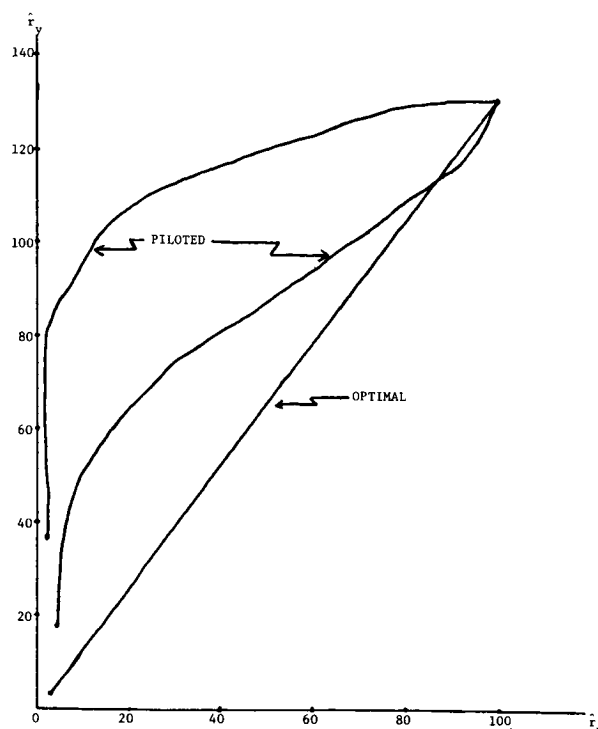


Figure 4.— Comparison of typical piloted trajectories with optimal trajectory for case 1.



The idea of "doing battle" with an intelligent adversary seemed to provide excellent motivation for the pilot. In fact, the "game" nature of the problem resulted in a large number of untrained "volunteers" for the experiment.

Several runs were tried with "unskilled" subjects. Their performance was, as could be expected, quite inferior to that of the pilot. As an additional cue, these subjects were displayed the optimal trajectory in  $\hat{r}_x$ - $\hat{r}_y$  coordinates and given the task of "tracking" this trajectory. It soon became apparent that a timing reference was needed for such a display to be effective. However, this approach was not pursued further.

## CONCLUSION

A simple pursuit-evasion differential game has been solved by variational methods. The results of a limited investigation comparing a pilot's performance with that of an optimal pursuer indicate that differential game problems could be useful in the study of manual control. Since optimal control problems are simply one-player differential games, it is apparent that the "game" will provide at least as much information, from a manual control standpoint, as will a similar optimal control problem; the "game" has the additional advantages of providing excellent motivation for the subject pilot and allowing the study of performance subject to worst case disturbances. In fairness, it should be noted that differential game problems will, in general, be more complicated theoretically than their optimal control counterparts.

## REFERENCES

1. Isaacs, R.: Differential Games I, II, III, IV. Res. Memo. RM-1391, RM-1399, RM-1411, RM-1468, Rand Corp., 1954-56.
2. Berkowitz, L. D.; and Fleming, W. H.: On Differential Games with Integral Payoff. Annals of Math. Study No. 39, Princeton University Press, 1957, pp. 413-435.
3. Berkowitz, L. D.: A Variational Approach to Differential Games. Advances in Game Theory, Annals of Math. Study No. 52, Princeton University Press, 1964, pp. 127-173.
4. Ho, Y. C.; Bryson, A. E.; and Baron, S.: Differential Games and Optimal Pursuit-Evasion Strategies. IEEE Trans. on Automatic Control, vol. AC-10, no. 4, Oct. 1965.
5. Obermayer, R. W.; and Muckler, F. A.: Modern Control System Theory and Human Control Functions. NASA CR-256, July 1965.

252  
N67-15876

## 25. DYNAMICAL SYSTEM MODELING OF HUMAN OPERATORS—A PRELIMINARY REPORT

*Peter L. Falb*  
*University of Michigan*  
*and*  
*Electronics Research Center, NASA*  
*and*  
*George Kovatch*  
*Electronics Research Center, NASA*

Results from control theory are applied to the development of dynamical system models for human operators in a control loop. Linear differential equation models are examined using a procedure of B. L. Ho to determine the model from estimates of the impulse response. The system order, the system matrix, and the system gains are adjusted. Nonlinear Volterra series models are also considered and an identification method of A. V. Balakrishnan is used to estimate the kernels.

The representation of human operator response characteristics in terms of transfer functions, ratios and cross-spectral densities, and describing functions, has been the subject of many investigations (see, for example, refs. 1 to 5). In this preliminary report, we suggest the possibility of using results from modern control theory in developing dynamical system, that is, differential, difference, and integral equation models for human operator behavior in a control loop, and we discuss several implementations of this possibility. In particular, we (1) examine linear models using a procedure of B. L. Ho (see refs. 6 and 7) to determine the model from estimates of the impulse response; (2) consider nonlinear Volterra series models and use an identification method of A. V. Balakrishnan (see ref. 8) to find the kernels; (3) apply the Ho identification procedure in some simulation studies and to experimental data previously obtained by J. I. Elkind, et al. (see ref. 2); and (4) suggest some experiments for testing the viability and usefulness of nonlinear models in some simple tracking tasks. Throughout, we have used the model adjustment technique as our basic analysis method; in other words, assuming a type of model, we have adjusted the model "parameters" until a satisfactory match between the operator output and the model output was obtained. Since this report is of a preliminary nature, our treatment is neither exhaustive nor complete; however, the results obtained do indicate considerable potential for the use of a dynamical system approach.

After making some brief general remarks on identification in the next section, we discuss linear models. Then, we examine nonlinear models and indicate some experiments, currently in process, relating to these models.

### REMARKS ON IDENTIFICATION

Loosely speaking, the identification problem may be phrased as follows: "determine" an unknown system on the basis of measured input-output data. More precisely, we deal with the following problem:

Given a physical system  $P$  and a set  $M$  of potential models (or representations) of  $P$ , find the element of  $M$  whose input-output behavior is closest to the input-output behavior of  $P$ . Here the physical systems that we shall consider are manned plants as illustrated in the block diagram of figure 1. We shall suppose that the plant (or vehicle) dynamics are known, that the operator is attempting to track the input  $i(t)$ , and the measured quantity  $z(t)$  is the true system output  $y(t)$  corrupted by additive noise  $w(t)$  (i.e.,  $z(t) = y(t) + w(t)$ ). Knowing  $i(t)$  and  $z(t)$ , we shall attempt to identify the "closed-loop" behavior of the manned plant. We note that it would also be possible to apply the techniques discussed here to the signals  $e(t)$  and  $m(t)$  in an effort to identify the "open-loop" behavior of the operator.

We consider several classes of models in the sequel, namely: (1) the class of linear time-invariant differential equations with sampled inputs (preceded by a delay to account for the operator "reaction time"); and (2) the class of (possibly) nonlinear functionals representable by "physically realizable" Volterra series. In other words, we examine models of the form

$$\left. \begin{aligned} \dot{\underline{x}}(t) &= \underline{A}\underline{x}(t) + \underline{b}u(t) \\ y(t) &= \underline{c}'\underline{x}(t) \end{aligned} \right\} \quad (1)$$

(where  $u(t)$  is  $i(t-\tau)$  for some delay  $\tau$ ) and of the form

$$y(t) = \sum_1^{\infty} \frac{1}{n!} \int_0^t \cdots \int_0^t h_n(\tau_1, \dots, \tau_n) i(t-\tau_1) \cdots i(t-\tau_n) d\tau_1 \cdots d\tau_n \quad (2)$$

More explicit details concerning the actual models are given in the sequel.

No matter what the class of models, our approach to the identification of the manned plant will be structurally the same. As illustrated in figure 2, the model is connected in parallel with the unknown manned plant and adjusted, on the basis of the "error,"  $e(t)$ , between the model output and the measured output, by the "identifier." The structure of the "identifier" will, of course, depend upon the particular class of models. In point of fact, most of our theoretical discussion will revolve around the description of the "identifier."

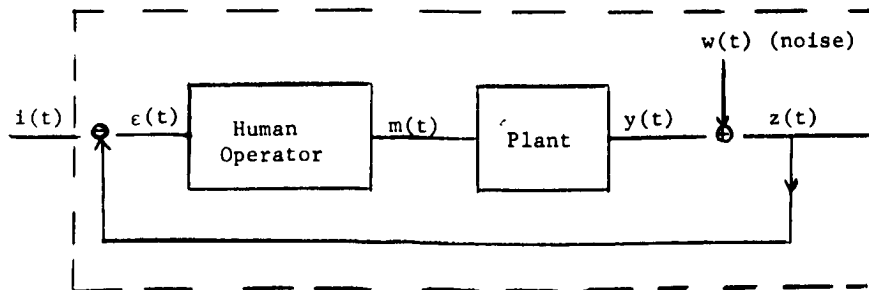


Figure 1.—Manned plant.

## LINEAR MODELS

Here we suppose that the manned plant can be described by a time-invariant linear differential equation preceded by a delay as indicated in figure 3. Assuming that the delay  $\tau$  is known<sup>1</sup>, the behavior of the model is characterized by the equation

$$\left. \begin{aligned} \dot{\underline{x}}(t) &= \underline{A} \underline{x}(t) + \underline{b}u(t) \\ y(t) &= \underline{c}'\underline{x}(t) \end{aligned} \right\} \quad (3)$$

where  $\underline{x}(t)$  is an  $n$ -column vector (called the state),  $\underline{A}$  is a constant  $n \times n$ -matrix,  $u(t)$  is the (delayed) scalar input, and  $\underline{b}$  and  $\underline{c}$  are  $n$ -column vectors. In view of some results of Kalman (see ref. 8), we shall assume that

$$\underline{c}' = (1 \ 0 \ \dots \ 0) \quad (4)$$

that  $\underline{A}$  is in "companion form," that is,

$$\underline{A} = \begin{bmatrix} 0 & 1 & 0 & \dots & 0 \\ 0 & 0 & 1 & \dots & 0 \\ \cdot & \cdot & \cdot & & \cdot \\ \cdot & \cdot & \cdot & & \cdot \\ \cdot & \cdot & \cdot & & \cdot \\ 0 & 0 & 0 & & 1 \\ a_1 & a_2 & a_3 & \dots & a_n \end{bmatrix} \quad (5)$$

and that  $\underline{b} \neq 0$ . (Actually we are supposing that eq. (3) is both completely controllable and completely observable as this is the only part of the system that can be determined from input-output measurements (see ref. 9).) We observe that the transfer function of equation (3) is given by

$$\underline{c}' (s\mathbf{I} - \underline{A})^{-1} \underline{b} \quad (6)$$

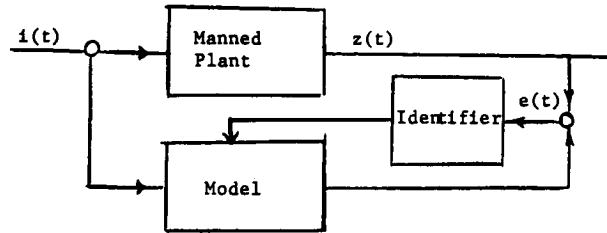


Figure 2.—Model connection in parallel with the unknown manned plant.

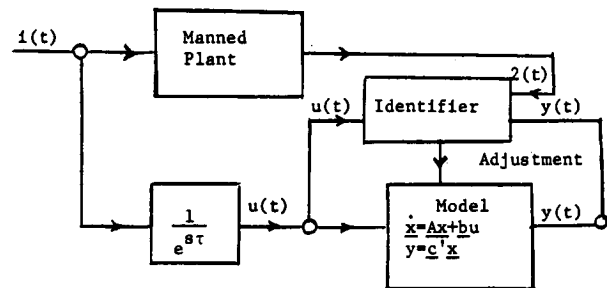


Figure 3.—Manned plant described by a time-invariant linear differential equation preceded by a delay.

<sup>1</sup>It is possible to estimate  $\tau$  by using several models in parallel (cf. ref. 2).

so that the overall transfer function of our model is given by

$$e^{-s\tau} \underline{c}' (s\underline{I} - \underline{A})^{-1} \underline{b} \quad (7)$$

This facilitates comparison with previous modeling methods.

Now our goal is the determination of the system order  $n$  and the parameters  $a_1, \dots, a_n$  and  $b_1, \dots, b_n$  (where the  $b_i$  are the components of  $\underline{b}$ ). With a view towards attaining our goal we observe that the impulse response function  $h(t)$  of equation (3), which is given by

$$h(t) = \underline{c}' e^{\underline{A}t} \underline{b} \quad (8)$$

can be expanded in a power series in  $t$  of the form

$$h(t) = \sum_0^{\infty} s_k t^k / k! \quad (9)$$

Conversely, given the expansion of equation (9) or equivalently the numbers  $s_k$ ,  $k = 0, 1, \dots$  (actually only a finite set of  $s_k$  is required) it is possible, using a method of B. L. Ho (see refs. 6 and 7 and the appendix), to determine  $n$ ,  $\underline{A}$ , and  $\underline{b}$ . This forms the basis for our identification procedure.

Again let us consider figure 3. On the basis of the measured output  $z(t)$  and the input  $u(t)$ , the identifier block adjusts the model order  $n$ , the model system matrix  $\underline{A}$ , and the model gain vector  $\underline{b}$ . The adjustment depends on a (running) estimate of the coefficients  $s_k$  of the expansion of the impulse response. To be more precise, we suppose that equation (9) can be approximated by

$$h(t) \sim \sum_0^N s_k t^k / k! \quad (10)$$

and we let  $\underline{s}$  denote the  $N+1$  vector of coefficients  $s_k$

$$\underline{s} = \begin{bmatrix} s_0 \\ s_1 \\ \cdot \\ \cdot \\ s_N \end{bmatrix} \quad (11)$$

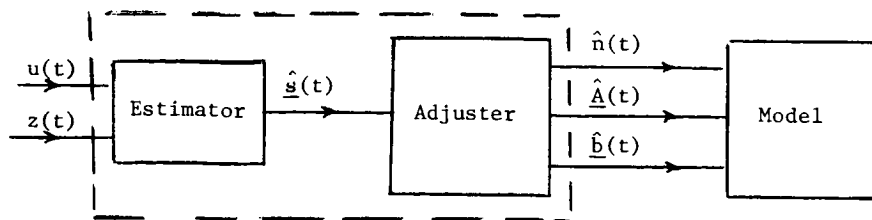


Figure 4.—Identifier.

Then, as illustrated in figure 4, the identifier consists of two parts, an estimator and an adjuster. The estimator generates estimates  $\hat{s}(\cdot)$  of  $\underline{s}$  based on  $u(\cdot)$  and  $z(\cdot)$ ; these estimates are the input to the adjuster. The adjuster computes estimates  $\hat{n}(\cdot)$ ,  $\hat{A}(\cdot)$ , and  $\hat{b}(\cdot)$  from  $\hat{s}(\cdot)$  using the B. L. Ho method. We observe that the procedure is suitable for both on- and off-line computations.

We use two types of estimators: one is based on direct least squares fitting and the other is based on a slightly modified Kalman filter. We shall examine each type of estimator in turn.

**DIRECT LEAST SQUARES FITTING.**—Let us suppose that  $T$  is the length of our sample interval and that the initial conditions are zero. Then, if there were no noise and if  $\underline{A}$ ,  $\underline{b}$ , and  $\underline{c}$  were the actual quantities characterizing the system, the output  $y(t)$  would be given by

$$y(t) = \int_0^t \underline{c}' e^{\underline{A}\tau} \underline{b} u(t-\tau) d\tau \quad (12)$$

$$= \sum_{k=0}^{\infty} s_k \int_0^t \frac{\tau^k}{k!} u(t-\tau) d\tau \quad (13)$$

Therefore, after setting

$$f_k(t) = \int_0^t \frac{\tau^k}{k!} u(t-\tau) d\tau \quad (14)$$

we write equation (13) as  $y(t) = \sum_{k=0}^{\infty} s_k f_k(t)$

Now, for practical reasons, we must approximate the impulse response by a finite sum; moreover, our measured output is the true output corrupted by noise. Thus, we are led to the problem of determining the estimate  $\hat{s}$  of  $\underline{s}$  which gives the least mean-square error over the interval  $(0, T)$ . In other words,  $\hat{s}$  is chosen in such a way as to minimize the quantity

$$\overline{e^2} = \frac{1}{T} \int_0^t e^2(t) dt = \overline{\left\{ z(t) - \sum_{k=0}^N s_k f_k(t) \right\}^2} \quad (15)$$

where

$$e(t) = \left\{ z(t) - \sum_{k=0}^N s_k f_k(t) \right\}$$

This is a standard least squares fitting problem, and the solution  $\hat{\underline{s}}$  is the solution of the equation

$$\underline{F} \underline{s} = \underline{z} \quad (16)$$

where  $\underline{F}$  is the  $N+1 \times N+1$  matrix whose entries  $F_{ij}$  are given by

$$F_{ij} = \overline{f_i f_j} = \frac{1}{T} \int_0^t f_i(t) f_j(t) dt \quad (17)$$

$i, j = 0, \dots, N$  and where  $\underline{z}$  is the  $N+1$  vector whose components  $z_i$  are given by

$$z_i = \overline{f_i z} = \frac{1}{T} \int_0^t f_i(t) z(t) dt \quad (18)$$

$i = 0, 1, \dots, N$ . Standard calculations can be made to determine confidence intervals for the estimate  $\hat{\underline{s}}$ .

**THE MODIFIED KALMAN FILTER.**<sup>2</sup>—The estimator discussed is recursive in nature and is better suited to handling potential time variation than the least squares estimator. Since the actual data are in digital form, we shall base our estimation of  $\underline{s}$  on the quantities  $u(j\delta)$ ,  $z(j\delta)$ ,  $j = 0, 1, \dots$ , where  $\delta$  is the time between measurements. For simplicity, we write  $u(j)$  and  $z(j)$  in place of  $u(j\delta)$  and  $z(j\delta)$ . The estimation begins with an initialization and then proceeds recursively.

The initial estimate  $\hat{\underline{s}}(1)$  is determined as a least squares estimate based on  $u(j)$ ,  $z(j)$ ,  $j=0, \dots, N$  via equation (16). From the estimate  $\hat{\underline{s}}(1)$ , we deduce via the Ho method, estimates  $\hat{\underline{A}}(1)$ ,  $\hat{\underline{b}}(1)$  of the system dynamics and then, an estimate  $\hat{\underline{x}}(1)$  of the state from the equation

<sup>2</sup>See reference 10.

$$\hat{\underline{x}}(1) = \sum_{j=0}^N \left( e^{\hat{\underline{A}}(1)\delta} \right)^{N-j} \left( \int_0^\delta e^{\hat{\underline{A}}(1)\tau} d\tau \right) \hat{\underline{b}}(1) u(j) \quad (19)$$

This completes the initialization.

The estimate of  $\underline{s}$  is updated in accordance with the following formula:

$$\hat{\underline{s}}(k+1) = \hat{\underline{s}}(k) + \underline{L}_k \underline{g}(N+k) r_k^{-1} \{ z(N+k+1) - \hat{\underline{c}}'(k) e^{\hat{\underline{A}}(k)\delta} \hat{\underline{x}}(k) - \underline{g}'(N+k) \hat{\underline{s}}(k) \} \quad (20)$$

where  $\underline{g}(N+k)$  is the  $N+1$ -vector with components  $g_i(N+k)$ ,  $i=0, \dots, N$  given

$$g_i(N+k) = \int_0^\delta \frac{\tau^i}{i!} u(N+k) d\tau \quad (21)$$

The  $N+1 \times N+1$ -matrix  $\underline{L}_k$  is the solution of the Riccati type equation

$$\underline{L}_k = \underline{L}_{k-1} - \underline{L}_{k-1} \underline{g}(N+k) \{ \underline{g}'(N+k) \underline{L}_{k-1} \underline{g}(N+k) + r_k \}^{-1} \underline{g}'(N+k) \underline{L}_{k-1} \quad (22)$$

the scalar  $r_k$  is the variance of the noise  $w(N+k)$  and is approximated by the sample variance of the numbers  $z(N+j) - \hat{\underline{c}}'(j) \hat{\underline{x}}(j)$ ;  $\hat{\underline{A}}(k)$  is the estimate of the system matrix at the  $k$ th step; and  $\hat{\underline{x}}(k)$  is the estimate of the state at the  $k$ th step and is computed by the formula

$$\hat{\underline{x}}(k) = e^{\hat{\underline{A}}(k)\delta} \hat{\underline{x}}(k-1) + \left( \int_0^\delta e^{\hat{\underline{A}}(k)\tau} d\tau \right) \hat{\underline{b}}(k) u(N+k) \quad (23)$$

if  $n(k) = n(k-1)$ , and by the formula

$$\hat{\underline{x}}(k) = \sum_{j=0}^{n+k-1} \left( e^{\hat{\underline{A}}(k)\tau} \right)^{N+k-1-j} \left( \int_0^\tau e^{\hat{\underline{A}}(k)\tau} d\tau \right) \hat{\underline{b}}(k) u(j) \quad (24)$$

if  $\hat{n}(k) \neq \hat{n}(k-1)$  where  $\hat{\underline{b}}(k)$  is the estimate of the gain vector and  $\hat{n}(k)$  is the estimate of the order at the  $k$ th step.

Although this estimator is not necessarily optimum and although we cannot give a convergence proof, our simulation studies indicate the practical effectiveness of the procedure, particularly in tracking parameter changes.



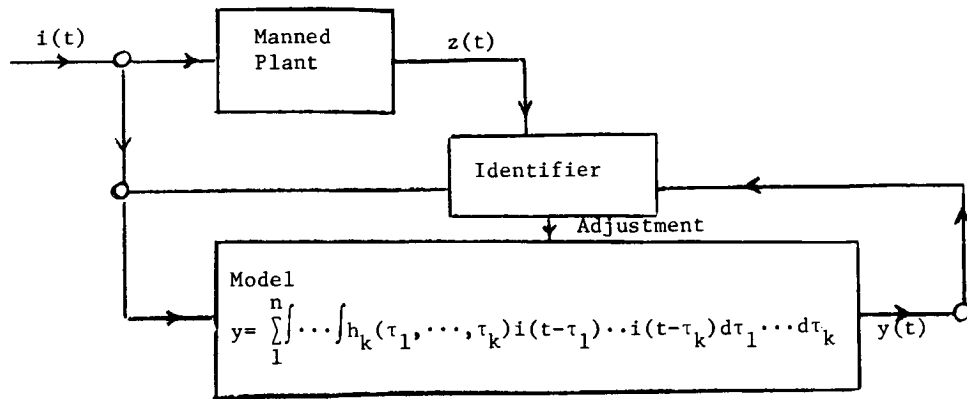


Figure 5.—Manned plant described by a time-invariant Volterra expansion of finite order.

## NONLINEAR MODELS

We suppose now that the manned plant can be described by a time-invariant Volterra expansion of finite order as indicated in figure 5. Thus, the behavior of the model, neglecting initial conditions, is characterized by the equation

$$y_m(t) = \sum_{k=1}^n \int_0^t \dots \int_0^t h_k(\tau_1, \dots, \tau_k) i(t-\tau_1) \dots i(t-\tau_k) d\tau_1 \dots d\tau_k \quad (25)$$

where the functions  $h_k(\tau_1, \dots, \tau_k)$ , which are called the  $k$ th order kernels, are the "parameters" of the model. Recalling that the output  $z(t)$  of the manned plant is given by  $y(t) + w(t)$  where  $w(t)$  is the noise and assuming that  $w(t)$  is "white gaussian," we let

$$E[w(t)^2] = 1/\sigma(t) \quad (26)$$

be the noise variance and we seek to determine the  $h_k(\dots, \dots)$  which minimize the quantity  $\epsilon(h_1, \dots, h_n)$  given by

$$\epsilon(h_1, \dots, h_n) = \int_0^T \{z(t) - y_m(t)\}^2 \sigma(t) dt \quad (27)$$

where  $(0, T)$  is the sampling interval (cf. ref. 8). An iterative procedure for determining a sequence  $(h_1^v, \dots, h_n^v)$  of "kernel vectors" such that

$$\inf \epsilon(h_1, \dots, h_n) = \lim_{v \rightarrow \infty} (h_1^v, \dots, h_n^v) \quad (28)$$

is given in reference 8. We illustrate that procedure here for the second-order case, that is, for  $n=2$ .

So we now suppose that the behavior of the model is characterized by the equation

$$y_m(t) = \int_0^t h_1(\rho) i(t-\rho) d\rho + \int_0^t \int_0^t h_2(\rho, \tau) i(t-\rho) i(t-\tau) d\rho d\tau \quad (29)$$

and we wish to determine a sequence  $(h_1^\vee, h_2^\vee)$  such that equation (28) is satisfied. On the basis of a steepest descent approach, it is shown in reference 8 that the following sequence accomplishes this task:

$$h_1^\vee(\rho) = \int_0^T z_v(t) i(t-\rho) \sigma(t) dt \quad (30a)$$

$$h_2^\vee(\rho, \tau) = \int_0^T z_v(t) i(t-\rho) i(t-\tau) \sigma(t) dt \quad (30b)$$

where

$$z_1(t) = z(t) \quad (31)$$

and

$$z_{v+1}(t) = z_v(t) - \delta_v x_v(t) \quad (32)$$

with

$$\begin{aligned} x_v(t) = & \int_0^t \left\{ \int_0^T z_v(s) i(s-\rho) \sigma(s) ds \right\} i(t-\rho) d\rho \\ & + \int_0^t \int_0^t \left\{ \int_0^T z_v(s) i(s-\rho) i(s-\tau) \sigma(s) ds \right\} i(t-\rho) i(t-\tau) d\rho d\tau \end{aligned} \quad (33)$$

and

$$\delta_v = \int_0^T \phi_v(t) x_v(t) \sigma(t) dt / \int_0^T \phi_v(t)^2 \sigma(t) dt \quad (34)$$

where

$$\phi_v(t) = \int_0^t \left\{ \int_0^T x_v(s) i(s-\rho) \sigma(s) ds \right\} i(t-\rho) d\rho$$

$$+ \int_0^t \int_0^t \left\{ \int_0^T x_v(s) i(s-\rho) i(s-\tau) \sigma(s) ds \right\} i(t-\rho) i(t-\tau) d\rho d\tau \quad (35)$$

and  $i(\cdot)$  is the input to our system. We observe that this iteration procedure forms the basis for our identification method and that a program to carry out the necessary computations (for the 2nd and 3rd order cases) is currently being developed.

Again let us consider figure 5. On the basis of  $z(t)$  and  $i(t)$ , the identifier block adjusts the kernels of the model via the iteration procedure indicated previously. The adjustment depends on an estimate of the noise variance which is made a priori (e.g., by running a zero input through the system for a sampling interval and using the resulting sample variance) and updated after each sampling interval on the basis of the variance of  $z(t) - y_m(t)$  over that interval, where  $y_m(t)$  is the model output. Now, the identifier does not work recursively relative to the sampling intervals. In other words, given  $z(t)$  and  $i(t)$  for  $t$  in  $(0, T)$  and  $(T, 2T)$ , the identifier will obtain an estimate of the kernels using integrals from 0 to  $T$  and then on the basis of the additional data over  $(T, 2T)$  obtain an estimate of the kernels using integrals from 0 to  $2T$ . Thus, the current model kernels depend upon all the past data.

Some simple experiments are currently being set up to test the usefulness of this modeling method. The experiments are based on the idea that the human operator will behave as an approximately optimal system in a simple control task (cf. ref. 4). For example, in one experiment the operator is attempting to control a double integral plant in a time-optimal fashion and it is expected that his behavior in this task will be adequately modeled by a 3rd order expansion. However, as yet, we have no substantive numerical results to report.

## CONCLUDING REMARKS

In this preliminary report, we have indicated several ways in which results from modern system theory can be applied to the modeling of human operator behavior with dynamical systems. As regards linear models, our approach allows the estimation of both the order and the poles of the human operator in contradistinction to approaches in which the order was fixed a priori and suitable poles chosen for the model. For the case of nonlinear models, we discussed a method for identification which we feel merits further investigation. In general, we admit our results are preliminary and fragmentary; however, we do think that the dynamical system approach has considerable potential in the modeling of human operator behavior in control tasks.

## APPENDIX - THE B.L. HO PROCEDURE<sup>3</sup>

Let  $s_0, s_1, \dots$  be the coefficients of the expansion of the impulse response of a time-invariant linear system. We wish to determine the system order  $n$ , the system matrix  $\underline{A}$ ,

<sup>3</sup>See references 6 and 7.

and the system gain vector  $\underline{b}$  from  $s_0, s_1, \dots$ . To this end we consider the  $r \times r$ -matrix  $\underline{s}_r$  given by

$$\underline{s}_r = \begin{bmatrix} s_0 & s_1 & \dots & s_{r-1} \\ s_1 & s_2 & \dots & s_r \\ \cdot & \cdot & & \cdot \\ \cdot & \cdot & & \cdot \\ \cdot & \cdot & & \cdot \\ s_{r-1} & s_r & \dots & s_{2r-2} \end{bmatrix} \quad (\text{A1})$$

and we let  $\rho(r)$  denote its rank. Since the  $s_k$  come from a finite dimensional system, it will follow (by the Cayley-Hamilton theorem) that there is an  $\hat{r}$  such that  $\rho(r) = \rho(\hat{r})$  for  $r \geq \hat{r}$ . We let  $n = \rho(\hat{r})$  (that  $n$  is actually the desired system order is proven in reference 6). Then we know that there are nonsingular matrices  $\underline{P}$  and  $\underline{Q}$ , which may be taken in triangular form, such that

$$\underline{P} \underline{s}_{\hat{r}} \underline{Q} = \begin{bmatrix} \underline{I}_n & \underline{0} \\ \underline{0} & \underline{0} \end{bmatrix} \quad (\text{A2})$$

where  $\underline{I}_n$  is the  $n \times n$  identity matrix. Letting  $\underline{e}' = (1 \ 0 \dots 0)$  and letting  $\tau \underline{s}_{\hat{r}}$  be the  $\hat{r} \times \hat{r}$  matrix given by

$$\tau \underline{s}_{\hat{r}} = \begin{bmatrix} s_1 & s_2 & \dots & s_{\hat{r}} \\ s_2 & s_3 & & s_{\hat{r}+1} \\ \cdot & \cdot & & \cdot \\ \cdot & \cdot & & \cdot \\ \cdot & \cdot & & \cdot \\ s_{\hat{r}} & s_{\hat{r}+1} & & s_{2\hat{r}} \end{bmatrix} \quad (\text{A3})$$

we have (theorem 1 of ref. 6):  $\{\tilde{\underline{A}}, \tilde{\underline{b}}, \tilde{\underline{c}}\}$  is a minimal realization of our system where  $\tilde{\underline{A}}$  is the upper left-hand  $n \times n$  block of the matrix  $\underline{P} (\tau \underline{s}_{\hat{r}}) \underline{Q}$ ;  $\tilde{\underline{b}}$  is the upper  $n$ -column vector of the column vector  $\underline{P} \underline{s}_{\hat{r}} \underline{e}$ ; and,  $\tilde{\underline{c}}$  is the left-hand  $n$ -row vector of the row vector  $\underline{e}' \underline{s}_{\hat{r}} \underline{Q}$ . If  $\tilde{\underline{A}}$ ,  $\tilde{\underline{b}}$  and  $\tilde{\underline{c}}$  are determined in this way, then  $\underline{A}$  and  $\underline{b}$  are given by

$$\underline{A} = \underline{T}^{-1} \tilde{\underline{A}} \underline{T}, \quad \underline{b} = \underline{T} \tilde{\underline{b}}$$



$$\tilde{\underline{b}} = \begin{bmatrix} \underline{b_1} \\ \underline{0} \\ \underline{b_2} \\ \underline{0} \\ \underline{b_3} \\ . \\ . \\ . \end{bmatrix} \begin{matrix} \} k_1 \\ \\ \} k_1 + k_2 \end{matrix} \quad \tilde{\underline{c}} = \begin{bmatrix} \underline{c_1} \\ \underline{c_2} \\ \underline{0} \\ \underline{c_3} \\ \underline{0} \\ . \\ . \\ . \end{bmatrix} \begin{matrix} \\ \} k_1 \\ \\ \} k_1 + k_2 \end{matrix} \quad (A7)$$

The final model is determined from  $\tilde{\underline{A}}$ ,  $\tilde{\underline{b}}$ , and  $\tilde{\underline{c}}$  by use of (A5). We note that the final system order  $n$  is given by

$$n = n_1 + k_1 + n_2 + k_1 + k_2 + \dots \quad (A8)$$

## REFERENCES

1. Bekey, G.: The Human Operator as a Sampled-Data System. IRE Trans. HFE-3, 1962, pp. 43-51.
2. Elkind, J.; Starr, E.; Green, D.; and Darley, D.: Evaluation of a Technique for Determining Time-Invariant and Time-Variant Dynamic Characteristics of Human Pilots. NASA TN D-1897, 1963.
3. McRuer, D.; Graham, D.; Krendel, E.; and Reisener, W.: Human Pilot Dynamics in Compensatory Systems—Theory, Models, and Experiments with Controlled Element and Forcing Function Variations. Wright-Patterson AFB, Tech. Rep. AFFDL-TR 65-15, 1965.
4. Pew, R.: Temporal Organization in Skilled Performance. Doctoral Dissertation, Univ. of Michigan, 1963.
5. Wierwille, W.: A Theory for Optimal Deterministic Characterization of Time-Varying Human Operator Dynamics. IEEE Trans. HFE-6, 1965, pp. 53-61.
6. Ho, B.; and Kalman, R.: Effective Construction of Linear State Variable Models From Input/Output Data. Proc. Third Annual Allerton Symposium on Circuit and System Theory, Allerton House, Univ. of Illinois, 1965.
7. Ho, B.: Doctoral Dissertation, Stanford Univ., 1966.
8. Balakrishnan, A.: Determination of Nonlinear Systems From Input/Output Data. Proc. of Princeton Conf. on Identification and Prediction, 1961.

9. Kalman, R.: Mathematical Description of Linear Dynamical Systems. J. SIAM Control, vol. 1, 1963, pp. 152-192.
10. Lee, R.: Optimal Estimation, Identification, and Control. MIT Press, Cambridge, Mass., 1964.

# **ANALYSIS AND DESIGN METHODS**



N67-15877

## 26. A "CRITICAL" TRACKING TASK FOR MAN-MACHINE RESEARCH RELATED TO OPERATOR'S EFFECTIVE DELAY TIME\*

H.R. Jex, J.D. McDonnell, and A.V. Phatak  
*Systems Technology, Inc.*

A closed-loop compensatory tracking task has been developed which yields a measure of the human operator's time delay characteristics while tracking, constrains his behavior to within very narrow limits, and provides a low variability indicator of the operator's tracking ability. The procedure is called the critical task because the operator is required to stabilize an increasingly unstable controlled element up to the critical point of loss of control.

Based on recent human response research, a theoretical analysis of this man-machine system is performed, and the results of an experimental program are described, which enables describing function and critical task measures to be compared. An "autopaced" critical task mechanization and operating procedure is described which yields consistent, reliable, and very low variance measurements of the critical levels of instability.

An analysis of the measured human operator describing functions shows that, when operating near criticality, the subject's behavior is adequately represented by the most recent human-operator describing-function models and adaptation laws. Further, the extrapolation of describing function data to the critical level of instability shows that the operator is constrained by the vanishing stability margins. The just-controllable first-order divergence is shown to be related dominantly to the operator's effective time delay, and secondarily to low-frequency neuromuscular adaptation effects. Very good agreement is demonstrated between theory and experiment for both stability and performance parameters.

A number of applications for the critical task are reviewed, including secondary workload research, control and measurement of operator and controlled-element gain, and display research.

This paper traces the development of a new psychomotor tracking task for use in a variety of man-machine research applications. The motivation and roots of this development go back several years into the fields of aircraft handling qualities and engineering psychology. The manual control of statically unstable aircraft and launch vehicles has been under experimental investigation for a number of years by aircraft engineers. Notable among this research is the work of Phillips and Cheatham in a statically unstable yaw chair (e.g., ref. 1); of Brissenden et al. in the variable-lift Beechcraft (e.g., ref. 2); the work of Sadoff and McFadden at the Ames Research Center on aircraft dutch-roll instability (e.g., ref. 3); the work of Taylor at the NASA Flight Research Center on statically unstable high speed aircraft (ref. 4); and the control of statically unstable launch vehicles by Holleman (ref. 5) and Hardy,

---

\*This work has been sponsored by the NASA Ames Research Center under Contract NAS2-2288 and the U.S. Air Force Aeromedical Laboratory at Wright-Patterson Air Force Base under Contract AF 33(615)-2826.

et al. (ref. 6). More recently L. Young at MIT has investigated the manual control of the statically unstable inverted pendulum using visual and/or motion cues (ref. 7). However, relatively little analysis has been done.

In the engineering psychology field, the use of difficult tracking tasks has a long history and, more recently, the concept of "self-paced" tracking tasks has been exploited. Review of several concepts is given by Kelly (ref. 8). Of the various concepts proposed, the most pertinent to the work here is that proposed by Birmingham and Chernikoff in reference 9, wherein a parameter of the controlled element itself is varied and its limiting value is used to measure some aspect of the operator's tracking skill.

Our interest in this field at Systems Technology, Inc., started as a result of extensive work in the analytical treatment of aircraft handling qualities (e.g., ref. 10). In 1958 McRuer showed, by a very simple analysis in reference 11 (which still forms the basis for the theory described here), that the controllable spiral mode divergence would be limited primarily by the effective delay times in the pilot and manual control system. Ashkenas in 1960 (ref. 12) computed the just-controllable aircraft short-period static instability and showed that this was dominantly related to the pilot's effective delay time. At this time STI proposed to the FAA that this type of controlled element be employed in a "critical task" to evaluate pilot proficiency, but nothing came of this proposal (ref. 13). In subsequent reports, Jex, Cromwell, and Durand validated the initial predictions of Ashkenas both by further analysis and by experimental tests with pilots, and showed that near the just-controllable instability, the pilot's behavior would be tightly constrained by the nature of the aircraft short-period dynamics (refs. 14 and 15). In May 1961 Durand discovered that a first-order divergence as a controlled element would provide an ideal constraint on the operator's dynamic behavior, and that the just-controllable divergence would be closely related to the operator's effective time delay. Consequently, both first- and second-order divergent controlled elements were included in some experiments, performed jointly by Systems Technology, Inc., and The Franklin Institute in 1962, on a wide variety of human-operator/controlled-element combinations (ref. 16). Measurements of the human operator's describing function in these experiments showed that the basic theoretical assumptions were justified, and provided impetus for further development of the critical task concepts.

The goal of the work reported here (ref. 17) was to develop a critical tracking task for psychomotor research applications, and, in particular—

- (1) To provide a sound theoretical foundation for the task
- (2) To validate experimentally the assumptions and operator behavior
- (3) To evolve a suitable operational configuration for the test.

## EFFECTIVE TIME DELAY

In the subsequent discussion we will make frequent use of the term "effective time delay,"  $\tau_e$ . It is important to understand the components of the effective time delay when interpreting the assumptions and measurements made. The effective time delay is defined below:

(1)

It is seen that  $\tau_e$  comprises several components:  $\bar{\tau}_d$  includes all of the pure transport delays (e.g., perceptual, neural transmission, pulse coding delays, and central nervous system latencies), and is defined as an average value over some run length;  $\tau_r(t)$  is the time-varying component of this, whose time average is zero by definition. The next two terms,  $T_{N_1}$  and  $2\zeta_N/\omega_N$ , are associated with the high frequency neuromuscular lags, which in turn depend on the limb in use, the neuromuscular tension involved, and the mass, damping, and spring characteristics of the device being manipulated by the operator. The last term,  $T_{L_{hi}}$ , represents high-frequency lead equalization which the operator sometimes can use to help cancel some of the neuromuscular system lags, but which is beyond the bandwidth of the input measurements and, therefore, is not directly resolvable in measurements. Not shown in equation (1), but referred to later, is an additional effective delay,  $T_s$ , due to the operator's sampling behavior among several displays when placed in a multiloop control situation.

## MECHANICAL ANALOG

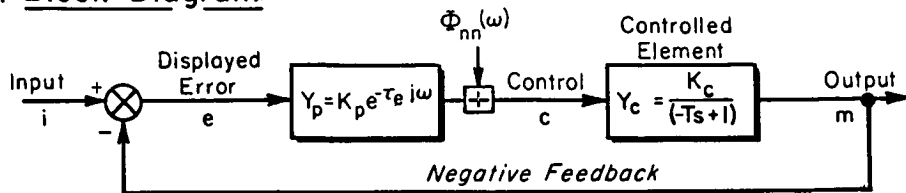
The controlled element used for the critical task is a first-order divergent system. Before proceeding with the theoretical development, it is helpful to consider the mechanical analog of this system and its implications.

The mechanical analog of a first-order divergence is a forward-facing caster. If a forward-facing caster is pushed along a table, the point of contact of the tire is ahead of the pivot point, and the motion of the caster is unstable; that is, the tire will diverge from a straight path unless the pivot point is controlled to bring it back onto the path. The time constant of this divergence is decreased as the speed of motion across the table is increased, or, in other words, the level of instability is increased as the speed of motion is increased. In order to steer a forward-facing caster back to a given line, the pivot point must be moved farther away from the line than the error between the line and tire contact point; that is, a control gain of greater than unity is required to stabilize the system. If an attempt is made to steer the tire precisely to the line, it will be noted that an oscillatory divergence appears; that is, at high gain the forward-facing-caster-plus-human-operator system becomes unstable in an oscillatory manner. This instability is governed primarily by the operator's effective time delay. If the speed of the caster along the table is gradually increased, there will be some speed at which control can no longer be maintained. This is the critical condition, and it will be shown that the time constant of the caster's first-order divergence closely approximates the effective delay time of the operator at this critical condition.

## THEORY

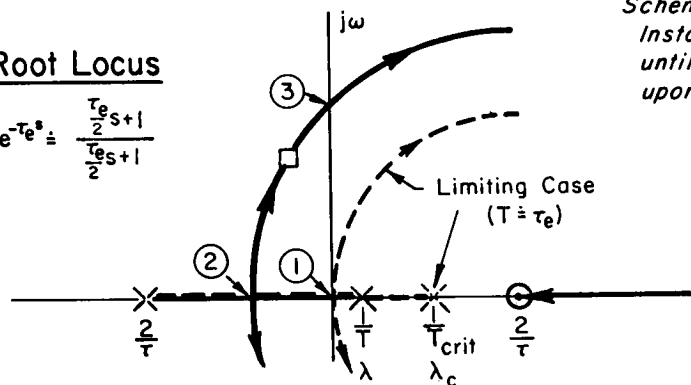
Complete theoretical analyses of the manual control of a first-order instability are given in references 16 and 17, and only a brief and somewhat over-simplified version is given here. However, it illustrates most of the features of the more precise analyses. Figure 1 shows the theoretical considerations. Figure 1(a) is a block diagram showing the operator manually stabilizing a first-order divergence in closed-loop operation. He is presented only with the error; that is, it is a compensatory control task. A random input is provided in most cases, although the system is also excited by the operator-injected remnant, or noise, represented in figure 1(a) by  $\Phi_{nn}$ . The divergent time constant is  $T$  (seconds), and the level of instability is represented by  $\lambda = 1/T$ . The controlled element is set up so that the static gain does not change as the instability is increased. The pilot is represented as a pure gain with effective time delay,  $\tau_e$ . The justification for this simplified form of operator behavior is presented subsequently.

### a. Block Diagram



### b. Root Locus

$$e^{-\tau_e s} \approx \frac{\frac{\tau_e}{2}s + 1}{\frac{\tau_e}{2}s + 1}$$



*Scheme:*

*Instability,  $\lambda$ , is increased until control is lost, whereupon  $\tau_e \approx T_c = 1/\lambda_c$*

### c. Bode Plot (for $Y_p \cdot Y_c$ )

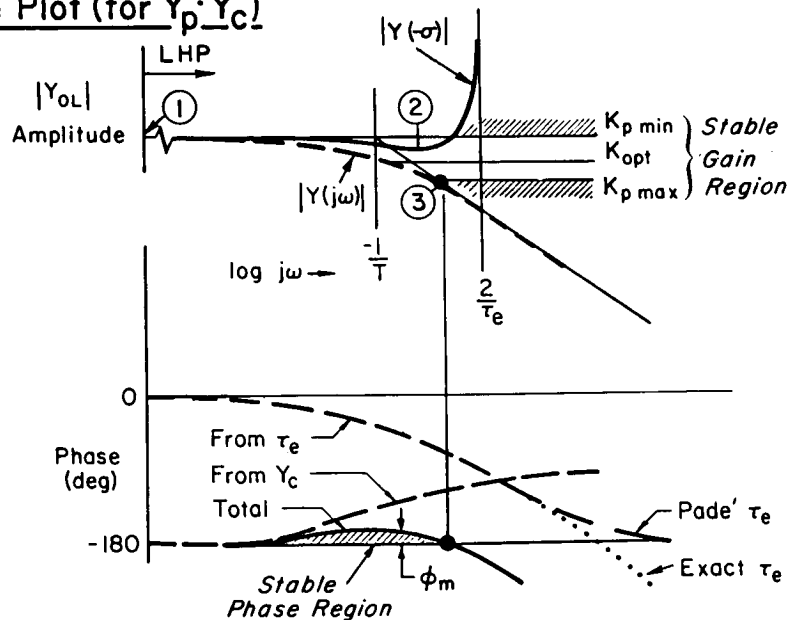


Figure 1.—Systems analysis of human operator control of a first-order divergent controlled element.

Figure 1(b) shows the root locus plot for this system as the loop gain is increased. First of all we note that the effective time delay has been represented for convenience by a first-order Padé approximation with the pole and zero at  $-2/\tau$  and  $+2/\tau$ , respectively. (The same results occur when the exact time delay effects are used.) As the gain is increased,

the unstable root, starting at  $1/T$  or  $\lambda$ , is stabilized at some minimum gain at point ①. As the gain is further increased, the system finally becomes unstable in an oscillatory manner at point ③. Between points ② and ③ there is an optimum gain at which the system is stable and controllable. This situation is, of course, analogous to the control of the forward-facing caster described previously. As the instability is increased, that is, the root at  $\lambda$  is moved to the right toward  $\lambda_c$ , the region of stable gains shrinks toward zero and, in the limit, no stable gain exists. This is the critical condition beyond which control is not possible.

Looking at the theory from the standpoint of frequency response, let us turn to figure 1(c) which gives the Bode plots for the open-loop system. Considering the bottom half first, we see that the net phase angle, which is the sum of the controlled element and the effective phase delays due to the delay time, has a limited region of stability, indicated by the shaded region. Projecting this upward to the amplitude ratio plot, we see that there is a corresponding limit on both the minimum and maximum gains for stability, corresponding to points ① and ③, respectively, in the root locus diagram. At some gain in between these limits, there are finite gain margins and a finite phase margin. Near the critical limits of  $\lambda$ , these margins become vanishingly small.

It can be shown by iterative analysis that the optimum operator equilization in near-critical cases is to adopt neither lead nor lag, but to operate as much as possible as a pure gain. Introduction of phase lead at low frequencies helps the phase limits, but detracts from the gain margin; conversely, adoption of lag equalization to help the gain margin situation reduces the phase margins. In the limit, then, the pilot is constrained to a nonequalized form of behavior over the frequency range near unity gain crossover, that is, from approximately 0.5 to 10 rad/sec.

As can be seen from this simple idealized analysis, control is ideally lost when the divergence time constant is made as short as the effective time delay, that is,  $T \dot{=} \tau_e$ . The essence of the critical task, then, is that the operator is given a compensatory tracking task with a first-order divergent controlled element. The instability,  $\lambda$ , is increased until control is just lost, whereupon the operator's effective delay time is measured by the critical instability.

## EXPERIMENTAL VALIDATION

A series of experiments were run to test the operator under nearly critical instability levels, to determine whether the behavior was constrained according to theory, and whether the behavior would change in kind or degree as the critical levels of instability were approached. Various fixed levels of instability were given to the operator for 4-minute runs, and his describing functions were measured by cross-spectral analysis techniques, described in reference 16. The order of presentation of the various configurations was randomized and balanced and repeated on different days, so that fairly valid averages could be obtained. Also measured on the same days were the subject's simple and disjunctive reaction time and the critical instability level. The correlation among these various measures is continuing and is nearly complete. Reference 17 gives further details.

Figure 2 shows some measurements of the open-loop describing function for a sub-critical task with the instability fixed at a level well below the critical level. The open symbols depict the average frequency response characteristics for a series of four pilots and one engineer tested in connection with the previous data in reference 16. Despite the fact that

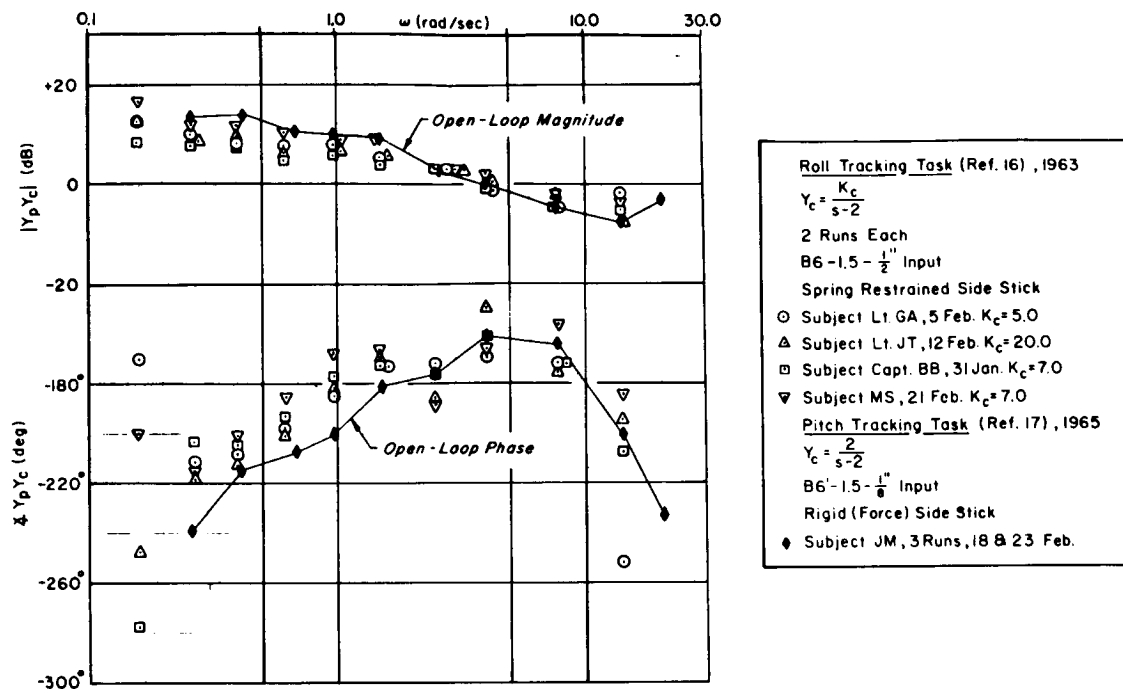


Figure 2.—Comparison of previous and present open-loop describing function data.

each of these operators was given a different controlled element gain, the similar magnitude plots show that they compensated, as would be predicted by theory, such that the loop gain was close to the level of  $K_{opt}$  shown in figure 1. It can also be seen that the shape of these curves is, in fact, similar to that predicted by the simple theory, with the exception that the low-frequency phase curve starts below the  $180^\circ$  level. This low frequency "droop" is commonly observed in human response measurements and has been attributed to proprioceptive accommodation, or "washout," characteristics, which are beyond the scope of this paper.

The second point of note is in the present experiments the operator (depicted by the solid symbols) behaved very similarly to those in previous experiments. The differences between the present and previous operator characteristics can be explained on the basis of the more rigid force stick used in the present experiments, which leads to a tighter neuromuscular loop. We thus conclude that the present subject is typical of all subjects tested to date (in his subcritical tracking behavior) and that the loop describing function is at least qualitatively similar to the simple model presented previously.

Let us now look at the measured describing function for the operator alone under more nearly critical conditions. This is shown in figure 3, where the level of instability is  $\lambda = 4$ , which is about two-thirds of the critical value and about as much as the operator can track continuously for 4 minutes. One of the first points to note is the very small variance from run to run, as indicated by the relatively small standard deviation marks relative to the mean values. Again, there is confirmation that the operator's behavior in the critical task is tightly constrained. The next important point is that the amplitude ratio in the important crossover region between  $\omega = 0.5$  and  $\omega = 10$  is nonequalized, that is, closely represented by

a pure gain. The rising data points at either end (which were also noted in the pilot describing functions for the five pilots of the experiments in fig. 2) have been traced to intrinsic neuromuscular characteristics of the operator.

**PRECISION MODEL.**—The precision describing-function model of reference 16 has been fitted to these data following the procedures referenced there, with the results shown by the solid line in figure 3. The resulting describing function is as follows (see ref. 17 for details):

$$Y_p = K_{\pi} e^{-j\omega\tau_d} \underbrace{\left( \frac{T_L j\omega + 1}{T_I j\omega + 1} \right) \left( j\omega + \frac{1}{T_K} \right)}_{\text{Equalization}} \underbrace{\frac{1}{(T_{N1} j\omega + 1) \left[ \left( \frac{j\omega}{\omega_N} \right)^2 + \frac{2\zeta_N j\omega}{\omega_N} + 1 \right]}}_{\text{Neuromuscular dynamics}} \quad (2)$$

Gain
Delay
Equalization

where

$$K_{\pi} = 1.9 \text{ cm/cm (mid-frequency gain)}^1$$

$$\tau_d = 0.065 \text{ sec}$$

$$T_L = 0.02 \text{ sec}$$

$$T_I = 0$$

$$T_K = 2.5 \text{ sec}$$

$$T'_K = 25 \text{ sec}$$

$$T_{N1} = 0.063 \text{ sec}$$

$$\omega_N = 23 \text{ rad/sec}$$

$$\zeta_N = 0.1$$

When all nine parameters of the complete precision model are used, the apparent deviations of the data from the simple nonequalized model are properly accounted for. Note that the lead and lag equalization parameters  $T_L$  and  $T_I$  are negligible, as predicted.

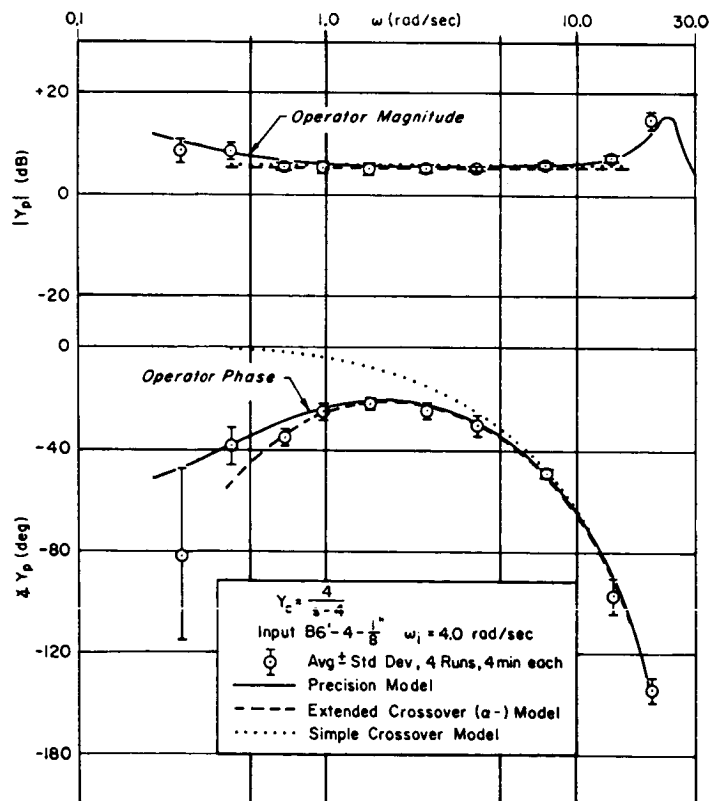


Figure 3.—Mean data and curve fits for one operator's describing function at  $\lambda = 4$ .

<sup>1</sup>The "pilot gain" plotted throughout this paper is the product of the pilot's force/error gain and the controlled-element static gain, the latter of which was constant at 8.7 cm/kg. Thus,  $K_p$  (or  $K_{\pi}$ ), in units cm/cm, is the effective loop static gain, for easier comparison with the theory.

**EXTENDED CROSSOVER MODEL ( $\alpha$ -MODEL).**—Since it was desired to cross-plot the results from different levels of instability, a simpler set of fitting parameters was in order, and for this purpose the "extended crossover" model of reference 16, or the " $\alpha$ -model," was picked. This is a three-parameter model designed to fit only in the extended crossover region, and the resulting fit is shown as the dashed line in figure 3. The resulting describing function is:

$$Y_p \doteq K_p e^{-j\left(\frac{\alpha}{\omega} + \omega\tau_e\right)} \quad (3)$$

↑ Gain
 ↑ Effective time delay  
↑ Low frequency phase droop

where

$$\begin{aligned} K_p &= K_\pi &&= 1.9 \text{ cm/cm} \\ \alpha &= 1/T_K - 1/T'_K &&= 0.36 \text{ rad/sec} \\ \tau_e &= \tau_d + T_{N_1} + (2\zeta_N/\omega_N) - T_L &&= 0.116 \text{ sec} \end{aligned}$$

It is seen in figure 3 that this model fits the data in the crossover region quite adequately.

**SIMPLE MODEL.**—Finally, as a point of comparison with the simple theory assumed in the beginning, the simple model assumed there is shown as the dotted line in figure 3. The describing function for this simple crossover model is given by:

$$Y_p \doteq K_p e^{-j\omega\tau_e} \quad (4)$$

where

$$\begin{aligned} K_p &= 1.9 \text{ cm/cm} \\ \tau_e &= 0.116 \text{ sec} \end{aligned}$$

Even the simple model fits the data reasonably well in the region near and just above crossover, that is, from 5 to 10 rad/sec, where  $\tau_e$  is most clearly defined by the phase data points.

The three parameters  $K_p$ ,  $\alpha$ , and  $\tau_e$  were fitted to the data by the  $\alpha$ -model, and the resulting stability margins were then cross-plotted versus the level of instability in order to determine whether the theoretically predicted trends were validated by the experiment. Figure 4 shows some of these cross-plots. Figure 4(a) shows that the level of  $\tau_e$  is very close to its irreducible minimum and is flattening out at the extreme instability reached in these experiments. The fitting parameter  $\alpha$  is a much less precisely defined quantity; however, it is roughly constant also. Both of these values are consistent with those previously reported in reference 16, considering that the neuromuscular system was tighter in the



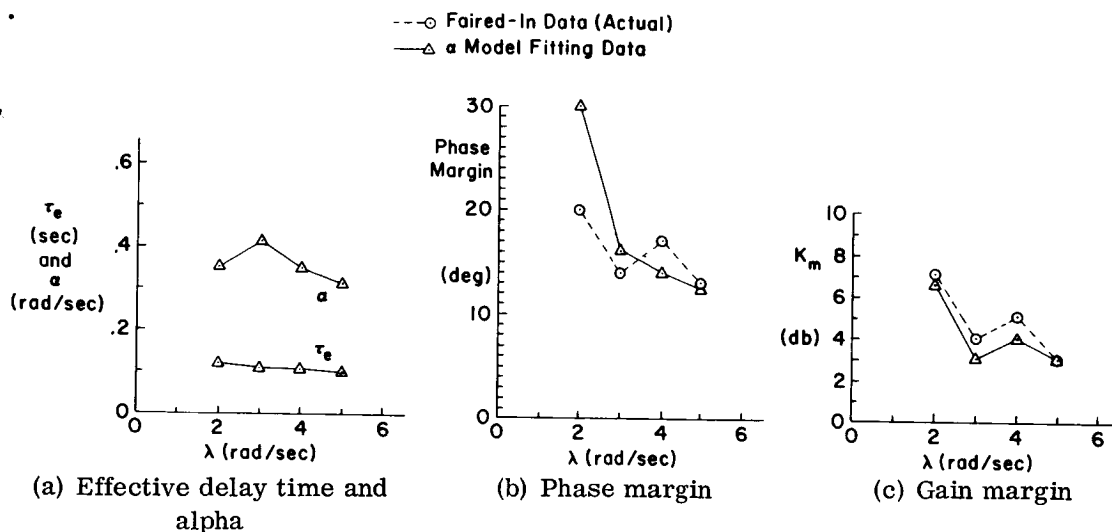


Figure 4.—Trends in fitted  $\tau_e$ ,  $\alpha$ ,  $\varphi_M$ , and  $K_M$  at various levels of instability.

present case (implying higher  $\alpha$  and lower  $\tau_e$ ). Figures 4(b) and 4(c) show that the phase and gain margins were reduced as the instability was increased, in accordance with the predictions. The dashed line in these figures shows the stability margins defined by direct hand fairings of the data points in the appropriate frequency regions, which, in some cases, differed slightly from the fitted curves. The same trends are seen in either case. For further details, including the actual plots for all experiments and more detailed tabulation of cross-plotted data, see reference 17.

Figure 5 more dramatically illustrates the constraining effect of the critical task. Here the gain used by the operator at each level of instability is plotted, along with the upper and lower gain limits. Shown for comparison are the theoretical gain boundaries which would result from using the  $\alpha$ -model in the closed-loop analysis, which is similar to the analysis in figure 1. The measured gain limits indicated by the triangular points closely approximate the theoretical boundary, and thus verify that the operator's gain limitations are drastically constrained as the critical limits are approached, in good accordance with the theory. The actual gain adopted by the operator, indicated by the circular points, closely follows the theoretical gain for maximum gain margin,  $K_{GM}$ , which is the geometric mean between the upper and lower gain boundaries. Notice from the lower right-hand portion of the figure that the low frequency phase terms (the  $\alpha$ -terms) have the effect of blunting the toe of the gain limits, and of reducing the critical instability at which control is lost (relative to the simple case).

In summarizing this section on experimental validation, the main points are as follows:

- (1) The operator's behavior is tightly constrained, as evidenced by the similarity among different operators in subcritical tasks and the small variance in the run-to-run describing functions seen in all of the data to date.
- (2) A relatively simple three-parameter model closely accounts for all of the data, and verifies that the pilot does not adopt equalization within the bandwidth of these measurements, in agreement with the theory.

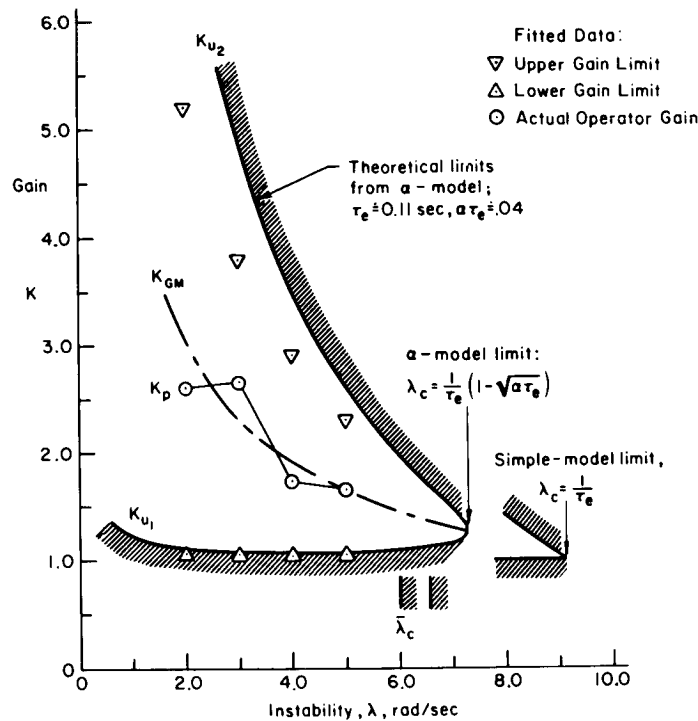


Figure 5.—Measured and theoretical operator gains at various levels of instability.

(3) There is good agreement between the theoretical and experimentally observed stability limits, which show a rapid convergence toward the limiting case.

(4) The actual gain adopted by the pilot appears to closely approximate the gain for maximum gain margin,  $K_{GM}$ .

In short, we believe that there is very good experimental validation of the theoretical assumptions and implications of the operator's behavior in the first-order critical task.

### THE AUTOPACED CRITICAL TASK

To measure the controllability limits of the operator, it is necessary to drive him into the toe of the stability region of figure 5. This is done by gradually increasing the level of instability during a run until control is lost and recording the critical value of instability as the task score. An automatic device for performing this increase in instability was developed in accordance with the arrangement shown in figure 6. Several schemes were investigated for pacing the level of instability, and are described in more detail in

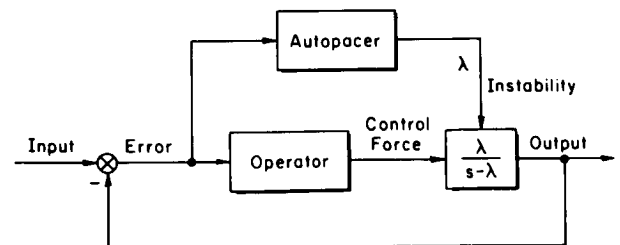


Figure 6.—Autopaced critical task.

Input Parameters (when used)

$$i_{rms} \leq 0.4 \text{ cm}$$

$$N_{01} \leq 3 \frac{\text{upward zero-crossings}}{\text{sec}}$$

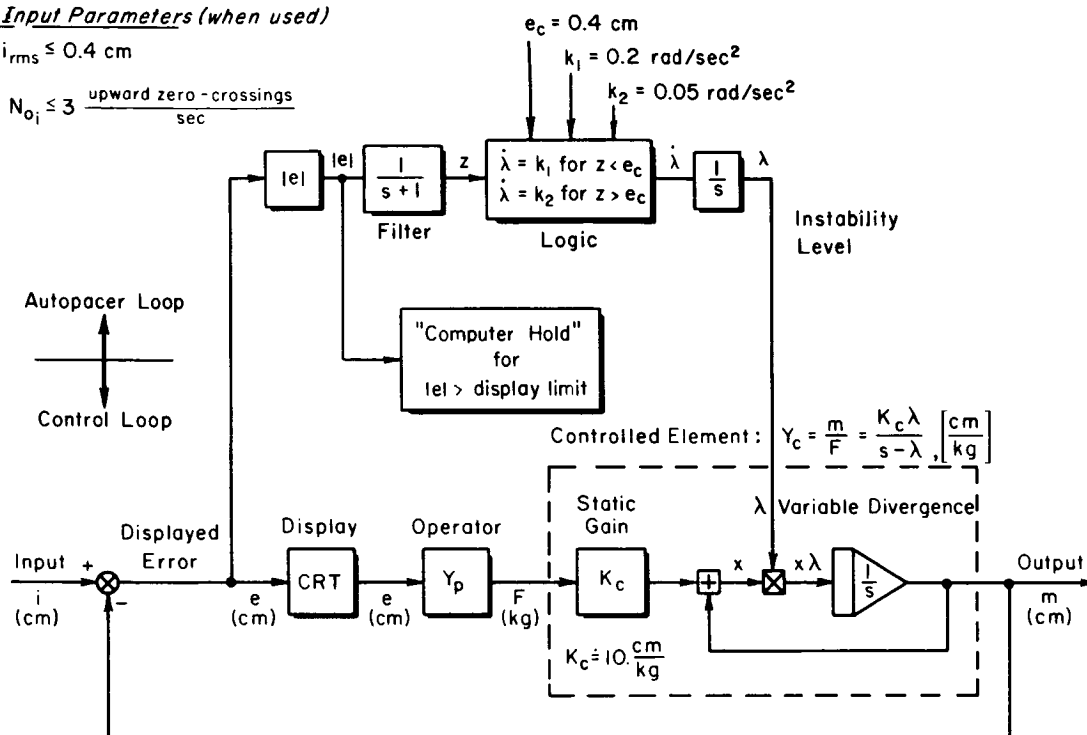


Figure 7.—Block diagram of critical task.

reference 17. To make a long story short, any schemes involving feedback of the error to adjust the instability to maintain continuous control were not successful. By relaxing his error tolerances, the operator can allow the errors to increase, whereby the instability is reduced, and the level of  $\lambda$  is not indicative of the operator's control limits. Instead, a monotonically increasing instability was found necessary, and it was mechanized, finally, according to the parameters given in figure 7. The scheme operates as follows: The instability is set at some small level at the beginning of the run and is increased rapidly as long as the operator has no difficulty controlling the task. When he gets in trouble, as indicated by an increase in the absolute error averaged over a 1-second interval, the rate of increase of instability is reduced to a creeping value for the remainder of the run, until control is lost. The operation of this autopacer is very similar to what a human operator instinctively does when probing human operator stability limits by manipulation of a  $\lambda$ -potentiometer. The parameters given in figure 7 are not critical, and may be varied by more than  $\pm 20$  percent without a significant effect on the measured critical instability. We have thus achieved a most desirable feature; that is, precise duplication of the experimental setup is not necessary to yield precise measures of the score,  $\lambda_c$ , which is an intrinsically operator-centered measure rather than an equipment-centered score.

Figure 8 shows typical time histories of autopaced critical task runs, first with no input and, second, with the same input as used in the describing function runs. In either case the task is subjectively very similar to the operator, that is, the error characteristics appear similar and the task has the same degree of difficulty. This is borne out by the time histories, which show similar qualitative characteristics in the critical region for either

Note:  $i, \epsilon, m$  Referred To CRT Display

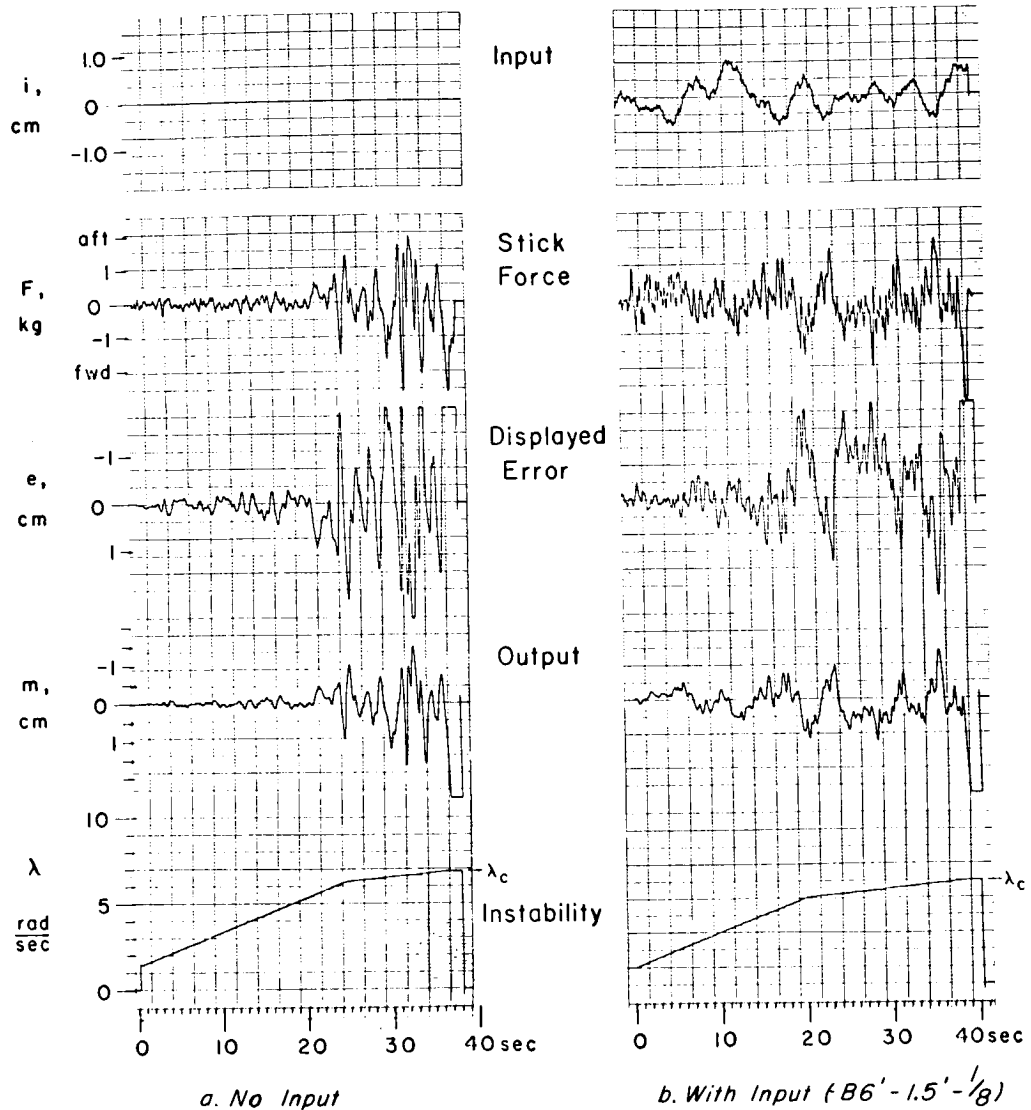


Figure 8.—Typical autopaced critical task time histories.

case. There is no evidence of bang-bang control force application in any of the records seen to date, implying quasi-linear operation (this is also borne out by the relatively high coherence levels measured between operator output and input). Tracing the operation of the autopacer shown in figure 8, we see that  $\lambda$  is increased at a high rate until the suddenly increasing error indicates trouble, at which time the rate is decreased to a creeping level until control is lost. Although the operator's control force appears to be wildly oscillating at the critical instability point, the level of the score is quite consistent, as is shown next.

Figure 9 shows the autopaced scores which were measured concurrently with the describing function measurements. Appreciable training had been given at the Hawthorne

facility of Systems Technology, Inc., before the operator performed these experiments at The Franklin Institute in Philadelphia. About 170 runs without input were given to the operator, who achieved the level indicated by the arrow at the left side of figure 9. The learning curves look conventional, and a fairly stable asymptote was realized for the last two dozen runs. First, it is apparent from figure 9 that the level achieved at The Franklin Institute was comparable to that achieved during practice, showing that a stable plateau had indeed been reached and that the task is repeatable on a completely different installation. Second, a small but finite effect of the input is noted, with the input reducing the critical

instability by a small amount. This is predictable by theory and is related to the fact that the error exceeds the display limits quicker with an input than with no input, and so it shuts off the task somewhat sooner. Although an input is necessary for describing-function measurements, it is felt that zero input may be preferable for most applications because the operator remnant can provide sufficient wide-band excitation of the system to ensure a valid tracking task.

One of the main results shown in figure 9 is that the standard deviation is a very small fraction of the mean score (approximately 4 to 7 percent). This is about one-half to one-third the variance experienced in reaction time measurements. A five-run sample seems to be the best compromise to give a stable level of the mean without an excessive number of runs.

Aside from the anomalously high points indicated in the next to last set of runs in figure 9, and the one low point at the beginning (which is associated with warm-up effects), the level of instability and (by implication) the effective time delay of the operator during these experiments seem to be quite stable. This has also been found to be true of other subjects who have been monitored over a large number of runs and a long period of time.

In summary, a relatively simple automatic pacing scheme for the critical task has been evolved which ensures repeatable results and is insensitive to the detailed pacing and mode-switching criteria involved. The resulting  $\lambda_c$  scores show rapid learning and stable asymptotes, with the standard deviation being approximately 5 percent of the mean. It is felt that the use of the critical instability as a psychomotor test score to replace the more standard error-scoring measures should result in significant improvements in precision, efficiency, and sensitivity, particularly in those cases where the operator's time delays are a dominant factor in his performance.

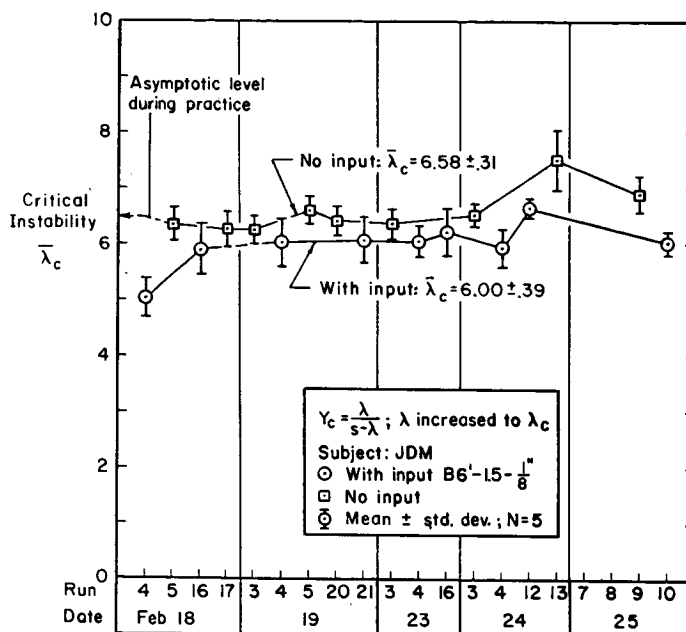


Figure 9.—Autopaced critical task scores.

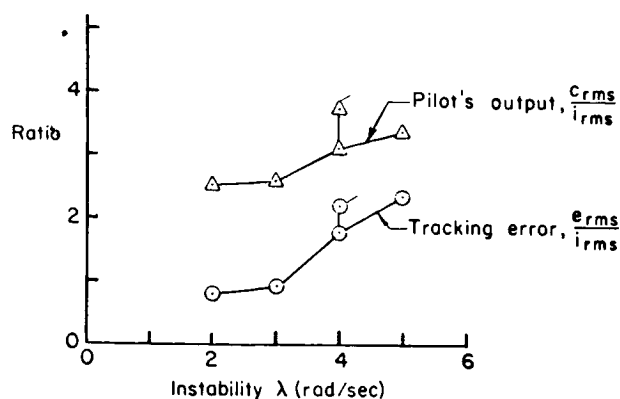
## APPLICATIONS

The autopaced critical task is applicable to a number of man-machine research applications, for the following reasons:

- (1) The critical instability score is operator-centered, rather than machine-centered; that is, it measures an intrinsic property of the operator, rather than some arbitrary scoring criterion of the machine.
- (2) The operator's behavior is constrained, resulting in less variability in the score. Consequently, the test is much more efficient than reaction time measurements, for example, and fewer runs are required to achieve a given level of precision.
- (3) The cause-effect relationships affecting the score (i.e., the components of effective time delay) are fairly well known, and the effects of such variables as manipulators, displays, and different limbs can thereby be predicted.
- (4) Only a few parameters are involved in the test configuration. None of these are particularly critical; the score is relatively independent of the fidelity to which the experimental setup is duplicated from one facility to another.
- (5) The score,  $\lambda_c$ , depends primarily on  $\tau_e$ , and so it is a relatively unconfounded metric. It does not measure a mixture of operator lead and time delay, as is the case, for example, with operator control of an inverted pendulum.
- (6) The controllable limit of an unstable system has a high face validity and motivational appeal as a psychomotor test.
- (7) Since the operator is always pushed to his limit, the initial rate of learning is very high, and the score approaches a stable asymptote after several dozen runs.

Numerous applications and further experiments immediately suggest themselves. Any experiment in which reaction time is a traditional measure is a candidate for the autopaced critical task. These include such fields as psychomotor tests for pilots and astronauts, training and proficiency checks, learning experiments, drug research, secondary workload effects, multichannel control tasks, display research, and control stick.

The fact that the operator is constrained to a pure-gain-like amplitude ratio over a wide frequency band has two implications. The first is that the ratio of the operator's control output to the displayed error should be roughly constant and equal to the gain:  $c_{rms}/e_{rms} \doteq K_p$ . The second is that this ratio should be constrained to the optimum gain level. This is borne out by figure 10. Figure 10(a) shows the measured control outputs and errors for the previous describing function data (the tagged points are for a wide-band input). Both the error and control output increase as instability is increased, in accordance with theoretical predictions. The ratio of the control output to error does indeed closely approximate the measured pilot gain, as shown in figure 10(b). Furthermore, this gain is closely approximated by the dotted line, which shows the gain for maximum gain margin,  $K_{GM}$ . This has the following simple formula (based on the simple-model analysis, see ref. 17):



a. Tracking and control measures

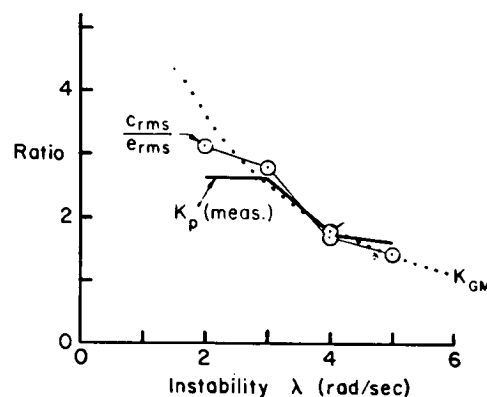
b. Comparison of  $c_{rms}/e_{rms}$ ,  $K_p$ , and  $K_{GM}$ 

Figure 10.—Relative rms tracking errors and control outputs versus the level of instability.

Thus, it seems possible to predict the loop gain adopted by the pilot. This predictability of the pilot gain in a subcritical task affords an independent check on the operation of parameter trackers or other cross-spectral measurement techniques.

It is also possible to control the pilot's (control force/error) gain by varying the controlled-element gain, since the loop gain must remain constant near  $K_{GM}$ , as was noted in connection with the five operators' data of figure 2. A subcritical task is set up and the controlled-element gain is then varied with the knowledge that  $K_p$  will be adjusted inversely by the operator such that the product  $K_p K_c \doteq K_{GM}$ . By this means it is possible to explore the operator's dynamic range of gain-adaptation capability. Finally, note that a very simple approximation of the pilot gain used in a given subcritical task can be obtained by simply dividing  $c_{rms}/e_{rms}$  or, even more simply, the ratio of mean absolute values  $|c|/|e|$ .

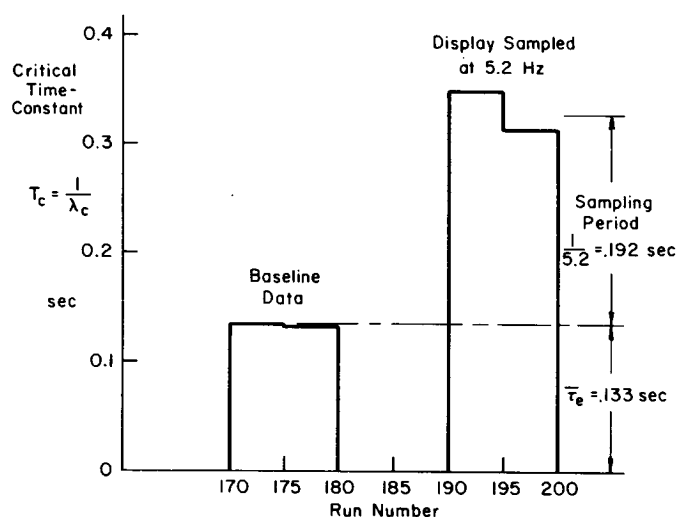


Figure 11.—Effect of display sampling on critical time constant.

An additional time delay due to the operator's sampling among more than one display, or sampling lags from a sampled display, will show up as an increased effective time delay in the loop and will result in a decrease in the critical instability. A very simple experiment was performed to check this application, as shown in figure 11. Here is plotted the critical divergence time constant ( $T_c = 1/\lambda_c$ ) for two situations: (1) the baseline case where there is no display sampling, and (2) a sampled case for which the display was blanked for 50 percent

of the duty cycle at the rate of 5.2 cycles/sec. Subjectively, this appears as a rapid flickering display dot. If the display sampling period of 0.19 second is added to the baseline effective time delay of 0.133 second, it is seen that the sum lies close to the just-controllable divergence time constant. Thus the sampling lag does produce a sensitive decrement in the critical task score. This experiment was too crude and isolated to validate conclusively this application of the critical task, but it merits further consideration as an indicator of sampled behavior.

A very subcritical task makes a novel and effective secondary workload because it demands frequent attention to avoid loss of control. Noting that the operator must sample and activate the control every  $1/\lambda$  seconds or so, the degree of secondary workload may be quantified by specifying the instability,  $\lambda$ . In this application the instability is set at a low level, permitting appreciable time away from the secondary task.

In a corollary application, the detrimental effect on the autopaced critical task score of a secondary workload can be measured. The decrease in critical instability is a measure of the time spent away from the critical task, thus affording a new metric for determining the effects of secondary workloads.

The autopaced critical task has been tentatively approved as one of the tests in a psychomotor test battery to be employed in the NASA Apollo Extension Experiments, and work is proceeding, under NASA sponsorship, toward establishing valid baseline data in laboratory and flight tests under various conditions. Finally, further validations and other applications of the critical task are currently being explored at Systems Technology, Inc., under Air Force sponsorship, toward possible application in the forthcoming Manned Orbiting Laboratory.

## REFERENCES

1. Cheatham, Donald C.: A Study of the Characteristics of Human-Pilot Control Response to Simulated Aircraft Lateral Motion. NACA TR.1197, 1954.
2. Brissenden, Roy F.; Alford, William L.; and Mallick, Donald L.: Flight Investigation of Pilot's Ability to Control an Airplane Having Positive and Negative Static Longitudinal Stability Coupled with Various Effective Lift-Curve Slopes. NASA TN D-211, 1960.
3. McFadden, N. M.; Vomaske, R. F.; and Heinle, D. R.: Flight Investigation Using Variable-Stability Airplanes of Minimum Stability Requirements for High-Speed, High-Altitude Vehicles. NASA TN D-779, 1961.
4. Taylor, L. W.; and Day, R. E.: Flight Controllability Limits and Related Human Transfer Functions as Determined From Simulator and Flight Tests. NASA TN D-746, May 1961.
5. Holleman, E. C.; Armstrong, N. A.; and Andrews, W. H.: Utilization of the Pilot in the Launch and Injection of a Multistage Orbital Vehicle. IAS Paper 60-16, Jan. 1960.
6. Hardy, G. H.; West, J. V.; and Gunderson, R. W.: Evaluation of Pilot's Ability to Stabilize a Flexible Launch Vehicle During First-Stage Boost. NASA TN D-2807, May 1965.



7. Young, L. R.; and Meiry, J. L.: Manual Control of an Unstable System with Visual and Motion Cues. IEEE Intern. Conven. Record, vol. 13, part 6, 1965, pp. 123-127.
8. Kelley, C. R.: Self-Adjusting Vehicle Simulators. Presented at the Intern. Congress on Human Factors in Electronics (Long Beach, Calif.), May 3-4, 1962.
9. Birmingham, H. P.; and Chernikoff, R.: The Concept of Equalization Ability in Operator Selection and Training. IRE-WEMA paper 39-1, 1961.
10. Ashkenas, I. L.; and McRuer, D. T.: A Theory of Handling Qualities Derived from Pilot-Vehicle System Considerations. Aerospace Eng., vol. 21, no. 2, Feb. 1962, pp. 60, 61, 83-102.
11. Ashkenas, I. L.; and McRuer, D. T.: The Determination of Lateral Handling Quality Requirements from Airframe/Human-Pilot System Studies. WADC-TR-59-135, June 1959.
12. McRuer, D. T.; Ashkenas, I. L.; and Guerre, C. L.: A Systems Analysis View of Longitudinal Flying Qualities. WADD-TR-60-43, Jan. 1960.
13. Ashkenas, I. L.: A Simple "Critical Task" Test Procedure To Yield Information on Pilot Fitness. TM-46, Systems Technology, Inc., Apr. 1960.
14. Jex, H. R.; and Cromwell, C. H.: Theoretical and Experimental Investigation of Some New Longitudinal Handling Quality Parameters. ASD-TR-61-26, Mar. 1961.
15. Durand, T. S.; and Jex, H. R.: Handling Qualities in Single-Loop Roll Tracking Tasks: Theory and Simulator Experiments. ASD-TDR-62-507, Nov. 1962.
16. McRuer, D.; Graham, D.; Krendel, E.; and Reisener, W., Jr.: Human Pilot Dynamics in Compensatory Systems—Theory, Models, and Experiments With Controlled Element and Forcing Function Variations. AFFDL-TR-65-15, Jan. 1965.
17. Jex, H. R.; McDonnell, J. D.; and Phatak, A. V.: A "Critical" Tracking Task For Man-Machine Research Related to the Operator's Effective Delay Time, Part I, Theory and Experiments with a First-Order Divergent Controlled Element. NASA CR-616, 1966.

N67-15878

## 27. DESIGN APPLICATIONS OF ADAPTIVE (SELF-ADJUSTING) SIMULATORS\*

*Charles R. Kelley  
Dunlap and Associates, Inc.*

Adaptive simulators have been previously applied to problems of training. This study explores their usefulness for manual control system design. The history and development of the field of adaptive vehicle simulation is reviewed. The technique of adaptation most suitable for design studies is one in which operator performance is kept at a preset criterion level by means of adaptive changes in task difficulty. This technique permits design variables to be assessed without the intervention of operator error scores.

The performance criterion used to measure operator performance is important in adaptive as well as nonadaptive simulation. Time-on-target scores were analyzed and found to be excessively imprecise. The recommended performance criterion for many applications is rms error in one axis and vector error in two or more independent axes.

Adaptive system changes are a compromise between speed of adjusting to change in operator performance and stability of the adaptive level achieved. The emphasis on speed versus stability can be changed by varying coefficients in the adjustment equation.

Example design data are presented with respect to (1) display gain, (2) continuous versus on-off control, and (3) one versus two versus three axes. Data were gathered in each case on an acceleration control task in which forcing function amplitude was varied adaptively. The relation of each design variable to forcing function amplitude, with operator error constant, is described for the example task.

In 1959 Henry Birmingham of the U.S. Naval Research Laboratories reported a technique for measuring "human operator bandwidth," in which he employed the operator's error to modify the gain of the integrators in a tracking system (ref. 1). This change in gain is equivalent to accelerating the time scale of the integrators. Birmingham employed the operator's error to adjust the system automatically so that, as the operator tracked more skillfully, the time scale grew faster. The limit reached was taken as indicative of the operator's "bandwidth," or the maximum frequency with which he was able to cope.

The technique as originally presented by Birmingham has not found wide application, perhaps because the "bandwidth" of the operator was already known quite precisely. However, an important concept was implicit in Birmingham's technique, that of modifying a tracking system or simulator automatically as a function of operator performance.

In 1962 the concept was made explicit and generalized in reference 2. This paper described how operator performance measurements could be used in a vehicle simulator or tracking system to adjust automatically such variables as forcing function amplitude, forcing function frequency, display gain, control gain, display quickening, display prediction span,

\*This study was supported by the Office of Naval Research under Contract Nonr-4986(00).

rate-aided time constant, and system stability (damping). Also described was a technique by means of which an automatic controller "taught" a subject operating in parallel with it by automatically taking control when the operator performed poorly and relinquishing control to the subject as his performance improved. The last half of the article discussed, in turn, the application of the technique to four areas: measuring operator skill, selection, training, and design. Example application data were given, especially with respect to uses of the technique for system design.

Later in the same year Birmingham (ref. 3), Hudson (ref. 4), and Chernikoff (ref. 5) described work with particular training devices utilizing self-adjusting circuitry. Hudson applied the term "adaptive" to his device, and it is this term that has been most favored in subsequent work. Among the subsequent major studies of adaptive vehicle trainers is Hudson's study for the U.S. Naval Training Device Center (ref. 6).

It was suggested in the first general paper on the subject that the technique comprised a highly sensitive means of assessing human performance, and was in important respects better for determining skill than the use of secondary tasks, stressors, or display blanking (ref. 2, p. 14). To quote:

The self-adjusting simulator...alone answers the question, "How difficult a system (or problem) can a subject be expected to manage at a specified level of accuracy?" The self-adjusting simulator can measure this important variable quickly and accurately without recourse to tricks or auxiliary experimental variables.

It is this aspect of the technique that suggested its use in designing an onboard test of piloting skill for extended space missions (ref. 7). Such a test subsequently has been developed for Air Force use aboard the Manned Orbital Laboratory (ref. 8).

Adaptive simulation, as the term is employed here, can apply to any man-operated vehicle simulator or tracking system in which one or more parameters which affect the difficulty of the task are varied automatically as a result of how well or poorly the task is performed. This adaptation can be done in many ways. Different parameters of the task may be adjusted, different criteria of performance may be employed, and there may be different relations between the two, that is, different equations describing the relation between the parameter adjusted and the performance criterion. These three aspects of the task—performance criterion, adjustment formula, and adjustment parameter—are discussed with respect to design applications.

## PERFORMANCE CRITERIA

The criterion of performance in tracking and vehicle control studies is the index of goodness or poorness of operation that is employed in the adjustment formula on which adaptation is based. The problem is essentially the same for adaptive and nonadaptive simulators. In a given system, it is important to select a measurement which reflects the performance desired. Thus time-on-target measurements appear appropriate for gunnery tracking, while error amplitude measurements such as rms error or mean absolute error

are the choice for many other tracking and most vehicle simulation studies.<sup>1</sup> Because of the inherent unreliability of time-on-target scoring, as analyzed below, it may sometimes be desirable for training and testing purposes to employ rms error even in a gunnery task.

**SINGLE-AXIS SCORING.**—The error amplitude distribution for many tracking tasks is gaussian in form, with a mean close to zero (ref. 9). Appropriate display scaling for such a task, if it is not otherwise constrained, would be linear, and such that some  $\pm 2$  to  $3\sigma$  (standard deviations) of the error amplitude distribution appear on the display. If less than a  $\pm 2\sigma$  range is displayed, scale will be exceeded too often, while if more than  $\pm 3\sigma$  are shown, the extremes of the display scale will be poorly utilized.

Most tracking data taken under a given set of conditions can be assumed to be a sample drawn from a hypothetical underlying distribution which is gaussian in form, and which has a mean of zero. A change in conditions results in a different underlying distribution from which data is drawn. With these assumptions, sampling statistics can be applied, and the concept of sampling error of tracking performance measurements becomes relevant.

A gaussian distribution is completely described by two numbers, for example, its mean and standard deviation. A gaussian tracking-error amplitude distribution with a mean of zero is completely described by one number, the rms error, which corresponds here to the standard deviation. The best description of such an underlying gaussian tracking distribution is the rms error of the sample. However, other tracking performance scores made on a sample can be employed to describe the hypothetical underlying distribution. Since they describe the same data, these scores can be converted from one to another. In order to evaluate their accuracy or precision, they may be employed to derive an estimate of the same number, that is, an estimate of spread or deviation of the underlying curve. The ratio of the rms error of the sample to the standard error of the estimate of rms error obtained via another score from the same sample is the accuracy or precision of the score in question, 1.00 then being the most precise possible. The square of the relative precision is then the power-efficiency of the measurement, in the usual sense employed in statistics. The reciprocal of the power efficiency is the relative sample size that is necessary in order to estimate the spread of the underlying distribution as accurately as does the rms error of the sample. The relative precision of the usual estimates of spread of a distribution is inversely proportional to the square root of the sample size, so that sample size must be quadrupled to double the precision (halve the error) of an estimate. Figures for three performance measurements are shown in table 1.

The median absolute error is the point which would divide the absolute-error amplitude distribution into equal areas. It is almost never measured in tracking, but it provides the same information as does the "time-on-target" score with a 50-percent target band, and so it estimates the spread of the underlying distribution with the same precision, that is 0.61. This low precision means that a tracking test employing a 50-percent time-on-target score must be 2.7 times as long to estimate the spread of a hypothetical underlying gaussian error amplitude distribution with the precision of an rms error score. The precision is much better, however, for target bands wider than 50 percent. This derives from the fact that highly

---

<sup>1</sup>Bahrack et al. (ref. 9) and Bilodeau and Bilodeau (ref. 10) review some of the traditional problems inherent in scoring performance in tracking type tasks. Obermayer and Muckler (ref. 11) and Miller (ref. 12) have contributed significant recent work in this area.

TABLE 1.—RELATIVE PRECISION, POWER EFFICIENCY, AND SAMPLE SIZE REQUIRED TO GIVE A PRECISION OF 1.0 FOR TWO TRACKING PERFORMANCE MEASUREMENTS AS COMPARED WITH RMS ERROR

[Computed from the relative sampling errors of the average deviation and semi-interquartile deviation, as compared with the sampling error of the standard deviation. (See ref. 13.)]

Performance measurement	Relative precision, $a$	Power efficiency, $a^2$	Sample size to yield relative precision of 1.0, $1/a^2$
rms error	1.00	1.00	1.00
Mean absolute error	.93	.88	1.14
Median absolute error	.61	.37	2.71

deviant scores of a sample are much more important in determining the spread of an underlying distribution than are scores near the mean. It reflects in the quite different relative precisions of time-on-target scores for different error bands, as shown in table 2. From this it can be seen that time-on-target scores have a reasonable precision when the target band includes between 70 and 95 percent of the sample, though even in this optimal range the trial length should be 50 to 85 percent again as long to give the precision yielded by rms error.

TABLE 2.—RELATIVE PRECISION, POWER EFFICIENCY, AND SAMPLE SIZE REQUIRED TO GIVE A PRECISION OF 1.0 FOR TIME-ON-TARGET SCORES

[The rms error used as a standard, with a precision of 1.0. The table assumes there is an underlying gaussian error amplitude distribution with a mean of zero. Computed to slide rule accuracy from the equation for relative sampling errors of interpoint-ranges (ref. 14).]

Proportion of error amplitude distribution within target band (TOT target zone)	Relative precision, $a$	Power efficiency, $a^2$	Proportionate sample size to yield relative precision of 1.0, $1/a^2$
0.20	0.35	0.12	8.2
.30	.44	.20	5.2
.50	.61	.37	2.7
.70	.74	.54	1.8
.80	.79	.63	1.6
.85	.81	.65	1.5
.90	.80	.64	1.6
.95	.75	.55	1.8
.98	.68	.46	2.2

Bahrick, Fitts, and Briggs (ref. 9) analyzed a different aspect of time-on-target scoring and arrived at conclusions as to the optimal TOT target band that are somewhat at variance with those presented here. These authors showed that because of the nonlinear relation between time-on-target scores and other measures of spread of a distribution (rms error, mean absolute error, etc.) incorrect conclusions regarding comparative tracking performance could be drawn from TOT data. Thus a perfectly linear learning curve in terms of change in rms error with training can yield a decidedly nonlinear curve in terms of time-on-target scores for the same data. Other comparative score data are similarly distorted. A simple example of the point made in reference 9 (but not used by the authors as an example) will serve to illustrate. The example appears in table 3. The data in the table are hypothetical, drawn from a table of normal curve. Each score for a given condition represents the identical level of performance, measured by rms error and by three time-on-target bands. Note that if time-on-target were linearly related to rms error, every difference in percent time-on-target score shown in any one column in the bottom half of table 3 would be identical, as the conditions all differ by the same amount (1 in.) in rms error. Note that any three experimental conditions, A, B and C, in a tracking study, could show much greater time-on-target differences between conditions A and B than between conditions B and C, and yet B and C could be more different in rms error terms.

Differences in time-on-target scores reflecting differences in tracking performance are largest when the target zone employed includes on the order of 68 percent of the tracking

TABLE 3.— TRACKING SCORES AND DIFFERENCE IN TRACKING SCORES  
AS MEASURED BY RMS ERROR AND BY FOUR TIME-ON-TARGET  
SCORES DIFFERING IN WIDTH OF TARGET ZONE

[Drawn from a table of the normal curve,  
based on the analysis of reference 9.]

Condition	rms error, in.	Time-on-target, percent, for -			
		Target zone, in.			
		1	2	3	4
1	4.0	20	38	55	68
2	3.0	26	50	68	82
3	2.0	38	68	87	95
4	1.0	68	95	99.7	100
Conditions compared	Difference in rms error	Difference, percent TOT			
1-2	1.0	6	12	13	14
2-3	1.0	12	18	19	13
3-4	1.0	30	37	13	5

error amplitude distributions. This is indicated by the dotted diagonal lines in table 3, which show larger differences in percent time-on-target for target zones which include close to 68 percent of the distribution than for wider or narrower zones. This is the point made by Bahrack et al. (ref. 9). It reflects the fact that when the target zone includes 68 percent of a gaussian distribution, the curve is sampled at its inflection points, or points of steepest slope, namely,  $\pm 1\sigma$  from the mean.

It does not follow, however, that a TOT target band should aim to include 68 percent of the tracking-error amplitude distribution. Every TOT measurement can be converted directly into rms error, based on the assumption of an underlying normal distribution. This conversion fully corrects for the nonlinearity problem that Bahrack et al. describe. The critical question is not how large are differences in time-on-target score as a function of target zone, but rather how accurate is the estimate of spread of the underlying distribution when made from time-on-target scores employing different target bands. To phrase it differently, the question is, what is the size of the sampling error of rms error estimates made from TOT scores, as a function of the width of the target band? But this is the question of precision or "power efficiency" of the time-on-target score, as shown in table 2.

A time-on-target zone which includes 68 percent of a distribution has greater "sensitivity" than any other; that is, there are greater differences in TOT score with small changes in level of performance than with any other target band. However, sampling errors with a 68 percent target band are enough greater than those with an 85 percent target band that, when they are used to estimate the spread of an underlying normal tracking error distribution, the time-on-target score using a 68 percent target zone does it less precisely than does the time-on-target score with an 85 percent target zone.

To conclude:

- (1) The best single measurement of tracking proficiency is rms error when an underlying error amplitude curve normally distributed about zero may be assumed.
- (2) Under the same conditions, mean absolute error is also a good tracking proficiency score. Its power efficiency is 0.88 as compared with rms error, and it requires a sample size 14 percent longer to estimate the distribution as precisely as does rms error.
- (3) Time-on-target scores are much less adequate as measures of tracking proficiency under the above conditions. The best time-on-target score will include some 85 percent of the distribution, in which case the measurement has a power efficiency of 0.65, indicating that a sample size some 53 percent longer than that used with an rms score is needed to make the estimate of the distribution as precise as that provided by rms error.
- (4) For nonoptimal target bands, time-on-target scores are extremely imprecise. Under the above conditions, a time-on-target score that includes 50 percent of the distribution has a power efficiency of 0.37, and requires a sample some 2.7 times as long to estimate the spread of the distribution as precisely as does an rms error score.

For the above reasons, rms error is the first choice as a performance measurement as long as normality of the error amplitude distribution can reasonably be assumed.

**MULTIAXIS SCORING.**—Multiaxis adaptive tasks can employ separate self-adjustment of each axis, in which case each axis is separately scored. Often, however, it is desirable to treat the task as an integrated whole, adjusting the difficulty level of all axes simultaneously. In this case, performance in the separate axes must be combined into some single score. This problem is considered briefly for the case of equivalent independent axes, since some of the data to be discussed are of this nature.

For multiaxis time-on-target scoring, a target zone may be established in each axis that for equivalent axes is the same.<sup>2</sup> Whenever the subject is within the target zone in any axis he is "on target"; when he is out of the target zone in any axis he is "off target." Considering the independent task axes as orthogonal with a common origin, this establishes a target zone that is a regular equal-sided figure in the N dimensions of the task, that is, square, cube, or N-dimensional "hypercube." An alternative is to sum the squares of each axis error and to compare the sum to a target zone signal corresponding to  $Nr^2$ , where  $\pm r$  is the target band in each axis. This results in a target figure which is the locus of all points in the N-dimensional space that are located r units from the origin, that is, a circle, sphere, or N-dimensional hypersphere. The difference in the two techniques is greatest along the diagonals to the task axes. The first technique permits greater excursions from the origin along the diagonals than along the axes, while the second allows equal excursions in all directions. The first technique sums the errors in each axis independently, while the second employs a vector sum.

In rms error scoring, either independent or vector summation of multiaxis errors may also be employed. When it makes sense to think of the separate axes in terms of a multiaxis space, vector summation has the nice feature of keeping the probability density distribution of the multiaxis error score symmetric about the origin. Vector error is also frequently most appropriate in multiaxis vehicle control.

The vector error from combined independent axis errors that are normally and symmetrically distributed about the origin is also normally distributed and has a variance equal to the sum of the variance of the individual axes. This error is the vector sum of the individual errors,  $\sqrt{N}\sigma$ , where N is the number of axes and  $\sigma$  is the rms error in each axis.

Data to be reported were obtained by employing time-on-target and rms performance criteria. When rms error is used in multiaxis scoring, a vector sum of errors in the individual axes of the task has been employed.

### ADJUSTMENT FORMULA

The adjustment formula originally proposed for generation in adaptive tasks (ref. 2) employed this formula for scoring:

$$C = K \int_0^t (e_L - e) dt + C_{\text{initial}}$$

<sup>2</sup>When axes are unequal in terms of scale units, they may be rendered equivalent by establishing the target zones on the basis of normalized or standard scores for each axis.



where

C the adaptive score, a higher value denoting better performance

$e_L$  the "error threshold," or error criterion the task is to meet

e the error, however it is defined (e.g., mean absolute error, vector error, etc.)

K a coefficient governing the rate of increase or decrease of C

Whenever the error is less than criterion ( $e > e_L$ ), system difficulty (C) increases. When error is greater than criterion, however, system difficulty (C) decreases and the system becomes easier. Thus the system adjusts to the difficulty level that produces  $e_L$  units or errors, and oscillates around that value. When K is large, the system reaches the desired value quickly, but oscillates widely upon reaching it. When K is small, the system approaches the desired value slowly, but is much more stable. For long test trials, lower values of K are more feasible than they are for short trials. For short trials, it is preferable to allow a substantial oscillation in C to be sure the appropriate level of difficulty is reached. In this case, it is best to use the average value of C, or its average over the latter part of a trial, as the trial score. For longer trials, it is equally satisfactory to use instead slow changes in C, with the final value of C as the score for the trial. Figure 1 is a typical graph of C for a 5-minute task. The task was acceleration control in two axes. The actual equation used was

$$C = 0.017 \int_0^{300} (0.33 - e_v / \sqrt{2}) dt + C_{\text{initial}}$$

where

$e_v$  two-axis vector error ( $\sqrt{x^2 + y^2}$ ), scaled in proportion to full-scale of the display

$C_{\text{initial}}$  0.40 and 0.70 for the two trials, as indicated in figure 1

The score for this trial needs to be averaged. Had initial conditions near the attained value been employed, the time average over the trial would have been an adequate score. Often (as here), because of the initial discrepancy and consequent period of "hunting" for the appropriate level, the time average of the last half of the trial would have been more adequate.

The adjustment techniques applied in studies of adaptive training (refs. 3 and 4) have employed an adaptive score in the form of a filtered error measurement which adjusted a servo controlling task difficulty. As filtered error reduced, the trainer increased its difficulty appropriately. The reduction in error with adaptation forms a primary point of difference between the technique of these authors and that employed here, which keeps the error at the same level by means of adaptive changes in the task. By keeping error at a fixed level, the variation in task performance is transferred entirely to the adaptive variable. It is then

possible to compare the adaptive variable with selected dependent variables, and the adaptive simulator will hold the error constant across the range of the two variables whose relationship is studied. This feature proves extremely valuable in design and research applications, as will become evident.

In gathering data under different conditions, each of which employs the same starting value for the adaptive score  $C$ , the time-averaged  $C$  score for the period of the trial, after due allowance for adaptive change to the region of appropriate task difficulty, is the best single score. A stability analysis to determine the rate at which  $C$  approaches an asymptotic level for various task conditions has not been made. The adjustment of the coefficient  $K$  in the equation for  $C$  must as yet be done empirically.

The general adjustment equations recommended for adaptive simulators for continuous control tasks for any number of equivalent independent axes are

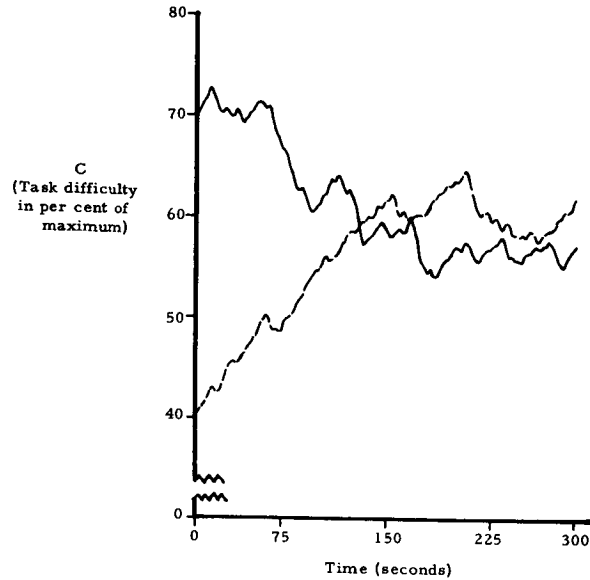


Figure 1. — Typical graphs of  $C$ , the "self-adjust" score, for 5-minute test runs. Scores for the two trials were purposely started at different initial values of  $C$ , to show the rates of convergence of  $C$ .

$$C = K \int_0^{T_2} \left( e_L - \sqrt{\frac{e_1^2 + e_2^2 \dots e_n^2}{N}} \right) dt + C_{\text{initial}} \quad (1)$$

and

$$\bar{C} = \frac{1}{T_2 - T_1} \int_{T_1}^{T_2} C dt \quad (2)$$

where

$C$  the instantaneous score which determines the difficulty of the adaptive task

$\bar{C}$  the average  $C$  score between  $T_1$  and  $T_2$  (the trial score)

K	the constant regulating the stability versus responsiveness of C to changes in task performance
$e_L$	desired level of rms error in each axis of the task, expressed as a proportion of display range
$e_1, e_2, \dots e_n$	actual errors in each axis, expressed in the same units as $e_L$ (errors may be scaled in standard score units to equate axes having different rms errors)
N	number of independent axes
$T_1$	"settling" time of C—the time required for C to change from $C_{\text{initial}}$ to a value corresponding to the appropriate level of task difficulty in the worst case to be measured
$T_2$	length of the trial

## THE ADAPTIVE VARIABLE

Any adjustment of the task that can be made automatically and that varies task difficulty is potentially suitable for use as an adaptive or adjustment variable in adaptive simulation. Six or eight such variables were considered briefly in the initial study (ref. 2), and will not be reviewed here. Very few adjustment variables have been investigated, although Hudson (ref. 6) presents interesting training data comparing control gain, quickening coefficients, and stabilizing feedback as adaptive variables. These proved to be equivalent for training purposes. The present study has employed forcing-function amplitude as an adaptive variable for some example experimental data. It has proved an excellent choice. It varies task difficulty in a straightforward manner, and it has proved to be linearly related to other variables studied to a surprising degree.

## EXPERIMENTAL BACKGROUND

The purpose of this study (including its experimental data) is to study applications of adaptive simulation to design problems in manual control. The relationships shown, though often of interest in their own right, are a byproduct and not the primary concern of the study.

**EQUIPMENT AND TASK CONFIGURATION.**—The basic manual control system employed for gathering data consisted of an analog computer-generated acceleration tracking task in one, two, or three independent axes, with a three-axis hand controller (either proportional or on-off), three compensatory display meters, and a score meter showing the current value of C, the self-adjust score. The full range of output in each axis was displayed. Displays were scaled to range,  $\pm 1.0$ ; the controller output,  $\pm 0.28$ ; and the forcing function,  $\pm 0.28C$ . A digital forcing function generator produced a random step output, which was integrated twice to form the forcing function as the operator tracked it. The random steps were rectangularly distributed about zero in 64 equal intervals. Their amplitude could be adjusted adaptively from zero to up to 168 percent of the controller output range ( $\pm 0.28$ ). At 100 percent, the largest amplitude step from the forcing function was so great that the controller could not overcome it. This served, therefore, as the effective task ceiling, although on the easier

tasks, skilled subjects could and did exceed "100 percent forcing function" ( $C = 1.0$ ) for brief periods, which made it necessary to permit  $C$  to become greater than 1.0 (maximum 1.68) for this task.

The equipment used was essentially that described in Kelley (ref. 6) as a test of space-craft piloting skill. Figure 2 is a block diagram of the task. The display configuration is shown in figure 3. Data were recorded on meters, a six-pen recorder, and an x-y plotter, as appropriate.

**SUBJECTS AND TRAINING.**—Training was carried out on two other projects (ref. 7) and is described here only as it relates to this project, and to the fact that the same subjects were employed. Subjects were two firemen, selected from a pool of five on the basis of equality in tracking skill on a screening test. Subjects were 33 and 35 years old, had normal vision, and were in good health. They were originally trained on alternate trials on (1) a two-axis adaptive version of the test with forcing function amplitude as the adjustment variable, and on (2) a closely comparable constant-difficulty task, in which performance was measured in terms of mean absolute error. In the second task, a forcing function was selected that had a range equal to "18 percent forcing function," or  $C = 0.18$  for the adaptive task. It was chosen because preliminary data indicated that the task was difficult, but could be learned to a reasonable level of proficiency in the available training time with this forcing function. Training was in 5-minute trials, four trials per hour for each subject, 5 hours per day for 9 days. Every other trial was adaptive. Thus the learning curves of figure 4 reflect the same level of skill at each point in training, but measured by the two different techniques. The adaptive task scores show the forcing function amplitude in percent of the controller output that the subjects were able to control with an rms error of 20 percent of the display scale. They are true ratio scores. The constant-difficulty scores represent score improvement in units of mean absolute error, scaled to reach the same final point on day 9 as the adaptive task scores. Thus the two curves of figure 4 were equated by beginning at zero and proceeding to the same day 9 means.

These learning curves demonstrate several points of importance for the present project. The linearity of the adaptive scores is striking, and indicates that growth in tracking skill shows a protracted linear increase over time when measured by the forcing function amplitude that a subject can handle at some fixed level of error. Note that subject error does not enter into the adaptive learning curve, as the adjustment formula used keeps error constant, and changes only the task difficulty.

The constant-difficulty task curve is interesting by comparison. The straight line denoting the forcing-function amplitude for the constant-difficulty task is critical for understanding the data. At the point where the adaptive curve crosses this line (day 8), the two tasks are of equal difficulty. Prior to that time, the constant-difficulty task is harder than the adaptive; after, it is easier. The constant-difficulty task learning curve is best understood as data for a task that is at first too hard, is mastered, and is becoming too easy. If the curves could have been extended, the constant-difficulty curve would have leveled off while the adaptive test continued to rise, as the slopes of figure 4 suggest.

Of equal interest for the present project is the variability of the adaptive and constant-difficulty scores. The much smaller variability of the former indicates their greater precision of measurement. This is best expressed in terms of relative power efficiency and its reciprocal, the proportionate length of test that is needed to provide the same precision of

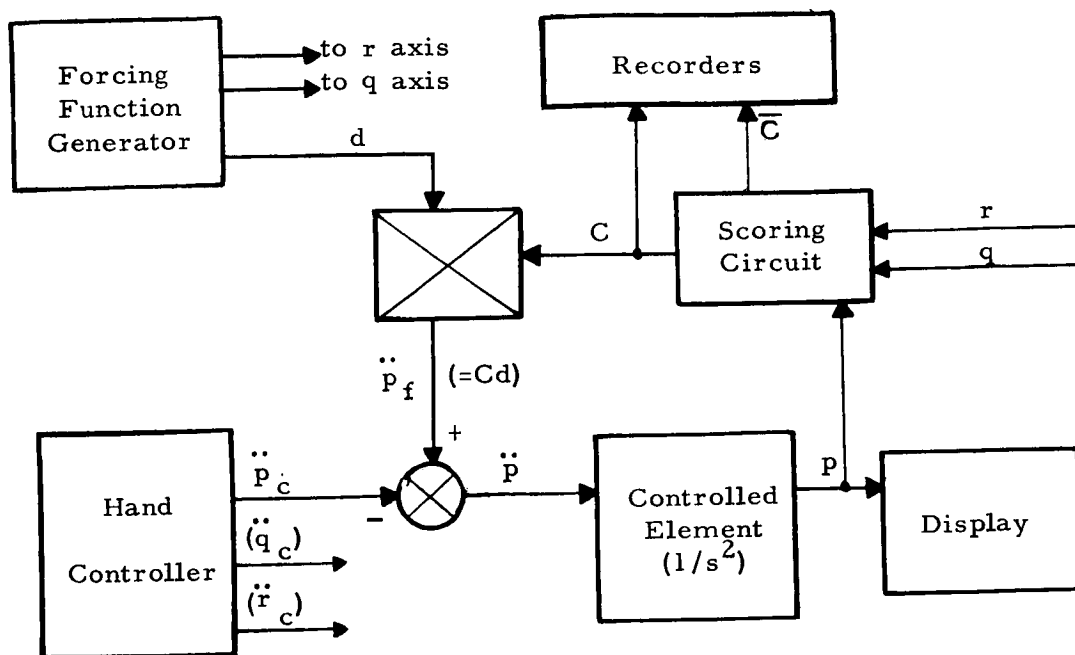


Figure 2.—Block diagram of one axis of example task.

$d$  = random step disturbances. Steps rectangularly distributed in 64 equal intervals in the range  $\pm 0.28$ . Every 2 seconds there is a 0.33 probability that the disturbance entering any axis will be changed.

$C$  and  $\bar{C}$  = adaptive score and mean adaptive score, respectively, computed according to equations (1) and (2).

$\ddot{p}_f = Cd$  = disturbances; acceleration to be tracked.

$\ddot{p}_c$  = controller output;  $+0.28$ ,  $0$ , or  $-0.28$  for on-off control;  
 $+0.28 > \ddot{p}_c > -0.28$  for continuous control.

$p$  = output in one axis ( $q$  and  $r$  axes identical); limited to  $\pm 1.0$ .

measurements. There are different techniques by which this can be done. Table 4 shows the coefficient of variation ( $\sigma/\bar{X}$ ) of both tests for each day and the increase in test length required for the constant-difficulty test to have the same coefficient of variation as the adaptive. The only assumption is that the variability of the mean score (standard error of the mean) decreases as the square root of the test length.

From table 4 it can be seen that the adaptive test has much greater power efficiency than the constant-difficulty throughout training. The adaptive test is, in fact, equivalent to a much longer test of constant-difficulty.

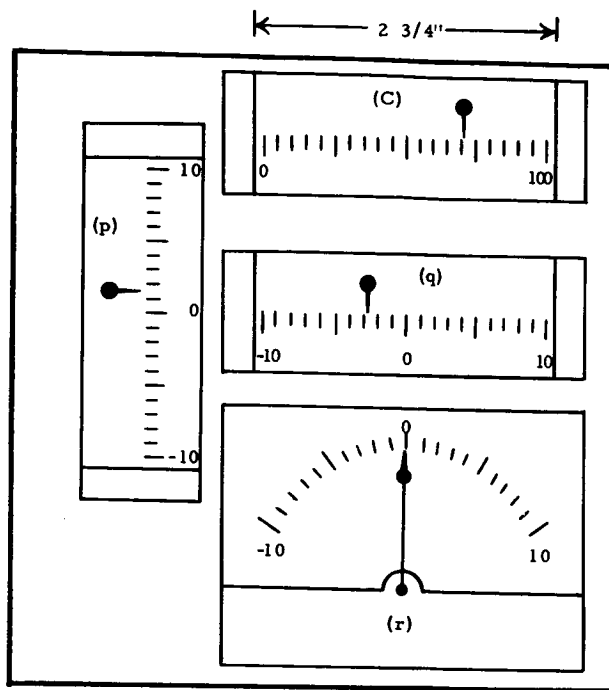


Figure 3.—Display panel employed for three-axis study; p, q, and r are the three axes of the task; C is the self-adjust score.

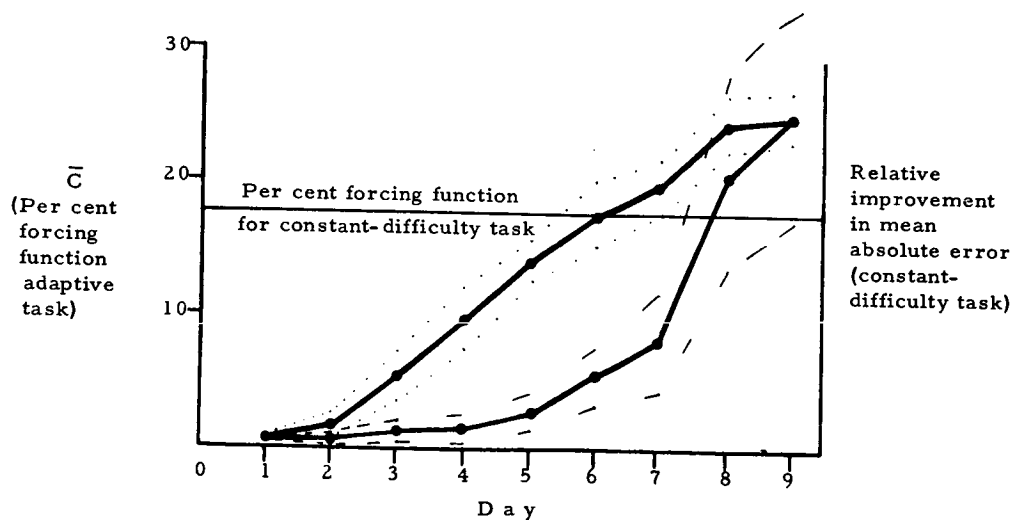


Figure 4.—Daily means  $\pm 1\sigma$  during training for adaptive (upper curve) and constant-difficulty (lower curve) two-axis tasks. Each point equals 10 trials.

TABLE 4. —POWER-EFFICIENCY OF CONSTANT-DIFFICULTY AS  
COMPARED TO ADAPTIVE TEST SCORES DURING TRAINING

Item	Day 1	Day 2	Day 3	Day 4	Day 5	Day 6	Day 7	Day 8	Day 9	$\bar{X}_{1-9}$
<u>Adaptive scores:</u>										
Mean ( $\bar{X}_a$ ) <sup>a</sup>	.437	1.77	5.43	9.77	14.07	17.64	19.77	24.29	25.0	13.13
Standard deviation, ( $\sigma_a$ ) <sup>a</sup>	(.350) <sup>b</sup>	(.980) <sup>b</sup>	1.91	2.32	1.60	2.46	2.11	2.17	1.74	1.74
Coefficient of variation, $V_a = \sigma_a / \bar{X}_a$	(.80) <sup>b</sup>	(.55) <sup>b</sup>	.35	.24	.11	.14	.11	.090	.070	.13
<u>Constant-difficulty scores:</u>										
Mean ( $\bar{X}_c$ ) <sup>a</sup>	.375	.780	1.16	1.59	2.84	5.67	8.09	20.96	25.0	13.13
Standard deviation ( $\sigma_c$ ) <sup>a</sup>	(.281) <sup>b</sup>	(.330) <sup>b</sup>	1.10	.86	1.30	2.18	3.78	7.14	7.64	2.74
Coefficient of variation, $V_c = \sigma_c / \bar{X}_c$	(.75) <sup>b</sup>	(.42) <sup>b</sup>	.95	.54	.46	.38	.47	.34	.31	.37
Ratio of constant-difficulty to adaptive test length that would yield equal coefficients of variation, $R = (V_c/V_a)^2$	(.883) <sup>b</sup>	(.588) <sup>b</sup>	7.32	5.24	16.26	7.60	19.13	14.49	19.32	7.82
Power-efficiency of constant- difficulty as compared to adaptive scores, $P = 1/R$	(1.13) <sup>b</sup>	(1.70) <sup>b</sup>	.14	.19	.06	.13	.05	.07	.05	.13

<sup>a</sup>Average for two subjects; ten trials for each condition for each day.

<sup>b</sup>Artifacts of data including many zero scores before any appreciable learning is in evidence.

The method of calculation employed in table 4 does not take into account differences in the slopes of the two learning curves at the various points of measurement. Thus it overestimates the power efficiency of the constant-difficulty task where the slope is less than that of the adaptive, and underestimates it where the slope is greater. The average slope of the two curves over training is, of course, the same. Correcting for this factor, the power efficiency of the constant-difficulty scores rises to its maximum (still well below the adaptive task) on day 8, when the slope of that curve is much greater than that of the adaptive. This represents an optimum for the constant-difficulty task. Its power efficiency is lower prior to and after day 8. It is on day 8 that the adaptive task adjusts itself through the level of difficulty maintained throughout on the constant-difficulty task as figure 4 shows. Prior to this day the constant-difficulty task was too difficult; after, it was too easy, in relation to the criterion of error set into the adaptive task. A principal virtue of the adaptive task is, of course, that it keeps an appropriate difficulty level, irrespective of the level of performance measured.

After the data of figure 4 and table 4 were gathered, the subjects were trained on a three-axis version of the adaptive task with an on-off three-axis hand controller. Their three-axis  $\bar{C}$  scores reached the same level as the best two-axis performance (25 percent forcing function) in 40 trials, and has progressed steadily for approximately an additional 250 trials, to a current level on the order of 70 percent forcing function for a performance criterion comparable to that of the two-axis task. They now handle a forcing function some three times as great as that which test pilots highly trained on three-axis control are able to cope with in 15 to 20 practice trials. They are still improving, though the slope of their learning curve has reduced. The variability of their performance has decreased with training. The standard deviation for various series of homogeneous three-axis trials is now at or under 5-percent forcing function, even though the mean score may be 70-percent forcing

function or higher. The coefficient of variation ( $\sigma/\bar{X}$ ) is 0.07 or less. This precision permitted design differences to be pinpointed accurately with few trials, as the experimental data will show.

## EXAMPLE EXPERIMENTAL DATA

**DISPLAY GAIN.**—In this study the gain of the display signal was systematically varied to reduce the output range to one-half, one-fourth, or one-eighth of its full-scale value in each axis. The three-axis output signals, ordinarily ranging across the entire display scales, were thus restricted to the central 50, 25, or 12.5 percent portions of these scales. The subject's line-of-sight distance to the display remained 2 feet on all trials. The display scale was 2.75 inches long, or  $6.6^\circ$  of visual angle for the normal display gain of 1.0 and correspondingly smaller for the other conditions. The on-off three-axis controller was employed. The task utilized vector error scoring using the following equation:

$$C = 0.021 \int_0^{300} \left( 0.33 - \sqrt{\frac{p^2 + r^2 + q^2}{3}} \right) dt + 0.5$$

where  $C$  is the ratio of the forcing function range to the controller range. The score taken was  $\bar{C}$ , the time-average of  $C$ . The controller output in each axis was integrated twice (range  $\pm 0.28/s^2$ ) as was the forcing function (range  $\pm 0.28C/s^2$  at each instant) to form  $p$ ,  $q$ , and  $r$ . In the above scoring equation  $e_L$ , the desired vector error, is set to allow three standard deviations of error on each axis display, assuming equal gaussian distributions of error in each axis. There were no practice trials under each condition, although the subject was warmed up and fully practiced on the standard (1.0) display gain condition. A warm-up effect was apparent in the data on the smallest gain, as the data of table 5 and figure 5 show. An x-y plot of  $C$  that was taken indicated little practice effect during the second trial, however. The better score under this one condition may be considered more representative than the mean. The dotted line of figure 5 is the best estimate of the actual underlying function, taking this factor into account.

Some data obtained in quite a different way and for a different purpose provided an indication of the accuracy of the curve of figure 5. In studying scoring, different settings of desired vector error ( $e_L$  in the equation for this task) were used. These settings were made to examine the score with the displays showing  $3\sigma$ ,  $4\sigma$ ,  $6\sigma$ , and  $10\sigma$  of the error amplitude distribution. Since this confines the error amplitude distribution within a predetermined proportion of the display, the result is, in effect, a change in display gain. Thus, for example, if  $C$  (percent forcing function) adjusts to the point that  $\pm 6\sigma$  of the error-amplitude distribution appears on the same scale that previously showed a  $\pm 3\sigma$ , the net effect is a reduction in display gain to 0.5 of its  $3\sigma$  value. A difference is that the (unusual) errors between  $3$  and  $6\sigma$  are shown in the second case. Despite this difference, the data obtained by the second technique are virtually the same as by the first, as table 6 indicates. The data from the second technique are plotted as triangles in figure 5. Note that the four triangles fall virtually on the curve drawn to fit the previous data.



TABLE 5.—PERCENT FORCING FUNCTION ( $\bar{C}$ ) IN A THREE-AXIS ADAPTIVE ACCELERATION CONTROL TASK AS AFFECTED BY REDUCING THE GAIN OF DISPLAY METER SIGNALS

Trial	Display gain	Score
1	1.000	79.0
2	.500	65.5
3	.250	47.2
4	.125	21.2
5	.125	38.4
6	.250	53.5
7	.500	68.7
8	1.000	74.2
		<u>Mean score</u>
4 and 5	.125	29.7
3 and 6	.250	50.4
2 and 7	.500	67.1
1 and 8	1.000	76.6

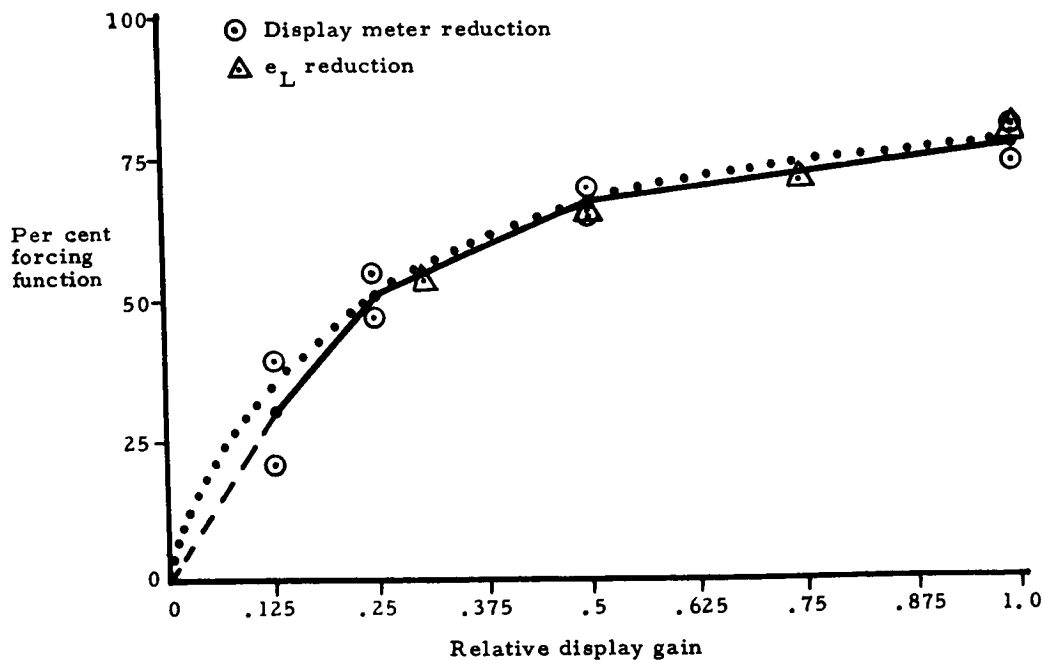


Figure 5.—Percent forcing function ( $\bar{C}$ ) in a three-axis adaptive acceleration control task. The display scale length corresponding to a gain of 1.0 subtended  $6.6^\circ$  of visual angle. The dotted curve is the best estimate of the underlying function. (Data from tables 5 and 6.)

TABLE 6. —PERCENT FORCING FUNCTION ( $\bar{C}$ ) VERSUS DISPLAY GAIN IN A THREE-AXIS ADAPTIVE ACCELERATION CONTROL TASK AS AFFECTED BY REDUCING THE ERROR AMPLITUDE BY ADJUSTING  $e_L$  IN THE ADJUSTMENT EQUATION  
[see fig. 5]

Trial	Desired vector error, three axes ( $e_L$ ) <sup>a</sup>	Desired rms error, each axis in proportion of display scale	Score ( $\bar{C}$ ) in percent forcing function	Relative display gain	Comparative score from table 5
1	0.17 ( $= \sqrt{3}/10$ )	0.10	53.4	$\begin{Bmatrix} 0.25 \\ .30 \end{Bmatrix}$	50.4
2	.29 ( $= \sqrt{3}/6$ )	.17	66.0	.50	67.1
3	.43 ( $= \sqrt{3}/4$ )	.25	70.2	.75	-
4	.58 ( $= \sqrt{3}/3$ )	.33	78.8	1.00	76.6

<sup>a</sup> It is more convenient to divide the error-squared score by the number of axes according to equation (1) than to increase the desired vector error by the square root of that number as done here, although the effect is very much the same. The experimental data were gathered before scoring equations (1) and (2) were developed.

This example illustrates many of the virtues of the adaptive approach recommended here. The elimination of variations in task error scores allows the variables of interest to be compared directly, as forcing function amplitude and display gain are compared in figure 5. Operator error does not enter the picture. The precision of the technique as a measuring instrument makes for a great economy in taking data. All the data for the display gain study were gathered in half a day, and the total actual running time was only 60 minutes. The designer can employ data such as provided by figure 5 to determine display scale, and to see what loss in precision of control would result from reducing either the physical size of display scales or the gain of display signals.

It is instructive to consider how the information in figure 5 (which traces quite precisely the relation between display gain and forcing-function amplitude in a three-axis acceleration control task) could be obtained by employing constant-difficulty simulation. First, the relation between forcing-function amplitude and operator error would have to be traced by gathering data at several different forcing-function amplitudes. Next, the relation between display gain and operator error would have to be defined experimentally in the same way. The relative imprecision of constant-difficulty tasks would require substantial amounts of data if the two relations were to be accurately defined. The two relations would each be highly nonlinear (as figs. 4 and 5 indicate) and direct comparison would be possible only at points where similar error scores were obtained with different combinations of forcing-function amplitude and display gain. In practical terms, to show the relation depicted in figure 5 to the same accuracy, at least several weeks of data collection via constant-difficulty tasks would appear necessary.

CONTINUOUS VERSUS ON-OFF CONTROL. —Subjects were originally trained for 180 trials on a two-axis continuous controller, after which they switched to a three-axis on-off controller and were trained for some 250 more trials. Because the change to on-off control

and to three-axis control was done simultaneously, the effects could not be separated. Since these are typical design variables, data were gathered on them for this study.

Prior to the run, a Monte Carlo run on a digital computer was made to determine the coefficients of a McRuer and Krendell-type model optimum for one axis of this task. The "Pactolus" analog program of the SDS 920 was employed to optimize gain, lead, and lag terms in the following standard human operator model:

$$H(s) = \frac{Ke^{-0.15s}(1+T_L s)}{(1+0.1s)(1+T_I s)}$$

where

$H(s)$  linear approximation to the human operator transfer function

$K$ ,  $T_L$ , and  $T_I$  operator gain, lead, and lag terms, respectively

$s$  the Laplace operator

The task as shown in figure 2 was represented in digital form as described, including its nonlinearities. The output of the controller was continuous and was limited to  $\pm 0.28$ , so that changes in gain affected only the slope of the controller function. An on-off controller thus would have had a limited output, but an infinite slope of output versus displacement. Under these conditions it was uncertain whether or not the gain term  $K$  would go toward infinity on the optimization runs. It did not, however; instead it reached an optimum close to 3.0 and produced worse performance for higher and lower values. At this gain, the limit of controller output was frequently reached. It thus appeared that continuous control should be somewhat superior to on-off control for this task. This is by no means a foregone conclusion, as skilled operators often adopt a "bang-bang" form of operation with continuous controllers in acceleration-control tasks.

The actual three-axis hand controller employed for gathering data in these studies had a basic continuous output that could be converted to "on-off" electronically by the use of appropriate comparators and limiters. A small deadzone protected against accidental activation of one axis while making corrections in another. Figure 6 shows the curves of controller output for on-off versus continuous operation.

Because the subject had been trained originally for 180 trials on a continuous two-axis task, and for 250 subsequent trials on the on-off three-axis task, the training situation perhaps favored on-off control. The data gathered consisted of one trial in each of the three axes individually, one trial in each of the three possible pairs of axes, and five trials on the three-axis task. This balanced out effects of differences among axes, although it added the variance due to such differences to each of the main effects studied. These differences were not large, and the use of different axes and combinations of axes contributed to the generality of the data. The "on-off" series was run first; the continuous series, second.

Because one-axis performance would bring the score close to or exceeding 100 percent forcing function with an rms error of  $\pm 0.33$  display scale, a desired rms error of 0.10 display scale was selected. This reduced the scores by the desired amount. For the two- and three-axis tasks,  $e_L$  was multiplied by  $\sqrt{2}$  and  $\sqrt{3}$ , respectively, to keep the same desired rms error (0.10) for the individual axes, that is,  $e_L$  was 0.10, 0.14, or 0.17 for one, two, and three axes, respectively.<sup>3</sup>

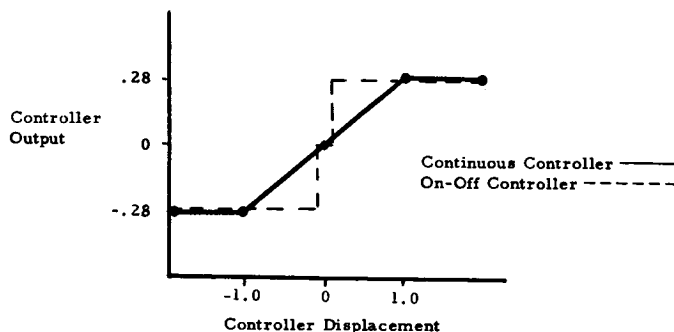


Figure 6. —Curve of controller displacement versus output for each axis of the three-axis task.

Table 7 shows the results, which are plotted in figure 7. There is a relative advantage of about 9 percent for the continuous controller, even though the subject was so highly practiced using the on-off. It is interesting that this difference is virtually the same for one-, two-, and three-axis acceleration control. It might seem that in three-axis tracking the subject would have less time to develop appropriate continuous output signals in each axis, and would tend toward on-off control under this one condition. If this were true, the continuous controller would be of less relative value in three-axes tracking. Figure 7 does not support this hypothesis.

Figure 8 is two typical 30-second pen-recorder samples of the controller response in each axis on one of the three-axis trials. Unfortunately, pen records were not made of corresponding one- and two-axis trials.

#### ONE- VERSUS TWO-AXIS

**TRACKING.** —The score for different axes and axis combinations of table 7 and figure 7 may be less than typical differences, due to the fact that the subject had more than 20 times as much training on multiaxis as on single-axis versions of the task. He was relatively much more proficient with three than two axes and with two than with a single axis. The score differences between one and two and three axes are very likely smaller than would have been found using subjects equally practiced on one-, two-, and three-axis trials. It is, of course, no reflection on the adaptive technique, which accurately portrayed the true level of skill of the subject on each task.

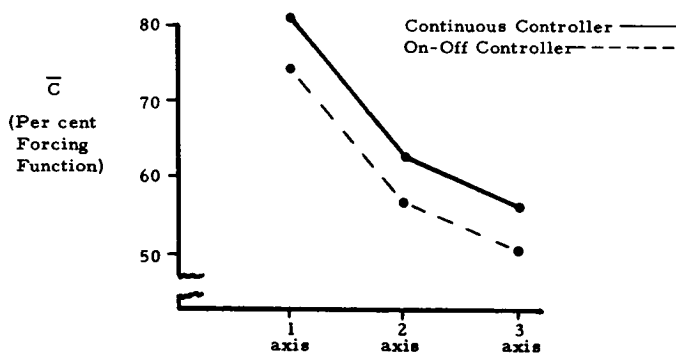


Figure 7. —Continuous versus on-off control in 1, 2, and 3 axes.

<sup>3</sup>As previously noted, it is better to divide the error-squared scores by  $N$ , the number of axes, than to multiply  $e_L$  by  $\sqrt{N}$ . The latter has the effect of increasing  $K$  in equation (1) by  $\sqrt{N}$ ; this probably did not change the mean scores ( $\bar{C}$ ) of this study.

TABLE 7.—ADAPTIVE TASK SCORES IN PERCENT FORCING FUNCTION FOR ONE-, TWO-, AND THREE-AXIS ACCELERATION CONTROL, FOR BOTH ON-OFF AND CONTINUOUS CONTROLLER OUTPUT

[All main effects (continuous versus on-off, one versus two axes, and two versus three axes) are statistically significant, with critical ratios greater than 3.0.]

On-off trials				Continuous trials			
Trial	Axes (a)	$e_L$	$\bar{C}$ , percent	Trial	Axes (a)	$e_L$	$\bar{C}$ , percent
1	p	0.10	68.4	12	pqr	0.17	61.7
2	q	.10	73.9	13	pqr	.17	56.4
3	r	.10	81.0	14	pqr	.17	55.5
4	pq	.14	54.6	15	pqr	.17	56.4
5	qr	.14	56.4	16	pqr	.17	50.3
6	pr	.14	59.5	17	pr	.14	66.6
7	pqr	.17	51.8	18	pr	.14	59.5
8	pqr	.17	49.7	19	pq	.14	61.0
9	pqr	.17	52.1	20	r	.10	83.4
10	pqr	.17	50.3	21	q	.10	79.1
11	pqr	.17	48.5	22	p	.10	80.4
$\bar{X}$ , 1-3 (single axis) 74.4				$\bar{X}$ , 20-22 (single axis) 81.0			
$\bar{X}$ , 4-6 (double axis) 56.8				$\bar{X}$ , 17-19 (double axis) 62.4			
$\bar{X}$ , 7-11 (three-axis) 50.5				$\bar{X}$ , 12-16 (three-axis) 56.1			
$\bar{X}$ , 1-11 (all on-off trials) 58.84				$\bar{X}$ , 12-22 (all continuous trials) 64.57			
$\bar{X}$ , (1-3 + 20-22) (all single axis trials) 77.7							
$\bar{X}$ , (4-6 + 17-19) (all double axis trials) 59.6							
$\bar{X}$ , (7-16) (all three-axis trials)				53.3			

<sup>a</sup>p equals fore-aft axis; q equals side-side axis; r equals twist axis of controller.

These data illustrate again how design data of importance can be obtained via adaptive simulation with relatively little expenditure of effort. Although the differences between one- and two-axis and two- and three-axis control were not large, they were determined with sufficient precision with but a few trials that the results are statistically significant. In studies of the same question by other investigators, differences between one- and two-axis performance have not been demonstrated except when the controlled element dynamics are unlike in the two axes. Chernikoff et al. (ref. 15) tested one- and two-axis control for position, rate, and acceleration tracking, and found no differences in one- versus two-axis performance except when the controlled element dynamics were different in the two

axes.<sup>4</sup> These data perhaps represent a fair test of the power of adaptive simulation in studies of this kind. All the data of table 7 comparing one, two, and three axes and continuous versus on-off control were gathered in 1 day, with 22 five-minute trials on one subject.<sup>5</sup> Yet the relationships of interest were established quantitatively with a satisfying degree of precision.

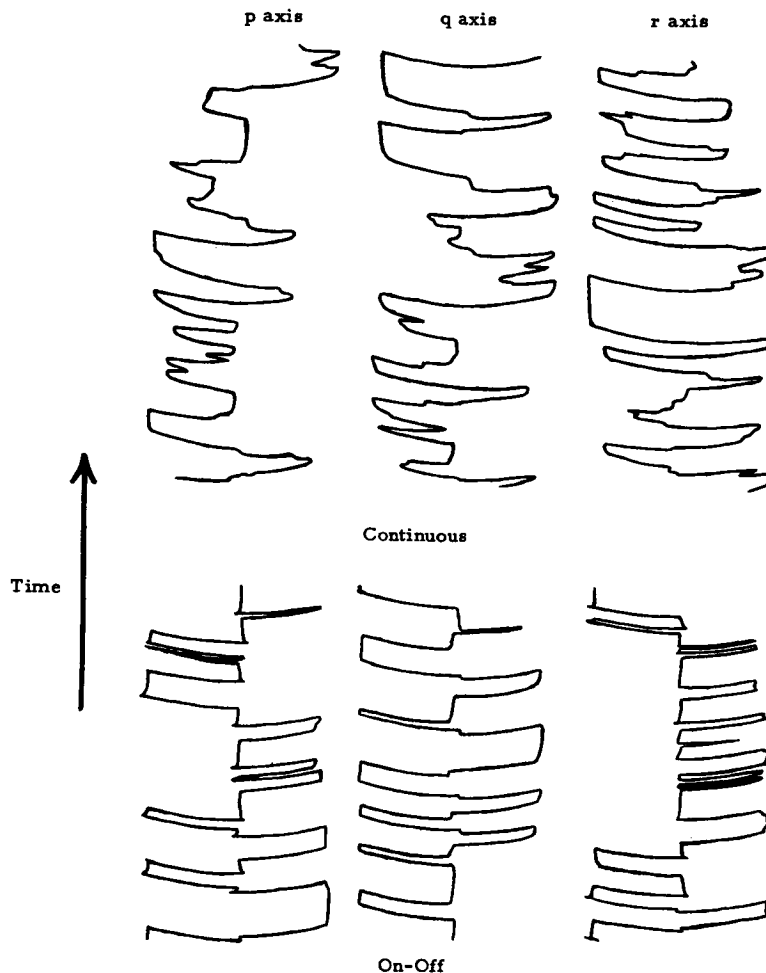


Figure 8.—Pen record of controller output signals for typical 30-second segments of continuous and discrete three-axis trials.

<sup>4</sup>The studies of Todosiev, et al. (paper 11) and of Levinson (paper 12) in the present volume also failed to establish differences between one- and two-axis performance with identical controlled element dynamics of the two axes. All of these studies (Chernikoff et al. (ref. 15), Todosiev et al., and Levinson) differed principally from the present one in their use of fixed difficulty simulators.

<sup>5</sup>Adaptive tracking such as employed in this study is so trying that no more than five or six 5-minute trials per hour and about 25 trials per day can be run without danger of encountering large fatigue effects.

## CONCLUDING REMARKS

The above examples illustrate certain straightforward applications of adaptive simulation to typical design problems in manual control. In each case the design variable of interest (display gain, on-off versus continuous control, one- versus two- versus three-axis control) was related to an adaptive variable (forcing function amplitude) with precision and economy of experimental effort.

A major feature of the particular adaptive simulation technique illustrated here is that it uses adaptation to keep operator performance at a preestablished criterion level. This permits the exploration of the relations among manual control design variables without first exploring the often imprecise and nonlinear relation of each variable to operator error and then attempting to adduce their relations to each other. By holding error constant adaptively, design variables can be compared directly, as the example experimental data have illustrated.

Studies now in progress are extending the technique to other design variables, such as control and display lags. Other ways of applying the technique are also explored, including these two, in particular:

(1) The use of design variables as adaptive parameters, in the technique defined in the original paper (ref. 2).

(2) The use of an adaptive secondary or operator loading task technique, in which performance on one task is employed to adjust ("adapt") another.

Either primary or secondary tasks may be adjusted in the latter technique. Its virtue is to hold performance on one of the tasks to a preset standard, transferring the variance entirely to the other by means of adaptive task changes.

For one working with it, adaptive simulation appears to be a tool of great power, deserving much wider use than is being made of it at present.

## REFERENCES

1. Birmingham, H. P.: The Instantaneous Measurement of Human Operator Bandwidth. Presented at 8th Annual Conference on Manual Control, 1959.
2. Kelley, C. R.: Self-Adjusting Vehicle Simulators. The Predictor Instrument: Final Report and Summary of Project Activities During 1961. Dunlap and Associates, Inc., Jan. 1962. (Also presented at IRE Internat. Cong. on Human Factors in Electronics (Long Beach, Calif.), May 3-4, 1962).
3. Birmingham, H. P.; Chernikoff, R.; and Ziegler, P. N.: The Design and Use of "Equalization" Teaching Machines. Presented at IRE Internat. Cong. on Human Factors in Electronics (Long Beach, Calif.), May 3-4, 1962.
4. Hudson, E. M.: An Adaptive Tracking Simulator. Presented at IRE Internat. Cong. on Human Factors in Electronics (Long Beach, Calif.), May 3-4, 1962.

5. Chernikoff, R.: Human Equalization: Concept Machine and Measurement. Proceedings of ONR Symposium on Complex Vehicular Controls, May 1962.
6. Hudson, E. M.: Adaptive Training and Nonverbal Behavior. NAVTRADEVCCEN-1395-1, Naval Training Device Center, 1964.
7. Kelley, C. R.: Testing the Effects of Extended Space Missions on Piloting Skill. Proceedings of a Symposium, Physiological and Performance Determinants of Manned Space System Design, Am. Astron. Soc., 1965.
8. Kelley, C. R.; Mitchell, M. B.; and Strudwick, P. H.: The MOL Tracking Task: Development of a Test of Tracking Skill for Inclusion in the General Performance Battery of the Air Force Manned Orbital Laboratory. Preliminary Technical Report, Dunlap and Associates, Inc., June 1965.
9. Bahrick, H. P.; Fitts, P. M.; and Briggs, G. E.: Learning Curves—Facts or Artifacts? Psychol. Bull., vol. 54, 1957, pp. 256-268.
10. Bilodeau, E. A.; and Bilodeau, Ina, McD.: Motor Skills Learning. Ann. Rev. Psychol., vol. 12, 1961, pp. 243-280.
11. Obermayer, R. W.; and Muckler, F. A.: Performance Measures in Flight Simulation Studies. AIAA Simulation for Aerospace Flight Conference, Aug. 26-28, 1963.
12. Miller, D. C.: The Effects of Performance-Scoring Criteria on Compensatory Tracking Behavior. IEEE Trans. on Human Factors in Electronics, vol. HFE-6, no. 1, 1965, pp. 62-65.
13. McNemar, Q.: Psychological Statistics. John Wiley & Sons, 1955.
14. Peters, C. C.; and Van Voorhis, W. R.: Statistical Procedures and Their Mathematical Basis. McGraw-Hill Book Co., Inc., 1940.
15. Chernikoff, R.; Duey, J. W.; and Taylor, F. W.: Two-Dimensional Tracking with Identical and Different Control Dynamics in Each Coordinate. J. Exp. Psychol., vol. 60, 1960.



N67-15879

PRECEDING PAGE BLANK NOT FILMED.

## 28. DISCUSSION OF SPECTRAL HUMAN-RESPONSE ANALYSIS

*Lawrence W. Taylor, Jr.*  
*Flight Research Center, NASA*

Estimates of describing functions and associated parameters that represent a human pilot performing a compensatory tracking task, while being subjected to a random-appearing input, are expressed in terms of cross- and power-spectral-density functions. The expression most commonly used for spectral densities is the Fourier transform of the autocorrelation and cross-correlation functions. Use of an equivalent expression for spectral-density functions, the product of the Fourier transforms of the signals divided by the record length, makes several simplifications become evident.

The estimates of the human describing function are seen to be unchanged by correlation with other signals and are shown to be equal to the ratio of the Fourier transforms of the pilot's output and error. The expression for the linear-correlation coefficient is shown to be ill-defined, since it equals 1 under all circumstances. Alternate definitions of this parameter are discussed. The need for a sum of sine waves for an input is also discussed, and the technique for making measurements of the remnant is outlined. In addition to the analytical considerations, a computational advantage results which enables improvements in accuracy.

About a year and a half ago, the NASA Flight Research Center became interested in human-response analysis when it was decided to record human-response data as part of a NASA-USAF-Cornell Aeronautical Laboratory (CAL) handling-qualities program. The program was originally conceived as a study of a number of configurations which were simulated by using a USAF-CAL variable-stability airplane. The decision to collect human-response data was made primarily because of the wealth of data that could be gained with a relatively small extension of the handling-qualities program. The results of the human-response-analysis portion of this program are reported in paper 20 of this volume. The development of the methods used to analyze the data collected is discussed in this paper.

### SYMBOLS

$A_k$	power of the pilot linear output 0 at the $k$ th input frequency
$A_{kn}$	power of the $n$ th harmonic of the input frequency $\omega_k$ of the pilot output
$c$	total output of pilot
$e$	error
$F[x(t)]$	Fourier transform, $\int_0^T x(t)e^{-j\omega t} dt$
$i$	tracking-task input
$j=\sqrt{-1}$	
$k$	identification of input frequency
$M$	number of input frequencies
$m$	response of controlled element

N	nonlinear element
n	identification of harmonic
o	linear output of pilot
r	remnant
T	half of total record length
t	time
$x(t), y(t)$	signals
$Y_c$	controlled-element transfer function
$Y_p$	human describing function
$\alpha$	variable of substitution
$\rho$	linear-correlation coefficient, $\frac{\bar{\phi}_{ee}  Y_p ^2}{\bar{\phi}_{cc}}$
$\rho_a$	average linear-coherence coefficient
$\sigma_x$	standard deviation, $\sqrt{x^2 - \bar{x}^2}$
$\tau$	lag time
$\bar{\phi}_{xx}(\omega)$	power-spectral-density-function estimate, $F[\bar{\phi}_{xx}(\tau)]$ or $\frac{F^*(x)F(x)}{2T}$
$\bar{\phi}_{xy}(\omega)$	cross spectral-density-function estimate, $F[\bar{\phi}_{xy}(\tau)]$ or $\frac{F^*(x)F(y)}{2T}$
$\bar{\phi}_{xx}(\tau)$	autocorrelation-function estimate, $\frac{1}{2T} \int_{-T}^T x(t)x(t + \tau)dt$
$\bar{\phi}_{xy}(\tau)$	cross-correlation-function estimate, $\frac{1}{2T} \int_{-T}^T x(t)y(t + \tau)dt$
$\omega$	frequency

Subscripts:

auto autopilot

A bar over a variable denotes a time average. An asterisk denotes a complex conjugate.

## DISCUSSION

In preparation for the analysis of the data, a review was made of the various techniques that have been used to determine the pilot's describing-function input  $Y_p$  under the conditions illustrated in figure 1. A random-appearing sum of 10 sine waves serves to disturb the pilot in his effort to stabilize the airplane in a wings-level attitude. The linear portion of the pilot output is attributed to  $Y_p$ , and the nonlinear and random portion to the remnant  $r$ . If the pilot were indeed quasi-linear, as an airplane, we need only find the Fourier transforms of the pilot's output  $c$  and input  $e$  and determine their ratio for  $Y_p$ . This type of analysis had been made at the Flight Research Center for many years, so that we were familiar with it. The pilot, however, was known to be nonlinear and nondeterministic, which was understood to require a somewhat different analysis. Specifically, the literature (ref. 1) suggested that the best estimate of  $Y_p$  was the ratio of the cross spectra of the tracking-task input  $i$  to the

pilot output  $c$  and the tracking-task input  $i$  to the error  $e$ . That is,

$$Y_p = \frac{\Phi_{ic}}{\Phi_{ie}}$$

There are, however, two commonly used estimates of the power-spectral-density function. The first expression of the cross-spectral density is the equation that is almost always used for random signals and consists of the Fourier transform of the autocorrelation of the two signals involved

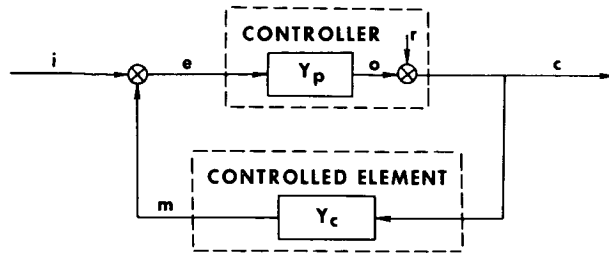


Figure 1.—Describing function model of a human controller.

$$\Phi_{xy}(\omega) = F\left[\varphi_{xy}(\tau)\right] = \int_{-T}^T \left[ \frac{1}{2T} \int_{-T}^T x(t)y(t+\tau)dt \right] e^{-j\omega\tau}d\tau \quad (1)$$

The second expression is the product of the Fourier transforms of the signals divided by the record length:

$$\Phi_{xy}(\omega) = \frac{F^*[x]F[y]}{2T} = \left[ \int_{-T}^T x(t)e^{j\omega t}dt \right] \left[ \int_{-T}^T y(\tau)e^{-j\omega\tau}d\tau \right] \frac{1}{2T} \quad (2)$$

Because of our experience in Fourier analysis and because we believed the two expressions to be equivalent, we chose to use the second expression and wrote a digital computer program to analyze the data. While the program was being written, we realized that part of the computation was superfluous. If the second expression for the cross-spectral density is substituted into the expression for  $Y_p$ , identical factors appear in the numerator and denominator. Cancellation of these terms results in the estimate of  $Y_p$  again being simply the ratio of the Fourier transforms, as for a quasi-linear system

$$Y_{p\text{estimate}} = \frac{\Phi_{ic}}{\Phi_{ie}} = \frac{\frac{1}{2T}F^*[i]F[c]}{\frac{1}{2T}F^*[i]F[e]} = \frac{F[c]}{F[e]}$$

This result was questionable, since it did not agree with certain mathematical arguments and experimental evidence in the literature, which are discussed subsequently. A similar result occurred when similar expressions for the cross and power spectra were substituted into the equation used for the linear-correlation coefficient  $\rho$ . The numerator and denominator become identical, with the result that the value of  $\rho$  equals 1.0 for all signals, erroneously indicating linearity under all circumstances:

$$\rho^2 = \frac{|\bar{\phi}_{ic}|^2}{\bar{\phi}_{ii}\bar{\phi}_{cc}} = \frac{F^*[i]F[c]F[i]F^*[c]}{F^*[i]F[i]F^*[c]F[c]} = 1.0$$

At this point help was sought through meetings with individuals who had performed such analysis before, through letters, and by a literature search. In fact, several human-response analysts and experts in related fields helped resolve this problem. This is, therefore, a report of the results of a cooperative effort rather than just the work at the Flight Research Center.

ESTIMATES OF POWER-SPECTRAL DENSITY.—Nelson of MIT was quick to point out that the two expressions were equivalent, a fact which has considerable coverage in the literature on statistical analysis (refs. 2 to 5). A proof of this equivalence is offered as follows: The first expression for cross-spectral density is expanded to show the integral expressions of the Fourier transform and the cross-correlation function

$$\begin{aligned}\bar{\phi}_{xy}(\omega) &= F\left[\varphi_{xy}(\tau)\right] = \int_{-T}^T e^{-j\omega\tau} \left[ \frac{1}{2T} \int_{-T}^T x(t)y(t+\tau)dt \right] d\tau \\ &= \frac{1}{2T} \int_{-T}^T \left[ \int_{-T}^T y(t+\tau)e^{-j\omega(t+\tau)}d\tau \right] x(t)e^{j\omega t}dt\end{aligned}$$

Then, by a variable substitution and rearrangement, a product of Fourier transform integrals is obtained, thereby showing it to be equal to the second expression of cross-spectral density

$$\bar{\phi}_{xy}(\omega) = \frac{1}{2T} \left[ \int_{-T}^T x(t)e^{j\omega t}dt \right] \left[ \int_{-T}^T y(\alpha)e^{-j\omega\alpha}d\alpha \right] = \frac{1}{2T} F^*(x)F(y)$$

where  $\alpha = t + \tau$

Therefore

$$\begin{aligned}\bar{\phi}_{xy}(\omega) &= \bar{\phi}_{xy}(\omega) \\ (1) \quad & (2)\end{aligned}$$

This means that the  $Y_p$  estimate in the literature is actually equal to the ratio of the Fourier transforms and that  $\rho$ , as presently defined, does equal 1 in spite of experimental evidence that indicates otherwise.

In addition to the analytical considerations of expressing  $Y_p$  in terms of the Fourier transforms, there is a real computational advantage. In order to determine cross-correlation functions, virtually all points of one time history are multiplied by those of another time history, which requires that considerable information be contained in the computer's memory. For one application this necessitated extensive thinning of the data, which caused a noticeable loss in accuracy. Fourier transforms, on the other hand, can be determined without storing the time histories, thereby removing the restriction on the amount of data processed and allowing an improvement in accuracy. Figure 2 shows

a comparison of estimates of  $Y_p$  for a known "autopilot" whose describing function is given by the curve. The open symbols show the result of using the cross-correlation function as an intermediate step (see eq. (1)) and applying a Hamming lag window, and the solid symbols show the alternate Fourier transform approach of equation (2). The latter is obviously superior because of the increased amount of data that was processed, the better resolution in frequency by not smoothing, and possibly the more straightforward numerical methods involved. (Different estimates of  $Y_p$  at the same frequency resulted when the analysis was repeated using different time intervals to obtain the desired frequency range.)

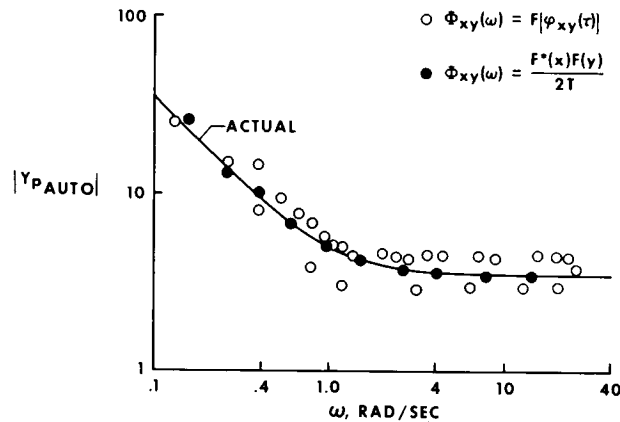


Figure 2.—Comparison of measured and actual autopilot gain.

**HUMAN DESCRIBING FUNCTION.**—Elkind (ref. 6) had indicated a different result in the estimate of  $Y_p$  if the correlation of the pilot's error and output is made with respect to the pilot error rather than the tracking-task input:

$$Y_{p_{\text{error}}} = \frac{\bar{\phi}_{ec}}{\bar{\phi}_{ee}} \neq Y_{p_{\text{input}}} = \frac{\bar{\phi}_{ic}}{\bar{\phi}_{ie}}$$

In the latter case, it was maintained that no bias would result because of the lack of any correlation between the remnant and the tracking-task input:

$$Y_{p_{\text{input}}} = \frac{\bar{\phi}_{io}}{\bar{\phi}_{ie}} + \frac{\bar{\phi}_{ir}}{\bar{\phi}_{ie}} = Y_{p_{\text{actual}}}$$

if  $\bar{\phi}_{ir} = 0$ .

If the Fourier transform expressions of the cross-spectral-density functions are used, however, both estimates are equal

$$Y_{p_{\text{error}}} = \frac{\phi_{ec}}{\phi_{ee}} = Y_{p_{\text{actual}}} + \frac{\phi_{er}}{\phi_{ee}} = Y_{p_{\text{actual}}} + \frac{F(r)}{F(e)}$$

$$Y_{p_{\text{input}}} = \frac{\phi_{ic}}{\phi_{ie}} = Y_{p_{\text{actual}}} + \frac{\phi_{ir}}{\phi_{ie}} = Y_{p_{\text{actual}}} + \frac{F(r)}{F(e)}$$

If the remnant is uncorrelated with the input, its Fourier transform will equal zero so that both estimates will be unbiased:

$$Y_{p_{\text{error}}} = Y_{p_{\text{input}}} = Y_{p_{\text{actual}}}$$

if  $F(r) = 0$ .

Heretofore, the first estimate (that correlated to the error) was not recognized to be unbiased for the same conditions which made the second estimate (that correlated to the input) unbiased. The conclusion, then, is that both estimates are identical and both equal simply the ratio of the Fourier transform of  $c$  to that of  $e$ . If the remnant is uncorrelated to the input, the Fourier transform of the remnant will be zero at input frequencies, making the estimates of  $Y_p$  unbiased.

It might be well to point out that there is at least one way that bias can be present. In almost all nonlinearities, harmonics are generated at frequencies which are multiples of the input frequencies. Figure 3 shows the multitude of frequencies that are generated. First, the input frequencies are adequately spaced relative to the resolution in frequency that can be realized with the limitation resulting from the length of record to be analyzed. After the loop is closed, frequencies having multiples of each input frequency are generated, making it impossible to discriminate at the higher frequencies between linear response to the input frequencies and the remnant. This fact raises the question of the advisability of using a lag window or other smoothing technique, since they result in poorer resolution in frequency as a result of the broader bandwidth of the spectral-density estimate. Measures of the remnant are also involved in the calculation of the linear-correlation coefficient.

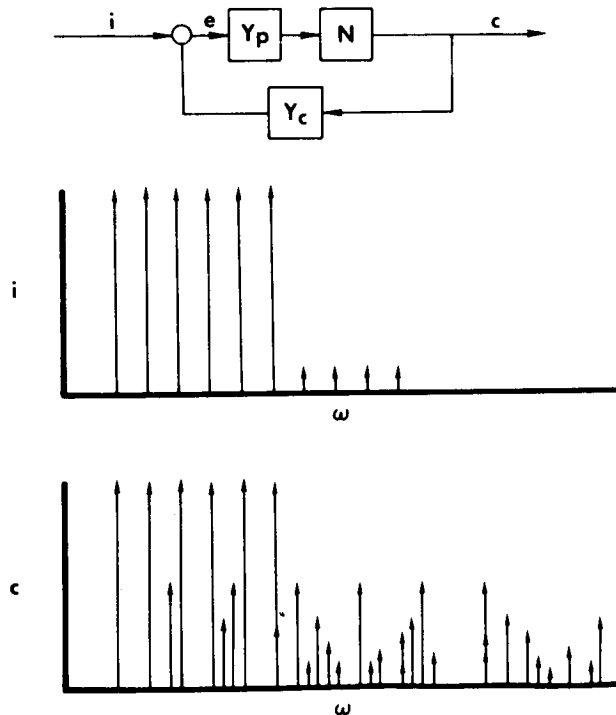


Figure 3.—Frequencies generated by a nonlinearity.

LINEAR-CORRELATION COEFFICIENT.—It was shown earlier that the linear-correlation coefficient  $\rho$  is equal to 1.0 for all signals when defined as

$$\rho^2 = \frac{|\bar{\Phi}_{ic}|^2}{\bar{\Phi}_{ii}\bar{\Phi}_{cc}} = \frac{F^*(i)F(c)F(i)F^*(c)}{F^*(i)F(i)F^*(c)F(c)} = 1.0$$

Let us consider what caused this definition of  $\rho$  to fail.

The linear-correlation coefficient was conceived as the square root of the ratio of the power of the linear part of the pilot's output to the total:

$$\rho = \sqrt{\frac{|Y_p|^2 \bar{\Phi}_{ee}}{\bar{\Phi}_{cc}}}$$

This is a meaningful measure of linearity, but, unfortunately, it is difficult to determine. The error made was the substitution of an expression for  $Y_p$  which makes  $\rho = 1$

$$Y_p = \frac{\bar{\Phi}_{ic}}{\bar{\Phi}_{ie}} = \frac{F(c)}{F(e)}$$

$$\rho = \sqrt{\frac{\frac{|F^*(c)F(c)|}{|F^*(e)F(e)|} F^*(e)F(e)}{F^*(c)F(c)}} = 1$$

It is, therefore, the bias of the estimate of  $Y_p$  that caused  $\rho$  to equal 1.0. It may be possible to determine meaningful values of  $\rho$  if the power at the harmonics of specific input frequencies can be assessed, in which case

$$\rho(\omega_k) = \sqrt{\frac{A_{k1}}{\sum_{n=1}^{\infty} A_{kn}}}$$

where

$$A_{kn} = \frac{F^*(c)F(c)}{2T^2} \text{ at } \omega = n\omega_k$$

Difficulties are anticipated in trying to use this expression of the linear-correlation coefficient because of the inability to discriminate and identify harmonics at the higher

frequencies. Kalman of Stanford University has suggested that the definition of  $\rho$  be changed to a ratio of expected values of cross and power spectra based upon a suitable probability distribution of the input amplitudes. He points out the need for repeated or at least partitioned experiments in which the input amplitudes are changed and the results of each part weighed. These ideas have not been tried, however, so it would be premature to publish or suggest the use of such a parameter until it has been proven to be a proper measure of linearity.

**REMNANT.**—Although the previous definition of  $\rho$  has no significance, there are certain measures that can be made of the remnant. The first requirement is that the input spectrum must have "holes" in it; that is to say, there must be ranges of frequency for which there is no input power. The reason for this requirement is that the remnant cannot be measured at frequencies for which there is input power because our estimate of  $Y_p$  assumes negligible remnant and, when that estimate is used to express remnant, the result is zero.

$$r = c - o = c - Y_p e$$

since

$$Y_p = \frac{F(c)}{F(e)}$$

$$F(r) = F(c) - \frac{F(c)}{F(e)} F(e) = 0$$

It is necessary, therefore, to use the  $Y_p$  estimate defined at nearby frequencies to measure the remnant at the intermediate frequencies. This point is illustrated in figure 4. The tracking-task input has power at the discrete frequencies indicated, and  $Y_p$  estimates have been determined at these frequencies. At the intermediate frequencies which fall between

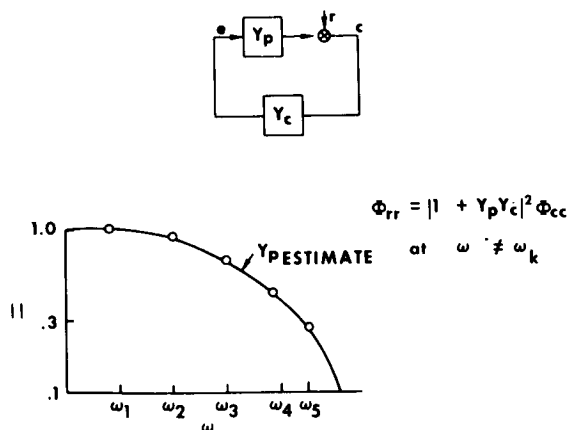


Figure 4.—Determination of remnant power-spectral density.

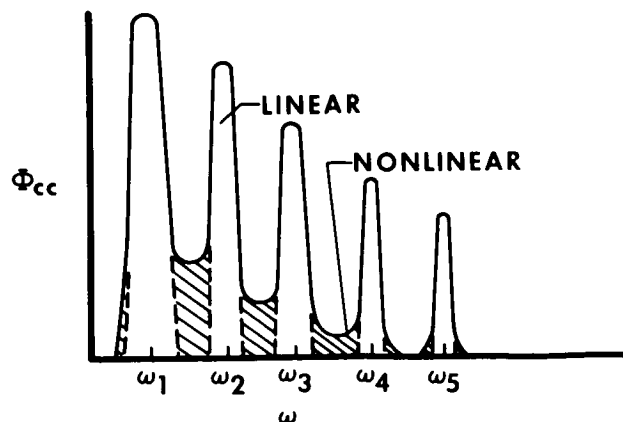


Figure 5.—Pilot's output power-spectral density.



these discrete frequencies, the power-spectral density of the remnant can be determined by using the expression shown. Note that it was possible to obtain an expression for the remnant only by knowing that there was no input at these frequencies.

Let us turn now to the power-spectral density of the total output of the pilot  $\Phi_{cc}$ . A typical result might be that shown in figure 5. The peaks occur at the input frequencies, and, if the pilot were linear, power would occur at only these frequencies. This fact would suggest that a measure of linearity consists of the ratio of the power at the input frequencies to the total power:

$$\rho_a^2 = \frac{\sigma_o^2}{\sigma_c^2} = \frac{\sum_{k=1}^M A_k}{c^2 - \bar{c}^2}$$

where

$$A_k = \frac{F^*(c)F(c)}{2T^2} \text{ at } \omega = \omega_k$$

The square root of this ratio has been termed  $\rho_a$  (ref. 7) and an overall measure of linearity. This expression is unchanged conceptually but is presented for information or review. The total power or variance is given by the mean square minus the square of the mean of the total pilot-output signal  $c$ . The linear response equals the sum of the powers at each input frequency, which is given in terms of the Fourier transform of  $c$  as expressed in figure 5. Again, one would be at a loss if a continuous input spectra were used, since the power at the input frequencies would equal the total power output of the pilot, giving an erroneous indication of linearity.

### CONCLUDING REMARKS

It has been shown that discrete sine-wave inputs must be used if meaningful measures of the remnant are to be made. The method of estimating  $Y_p$  has not been changed except that it can be expressed more simply, namely, as the ratio of the Fourier transforms of  $c$  and  $e$ . This form results in increased accuracy by removing the restriction on the amount of data that can be processed.

The linear-correlation coefficient  $\rho$  as presently defined is useless, since it always equals unity. This was shown to result from the bias of the estimate of  $Y_p$ . Suggested modifications of the parameter must be scrutinized and tested before they can be used with confidence.

The parameter  $\rho_a$ , which has been used as an overall measure of linearity, is derived from the ratio of the powers of the linear portion of the pilot's output  $o$  to the total pilot output  $c$ . This parameter has not been altered by these developments except that discrete sine-wave inputs must be used in the experiments to enable it to be calculated.

The incorporation of these findings should result in more accurate measures and models of human response, a goal toward which the Flight Research Center will continue to work.

## REFERENCES

1. Graham, Dunstan; and McRuer, Duane: Analysis of Nonlinear Control Systems. John Wiley & Sons, 1961.
2. James, H. M.; Nichols, N. B.; and Phillips, R. S.: Theory of Servomechanisms. McGraw-Hill Book Co., Inc., 1947.
3. Solodovnikov, V. V. (John B. Thomas and Lofti A. Zadeh, trans. ed.): Introduction to the Statistical Dynamics of Automatic Control Systems. Dover Publications, Inc. (New York), 1960.
4. Bartlett, M. S.: An Introduction to Stochastic Processes with Special Reference to Methods and Applications. The Syndics of the Cambridge University Press (New York), 1955.
5. Grenander, Ulf; and Rosenblatt, Murray: Statistical Analysis of the Stationary Time Series. John Wiley & Sons, 1957.
6. Elkind, Jerome I.: Further Studies of Multiple Regression Analysis of Human Pilot Dynamic Response: A Comparison of Analysis Techniques and Evaluation of Time-Varying Measurements. WADD Rep. ASD-TDR-63-618, Wright Air Development Division, U.S. Air Force, Mar. 1964.
7. McRuer, Duane; Graham, Dustan; Krendel, Ezra; and Reisener, William, Jr.: Human Pilot Dynamics in Compensatory Systems. Tech. Rep. AFFDL TR-65-15, U.S. Air Force, July 1965.

## 29. ANALYSIS AND PREDICTION OF PERFORMANCE OF A DIGITAL COMPUTER FACILITY FOR FLIGHT SIMULATION STUDIES

*M.C. Grignetti and J.I. Elkind  
Bolt Beranek and Newman*

We are concerned with the design of a digital computer facility for use in manual control and flight simulation studies. The facility will provide a group of experimenters with the means of monitoring the signals and data obtained from their experiments while they are being run, for extracting information from these signals in order to control the experiments, for recording the data and signals in permanent files, for editing these data, and for applying a variety of different analysis techniques to the edited data.

Let us try to depict the situation with which we are concerned. Suppose a large experimental program is to be carried out by a research group. We can expect that several experiments will be running simultaneously and will give rise to simultaneous demands for real-time computations that will have to be performed immediately after each run, and thus, there will occur simultaneous demands for high-priority, non-real-time computations. In addition, experimenters who have completed their experiments, or who are planning new experiments, will want to examine their data files using a conversational mode of interaction with the computer. These users will generate low-priority demands for non-real-time computations. For the most part, the demands for service will be random, and certainly subject to unpredictable interruptions and delays. Thus, the system must be designed to service a non-predictable, randomly varying load.

Two main sources of randomness can be readily singled out: (1) the times at which the demands for service are initiated are not predictable; and (2) the time required to service a demand, that is, to perform the computations requested by the user, will vary in some non-predictable way from demand to demand. Viewed in this light, the appropriate models to use to represent and analyze the system's behavior are the Markov models that form the basis of queueing theory.

We would like to emphasize this last statement since we think it is of considerable importance. To analyze complex man-machine systems, use methods of operations research. It is this message we are trying to convey, rather than the scarce and partial results that are presented subsequently. In the following paragraphs a preliminary attempt is presented to apply these notions to the rationalization of the design of a digital computer facility of the indicated type.

The specific problem we shall be concerned with is the allocation of computer capacity among the different computer functions so that certain user performance criteria are satisfied.

Let us concentrate on two of the computer functions that were outlined before, that is, (1) real-time computations, and (2) high-priority computations.

When a real-time user is given service, he is assured of receiving as much processor capacity as he may need. This is necessary for he otherwise would not be able to cope with his data rate, that is, he would not be a "real-time" user. However, when a high-priority user enters the system, he gets only the processor capacity that was left over by the real-time users. As soon as the demands for central processing by both real-time and high-priority users exceed the central processor's capacity, the high-priority users' service rate is diminished. This dependence of the high-priority users' service rate on the number of real-time users being simultaneously served introduces a fair amount of complication in the analysis.

The data we have concerning the demands made on systems of this nature is very scarce and there is little justification for using any but the simplest models to represent the stochastic nature of these demands. The simplest assumption that we can make is that they are of Poisson distribution. This is equivalent to saying that the time interval between demands for service and the time to service a demand is exponentially distributed; for example

$$\rho(t) = \lambda e^{-\lambda t}$$

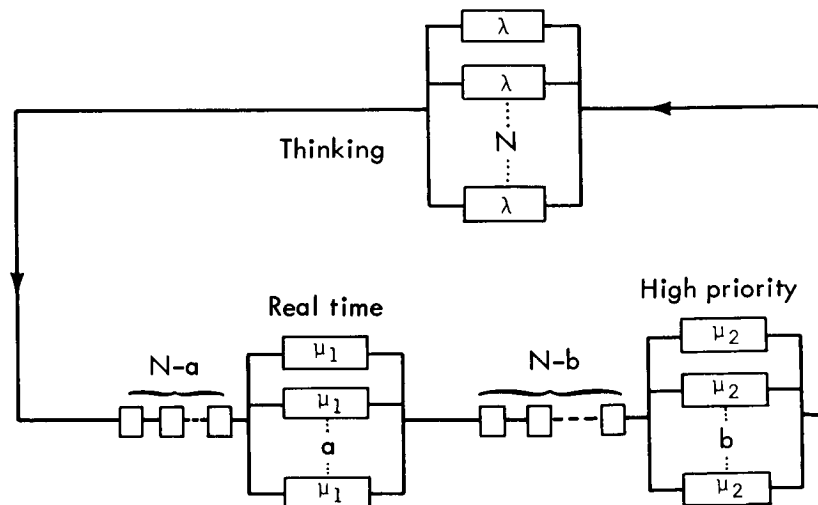
where

$\rho(t)$  probability density that the interarrival time be  $t$

$\lambda$  mean rate of arrivals

The simplicity of this description is evident in that it requires only one parameter.

A model that represents fairly accurately the behavior of the system we are describing is given below:



where

- N    number of users in the group
- $\lambda$     mean rate of user's demand for service
- $\mu_1$     mean service rate for real-time users
- $\mu_2$     mean service rate for high-priority users
- a    number of real-time service channels
- b    number of high-priority service channels

Each box on the bottom branch of the main loop represents a service channel to which a fixed amount of computation capacity is assigned. Queues can be formed before each computer function.

The model operates as follows: A given user occupies one of the  $\lambda$  boxes; he is thinking. When he demands service he lines up in front of the real-time service facility. The number of channels allocated to this computer function is a, while b is the number of channels allocated to the high-priority users. The two integers a and b can change, but they are subjected to the condition

$$a + kb = C$$

that represents the fixed total capacity of the system.

Once the user exits the real-time service facility, he lines up for high-priority service; and when he has finished, he goes back to his cubicle to "think" again. Observe that there are N such "thinking" channels, so that no queues are formed.

The behavior of models of this type is described by the steady-state probabilities  $P_{n,m}$  that n real-time and m high-priority users will be simultaneously waiting or being serviced at each facility. With the probabilities  $P_{n,m}$  we can then calculate user performance indexes like average waiting times and queue lengths and manipulate a and b so that user performance criteria based on waiting times, for example, can be satisfied. These probabilities may be very difficult to determine. Generally speaking, two avenues of approach are available, namely, analytical and Monte Carlo methods.

By the analytical method, the steady-state probabilities are determined using the resources of mathematical analysis. In our model, the probabilities are obtained by solving the following equation of partial differences:

$$[(N-m-n)\lambda + \mu_1(n) + \mu_2(m)] P_{n,m} = (N-m-n+1)\lambda P_{n-1,m} + \mu_1(m) P_{n+1,m-1} + \mu_2(m) P_{n,m+1}$$

where

$$\mu(n) = \begin{cases} n\mu_1 & \text{for } 0 \leq n \leq a \\ a\mu_1 & \text{for } n > a \end{cases}$$

$$\mu_2(m) = \begin{cases} m\mu_2 & \text{for } 0 \leq m \leq b \\ b\mu_2 & \text{for } m > b \end{cases}$$

Despite the innocent looking aspect of this equation, it has proved exceedingly difficult to solve. Its solution is

$$P_{n,m} = \frac{P_{00}}{(N-n-m)!} p(n, a, \mu_1) p(m, b, \mu_2)$$

where

$$p(n, a, \mu_1) = \begin{cases} \frac{(\lambda/\mu_1)^n}{n!} & \text{for } n \leq a \\ \frac{a(\lambda/\mu_1 a)^n}{a!} & \text{for } n > a \end{cases}$$

and where  $P_{00}$  is determined so that

$$\sum_{m=0}^N \sum_{n=0}^{N-m} P_{nm} = 1$$

The other approach, known for a long time but only recently resuscitated with the advent of high-speed computation machines, is to use Monte Carlo methods.

In following this approach the model is simulated and then is subjected to simulated inputs, with the goal of determining the probabilities by sheer frequency count.

We have followed this approach while attempting to determine the behavior of a more complicated model, where users require not only computation service, but part of the system's hardware as well. For example, let us suppose that the system has  $I$  data inputs and each user requires a randomly varying number  $i$  of data inputs, so that to service a user the system must now be able to provide not only the required computation service, but must have available at least  $i$  data input channels as well.

A Monte Carlo program like the one required by the simple example above can be readily put together using our TELCOMP facilities. The following is a typical output page.

T = 583.0409  
 M = 2.623797  
 U = 6  
 AVC = 13  
 W = 0

T = 615.3456  
 M = 2.514103  
 U = 6  
 AVC = 15  
 W = 2

T = 585.9525  
 M = 2.488071  
 U = 6  
 AVC = 13  
 W = 1

T = 640.6175  
 M = 2.514103  
 U = 6  
 AVC = 15  
 W = 3

T = 597.5138  
 M = 2.488071  
 U = 6  
 AVC = 13  
 W = 8  
 T-TEX(U) = 22.44865

T-TEX(U) = 52.42552  
 T = 649.9393  
 M = 2.514103  
 U = 6  
 AVC = 16  
 W = 2

T = 608.4011  
 M = 2.488071  
 U = 6  
 AVC = 15  
 W = 1

T = 660.7608  
 M = 2.52732  
 U = 6  
 AVC = 16  
 W = 3

T = 664.454

The meaning of the symbols is as follows:

T            time, seconds  
 M            number of time-sharing cycles  
 U            number of users being serviced  
 AVC          number of input data lines still available  
 W            number of users in waiting line  
 T-TEX(U)    time in waiting line, seconds

Letting the program run for a sufficiently long time, the probabilities  $P_{n,m}$  and other statistics can be computed by frequency count.

In closing, as a word of caution in the use of these methods, we quote from Hamming: "The purpose of computing is insight, not numbers." Hence, without at least a couple of failures in the analytical approach, it is not worthwhile to "Monte Carlo" the problem. This, we know by experience.

01701  
5284  
3-2-67

*"The aeronautical and space activities of the United States shall be conducted so as to contribute . . . to the expansion of human knowledge of phenomena in the atmosphere and space. The Administration shall provide for the widest practicable and appropriate dissemination of information concerning its activities and the results thereof."*

—NATIONAL AERONAUTICS AND SPACE ACT OF 1958

## NASA SCIENTIFIC AND TECHNICAL PUBLICATIONS

**TECHNICAL REPORTS:** Scientific and technical information considered important, complete, and a lasting contribution to existing knowledge.

**TECHNICAL NOTES:** Information less broad in scope but nevertheless of importance as a contribution to existing knowledge.

**TECHNICAL MEMORANDUMS:** Information receiving limited distribution because of preliminary data, security classification, or other reasons.

**CONTRACTOR REPORTS:** Scientific and technical information generated under a NASA contract or grant and considered an important contribution to existing knowledge.

**TECHNICAL TRANSLATIONS:** Information published in a foreign language considered to merit NASA distribution in English.

**SPECIAL PUBLICATIONS:** Information derived from or of value to NASA activities. Publications include conference proceedings, monographs, data compilations, handbooks, sourcebooks, and special bibliographies.

**TECHNOLOGY UTILIZATION PUBLICATIONS:** Information on technology used by NASA that may be of particular interest in commercial and other non-aerospace applications. Publications include Tech Briefs, Technology Utilization Reports and Notes, and Technology Surveys.

*Details on the availability of these publications may be obtained from:*

SCIENTIFIC AND TECHNICAL INFORMATION DIVISION  
NATIONAL AERONAUTICS AND SPACE ADMINISTRATION  
Washington, D.C. 20546